

29TH ANNUAL PRECISE TIME AND TIME INTERVAL (PTTI) SYSTEMS AND APPLICATIONS MEETING



DISTRIBUTION STATEMENT A
Approved for Public Release
Distribution Unlimited

*Proceedings of a meeting held at
The Sheraton Long Beach Hotel
Long Beach, California
2 — 4 December 1997*

20031103 138

*The U.S. Naval Observatory
Washington, DC*



NONPRINT FORM

1. Type of Product: softcover book	2. Operating System/Version:	3. New Product or Replacement: New	4. Type of File: Text
5. Language/Utility Program:			
6. # of Files/# of Products:	7. Character Set:	8. Disk Capacity:	
	9. Compatibility:	10. Disk Size:	
11. Title: Proceedings of the 29th Annual Precise Time and Time Interval (PTTI) Systems and Applications Meeting			
12. Performing Organization: U.S. Naval Observatory 3450 Massachusetts Ave., NW Washington, DC 20392-5420	13. Performing Report #:	14. Contract #:	
		15. Program Element #:	
16. Sponsor/Monitor: U.S. Naval Observatory 3450 Massachusetts Ave., NW Washington, DC 20392-5420	17. Sponsor/Monitor # Acronym:	19. Project #:	
	18. Sponsor/Monitor #:	20. Task #:	
		21. Work Unit #:	
22. Date: 1998		23. Classification of Product: Unclassified	
24. Security Classification Authority: DOD		25. Declassification/Downgrade Schedule: none	
26. Distribution/Availability: A Approved for public release; distribution is unlimited.			

27. Abstract: This document is a compilation of technical papers presented at the 29th Annual Precise Time and Time Interval (PTTI) Systems and Applications Meeting held 2-4 December 1997 at the Sheraton Long Beach Hotel at Long Beach, California. Papers are in the following categories:

- Recent developments in rubidium, cesium, and hydrogen-based atomic frequency standards, and in trapped-ion and space clock technology;
- National and international applications of PTTI technology with emphasis on GPS and GLONASS timing, atomic time scales, and telecommunications;
- Applications of PTTI technology to evolving military navigation and communication systems; geodesy; aviation; and pulsars;
- Dissemination of precise time and frequency by means of GPS, geosynchronous communication satellites, and computer networks.

28. Classification of Abstract:
Unclassified

29. Limitation of Abstract:
Unclassified Unlimited

30. Subject Terms: time, atomic time, time scales, precise time, frequency standards, precision oscillators, cesium, rubidium, hydrogen masers, trapped ion, time transfer, frequency transfer, synchronization, GPS, navigation, telecommunications, communication satellites, computer networks, geodesy, relativity

30a. Classification of Subject Terms:
Unclassified

31. Required Peripherals:

32. # of Physical Records:

33. # of Logical Records:

34. # of Tracks:

35. Record Type:

36. Color:
Black and White

37. Recording System:

38. Recording Density:

39. Parity:

40. Playtime:

41. Playback Speed:

42. Video:
No

43. Text:
Yes

44. Still Photos:
No

45. Audio:
No

46. Other:

47. Documentation/Supplemental Information:

Bound hardcopies are available from POC. Hardcopies may also be ordered via <http://tycho.usno.navy.mil/ptti/orderform.html>. Table of contents available at <http://tycho.usno.navy.mil/ptti/index.html>.

48. Point of Contact and Telephone Number: Lee A. Breakiron
Time Service Department, U.S. Naval Observatory, 3450 Massachusetts Ave., NW, Washington, DC 20392-5420
(202) 762-1092
lab@kepler.usno.navy.mil

29TH ANNUAL PRECISE TIME AND TIME INTERVAL (PTTI) SYSTEMS AND APPLICATIONS MEETING

Editor
Lee A. Breakiron
U.S. Naval Observatory

Proceedings of a meeting sponsored by
the U.S. Naval Observatory
the U.S. Naval Research Laboratory
NASA Headquarters
the NASA Jet Propulsion Laboratory
the Space and Naval Warfare Systems Command
the Air Force Office of Scientific Research
and the U.S. Air Force Space Command

and held at
The Sheraton Long Beach Hotel
Long Beach, California
2 — 4 December 1997



United States Naval Observatory
Washington, DC 20392-5420

1998

ORDER FORM FOR PROCEEDINGS

You can order back issues of the Proceedings from either PTTI or NTIS

Year	PTTI Price	NTIS Number	NTIS Price subject to change without notice
1 - 1969*		unavailable	
2 - 1970**	\$ 25.00	AD-881014 (incl. Vols. 1 and 2)	\$ 44.00
3 - 1971**	\$ 25.00	AD-758739	\$ 71.50
4 - 1972**	\$ 25.00	AD-A010785/4	\$ 61.50
5 - 1973**	\$ 25.00	AD-A010786/2	\$ 84.00
6 - 1974	\$ 25.00	AD-A018192/5	\$ 84.00
7 - 1975	\$ 25.00	AD-A040774/2	\$ 115.00
8 - 1976**	\$ 25.00	AD-A043856/4	\$ 115.00
9 - 1977**	\$ 25.00	AD-A123920/1	\$ 84.00
10 - 1978	\$ 25.00	N79-24731/8	\$ 125.00
11 - 1979	\$ 25.00	N80-29096/8	\$ 115.00
12 - 1980	\$ 25.00	N81-27467/2	\$ 125.00
13 - 1981	\$ 25.00	N82-20494/2	\$ 125.00
14 - 1982**	\$ 25.00	N83-35351/6	\$ 106.00
15 - 1983**	\$ 25.00	AD-A149163/8	\$ 115.00
16 - 1984	\$ 25.00	N85-29221/7	\$ 71.50
17 - 1985	\$ 25.00	unavailable	
18 - 1986	\$ 25.00	unavailable	
19 - 1987***	\$ 25.00	unavailable	
20 - 1988	\$ 35.00	AD-A217145/2	\$ 61.50
21 - 1989	\$ 65.00	unavailable	
22 - 1990	\$ 70.00	N91-25755/0	\$ 106.00
23 - 1991	\$ 85.00	AD-A255837/7	\$ 57.00
23 - Tutorial	included	AD-A254745/3	\$ 39.00
24 - 1992	\$ 85.00	AD-A267301/0	\$ 57.00
25 - 1993	\$ 85.00	N94-30639/6	\$ 67.00
26 - 1994***	\$ 95.00	N95-32319/2	\$ 57.00
27 - 1995	\$ 115.00	unavailable	
28 - 1996	\$ 115.00	unavailable	
28 - Tutorial	\$ 35.00	unavailable	
29 - 1997	\$ 135.00	unavailable	

*The Proceedings of the 1st PTTI meeting consists of an 8-page report.

**Original Proceedings no longer available for sale; however, copies made from the original can be purchased from PTTI.

***Includes an Errata volume

When ordering from PTTI, return order form with payment to:

PTTI Executive Committee
U.S. Naval Observatory
3450 Massachusetts Avenue, NW
Washington, DC 20392-5420
Tel: 202-762-1414, Fax: 202-762-1511

When ordering from NTIS, contact:

U.S. Department of Commerce
Technology Administration
National Technical Information Service
Springfield, VA 22161
Tel: 703-487-4630

Make checks payable to "Treasurer, PTTI." Do not send cash. We cannot accept credit card orders. When you register for the PTTI meeting or order the Proceedings, your name is added to the PTTI mailing list to receive future meeting information.

EXECUTIVE COMMITTEE

DR. JOSEPH D. WHITE, CHAIRMAN
U.S. Naval Research Laboratory

MR. RONALD L. BEARD
U.S. Naval Research Laboratory

DR. LEE A. BREAKIRON
U.S. Naval Observatory

(VACANT)
U.S. Air Force Space Command

DR. HELMUT HELLWIG
Deputy Assistant Secretary Air Force/AQR

MR. PAUL F. KUHNLE
Jet Propulsion Laboratory

DR. DENNIS D. MCCARTHY
U.S. Naval Observatory

MR. JOHN R. RUSH
NASA Headquarters

COMMANDER TIMOTHY F. SHERIDAN, USN
Space and Naval Warfare Systems Command

DR. RICHARD L. SYDNOR
Jet Propulsion Laboratory (Retired)

MS. FRANCINE M. VANNICOLA
U.S. Naval Observatory

MS. NICOLETTE M. JARDINE
Administrative Assistant
U.S. Naval Observatory

OFFICERS

GENERAL CHAIRMAN
Ms. FRANCINE M. VANNICOLA
U.S. Naval Observatory

TECHNICAL PROGRAM COMMITTEE CHAIRMAN
MR. DONALD H. MITCHELL
TrueTime, Inc.

TECHNICAL PROGRAM COMMITTEE
DR. HENRY F. FLIEGEL
The Aerospace Corporation

MR. PAUL F. KUHNLE
Jet Propulsion Laboratory

DR. RICHARD L. SYDNOR
Jet Propulsion Laboratory

MR. S. CLARK WARDRIP
AlliedSignal Technical Services Corporation

EDITOR
DR. LEE A. BREAKIRON
U.S. Naval Observatory

TREASURER
DR. LEE A. BREAKIRON
U.S. Naval Observatory

EXHIBITS AND PUBLICITY COMMITTEE CHAIRMAN
MR. DONALD H. MITCHELL
TrueTime, Inc.

TECHNICAL ASSISTANCE
MR. JEFFREY S. INGOLD
MR. S. CLARK WARDRIP
AlliedSignal Technical Services Corporation

PTTI AWARD COMMITTEE

DR. LEONARD S. CUTLER, CHAIRMAN
Hewlett-Packard Company

DR. HENRY F. FLIEGEL
The Aerospace Corporation

DR. RICHARD L. SYDNOR
Jet Propulsion Laboratory

PAST RECIPIENTS OF THE DISTINGUISHED PTTI SERVICE AWARD

1994

DR. GERNOT M. R. WINKLER
U.S. Naval Observatory
(Retired)

1995

DR. JAMES A. BARNES
National Institute of
Standards and Technology
(Retired)

1996

DR. SIGFRIDO LESCHIUTTA
Politenico di Torino and
Istituto Elettrotecnico Nazionale G. Ferraris

SESSION CHAIRMEN

SESSION I

DR. GERRIT DE JONG
NMI Van Swinden Laboratorium

SESSION VI

DR. ROBERT J. DOUGLAS
National Research Council of Canada

SESSION II

MR. GARY GEIL
Geil Marketing Associates

SESSION VII

DR. CLAUDINE THOMAS
Bureau International des
Poids et Mesures

SESSION III

DR. WILLIAM J. KLEPCZYNSKI
Innovative Solutions International

SESSION VIII

MR. BRUCE PROCTOR
U.S. Army Yuma Proving Group

SESSION IV

MR. MARNIUS J. VAN MELLE
Boeing North American Space
Operations Company

SESSION IX

MR. RICHARD E. SCHMIDT
U.S. Naval Observatory

SESSION V

Ms. LISA M. NELSON
National Institute of
Standards and Technology

SESSION X

MR. MALCOLM D. CALHOUN
Jet Propulsion Laboratory

POSTER SESSION

MR. JEFFREY S. INGOLD
AlliedSignal Technical Services Corporation

ARRANGEMENTS

**MRS. SHEILA FAULKNER
MR. PAUL F. KUHNLE**

FINANCE COMMITTEE

**MR. RONALD L. BEARD
DR. JOSEPH D. WHITE
DR. LEE A. BREAKIRON**

THE RECEPTIONISTS FOR THE 29TH ANNUAL PTTI MEETING WERE:

**MRS. KATHY HIBBARD
MS. BRENDA HICKS
MS. NICOLETTE JARDINE
MRS. ALINE KUHNLE
MRS. BETTY WARDRIP
MS. JAIMIE WHITE**

ADVISORY BOARD MEMBERS

MR. S. CLARK WARDRIP, CHAIRMAN

AlliedSignal Technical Services Corporation

Professor Carroll O. Alley
University of Maryland

Mr. Martin B. Bloch
Frequency Electronics, Inc.

Mr. Peter E. Cash
Frequency and Time Systems
Datum, Inc.

Mrs. Mary Chiu
The Johns Hopkins University
Applied Physics Laboratory

Lt. Col. Michael Cimafronte, USAF (Ret.)
System Technology Associates, Inc.

Dr. Leonard S. Cutler
Hewlett-Packard Company

Mrs. Sheila C. Faulkner
Meetings Consultant

Dr. Henry F. Fliegel
The Aerospace Corporation

Mr. Jeffrey S. Ingold
AlliedSignal Technical Services
Corporation

Mr. Robert H. Kern
KERNCO, Inc.

Dr. William J. Klepczynski
Innovative Solutions, Inc.

Dr. Paul A. Koppang
Sigma Tau Standards Group

Mr. Pete R. Lopez
TRAK Systems

Mr. Donald H. Mitchell
TrueTime, Inc.

Mr. Jerry R. Norton
The Johns Hopkins University
Applied Physics Laboratory

Mr. Allen W. Osborne, III
Allen Osborne Associates

Mr. Terry N. Osterdock
Absolute Time

Dr. Bradford W. Parkinson
Stanford University

Dr. Victor S. Reinhardt
Hughes Aircraft

Mr. William J. Riley
EG&G, Inc.

Dr. Henry Robinson
Duke University

Mr. Ronald C. Roloff
Advanced Technology Resources

Dr. Samuel R. Stein
Timing Solutions Corporation

Dr. Richard L. Sydnor (Ret.)
Jet Propulsion Laboratory

Mr. Michael R. Tope
TrueTime, Inc.

Mr. James L. Wright
Computer Sciences Raytheon

TABLE OF CONTENTS

PTTI OPENING ADDRESS	1
-----------------------------------	----------

**Dr. Joseph D. White, U.S. Naval Research Laboratory; and
Dr. Dennis D. McCarthy, U.S. Naval Observatory**

PTTI DISTINGUISHED SERVICE AWARD	3
---	----------

**Presented by
Dr. Leonard S. Cutler
Hewlett-Packard Company
to
Prof. Bernard René Guinot
Paris Observatory**

SESSION I

INTERNATIONAL PTTI REPORTS

**Dr. Gerrit de Jong, Chairman
NMI Van Swinden Laboratorium**

Proposals for Updating TAI Algorithm C. Thomas and J. Azoubib, Bureau International des Poids et Mesures ..	7
--	----------

The Accuracy of TAI C. Thomas, Bureau International des Poids et Mesures	19
---	-----------

SESSION II

NEW PRODUCTS FOR THE TIMING COMMUNITY

**Mr. Gary Geil, Chairman
Geil Marketing Associates**

Presentations were made by representatives of Absolute Time Corporation; Brandywine Communications; Datum, Inc.; EG&G Frequency Products; Femtosecond Systems; Guide Technology; Starlink, Inc.; 3S Navigation; TimeTech GmbH; TRAK Systems; TrueTime, Inc.; and WR, Inc.

Panel Discussion: Timing Systems

J. D. White, U.S. Naval Research Laboratory (moderator) 27

SESSION III

STANDARDS AND ANALYSIS

Dr. William J. Klepczynski, Chairman
Innovative Solutions International

**Relationships Between Drift Coefficient Uncertainties and Noise Levels:
Application to Time Error Prediction**

F. Vernotte and M. Vincent, Observatoire de Besançon, France 29

**Total Variance: A Progress Report on a New Frequency Stability
Characterization**

D. A. Howe, National Institute of Standards and Technology; and C. A.
Greenhall, Jet Propulsion Laboratory 39

Maintenance of HP 5071A Primary Frequency Standards at USNO

H. Chadsey and A. Kubik, U.S. Naval Observatory 49

**The SHM Hydrogen Atomic Clock for Space Applications: Development
and Test of the PEM Physics Package**

L. G. Bernier, A. Jornod, H. Schweda, R. Gentsch, and G. Busca,
Observatoire Cantonal de Neuchâtel, Switzerland 61

GPS Receivers and Relativity

M. Weiss, National Institute of Standards and Technology; and N. Ashby,
University of Colorado 69

**The CCTF Working Group on the Expression of Uncertainties in Primary
Frequency Standards**

R. J. Douglas, National Research Council of Canada; and C. Thomas,
Bureau International des Poids et Mesures 85

Total Variance as an Exact Analysis of the Sample Variance

D. B. Percival, University of Washington; and D. A. Howe, National
Institute of Standards and Technology 97

**Narrow-band Searches for Gravitational Radiation with Spacecraft
Doppler Tracking**

M. Tinto and J. W. Armstrong, Jet Propulsion Laboratory 107

POSTER SESSION

Mr. Jeffrey S. Ingold, Chairman
AlliedSignal Technical Services Corporation
(papers have been reassigned to Sessions III, IV, V, and VI)

SESSION IV

GPS APPLICATIONS

Mr. Marnius J. Van Melle, Chairman
Boeing North American Space Operations Company

- The 2 SOPS Ephemeris Enhancement Endeavor (EEE)**
Capt. J. D. Crum, USAF, 2nd Space Operations Squadron; S. T. Hutsell,
U.S. Naval Observatory Alternate Master Clock; and R. T. Smetek, Jr.,
Boeing North American Space Operations Company 117
- Refining Monitor Station Weighting in the GPS Composite Clock**
Lt. H. S. Mobbs, USAF, 2nd Space Operations Squadron; and S. T.
Hutsell, U.S. Naval Observatory Alternate Master Clock 131
- A New Approach to Ionospheric Delay Corrections in Single Frequency
GPS Receivers**
G. Mirena, V. Pettiti, F. Cordara, Istituto Elettrotecnico Nazionale
"Galileo Ferraris," Italy; and L. Ciraolo, Istituto di Ricerca sulle Onde
Elettromagnetiche "Nello Carrara," Italy 143
- Performance of the Kalman Filter of the Global Positioning System
Operational Control Segment during January - March 1997**
M. Weiss and A. Zarr, National Institute of Standards and Technology . 155
- Long-Term Evaluation of GPS Timing Receiver Failures**
D. Höchtl and U. Schmid, Technische Universität Wien, Austria 165
- SVN 20 End-Of-Life Frequency Standard Test Results**
Lt. R. E. Bower, USAF, 2nd Space Operations Squadron; G. L. Dieter, and
M. J. Van Melle, Boeing North American Space Operations Company . 181
- Absolute Time Error Calibration of GPS Receivers Using Advanced
GPS Simulators**
E. D. Powers and M. Miranian, U.S. Naval Observatory 193
- Atomic Frequency Standards for the GPS IIF Satellites**
W. Emmer and E. Watts, Boeing North American Space Operations
Company 201
- Early In-Orbit Performance of GPS Block IIR Rubidium Clocks**
W. J. Riley, EG&G Frequency Products 213

SESSION V

TIME TRANSFER TECHNIQUES

Ms. Lisa M. Nelson, Chairman
National Institute of Standards and Technology

- Time Transfer Using GPS Carrier Phase Methods**
K. M. Larson, University of Colorado; and J. Levine, National Institute of Standards and Technology 221
- GLONASS/GPS Time Transfer and the Problem of the Determination of Receiver Delays**
G. de Jong, NMI van Swinden Laboratorium; and W. Lewandowski, Bureau International des Poids et Mesures 229
- Delay Stability of the TWSTFT Earth Station at VSL**
G. de Jong, NMI van Swinden Laboratorium, the Netherlands 241
- C- and Ku-Band Two-Way Satellite Time Transfer Comparison Experiment**
R. Beard, I. Galysh, J. Oaks, M. Largay, P. Landis, W. Reid, U.S. Naval Research Laboratory; M. Ehnert, R. Eisenhauer, USAF, Space and Missile Systems Center; W. Hanson, L. Nelson, A. Clements, National Institute of Standards and Technology; J. Durden, L. Brownhill, Comlink, Inc.; J. Wright, C. Duffy, Computer Sciences Raytheon; J. Kasik, COMSAT; and J. Buisson, Antoine Enterprises, Inc. 253
- An Operational TWSTT Monitoring System**
P. Mai and J. DeYoung, U.S. Naval Observatory 265

SESSION VI

MULTI-CHANNEL GPS APPLICATIONS

Dr. Robert J. Douglas, Chairman
National Research Council of Canada

- Common-View Time Transfer Using Multi-Channel GPS Receivers**
L. Schmidt and M. Miranian, U.S. Naval Observatory 269
- Multi-Channel vs. Common-View GPS Frequency Transfer Comparison in the Asia-Pacific Region**
P. T. H. Fisk, M. A. Lawn, S. Quigg, J. S. Thorn, National Measurement Laboratory, Australia; T. Armstrong, Measurement Standards Laboratory of New Zealand; J. McK. Luck, J. R. Woodger, Ororol Geodetic Observatory, Australia; and M. M. Ruiz, Industrial Technology Development Institute, Philippines 277

On Improvements Of and Suggestions About GPS "Common-View" with Multi-Channel Time Receivers - First Results	
J. Hahn, H. Nau, Institut für Hochfrequenztechnik, Germany; and P. Moussay, Bureau International des Poids et Mesures	287
A New Approach to Common-View Time Transfer Using "All-In-View" Multi-Channel GPS and GLONASS Observations	
J. Azoubib, W. Lewandowski, Bureau International des Poids et Mesures; G. de Jong, NMi van Swinden Laboratorium, the Netherlands; and J. Danaher, 3S Navigation	299
Multi-Channel GPS Common-View Time Transfer Experiments: First Results and Uncertainty Study	
G. Petit, C. Thomas, P. Moussay, Bureau International des Poids et Mesures; J. A. Davis, National Physical Laboratory, UK; M. Miranian, U.S. Naval Observatory; and J. Palacio, Real Instituto y Observatorio de la Armada, Spain	309
Time Transfer with GPS Multi-Channel Motorola Oncore Receiver Using CCDS Standards	
J. Nawrocki, Astrogeodynamical Observatory, Poland; W. Lewandowski, and J. Azoubib, Bureau International des Poids et Mesures	319

SESSION VII

INTERNATIONAL TIMING AND SYNCHRONIZATION

Dr. Claudine Thomas, Chairman
Bureau International des Poids et Mesures

A Study Examining the Possibility of Obtaining Traceability to UK National Standards of Time and Frequency Using GPS-Disciplined Oscillators	
J. A. Davis and J. M. Furlong, National Physical Laboratory, UK	329

SESSION VIII

RANGE AND TIMING COUNTDOWN

Mr. Bruce Proctor
U.S. Army Yuma Proving Ground

Utilization of the Global Positioning System (GPS) for Timing Systems Under Range Standardization & Automation Phase-IIA Program	
M. C. Lee, Lockheed Martin Space Mission Systems & Services	345

The WSMR Timing System: Approaching the Horizon	
W. A. Gilbert, White Sands Missile Range	357

SESSION IX

NETWORK AND TELECOMMUNICATIONS TIMING AND SYNCHRONIZATION

Mr. Richard E. Schmidt, Chairman
U.S. Naval Observatory

Internet Timekeeping Around the Globe	
D. L. Mills, A. Thyagarjan; and B. C. Huffman, University of Delaware ..	365
SIPRNET Network Time Service	
R. E. Schmidt, U.S. Naval Observatory	373
The Application of NTP to Navy Platforms	
K. F. O'Donoghue and D. T. Marlow, Naval Surface Warfare Center ...	381
Benefits and Issues on the Integration of GPS with a Wireless Communications Link	
R. DiEsposti, S. Saks, L. Jovic, The Aerospace Corporation; and J. Kayloe, USAF, Space and Missile Center	391
Panel Discussion: Time Rollover Events: Year 2000 (Y2K), GPS Week 1024, Leap Second, and Leap Year	
J. Levine, National Institute of Standards and Technology (moderator) .	399

SESSION X

FIBER OPTIC TIMING APPLICATIONS

Mr. Malcolm D. Calhoun, Chairman
Jet Propulsion Laboratory

Long-Term Time Transfer Stability of a Fiber Optic Link	
O. Buzek, Czech Institute of Radio Engineering and Electronics	405
Two-Way Time Transfer Through 2.4 Gbit/s Optical SDH System	
M. Kihara, A. Imaoka, NTT Optical Network Systems Laboratories, Japan; M. Imae and K. Imamura, Communications Research Laboratory, Japan	415

Results from Proof-Of-Concept Time-Based Communications Testing T. P. Celano, S. R. Stein, Timing Solutions Corporation; G. A. Gifford, U.S. Naval Observatory; E. A. Swanson, B. R. Hemenway, Jr., and J. C. Carney, MIT Lincoln Laboratory	423
List of Attendees	435

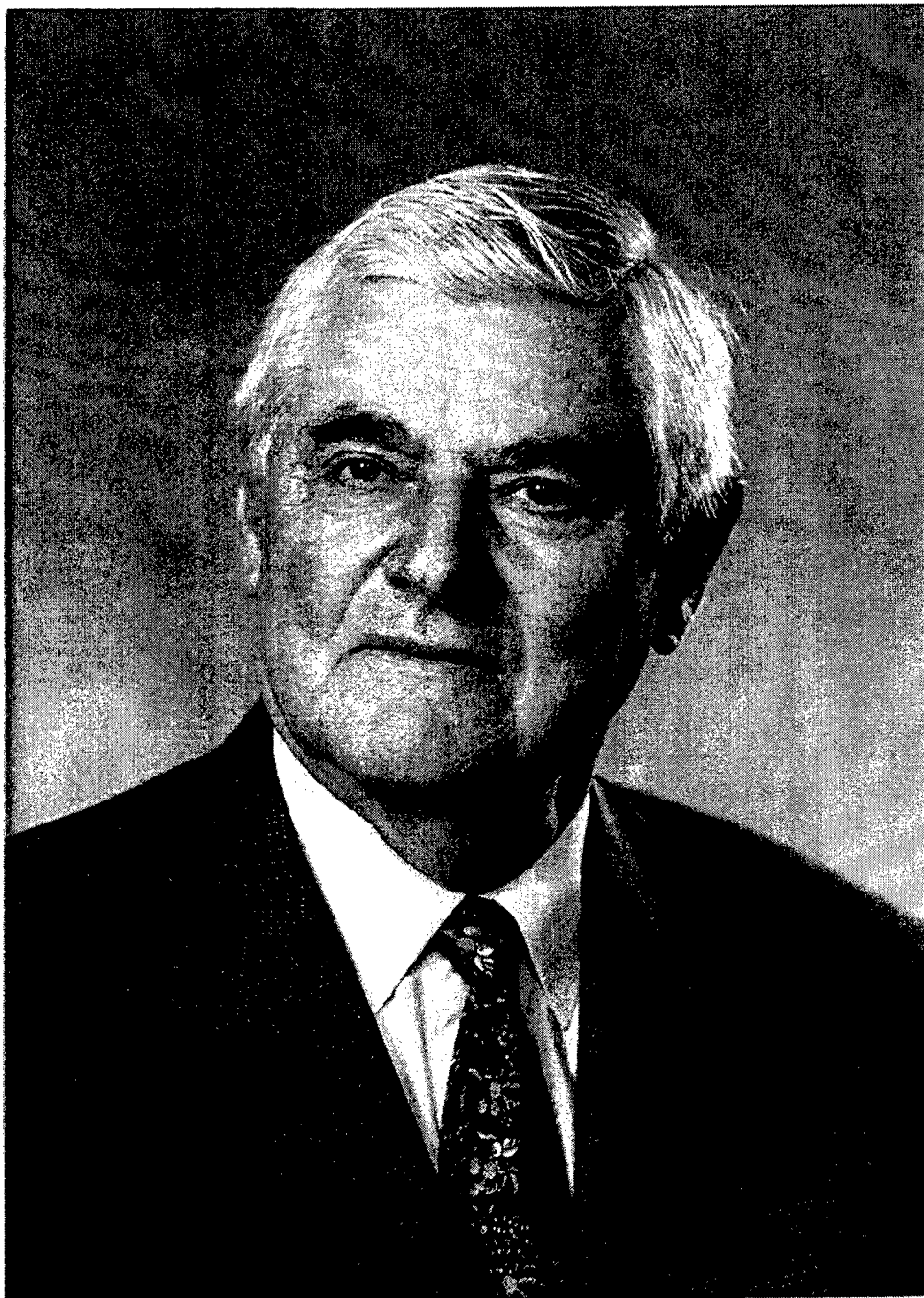
PTTI OPENING ADDRESS: THE FUTURE OF THE PTTI MEETING

Joseph D. White
U.S. Naval Research Laboratory
Washington, DC 20375

Dennis D. McCarthy
U.S. Naval Observatory
Washington, DC 20392

At the meeting of the PTTI Executive Committee on 30 January 1997, it was decided that the following principles would be implemented in the planning of all future PTTI Meetings:

- The purpose of the PTTI Meeting is to inform users about state-of-the-art capabilities in PTTI and inform government system managers and engineers and sponsoring agencies about new opportunities, programs, and technical challenges requiring PTTI.
- To emphasize the fact that system managers and engineers comprise the majority of the attendees desired, the meeting name has been changed from "The Precise Time and Time Interval Applications and Planning Meeting" to "The Precise Time and Time Interval Systems and Applications Meeting."
- The PTTI Meeting is and will remain an open meeting. This means that it will not be by invitation only. It will be advertised widely and vendors will always be able to participate.
- The PTTI Meeting will be managed more aggressively with regard to its program. A theme and a "matching" Program Committee chair will be selected for each meeting; papers not appropriate to the theme will be rejected. The Program Committee will recruit invited papers and arrange discussions and workshops in keeping with the theme. Details of the mechanics of the meeting organization will be left to the Program Committee, but the program must be approved by the Executive Committee. Each sponsoring agency will have the option of naming a representative to the Program Committee. Classified sessions may be arranged if appropriate. The meeting should be no longer than 3 days in length.
- The PTTI Meeting will continue as an annual meeting independent of other meetings, but the Executive Committee shall have the option to plan joint meetings if it feels that a joint meeting would contribute positively to the theme of the PTTI Meeting.



PTTI DISTINGUISHED SERVICE AWARD

Presented to
Prof. Bernard René Guinot
Honorary Astronomer
Paris Observatory
by

Dr. Leonard S. Cutler
Hewlett-Packard Co.

It is again a particular honor and a great pleasure for me to help recognize past achievements in the time and frequency arena. I am very happy, with inputs from Dr. Claudine Thomas, to do this for Bernard Guinot, a distinguished scientist, astronomer, and friend for many years. I am certain everyone agrees that he is very well qualified to receive this award, as evidenced by an impressive list of important contributions, accomplishments, and awards.

Bernard was born in Livarot, France, in 1925. From 1945 to 1952, he was an Officer in the Merchant Navy. In 1946-47, he was on a small freighter in the Far East with a Chinese crew. The ship's radio officer was drunk 24 hours a day and, for a full year, was not able to get a single time signal. This is where Bernard had his first contact with time determination and comparison. He did this by astronomical determination of Universal Time at sea in view of the coast, clock transportation to nearby ships in a harbor, and even synchronization by light signals with ships upon the open sea. This was an early, and very practical, introduction for him to clock synchronization. Later, on more comfortable ships, he resumed his studies in mathematics, thus gaining respect from some of the captains, but also some complaints about not being seen enough among the passengers.

Bernard says that, probably because he was a seaman, the Director of the Paris Observatory, A. Danjon, recruited him to be his assistant in 1952. His first scientific work was to make determinations of Universal Time and latitude by observing the altitude of stars with an astrolabe, invented by Danjon, enabling 1,000 times less uncertainty than with a sextant. The nighttime observations in the open air were often very uncomfortable and sometimes disappointing, as was the case when, after a full winter night of data-taking, Bernard discovered that the janitorial staff had thrown the chronograph tape away.

In 1958, while at the Observatory, he received his Doctor's degree. While there from 1952 to 1984, his title was Astronomer, Paris Observatory. During that time he had two books published: *The Measurement of Time* and *The Equal Altitude Method in Astronomy*.

From 1984 to 1992, he was Physicist, Bureau International des Poids et Mesures. He retired from the BIPM in 1992 and, since then, has been Honorary Astronomer, Paris Observatory. Recently he has written, with Claude Audoin, a third book, *Fundamentals of the Measurement of Time*, to be published in December, 1997.

Some of his accomplishments include:

- Determination of star position by a new method, the equal altitude method, using astrolabes
- Studies and determination of the astronomical constants of aberration and nutation
- Relativistic definition of reference systems
- Introduction of a new concept, the non-rotating origin, allowing a rigorous definition of the earth's rotation about the moving rotation axis
- Work in many aspects of earth rotation and geodesy, including the definition of Universal Time
- Creation of International Atomic Time, TAI, including:
 - Organization of the network of contributing clocks and time comparisons
 - Establishment of stability and accuracy algorithms
 - Organization of TAI dissemination
 - Relativistic definition of TAI
- Promotion of the UTC system and the introduction of a mathematical relation between UTC and TAI
- Transfer of the activities on TAI to the BIPM.

Bernard considers his creation of TAI and the concept of the non-rotating origin his most important contributions. He is presently working on applications of general relativity to fundamental astronomy, geodesy, and metrology and continuation of his research on the non-rotating origin.

His affiliations and awards include:

- Corresponding Member, French Academy of Sciences
- Member, Bureau des Longitudes (President, 1984-1986)
- Member, Academia Europaea
- Prix du Commissariat de l'Énergie Atomique (1991)
- Tompion Gold Medal of the Worshipful Company of Clockmakers, London (1997)
- Prix Émile Girardeau, Académie de Marine (1991) (This was very pleasing to Bernard, the former sailor.).

Bernard's interests include diving and, not surprisingly, sailing. One time he was invited to attend a meeting on time dissemination at the Cagliari University, Italy. To get there he rented a sailboat and spent five days navigating from France to Cagliari. This caused some complications for the reimbursement of travel expenses.

Once, when arriving in New York coming from France, he was going through immigration and got to a severe-looking customs officer who examined his passport with a frown. He

motioned Bernard to follow him. They went to the office and Bernard, expecting a search, was discouraged. The officer then said his first words: "What do you think about black holes?" He had seen "Astronomer" on the passport.

Bernard has clearly made many important contributions to astronomy, physics, and the time and frequency community. He is a capable, dedicated, and highly productive individual as well as being a fine person.

With great pleasure we now give him his award and express our congratulations and appreciation for his outstanding contributions and service to our community. Bernard, will you please come up?

PROPOSALS FOR UPDATING TAI ALGORITHM

C. Thomas and J. Azoubib
Bureau International des Poids et Mesures
Pavillon de Breteuil
92312 Sèvres Cedex
France

Abstract

The conditions of computation of TAI and UTC are in constant evolution. The replacement of clocks of older design by new ones of type HP 5071A, started in 1993, continues with consequent improvement in the stability of the free atomic time scale EAL, the first step in the calculation of TAI. To further improve the stability of EAL and to further reduce the delay of access to TAI and UTC, the algorithm which produces them may need to be revised. With this in view, experiments on real clock data collected at the BIPM have been carried out to show the advantage of simultaneously using an upper limit on relative weights, rather than one on absolute weights, and a basic interval of computation of one month, rather than one of two months. Results of these tests are positive, so the BIPM reported on these studies to the Working Group on TAI of the Comité Consultatif du Temps et des Fréquences (CCTF) in view of implementing consequent changes in January 1998. A decision is being made.*

INTRODUCTION

Since the end of 1992, the quality of the timing data received at the BIPM has evolved rapidly thanks to the wide use of GPS time transfer and to the extensive replacement of older designs of commercial clocks by the new HP 5071A clocks. Consequently, the stability of the free atomic time scale EAL, the first step in the calculation of TAI, has improved significantly. The medium-term stability of EAL, expressed in terms of the Allan standard deviation σ_y , is estimated to be 1.3×10^{-15} for averaging times of about 40 d. This improves the predictability of UTC for averaging times of between 1 and 2 months, a scale attribute of fundamental importance for institutions charged with the dissemination of real-time time scales.

For further improvement, the stability algorithm which produces EAL may need to be revised. Given this prospect, several changes, all guided by physical considerations, have been brought to the existing algorithm. These make it possible to compute, in parallel with the published EAL, an experimental time scale E, using the real clock data collected at the BIPM from January 1996 until August 1997.

* At its 1997 meeting, the Comité International des Poids et Mesures (CIPM) decided to change the name of the Comité Consultatif pour la Définition de la Seconde (CCDS) to that of Comité Consultatif du Temps et des Fréquences (CCTF).

The experimental algorithm uses the same defining equations and same fundamental procedure as the usual algorithm [1, 2, 3, 4], but the definitive computation time of the time scale is shortened from two months to one month. Another change is the imposition of an upper limit on the relative weights attributed to contributing clocks, rather than one of absolute weights.

In the following, we recall some fundamental features of the usual algorithm, then we explain the advantages of implementing the above changes and outline some possible objections. The results of the experiment carried out at the BIPM since January 1996 are then analyzed in terms of stability and accuracy.

USUAL ALGORITHM

The free atomic time scale EAL is basically a weighted averaged of data from comparison of clocks, mostly of commercial type, maintained in national timing laboratories [1]. Though timing measurements are taken and reported to the BIPM for MJDs ending in 4 and 9, *i.e.* for dates separated by 5 d, the computation treats as a whole two-month blocks of data. The reference time scale TAI is thus a deferred-time time scale available to user with a delay which can reach two months.

Treating two-month blocks of data as a whole means that the weight p_i of a given clock H_i is maintained constant over a given two-month interval and cannot change before the next one. For a given interval of computation the weight p_i , referred to as 'absolute weight', is written as:

$$p_i = \frac{C}{\sigma_i^2},$$

where σ_i^2 is the variance (over one year) of the mean frequencies of clock H_i , relative to the time scale, and estimated over two-month periods. C is a constant, the value of which is arbitrary since the contribution of clock H_i to the weighted average, referred to as 'relative weight', is given by:

$$\omega_i = \frac{p_i}{\sum_i p_i}$$

and thus is independent of the value of C .

The weighting procedure introduces an upper limit of absolute weights, p_{MAX} , such as, if over a given two-month interval

$$p_i \geq p_{\text{MAX}}, \text{ then } p_i = p_{\text{MAX}}.$$

A given clock thus receives the maximal weight according to its own stability independently of the stability of the other clocks constituting the ensemble. Keeping the value p_{MAX} constant makes the maximum contribution ω_{MAX} of a given clock vary with time.

WHY CHANGE THE ALGORITHM?

The reason for changing the algorithm is very natural: the quality of the contributing clocks has changed and the algorithm should be adapted.

The most important change is the massive replacement of older designs of clocks by the new HP 5071A clocks which are more stable and which reach their maximum of stability for shorter averaging time. Fig. 1 shows the typical stability curve of these clocks with a flicker floor level of about 6×10^{-15} for averaging times in between 20 and 40 days [5].

Since January 1993, we have observed the progressive entry of about 100 HP 5071A units in the computation and nearly all of them have been assigned the upper weight. No discrimination among these stable clocks is thus effected with the consequence that full advantage of the best ones is not taken. We alerted the CCDS Working Group on TAI to this problem, and the decision was taken in March 1995 [6] to rise the upper limit of absolute weight by a factor 2.5 on 2 May 1995. This induced a punctual increase of the maximum contribution ω_{MAX} on this date (see Fig. 2) above a general trend which is a decrease from 1.4% to 0.7%. The problem is now reappearing and we suggest that a limit should be imposed on the relative contribution made by any clock to the scale.

Another point concerns the two-month period of observation for frequency estimation. This does not appear to be optimum with a set of contributing clocks which globally present their best stability for smaller averaging times. We thus suggest to shorten the computation time of the scale to one month.

UPPER LIMIT OF RELATIVE WEIGHTS

The detailed computational process used to implement an upper limit of relative weights in the algorithm is given in Ref. 4.

ADVANTAGES

- The most important feature of this process is that it does not independently assign a weight to each clock, rather the set of clocks is treated globally. With the progressive entrance of very stable clocks fixing an upper limit of relative weight removes from the highest weight category some of those with the weakest stability. The time scale thus relies more heavily upon the very best clocks.
- This new weight determination is also more robust. One can reasonably expect that the stability of clocks contributing to TAI will still improve in coming years. This will be correctly handled by an algorithm which selects the best clocks, the criteria of stability for reaching the upper relative weight becoming more severe.
- The use of an upper limit of relative weights is already implemented in some algorithms for the generation of local time scales [3] and this technique has already proved its efficiency. In addition, following the suggestion of using an upper relative contribution for individual clocks expressed at the meeting of the CCDS Working Group on TAI in 1995, several experimental studies have already been carried out on real clock data collected at the BIPM over different periods, and have produced successful results [4].

ONE CONSTRAINT

At present, the number of clocks receiving the upper limit of absolute weight is increasing from one computation to the next with a consequent decrease of the upper contribution. At the date of implementation of the upper limit of relative weight, we will have to fix this limit in continuity with the previous computation. If we wait too long, this value will be too small to discriminate efficiently among the best clocks. For this reason we propose the implementation of the alternative algorithm as soon as possible (January 1998).

SHORTENING OF THE COMPUTATION TIME

The change proposed here is to shorten the computation time for TAI from two months to one month [7] keeping this computation time in phase with the calendar months (the interval of computation then has a length of 30 d or 35 d).

ADVANTAGES

- This shortening corresponds to an adaptation of the algorithm to the statistical properties of the clocks we have at our disposal.
- The delay of access to the time scale is reduced. The definitive computation for any month is available by the 13th of the following month. The procedure used until now (provisional results one month in two) is abandoned and each issue of *Circular T* provides final values. The question of reducing the delay of access is important since it facilitates procedures for UTC prediction implemented in time laboratories charged with the dissemination of real-time time scales.
- The work of the BIPM Time Section is simplified, a non-negligible point if the decision to update TAI every 2 or 3 d, rather than 5 d, is taken in future.

ONE PRACTICAL CONSTRAINT

Time transfer and clock data used in the TAI computation covering month n must necessarily reach the BIPM at the beginning of month $(n+1)$, since the final computation is made some days later. Data arriving too late cannot be included in the computation and those working in time laboratories should be aware of it.

ONE OBJECTION

Shortening from two months to one month the averaging time for estimation of clock frequencies, and of their variances, optimizes the stability of the time scale over a duration of one month, which may appear to conflict with the requirement of long-term stability for reference time scales. This argument has been developed fully in the past, but the current approach to the problem is different:

- The requirement is high predictability for the reference time scale in order to implement an efficient steering of local representations of UTC. Timing laboratories thus need high stability between successive computations and rapid access.
- The long-term stability of the scale mainly relies upon its accuracy, *i.e.* the quality of the measurements provided by primary frequency standards. This is on a promising path: several very accurate primary frequency standards are under development with expected type B standard uncertainties of several parts in 10^{15} , and frequency transfer techniques, such as those using two-way or GPS phase measurements, are expected soon to reach the level of 1×10^{-15} over one day.

THE EXPERIMENT

The two changes detailed above have been implemented in our usual algorithm for computation of an alternative free atomic time scale E, using real clock data collected at the BIPM from January 1996 to August 1997.

The starting date of computation (MJD = 50079, 28 December 1995) corresponds to the first date of implementation of the 5 d, rather than 10 d, recurrence of TAI updates. Each month, clock frequencies are estimated as slopes of linear fits over 7 or 8 time data, while only 4 points were available before.

This improves our confidence in the frequency estimation.

The closing date (MJD = 50689, 29 August 1997) corresponds to the last date included in the last complete two-month interval of computation available when writing this paper with the intention to implement the new algorithm in January 1998.

For this exercise the upper limit of relative weight was set at 0.8%, which corresponds closely to the upper limit of relative weight given to the best clocks in November-December 1995.

The time scale E is compared with the published EAL over the period under study. A time scale TE is deduced from E using the steering frequency corrections applied to EAL to obtain TAI. TE is then comparable with the published TAI over the same period.

Several other time scales, using only one of the two changes described here or testing other possibilities, have been computed in parallel with E. The time scale E is the one which led to the most significant results, this being the reason why it is recommended here.

RESULTS

STABILITY

Values of the stability of the time scales E and EAL are estimated by application of the 3-cornered-hat technique to data obtained from January 1996 to August 1997 in comparisons between E (or EAL) and two of the best time scales in the world, maintained at the NIST and at the USNO. This leads to the values for the Allan standard deviation $\sigma_y(\tau)$ shown in Fig. 3.

Fig. 3 calls for some remarks:

- Stability is estimated for averaging times not exceeding 80 d. Evaluating Allan standard deviation values, with reasonable confidence, for longer averaging times is very difficult: we have at our disposal only 20 months of data and the time scales considered may be subject to variations which are correlated in the long term, a circumstance sufficient to prevent the use of the N -cornered-hat technique. It is probable, however, that E and EAL are subject to a residual annual variation which would appear in Fig. 3 as a 'bump' for averaging times of about 180 d.
- The time scales E and EAL present white frequency noise for averaging times between 5 and 40 days, with no residual trace of noise coming from time transfer methods.
- The time scale E is more stable than EAL for all averaging times*.
- The best performance is:

$$\begin{aligned}\sigma_{yEAL}(\tau = 40 \text{ d}) &= 1.3 \times 10^{-15}, \\ \sigma_{yE}(\tau = 40 \text{ d}) &= 1.1 \times 10^{-15}.\end{aligned}$$

* Another stability estimation computed with the 9-cornered-hat technique, involving the 8 best HP 5071A clocks reported to the BIPM, gives the same result.

ACCURACY

To characterize the accuracy of TE and TAI, estimates are made of the relative departures d_T , and of their uncertainties σ_T , of the durations of the TE and TAI scale intervals, u_T , from the SI second, u_0 , as produced on the rotating geoid by primary frequency standards:

$$d_T = \frac{u_T - u_0}{u_0},$$

with $T = \text{TE or TAI}$.

Since January 1996, individual measurements of the TE and TAI frequencies have been provided by five primary frequency standards:

- LPTF-FO1, which is a cesium fountain developed at the BNM-LPTF, Paris, France. The preliminary evaluation of its accuracy led to a type B standard uncertainty of 3×10^{-15} , a value never reached before. Three measurements taken in May 1996 and averaged over periods of about 10 hours were sent to the BIPM.
- NIST-7, which is the optically pumped primary frequency standard developed at the NIST, Boulder, Colorado, USA. In the period covered by this report, it provided four measurements which cover a 5 day period in March 1996 and three 10 day periods in May 1996, December 1996 and June 1997. The type B standard uncertainty of NIST-7 is 1×10^{-14} for the first two measurements and 7×10^{-15} for the last two measurements.
- PTB CS2 and PTB CS3, which are classical primary frequency standards operating continuously as clocks at the PTB, Braunschweig, Germany. Frequency measurements are taken continuously and can be reported over successive one-month or two-month periods. The type B standard uncertainties
- SU MCsR 102, which is a classical primary frequency standard operated at the VNIIFTRI, Moscow, Russia. It delivered two measurements, both averaged over two-month periods, in February and March 1996. The type B standard uncertainty of this standard is 5×10^{-14} .

Values of d_{TE} and d_{TAI} deduced from these individual measurements are reported in Figs. 4 and 5, where results from PTB CS2 and PTB CS3 are treated over one-month intervals to assess the accuracy of TE, and over two-month intervals for TAI. The number of points in Fig. 5 is thus larger than in Fig. 4. Values over one-month intervals are not available for SU MCsR 102, which explains that the number of points concerning this standard is the same in both figures. Points deduced from LPTF-FO1, NIST-7 and SU MCsR 102 cannot be exactly superposed in the two figures because they are not related to the same time scale.

The uncertainty of each point in Figs. 4 and 5, except those from LPTF-FO1, is close to the type B uncertainty of the primary frequency standard since the uncertainty caused by the transfer to TAI is negligible. For LPTF-FO1, an additional uncertainty of about 5×10^{-15} must be taken into account for the link to TAI.

Estimates of TE and TAI accuracy obtained by global treatment of individual measurements [8] are added in Figs. 4 and 5. Measurements from PTB CS3 are not used in the processing because this standard experienced frequency steps of several parts in 10^{14} over the period under study. This global treatment can provide mean values of d_T estimated over durations of one or two months. The continuous lines of Figs. 4 and 5 correspond to two-month estimates of d_{TAI} and d_{TE} and are thus directly comparable. They appear to be nearly identical, the largest discrepancy between the two is

observed over July-August 1997:

$$\begin{aligned}d_{TE} &= 1.7 \times 10^{-14}, \sigma_{TE} = 1.0 \times 10^{-14}, \\d_{TAI} &= 1.8 \times 10^{-14}, \sigma_{TAI} = 1.0 \times 10^{-14},\end{aligned}$$

and is much smaller than the corresponding uncertainties. Over the whole period under study the obtained values of σ_{TE} and σ_{TAI} are very close to each other and vary from 0.6×10^{-14} to 1.0×10^{-14} .

The accuracy of the time scale is thus nearly unchanged by the alternative algorithm. The discrepancy obtained is close to that resulting from uniform application of the correction for the black-body radiation frequency shift in 1995, for which a procedure for compensation was applied immediately (cumulative frequency steering corrections, each of relative amplitude 1×10^{-15} applied on dates separated by 60-day intervals). Current results suggest that this procedure has compensated only for the natural drift of the scale and that it should be reinforced, keeping in mind that the middle-term stability of the scale should not be degraded. For this reason successive frequency steering corrections of greater amplitude, 2×10^{-15} , have been applied since May 1997. This conclusion does not depend on the choice of algorithm.

CONCLUSIONS

We propose to the CCTF Working Group on TAI the implementation of an alternative algorithm for TAI computation. This algorithm is based on the same defining equations as the one in use at present, but includes two changes: shortening of the computation time of the time scale from two months to one month and use of an upper limit to the relative weights attributed to contributing clocks. Tests show that the middle-term stability of the resulting scale is improved and that its accuracy is unchanged, when compared with the published TAI. In addition, the delay of access to the time scale is reduced and the algorithm is more robust in response to global changes in the quality of the clocks, of the kind we experienced since the entry of the HP 5071A units into the computation.

The BIPM is ready to implement this alternative algorithm for the computation covering the month of January 1998.

REFERENCES

- [1] B. Guinot, C. Thomas, Establishment of International Atomic Time, *Annual Report of the BIPM Time Section*, 1988, 1, D1-D22.
- [2] P. Tavella, C. Thomas, Comparative study of time scale algorithms, *Metrologia*, 1991, 28, 57-63.
- [3] C. Thomas, P. Wolf, P. Tavella, Time Scales, *Monographie BIPM 94/1*, 1994, 52 p.
- [4] C. Thomas, J. Azoubib, TAI Computation: study of an alternative choice for implementing an upper limit of clock weights, *Metrologia*, 1996, 33, 227-240.
- [5] C. Thomas, Impact of New Clock Technologies on the Stability and Accuracy of the International Atomic Time, *IEEE Trans. Ultras. Fer. and Freq. Cont.*, 1997, 44, 3, 696-700.

- [6] G. Petit, Report on the discussions and decisions of the meeting of the CCDS Working Group on TAI, 13 and 14 March 1995, *BIPM Publication*, 1995, 10 p.
- [7] J. Azoubib, C. Thomas, Shortening of the definitive computation time of TAI, *Report to the CCDS Working Group on TAI*, GT-TAI/95-7, 1995, 28 p.
- [8] J. Azoubib, M. Granveaud, B. Guinot, Estimation of the scale unit duration of time scales, *Metrologia*, 1977, **13**, 87-93.

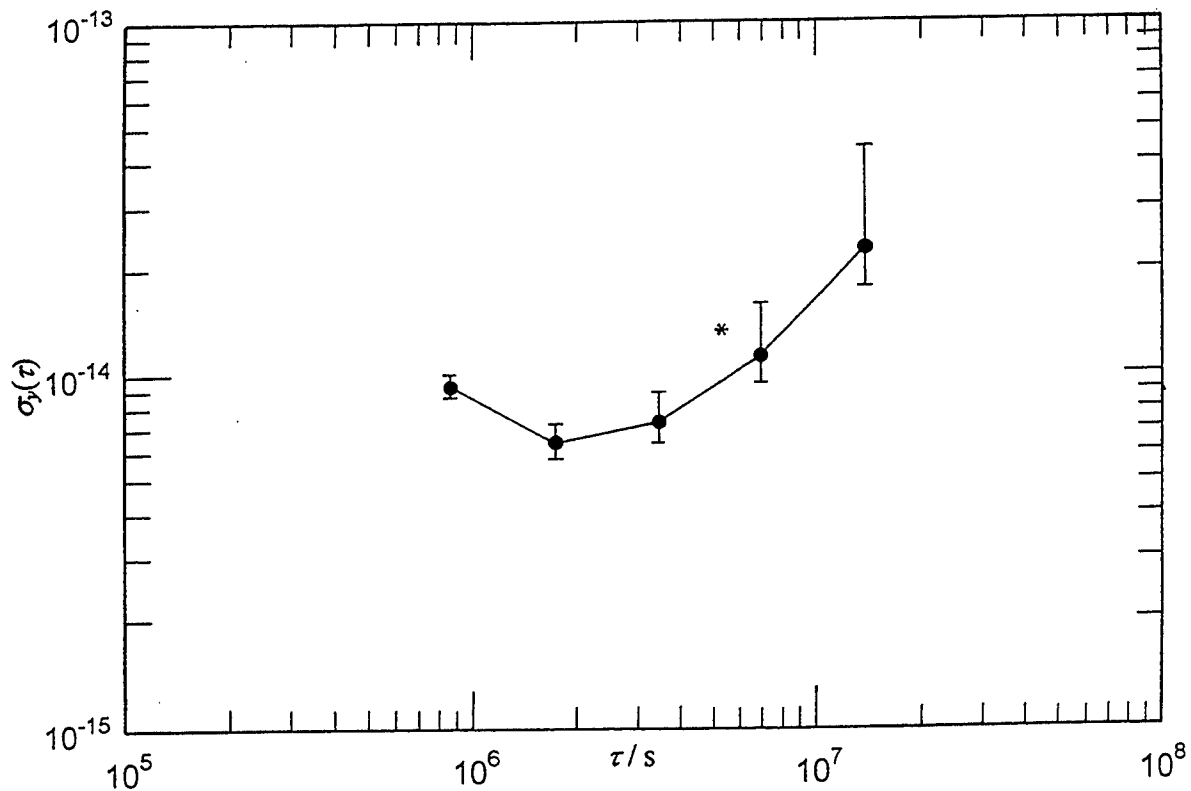


Figure 1. Typical stability curve of a HP 5071A clock in terms of variation of the Allan standard deviation σ_y with the averaging time τ . * indicates the value $\sigma_y(\tau = 60 \text{ d})$ sufficient for a given clock to be assigned the upper limit of absolute weight p_{MAX} in TAI computation.

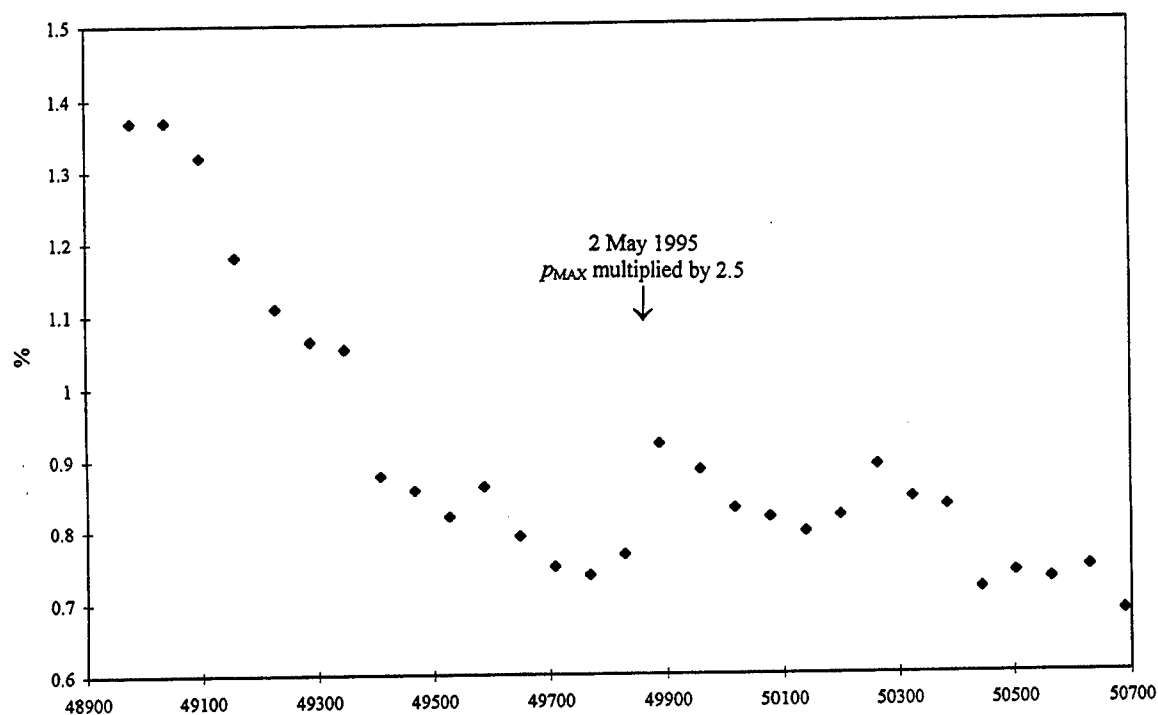


Figure 2. Maximum relative contribution ω_{MAX} taken by an individual clock in TAI computation from January 1993 to

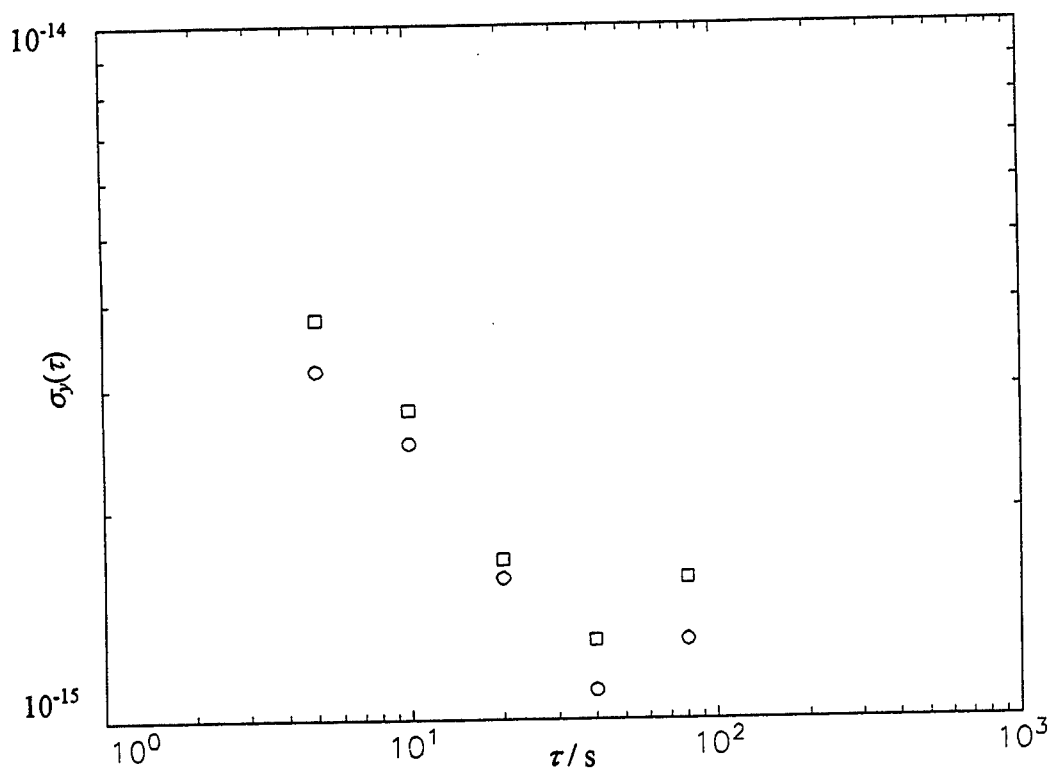


Figure 3. Stability of the time scales E (O) and EAL (□) estimated by application of the 3-cornered-hat technique to data obtained from January 1996 to August 1997 in comparisons between the time scales E or EAL, AT1 (maintained at the NIST), and A. IMEAN (maintained at the USNO).

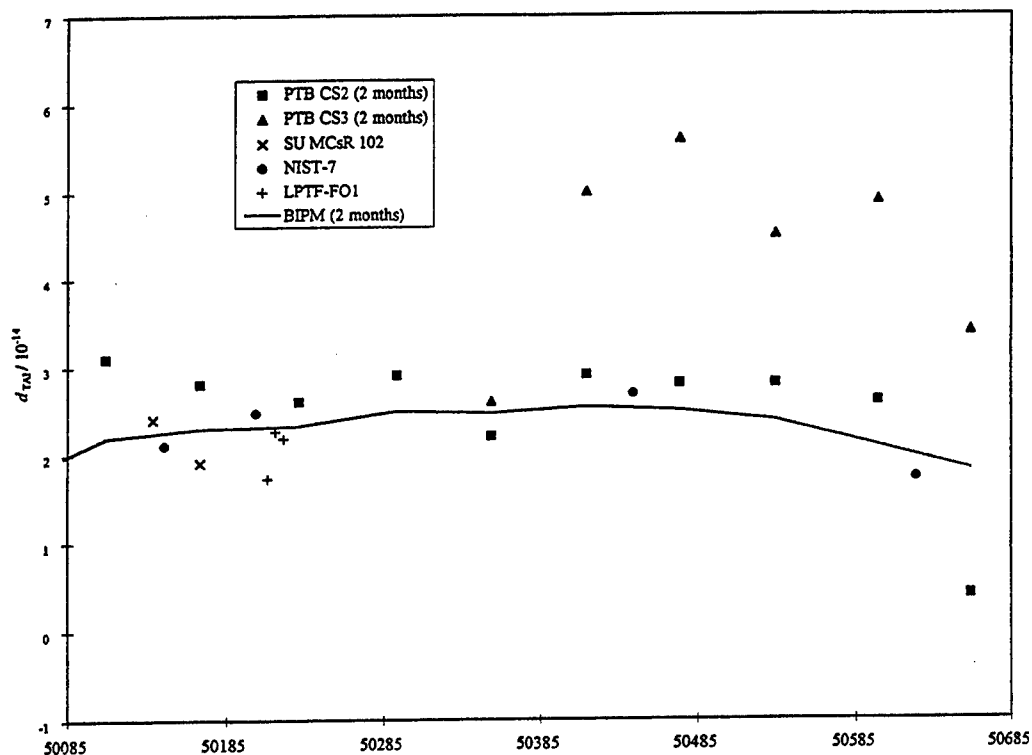


Figure 4. Accuracy of TAI over the period January 1996 to August 1997.

The quantity reported is the relative departure, d_{TAI} , of the duration of the TAI scale interval from the SI second as produced on the rotating geoid by primary frequency standards. The continuous curve corresponds to BIPM estimates of d_{TAI} over two-month intervals.

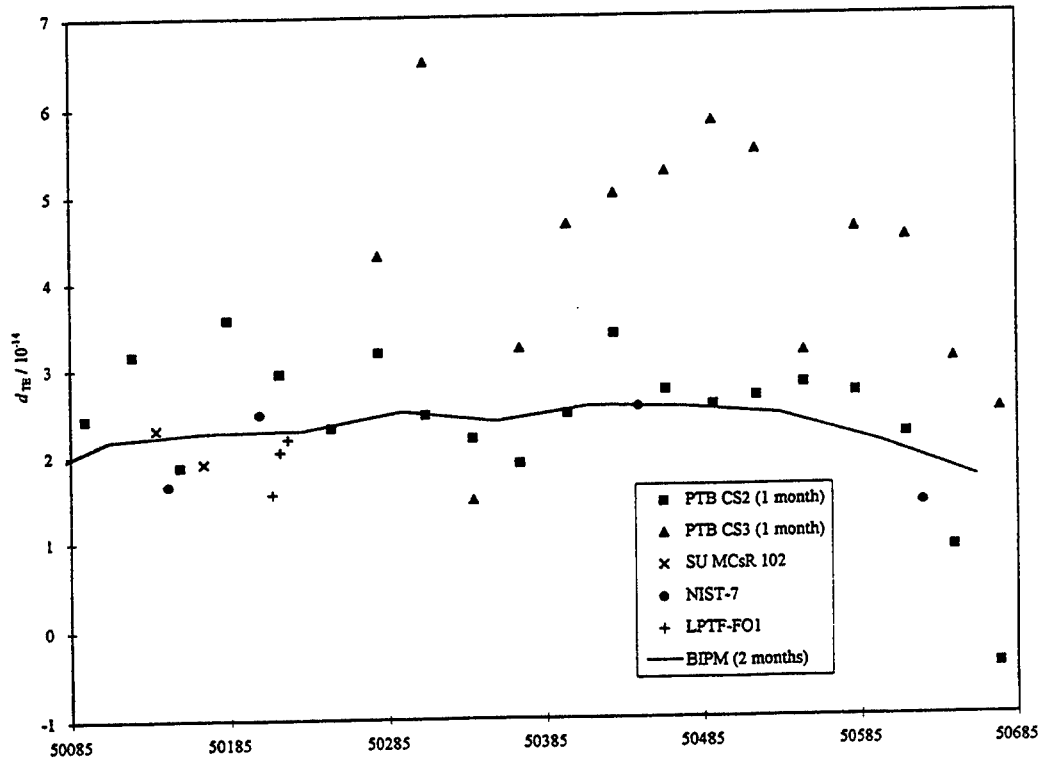


Figure 5. Accuracy of TE over the period January 1996 to August 1997.

The quantity reported is the relative departure, d_{TE} , of the duration of the TE scale interval from the SI second as produced on the rotating geoid by primary frequency standards. The continuous curve corresponds to BIPM estimates of d_{TE} over two-month intervals.

Questions and Answers

JUDAH LEVINE (NIST): We think it is a very good idea. We have said that to BIPM in writing. I think we would not be too concerned about the possible correlation between AT-1 and EAL because we have a relatively small number of clocks that contribute to EAL, and I would guess that the correlation between AT-1 and EAL is very small. I think the results of the three-corner hat using AT-1 are just fine.

THE ACCURACY OF TAI

C. Thomas
Bureau International des Poids et Mesures
Pavillon de Breteuil
92312 Sèvres Cedex
France

Abstract

By definition, the duration of the TAI scale unit should be as close as possible to the SI second on the rotating geoid. The frequency of the free atomic time scale, computed at the BIPM as a weighted average of commercial clock data obtained from time laboratories, was carefully steered for more than ten years in order to generate an international time reference which conforms with this definition. In 1995, uniform application of the correction compensating for the black-body frequency shift in primary frequency standards artificially degraded the accuracy of TAI. A procedure to compensate for this effect was immediately implemented, but only compensated for the natural drift of the free atomic time scale over the first two years, leading to the uncomfortable condition that TAI was not sufficiently accurate. Since April 1997, an improvement in the accuracy of TAI has been detected, but has still to be confirmed. For this purpose results from very accurate primary frequency standards, such as the new cesium fountains now under development, would be very helpful.

INTRODUCTION

From a declaration of the Comité Consultatif pour la Définition de la Seconde, CCDS, in 1980 [1] International Atomic Time, TAI, is

a coordinate time scale defined in a geocentric reference frame with the SI second as realized on the rotating geoid as the scale unit.

Since 1 January 1988, the Bureau International des Poids et Mesures, BIPM, has been responsible for the generation and dissemination of TAI, which is a world-wide reference time scale and thus should be maintained in such a way as to be as reliable, stable and accurate as possible.

TAI relies on measurements taken on a regular basis from commercial atomic clocks and primary frequency standards maintained in national timing centers spread world-wide. Reliability and stability are optimized in the first step of the procedure used for combining these data. In this, a free atomic time scale, EAL (échelle atomique libre), is computed as a weighted average of data from a large number of free-running and independent atomic clocks [2]. The weight attributed to a given contributing clock increases with its stability which makes it possible to improve the stability of the resulting average (over the period January 1996 - August 1997, the stability of EAL was characterized by an Allan deviation close to 1×10^{-15} for averaging times of 40 d [3]). No attempt is made to ensure the conformity of the EAL scale unit with the SI second as realized on the rotating geoid.

In a second step, the duration of the scale unit of EAL is evaluated by comparison with data from primary cesium standards which realize the SI second. TAI is then derived from EAL by adding a linear function of time with a slope designed to bring the TAI scale unit close to the SI second on the surface of the rotating geoid. To maintain accuracy the frequency offset between TAI and EAL is changed when necessary [4], the magnitude of the changes being of the same order as the frequency fluctuations resulting from the instability of EAL. This operation is referred to as the 'steering of TAI'.

In the first section of this paper we compare the frequency of EAL, over the last twelve years, to the frequencies of the two continuously operating primary frequency standards PTB CS1 and PTB CS2. We also justify the frequency steering corrections which were applied over this period. The second section describes how the accuracy of TAI is estimated and, in the third section, comments are given on individual and global estimations of the accuracy of TAI for the period January 1996 - October 1997.

FREQUENCY OF EAL SINCE 1985

Figure 1 shows the frequency of the free atomic time scale EAL, computed over successive two-month intervals, relative to the continuously operating primary frequency standards PTB CS1 and PTB CS2, maintained at the PTB, Braunschweig, Germany. It includes data taken since January 1985 when only PTB CS1 was in operation. First measurements from PTB CS2 were provided in 1986. PTB CS1 ceased operation in March 1995. The type B standard uncertainties of PTB CS1 and PTB CS2 are respectively 3×10^{-14} and 1.5×10^{-14} . The dashed line added to Fig. 1 shows the frequency of EAL relative to TAI, each step corresponding to an additive steering correction.

The step observed in the values relative to PTB CS2 in April 1995 comes from the application of a correction compensating for the black-body frequency shift experienced by the standard: under the influence of the radiation from the walls surrounding the atoms inside the clock at temperature T , the clock transition frequency is reduced with respect to its value at $T = 0$ K. From the formula provided by Itano *et al.* [5] the amplitude of the effect is 1.7×10^{-14} for $T = 299$ K, with an uncertainty conservatively estimated at 1×10^{-15} . The uniform application of this correction to results provided by primary frequency standards is recommended by the Comité Consultatif pour la Définition de la Seconde [6].

Figure 1 calls for some remarks:

- The values relative to PTB CS1 and PTB CS2 agree within their uncertainty bars, but a systematic difference of about 2×10^{-14} may be observed between them.
- The instability of the frequency values of EAL relative to PTB CS1 may be entirely due to the intrinsic instability of the standard. Alternatively, one may note that the dispersion of the values relative to PTB CS2 falls so that it approaches the intrinsic instability of the standard at the beginning of 1995.
- If we except the step due to the application of the black-body correction from April 1995, one can distinguish two successive phases in the behavior of EAL relatively to the primary frequency standards:
 - a) for the period January 1985 - June 1993, EAL presented a drift of about $1.5 \times 10^{-14}/y$,
 - b) from mid-1993, the amplitude of the drift has been much smaller.

The epoch separating these phases corresponds to that at which replacement of clocks of older design by the new HP 5071A units began to take place in the time laboratories contributing to TAI.

- The first drift was compensated by a series of 12 cumulative frequency steering corrections, each of amplitude 5×10^{-15} , applied between 1989 and 1992.

- The application of the black-body correction has required the implementation of a compensation procedure starting at the beginning of 1995, and which still continues. This takes the form of cumulative steering corrections applied at 60-day intervals and of increasing amplitude (1×10^{-15} from January 1995 to June 1996, 1.5×10^{-15} from July 1996 to February 1997, and 2×10^{-15} starting March 1997).

The following conclusions can be drawn for the long-term behavior of the EAL frequency:

- In the period 1985-1992, the time scale EAL presented a nearly constant frequency drift which was compensated through cumulative steering corrections between 1989 and 1992.
- Since 1993 the introduction of HP 5071A clocks has reduced the drift of EAL and no other frequency corrections have been applied, except those which compensate the additional step due to the application of the black-body correction.
- The procedure for compensating the black-body step, accelerated in 1996, now progresses faster than the natural drift of EAL.

It follows that over the last 12 years the applied frequency steering corrections have been appropriate and have contributed to improvement of the accuracy of TAI. The studies presented in the following focus on more recent years; they cover the period January 1996 - October 1997.

HOW CAN WE ESTIMATE THE ACCURACY OF TAI?

From its definition, the duration of the TAI scale unit, u , should be as close as possible to the duration of the SI second, u_0 , on the rotating geoid. The accuracy of TAI may thus be characterized by the relative departure, d , defined as:

$$d = \frac{u - u_0}{u_0}, \quad (1)$$

and its uncertainty σ .

In (1) u is expressed in seconds and $u_0 = 1$ s is the period of the 1 Hz signal provided by a primary frequency standard, after all frequency corrections, especially those compensating for the black-body shift and the gravitational red shift, have been applied.

Individual values d_i of d are provided by comparing the frequency of TAI with that of primary frequency standard i over a given time interval I_{Ci} , designed as the calibration interval and defined by its length τ_{Ci} and its central date t_{Ci} . The corresponding uncertainty, σ_i , is generally close to the type B uncertainty (1σ) of the primary standard, σ_{Bi} , however, it may happen that the uncertainty introduced by the transfer to TAI (local comparison inside the laboratory and GPS transfer) is not negligible when compared to σ_{Bi} and should be accounted for.

The individual estimations can also be treated in a global way in order to deliver a more precise value of d for any interval of estimation I_E , defined by its length τ_E and its central date t_E . This global treatment operates with preceding and following calibrations taking place over intervals I_{Ci} included or not in I_E , even partially overlapping with I_E , and for which $t_E - t_{Ci}$ may be positive or negative. It is thus necessary to transfer the individual calibrations (d_i, σ_i) temporally over $|t_E - t_{Ci}|$. In the temporal transfer the values d_i are kept constant but the values σ_i are increased. In fact, the temporal transfer is carried out by the time scale itself, which, because it is continuous, can temporally link calibration and estimation intervals. Its instability over $|t_E - t_{Ci}|$ thus creates a new component of uncertainty.

After temporal transfer to the chosen interval I_E , calibrations are combined to obtain d and σ valid over I_E . In practice, this global treatment is not an easy task because the time scale is affected by different types of noise according to the length of time involved, and because the system is not stationary since the time scale stability improves with the passing of time. In addition, the combination of transferred calibrations should be optimized in order to obtain the best global estimate (with the smallest possible uncertainty). This problem was solved in 1977 by Azoubib, Granveaud and Guinot [7], the question of temporal transfer is also treated in [8]. Post-processing allows d to be estimated over a given I_E through a weighted average of all individual measurements which have occurred before and after t_E . An expression of the error made in the estimation process is given in [7] (page 89). It involves the weights and a number of other parameters:

- the uncertainty σ_i of each measurement d_i ,
- a model for the stability of the time scale,
- the length of individual calibration intervals τ_{Ci} ,
- the length of the estimation interval τ_E ,
- the length of the time interval $|t_E - t_{Ci}|$ separating the calibration intervals and the estimation interval.

Minimizing this error makes it possible to determine the weights (the sum of which is equal to 1) and to obtain the value of σ which corresponds to the computed minimum error.

The method described in [7] is applied at the BIPM and provides the regular estimates of d and σ which are published in successive issues of *Circular T* and of the *Annual Report of the BIPM Time Section*. We give results of this treatment for the period January 1996 - October 1997 in the following section.

ESTIMATION OF TAI ACCURACY SINCE JANUARY 1996

Since January 1996, individual measurements of the TAI frequency have been provided by five primary frequency standards:

- LPTF-FO1, which is a cesium fountain developed at the BNM-LPTF, Paris, France [9]. The preliminary evaluation of its accuracy led to $\sigma_{B\text{ FO1}} = 3 \times 10^{-15}$, a value never reached before. Three measurements, taken in May 1996 and averaged over $\tau_{C\text{ FO1}} \approx 10$ h, were sent to the BIPM.
- NIST-7, which is the optically pumped primary frequency standard developed at the NIST, Boulder, Colorado, USA [10]. In the period covered by this report, it provided five measurements which cover a 5-day period in March 1996 and four 10-day periods in May 1996, December 1996, June 1997 and October 1997; $\sigma_{B\text{ NIST-7}} = 1 \times 10^{-14}$ for the first two and the last measurements, 7×10^{-15} for the third and fourth measurements.
- PTB CS2 and PTB CS3, which are classical primary frequency standards operating continuously as clocks at the PTB, Braunschweig, Germany. Frequency measurements are taken continuously and are used over successive two-month periods; $\sigma_{B\text{ PTB CS2}} = 1.5 \times 10^{-14}$, except for the measurement covering the period July-August 1997 for which $\sigma_{B\text{ PTB CS2}} = 2.7 \times 10^{-14}$, and $\sigma_{B\text{ PTB CS3}} = 1.4 \times 10^{-14}$.
- SU MCsR 102, which is a classical primary frequency standard operated at the VNIIFTRI, Moscow, Russia. It delivered two measurements, both averaged over two-month periods, in February and March 1996; $\sigma_{B\text{ MCsR}} = 5 \times 10^{-14}$.

Values of d_i deduced from these individual measurements are given in Fig. 2. The corresponding uncertainties σ_i are close to σ_{Bi} except for points originating from LPTF-FO1 data, for which an additional uncertainty of about 5×10^{-15} must be taken into account for the link to TAI.

Estimates of d obtained by global treatment of individual measurements are added as a continuous line in Fig. 1. The chosen intervals of estimation I_E correspond to successive two-month periods in phase with the calendar bimesters. For the year 1997, the uncertainty σ on d values is about 1×10^{-14} .

Comments on Fig. 2 are as follows:

- The transfer of the LPTF-FO1 measurements to TAI is not optimized and it has not produced new results since May 1996; TAI thus does not take advantage of its outstanding accuracy.
- The relatively high uncertainty of the primary standard SU MCsR 102 makes its weight very low in the estimation of values for d .
- Measurements from PTB CS3 are not used in the computation of d values because this standard experienced frequency steps of several parts in 10^{14} over the period under study.
- Results provided by PTB CS2 show a high stability except for the measurement covering the two month interval July-August 1997 over which $d_{PTB\ CS2}$ experienced a step of about 2×10^{-14} . The PTB informed the BIPM that this measurement should be used with a higher value of type B uncertainty. If we except this particular measurement, we observe a decrease of the duration of the TAI scale unit when compared to the SI second as produced on the rotating geoid by PTB CS2 in September-October 1997: $d_{PTB\ CS2} = 1.4 \times 10^{-14}$ and $\sigma_{PTB\ CS2} = 1.5 \times 10^{-14}$.
- Measurements from NIST-7 cover five or ten day intervals and have calibration dates spaced at nearly equal intervals of six months. The last three results seem to indicate a decreasing trend in the relative duration of the TAI scale unit. The decrease progresses much faster than that observed in the PTB CS2 results, so the two standards are not in such close agreement as they were before January 1997. Nevertheless, they agree within their uncertainty bars.

Over the period under study, estimates of TAI accuracy mainly relied on measurements provided by two primary frequency standards PTB CS2 and NIST-7. These two provide results on a regular basis and so are particularly helpful for the estimation of TAI accuracy. The situation is thus comparable with the one we experienced earlier when we had at our disposal both PTB CS1 and PTB CS2, but with a greatly improved level of stability in the data.

Until April 1997, the average d value was close to 2×10^{-14} , a discrepancy nearly equal to that resulting from uniform application of the correction for the black-body radiation frequency shift in 1995. The successive frequency steering corrections thus simply compensated for the natural drift of the scale. The accuracy of TAI was thus not as good as desired so we progressively reinforced the amplitude of the frequency steering correction from 1×10^{-15} to 1.5×10^{-15} and 2×10^{-15} (see the second section of the paper).

Since April 1997, it appears that the duration of the TAI scale unit is decreasing as if the steering frequency corrections were progressively compensating the 'black-body' step. At first sight the accuracy of TAI may be thought to be improving, but the trend is still slight and we must wait for new measurements from PTB CS2 and NIST-7 to confirm it. In addition, the uncertainty σ affecting the values of d is still rather large, 1×10^{-14} , and is difficult to reduce given the type B uncertainties of these two standards. Results from new cesium fountains under development in a number of laboratories should confirm the decreasing trend of d values and also reduce the uncertainty in these values.

CONCLUSIONS

The accuracy of TAI is estimated by computation of the relative departure d , together with its uncertainty σ , of the duration of its scale unit from the SI second as produced by primary frequency

standards on the rotating geoid. The frequency of the free atomic time scale, computed at the BIPM as a weighted average of commercial clock data provided by time laboratories, was carefully steered for more than ten years in order to generate an international atomic time which conforms with its definition. At the end of 1994, $d = 0.2 \times 10^{-14}$ and $\sigma = 2.0 \times 10^{-14}$.

In 1995, the uniform application of the correction compensating for the black-body frequency shift in primary frequency standards artificially degraded the accuracy of TAI: over May - June 1995, $d = 2.3 \times 10^{-14}$ and $\sigma = 1.0 \times 10^{-14}$. A procedure to compensate for this effect was immediately implemented, but, over the first two years, merely compensated for the natural drift of the free atomic time scale, leading to the uncomfortable conclusion that TAI was not sufficiently accurate.

Since April 1997, an improvement in TAI accuracy has been observed: over September - October 1997, $d = 1.2 \times 10^{-14}$ and $\sigma = 1.0 \times 10^{-14}$, but this has still to be confirmed. For this purpose data from the very accurate primary frequency standards, among them the new cesium fountains now in development in time laboratories, would be very helpful.

REFERENCES

- [1] BIPM Com. Cons. Déf. Seconde, 1980, 9, p S15.
- [2] C. Thomas, J. Azoubib, 1996, *Metrologia*, 33, 227-240.
- [3] C. Thomas, J. Azoubib, these proceedings.
- [4] Differences between the normalized frequencies of EAL and TAI, 1996, *Annual Report of the BIPM Time Section*, 9, Table 5, p 35.
- [5] W.M. Itano, L.L. Lewis, D.J. Wineland, *Phys. Rev. A*, 1982, 25, 1233-1235.
- [6] BIPM Com. Cons. Déf. Seconde, 1996, 13, p S75.
- [7] J. Azoubib, M. Granveaud, B. Guinot, *Metrologia*, 1977, 13, 87-93.
- [8] R.J. Douglas, J.-S. Boulanger, S. Cundy, M.-C. Gagné, W. Cazemier, B. Hoger, R. Pelletier, J. Bernard, A.A. Madej, L. Marmet, K. Siemsen, B.G. Whitford, *Proc. 28th PTTI Meeting*, 1996, 65-74.
- [9] A. Clairon, S. Ghezali, G. Santarelli, P. Laurent., S.N. Lea, M. Bahoura, E. Simon, S. Weyers, K. Szymaniec, *Proc. 5th Symposium on Frequency Standards and Metrology*, Ed. James C. Berquist, World Scientific, 1995, 49-59.
- [10] W.D. Lee, J.H. Shirley, J.P. Lowe, R.E. Drullinger, *IEEE Trans. Instrum. Meas.*, 1995, 44, 120-123.
- [11] A. Bauch, T. Heindorff, R. Schröder, B. Fischer, *Metrologia*, 1996, 33, 249-259.

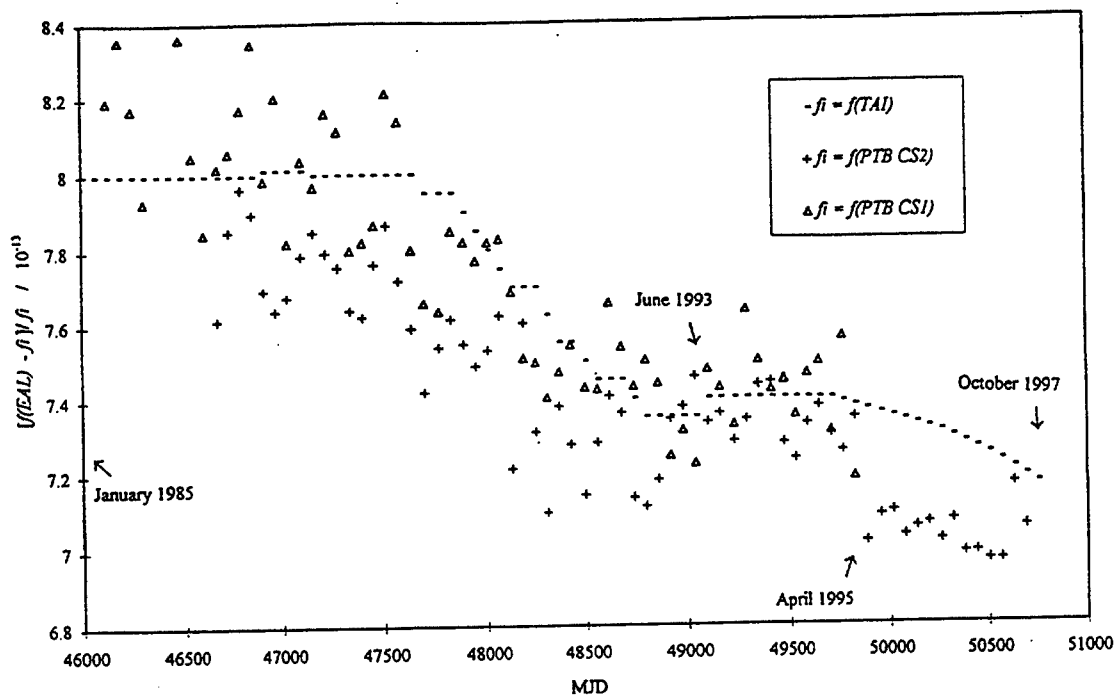


Figure 1. Frequency of the free atomic time scale EAL relative to PTB CS1, PTB CS2 and TAI over the last 12 years.

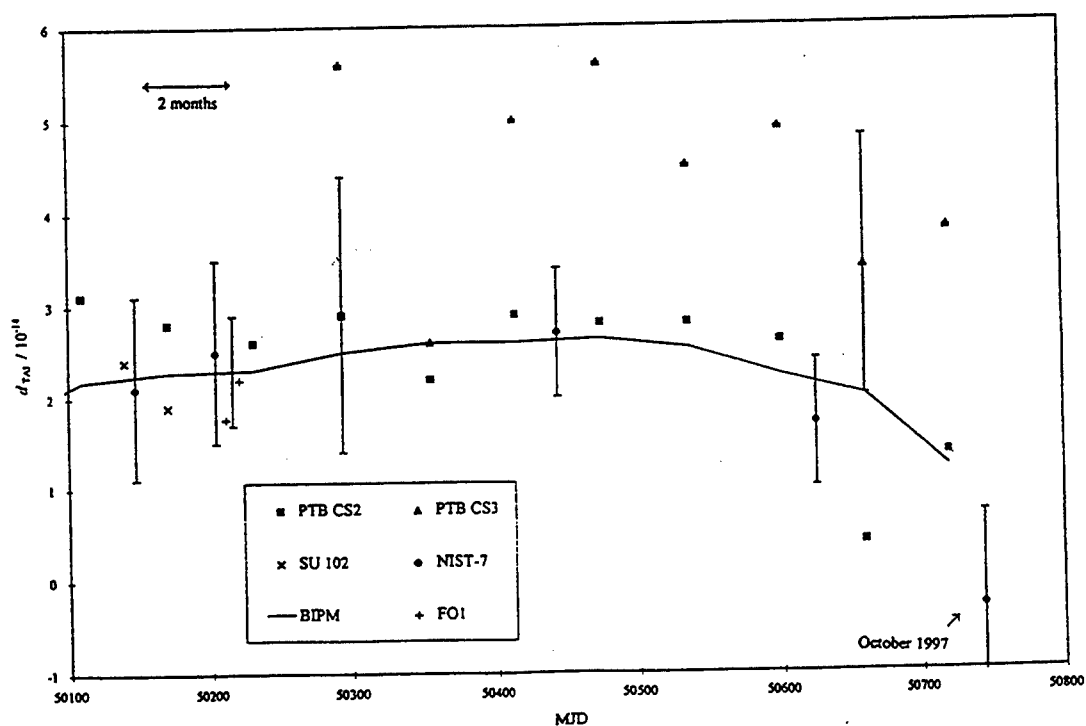


Figure 2. Estimates of the relative departure d of the TAI scale unit from the SI second as produced by primary frequency standards on the rotating geoid. The black curve corresponds to the BIPM global estimate.

Questions and Answers

BERNARD GUINOT (OBSERVATOIRE de PARIS): You mentioned the need of other primary standards. I would say that there should be a need of other operating primary standards. The pity is that there are some standards which are not really used in forming the current measurement of the frequency of TAI; it was already recommended that the standard as a primary standard be operated on the operational basis. Could we insist on the importance of that?

CLAUDINE THOMAS (BIPM): Yes, thank you. It is true that the BIPM needs measurements. But what we need is regular measurements. For instance, the example of NIST-7 is very important. We have measurements, I would say, every four or five months, but it comes regularly. So each time it comes, we have new information and this is very helpful for us. One measurement, even very accurate, is not very useful if it does not come on a regular basis. That is something which is very important for us. Thank you for this remark.

TIMING SYSTEMS PANEL DISCUSSION

PANEL MEMBERS

Ronald Beard, Joe White (Moderator)
U.S. Naval Research Laboratory
Washington, DC

James Bleich
U.S. Navy Logistics Engineering Office
Bremerton, OR

Edgar Butterline
Telecomm Solutions Incorporated
North Brunswick, NJ

Michael Cimafonte
Systems Technology Associates
Colorado Springs, CO

The purpose of this panel was to discuss practical issues of designing, building, operating and maintaining remote precise timing systems. Mr. Beard's organization has been a leader in designing and fielding precise timing systems. Mr. Cimafonte's experience has been high level military operation of systems requiring precise time. Mr. Butterline comes from the civil telecommunications industry as a user of these systems. Mr. Bleich represents the operations and maintenance side of the technology.

The panel began the discussion with the issue of documentation for new systems and upgrades. Mr. Cimafonte started the discussion with the comment that any new system or upgrade must start with a requirement. Upgrades driven by these needs may start from well-documented systems, but in at least some cases, the quality and quantity of documentation drops in the process of the upgrade. Mr. Cimafonte made the point that involvement of the user and maintainer community in the development of the upgrade is essential to making the process work. It was agreed that while the commercial instruments (clocks, receivers, etc.) were usually well covered by the manufacturer's operation and service manuals, the overall systems and specially made instruments often were not well documented. This was particularly true where only a few of the systems were built. The problem is worst for the maintainer. Mr. Beard pointed out the need for the developer to describe not only the details of the system hardware, but also to describe how the system is supposed to work. This gives the maintainer a "feel" for the system that gives insight into the operations and maintenance aspects.

The other key issue discussed was the problem created by the rapid technology turnover in

modern instruments. The panel felt that many devices used in timing systems were obsolete soon after the systems were designed. The problem comes in deciding whether to try to preserve the integrity of the system, freezing the design, or to allow system "upgrades." Mr. Butterline said that his experience had been that freezing the design was an effective way of dealing with the problem. It meant that all of the systems always looked the same to maintainers and the inventory of replacement parts was smaller and better defined. This allowed the carrier to provide maintenance with a small core technical staff. Mr. Cimafronte responded that the downside of freezing the configuration was that systems as a whole became obsolete much quicker and that replacement parts for the obsolete components become very hard to find. It often becomes more expensive to maintain antiquated equipment than to replace it. Mr. Beard described an NRL-designed system that was built with the latest model computer. The computer was obsolete before fielding of the system was completed. All agreed that there were no clean solutions to the problem.

RELATIONSHIPS BETWEEN DRIFT COEFFICIENT UNCERTAINTIES AND NOISE LEVELS : APPLICATION TO TIME ERROR PREDICTION

F. Vernotte, M. Vincent
Observatoire de Besançon

41 bis avenue de l'Observatoire - BP 1615 - 25010 BESANCON Cedex - FRANCE
Phone : +333.81.66.69.22 - Fax : +333.81.66.69.44 - E-mail : francois@obs-besancon.fr

Abstract

Oscillators are affected by drifts (linear phase drift, linear frequency drift, i.e. quadratic phase drift) and different types of noise according to the power law model of power spectral density (from f^{-2} to f^{+2} frequency noise, i.e. f^{-4} to f^0 phase noise). Generally, for long-term instability characterization (duration greater than one hour), drift coefficients are estimated by using least squares whereas noise levels are obtained from the residuals by using variances (AVAR, MVAR, TVAR, ...).

However, the low frequency noises, such as random walk FM, induce very long term fluctuations which may be confused with deterministic drifts. This effect, due to the non-stationarity of these noises, depends on the low cut-off frequency which must be introduced in order to ensure power convergence for low frequencies. We calculate the standard deviation of "artificial" drifts due to long-term random fluctuations, versus the noise levels.

The first interest of these results concerns the estimation of the measurement uncertainty of drift coefficients : knowing the noise levels of an oscillator we calculate the standard deviation of the artificial drift coefficient due to these noises; thus, if a "real" deterministic drift is identified in the signal, its coefficients are determined plus or minus the artificial drift coefficients. The standard deviation of the artificial drift coefficients may be considered as the measurement uncertainty of the deterministic drift coefficient.

The second interest concerns the predictability of an oscillator affected by a deterministic drift. Thus, the knowledge of the drift coefficient uncertainties yields a criterion for quantifying the reliability of a time error prediction.

1 INTRODUCTION

We consider a sequence of frequency deviation samples composed of a deterministic part, i.e. a linear frequency drift, and a random part:

$$y(t_k) = C_1 t_k + C_0 + \epsilon_k. \quad (1)$$

An estimation by least squares yields estimates \hat{C}_0 and \hat{C}_1 of the real coefficients C_0 and C_1 . Denoting the interpolated samples by $\hat{y}(t)$, we obtain:

$$\hat{y}(t_k) = \hat{C}_1 t_k + \hat{C}_0. \quad (2)$$

The residuals are defined as:

$$e_k = y(t_k) - \hat{y}(t_k) \quad (3)$$

1.1 Random Fluctuations and Deterministic Drifts

The instantaneous frequency is defined from the nominal frequency and the frequency deviation samples by:

$$\nu_k = \nu_0 (1 + y_k) \quad (4)$$

If the sequence y_k is not centered, there are two possibilities:

- the real nominal frequency is different from the assumed nominal frequency: this is a problem of inaccuracy of the oscillator;
- there are long-term random fluctuations (with period much longer than the duration of the sequence) which are seen as constant over the sequence[1].

The same problem may occur with linear frequency drift.

It is impossible to distinguish a “true” deterministic drift from a “false” random drift.

1.2 Statement of the Problem

The Power Spectral Density (PSD) may be modelled as:

$$S_y(f) = \sum_{\alpha=-2}^{+2} h_{\alpha} \cdot f^{\alpha} \quad (5)$$

- If no deterministic drift exists, what are the relationships between the noise levels h_{α} and the estimated drift coefficients \hat{C}_0 and \hat{C}_1 ?
- If a deterministic drift exists, what are the uncertainties of the estimated drift coefficients \hat{C}_0 and \hat{C}_1 ?
- In both cases, what is the Time Interval Error (TIE) due to an extrapolation of the linear frequency drift?

2 LINEAR REGRESSION

2.1 Coefficient Calculation

We consider N measurements (t_i, y_i) : $\{(t_0, y_0), \dots, (t_{N-1}, y_{N-1})\}$, regularly spaced with a sampling period τ_0 :

$$t_k = t_0 + k \cdot \tau_0 \quad (6)$$

We need to know the coefficient of the linear model:

$$y_k = \hat{C}_1 t_k + \hat{C}_0 + e_k \quad (7)$$

The most probable coefficient values, in the sense of the least squares, are given by:

$$\hat{C}_0 = \frac{2(2N-1)}{N(N+1)} \sum_{i=0}^{N-1} y_i + \frac{-6}{N(N+1)\tau_0} \sum_i t_i \cdot y_i \quad (8)$$

$$\hat{C}_1 = \frac{-6}{N(N+1)\tau_0} \sum_i y_i + \frac{12}{N(N-1)(N+1)\tau_0^2} \sum_i t_i \cdot y_i \quad (9)$$

2.2 Estimation of the Uncertainties

From (8) and (9), it is possible to calculate $\sigma^2(C_0)$ and $\sigma^2(C_1)$:

$$\begin{aligned} \sigma^2(C_0) = & \frac{4(2N-1)^2}{N^2(N+1)^2} \sigma^2 \left(\sum y_i \right) + \frac{36}{N^2(N+1)^2 \tau_0^2} \sigma^2 \left(\sum t_i \cdot y_i \right) \\ & - \frac{24(2N-1)}{N^2(N+1)^2 \tau_0} \text{Cov} \left(\sum y_i, \sum t_i \cdot y_i \right) \end{aligned} \quad (10)$$

$$\begin{aligned} \sigma^2(C_1) = & \frac{36}{N^2(N+1)^2 \tau_0^2} \sigma^2 \left(\sum y_i \right) + \frac{144}{N^2(N-1)^2(N+1)^2 \tau_0^4} \sigma^2 \left(\sum t_i \cdot y_i \right) \\ & - \frac{144}{(N-1)N^2(N+1)^2 \tau_0^3} \text{Cov} \left(\sum y_i, \sum t_i \cdot y_i \right) \end{aligned} \quad (11)$$

with

$$\sigma^2 \left(\sum y_i \right) = \sum_i \sum_j \langle y_i \cdot y_j \rangle \quad (12)$$

$$\sigma^2 \left(\sum t_i \cdot y_i \right) = \tau_0^2 \sum_i \sum_j i \cdot j \cdot \langle y_i \cdot y_j \rangle \quad (13)$$

$$\text{Cov} \left(\sum y_i, \sum t_j \cdot y_j \right) = \tau_0 \sum_i \sum_j i \cdot \langle y_i \cdot y_j \rangle \quad (14)$$

where $\langle \rangle$ denotes an average over an infinite number of identical processes (ensemble average).

2.3 Correlation of the Samples

$S_y(f)$	R_{ij} (with $i \neq j$)	R_{ii}
$h_{-2} \cdot f^{-2}$	$h_{-2} \left[\frac{1}{f_l} + \pi^2 t_j - t_i \right]$	$\frac{h_{-2}}{f_l}$
$h_{-1} \cdot f^{-1}$	$-h_{-1} [C + \ln(2\pi f_l) + \ln t_j - t_i]$	$-h_{-1} \ln(2\tau_0 f_l)$
$h_0 \cdot f^0$	0	$h_0 f_h$
$h_{+1} \cdot f^{+1}$	$h_{+1} \frac{(-1)^{(j-i)} - 1}{4\pi^2 (t_j - t_i)^2}$	$h_{+1} \frac{f_h^2}{2}$
$h_{+2} \cdot f^{+2}$	$h_{+2} \frac{f_h \cos[2\pi f_h (t_j - t_i)]}{2\pi^2 (t_j - t_i)^2}$	$h_{+2} \frac{f_h^3}{3}$

Table 1: Correlations of the y_k samples versus the noise levels h_α . C is the Euler constant: $C \approx 0,5772$. Assuming a sampling satisfying the Shannon rule, the high cut-off frequency is $f_h = \frac{1}{2\tau_0}$. f_l is the low cut-off frequency.

The PSD $S_y(f)$ is the Fourier Transform of the autocorrelation function. Thus, if no real drift exists in the sequence, we have:

$$\begin{aligned}
\langle y_i \cdot y_j \rangle &= \int_{-\infty}^{+\infty} S_y^{2S}(f) e^{j2\pi f(t_j - t_i)} df \\
&= \int_0^{+\infty} S_y(f) \cos[2\pi f(t_j - t_i)] df = R_{ij}
\end{aligned} \tag{15}$$

which leads to the results given in Table 1.

2.4 Mean Value Subtraction

Table 1 shows that, for low frequency noises (f^{-2} and f^{-1} FM), the correlations of the samples depend on the low cut-off frequency f_l . This cut-off frequency must be introduced in order to ensure the power convergence.

If the inverse of the low cut-off frequency is much larger than the duration of the sequence $[t_0, t_N]$, the very long term fluctuations (period $\approx \frac{1}{f_l}$) are seen as a constant[1] (see Figure 1).

On the other hand, the subtraction of the mean value of the sequence cancels the dependence on f_l . Denoting the mean value of the sequence by \bar{y} and the centered sequence samples by y'_k :

$$\bar{y} = \frac{1}{N} \sum_{j=0}^{N-1} y_j \tag{16}$$

$$y'_k = y_k - \bar{y} \tag{17}$$

The subtraction of the mean value is equivalent to a correction of the nominal frequency by a factor $(1 + \bar{y})$:

$$\nu_k \approx \nu_0(1 + \bar{y})(1 + y'_k) \tag{18}$$

After subtraction of the mean value, it follows that:

$$\sum_{i=0}^{N-1} y'_i = 0 \tag{19}$$

$$\sum_{i=0}^{N-1} t_i \cdot y'_i = \tau_0 \left[\sum_i i \cdot y_i - \frac{N+1}{2} \sum_j y_j \right] \tag{20}$$

Thus:

$$\sigma^2 \left(\sum t_i \cdot y'_i \right) = \tau_0^2 \left[\sum_i \sum_j i \cdot j \cdot R_{ij} - (N+1) \sum_i \sum_j i \cdot R_{ij} + \frac{N(N+1)}{4} \sum_i \sum_j R_{ij} \right] \tag{21}$$

Considering the new linear frequency drift model:

$$y'_k = \hat{C}'_1 t_k + \hat{C}'_0 + e'_k \tag{22}$$

we have:

$$\sigma^2(C'_0) = \frac{36}{N^2(N+1)^2\tau_0^2} \sigma^2 \left(\sum t_i \cdot y'_i \right) \tag{23}$$

$$\sigma^2(C'_1) = \frac{144}{N^2(N-1)^2(N+1)^2\tau_0^4} \sigma^2 \left(\sum t_i \cdot y'_i \right) \tag{24}$$

It may be demonstrated that $\hat{C}'_1 = \hat{C}_1$ and then $\sigma^2(C'_1) = \sigma^2(C_1)$.

2.5 Estimation of the Residuals

The differences between the estimated drift and the y_k samples are:

$$e_k = y_k - \hat{C}_1 t_k - \hat{C}_0 \quad (25)$$

The variance of the residuals is given by:

$$\begin{aligned} \sigma^2(e) = & \sigma^2(y) + \frac{(N-1)(2N-1)\tau_0^2}{6} \sigma^2(C_1) + \sigma^2(C_0) \\ & - \frac{2}{N} \text{Cov} \left(\sum y_k, C_0 \right) - \frac{2}{N} \text{Cov} \left(\sum t_k y_k, C_1 \right) + (N-1)\tau_0 \text{Cov}(C_0, C_1) \end{aligned} \quad (26)$$

The residuals don't depend on the subtraction of the mean value:

$$e_k = y_k - \hat{C}_1 t_k - \hat{C}_0 = y'_k - \hat{C}'_1 t_k - \hat{C}'_0 \quad (27)$$

3 RESULTS

$S_y(f)$	$\sigma(C_0)$	$\sigma(C'_0)$	$\sigma(C_1)$	$\sigma(e)$
$h_{-2}.f^{-2}$	$\sqrt{\frac{h_{-2}}{f_l}}$	$\sqrt{\frac{3\pi^2 \tau h_{-2}}{5}}$	$\sqrt{\frac{12\pi^2 h_{-2}}{5\tau}}$	$\sqrt{\frac{2\pi^2 \tau}{15} h_{-2}}$
$h_{-1}.f^{-1}$	$\sqrt{\left[\frac{3}{2} - \frac{1}{4} \ln(2f_l \tau)\right] h_{-1}}$	$\frac{3\sqrt{h_{-1}}}{2}$	$\frac{3\sqrt{h_{-1}}}{\tau}$	$\sqrt{[C + \ln(\pi\tau)] h_{-1}}$
$h_0.f^0$	$\sqrt{\frac{2h_0}{\tau}}$	$\sqrt{\frac{3h_0}{2\tau}}$	$\sqrt{\frac{6h_0}{\tau^3}}$	$\sqrt{\frac{h_0}{2\tau_0}} = \sqrt{f_h h_0}$
$h_{+1}.f^{+1}$	$\sqrt{\frac{5[1.37 + \ln(2f_h \tau)] h_{+1}}{\pi^2 \tau^2}}$	$\sqrt{\frac{9[1.27 + \ln(2f_h \tau)] h_{+1}}{2\pi^2 \tau^2}}$	$\sqrt{\frac{18[1.27 + \ln(2f_h \tau)] h_{+1}}{\pi^2 \tau^4}}$	$\sqrt{\frac{f_h^2}{2} h_{+1}}$
$h_{+2}.f^{+2}$	$\sqrt{\frac{10f_h \ln(2) h_{+2}}{\pi^2 \tau^2}}$	$\sqrt{\frac{9f_h \ln(2) h_{+2}}{\pi^2 \tau^2}}$	$\sqrt{\frac{36f_h \ln(2) h_{+2}}{\pi^2 \tau^4}}$	$\sqrt{\frac{f_h^3}{3} h_{+2}}$

Table 2: Standard deviation of the drift coefficients and of the residuals versus the noise level h_α and the duration of the sequence τ . The high cut-off frequency is $f_h = \frac{1}{2\tau_0}$ and the low cut-off frequency is f_l .

Thus, after measuring the h_α noise levels, we may estimate the uncertainties $\sigma(C_0)$ and $\sigma(C_1)$ by using Table 2.

This table shows that the subtraction of the mean value cancels the dependence of C_0 on f_h . For high frequency noises, $\sigma(C_0)$ remains very close to $\sigma(C'_0)$. Moreover, neither $\sigma(C_1)$ nor $\sigma(e)$ are modified by this subtraction.

3.1 Measurement Uncertainties of Drift Coefficients

If no real deterministic drift exists, the determination of the drift coefficients yields:

$$\begin{aligned} -2\sigma(C_0) < \hat{C}_0 < 2\sigma(C_0) & \quad \text{with 95.5\% confidence} \\ -2\sigma(C_1) < \hat{C}_1 < 2\sigma(C_1) & \quad \text{with 95.5\% confidence} \end{aligned}$$

Thus, measuring a drift coefficient C within the interval $[-2\sigma(C), +2\sigma(C)]$ is compatible with a null drift hypothesis (with a risk of the second kind of 4.5%).

On the other hand, if a real deterministic drift exists, the estimates \hat{C}_0 and \hat{C}_1 converge toward the real coefficients C_0 and C_1 :

$$\langle \hat{C}_0 \rangle = C_0 \quad \text{and} \quad \langle \hat{C}_1 \rangle = C_1.$$

The uncertainty domains of the coefficients C_0 and C_1 are:

$$C_0 = \hat{C}_0 \pm 2\sigma(C_0) \quad \text{with 95.5\% confidence}$$

$$C_1 = \hat{C}_1 \pm 2\sigma(C_1) \quad \text{with 95.5\% confidence}$$

3.2 Frequency and Time Error Prediction

3.2.1 Frequency error prediction

If \hat{C}_0 and \hat{C}_1 are estimated over a sequence of N samples (duration $\tau = N\tau_0$), what error results from an extrapolation of the linear model to $t_N + T$?

$$\hat{y}(t_N + T) = \hat{C}_1 \cdot (t_N + T) + \hat{C}_0 \quad (28)$$

The Total Frequency Error (TFE) may be defined as:

$$TFE(T) = y(t_N + T) - \hat{y}(t_N + T) \quad (29)$$

The TFE is composed of a Deterministic Frequency Error (DFE):

$$DFE(T) = (C_1 - \hat{C}_1)(t_N + T) - (C_0 - \hat{C}_0) \quad (30)$$

plus a random error (see Figure 2):

$$TFE(T) = DFE(T) + y_r(t_N + T) \quad (31)$$

$y_r(t_i)$ is a centered random variable without drift, with a variance $\sigma^2(y_r) = R_{ii}$.

Thus, denoting $t' = t_N + T$, we obtain:

$$\begin{aligned} \langle TFE^2(T) \rangle = & \sigma^2(C_0) + \sigma^2(C_1) \cdot t'^2 + \sigma^2(y_r) \\ & - 2Cov(C_0, y_r(t')) - 2Cov(C_1, y_r(t')) \cdot t' + 2Cov(C_0, C_1) \cdot t' \end{aligned} \quad (32)$$

$Cov(C_0, y_r(t'))$ is the covariance between the parameter C_0 estimated over the sequence $[t_0, t_N]$ and the random sample y_r at the date $t' = t_N + T$.

3.2.2 Time error prediction

If a sequence of $x(t_k)$ is known over a duration τ (from t_0 to $t_N = t_0 + \tau$), the Time Interval Error (TIE) at $t_N + T$ may be defined as [2, 3]:

$$TIE(T) = x(t_N + T) - x(t_N) - T\bar{\dot{y}}_{t_N, T} \quad (33)$$

with

$$\begin{aligned}\bar{y}_{t_N, T} &= \frac{1}{T} \int_{t_N}^{t_N+T} \hat{y}(t) dt \\ &\approx \frac{1}{M} \sum_{i=N}^{N+M-1} \hat{y}_i\end{aligned}\quad (34)$$

where \hat{y}_i is the extrapolated frequency deviation at t_i and M is defined as $T = M\tau_0$.

$$TIE(T) = \tau_0 \sum_{i=N}^{N+M-1} (y_i - \hat{y}_i) \quad (35)$$

Thus, denoting $M' = N + M - 1$, we obtain:

$$\begin{aligned}\langle TIE^2(T) \rangle &= \tau_0^2 \sum_{i=N}^{M'} \sum_{j=N}^{M'} R_{ij} + t_M^2 \sigma^2(C_0) + t_M^2 \left(t_N + \frac{T}{2}\right)^2 \sigma^2(C_1) \\ &\quad + 2t_M^2 \left(t_N + \frac{T}{2}\right) Cov(C_0, C_1) \\ &\quad - 2\tau_0^2 \sum_{i=N}^{M'} \sum_{j=N}^{M'} Cov(y_i, C_0) - 2\tau_0^2 \sum_{i=N}^{M'} \sum_{j=N}^{M'} t_j Cov(y_i, C_1)\end{aligned}\quad (36)$$

3.2.3 Example of f^{-2} frequency noise

In order to use (32) the covariances $Cov(C_0, y_r(t'))$ and $Cov(C_1, y_r(t'))$ must be calculated:

$$\begin{aligned}\langle C_0, y_{rM'} \rangle &= \frac{2(2N-1)}{N(N+1)} \sum_{i=0}^{N-1} \langle y_i, y_{rM'} \rangle - \frac{6}{N(N+1)} \sum_{i=0}^{N-1} i \langle y_i, y_{rM'} \rangle \\ &= \frac{2(2N-1)}{N(N+1)} \sum_{i=0}^{N-1} R_{iM'} - \frac{6}{N(N+1)} \sum_{i=0}^{N-1} i R_{iM'} \\ &= h_{-2} \left[\frac{1}{f_l} - \pi^2(t_N + T) \right]\end{aligned}\quad (37)$$

For $Cov(C_1, y_r(t'))$, we obtain:

$$Cov(C_1, y_r(t')) = \frac{h_{-2}\pi^2}{\tau_0} \quad (38)$$

Therefore, for an f^{-2} frequency noise, the standard deviation of the TFE is:

$$\sqrt{\langle TFE^2(T) \rangle} = \sqrt{h_{-2} \left[\frac{4\pi^2 t_N}{15} + \frac{12\pi^2 T}{5t_N} (t_N + T) \right]} \quad (39)$$

It is interesting to notice that the DFE and the Random Frequency Error are fully separated:

$$\sqrt{\langle TFE^2(T) \rangle} = \sqrt{2\sigma^2(e) + \sigma^2(C_1)(t_N + T)} \quad (40)$$

Thus, if $T = 0$ (interpolation), the standard deviation of the TFE is $\sqrt{2}$ times the standard deviation of the residuals, i.e. it is the standard deviation between two residuals.

Concerning the TIE, from (36), (37) and (38), we obtain:

$$\sqrt{\langle TIE^2(T) \rangle} = \sqrt{\frac{\pi^2 h_{-2} T^2}{15 t_N} (9 t_N^2 + 13 t_N T + 4 T^2)} \quad (41)$$

4 CONCLUSION: CHOICE OF THE FREQUENCY MODEL

What is the physical meaning of the low cut-off frequency of an oscillator? Is it a real feature of low frequency noises or a mathematical trick? In practice, it is possible to avoid its use.

For an f^{-2} frequency noise, the derivative of the frequency deviation, the ageing $z(t)$, is a white noise:

$$y(t) = \int_{t_0}^t z(\theta) d\theta \quad (42)$$

where t_0 is the switch-on date of the oscillator. In this case, we have assumed that the oscillator was syntonized and synchronized at t_0 . f_1 is no longer necessary, $y(t)$ is a centered random variable whose standard deviation increases with Θ :

$$f_1 \equiv \frac{1}{\Theta} \quad (43)$$

What is the "real" frequency of the oscillator over $T \ll \Theta$: its nominal frequency or its mean frequency over T ?

The answer depends on the frequency model:

- the use of the power law PSD model implies that the nominal frequency and the h_α noise levels are time-independent: they are the constants of this model. This model is suitable for free-running oscillators, e.g. frequency standards involved in the TAI computation;
- the determination of the nominal frequency as the mean frequency over a sequence of finite duration implies that the nominal frequency is time-dependent: this nominal frequency is only valid over this whole sequence but neither over a part of this sequence nor over another sequence. This model is suitable for oscillators used for an experiment of well-defined duration.

References

- [1] F. Vernotte and M. Vincent. Estimation of the uncertainty of a mean frequency measurement. In *11th European Frequency and Time Forum*, pages 553–556, Neuchâtel, Switzerland, March 1997.
- [2] C. A. Greenhall. Initializing a flicker noise generator. *IEEE Trans. on Instrum. and Meas.*, IM-35(2):222–224, June 1986.
- [3] L. G. Bernier. Linear prediction of the non-stationarity clock error function. In *European Frequency and Time Forum 1988*, pages 125–137, Neuchâtel, Switzerland, March 1988.

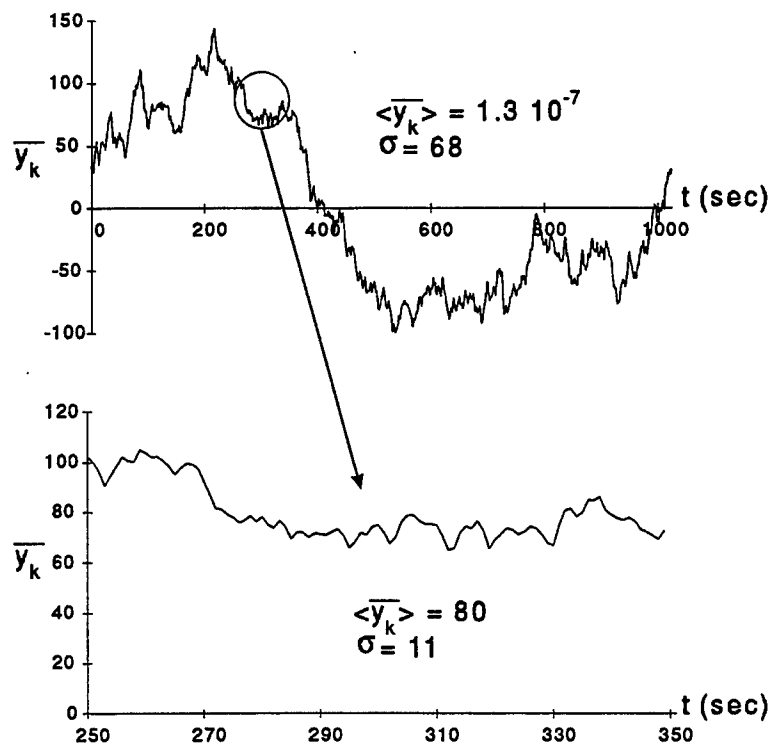


Figure 1: Sequence of frequency deviation samples for an f^{-2} FM noise. Above, the duration of the sequence is about the inverse of the low cut-off frequency. Below is an enlargement of a part of this graph: the inverse of the low cut-off frequency is far larger than the duration of the sequence, and the samples are no longer centered

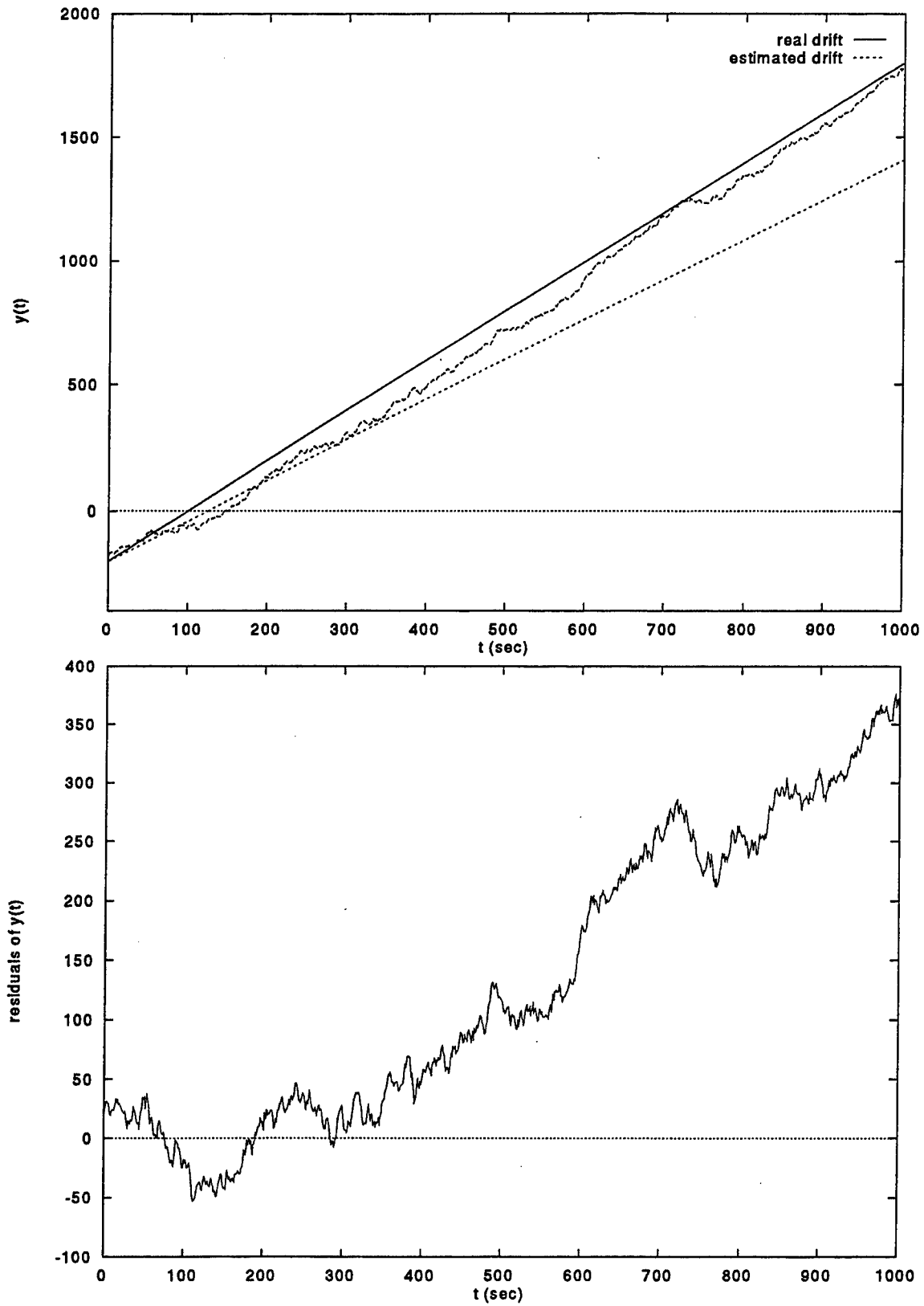


Figure 2: Estimation of the drift over a sequence of frequency deviation altered by f^{-2} FM noise (above). The drift was estimated over the first 256 samples (256 sec). After this time, the sequence moves away from the estimated drift. This effect is more obvious in the residuals (below).

Total Variance: a Progress Report on a New Frequency Stability Characterization*

D. A. Howe †

National Institute of Standards and Technology
325 Broadway
Boulder, CO 80303

C. A. Greenhall ‡

Jet Propulsion Laboratory (Caltech)
4800 Oak Grove Dr., MS 298-100
Pasadena, CA 91109

Abstract

We give results of recent work on a newly developed frequency stability characterization, called Total variance, whose main advantages are improved confidence at and near the longest averaging time of half the data duration, and lower sensitivity to drift removal. Properties given here, for the standard FM noise types, include mean, degrees of freedom, frequency response, and empirical distribution function.

1 Introduction and Conclusions

This paper is about characterizing common, difficult to characterize frequency noise modulations found at long-term averaging time τ in the output signal of many laboratory frequency standards. It assumes a familiarity with the Allan variance and its characterizations of white, flicker, and random walk FM noise models (WHFM, FLFM, and RWFM) [1].

A shortfall of the currently recommended [2] Allan variance for τ , denoted here by $Avar(\tau)$, is that the usual estimators of it are highly variable at large τ [1, 3, 4] and are sensitive to the method of drift removal [5]. We report statistical properties of a new kind of frequency variance, inherently dependent on measurement duration T as well as τ , called Total variance and denoted hereafter by $Totvar(\tau, T)$ (pronounced töt'-vär). We quantify the improvement in the uncertainty on frequency-stability estimation from the use of $Totvar(\tau, T)$ rather than $Avar(\tau)$ in the presence of FM noises. The square root of this variance, called Total deviation and denoted by $Totdev(\tau, T)$ or the recommended [2] notation $\sigma_{y,TOTAL}(\tau)$, can be interpreted like the Allan deviation $\sigma_y(\tau)$, but with improved confidence at long-term τ , as pointed out in earlier papers [6, 7] and quantified in this paper for FM noises. We do not address the important property that $Totvar(\tau, T)$ appears to have considerably less sensitivity to the method of drift removal than $Avar(\tau)$ [8].

The main advantages of $Totvar$ over $Avar$ are improved confidence at and near the longest averaging time of $\tau = T/2$, and lower sensitivity to drift removal. By theory and simulation we have computed its mean, variance, and empirical probability distribution in the presence of the three FM noise types. Variance results are given in terms of equivalent degrees of freedom [9]. In

*Contribution of the U. S. Government, not subject to copyright.

†This author is with the Time and Frequency Division; E-mail: dhowe@nist.gov.

‡The work of this author was performed at the Jet Propulsion Laboratory, California Institute of Technology, under a contract with the National Aeronautics and Space Administration; E-mail: Charles.Greenhall@jpl.nasa.gov.

the presence of white FM noise modulation, Total variance is an unbiased estimate of the Allan variance for all τ , yet has three degrees of freedom instead of one at $\tau = T/2$. For all three noise types, the mean and edf of Totvar are given by simple exact or empirical formulas. A comparison of the empirical distribution of Totvar($T/2, T$) with the appropriate chi-squared distribution indicates that confidence intervals based on chi-squared levels are conservative.

In the established tradition of time and frequency statistics, frequency stability is described in terms of finite-difference variances that are ensemble or infinite-time averages of stationary, ergodic increments of phase [12, 13, 14]. In particular, the theoretical Allan variance is a number that depends only on τ , while its conventional estimators are random variables that depend on both τ and T , the largest possible τ being $T/2$. Total variance is a random variable that, along with all its properties, inherently depends on both τ and T . Moreover, Total variance can report values beyond the usual Allan variance last- τ value of $\tau = T/2$; its values at $\tau > T/2$ might be used to augment the normal last- τ value of frequency stability reported at $\tau = T/2$.

We compute the frequency response of Total variance as a function of τ by averaging the squares of the Fourier transforms of Total variance sampling functions, and find that it resembles the frequency response of Allan variance. The results of these investigations indicate that Total variance, while it has an interpretation like that of the Allan variance, also has lower variability and less sensitivity to drift removal.

2 Equations for Totvar(τ, T)

The purpose of this section is to give a precise definition of Totvar(τ, T) for an N_x -point time deviation record with sample period τ_0 . In the following description, the indices m, n , and N_x are related to time by $\tau = m\tau_0$, $t = t_0 + n\tau_0$, and $T = N_x\tau_0$, where t_0 is the time origin and without loss may be made equal to 0.

We start with time-deviation data x_n , $n = 1$ to N_x , with normalized frequency deviations $y_n = (x_{n+1} - x_n)/\tau_0$, $n = 1$ to $N_y = N_x - 1$. Extend the sequence $\{y_n\}$ to a new, longer virtual sequence $\{y_n^*\}$ by reflection as follows: for $n = 1$ to N_y let $y_n^* = y_n$; for $j = 1$ to $N_y - 1$ let

$$y_{1-j}^* = y_j, \quad y_{N_y+j}^* = y_{N_y+1-j}. \quad (1)$$

An equivalent operation can be performed on the original time-deviation sequence $\{x_n\}$ to produce an extended virtual sequence $\{x_n^*\}$ as follows: for $n = 1$ to N_x let $x_n^* = x_n$; for $j = 1$ to $N_x - 2$ let

$$x_{1-j}^* = 2x_1 - x_{1+j}, \quad x_{N_x+j}^* = 2x_{N_x} - x_{N_x-j}. \quad (2)$$

This operation, depicted in Figure 1, is called *extension by reflection about both endpoints*. The result of this extension is a virtual data sequence x_n^* , $n = 3 - N_x$ to $2N_x - 2$, having length $3N_x - 4$ and satisfying $y_n^* = (x_{n+1}^* - x_n^*)/\tau_0$, $n = 3 - N_x$ to $2N_x - 3$.

We now define

$$\text{Totvar}(m, N_x, \tau_0) = \frac{1}{2(m\tau_0)^2(N_x - 2)} \sum_{n=2}^{N_x-1} (x_{n-m}^* - 2x_n^* + x_{n+m}^*)^2, \quad (3)$$

for $1 \leq m \leq N_x - 1$, that is, τ can go to $(N_x - 1)\tau_0$ instead of the usual limit of $\lfloor (N_x - 1)/2 \rfloor \tau_0$. The previous notation Totvar(τ, T) is to be regarded as equivalent to (3) with the dependence on τ_0 suppressed. Totvar can also be represented in terms of extended fractional frequency fluctuation averages as

$$\text{Totvar}(m, N_y, \tau_0) = \frac{1}{2(N_y - 1)} \sum_{n=1}^{N_y-1} (\bar{y}_n^*(m) - \bar{y}_{n-m}^*(m))^2, \quad (4)$$

where $\bar{y}_n^*(m) \doteq (x_{n+m}^* - x_n^*) / (m\tau_0)$.

It can be verified that Totvar, like Avar and its estimators, is invariant to an overall shift in phase and frequency; that is, if a first-degree polynomial $c_0 + c_1 n$ is added to the original data set x_n , then Totvar does not change.

We expect the Total variance to be applied mostly to long phase records in which the FM noises dominate the PM noises (white and flicker PM). Then, it is convenient for theoretical purposes to approximate Totvar(m, N_x, τ_0) by a continuous-time analog called Totvarc(τ, T), in which the sum in (3) is replaced by an integral and dependence on τ_0 is eliminated. The time deviation is now a continuous-time process $x(t)$, given for $0 \leq t \leq T$. Extend $x(t)$ to $x^*(t)$ as follows: for $0 \leq t \leq T$ let $x^*(t) = x(t)$; for $0 < u \leq T$ let $x^*(-u) = 2x(0) - x(u)$ and $x^*(T+u) = 2x(T) - x(T-u)$. Then $x^*(t)$ is given for $-T \leq t \leq 2T$. The continuous analog of Totvar is defined by

$$\text{Totvarc}(\tau, T) = \frac{1}{2\tau^2 T} \int_0^T [x^*(t-\tau) - 2x^*(t) + x^*(t+\tau)]^2 dt, \quad (5)$$

for $0 < \tau \leq T$.

The expressions above are quite different from their equivalent Allan variance expressions. Mainly, Totvar(τ, T) reports a value for an interval τ within data length T based on more samples of the second-difference of phase (or first-difference of average frequency) using a rearranged and extended series of the original data series $\{x_n\}$. It does this by a multiple sample on the phase using a larger, virtual set of data which is an odd, or reflected, extension at the beginning and end (left and right) of the original real set. Figure 1 illustrates the extension and, hence, the resulting circular or repeating representation.

Analyzing a larger virtual data set built from the original data set has been a tool in frequency-domain signal processing for many years. An assumption of periodicity replaces the recurrent behavior (in a time-series sense), a consequence of the ergodic principle [15]. In particular, a range of frequency values (Fourier components) from $0 < f < f_h$ can be extended by a mirror reflection through $f = 0$ so that "negative frequencies" are added to an original data set, resulting in $-f_h < f < f_h$. In the context of time-series analysis, rather than doing extensions of the original vector $\{x_n\}$ and applying the straight second-difference, we alternatively can resample within the original vector; see Section 4 for an algorithm that requires no extension of the data array.

3 Totvarc(τ, T) as an Estimator of Avar(τ)

3.1 Mean and Variance

For computing theoretical moments it is convenient to use the continuous-time random variable Totvarc(τ, T) as a surrogate for the discrete-time random variable Totvar(τ, T), for the same reason that the calculus of integrals and derivatives is less intricate than the calculus of sums and differences. The mean and variance of Totvarc(τ, T) in the presence of the three standard power-law FM noises were computed by the generalized autocovariance method [4] under the assumption of Gaussian, mean-zero second differences of phase; no frequency drift or drift removal is allowed. The mean $E[\text{Totvarc}(\tau, T)]$ is compared to Avar(τ); the variance is most conveniently communicated through the equivalent degrees of freedom (edf), defined for a random variable V by

$$\text{edf}(V) = \frac{2(EV)^2}{\text{var}(V)}. \quad (6)$$

The results, some of which are exact and some of which are empirical fits to numerically computed results, can be expressed as

$$\frac{E[\text{Totvar}(\tau, T)]}{\text{Avar}(\tau)} = 1 - a\frac{\tau}{T}, \quad 0 < \tau \leq \frac{T}{2}, \quad (7)$$

$$\text{edf}[\text{Totvar}(\tau, T)] = b\frac{T}{\tau} - c, \quad 0 < \tau \leq \frac{T}{2}, \quad (8)$$

where a , b , and c are given in Table I. These results were checked by simulations of Totvar (m, N_x, τ_0), with $N_x = 101$.

Table I. Values of a , b and c for FM noises

Noise	a	b	c
WHFM	0	$3/2$	0
FLFM	$1/(3 \ln(2))$	$24 (\ln(2)/\pi)^2$	0.222
RWFM	$3/4$	$140/151$	0.358

The simple, exact form (7) for the mean of Totvar can be interpreted as a scaling property of power-law noise. It turns out this way because the shapes of the sample functions for Totvar and Avar (see Section 4) depend only on τ . For $T/2 < \tau \leq T$ the sampling function shapes depend also on T ; yet, it is noteworthy that (7) persists all the way to T , but only for white FM and random walk FM. The edf results are empirical, with an observed error below 1.2% of numerically computed values; for white FM, though, the edf result appears to be exact, although this is unverified.

For white FM noise processes, Total Variance is an unbiased estimate of the traditional Allan Variance (square of frequency change vs. τ) for all averaging times (τ 's). Its primary advantage, as surmised from (8) and Table I, is a considerable improvement in the confidence of that estimate at longer averaging times. For example, 10 000 seconds of frequency measurements means that τ can't go beyond 5000 seconds ($T/2$) to get one single estimate of frequency-change over the data duration (last half minus first half) using Avar. The edf result (8) for white FM yields the equivalent of three independent estimates ($\text{edf} = 3$) by using Totvar and its multi-sampling function, which is discussed in the next section. The improvement of edf in the presence of FLFM and RWFM (2.097 and 1.514, respectively) is not as dramatic, but substantial nevertheless. For $\tau = T/4, T/8$, etc., the confidence measures of Allan and Total confidence approach each other, until they are essentially the same at $T/16$. For small values of τ/T , the time-deviation record is extended only a short distance at both ends, and hence Totvar (τ, T) differs little from the fully overlapped estimator of Avar (τ) [9].

3.2 Distribution Functions

In the tradition of time and frequency statistics, it is customary to derive confidence intervals for frequency stability on the basis of the assumption that the probability distribution of a frequency stability estimator V , when scaled appropriately, follows the chi-squared distribution with the same edf as V ; see [9]. The chi-squared assumption has been investigated in a limited way for conventional estimators of Allan variance [10, 11]; in view of the greater complexity of Total variance, some investigation of its distribution is appropriate.

Let V denote the Totvar estimator of Allan variance σ^2 , for some τ , and let $r = E(V)/\sigma^2$, $\nu = \text{edf}(V)$, which are presumed known from the previous results. Then the random variable

$$X = \frac{\nu V}{r \sigma^2}$$

has the same mean and edf as does a χ^2_ν , namely, ν . If X had the χ^2_ν distribution, then one could derive confidence intervals for σ^2 based on one observation of V .

We carried out a brief investigation of the chi-squared assumption for the most important case of $\tau = T/2$. One thousand independent trials of Totvar (50, 101) were simulated for the three FM noise types, and the empirical distribution functions of X were plotted along with the theoretical chi-squared distribution functions. The chi-squared distributions were good fits to the empirical distributions except at the lower tails, expanded views of which are shown in Figure 2. The empirical tail always lies below the chi-squared tail. Thus, for a probability $p \leq 0.2$, if $x_\nu(p)$ is the chi-squared level for p , and $x_\nu^*(p)$ the level of the scaled Totvar X , we have $x_\nu(p) < x_\nu^*(p)$. Because the upper end of a true confidence interval for σ^2 is proportional to $1/x_\nu^*(p)$ for an appropriate value of p , using $x(p)$ for this purpose gives a conservative confidence interval. For example, suppose we want a 90% confidence interval for σ^2 at $\tau = T/2$ based on $V = \text{Totvar}(T/2, T)$ and a white-FM noise assumption. Then $r = 1$, $\nu = 3$; the 5% and 95% χ^2_3 levels are 0.352 and 7.81; and a 90% confidence interval for σ^2 based on chi-squared is $[3V/7.81, 3V/.352] = [0.384V, 8.52V]$. (Take square roots for σ .) The more realistic value of 0.60 for the 5% Totvar level from Figure 2(a) reduces the upper end of the confidence interval to $5V$.

4 Sampling Functions and Frequency Responses

Extending by reflection an original $\{x_n\}$ vector at both ends and then applying a second difference can be equivalently represented as four different types of differencing on $\{x_n : n = 1, \dots, N_x\}$ directly. The summand of Totvar(m, N_x, τ_0) in the following equation takes on four forms that depend on the relationship of n to a given m and N_x :

$$\text{Totvar}(m, N_x, \tau_0) = \frac{1}{2(m\tau_0)^2(N_x - 2)} \sum_{n=2}^{N_x-1} D_n^2, \quad (9)$$

where

$$\begin{aligned} D_n &= x_{n-m} - 2x_n + x_{n+m} & : & \quad m - n \geq 1, \quad m + n \leq N_x, \\ D_n &= 2x_1 - x_{2-n+m} - 2x_n + x_{n+m} & : & \quad m - n < 1, \quad m + n \leq N_x, \\ D_n &= x_{n-m} - 2x_n + 2x_{N_x} - x_{2N_x-n-m} & : & \quad m - n \geq 1, \quad m + n > N_x, \\ D_n &= 2x_1 - x_{2-n+m} - 2x_n + 2x_{N_x} - x_{2N_x-n-m} & : & \quad m - n < 1, \quad m + n > N_x. \end{aligned}$$

We can derive from these expressions the frequency sampling functions associated with Totvar(τ, T), that is, how its terms act on $y_n = (x_n - x_{n-1})/\tau_0$, and contrast them with the simpler sampling function associated with Avar(τ) (see Figure 3), which gives the change in average frequency from one τ interval to the next [7]. The augmentation incorporated in Totvar(τ, T) combines the sequential sampling function with others, which makes its sampling technique bizarre, but nevertheless shown in Figure 4.

Although the time-domain presentation of the action of Totvar on frequency residuals seems to give little insight, we can use the Fourier transform of these sampling functions to derive frequency responses that perhaps convey more meaning. The continuous analog version of Totvar(τ, T) can be written in the form

$$\text{Totvarc}(\tau, T) = \frac{1}{2\tau^2 T} \int_0^T dt \left[\int_0^T du y(u) h_y(u; t, \tau) \right]^2, \quad (10)$$

where $h_y(u; t; \tau)$ is the sampling function for $\nabla_\tau^2 x^*(t)$ (for the extended $x^*(\cdot)$ record) in terms of $y(u) = dx(u)/du$, $0 < u < T$. Let $H_y(f; t, \tau) = \int_0^T h_y(u; t, \tau) e^{-i2\pi fu} du$. We can show that the expected value is given in terms of $S_y(f)$, the one-sided spectral density of $y(t)$, by

$$E[\text{Totvarc}(\tau, T)] = \int_0^\infty W_y(f; \tau, T) S_y(f) df, \quad (11)$$

where

$$W_y(f; \tau, T) = \frac{1}{2\tau^2 T} \int_0^T |H_y(f; t, \tau)|^2 dt. \quad (12)$$

$W_y(f; \tau, T)$ can therefore be regarded as the mean frequency response of Totvar as an action on $y(t)$. Figure 5 shows this frequency response plotted against $f\tau$ for $\tau/T = 0.1, 0.2, \dots, 0.5$. The frequency response of Allan variance (dotted curve) is the limit of Totvar response as $\tau/T \rightarrow 0$. Also shown (dashed curve) is the frequency response of $2 \cdot \text{Totvarc}(T, T)$, regarded as an estimator of $\text{Avar}(T/2)$ (see Section 5 below).

$\text{Totvarc}(\tau, T)$ has an approximate Allan-like response; more importantly, Totvar does not have the deep nulls encountered with $\text{Avar}(\tau)$ near $\tau = T/2$; consequently it has less variability and hence better confidence as indicated by an increased edf. We showed that the estimate (*vis-à-vis* $E[\text{Totvarc}(\tau, T)]$) is an unbiased estimate of $\text{Avar}(\tau)$ for WHFM noise and slightly biased for FLFM and RWFM noise. This may be somewhat evidenced by noting the slight reduction in the amplitudes of the main lobes of the frequency responses in Figure 5.

5 Properties of Totvarc(T, T)

Although we have defined Totvar for τ all the way up to $(N_x - 1)\tau_0$, we can realistically expect to obtain meaningful frequency stability results only $\tau \leq T/2$. Nevertheless, we computed the mean and edf of $\text{Totvarc}(\tau, T)$ for $T/2 < \tau \leq T$. For white and random walk FM, *twice* $\text{Totvarc}(T, T)$ is unbiased for $\text{Avar}(T/2)$ and is almost unbiased (within a factor of $2/(3 \ln(2)) = 0.9618$) for flicker FM. This result was motivated by comparing the frequency responses of $2 \cdot \text{Totvarc}(T, T)$ and $\text{Avar}(T/2)$, as seen in Figure 5. Unfortunately, $\text{Totvarc}(T, T)$ has a smaller edf (1.5, 1.126, and 1.029 for WHFM, FLFM, and RWFM) than $\text{Totvarc}(T/2, T)$ does, and hence the mean-squared error (bias² + variance) of $2 \cdot \text{Totvarc}(T, T)$ as an estimator of $\text{Avar}(T/2)$ is greater than that of $\text{Totvarc}(T/2, T)$, so we might still prefer $\text{Totvarc}(T/2, T)$, or perhaps some linear combination of the two. This possibility has yet to be investigated, but other work indicates that Total variance coefficients beyond $\tau = T/2$ could justifiably be incorporated in the last $T/2$ value usually reported. Summing all the familiar “power-of-2” τ -values in a Total variance plot leads to exactly twice the standard sample variance, much in the same way that integrating an estimate of a spectrum also yields the sample variance [18].

References

- [1] D.B. Sullivan, D.W. Allan, D.A. Howe, and F.L. Walls (Editors), *Characterization of Clocks and Oscillators*, Natl. Inst. Stand. Technol. Technical Note 1337 (1990; available from NIST, 325 Broadway, Boulder, CO 80303-3328).
- [2] E.S. Ferre-Pikal, J.R. Vig, et al., “Draft Revision of IEEE Std 1139-1988: Standard Definitions of Physical Quantities for Fundamental Frequency and Time Metrology—Random Instabilities,” *Proc. 1997 IEEE Int. Freq. Cont. Symp.*, 338–357 (1997; in revision).

- [3] D.A. Howe and D.B. Percival, "Wavelet Variance, Allan Variance, and Leakage," *IEEE Trans. Instrum. Meas.*, IM-44, 94-97 (1995).
- [4] C.A. Greenhall, "A Structure Function Representation Theorem with Applications to Frequency Stability Estimation," *IEEE Trans. Instrum. Meas.*, IM-32, 364-370 (1983).
- [5] M.A. Weiss and C. Hackman, "Confidence on the Three-Point Estimator of Frequency Drift," *Proc. 24th Ann. PTTI Meeting*, 451-460 (1992).
- [6] D.A. Howe, "An Extension of the Allan Variance with Increased Confidence at Long Term," *Proc. 1995 IEEE Int. Freq. Cont. Symp.*, 321-329.
- [7] D.A. Howe, "Methods of Improving the Estimation of Long-term Frequency Variance," *Proc. 1997 European Frequency and Time Forum*, 91-99.
- [8] D.A. Howe and K.J. Lainson, "Effect of Drift on TOTALDEV," *Proc. 1996 IEEE Intl. Freq. Control Symp.* 883-889.
- [9] D.A. Howe, D.W. Allan, and J.A. Barnes, "Properties of Signal Sources and Measurement Methods," *Proc. 35th Freq. Cont. Symp.*, 1-47 (1981; reprinted in [1]).
- [10] K. Yoshimura, "Characterization of Frequency Stability: Uncertainty Due to the Autocorrelation of the Frequency Fluctuations," *IEEE Trans. Instrum. Meas.*, IM-27, 1-7 (1978).
- [11] W.V. Prestwich and T.J. Kennett, "The Statistical Properties of Allan Variance," *Can. J. Phys.* 69, 1405-1415 (1991).
- [12] J.A. Barnes, "Atomic Timekeeping and the Statistics of Precision Signal Generators," *Proc. IEEE* 54, 207-220 (1966).
- [13] J.A. Barnes, A.R. Chi, L.S. Cutler, D.J. Healy, D.B. Leeson, T.E. McGunigal, J.A. Mullen, Jr., W.L. Smith, R.L. Sydnor, R.F.C Vessot, G.M.R. Winkler, "Characterization of frequency stability," *IEEE Trans. Instrum. Meas.*, IM-20, 105-120 (1971).
- [14] J. Rutman, "Characterization of Phase and Frequency Instabilities in Precision Frequency Sources: Fifteen Years of Progress," *Proc. IEEE* 66, 1048-1075 (1978).
- [15] D.A. Howe, "Circular Representation of Infinitely Extended Sequences," *Proc. 1995 IEEE Intl. Freq. Cont. Symp.* 337-345.
- [16] D.W. Allan, M.A. Weiss, and J.L. Jespersen, "A Frequency-domain View of Time-domain Characterizations of Clocks and Time and Frequency Distribution Systems," *Proc. 45th Freq. Cont. Symp.*, 667-678 (1991).
- [17] D.A. Howe and K.J. Lainson, "Simulation Study Using a New Type of Sample Variance," *Proc. 1995 PTTI Meeting*, 279-290.
- [18] D.B. Percival and D.A. Howe, "Total Variance as an Exact Analysis of the Sample Variance," *Proc. 1997 PTTI Meeting*, this issue.

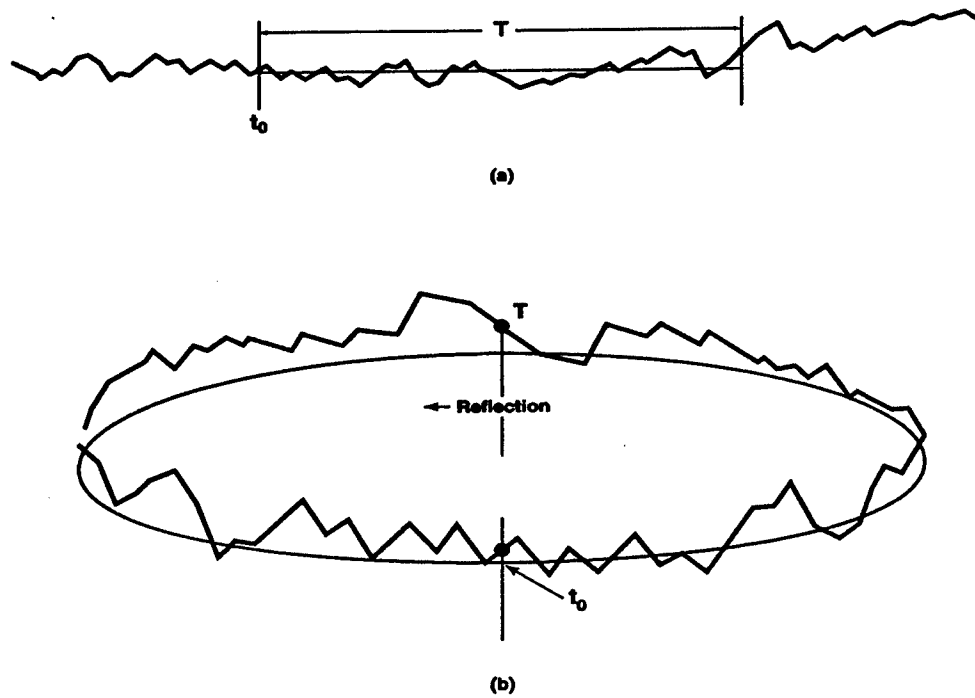


Figure 1: (a) Extension of a phase record by reflection at both ends; (b) circular representation of extended phase record

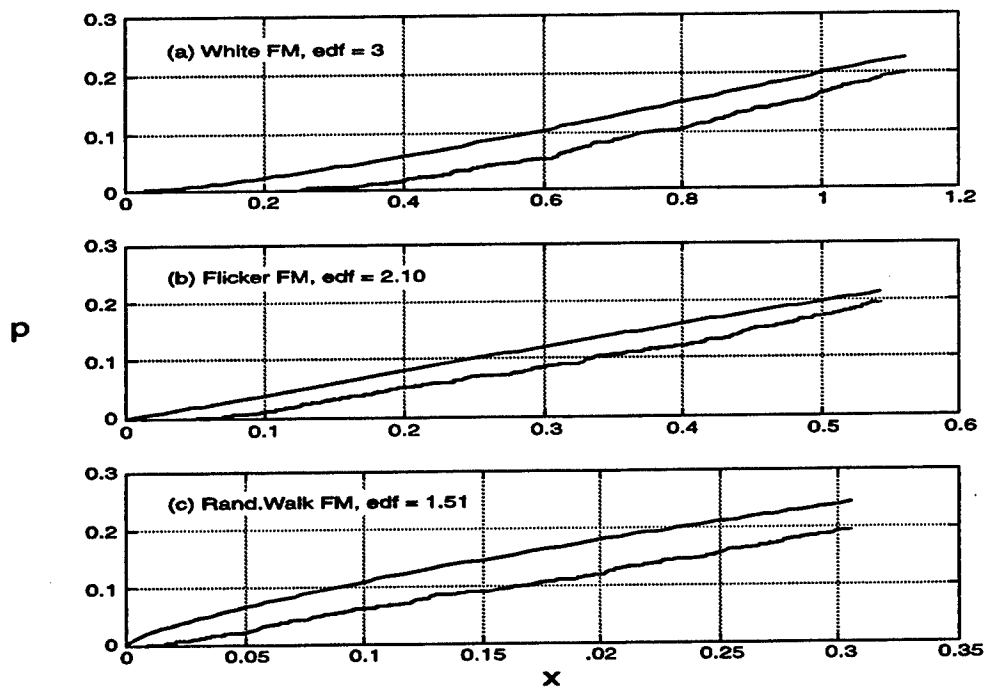


Figure 2: Expanded views of the lower tails of empirical Totvar distribution functions (lower curves), and the corresponding chi-squared distribution functions (upper curves)

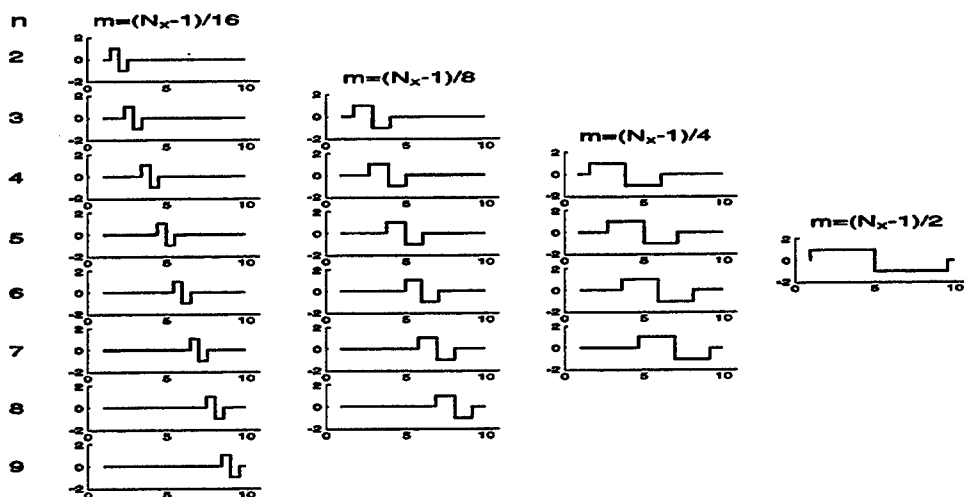


Figure 3: Usual sampling given by Avar for values of m and n when $N_x=10$, $m \leq (N_x - 1)/2$

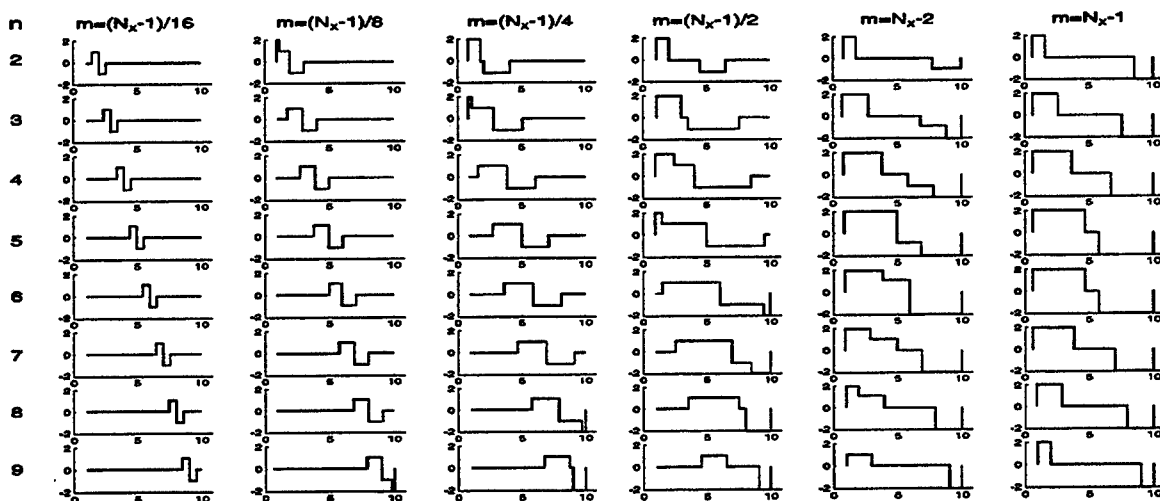


Figure 4: Sampling given by Totvar for values of m and n when $N_x=10$; note that m is not restricted to $m \leq (N_x - 1)/2$ as with Avar

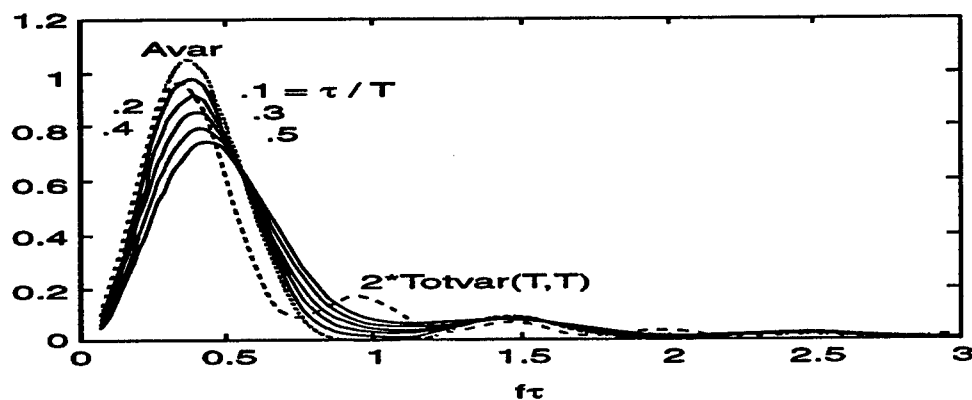


Figure 5: Mean frequency responses of Avar and Totvar as operations on $y(t)$

Questions and Answers

CLAUDINE THOMAS (BIPM): If we want to use the total variance, we must first be sure that there is no frequency drift in the data.

DAVE HOWE (NIST): Oh, that is not true. We no longer have to remove the drift or some coefficient, at any rate. We never know the drift in real data; in simulation we, of course, can –

CLAUDINE THOMAS: But, when you circle the data, if you have a frequency drift, of course, you will have an offset.

DAVE HOWE: Well, no. As a matter of fact – let me put that slide back on here, that is a very good question. I will put this up. This is the original data, this is 20 simulations of random walk FM. So the data duration extends with Index 1 to 1025. The procedure calls for extending that at both ends. So, the vector that you actually work on is going to look like that.

Now, in the presence of drift, because it is a mirrored reflection, if there is a trend in the data at the adjoin, when you are adding or extending the data set, then there will not be any discontinuity by taking the second difference. Yes, you have to think about it a little bit, but what we do is we actually reverse the data set and we also mirror it. So, even if there is a racing trend through that last point, or the first point, then there's no discontinuity in looking at the variance, which would be the second difference in that.

CLAUDINE THOMAS: Thank you for your answer. I also have another question. Does the use of the total variance suppose that your system is more or less stationary; that at the beginning and the end of the Tau, of the big T lines, the statistical properties of the system should be the same? Because, when you circle, the statistical properties are completely different. I am thinking about the total time scale of course.

DAVE HOWE: Yes. First of all, by construction, we have a situation where the variance for the original data has to be the same as the variance for the extended data, and that again is by construction. We have not added any additional data; we are using the original data; and constructed it in a way that added more terms, what we call "surrogate terms," which will contribute to the answer that you get in the long term. Nevertheless, getting back to your remark about circularizing the data –

CLAUDINE THOMAS: My question was you have a span of data –

DAVE HOWE: The treatment that we apply does not have any restriction regarding stationarity.

MAINTENANCE OF HP 5071A PRIMARY FREQUENCY STANDARDS AT USNO

H. Chadsey (hc@planck.usno.navy.mil)

A. Kubik (tony@simon.usno.navy.mil)

Time Service Department

U.S. Naval Observatory

Washington, D.C. 20392

Abstract

The U.S. Naval Observatory (USNO) has been operating Hewlett-Packard model 5071A cesium-beam frequency standards for over five years. During that period, there have been a variety of failures and these devices have shown frequency and phase changes.

The HP 5071A model primary frequency standard offers a very useful troubleshooting tool by outputting the status of 22 different operating parameters. This paper will present an explanation of the parameters and show any correlation of them with the time, frequency, and environmental changes. This paper will also offer some indicators to predict future device problems.

INTRODUCTION

The Hewlett-Packard (HP) model 5071A Primary Frequency Standard is a quantum leap forward compared to the HP model 5061B. Among the improvements is the greater frequency stability through a broader temperature and humidity range. HP also improved the device's operational parameter monitoring capabilities. No longer must people enter the room housing the device (disrupting its environment) and physically make the measurements on the device. The new standards can output their parameters via an RS-232 connection to a computer for permanent filing and analysis.

The analysis of these permanent files can range from a snapshot picture of the parameters to a time series analysis with plotting. Having the extreme long-term history of the parameters has additional benefits, especially if that history extends throughout the life of the standard. USNO has 45 standards from the 100, 200, 300, 400, 500, 700, and 1000 production series. Each device has its own "personality." Some characteristics have been correlated with production series. This paper will present the general characteristics of the USNO devices and note where they may differ. The parameters will be discussed in the order of their output. The more important parameters will be noted and discussed in greater detail.

THE PARAMETERS

There are 22 parameter values available via the RS-232 connection. These parameters are: frequency offset, oscillator control percentage, rf amplitude 1 percentage, rf amplitude 2 percentage, Zeeman frequency, C field current, electron multiplier voltage, signal gain percentage, tube oven voltage, tube oven temperature error, oscillator oven voltage, ion pump current, hot wire ionizer voltage, mass spectrometer voltage, SAW tuning voltage, DRO tuning voltage, 87 MHz PLL voltage, uP clock PLL voltage, +12 volt supply voltage, -12 volt supply voltage, 5 volt supply voltage, and internal temperature. USNO collects these data once per hour. The information appears as:

MJD 48587 21:03:42

CBT ID: 6-temp

Status summary: Operating normally

Power source: AC

Log status: Empty

Freq Offset:	0e-15	Osc. control:	-1.67 %
RF amplitude 1:	20.2 %	RF amplitude 2:	19.9 %
Zeeman Freq.	39949 Hz	C-field curr:	12.137 mA
E-multiplier:	1870 V	Signal Gain:	28.8 %

CBT Oven:	6.2 V	CBT Oven Err:	0.00 C
Osc. Oven:	-8.8 V	Ion Pump	0.2 uA
HW Ionizer:	1.0 V	Mass spec:	9.1 V
SAW Tuning:	3.5 V	DRO Tuning	6.8 V
87MHz PLL:	-0.8 V	uP clock PLL:	2.9 V
+12V supply:	12.3 V	-12V supply:	-12.4 V
+5V supply:	5.3 V	Thermometer:	35.0 C

USNO permanently files these values as:

50717.007569 CBT ID: 3128A00110(H) /Status summary: Operating
normally /Power source: AC /Log status: Empty 0e-15 29.94 26.5 25.4
39949 12.166 2553 15.4 8.3 0.00 -8.7 0.0 0.8 12.8 1.8 5.8 1.7
2.6 12.3 -12.3 5.2 41.3

A computer program can sort and display the information in whatever format is needed. One might want several devices listed on one page when looking at snapshot pictures. On the other hand, one might want several consecutive readings for a particular device listed on one page to look for trends. Outputting the values to a plotting program is better for trend observation. Although the snapshot pictures will tell if a device is operating normally, it is the plot of the parameters' history that will help most in detecting the onset of problems and in fixing the device when a failure occurs.

CLOCK PERFORMANCE

The frequency offset can be set by either the manufacturer or the user. Typically, it is set to 0e-15.

Oscillator control percentage is a very important value to monitor. The value can be positive or negative and like most of the other parameters, the value is very characteristic of the device. One standard may have an oscillator control value of -8.6% and another standard may have a value of -43.1%. Neither of these values alone means that the clock is performing (or will perform) poorly. A variation in the value may suggest a future failure, and that will be covered in the next section. What is important about the oscillator control percentage for performance is its frequency and amount of change. This is an example of when continuous, periodic readings are needed. For example, USNO has had at least two standards that exhibit a phase or rate change that was coincident with a change in its oscillator control percentage. Such an occurrence may be due to the standard experiencing an environmental change (temperature and/or humidity), a Cesium Beam Tube (CBT) change, or a CBT controller board change, or it may be a precursor to a failure.

The rf amps have been found to have relatively constant values between 20.0 and 31.0 for each standard after initial burn-in. (The values may change somewhat during the first 1 1/2 to 2 years of operation.) The values will differ slightly from

one device to another. The Zeeman frequency is set at the factory and should be 39949.0. The C field current should be between 12.0 and 12.2 milliamps and remain fairly constant. Again, the exact value will differ between standards.

The electron multiplier voltage is another very important parameter to watch. There is a limit at 2553 volts. USNO does have a standard performing quite well below the 1000 volt specification found in the 5071A owner's manual. (Its startup voltage was about 440 volts.) Typically, our standards have a startup voltage between 1150 and 1500. The voltage will decrease slightly and then begin to rise slowly during the first two years of operation. The total change will usually range from 150 to 200 volts. The voltage should continue to increase slowly after this initial startup period. The absolute value is characteristic of the device. The standard should be performing well if the value is changing slowly and CONSISTENTLY during the entire life time of the CBT.

The signal gain should be constant at 14.4 percent as long as the standard is below its maximum electron multiplier voltage. When the electron multiplier voltage reaches its limit, the signal gain will increase to keep the overall gain constant.

The cesium-beam oven voltage depends on ambient temperature. The USNO standards values are consistent between 7.5 and 8.0 volts. Actual values differ between devices. The cesium-beam tube error must be small (± 0.1 volts) for the standard to be operating properly.

The oscillator oven voltage typically has a value of -8.7 to -8.8 volts during normal operation. It should change by no more than 0.1 volts throughout the life of the device.

The ion pump current should have a low startup value (typically near 0.0) and remain constant. Some devices, however, are working quite well with constant values of 10, 20, or higher. (USNO has one device working well with an ion pump current of 36.0 microamps.) This value is another one of those "personality" characteristics of each device. A high current value can indicate a vacuum or electrical leak, that the tube has been off for a long period, or that the tube is contaminated. A current greater than 50 microamps will cause shutdown.

The hot wire ionizer voltage references the voltage across the ionizer ribbon. A value of 1.0 is ideal and it should be between 0.9 and 1.1 volts.

The mass spectrometer value will range from 10.0 to 14.0 volts. It should remain the same value during normal performance due to environmental changes.

The SAW and DRO tuning, 87 MHz PLL, uP clock PLL, +/-12 volt supply, and 5 volt supply values should be relatively constant from initial startup. All may vary by +/- 0.1 volts during normal operation.

The temperature value is the internal temperature of the standard. The value should typically range from 35 to 45 degrees Celsius and should remain constant. It will change as the standard's environment changes.

CLOCK FAILURES

The recording of the parameters once per hour, every hour, and retaining the information in permanent data files has a great benefit for detecting and analyzing failures. It also allows for the prediction of some future failures. Usually, analysis of the historical parameters may only indicate that a failure will occur, but not when. USNO has experienced a few problems with the standards and often looking at the parameters has pointed directly to the needed repair. By taking hourly readings of the parameters, one can watch a standard fail and prevent a related system disaster.

An example of a minor problem that can be seen in the parameters is a significant change in the standard's environmental temperature. A change in the environmental temperature can show up as an unusually large change in the electron multiplier voltage (see Figures 1, 2, and 3).

More serious problems are seen when an electronic card inside the standard fails. USNO has had some problems with the A2 and A6 cards failing and has documented the parameters showing the indications of a failure.

A failure in the A2 CBT controller card shows up as a significant change in only one parameter. The electron multiplier voltage will jump more than 10 volts. This greater than 10-volt change will occur over a 12- to 24-hour period (see Figure 4). Although a step in this parameter is not always an indication of an A2 card failure, the change is an indication that it is probable. No parameter changes seem to foretell this problem.

A failure in the A6 servo card causes the clock to lose frequency lock and shows up as a change in most of the parameters. The failure is most notable in the oscillator control, rf amplitudes, and CBT parameters. The oscillator control will jump more than 5 percent when the failure occurs (see Figure 5). The rf

amplitudes will jump and remain at a constant value (see Figure 6). The CBT oven voltage will go to 0.0 volts (see Figure 7). The CBT temperature error will step more than 1 degree Celsius and remain constant (see Figure 8). These jumps occur within a few hours and can occur between two consecutive hourly readings. Again, although a step in these parameters is not always an indication of an A6 card failure, the change suggests that it is probable. The occurrence of this failure is sometimes predictable. One cannot, however, foretell when it will occur. The signs are in the CBT parameters. The CBT oven voltage will vary more than ± 0.4 volts, rather than the normal less than ± 0.1 volts (see Figure 7). The CBT temperature error values will also show an abnormally large variation. They will vary more than ± 0.15 degree Celsius rather than the normal less than ± 0.1 degree Celsius (see Figure 8). Another type of failure in the A6 card normally occurs only at startup. A short can cause a fuse to fail on the A6 card. Notice that after repair, the rf amplitudes have returned to their prefailure characteristics (see Figure 6) and the CBT parameters show a "normal" amount of variation (see Figures 7 and 8). It is also worth noting that the oscillator control and electron multiplier have assumed new initial states after repair (see Figures 5 and 9).

The standards at USNO are now getting old enough so that we are starting to see end-of-life CBT failures. This is probably the only failure that every organization will see if they keep the standard for a long time or receive an old standard. The Hewlett-Packard manual says that the standard CBT should last about 5 years. The high performance is warranted for 3 years. USNO's experience is that the high performance CBT lasts on average more than 5 years. Two parameters that say the CBT has failed are the electron multiplier voltage and the signal gain percentage. The electron multiplier voltage will rise quickly during the failure. It will read 2553 (the limit) when the failure has occurred (see Figure 10). The signal gain will very quickly rise to 100% after the electron multiplier voltage has hit its limit (see Figure 11). The alarm light should but will NOT always be lit after the CBT failure has occurred.

The oscillator control percentage will slowly increase its amount of variation during the failure. The size of the variation will increase as time passes after the CBT failure (see Figure 12).

The failure will also be observed in the rf amplitude 1 and 2 parameters. They will both show a large increase in variation either at the time of CBT failure or shortly thereafter.

There seem to be three parameters that suggest a CBT failure will occur. These are the electron multiplier and rf amplitudes 1 and 2. (Although the signal gain does show that the CBT has failed, it does not show any sign of when the failure will occur.) The first and most obvious foretelling event is a rapid increase in the electron multiplier voltage (see Figure 10, MJD 50712 to 50716). USNO found

that the clock is sometimes already outside our performance criteria during this period. The step in the electron multiplier voltage (see Figure 10 at MJD 50708) indicates that the failure is about to begin. This step will usually occur between 2 weeks and 2 days before the electron multiplier voltage reaches its limiting value of 2553 volts and indicates that end-of-life is inevitable. This is, however, not much advance warning.

Advance warning is provided by the rf amplitude 1 and 2 parameters. The variation of the rf amplitude values is very large (see Figures 13 and 14 after MJD 50716). However, notice how the percentage values decrease just before the failure. This allows for some lead time before the failure. More lead time is provided by the rf amplitudes starting to show a tendency to change. For rf amplitude 1, this can occur about a week before the failure (see Figure 13 at MJD 50708). RF amplitude 2 can show this tendency as much as 25 days before the failure (see Figure 14 at MJD 50689). Both rf amplitudes can be either a more positive or negative variation. Either way, they will show an average decrease just before the CBT failure occurs. A word of caution, though: just because the rf amplitudes are showing these early signs does not mean that the CBT will fail in less than 30 days. It should be taken as a warning that the device needs to be watched more closely. More concern should be used when the tendency becomes more pronounced (see Figure 14 after MJD 50706). Although this is not a great amount of notice before the inevitable failure, some notice is better than none. The notice will hopefully be enough to avoid a system crash or other operational failures.

CONCLUSIONS

The Hewlett-Packard model 5071A primary frequency standard is a great operational improvement over the model 5061B. This operational improvement is enhanced further by the device's ability to output its operating parameters to a computer for analysis. The analysis can help in the diagnosis of problems (e.g., cards gone bad).

Close analysis of the parameters and their historical values will in some cases allow the foretelling of failures. These clues can be as simple as seeing extreme environmental effects on the device and/or a change in a card's operation. If the parameters are watched closely enough, the inevitable CBT failure can be anticipated and corrective measures taken.

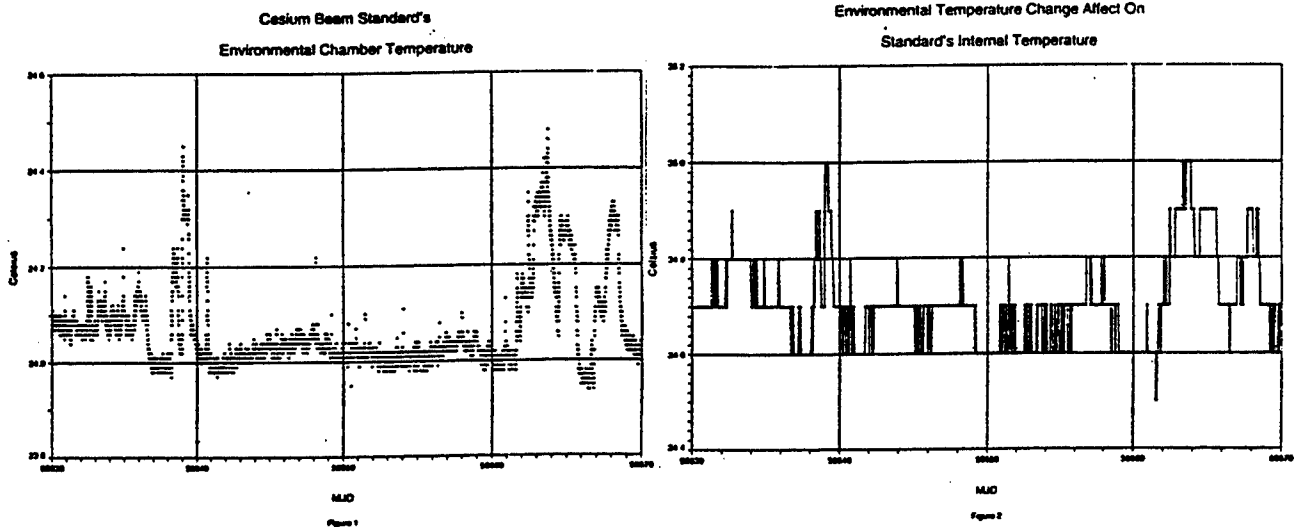
Most of the time, the important parameters to be watched are: electron multiplier voltage, ion pump current, oscillator control percentage, signal gain percentage, internal temperature, and readings of rf amplitude 1 and 2 percentages. These seven should enable a person to predict the performance and life of a frequency standard.

ACKNOWLEDGMENTS

The authors would like to thank Randolph Clarke for clock performance analysis assistance, and Edward Powers for providing historical clock parameter data. A special thanks to Wendy King for the parameter information collection programming.

REFERENCE

Hewlett-Packard Company, HP 5071A Primary Frequency Standard Operating and Programming Manual, 1992.



Servo Card Failure Affect on
CBT Temperature Error

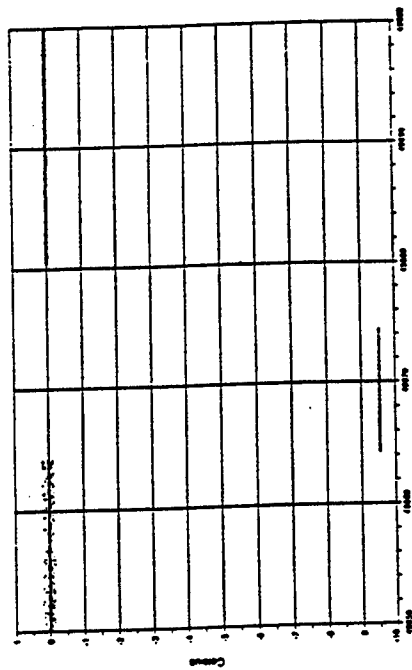


Figure 3
MJD

Cesium Beam Tube End Of Life
Electron Multiplier Voltage

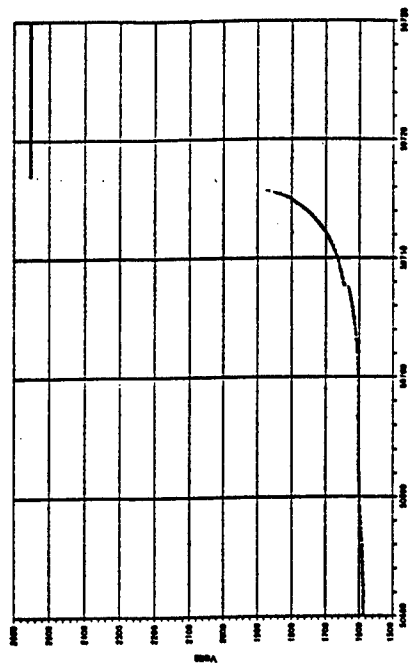


Figure 4
MJD

Servo Card Failure Affect On
CBT Oven Voltage

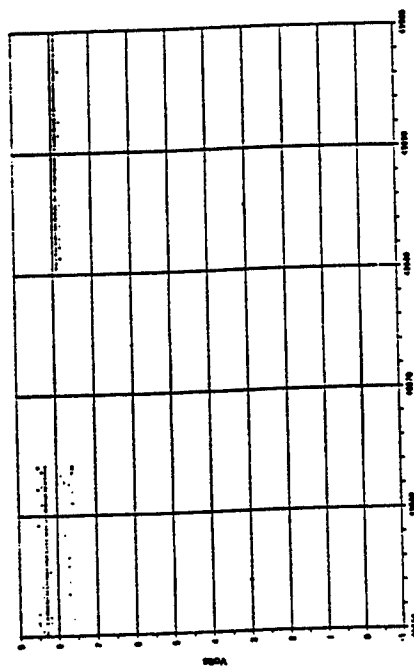


Figure 5
MJD

Servo Card Change Affect On
Electron Multiplier Voltage

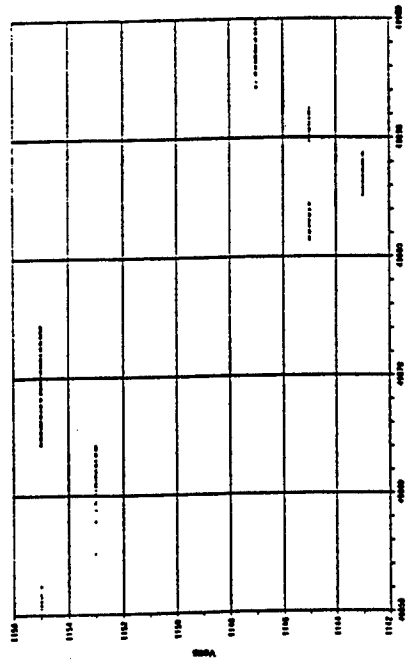
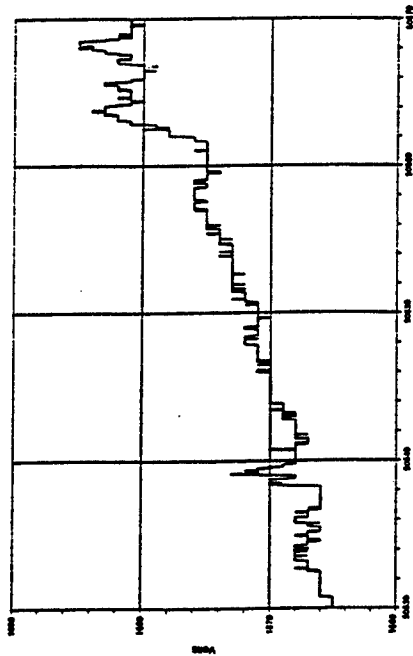


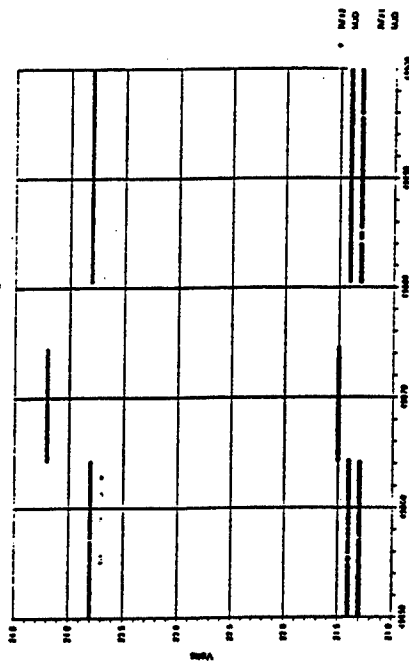
Figure 6
MJD

Environmental Temperature Affect On
Electron Multiplier Voltage



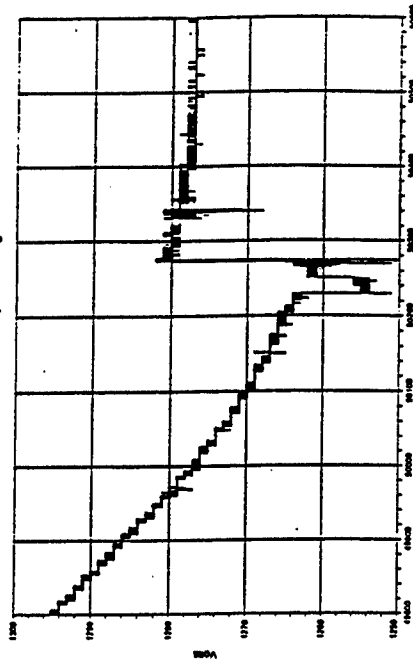
MJD
Figure 2

Servo Card Failure Affect On
RF Amplitude Voltages



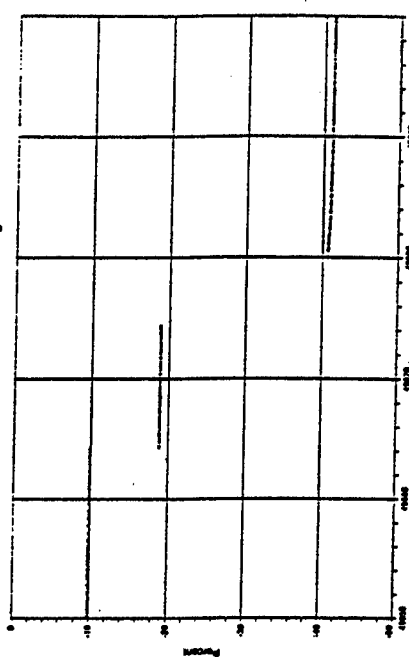
MJD
Figure 3

CBT Controller Card Failure Affect On
Electron Multiplier Voltage



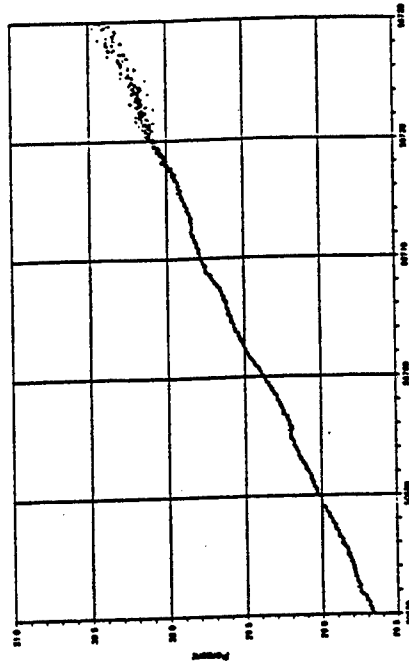
MJD
Figure 4

Servo Card Failure Affect On
Oscillator Control Percentage



MJD
Figure 5

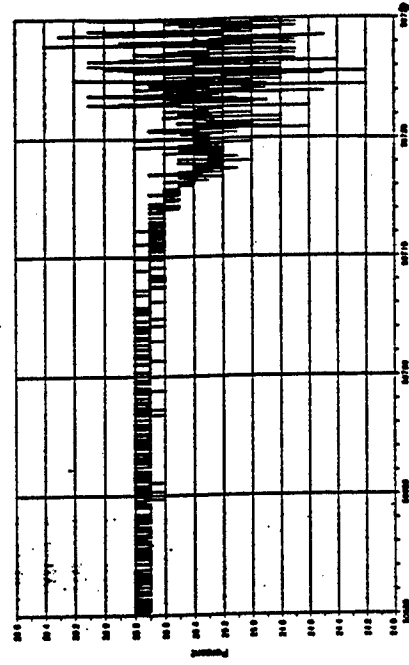
Cesium Beam Tube End Of Life
Oscillator Control Percentage



SLD

Page 10

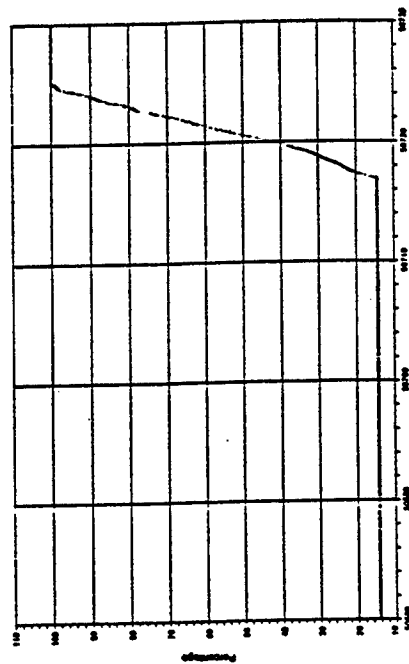
Cesium Beam Tube End Of Life
RF Amplitude #2



SLD

Page 10

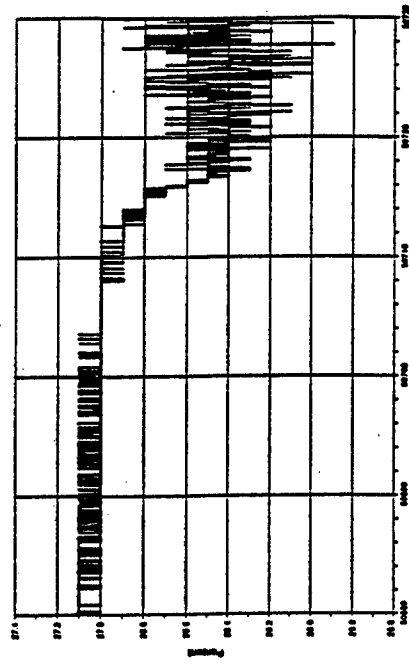
Cesium Beam Tube End Of Life
Signal Gain Percentage



SLD

Page 11

Cesium Beam Tube End Of Life
RF Amplitude #1



SLD

Page 10

THE SHM HYDROGEN ATOMIC CLOCK FOR SPACE APPLICATIONS

DEVELOPMENT AND TEST OF THE PEM PHYSICS PACKAGE

L.G. Bernier, A. Jornod, H. Schweda, R. Gentsch, G. Busca

Observatoire Cantonal de Neuchâtel, Observatoire 58, Neuchâtel, 2000 Switzerland

tel (+41) (32) 889 68 70, fax (+41) (32) 889 62 81

e-mail : Laurent-Guy.Bernier@on.unine.ch

Abstract

A compact Space-borne active Hydrogen Maser (SHM) frequency standard is being developed by the Observatory of Neuchâtel under the Swiss PRODEX program of ESA. The SHM instrument will be flown on the Radioastron (RA) mission in 2000 to be used as the reference clock for orbital Very Long Baseline Interferometry (VLBI) and for the red-shift experiment CRONOS.

The SHM design is based on a miniature sapphire loaded microwave cavity which makes possible an active hydrogen maser with a 1.7 liter storage volume for atomic hydrogen within a 50 kg space qualified instrument.

A preliminary measurement of the SHM instrument frequency stability using breadboard electronics has yielded an Allan deviation of $\sigma_y(1000s) = 3 \times 10^{-15}$ which is already close to the $\sigma_y(1000s) < 1.5 \times 10^{-15}$ instrument specification. An extensive program for the design verification by test & analysis of the PEM-PP was performed in 1997 and is now near completion.

Potential space applications of a compact active hydrogen maser instrument include scientific experiments related to relativity, precise ranging and navigation, time dissemination and synchronization. Present plans are to push miniaturization even further with the development of a 35 kg active hydrogen MASer for Navigation (MAN) for GNSS applications.

THE SHM INSTRUMENT

INTRODUCTION

The Observatory of Neuchâtel (ON) is developing a compact hydrogen maser for space applications, based on a miniature sapphire loaded microwave cavity. The hydrogen maser is a high performance frequency standard capable of a frequency stability of about 1×10^{-15} over averaging intervals from 1,000s to 10,000 s. If used as a clock, this is equivalent to a time stability of 0.7 ps over a 1,000 s time interval or 7 ps over a 10,000 s time interval. The SHM instrument was developed to fly on the international Radioastron (RA) orbital VLBI mission to be used as the alternate master clock. The SHM instrument was also designed to be used for an accurate measurement of the red-shift effect, i.e. the time dilatation due to the gravitational field. This is the purpose of the CRONOS experiment proposed by ON and sponsored by the Swiss PRODEX program of ESA. The RA mission and the CRONOS experiment were reported previously in references [1], [2], [6].

DEVELOPMENT STEPS

The SHM compact hydrogen maser frequency standard is based on a Miniature sapphire loaded Microwave Cavity (MMC) designed by ON in 1993 under a first ESTEC contract for the development of the SHM instrument [3], [5]. The development was continued up to now through several design and breadboarding steps that are reported in references [3] to [6]. The design of the SHM Physics Package (PP) makes use of several sophisticated technologies and many problems had to be overcome in the course of development. Technologies and development activities worth to be mentioned are : the optimization of the atomic storage volume in the sapphire loaded microwave cavity, the manufacturing of a very large sapphire cylinder, the diffusion bonding of sapphire to titanium, the vapor deposition plating of the internal surface of a titanium cylinder, the machining by electro-erosion of the main titanium structural part, the teflon coating of the composite titanium-sapphire atomic storage bulb, the development of a special process of the magnetic shields that optimizes the permeability in zero field, the evaluation of the pumping speed, capacity and brittleness of the hydrogen getters.

PEM-PP DESIGN VERIFICATION PROGRAM

The last major step of development was the manufacturing and the first integration of the PEM-PP. The prototype Physics Package was manufactured during the first half of 1996 and first integrated in October and November 1996. The first atomic signal from the fully integrated PEM-PP was obtained in December 1996.

A first evaluation of the PEM-PP was performed in January and February 1997. The atomic quality factor, the atomic signal power and the short-term frequency stability characteristics of the PEM-PP were verified experimentally. The PEM-PP was then disassembled and several design modifications were implemented during the first half of 1997. These modifications were known to be necessary but had been postponed in order to allow for a quick first integration and evaluation.

A detailed structural analysis of the PEM design was performed in 1997 by CSEM, a Swiss engineering company. For the purpose of analysis CSEM has developed a finite elements structural model of the SHM

instrument with more than 7,000 nodes. The detailed structural analysis included : static loading, random vibration analysis, shock analysis, load safety margins, buckling analysis, thermal stress analysis and fracture control analysis. The main conclusion of CSEM's engineering analysis is that the PEM design is compliant with the Radioastron requirements without modifications. Several design improvements to the mechanical design were also suggested by CSEM.

The Reduced Microwave Cavity & magnetic Shields Assembly (RMCSA), the heart of the Physics Package which contains the atomic hydrogen storage bulb, is also the most complex part of the Physics Package from the structural point of view. A spare RMCSA unit, identical to the one used in the PEM-PP, was tested successfully for shocks (40 g shock response spectrum) and for random vibration (7 g rms) to the Radioastron qualification levels on May 14-15 1997. The same unit was also tested for random vibration to the GPS clocks qualification levels (14 g rms) on September 25 1997 in preparation to future applications of the SHM design for GNSS.

The Preliminary Design Review (PDR) of the PEM SHM instrument was opened on October 29 1997 under the technical supervision of ESA. The reviewed material include the design definition documents, the design verification by inspection and analysis, and the design verification by test on the PEM-PP. The PEM-PP PDR is scheduled to be closed at the end of 1997.

PERSPECTIVES FOR FUTURE DEVELOPMENT

After the closure of the PEM-PP PDR, the next step will be to kick-off a contract for the development of a PEM SHM space compatible Electronics Package (EP).

On the basis of the existing breadboard electronics, the development of the space compatible PEM-EP is expected to take one year. The fully integrated and tested PEM SHM instrument will then be delivered to Astro Space Center in Moscow for the purpose of ground testing the Radioastron payload. In particular it is planned to perform a VLBI session on the ground using the actual Radioastron payload.

Another flight opportunity for the SHM instrument is the ACES atomic clocks experiment proposed by a team of French scientists for the early utilization of the International Space Station. The ACES experiment is yet to be officially endorsed by ESA and involves the demonstration in space of a cold atom cesium fountain and other atomic clocks [7], [8]. The ACES SHM design would be very close to the Radioastron design. The extra effort of development would concern mainly the adaptation of the instrument interfaces. A system study of the ACES Concept has already been performed by CNES for the Space Station Applications and Promotion Office of ESA [9], [10]. The study considers the SHM instrument as one of the necessary components of the ACES experiment.

Besides, a collaboration of ON with the Naval Research Laboratory (NRL) is in preparation for the joint development of a 35 kg active hydrogen Maser for Navigation (MAN). This new development will take advantage of the technologies already developed for the SHM instrument in the course of the Radioastron & CRONOS project. It is foreseen to test the MAN maser for navigation on an experimental basis as a Reserve Auxiliary Payload (RAP) on a Block IIF GPS satellite.

SHM-RA INSTRUMENT DESIGN

CONDENSED SPECIFICATION

- long-term drift: $< 3 \times 10^{-12}$ year⁻¹
- output levels: 0.4 V_{rms} in 50 Ω
- operating temp. range: 10°C to 35°C
- thermal sensitivity: $\leq 3 \times 10^{-15}$ °C⁻¹
- magnetic field range: ± 1 gauss
- magnetic sensitivity: $\leq 2 \times 10^{-14}$ G⁻¹
- DC input voltage: 22 to 50 V
- power consumption: < 70W
- largest diameter (horizontal) 460 mm
- full height (vertical) 600 mm
- mass 50 kg
- mission lifetime > 3 years

τ [s]	Allan deviation
1	$< 1.5 \times 10^{-13}$
10	$< 2.1 \times 10^{-14}$
100	$< 5.1 \times 10^{-15}$
1'000	$< 2.1 \times 10^{-15}$
10'000	$< 1.5 \times 10^{-15}$

Table 1
Frequency Stability

	14.71 MHz output	5 MHz output
f [Hz]	L (f) [dBc]	L (f) [dBc]
1	< -100	< -110
10	< -122	< -132
100	< -132	< -143
1'000	< -141	< -151
10'000	< -145	< -155

Table 2
Phase Noise

MASER PHYSICS DESIGN

The heart of the PP design concept is the sapphire loaded MMC. The internal volume of the MMC is 4.4 liters. This is to be compared with the 20 liters of a conventional circular microwave cavity tuned to the hydrogen hyperfine frequency. The storage volume for hydrogen is 1.7 liter which is comparable to a conventional design based on a full size cavity. It is basically the size reduction of the microwave cavity that has made possible the realization of a 50 kg SHM instrument. The sapphire cylinder of the MMC has both a microwave function, the dielectric loading of the cavity, and a maser physics function since, together with the bonded titanium covers, it also constitutes the hydrogen storage bulb.

State selection is performed by a conventional quadrupole magnetic state selector. The dissociator is a small fused quartz bulb. The solid-state hydrogen supply is stored in a container filled with 90 g of hydride material Hydralloy C20. Magnetic shielding is performed by a set of four 0.5 mm magnetic shields around the MMC and by a fifth 0.5 mm magnetic shield that surrounds the whole instrument.

There are two vacuum systems : the hydrogen vacuum enclosure and the thermal vacuum enclosure. Each enclosure is pumped by a set of getters and by a set of two 2 l/s ion pumps. For each enclosure, one ion pumps would be sufficient. The second pump is there for redundancy. The sealed part of the PP is closed by an aluminum bell jar that closes the thermal vacuum enclosure.

MECHANICAL DESIGN

The SHM instrument is designed to pass the Radioastron qualification requirements for shocks (40g) and random vibration (7 g rms).

THERMAL DESIGN

In orbit the instrument is covered by a MLI thermal insulation blanket. All thermal exchanges are performed by conduction to a dedicated thermally controlled base plate which is part of the spacecraft.

The temperature of the MMC is stabilized by three concentric pairs of electronic thermal control loops. The first layer of thermal control is the MMC itself, the second layer is the c-field thermal shield and the third layer is the intermediate thermal shield. All these elements are inside the thermal vacuum system. The vacuum bell jar is not thermally controlled and follows passively the base plate temperature.

ELECTRONICS DESIGN

The ACT (Automatic Cavity Tuning) system is the most important performance critical element of the electronics package. Because of the cavity pulling effect, and given the $-65 \text{ kHz}/^\circ\text{C}$ thermal sensitivity of the MMC, it is not possible to achieve the frequency stability and the thermal coefficient specified at the instrument level with only a thermal frequency control of the MMC. The function of the ACT system is to complement the thermal frequency control of the MMC by a varactor electronics frequency control.

EVALUATION OF THE PEM PHYSICS PACKAGE

MICROWAVE CAVITY

The measured loaded quality factor of the MMC is 34,000. The thermal coefficient of the TE_{011} mode is minus $65 \text{ kHz}/^\circ\text{C}$.

ATOMIC QUALITY FACTOR

The operating atomic quality factor at -105 dBm of atomic signal output is 1.7×10^9 .

THERMAL CONTROL

The thermal stability of the MMC is such that an Allan deviation of $\sigma_y(1,000s) = 2.2 \times 10^{-14}$ is achieved without ACT, i.e. with only a thermal frequency control of the MMC. This is equivalent to a thermal stability of $\sigma_T(1,000s) = 26 \mu^\circ\text{C}$ at the MMC level. Only 7.5 W of electrical power is necessary for the thermal control of the physics package in air with the MMC at 47°C , an ambient temperature of 20°C ,

and with no thermal insulation of the thermal vacuum bell jar. In vacuum, with the physics package protected by its MLI blanket, the power consumption will be even smaller.

BREADBOARD ACT

The breadboard ACT is still in development and does not reach yet the specified thermal sensitivity. Without ACT, i.e. with only a thermal frequency control of the MMC, the measured thermal coefficient is $5 \times 10^{-12} \text{ }^{\circ}\text{C}^{-1}$. The thermal coefficient improves to $3 \times 10^{-14} \text{ }^{\circ}\text{C}^{-1}$ when the breadboard ACT is put into operation. Note that, in this experiment, the breadboard electronics were maintained at a constant room temperature while the temperature of the PP was varied. Therefore long cables linking the PP to the EP were involved. A new iteration of the ACT breadboard electronics, better integrated and more compact, is in preparation and is expected to improve the thermal sensitivity up to the specified level.

Regarding the frequency stability specification, on the other hand, the Allan deviation measured with the breadboard ACT is $\sigma_y(1'000s) = 3 \times 10^{-15}$. This is already quite close to the specification.

MAGNETIC SHIELDING

The shielding factor measured with only the four cavity shields is 20,000. A global shielding factor of 200,000 is expected with 5 shields.

GETTERS & ION PUMPS

It was verified that the vacuum system has an autonomy of at least 10 days without electrical power to the ion pumps (getters only). This requirement is specific to the Radioastron mission and is motivated by the fact that during several critical phases of the payload integration, connection of the instruments to a power supply is not allowed. Regarding the operational lifetime of the vacuum system, on the other hand, it is worth mentioning that the vacuum getters are known to become brittle after absorbing a large quantity of hydrogen. In order to avoid this drawback, the supply of hydrogen getters was designed in such a way that only 10% of their nominal capacity for hydrogen is used during the operational lifetime.

CONCLUSION

The evaluation of the PEM SHM-PP reported in this paper is still in progress but most of the important conclusions have been drawn already. Most of the design parameters have been measured and analyzed and have been shown to be compliant with the specifications. In particular the maser physics parameters, i.e. atomic quality factor and short-term stability, have been verified and the detailed structural analysis performed by CSEM has shown that the design is compliant with the random vibration and shock requirements of Radioastron. The shock and random vibration tests of the spare RMCSA assembly have validated the finite elements model of CSEM and confirmed the conclusions of the structural analysis.

On the other hand, the breadboard electronics package is still in development and does not reach yet all the performance goals set by the instrument specifications. A new iteration of the breadboard ACT is in preparation and is expected to comply with the thermal sensitivity and frequency stability requirements.

REFERENCES

- [1] Valtaoja E., « *The Radioastron Space VLBI Project* », Proc. 4th European Frequency & Time Forum, Neuchâtel, March 13-15, 1990, pp. 707-710.
- [2] Andreyanov V.V., « *Time-Frequency Synchronization in Radioastron OVLBI Project* », Proc. 7th European Frequency and Time Forum, Neuchâtel, March 16-18, 1993, pp. 33-38.
- [3] Bernier L.G., « *Preliminary Design and Bread-Boarding of a Compact Space Qualified Hydrogen Maser Based on a Sapphire Loaded Microwave Cavity* », Proc. 8th European Frequency & Time Forum, Munich, March 9-11, 1994, pp. 965-980.
- [4] Couplet C., Bernier L.G., « *Proton Irradiation Test of the Teflon Wall Coating in the Atomic Hydrogen Maser in Preparation to Space Applications* », Proc. 8th European Frequency and Time Forum, Munich, March 9-11, 1994, pp. 952-958.
- [5] Bernier L.G., « *Preliminary Design and Bread-Boarding of a Compact Space Qualified Hydrogen Maser Based on a Sapphire Loaded Microwave Cavity* », Proc. 5th Time & Space Metrology Symposium, Mendeleevo, Russia, October 11-13, 1994, pp. 412-417.
- [6] Bernier L.G., Busca G., Jornod A., Schweda H., « *The SHM Space Borne Hydrogen Maser : First Evaluation of the PEM Physics Package* », Proc. 11th European Time & Frequency Forum, Neuchâtel, March 4-7, 1997, pp. 664-667.
- [7] Lemonde P., Salomon C., Laurent P., Simon E., Santarelli G., Clairon A., Dimarcq N., Petit P., Audoin C., Jamin-Changeart F., Gonzales F., « *PHARAO : A compact Clock Using Laser Cooled Cesium Atoms* », Proc. 11th European Time & Frequency Forum, Neuchâtel, March 4-7, 1997, pp. 646-650.
- [8] Feustel-Büechl J., Isakeit D., « *The International Space Station - A Challenge for Global Cooperation* », Proc. 11th European Time & Frequency Forum, Neuchâtel, March 4-7, 1997, pp. 3-11.
- [9] « *ACES Concept - Programme, Organisation and Development Plan* », CNES report ACES-MS-0-1-CNS, issue 1, revision 0 of 10.06.1997.
- [10] « *ACES Concept - Accommodation on the Express Pallet Adapter & Related Interface Constraints* », MATRA MARCONI SPACE report, EXT/PP/NT/062.97 issue 1, revision 0 of 29.05.1997.

GPS RECEIVERS AND RELATIVITY*

Marc Weiss
National Institute of Standards and Technology
Time and Frequency Division
325 Broadway, Boulder, CO 80303

Neil Ashby
Department of Physics, Campus Box 390
University of Colorado
Boulder, CO 80309-0390

Abstract

We illustrate the general methods for applying relativistic corrections needed by a GPS receiver in providing time or position to a user. We focus on estimating the time interval it takes for GPS signals to propagate from the transmitter to the receiver, the geometric range delay. We present a few cases which apply to many common uses of GPS. The most common case for positioning is illustrated numerically.

INTRODUCTION

A GPS receiver needs to make two corrections that are related to relativity in order to provide time or position to a user. We discuss these corrections and focus mostly on estimating the geometric range delay, Δt_D , the time for GPS signals to propagate from the transmitter to the receiver. Proper estimation of Δt_D is essential for solving for position or time. This is an application of the relativistic principle of the constancy of the velocity of light which states that electromagnetic signals travel in Euclidean straight lines with velocity c relative to an inertial reference frame. We present a few cases which apply to many common uses of GPS. The case where measurements of satellite signals are time-tagged at the receiver for positioning, probably the most common GPS application, is illustrated numerically.

The theory behind corrections is presented with references given for any derivations not done here. Through our theoretical discussion we show that the Interface Control Document (ICD-GPS-200) specifications, as issued by the Joint Program Office of the Global Positioning System [1], consistently cover the requirements of relativity down to the sub-nanosecond level for time. We respond to questions in the literature [2,3] as to whether the ICD specifications include relativity corrections with enough accuracy for certain applications. In particular we discuss the relativistic Doppler effect, the formula for its instantaneous magnitude, and its relationship with typical GPS receiver operation. We also address the use of carrier-phase measurements, which is not discussed in the ICD.

THEORY

Generally, a GPS navigation user measures the arrival times, on a local clock, of timing signals from at least

* Contribution of U.S. Government, not subject to copyright.

four different satellites, then solves for four unknowns: user position x, y, z and the receiver clock offset from GPS time t . The signals from the satellites can be thought of effectively as continuous timing signals from the satellite clocks arriving at the receiver. The receiver has its own local clock for comparison. The user measures either 1) the times in the received timing signals at a specific local clock time, or 2) the arrival times on the local clock of a specific time-tag in the received timing signals. The reception time (according to the local clock) minus the transmission time at one satellite (according to GPS time) is called the *pseudorange*. These pseudoranges are used to solve for user position and time.

For the ordinary user of broadcast ephemerides, there are two and only two relativistic effects that must be considered. First, the receiver must apply a correction to the transmitted time to account for relativistic effects arising from orbit eccentricity of the transmitting satellite. This is the Δt_r term defined in the ICD. Second, the finite and universally constant speed c of signals propagating from transmitter to receiver, relative to an inertial frame (the geometric path delay), must be accounted for.

RELEVANT RELATIVITY

Three effects in relativity are germane to GPS. Rates of clocks in GPS are adjusted (as for International Atomic Time) to match the rate that clocks would run on the geoid of the earth. This is a surface of gravitational equipotential in the rotating frame in which the effects 2) and 3) below add to a constant value. The relativity effects are as follows.

1) GPS time is defined using the principle of the constancy of c to synchronize an imagined system of clocks everywhere in space in the neighborhood of the earth (Einstein synchronization). GPS satellite clocks are in principle adjusted to agree with this imagined system of clocks. This network of synchronized GPS clocks realize a coordinate time. This definition of GPS time requires a locally inertial coordinate system. GPS time is thus defined relative to an earth-centered inertial coordinate system (an ECI), but the rate is set to match the rate at which clocks would run on the geoid. An ECI is also used to simplify the paths of signals propagating from satellites, since they move in Euclidean straight lines at the velocity c in vacuum relative to such inertial frames.

2) A clock moving with respect to an ECI runs slower relative to coordinate time than if it were at rest in the ECI. This is the time dilation effect due to the magnitude of the relative velocity, sometimes called the second-order Doppler effect. For satellites in GPS orbits, the fractional frequency offset needed to compensate for this is approximately $+8.3 \cdot 10^{-11}$ relative to the rate of clocks on the earth's geoid.

3) A clock in a lower gravitational potential runs slower relative to coordinate time than if it were at rest in a higher potential. This is called the gravitational red shift. Thus, standard clocks closer to the earth run slower than standard clocks farther away, since the potential becomes more negative closer to the earth. Clocks on GPS satellites need to be adjusted by about $-5.3 \cdot 10^{-10}$ relative to the earth's geoid, to compensate for this effect.

Atomic clocks in GPS satellites are given a fixed rate offset of $-4.4645 \cdot 10^{-10}$ as a consequence of the requirement that GPS satellite clocks run at the rate that a standard clock on the geoid would run, and of the relativistic effects in 2) and 3) for circular orbits. These three relativistic effects explain the reasons for the

two corrections the user must apply. The first relativity correction is the Δt_r term defined in the ICD. This term corrects the satellite vehicle (SV) clock offset due to any eccentricity in GPS orbits. Eccentricity produces frequency offsets from the nominal fixed rate offset of $-4.4645 \cdot 10^{-10}$ due to the combined effects of 2) and 3) on the SV clock rate. The second correction applies to users' estimates of the geometric range delay, the time delay from the transmitter to the receiver if the signal traveled in vacuum. This is most easily calculated in an ECI where signals travel in Euclidean straight lines at the speed of light, the constant c .

There can be many ECI coordinate systems, differing by constant spatial rotations from each other, which serve these purposes. All frames with the same origin at the earth's center, and non-rotating with respect to the "fixed" stars, will define simultaneity in the same way. All such frames are equivalent for determining the propagation delay. Yet users need to reference their positions to the earth. Satellites broadcast their positions relative to an earth-centered, earth-fixed coordinate system (an ECEF), the WGS-84 coordinate system. Users fixed on the earth often know their coordinates as constants in the ECEF frame.

USER CORRECTIONS

At any arbitrarily chosen instant the ECEF frame coincides with an ECI frame having identical x -, y -, and z -axes, but not rotating. Removing the rotation of the earth from the ECEF defines a coordinate system that is close enough to an inertial frame to serve for estimating the path delay. As time passes the ECEF system rotates, while this ECI system remains behind, so to speak. Any such coordinate system may serve as an ECI for estimating geometric range by using the Euclidean distance between the coordinates in the ECI of the satellite at transmission and the coordinates of reception. The time for the signal to travel this path, the geometric path delay, may be estimated as the geometric range divided by the defined velocity of light, c , to better than 200 ps [4].

The principle of the constancy of the speed of light in an inertial frame requires that an ECI be used for geometric path delay if it is calculated by dividing the Euclidean distance by c . Using such an ECI greatly simplifies the problem of solving for a GPS user's position or time. Whereas GPS is intended to provide users with their position or time in the ECEF system, if we use those coordinates for geometric range with the simple Euclidean distance metric and divide by c to obtain geometric path delay, we will make significant errors.

In general, a navigation solution requires pseudo-range measurements to at least four satellites. These are used to obtain geometric range delay estimates, which in turn are used to solve for position. To use the simplicity of the Euclidean distance metric that comes with an ECI, all satellite positions at the transmission epochs must be transformed into the common ECI frame. The user may then solve for the receiver position in this coordinate frame, and for the GPS time, t , corresponding to this solution. Finally, the user must find the receiver coordinates in the ECEF at the GPS time t by accounting for the rotation of the ECEF between the chosen moment t_c at which the ECI frame is defined, and the GPS time t .

With a receiver using four satellites we generally have five different times of interest as candidates for t_c : either a single GPS transmission time and four different reception times (time tagging at transmission time), or a single reception time and four different transmission times (time tagging at reception time). In any case an ECI frame can always be found which coincides with the ECEF frame at a chosen instant of time, and in this sense the ECEF can determine an inertial coordinate system. This answers the need for a coordinate system in which

the speed of light is c in vacuum during the transmission of the signals, and in which all the GPS satellite clocks can in principle be synchronized. We will give a number of examples below for using this general prescription.

Our focus here will remain on relativistic corrections for GPS users. We do not consider corrections for non-relativistic delays: ionospheric plasma delays, tropospheric delays due to water vapor, multipath interference, or receiver system delays. Non-relativistic delays must certainly be accounted for; however here our topic is relativity.

DOPPLER EFFECT

A receiver system that uses the instantaneous Doppler shift of the received carrier signal must also correct for the frequency shift of the received signal within the framework of relativity. As the true range between the satellite and receiver changes due to relative motion, the carrier frequency changes due to the Doppler effect. The relationship between the received frequency F , and the transmitted frequency, the proper frequency f , is [4,5,6,7]:

$$f = F \frac{\gamma(v) \left(1 - \frac{N \cdot v}{c} \right)}{\gamma(V) \left(1 - \frac{N \cdot V}{c} \right)}, \quad (1)$$

where

v = transmitter velocity in ECI coordinates,

V = receiver velocity in ECI coordinates,

N = ECI unit vector in the direction of propagation of the signal, and

$$\gamma(v) = \frac{1}{\sqrt{1 - \frac{v^2}{c^2}}}. \quad (2)$$

The change in frequency is closely related to the rate of change of range. In fact the relativistic Doppler frequency shift equation can be derived by differentiating the geometric path delay [4,6]. This proves the conceptual equivalence, within the framework of Special and General Relativity, of the methods of pseudorange (to obtain an instantaneous position solution) and integrated Doppler frequency (to obtain changes in position). A user of integrated Doppler frequency can account for the relativistic Doppler shift by accounting for the geometric path delay.

THE ROTATION MATRIX

Almost always the user of the broadcast ephemerides will want to use coordinate transformations which correspond to rotations of the coordinate system about the z -axis. For convenience we write out here an example of such a rotation matrix. Consider an ECI frame with z -axis which coincides with the WGS-84 axis. Let the position coordinates of some point of interest in these ECI coordinates be denoted by

$$X_{ECI} = \begin{bmatrix} x_{ECI} \\ y_{ECI} \\ z_{ECI} \end{bmatrix}. \quad (3)$$

Suppose that the ECI axes coincide with the ECEF axes at the time t_C . The angle through which the ECEF coordinates rotate relative to the ECI during the time interval $t-t_C$ is

$$\begin{aligned} \theta &= \dot{\Omega}_e (t-t_C), \\ \text{where:} \\ \dot{\Omega}_e &= 7.292115 \cdot 10^{-5} \text{ rad/s,} \\ &\text{the WGS84 earth rotation rate.} \end{aligned} \quad (4)$$

The time interval $t-t_C$ must be small since the earth rotation rate varies. With $t-t_C$ as large as 3 s, errors no larger than 0.05 mm are introduced [4]. With this rotation, the point denoted X_{ECI} in ECI coordinates has coordinates in the ECEF of

$$X_{ECEF} = R^S(t-t_C) X_{ECI} = \begin{bmatrix} \cos\theta & \sin\theta & 0 \\ -\sin\theta & \cos\theta & 0 \\ 0 & 0 & 1 \end{bmatrix} \begin{bmatrix} x_{ECI} \\ y_{ECI} \\ z_{ECI} \end{bmatrix}, \quad (5)$$

where R^S is the sidereal rotation matrix. This is an example of a "passive" rotation, a rotation of the coordinate axes keeping physical position vectors unchanged.

CASES

Generally, a GPS navigation user measures the arrival times of signals from four different satellites, and uses them to solve for four unknowns: position x, y, z and time t . A common way of doing so is to make the four measurements at one instant at the receiver ("time-tagging at the receiver"). A less common method is to use signals which left the satellites at a common GPS time ("time-tagging at the transmitters"). The latter method is more complex both because the signals are not received simultaneously, and because the clocks on the satellites are synchronized for the user by adding a transmitted clock correction. The clocks themselves may differ by no more than 1 ms [1]. Thus we must account both for the motion of the user during the intervals between transmission and reception, and the differences in transmission time of a common GPS time due to clock offsets from system time.

TIME-TAGGING AT THE RECEIVER: GENERAL PRESCRIPTION

1. At a chosen reception time, measure the transmission times using the received pseudo-random noise (PRN) codes from four satellites. This gives us the time t_{SV} according to the SV clock at transmission for the signals received at the chosen reception time.

We need the GPS time of transmission for each satellite and the common reception time according to

the (possibly biased) local clock. We obtain the time of reception from our local clock. The transmission time is encoded in the received signal. Since we are locked to the code, we can determine the offset of the locally generated PRN sequence required to maintain lock.

2. Apply the prescription for corrections to obtain GPS system time t of Table 20-IV, at transmission.

This includes the eccentricity correction, Δt_e , from section 20.3.3.3.1, an effect due to relativity. Δt_r is a correction which applies to the SV clock; it is the same correction no matter where the receiver is or how the receiver is moving. The value of Δt_r will generally be different for the clocks in different satellites.

3. Compute each satellite's position in the ECEF at its transmission time.

This is a straightforward application of the equations of Table 20-IV for determining the x -, y -, z -coordinates of the satellite at the instant of transmission. Note that the broadcast message gives the satellite positions in ECEF coordinates--specifically in the WGS84 reference frame.

4. Choose an ECI frame for computation of the path delays.

This choice is arbitrary, but some choices are more convenient than others. Simplification may sometimes occur if the choice is appropriately made. A natural choice for the case of time-tagging at the receiver is the GPS time equal to the local clock time of reception.

5. Transform the ECEF coordinates of each SV obtained in step 3 into the chosen ECI.

This will normally require at least three, and perhaps four, of such ECEF position vectors to be rotated. We may freeze the ECEF at any instant to define an earth-centered inertial system. If we choose the GPS time equal to the local clock's reception time, the later corrections may be small. If the local clock is sufficiently close to GPS time at the instant of reception, then the last step below, 7, would not need to be done. Alternatively we might choose an ECI frame which matches the ECEF frame at the instant of transmission from one of the satellites.

6. Solve the path delay equations for the receiver's position and time.

This can be done by linearizing the propagation delay equations and solving them iteratively. Note that other contributions to path delay, ionospheric and tropospheric delays, should be incorporated in this process. We use an initial estimate of position to solve for the linearized corrections to receiver position and the time offset. If these corrections are not small enough for the user, they may be used to obtain a next estimate of position and time. This, in turn, may be used to obtain the next linearized correction for position and time offset.

7. Rotate the user's position coordinates into the ECEF reference frame.

After finding the user's position in the chosen ECI coordinate system and the correct GPS system time, the receiver's ECI position coordinates are rotated into the ECEF reference frame at the instant corresponding to the measured reception time.

TIME-TAGGING AT THE TRANSMITTER: GENERAL PRESCRIPTION

Let us now consider time-tagging at the transmitter with four satellites. This approach requires an estimate

of velocity and perhaps acceleration over the interval of signal reception. If all signals leave satellites simultaneously with respect to the ECEF, most users will receive these signals within a 100 ms interval. For most users acceleration will contribute negligibly. We parallel the seven steps above.

1. Measure the time on the local clock at the reception of a given GPS time from each of four satellites.

Each SV clock is generally offset from each other and from GPS time. We measure the time of reception of a given epoch in the code from each satellite. This, then, needs to be corrected according to the ICD by the relativistic correction Δt_r and the broadcast second-order polynomial correction for the SV clock offset from GPS time.

2. Apply the prescription for corrections to obtain GPS system time t of Table 20-IV at transmission.

The difference here from example A is that the GPS system time t will be the same for the clocks in all satellites.

3. Compute each satellite's position in the ECEF at its transmission time.

This is a straightforward application of the equations of Table 20-IV, for determining the x -, y -, z -coordinates of the satellite at the instant of transmission.

4. Choose an ECI frame for computation of the one-way light times.

In this case the natural choice is to freeze the ECEF at the GPS transmission time, t . Note that the actual time of transmission will differ for each satellite, since it is determined by the SV clocks. The difference will be less than 1 ms.

5. If the ECI is defined by freezing the ECEF at GPS transmission time, the coordinates of each satellite will need to be rotated due to the time offset, Δt_{sv} , of the SV clock from GPS time. We also need to transform the estimated receiver positions at the arrival times into the ECI.

We may use a deterministic estimate of the change in receiver position over the reception interval. Since this model is usually a velocity, we will refer to it that way here for simplicity. This velocity estimate does not change during the solution of user position and time. It is necessary to obtain the velocity estimate in the coordinates of the chosen ECI. Now we may rotate the estimated user coordinates into the chosen ECI at the first instant of reception, and use the velocity to extend to the other reception times. We assume the user clock offset from GPS time is constant over the interval of reception.

6. Solve the equations for the geometric path delays to find the receiver's position and time offset at a specific time.

Again we linearize the propagation delay equations and solve them iteratively. We may iterate to find the position at the first reception time, using the velocity estimate to extend to the other reception times. This iteration is similar to step 6 in the of time-tagging at the receiver example.

7. Rotate the user's position coordinates into the ECEF reference frame for each of the reception times.

If we have chosen the ECI coordinate system coinciding with the ECEF at the transmission time, we will most certainly have to perform these final rotations. For, the reception times will be at least of

order 100 ms from the transmission time, and the ECEF will have changed significantly. We could perform only one rotation for the user position at the first reception time if we have the velocity vector in the ECEF as well as in the ECI. We could then use the ECEF velocity to obtain the coordinates for the other positions.

It would be possible to update the velocity estimate using positions obtained from two transmission time tags. This leads into other concerns and options associated with using GPS: filtering estimates over time. Techniques for estimating position, velocity, and acceleration could be coupled with strategies for filtering these estimates over time. We will not discuss these options here. We will mention, however, that if there are infrequent measurements of GPS signals from individual satellites, the local clock may be used to flywheel between them and find a solution. This may require careful filtering algorithms for estimation of the local clock frequency. In particular, relativistic effects on the local clock frequency due to velocity or gravitational potential may have to be considered.

GPS TIME TRANSFER WITH POSITION KNOWN

In this case we may use each pseudo-range measurement from each satellite separately to estimate our clock offset from GPS time. We either time-tag measurements at a transmission time and measure time of reception, or time-tag measurements at a reception time and determine time of transmission from the code lock of the receiver. We then use the prescriptions from Table 20-IV to obtain the satellite position in the ECEF. We must estimate the geometric path delay Δt_D in addition to the ionospheric and tropospheric corrections. Since we know the receiver position we may compute Δt_D as follows.

If ECI position vectors are referenced to the time of signal transmission, then

$$\Delta t_{GPD} = \frac{|r(t_T) - R(t_R)|}{c} \sim \frac{|r(t_T) - R(t_T)|}{c} + [R(t_T) - r(t_T)] \cdot \frac{V}{c^2}, \quad (6)$$

where:

r is the SV position vector,

R is the receiver position vector,

t_T and t_R are GPS time at respectively transmit and receive times, and

V is the receiver velocity vector in the ECI.

In the case of an earth-fixed user,

$$V = \dot{\Omega} \times R. \quad (7)$$

If ECI position vectors are referenced to the time of signal reception (instead of satellite transmission time), then

$$\Delta t_D = \frac{|r(t_T) - R(t_R)|}{c} \sim \frac{|r(t_R) - R(t_R)|}{c} + [R(t_R) - r(t_R)] \cdot \frac{v}{c^2}, \quad (8)$$

where v is the satellite velocity vector in the ECI.

EXAMPLE: MULTI-CHANNEL RECEIVER, TIME-TAGGING AT THE RECEIVER

In this example we simulate a navigation solution using an example receiver position and data from the GPS constellation as it was late 1995. We choose four satellites from this constellation in view from our receiver location with elevations above 20° . Suppose the receiver is truly at ECEF latitude and longitude 35°N , 0°E , with elevation on the reference ellipsoid, and the operator desires to make a measurement of position and GPS time at $t=37\,240.000\,000\,000\,0$ s of the week.

The receiver ECEF coordinates at this instant will be

$$X_{WGS84} = \begin{bmatrix} R \cos 35^\circ \\ 0 \\ R \sin 35^\circ \end{bmatrix} = \begin{bmatrix} 5\,224\,663.389 \text{ m} \\ 0 \\ 3\,658\,348.690 \text{ m} \end{bmatrix}, \quad (9)$$

where $R=6378136.300$ m. Such accuracy is not justified, but we are giving positions to a millimeter so that the convergence of the algorithms can be checked. The actual position is given here for comparison with the navigation solution.

We follow the step numbering from the cases section above, for this case.

1. Suppose we already have the SV clock time t_{sv} for the signals received at the chosen reception time.
2. We apply the prescription from ICD-GPS-200 according to Section 20.3.3.3.1 describing the user algorithm, to obtain the system time t_i for each satellite i , the GPS time of transmission. The relativistic eccentricity correction is part of this calculation. The subscript i is not used in the ICD, but is added here for clarity.
3. We obtain the ECEF coordinates of the satellites from the prescriptions given in Table 20-IV of the ICD-GPS-200. From the GPS time t_i , the time interval $t_k = t_i - t_{oe}$ from ephemeris reference epoch is calculated. Then t_k may then be used in the algorithm for computation of ephemerides. This gives the x -, y -, z -coordinates of the satellite, in the ECEF frame, at its transmission epoch.

Table I gives the results after these steps. Note that in Table I, GPS system times t_i rather than the time intervals $t_k = t_i - t_{oe}$ from ephemeris reference epoch, are used to label the events. The subscript i varying from 1 to 4 labels data from the different satellites.

Table I. GPS satellite positions in ECEF coordinates

SV#	Transmission Epoch t_i	x_i	y_i	z_i
1	37 239.924 422 365 6 s	13 005 878.255 m	18 996 947.213 m	13 246 718.721 m
2	37 239.920 713 391 8 s	20 451 225.952 m	16 359 086.310 m	-4 436 309.875 m
3	37 239.925 307 870 0 s	20 983 704.633 m	15 906 974.416 m	3 486 595.546 m
4	37 239.929 346 353 9 s	13 798 849.321 m	-8 706 113.822 m	20 959 777.407 m

4. We choose an ECI by fixing the rotation of the ECEF at $t_C = 37\,239.000\,000\,000\,0$ s for purposes of this example. We stress that this choice is arbitrary--much better choices are usually available. The purpose of the present choice is to illustrate its arbitrariness, and also to illustrate how rapidly the iteration algorithm converges.

5. We transform the coordinates in Table I into this ECI. The rotation matrix is different for each transmission epoch. To rotate from ECEF to ECI coordinates, the inverse of the rotation matrix of equation 5 is required. Thus we need $(R^S(t_i - t_C))^{-1}$, which must be calculated and applied to the coordinates of each satellite individually. The subscript j labels data from the different satellites after transforming to the chosen ECI. t_j will be different for each satellite, but t_C is the same for all satellites. We use a subscript C to indicate that the inertial system has been arbitrarily chosen. The results from transforming to the ECI frame are given in Table II.

Table II. Transmitted Data Transformed to the Chosen ECI System

SV #	Transmission Epoch t_i	x_j	y_j	z_j
1	37 239.924 422 365 6 s	13 004 597.642 m	18 997 823.895 m	13 246 718.721 m
2	37 239.920 713 391 8 s	20 450 127.566 m	16 360 459.358 m	-4 436 309.875 m
3	37 239.925 307 870 0 s	20 982 631.270 m	15 908 390.245 m	3 486 595.546 m
4	37 239.929 346 353 9 s	13 799 439.294 m	-8 705 178.668 m	20 959 777.407 m

6. We now solve the equations for the geometric path delays simultaneously to solving for the receiver's position and time. The notation is as follows. The four GPS satellites, at GPS times t_j , send out signals from the ECI locations r_j . These four signals are received simultaneously at GPS time t by a receiver at position R . The problem is to determine t and R at the receiver. The velocity of the receiver does not enter in the problem. The receiver's position R at the time of reception t will be determined by the solution of four equations which express the condition that the speed of propagation is c . The four equations to be solved are

$$(R - r_j)^2 - c^2(t - t_j)^2 = 0; \quad j = 1, 2, 3, 4. \quad (10)$$

However, if the position R and time t are known approximately, the equations can be reduced to a system of four linear equations which can be solved by standard matrix inversion techniques. These equations are derived in [4], and are

$$(R^{(i)} - r_j) \cdot \Delta R - c^2(t^{(i)} - t_j)\Delta t = \frac{1}{2}(c^2(t^{(i)} - t_j)^2 - (R^{(i)} - r_j)^2). \quad (11)$$

In equation 11, the quantity $c(t^{(i)} - t_j)$ is the i^{th} estimate of the pseudorange from the receiver to the j^{th} satellite, and $R^{(i)}$ is the i^{th} estimate of the receiver position in ECI coordinates. The equations (11) form a system of linear inhomogeneous equations in the corrections ΔR , Δt , which can be solved by matrix inversion. The matrix of coefficients of the unknowns ΔR , Δt will usually be nonsingular, unless the configuration of satellites is so unfavorable that the equations do not have a solution (it is possible for this to occur). The solutions obtained will be approximate, but can be used to obtain new trial values; the process of iteration can be repeated as many times as necessary to obtain the accuracy required.

To illustrate this process in the present case, as our initial guess at receiver position we take a worst case and assume the receiver is at the center of the earth. Also, we do not know the receiver clock bias so we guess that the time at the reception event is the time of the first transmission event plus some reasonable estimate of the propagation delay. In this case we set $t = t_1 + 0.07500$ s. Table III gives the results at each stage of the iteration.

Table III. Results of Iterative Solution of Propagation Delay Equations

Trial #	user x-position	user y-position	user z-position	user clock time
0 (start)	0 m	0 m	0 m	37 239.999 421 454 1 s
1	5 057 363.392 m	2 355.126 m	3 541 092.792 m	37 239.997 532 305 8 s
2	5 226 931.551 m	354.224 m	3 659 938.391 m	37 240.000 033 455 9 s
3	5 224 663.780 m	380.983 m	3 658 348.973 m	37 240.000 000 006 0 s
4	5 224 663.374 m	380.988 m	3 658 348.689 m	37 240.000 000 000 0 s
5	5 224 663.374 m	380.988 m	3 658 348.689 m	37 240.000 000 000 0 s

The position converges to within 1 m after three iterations. The GPS time at reception, determined by the solution, is $t_R = 37\,240.000\,000\,000\,0$ s. Thus the receiver clock was off by exactly 1 s.

7. These results must lastly be transformed into the WGS84 system by applying the rotation $R^S(t_R - t_C)$. That is, to obtain WGS84 coordinates at the instant of reception, we must use a sidereal rotation corresponding to that instant. Upon applying this rotation to the position coordinates given in the last line of Table III, the measured values of the receiver position are

$$X_{WGS84} = \begin{bmatrix} 5\,224\,663.388 \text{ m} \\ 0 \\ 3\,658\,348.689 \text{ m} \end{bmatrix}. \quad (12)$$

These agree with the true position coordinates to within a millimeter.

OTHER CONSIDERATIONS

THE BENEFIT OF BETTER INITIALIZATION

It pays to be more careful with our initial guesses. To illustrate this, let us consider the following situation which is not unreasonable after the receiver has been working for a while. There may be a good local quartz oscillator which can predict time accurately between measurements. After a local history of navigation solutions has been computed by the receiver, we may suppose that the GPS time of the next solution can be predicted to within 10 ns. If the velocity of the receiver has been monitored a reasonable estimate of the receiver position could be accurate to a few hundred meters. (An earth-fixed user can usually do much better.) Suppose we follow our example above where we assume the user chooses to take measurements at a time on the local clock exactly equal to 37 240.000 000 000 0 s, but that due to quartz oscillator instability the measurement is actually taken 10 ns later. We suppose here that the instant chosen to define the ECI frame is 37 240.000 000 000 0 s. If we go through the iterations we find two improvements. First, there is more rapid convergence, than in the first example. Better estimates of the position could reduce the number of iterations down to one. Second, the final solution for GPS time at the receiver is so close to the estimated time that the final rotation into the ECEF would not introduce significant changes in the position solution. The receiver clock can be updated with no other changes.

ERRONEOUS USE OF ECEF COORDINATES

It might seem that earth rotation effects during the propagation times from the satellites to the receiver are sufficiently small that transforming to ECI coordinates is not necessary. We tested this with the example data given in Table I, initializing the iteration as in the example but using the ECEF coordinates of the satellites. No transformation to ECI coordinates were performed. The results of the iteration, using the same algorithm as before, were significantly in error. The receiver time was in error by 14 ns and the position was in error by almost 30 m. Thus, *it is an error to solve the geometric range delay equations in ECEF coordinates.*

ITERATION WITH A SUCCESSION OF INERTIAL FRAMES

Another approach to the iteration for solving for position and time might be to consider a succession of inertial frames in the iteration process, each of which is aligned with the WGS84 frame at the reception time as estimated at the previous stage of the iteration. The advantage here is that at the end of the iteration the ECI frame would be exactly aligned with the WGS84 frame so no final rotation would be necessary. The disadvantage is the ECI coordinates of the transmission events must be recomputed that at each stage of the iteration, so more computation is required. During actual use, we might have very good estimates of the receiver position available to start the iteration. Possibly few iterations will then yield receiver position with

sufficient accuracy. Then this approach might be better.

CONCLUSIONS

We have discussed the two relativity-related corrections that a GPS receiver needs to make in order to provide time or position to a user. We have explained where they come from and given general prescriptions for their application. We have illustrated these with a numerical example simulated from the actual GPS constellation. In particular we emphasize the importance of removing the rotation from earth-fixed coordinates in order to determine the geometric range delay. This allows us to be consistent with the relativistic principle of the constancy of the velocity of light. We have also presented the equation for the relativistic Doppler shift that a receiver must account for in order to make use of instantaneous carrier phase measurements. A receiver that uses measurements of the integrated Doppler shift can correct for the geometric range in the same way as a code receiver does. Thus we conclude that the requirements if the ICD-200 which include the relativity corrections we have discussed are consistent with the requirements of relativity for range delay measurements accurate to better than 200 ps.

REFERENCES

- [1] Navstar GPS Space Segment/Navigation User Interfaces, ICD-GPS-200, Revision C, Code Ident. No. 6Z691, ARINC Research Corporation, 4055 Hancock Street, San Diego, CA 92110 (Oct. 10, 1993).
- [2] Deines, S., "Missing Relativity Effects in GPS," paper presented at ION-GPS-90, Colorado Springs, CO, September 1990. See also "Missing Relativity Terms in the Current GPS Algorithm," S. Deines, Contract F04701-87-C-0027, (June 1990), and "Missing Relativity Terms in the GPS," *J. Inst. of Navigation*, 39, 111-131 (1992).
- [3] Fliegel, H., and R. DiEposti, *GPS and Relativity: an Engineering Overview*, Aerospace Report ATR-97(3389-1) (1997).
- [4] Ashby, N., and Weiss, M.A., *Relativity for GPS Users*, National Institute of Standards and Technology Technical Note 1385, to be published.
- [5] See Eq. (2) of "Lectures on Frequency Stability and Clocks," by R. F. C. Vessot, in *Experimental Gravitation*, ed. B. Bertotti, Academic Press, Inc., p. 155 (1974).
- [6] Nelson, R., *An Analysis of General Relativity in the Global Positioning System Time Transfer Algorithm*, Sachs/Freeman Associates, Inc., Landover, Md., Contract No. N00014-90-C-204, September, 1991.
- [7] Jorgenson, P.S., "Special Relativity and Intersatellite Tracking," *J. Inst. of Navigation*, 35 (4), 429 (Winter 1988-1989).

Questions and Answers

BERNARD GUINOT (OBERVATOIRE de PARIS): To say this is true, of course; but I have always had some reservations about the a priori separation of velocity effect, gravitational effect, Sagnac effect and so on. The reason for this is that it is a source of many errors. I would simply mention that very often there are misunderstandings about acceleration effects; I have seen papers, especially on GPS, about these acceleration effects.

There are also many discussions about Sagnac effects. I recently received two papers from people who say that we in the time community are totally wrong because we omit the Sagnac effect due to the motion of the earth. All this happens because we do not start with the very fundamental object of general relativity, which is a metric. If you start from the metric in its usual form, you very simply or naturally get all the terms you need, all those you have mentioned here, without any discussion, without any possibility of mistakes. I think it is much better to face the problem that general relativity is some fundamental object which is metric.

MARC WEISS (NIST): Yes, I agree in principle. For most users, that brings up complexities that they do not need to worry about. I also agree that there has been confusion about accelerations. Accelerations are not a fundamental, relativistic effect; it is velocity that is the effect, and it is the fact that the tangent to the curvature is always considered to be a flat space-time that allows you to see velocity as the effect and acceleration as instantaneous effects.

The Sagnac effect is included in what I discussed in the one-way light time. Another way of understanding the Sagnac effect in GPS is simply the motion of the user relative to an inertial frame, which is what I talked about. Yes, I agree in principle, but I'm trying to show that it's a simple problem.

JOE WHITE (NRL): Marc, I am sure you can see it being simple or not, but I think it is a fairly thorough presentation of it. But, let me try to make it simpler. If people here go out and buy an off-the-shelf GPS timing receiver, is there a relativity problem they are likely to run into using it on the ground for timing?

MARC WEISS: If the receiver manufacturer has done it right, there should be no problem using it anywhere.

JOE WHITE: Are you aware of any popular receivers, at least, that do have a problem in the area?

MARC WEISS: I am not aware of them, but I have not done a great survey of what the receivers out there do. But, I would think that it would show up very rapidly. If you are sitting on the earth, even at the equator, you get 400 meters worth of error.

JOE WHITE: It shows up pretty quick.

MARC WEISS: Yes.

JOE WHITE: Now, to make it a little bit worse. Suppose we are using the receiver on an aircraft, say, a military or civilian aircraft at 40,000 feet, MACH 1-type velocities or less. Do we have an issue there?

MARC WEISS: There is no issue anywhere as long as you are doing the GPS problem; that is you have four or more satellites in view; you are trying to get GPS time; you are not using your local clock as a flywheel except for very short time periods between receiver updates, say 10-20 seconds, a minute or two; there is no problem.

JOE WHITE: Okay, that is really what I was trying to get at to kind of put this in scope for the audience to get a feel for whether there is something that we as users, as opposed to designers, might need to worry about.

MARC WEISS: The only place where another relativity term comes in is if you have very infrequent receiver updates, and now you have to use your clock as flywheel as you go through velocities and

accelerations. But in that case, there are other concerns besides relativity that come in, I mean, clocks run at different rates due to shock and vibration and temperature, and you have really got a lot to keep track of, I think. You have a whole clock prediction problem in that case.

THE CCTF WORKING GROUP ON THE EXPRESSION OF UNCERTAINTIES IN PRIMARY FREQUENCY STANDARDS

R.J. Douglas¹ and C. Thomas²
on behalf of the Working Group members

¹National Research Council of Canada, Ottawa, Ontario, K1A 0R6,
Canada

²Bureau International des Poids et Mesures, Pavillon de Breteuil, 92312
Sèvres Cedex, France

Abstract

The Comité Consultatif pour la Définition de la Seconde (CCDS) created in March 1996 a Working Group on the expression of uncertainties in primary frequency standards. This paper presents the main topics included in the first report of the Working Group dated April 1997. This report gives a brief review of the conditions which led to the creation of the Working Group and a summary of the discussions which took place at its first meeting held in Neuchâtel, Switzerland, on 5 March 1997, and also during the following weeks. A main objective of the Working Group is a better understanding between laboratories which evaluate the accuracy of their primary frequency standards and their clients represented by the Bureau International des Poids et Mesures (BIPM) which uses the measurements provided by these standards for assessing the accuracy of TAI (Temps Atomique International, or International Atomic Time) and UTC. An important point for this purpose is the application to primary frequency standards of the guidelines expressed in the Guide to the Expression of Uncertainty in Measurement [1].*

CREATION OF THE WORKING GROUP

A primary frequency standard is an instrument which produces an output whose average frequency is based on the internationally accepted definition of the second, and is operated with its own independent implementation of the cesium second and a specified accuracy that does not rely on calibration to another frequency standard. Some national metrology laboratories design and operate large primary frequency standards whose main design objective is to facilitate the evaluation of their accuracy. These instruments are the most accurate devices ever made by humans. The question of quantifying and expressing the accuracy of primary frequency standards - that is "the expression of the uncertainty of primary frequency standards" - arose at the 13th meeting of the CCDS* in March 1996 [2]:

[Dr Quinn] observed that the *ISO Guide* to the expression of uncertainty in measurements recommends that uncertainties be expressed as a combination of statistical (type A) and others (type B) uncertainties. In view of this, he assumes that the uncertainties quoted for primary frequency standards are entirely type B, since no associated averaging times are quoted.

* At its 1997 meeting, the Comité International des Poids et Mesures (CIPM) decided to change the name of the Comité Consultatif pour la Définition de la Seconde (CCDS) to that of Comité Consultatif du Temps et des Fréquences (CCTF).

An extended discussion on the topic followed, which was summarized by Mr Allan who said that in time and frequency applications we usually analyse data in the form of a time series. This leads to the question of what is intended when an uncertainty is calculated, that is, is it the expected variation of a quantity over a period of time, or is it merely the uncertainty of a single measurement?...

Dr Winkler said that the evaluation of a frequency standard involves two steps: the determination of systematic effects and then the measurement of its frequency with respect to TAI. This second step involves the consideration of measurement times and instability. Prof. De Marchi agreed with Dr Winkler, saying that stability and accuracy are very different entities...

Dr Winkler gave the opinion that the *ISO Guide* is applicable so long as the distinction is made between stability and accuracy.

Dr Sullivan added that some of the effects encountered in the uncertainty budget of a primary standard may not be independent. In such a case the quadratic sum of the uncertainty components is not sufficient.

Dr Bauch added that it is sometimes difficult to distinguish between type A and type B uncertainties; for example, the uncertainty in the first order Doppler effect in the fountain frequency is evaluated by measurement and thus cannot be treated as a type B uncertainty.

... the President... suggested that the matter is of sufficient importance that the CCDS should form a Working Group to report on how the accuracy of primary frequency standards should be evaluated in accordance with the *ISO Guide*. He asked Dr Douglas to act as Chairman of the CCDS Working Group on the expression of uncertainties in primary frequency standards... the membership of the Working Group is... open to... experts from timing laboratories.

The first meeting of this Working Group was held on 5 March 1997 at the 11th European Forum on Time and Frequency, in Neuchâtel, Switzerland. A preliminary exchange had been carried out via e-mail between those attending the first meeting and several other experts.

SCOPE OF THE WORKING GROUP

The scope of the Working Group was approached by its Chair, in an e-mail dated 22 January 1997, addressed to the Group members:

...it has become evident to me that it is vital to choose the correct scope: one that could result in our recommending a way to communicate the basis for frequency metrology rigorously and widely, without overburdening or bypassing any particular part of the frequency metrology chain - from primary standard metrologist to end-user.

In this approach, it is emphasized that user needs for frequency sources, though not necessarily at the upper level of accuracy, are important and should be discussed by the Working Group. It was suggested that the word 'primary' be dropped from the group title.

However, the discussions inside and after the first meeting led to the conclusion that the first objective of the Working Group is to develop a better understanding between those who are building and evaluating primary frequency standards, and those who are using them, one of the main users being the BIPM. Direct users, and especially the BIPM would be more fully informed on the evaluation of primary frequency standards, to allow the standards' data to be used in an optimum way. The Working Group discussed extending the scope to include the use of the results of primary frequency standards for calibrating instruments (with reference to TAI or UTC, for example). It was decided to restrict the scope of the Working Group's report for the next CCTF meeting to the expression of uncertainty of primary frequency standards, particularly uncertainty budgets aimed at frequency transfer to TAI.

TYPE A AND TYPE B UNCERTAINTIES

There exists a formal and published recommendation, Recommendation INC-1 (adopted in 1980) on the statement of uncertainties. This recommendation, on the expression of experimental uncertainties is the basis of the *ISO Guide to the Expression of Uncertainty in Measurement* [item 0.7, p viii]:

1. The uncertainty in the result of a measurement generally consists of several components which may be grouped into two categories according to the way in which their numerical value is estimated:

- A. those which are evaluated by statistical methods,

- B. those which are evaluated by other means.

There is not always a simple correspondence between the classification into categories A or B and the previously used classification into 'random' and 'systematic' uncertainties. The term 'systematic uncertainty' can be misleading and should be avoided.

Any detailed report of the uncertainty should consist of a complete list of the components, specifying for each the method used to obtain its numerical value.

2. The components in category A are characterized by the estimated variances s_i^2 (or the estimated 'standard deviation' s_i) and the number of degrees of freedom ν_i . Where appropriate, the covariances should be given.

3. The components in category B should be characterized by quantities u_j^2 , which may be considered as approximations to the corresponding variances, the existence of which is assumed. The quantities u_j^2 may be treated like variances and the quantities u_j like standard deviations. Where appropriate, the covariances should be treated in a similar way.

4. The combined uncertainty should be characterized by the numerical value obtained by applying the usual method for the combination of variances. The combined uncertainty and its components should be expressed in the form of 'standard deviations' (referred to as *standard uncertainties* since the publication of the *ISO Guide* in 1993[1]).

5. If, for particular applications, it is necessary to multiply the combined uncertainty by a factor to obtain an overall uncertainty, the multiplying factor used must always be stated.

The division of evaluation methods for uncertainties into type A and type B methods is in part an echo of the "random" and "systematic" uncertainties of past decades. However, since there is no difference in the way the two types are to be used, the type A and type B classification is only an issue for communicating the methodology rather than the value of the uncertainty.

STABILITY OF PRIMARY FREQUENCY STANDARDS

Most of the *ISO Guide* takes the implicit condition that the system under study is stationary and affected only by white noise. This is obviously not the case for time measurements which often deliver time series affected by correlated noise such as random walk of frequency. Expressing a type A uncertainty in the form of a generic standard deviation s , as recommended by the Guide, makes no sense in this case. To construct a stationary standard uncertainty, a specific frequency holdover pattern can be considered, calibrated over one time interval τ_1 and used over another time interval τ_2 a time t later [3,4]. Used in this way, tools like the Allan variance, $\sigma_y^2(\tau)$ [5], are suitable for specifying the consequences of known non-white noise on the uncertainty of primary frequency standards where deterministic frequency drift is not a major effect. When it is important, deterministic drift can be handled in similar ways [6]. The question of the Allan variance in time measurements is evoked in item 4.2.7 of the *ISO Guide*:

If the random variations in the observations of an input quantity are correlated, for example, in time, the mean and experimental standard deviation of the mean ... may be inappropriate estimators of the desired statistics. In such cases, the observations should be analysed by statistical methods specially designed to treat a series of correlated, randomly-varying measurements.

NOTE - Such specialized methods are used to treat measurements of frequency standards... (See reference [5], for example, for a detailed discussion of the Allan variance).

Uncertainty related to stability is thus treated with type A methods, but it may be possible to classify other sources of uncertainty in primary frequency standards as being also of type A.

Applied to some evaluation methods used in modern primary frequency standards, the type A and type B classification is ambiguous. Working Group members report different interpretations which result in strikingly similar methods, used by different laboratories, being classified by some as of type A, and by others as of type B.

For a primary frequency standard, all perturbing effects are best determined by measurement. The measurements are repeated, and evaluated - usually with the aid of a theoretical model whose parameters are determined by fitting to measured values - and the correction to zero perturbation is determined from the fit. The fitting process is certainly a statistical method, and viewed in this way the derived uncertainty in the extrapolated correction can then be described as having been evaluated by a type A method. However, the use of a theoretical model, and perhaps ancillary apparatus for determining the correction, can lead to the view that the correction has been imported and not determined by statistical analysis of the primary measurand - and so it has been evaluated by a type B method.

This classification, meant to communicate information about the evaluation method, is actually obscuring the similarities of the methods used. Thus the Working Group will have to address the refinement of this classification system, or consider abandoning it altogether. Abandoning the classification has implications for other fields where statistical methods and other knowledge interact. Even the purest type A method imports the model of a stationary mean, so it too might be viewed as using in part an "other method". Of those who were helped develop this classification into type A and type B evaluation methods, there is a willingness to consider abandoning the distinction [7]. The essential element is that uncertainty components, evaluated by any method, are to be construed as probability distributions and combined in the same way. The type A and type B classification filled the important role of replacing the "random" and "systematic" nomenclature, which were not always treated together, and unifying the treatment of their uncertainty distributions in a single uncertainty. With this primary function largely completed, it may be time to consider de-emphasizing the classification.

AVERAGING TIME FOR PRIMARY STANDARD EVALUATION

An important point about the question of frequency measurements and the evaluation of the uncertainty budget for a primary frequency standard concerns the averaging time chosen for the operations of evaluating and reporting average frequencies. The situation is not the same for the diverse very accurate primary frequency standards in operation in the world:

- The averaging time chosen by the American national metrology laboratory, the National Institute for Standards and Technology (NIST) for its optically pumped thermal beam primary frequency standard, NIST-7, is basically set by the sampling of TAI, 10 days in 1994 and 1995 and 5 or 10 days since January 1996. This makes it possible to cancel the frequency variations of the local hydrogen maser to which NIST-7 is compared, and thus ensures an optimum link to TAI.
- The German national metrology laboratory, Physikalisch-Technische Bundesanstalt (PTB), operates thermal beam primary frequency standards which use magnetic state selectors in an axial field geometry. Their standards are operated continuously and their data are sent to the BIPM as for conventional clocks contributing to TAI. The choice of

two-month periods for the estimation of their frequencies relative to TAI was made by the BIPM, simply because TAI is computed with blocks of two-month data.

- The French national metrology organization, the Bureau National de Métrologie (BNM), through its Laboratoire Primaire du Temps et des Fréquences (LPTF), operates a cesium fountain primary frequency standard. It is not operated continuously. The averaging time chosen for the BNM-LPTF cesium fountain FO1 is not related to the sampling time of TAI. The level of white frequency noise in FO1 is so low that, for an averaging time of about 10 hours, its curve of stability is limited by the stability of the local hydrogen maser to which FO1 is compared. Complete evaluation of the standard cannot be carried out efficiently over longer averaging times.

It is often supposed that the accuracy of a primary frequency standard is evaluated in the range of averaging times corresponding to its best stability, but it is not always the case:

- It is not possible for FO1 since the stability of the local oscillator limits the measurements.
- For what concerns NIST-7, a complete evaluation is carried out each time a new frequency measurement is provided to the BIPM, and is thus valid over averaging times of 5 or 10 days. The part of the type A uncertainty coming from the lack of stability of the standard is usually small compared to some of the uncertainties associated with the different frequency corrections, but that this is not always or necessarily true.
- There is no search to make regular complete evaluations of the accuracy of the PTB standards each two months: this is done at the beginning and is well documented [8]. Some contributions are routinely and frequently re-evaluated (mean magnetic field, second order Doppler, electronics, microwave spectrum) and the claimed uncertainties are repeatedly verified. Others are estimated only once (magnetic field inhomogeneity, cavity pulling, Rabi pulling, gravity, black-body). For what concerns the end-to-end cavity phase shift, it is checked from beam reversals; this specific uncertainty, of type B, is based on mechanical measurements made during construction of the clock, which cannot be repeated unless the clock is dismantled.

TRANSFER OF FREQUENCY MEASUREMENTS TO TAI

One important use of primary frequency standard measurements is for the assessment of the accuracy of TAI. It is thus essential to optimize the internal link between the standard and the time-transfer measurement system, often a GPS time receiver, inside the laboratory, and to treat with precautions the time transfer data to TAI:

- Links are optimized for NIST-7 thanks to the choice of averaging periods which match the TAI time grid. However, the component of uncertainty due to the GPS transfer over 5 days may not be negligible when compared with the standard uncertainty of NIST-7 as given at the end of 1996 (5×10^{-15}).
- The standard PTB CS2 provides UTC(PTB) and is used directly as input to the PTB GPS receiver. Since data are averaged over two-month periods, TAI takes advantage of the full accuracy of the PTB standards.
- After transfer to TAI, the FO1 data of September-December 1995 show a huge dispersion of the measurements (peak-to-peak 2×10^{-14}) when compared to the total uncertainty of the standard at that time (3×10^{-15}). The internal laboratory link was not optimized at that period, but this should be done for future measurements.

A primary frequency standard measurement is carried out over a given time interval, defined by its duration and its central date. The measurement calibrates the rate of a local time scale, which is compared (largely by GPS common-view techniques) with the time scales of other laboratories in the pooling of comparisons for the determination of the paper time scale TAI. The measurement can thus be used to calibrate the rate of TAI over a time interval with

another duration and another central date. The frequency holdover is carried out using the stability of TAI itself: the frequency measurement is transferred without change, but an additional uncertainty term is included (added in quadrature using the root-sum-square) to account for the relative stability of the two time scales, scaled by an amount depending upon the noise characteristic of the time scale difference [3,4].

UNCERTAINTY BUDGETS FOR PRIMARY STANDARDS

It is agreed that the uncertainty of a primary frequency standard should be documented in tabular form. This table should list all corrections applied to the standard data, together with their respective uncertainties, and references to the procedures used for measuring influence parameters and references to the functional forms and numerical constants used for calculating corrections. These references are important for allowing the evaluation of correlations between the methods used in different primary standards. Where appropriate the degrees of freedom should also be specified, to indicate how well the uncertainty has been determined. Together, this information constitutes the 'uncertainty budget'. This procedure is in complete accord with the *ISO Guide*. The elements of the uncertainty budget for a primary frequency standard have more in common with a pure physics measurement of a fundamental constant (the hyperfine interval of ^{133}Cs) than with classical metrology. They are covered in extensive textbooks on the subject [9], and is an active area of continuing research. They are touched on below. The strength of the *ISO Guide* is evident in the ease and completeness with which it encompasses the expression of uncertainty for both fundamental constants and classical metrology. Much of the Working Group's discussions will use the *ISO Guide* as their primary reference.

On several occasions the BIPM has published in its regular *Circular T*, a value of the duration of the TAI scale unit obtained from a primary frequency standard measurement, with the uncertainty budget of the standard, before the corresponding evaluation of accuracy could be published or even submitted to an international journal. The BIPM thus serves as publisher for results which may be revealed later to be too optimistic or too quickly obtained. The Working Group may decide that the BIPM should always indicate the source of information containing the claimed uncertainty, or re-publish uncertainty budgets that it uses.

Returning to the general problem of drawing up the uncertainty budget for a primary frequency standard, one may wonder if there is a complete consensus about what corrections should be listed in the table. One example that illustrates how there can be a difference in practice, rooted in a philosophical difference, is the gravitational shift.

One view is that since a frequency standard produces a proper unit, the SI second, defined locally from an experiment within the dimensions of a laboratory, the gravitational shift is small enough so that it should not be included in the uncertainty budget. For the largest cesium fountains ever seriously considered [10,11], the effect within the standard has a maximum difference of 0.5×10^{-15} , while for horizontal thermal beam cesium standards the maximum difference may be smaller than 1×10^{-18} . The uncertainty in the difference in gravitational potential within the laboratory will normally be easily at a negligible level.

A second view is that in addition to these small corrections and even smaller uncertainties, the correction and its uncertainty should be taken into account when the SI second is transferred to the rotating geoid for assessing the accuracy of TAI. For clients of primary frequency standards to be served in this way, a laboratory takes the responsibility of estimating this part of the uncertainty (which they are best equipped to do) for the way their frequency standard is used outside the confines of their laboratory. Proper time users also

have a gravitational correction to estimate. These corrections [12] can be large - about 10^{-9} for some Earth orbits. Uncertainties can range from 1×10^{-18} in Earth orbit to 1×10^{-17} for carefully surveyed elevations on the Earth's surface, to 10^{-15} if one uses a topographic map or a simple ellipsoid to geoid conversion, and can approach 10^{-14} if elevation above the ellipsoid is used in place of elevation above the geoid (i.e. elevation above sea level).

Different laboratories do not treat this question in the same way: the gravitational correction appears as an additional line in the FO1 uncertainty budget, after the quadratic sum of the different uncertainties has been made; for other standards it is taken into account in the main table. A consensus on this question has not developed in the Working Group.

For some members, it is understood that if people are developing standards it is largely for use at other locations in the outside world, so a reference location is chosen to convert the produced SI second, a unit of proper time, to a unit of coordinate time. The rotating geoid is almost universally chosen for terrestrial applications, most often through TAI or UTC. In this perspective the laboratory estimates and applies the gravitational correction and its uncertainty as an intrinsic part of realizing the unit of TAI.

Other members recall that the second is defined as a proper unit, and would classify the gravitational uncertainty in the transfer to TAI as an issue removed from the generation of the scale unit of a proper time scale. Some have suggested that the uncertainty in the gravitational correction is so small that this problem is not yet important.

In principle there should be no problem in agreeing about the corrections to be considered in the uncertainty budget. However, it should be recalled that the correction for the black-body shift had been neglected for years: it has been applied uniformly since 1995, although the paper first describing the effect was published in 1982 [13]. The first formal action on the effect was by the 1985 meeting of the CCDS, which recalled that the definition of the second was for the limit of zero perturbations and called for studies on these matters [14]. Although the theoretical underpinning seemed solid enough, experimental verification that the effect scaled as expected with blackbody temperature was not available until 1996 [15,16]. This led to a situation where there were two approaches in use: one held that the theory (and the old low frequency Stark shift measurements on cesium [17,18]) was the best estimate of the blackbody radiation shift, and the other held that further experimental confirmation on cesium atoms with appropriate blackbody radiation was necessary before the correction should be applied. The typical shift (at 300 K about -2×10^{-14}) is small enough to be difficult to measure and yet large enough to become a major source of uncertainty if no correction is applied. The uncertainty budgets of primary frequency standards through the decade 1985-1995 were not always published frequently enough nor widely enough to make it easy to understand how the blackbody radiation was being treated for widely accessible standards.

About the correction for the black-body shift, discussions took place inside the first meeting of the Working Group on whether its uncertainty should be classified as type A or as type B. The evaluation is based on the formula given by Itano *et al* [13]:

$$[\nu(T) - \nu_0] / \nu_0 = - (169 \pm 4) \times 10^{-16} (T/300)^4,$$

with $\nu(T)$ the frequency at temperature T (T in K) and ν_0 the frequency at 0 K. At room temperature, the correction is -1.7×10^{-14} with a variation of -2.3×10^{-16} per K.

This shift has not yet been measured directly for the temperature of primary standards as compared to the unperturbed low temperature limit ($T=0$ K), and we do not have yet a complete understanding of the limitations of the formula. The uncertainty quoted above

arises partly from previous measurements of the scalar low frequency Stark effect but also makes some allowance for inadequacies of the theoretical treatment. Many kinds of expertise are needed to estimate the extent to which these are the only sources of uncertainty. The formula's uncertainty should incorporate tensor effects as well as the AC Zeeman shift effect. Estimating the effective temperature of the radiation calls for knowledge of the temperature of the surroundings, and if the temperature distribution is not uniform, a knowledge of the emissivity of the surfaces. The uncertainty of the correction for the black-body shift is generally estimated to be 1×10^{-15} for standards operating at 300 K. This is a conservative value relative to the uncertainties given in the formula and in the temperature, and should thus be regarded as of type B. Such a discussion should be undertaken for all of the uncertainty components which appear in the uncertainty budget of primary standards.

The largest correction term, which also has an associated uncertainty, is the Zeeman shift deliberately induced by a small magnetic field applied to the cesium atoms. The field is applied to isolate and use the most stable component of the cesium hyperfine transition (between $F=3, m_F=0$ and $F=4, m_F=0$), which has a quadratic field dependence and a shift that is typically 2×10^{-9} or less. Most often the magnetic field is measured with the neighboring components of the cesium hyperfine transition (such as between $F=3, m_F=0$ and $F=4, m_F=1$). Evaluating and describing the stability and homogeneity of the magnetic field, and the uncertainty of the correction which these variations generate, will not be done identically for different types of standard. The completeness of the Breit-Rabi formula [9] for these transitions is an interesting issue, since any revision here could affect, unequally, standards which use different fields, and yet if the corrections are properly documented today's biases from this type of uncertainty could be removed retrospectively in later redeterminations of TT for astronomical purposes.

The Stark shift is generally negligibly small, since to keep this correction less than 10^{-16} , the electric field only needs to be kept below 5 V/m.

The second-order Doppler shift or time dilation is the second largest correction to be applied for many thermal beam frequency standards, since for thermal cesium atoms at 300 m/s the effect is $v^2/c^2 \approx 10^{-12}$. Determining the speed distribution of the cesium atoms can be done in different ways, and can be done with an uncertainty of 10^{-15} for thermal beams. For laser-cooled cesium beams the correction is normally less than 10^{-15} and the speed distribution can usually be measured even more accurately so that this uncertainty could be 10^{-18} or less.

Collisions in the vacuum in which the cesium atoms drift can affect the resonance frequency. The largest, and to some extent unavoidable, effect arises from collisions of the beam with other cesium atoms in the beam which gives a density shift with an uncertainty which might be evaluated with an uncertainty of 10^{-16} for cesium fountains.

Distributed phase variations in the microwave cavity give a phase shift for the two passages of the atoms through the cavity, with care room temperature cavities can be evaluated to produce an uncertainty of 10^{-6} of the linewidth or less. The time-averaged Poynting vector can be reduced by selecting cavity design and wall materials. The critical element is the absence of net energy flow rather than the Q of the cavity. Ring cavities, symmetric feeds, and in the future perhaps superconducting cavities may be used.

Other transitions than the intended one (between $F=3, m_F=0$ and $F=4, m_F=0$), can also affect the uncertainty. The cesium hyperfine transition is not a two-level one, but there are seven Zeeman sublevels of $F=3$ and nine sublevels of the $F=4$ level. The sublevels are purposefully split by the applied magnetic field, and excitation of unwanted transitions can lead to Rabi pulling or Ramsey pulling of the apparent center of the intended transition. Evaluating the

unwanted transitions involves considering the purity of the initial state preparation, the parallelism of the applied static and microwave magnetic fields, the spectral purity of the microwaves and the ability of the final state analyzer to reveal the final superposition of states. Describing the procedures used to evaluate all this can clearly be a challenge.

Microwave cavity leakage can affect the standard, and the evaluation of any residual microwave fields in the drift space leads to another source of uncertainty.

The main frequency control servo must be carefully characterized in terms of its offset. Unwanted effects arise from any unwanted detector signal which is coherent with the frequency modulation or switching of the servo system, but are easy to characterize. For analog servos the inverter, chopper and zero offset of the main integrator must be examined particularly carefully. The effects of servo design, bandwidth and gain are also considered, and can be modelled with the local oscillator to give a predicted stability which can be considered as a part of the uncertainty budget, particularly when describing the variation, with averaging time, of the standard uncertainty of the primary frequency standard.

The local oscillator's phase and frequency noise combines with the shot noise of the interrogation of the cesium resonance to affect the stability component of the standard uncertainty of the primary frequency standard, changing the servo response and (usually) to a lesser extent changing the excitation of unwanted transitions and uncertainty budget.

Environmental effects alter the physical environment of the cesium atoms of a primary frequency standard in measurable ways - measurable through the way that they change the above influence parameters of the cesium atoms. Environmental variations which are unanticipated may not be fully captured and accounted for by scheduled measurements. For a primary frequency standard there will be strategies for identifying random, diurnal, and seasonal effects and re-measuring corrections varied by magnetic fields, RF interference, temperature, temperature gradients, humidity, and atmospheric pressure. These variations will be associated with uncertainty in the influence parameters and so in the final frequency.

The transfer characteristics of the average frequency of a primary frequency standard to TAI is another area for active discussion. The laboratory possessing a primary frequency standard which is to be used in steering TAI is best equipped both to design the transfer strategy and to evaluate the uncertainty associated with the transfer of the average frequency to TAI. The Working Group will likely consider ways of exploiting this expertise for documenting and perhaps improving the evaluation of the frequency of TAI relative to the SI second.

CONCLUSIONS

In the first meeting of the CCTF Working Group on the expression of uncertainties in primary frequency standards, it was clear that those who produce measurements from primary frequency standards and those who use them do not always have a complete appreciation on what has been done in other laboratories. The Working Group could recommend a framework for the publication of uncertainty budgets and other reports on primary frequency standards. Uncertainty budgets of primary frequency standards would be given in accordance with the *ISO Guide*, and with some supplementary material specific to frequency metrology. In this framework several topics remained to be studied, in particular the classification of uncertainties into types A and B, and the procedures by which uncertainty components should be combined and weighted averages taken.

MEMBERS OF THE WORKING GROUP

It is a pleasure to acknowledge those who have participated in the deliberations of the Working Group to date: D. Allan, A. Bauch, J.-S. Boulanger, A. Clairon, A. De Marchi, R. Drullinger, P. Fisk, A. Lepek, and T. Parker.

REFERENCES

- [1] *Guide to the Expression of Uncertainty in Measurement*, 101 p (International Organization for Standardization, ISBN 92-67-10188-9, 1993).
- [2] Report of the 13th Meeting of the CCDS, *BIPM Publications*, item 2.2 p S56, (1996).
- [3] J. Azoubib, M. Granveaud, B. Guinot, *Metrologia*, **13**, 87-93 (1977).
- [4] R.J. Douglas, J.-S. Boulanger, *Proc. 11th EFTF*, 345-349 (1997).
- [5] D.W. Allan, *IEEE Trans. Instrum. Meas.* **IM 36**, 646-654 (1987).
- [6] R.J. Douglas, J.-S. Boulanger and C. Jacques, *Proc. 25th PTTI*, 249-266 (1993).
- [7] P. Giacomo, personal communication to the Working Group, (1997).
- [8] A. Bauch, T. Heindorff, R. Schröder, B. Fischer, *Metrologia* **33**, 3, 249-259 (1996).
- [9] J. Vanier and C. Audouin, *The Quantum Physics of Atomic Frequency Standards* (Adam Hilger, Bristol and Philadelphia, 1987).
- [10] J.R. Zacharias, *Phys Rev* **94**, 751 (1954).
- [11] A. De Marchi, *Metrologia* **18**, 103-116 (1982).
- [12] P. Wolf, *Relativity and the Metrology of Time*, BIPM Monograph 97/1, (1997).
- [13] W.M. Itano, L.L. Lewis, D.J. Wineland, *Phys Rev A*, **25**, 1233-1235 (1982).
- [14] Report of the 10th Meeting of the CCDS, *BIPM Publications*, S10, S44, and S58 (1985).
- [15] A. Bauch and R. Schröder, *Phys Rev Lett* **78**, 662 (1997).
- [16] R. Augustin, A. Bauch and R. Schröder, *Proc. 11th EFTF*, 47-52 (1997).
- [17] R.D. Haun and J.R. Zacharias, *Phys Rev* **107**, 107 (1957); J.R. Mount, *Phys Rev A* **5**, 1059 (1972).
- [18] E. Simon, P. Laurent, C. Mandache and A. Clairon, *Proc. 11th EFTF*, 43-46 (1997).

Questions and Answers

CLAUDINE THOMAS (BIPM): Maybe I can make one comment. Thank you for showing us the guide on the expression of uncertainties. Please do it again.

ROB DOUGLAS (NRC): That is what it looks like in the light.

CLAUDINE THOMAS: It is a very important book for us, of course, because it explains how we must express our uncertainties and combine them, of course; so thank you for that.

TOTAL VARIANCE AS AN EXACT ANALYSIS OF THE SAMPLE VARIANCE*

Donald B. Percival
Applied Physics Laboratory
University of Washington
Box 355640
Seattle, WA 98195-5640 USA
E-mail: dbp@apl.washington.edu

David A. Howe
Time and Frequency Division
National Institute of
Standards and Technology
325 Broadway
Boulder, CO 80303 USA
E-mail: dhowe@nist.gov

Abstract

Given a sequence of fractional frequency deviates, we investigate the relationship between the sample variance of these deviates and the total variance (Totvar) estimator of the Allan variance. We demonstrate that we can recover exactly twice the sample variance by renormalizing the Totvar estimator and then summing it over dyadic averaging times 1, 2, 4, ..., 2^J along with one additional term that represents variations at all dyadic averaging times greater than 2^J . This decomposition of the sample variance mimics a similar theoretical decomposition in which summing the true Allan variance over all possible dyadic averaging times yields twice the process variance. We also establish a relationship between the Totvar estimator of the Allan variance and a biased maximal overlap estimator that uses a circularized version of the original fractional frequency deviates.

1 INTRODUCTION

The goal of this paper is to explore the relationship between the sample variance of a sequence of fractional frequency deviates $\{y_n : n = 1, \dots, N_y\}$, namely,

$$\hat{\sigma}_y^2 \equiv \frac{1}{N_y} \sum_{n=1}^{N_y} (y_n - \bar{y})^2, \text{ where } \bar{y} \equiv \frac{1}{N_y} \sum_{n=1}^{N_y} y_n,$$

and a new estimator of the Allan variance called "Totvar" ("total variance" – see the companion article by Howe and Greenhall [1] in these Proceedings for additional details). The Totvar estimator is based upon the hypothesis that reasonable surrogates for unobserved deviates y_n , $n < 1$ or $n > N_y$, can be formed by tacking on reversed versions of $\{y_n\}$ at the beginning and end of the original series. The Totvar estimator makes use of certain of these surrogate values in order to come up with a new estimator of the Allan variance that has better mean-squared error properties than the usual Allan variance estimator at the very largest sampling times (Howe and Greenhall [1]). Here we show that a renormalized version of the Totvar estimator can be used to exactly decompose twice the sample variance. Except for the factor of two (an historical artifact due to the original definition of the Allan variance), this decomposition of the sample variance is very much similar to the one afforded by traditional spectral analysis

*Contribution of the U. S. Government, not subject to copyright.

estimators, which exactly decompose the sample variance across different Fourier frequencies. By comparison our results show that the (renormalized) Totvar estimator decomposes the sample variance across dyadic averaging times (i.e., averaging times of the form $2^j \tau_0$, where τ_0 is the sample period for $\{y_n\}$). Our result thus says that the Allan variance can be regarded as an example of an analysis of variance technique, which is one of the most widely used data analysis methods in modern statistics.

The remainder of this paper is organized as follows. In Section 2 we recall that in fact a very early estimator of the Allan variance (the nonoverlapped estimator) exactly decomposes twice the sample variance for the special cases when N_y is a power of two. Because of its poor variance properties, the nonoverlapped estimator is very seldom used, so we discuss in Section 3 what is generally considered to be the preferred estimator, namely, the maximal overlap estimator. The usual formulation of this estimator does *not* yield a decomposition of twice the sample variance; however, if we view this estimator as the mean-squared output of a circular filtering operation, we can augment the estimator with additional terms (namely, ones that make explicit use of the circularity assumption) and come up with an biased version of the maximal overlap estimator that does yield a decomposition of twice the sample variance for any sample size N_y . Because of the potential mismatch between y_1 and y_{N_y} , this circularity assumption can lead to serious biases. Thus, in Section 4 we consider using the biased maximal overlap estimator with the series of length $2N_y$ formed by tacking on a reversed version of $\{y_n\}$ at the end of the original series. This new estimator can be written as a renormalized version of the Totvar estimator. In Section 5 we summarize our results and conclude with a few comments.

2 THE NONOVERLAPPED ESTIMATOR OF THE ALLAN VARIANCE

For this section only we assume that the sample size is a power of two ; i.e., we can write $N_y = 2^J$ for a positive integer J . Given a sequence of τ_0 -average fractional frequency deviates $\{y_n : n = 1, \dots, N_y\}$ with a sampling period between adjacent observations given by τ_0 also, let us define the $m\tau_0$ -average fractional frequency deviate as

$$\bar{y}_n(m) \equiv \frac{1}{m} \sum_{j=0}^{m-1} y_{n-j}.$$

If we regard $\{\bar{y}_n(m) : n = m, \dots, N_y\}$ as a realization of one portion of the stochastic process $\{\bar{Y}_n(m) : n = 0, \pm 1, \pm 2, \dots\}$, the Allan variance for averaging time $m\tau_0$ is defined as

$$\sigma_y^2(m) \equiv \frac{1}{2} E \left\{ [\bar{Y}_n(m) - \bar{Y}_{n-m}(m)]^2 \right\},$$

where we assume that the stochastic process is such that the expectation above in fact depends on the averaging time index m , but not on the time index n (this will be true if the first difference process $\{\bar{Y}_n(1) - \bar{Y}_{n-1}(1)\}$ is a stationary process).

For $m = 2^j$ for $j = 0, 1, \dots, J-1$, let us form the so-called nonoverlapped estimator of the Allan variance:

$$\hat{\sigma}_{y, \text{nono}}^2(2^j) \equiv \frac{2^j}{N_y} \sum_{k=1}^{\frac{N_y}{2^{j+1}}} [\bar{y}_{2k2^j}(2^j) - \bar{y}_{(2k-1)2^j}(2^j)]^2.$$

For example, if $j = 0$ so that $m = 1$, the above reduces to

$$\hat{\sigma}_{y, \text{nono}}^2(1) = \frac{1}{N_y} \sum_{k=1}^{\frac{N_y}{2}} [y_{2k} - y_{2k-1}]^2, \quad (1)$$

so that each y_n contributes to exactly one term in the sum of squares above (hence the origin of the name "nonoverlapped estimator"). At the other extreme when $j = J - 1$ so that $m = \frac{N_y}{2}$, we have

$$\hat{\sigma}_{y, \text{nono}}^2\left(\frac{N_y}{2}\right) = \frac{1}{2} \left[\bar{y}_{N_y}\left(\frac{N_y}{2}\right) - \bar{y}_{\frac{N_y}{2}}\left(\frac{N_y}{2}\right) \right]^2.$$

The nonoverlapped estimator can be interpreted in terms of an orthonormal transform of the column vector \mathbf{y} whose elements are given by $\{y_n\}$. For $N_y = 8$, this transform is given by the following 8×8 matrix:

$$\mathcal{W} \equiv \begin{bmatrix} -\frac{1}{\sqrt{2}} & \frac{1}{\sqrt{2}} & 0 & 0 & 0 & 0 & 0 & 0 \\ 0 & 0 & -\frac{1}{\sqrt{2}} & \frac{1}{\sqrt{2}} & 0 & 0 & 0 & 0 \\ 0 & 0 & 0 & 0 & -\frac{1}{\sqrt{2}} & \frac{1}{\sqrt{2}} & 0 & 0 \\ 0 & 0 & 0 & 0 & 0 & 0 & -\frac{1}{\sqrt{2}} & \frac{1}{\sqrt{2}} \\ -\frac{1}{2} & -\frac{1}{2} & \frac{1}{2} & \frac{1}{2} & 0 & 0 & 0 & 0 \\ 0 & 0 & 0 & 0 & -\frac{1}{2} & -\frac{1}{2} & \frac{1}{2} & \frac{1}{2} \\ -\frac{1}{\sqrt{8}} & -\frac{1}{\sqrt{8}} & -\frac{1}{\sqrt{8}} & -\frac{1}{\sqrt{8}} & \frac{1}{\sqrt{8}} & \frac{1}{\sqrt{8}} & \frac{1}{\sqrt{8}} & \frac{1}{\sqrt{8}} \\ \frac{1}{\sqrt{8}} & \frac{1}{\sqrt{8}} & \frac{1}{\sqrt{8}} & \frac{1}{\sqrt{8}} & -\frac{1}{\sqrt{8}} & -\frac{1}{\sqrt{8}} & -\frac{1}{\sqrt{8}} & -\frac{1}{\sqrt{8}} \end{bmatrix}$$

(for other N_y , the $N_y \times N_y$ matrix \mathcal{W} is formulated in an analogous manner and is one version of the discrete Haar wavelet transform – for details, see, e.g., [4]). Letting $\mathbf{w} = \mathcal{W}\mathbf{y}$ and letting $\{w_n\}$ denote the elements of \mathbf{w} , it follows that

$$\begin{aligned} w_1^2 + w_2^2 + w_3^2 + w_4^2 &= 4\hat{\sigma}_{y, \text{nono}}^2(1) \\ w_5^2 + w_6^2 &= 4\hat{\sigma}_{y, \text{nono}}^2(2) \\ w_7^2 &= 4\hat{\sigma}_{y, \text{nono}}^2(4) \\ w_8^2 &= 8\bar{y}^2 \end{aligned}$$

Because \mathcal{W} is an orthonormal transform, we must have $\|\mathbf{w}\|^2 = \|\mathbf{y}\|^2$, where $\|\mathbf{x}\|$ is the usual Euclidean norm of the vector \mathbf{x} . It follows that

$$\hat{\sigma}_y^2 \equiv \frac{1}{8} \sum_{n=1}^8 (y_n - \bar{y})^2 = \frac{1}{8} \sum_{n=1}^7 w_n^2 = \frac{1}{2} \sum_{j=0}^2 \hat{\sigma}_{y, \text{nono}}^2(2^j).$$

For general $N_y = 2^J$, the corresponding result is

$$\hat{\sigma}_y^2 = \frac{1}{2} \sum_{j=0}^{J-1} \hat{\sigma}_{y, \text{nono}}^2(2^j) \text{ or, equivalently, } \sum_{j=0}^{J-1} \hat{\sigma}_{y, \text{nono}}^2(2^j) = 2\hat{\sigma}_y^2;$$

i.e., summing the nonoverlapped Allan variance estimator over all dyadic averaging times less than or equal to $\frac{N_y}{2}$ yields exactly twice the sample variance (for additional details and some historical background, see Section III of [3]).

3 MAXIMAL OVERLAP ESTIMATORS OF THE ALLAN VARIANCE

The nonoverlapped estimator of the Allan variance is rarely used in practice because it does not take advantage of certain "information" regarding $\sigma_y^2(m)$. To see in what sense this is true, let us consider the form of the maximal overlap estimator for $m = 1$:

$$\hat{\sigma}_{y,\max}^2(1) = \frac{1}{2(N_y - 1)} \sum_{k=2}^{N_y} [y_k - y_{k-1}]^2.$$

Note that, whereas each y_n appears exactly once in the nonoverlapped estimator of Equation (1), the variables y_2, \dots, y_{N_y-1} appear twice because now, in addition to terms like $[y_2 - y_1]^2$, $[y_4 - y_3]^2$ and $[y_6 - y_5]^2$ that appear in $\hat{\sigma}_{y,\max}^2(1)$, the maximal overlap estimator also includes terms like $[y_3 - y_2]^2$ and $[y_5 - y_4]^2$. For general m the maximal overlap estimator takes the form

$$\hat{\sigma}_{y,\max}^2(m) = \frac{1}{2(N_y - 2m + 1)} \sum_{k=2m}^{N_y} [\bar{y}_k(m) - \bar{y}_{k-m}(m)]^2.$$

Even if we were to restrict the sample size N_y to be a power of two 2^J , it can be argued that in general

$$\sum_{j=0}^{J-1} \hat{\sigma}_{y,\max}^2(2^j) \neq 2\hat{\sigma}_y^2,$$

so the usual maximal overlap estimator does *not* constitute an analysis of twice the sample variance. There is, however, an interesting way to define a variation on the maximal overlap estimator that in fact does yield an exact analysis of variance, as the following argument shows.

We start with two filters $\{\tilde{h}_{0,l}\}$ and $\{\tilde{g}_{0,l}\}$ defined as follows:

$$\tilde{h}_{0,l} \equiv \begin{cases} \frac{1}{2}, & l = 0; \\ -\frac{1}{2}, & l = 1; \text{ and} \\ 0, & l < 0 \text{ or } l \geq 2; \end{cases} \quad \text{and} \quad \tilde{g}_{0,l} \equiv \begin{cases} \frac{1}{2}, & l = 0; \\ \frac{1}{2}, & l = 1; \text{ and} \\ 0, & l < 0 \text{ or } l \geq 2 \end{cases}$$

(in the wavelet literature, $\{\tilde{h}_{0,l}\}$ and $\{\tilde{g}_{0,l}\}$ are two versions of what are called the Haar wavelet and scaling filters – for details, see, e.g., [4]). Let $\tilde{H}_0(\cdot)$ and $\tilde{G}_0(\cdot)$ be the transfer functions for $\{\tilde{h}_{0,l}\}$ and $\{\tilde{g}_{0,l}\}$:

$$\tilde{H}_0(f) \equiv \sum_{l=-\infty}^{\infty} h_l e^{-i2\pi f l} = i e^{-i\pi f} \sin(\pi f) \quad \text{and} \quad \tilde{G}_0(f) \equiv \sum_{l=-\infty}^{\infty} g_l e^{-i2\pi f l} = e^{-i\pi f} \cos(\pi f);$$

i.e., $\tilde{H}_0(\cdot)$ is the discrete Fourier transform (DFT) of $\{\tilde{h}_{0,l}\}$. Note that we have

$$|\tilde{H}_0(f)|^2 + |\tilde{G}_0(f)|^2 = 1 \quad \text{for all } f. \quad (2)$$

We want to circularly filter $\{y_n\}$ separately using the filters $\{\tilde{h}_{0,l}\}$ and $\{\tilde{g}_{0,l}\}$. Formally, we do so by defining $\{\tilde{h}_{0,l}^\circ : l = 0, \dots, N_y - 1\}$ and $\{\tilde{g}_{0,l}^\circ : l = 0, \dots, N_y - 1\}$, which are said to be $\{\tilde{h}_{0,l}\}$ and $\{\tilde{g}_{0,l}\}$ periodized to length N_y . By definition,

$$\tilde{h}_{0,l}^\circ = \sum_{k=-\infty}^{\infty} \tilde{h}_{0,l+kN_y}, \quad l = 0, \dots, N_y - 1,$$

with a similar definition for $\{\tilde{g}_{0,l}^\circ\}$. If $N_y \geq 2$, we have

$$\tilde{h}_{0,l}^\circ \equiv \begin{cases} \frac{1}{2}, & l = 0; \\ -\frac{1}{2}, & l = 1; \text{ and} \\ 0, & 2 \leq l \leq N_y - 1; \end{cases} \quad \text{and} \quad \tilde{g}_{0,l}^\circ \equiv \begin{cases} \frac{1}{2}, & l = 0; \\ \frac{1}{2}, & l = 1; \text{ and} \\ 0, & 2 \leq l \leq N_y - 1; \end{cases}$$

if, however, $N_y = 1$ so that $\{\tilde{h}_{0,l}^\circ\}$ and $\{\tilde{g}_{0,l}^\circ\}$ each have but a single term, then $\tilde{h}_{0,0}^\circ = 0$ and $\tilde{g}_{0,0}^\circ = 1$. It is an easy exercise to show that the DFT of $\{\tilde{h}_{0,l}^\circ\}$ can be obtained by subsampling the DFT for $\{\tilde{h}_{0,l}\}$; i.e.,

$$\sum_{l=0}^{N_y-1} \tilde{h}_{0,l}^\circ e^{-i2\pi kl/N_y} = H_0\left(\frac{k}{N_y}\right), \quad k = 0, \dots, N_y - 1.$$

The finite sequences $\{\tilde{h}_{0,l}^\circ\}$ and $\{H_0(\frac{k}{N_y})\}$ thus constitute a Fourier transform pair, a relationship we will express as

$$\{\tilde{h}_{0,l}^\circ : l = 0, \dots, N_y - 1\} \longleftrightarrow \{H_0(\frac{k}{N_y}) : k = 0, \dots, N_y - 1\}.$$

Similarly we have

$$\{\tilde{g}_{0,l}^\circ : l = 0, \dots, N_y - 1\} \longleftrightarrow \{G_0(\frac{k}{N_y}) : k = 0, \dots, N_y - 1\}.$$

Let us now define

$$\tilde{w}_{0,n} \equiv \sum_{l=0}^{N_y-1} \tilde{h}_{0,l}^\circ y_{(n-l) \bmod N_y} \quad \text{and} \quad \tilde{v}_{0,n} \equiv \sum_{l=0}^{N_y-1} \tilde{g}_{0,l}^\circ y_{(n-l) \bmod N_y}, \quad n = 1, \dots, N_y,$$

where we define $n \bmod N_y$ to be n if $1 \leq n \leq N_y$ and to be $n + kN_y$ otherwise, where k is the unique nonzero integer such that $1 \leq n + kN_y \leq N_y$ (thus $-1 \bmod N_y = N_y - 1$; $0 \bmod N_y = N_y$; $1 \bmod N_y = 1$; \dots ; $N_y \bmod N_y = N_y$; $N_y + 1 \bmod N_y = 1$; etc.). By construction we have

$$\frac{2}{N_y - 1} \sum_{n=2}^{N_y} \tilde{w}_{0,n}^2 = \hat{\sigma}_{y,\max}^2(1); \quad (3)$$

i.e., we have expressed the maximal overlap estimator of the Allan variance for $m = 1$ in terms of a sum of squares of the output from circular filtering $\{y_n\}$ with $\{\tilde{h}_{0,l}^\circ\}$.

An important point to note is that $\hat{\sigma}_{y,\max}^2(1)$ does not involve the entire output from the filter: it is missing $\tilde{w}_{0,1} \propto y_{N_y} - y_1$, which is the only term that explicitly makes use of the circularity assumption. Inclusion of this term is one of the two keys to defining a version of the maximal overlap estimator that constitutes an analysis of variance. The other key is to recognize that $\hat{\sigma}_{y,\max}^2(2^j)$ for $j = 1, 2, \dots$ can be obtained by further filtering of $\{\tilde{w}_{0,n}\}$ so that, whereas $\{\tilde{w}_{0,n}\}$ contains information about the variations of $\{y_n\}$ at τ_0 averaging times, the series $\{\tilde{v}_{0,n}\}$ contains information about variations of $\{y_n\}$ at all dyadic averaging times higher than τ_0 (i.e., $2\tau_0$, $4\tau_0$, etc.). Accordingly, let \tilde{w}_0 be an N_y dimensional vector whose elements are $\{\tilde{w}_{0,n}\}$, and define \tilde{v}_0 to contain $\{\tilde{v}_{0,n}\}$. Letting $\{\mathcal{Y}_k\}$ be the DFT of $\{y_n\}$, we have (from a standard theorem in filtering theory)

$$\{\tilde{w}_{0,n}\} \longleftrightarrow \{\tilde{H}_0(\frac{k}{N_y})\mathcal{Y}_k\} \quad \text{and} \quad \{\tilde{v}_{0,n}\} \longleftrightarrow \{\tilde{G}_0(\frac{k}{N_y})\mathcal{Y}_k\}.$$

Parseval's theorem tells us that

$$\|\tilde{w}_0\|^2 = \frac{1}{N} \sum_{k=0}^{N_y-1} |\tilde{H}_0(\frac{k}{N_y})|^2 |\mathcal{Y}_k|^2 \text{ and } \|\tilde{v}_0\|^2 = \frac{1}{N} \sum_{k=0}^{N_y-1} |\tilde{G}_0(\frac{k}{N_y})|^2 |\mathcal{Y}_k|^2,$$

which in turn yields

$$\|\tilde{w}_0\|^2 + \|\tilde{v}_0\|^2 = \frac{1}{N} \sum_{k=0}^{N_y-1} |\mathcal{Y}_k|^2 \left(|\tilde{H}_0(\frac{k}{N_y})|^2 + |\tilde{G}_0(\frac{k}{N_y})|^2 \right) = \frac{1}{N} \sum_{k=0}^{N_y-1} |\mathcal{Y}_k|^2 = \|\tilde{y}\|^2,$$

where we have made use of Equation (2) and a second application of Parseval's theorem.

Let us now define the following estimator of the Allan variance for $m = 1$:

$$\tilde{\sigma}_{y,\max}^2(1) \equiv \frac{2}{N_y} \sum_{n=1}^{N_y} \tilde{w}_{0,n}^2 = \frac{2}{N_y} \|\tilde{w}_0\|^2.$$

We refer to this estimator as the biased maximal overlap estimator of $\sigma_y^2(1)$ based on $\{y_n\}$. It differs from the standard maximal overlap estimator (Equation (3)) because of an additional term proportional to $(y_{N_y} - y_1)^2$. Although this estimator is in general a biased estimator of the true Allan variance, it is in fact unbiased when $\{y_n\}$ is a white noise process. It satisfies the analysis of variance condition

$$\tilde{\sigma}_{y,\max}^2(1) + \tilde{\eta}_{y,\max}^2(2) = 2\hat{\sigma}_y^2, \text{ where } \tilde{\eta}_{y,\max}^2(2) \equiv \frac{2}{N_y} \|\tilde{v}_0\|^2 - 2\bar{y}^2.$$

We can regard the second piece of the decomposition $\tilde{\eta}_{y,\max}^2(2)$ as being related to variations in $\{y_n\}$ at dyadic averaging times of 2 and greater.

Just as $\{y_n\}$ was split into the components $\{\tilde{w}_{0,n}\}$ and $\{\tilde{v}_{0,n}\}$, we now split $\{\tilde{v}_{0,n}\}$ into two components, namely, $\{\tilde{w}_{1,n}\}$ and $\{\tilde{v}_{1,n}\}$. The first component $\{\tilde{w}_{1,n}\}$ will be used to construct an estimator of $\sigma_y^2(2)$, while the second component is related to variations in $\{y_n\}$ at dyadic averaging times of 4 and greater. The filters that accomplish the desired split are N_y -periodized versions of ones whose transfer functions are defined by $\tilde{H}_0(2f)$ and $\tilde{G}_0(2f)$ – the impulse response sequence for these filters can be formed by taking the original filters $\{\tilde{h}_{0,l}\}$ and $\{\tilde{g}_{0,l}\}$ and inserting a single zero after each element, a procedure that is known as upsampling in the engineering literature [4]. For example, since the $l = 0, 1, 2, 3$ and 4 values of the impulse response sequence for $\tilde{H}_0(f)$ are given by $\frac{1}{2}, -\frac{1}{2}, 0, 0$ and 0, the corresponding values for $\tilde{H}_0(2f)$ are given by $\frac{1}{2}, 0, -\frac{1}{2}, 0$ and 0. We can also obtain $\{\tilde{w}_{1,n}\}$ and $\{\tilde{v}_{1,n}\}$ by directly filtering $\{y_n\}$:

$$\tilde{w}_{1,n} = \sum_{l=0}^{N_y-1} \tilde{h}_{1,l}^\circ y_{(n-l) \bmod N_y} \text{ and } \tilde{v}_{1,n} = \sum_{l=0}^{N_y-1} \tilde{g}_{1,l}^\circ y_{(n-l) \bmod N_y}, \quad n = 1, \dots, N_y,$$

where $\{\tilde{h}_{1,l}^\circ\}$ is the circular filter such that

$$\{\tilde{h}_{1,l}^\circ\} \longleftrightarrow \{\tilde{H}_0(\frac{2k}{N_y})\tilde{G}_0(\frac{k}{N_y})\}; \text{ likewise, } \{\tilde{g}_{1,l}^\circ\} \longleftrightarrow \{\tilde{G}_0(\frac{2k}{N_y})\tilde{G}_0(\frac{k}{N_y})\}.$$

Note that the impulse response sequence for $\{\tilde{h}_{1,l}^\circ\}$ is the circular convolution of the impulse response sequence for $\tilde{G}_0(\frac{k}{N_y})$ and $\tilde{H}_0(\frac{2k}{N_y})$, i.e., $\frac{1}{2}, \frac{1}{2}, 0, \dots$ convolved with $\frac{1}{2}, 0, -\frac{1}{2}, 0$, which

yields $\frac{1}{4}, \frac{1}{4}, -\frac{1}{4}, -\frac{1}{4}, 0, \dots$ (as long as $N_y > 4$). This latter filter is seen to be proportional to the filtering operation commonly used in estimates of $\sigma_y^2(2)$.

Define \tilde{w}_1 as the N_y dimensional vector containing $\{\tilde{w}_{1,n}\}$, and let \tilde{v}_1 contain $\{\tilde{v}_{1,n}\}$. By a simple variation on the argument used to establish $\|\tilde{w}_0\|^2 + \|\tilde{v}_0\|^2 = \|\tilde{y}\|^2$, we have

$$\|\tilde{w}_1\|^2 + \|\tilde{v}_1\|^2 = \|\tilde{v}_0\|^2.$$

Now define the following estimator of the Allan variance for $m = 2$:

$$\tilde{\sigma}_{y,\max}^2(2) \equiv \frac{2}{N_y} \sum_{n=1}^{N_y} \tilde{w}_{1,n}^2 = \frac{2}{N_y} \|\tilde{w}_1\|^2.$$

This is the standard maximal overlap estimator with three additional terms – these are proportional to $(y_1 + y_{N_y} - y_{N_y-2} - y_{N_y-1})^2$, $(y_1 + y_2 - y_{N_y-1} - y_{N_y})^2$ and $(y_2 + y_3 - y_1 - y_{N_y})^2$. In general this estimator is a biased estimator of $\sigma_y^2(2)$. We have the analysis of variance condition

$$\tilde{\sigma}_{y,\max}^2(1) + \tilde{\sigma}_{y,\max}^2(2) + \tilde{\eta}_{y,\max}^2(4) = 2\hat{\sigma}_y^2, \text{ where } \tilde{\eta}_{y,\max}^2(4) \equiv \frac{2}{N_y} \|\tilde{v}_1\|^2 - 2\bar{y}^2.$$

We can now state the result for general J , a proof of which follows from an easy inductive argument. We define

$$\tilde{w}_{j,n} = \sum_{l=0}^{N_y-1} \tilde{h}_{j,l}^\circ y_{(n-l) \bmod N_y} \text{ and } \tilde{v}_{j,n} = \sum_{l=0}^{N_y-1} \tilde{g}_{j,l}^\circ y_{(n-l) \bmod N_y}, \quad n = 1, \dots, N_y,$$

where

$$\{\tilde{h}_{j,l}^\circ\} \longleftrightarrow \{\tilde{H}_0(\frac{2^j k}{N_y}) \tilde{G}_0(\frac{2^{j-1} k}{N_y}) \tilde{G}_0(\frac{2^{j-2} k}{N_y}) \dots \tilde{G}_0(\frac{k}{N_y})\}$$

and

$$\{\tilde{g}_{j,l}^\circ\} \longleftrightarrow \{\tilde{G}_0(\frac{2^j k}{N_y}) \tilde{G}_0(\frac{2^{j-1} k}{N_y}) \tilde{G}_0(\frac{2^{j-2} k}{N_y}) \dots \tilde{G}_0(\frac{k}{N_y})\}.$$

An inductive argument can be used to show that $\{\tilde{h}_{j,l}^\circ\}$ is the usual filter involved in estimating $\sigma_y^2(2^j)$. Letting \tilde{w}_j and \tilde{v}_j be N_y dimensional vectors containing $\{\tilde{w}_{j,n}\}$ and $\{\tilde{v}_{j,n}\}$, define

$$\tilde{\sigma}_{y,\max}^2(2^j) \equiv \frac{2}{N_y} \sum_{n=1}^{N_y} \tilde{w}_{j,n}^2 = \frac{2}{N_y} \|\tilde{w}_j\|^2,$$

which is the biased maximal overlap estimator of $\sigma_y^2(2^j)$ based upon $\{y_n\}$ – it differs from the standard maximal overlap estimator due to $2^{j+1} - 1$ additional terms involving explicit circular use of $\{y_n\}$. For any J , the biased maximal overlap estimators satisfy the analysis of variance condition

$$\sum_{j=0}^J \tilde{\sigma}_{y,\max}^2(2^j) + \tilde{\eta}_{y,\max}^2(2^{J+1}) = 2\hat{\sigma}_y^2 \text{ with } \tilde{\eta}_{y,\max}^2(2^{J+1}) \equiv \frac{2}{N_y} \|\tilde{v}_J\|^2 - 2\bar{y}^2,$$

where the term $\tilde{\eta}_{y,\max}^2(2^{J+1})$ represents variations in $\{y_n\}$ at dyadic averaging times of 2^{J+1} and greater.

4 ESTIMATION OF THE ALLAN VARIANCE USING A CIRCULARIZED SERIES

For most models for $\{y_n\}$ of interest for actual frequency standards, a circularity assumption can yield an unacceptably large bias in the estimator $\hat{\sigma}_{y,\max}^2(2^j)$ due to the fact that y_1 and y_{N_y} can be quite different. To solve this problem, we construct a series $\{y_n^*\}$ of length $2N_y$

$$y_n^* \equiv \begin{cases} y_n, & 1 \leq n \leq N_y; \text{ and} \\ y_{2N_y+1-n}, & N_y + 1 \leq n \leq 2N_y. \end{cases}$$

For example, if $N_y = 3$ so that only y_1, y_2 and y_3 are observed, the values of y_1^*, \dots, y_6^* are given, respectively, by $y_1, y_2, y_3, y_3, y_2, y_1$. Note that, by construction, the sample mean and variance of $\{y_n\}$ and $\{y_n^*\}$ are identical. We now apply the estimation procedure of Section 3 to $\{y_n^*\}$ to obtain the following estimator of $\sigma_y^2(2^j)$:

$$\hat{\sigma}_{y^*,\max}^2(2^j) \equiv \frac{1}{N_y} \|\tilde{w}_j^*\|^2,$$

where \tilde{w}_j^* is a vector of length $2N_y$ formed by circularly filtering $\{y_n^*\}$ with the circular filter of length $2N_y$ whose DFT is given by

$$\tilde{H}_0\left(\frac{2^j k}{2N_y}\right) \tilde{G}_0\left(\frac{2^{j-1} k}{2N_y}\right) \tilde{G}_0\left(\frac{2^{j-2} k}{2N_y}\right) \dots \tilde{G}_0\left(\frac{k}{2N_y}\right), \quad k = 0, \dots, 2N_y - 1.$$

We refer to $\hat{\sigma}_{y^*,\max}^2(2^j)$ as the biased maximal overlap estimator of $\sigma_y^2(2^j)$ based on the circularized series $\{y_n^*\}$ (note, however, that this estimator is in fact unbiased for the special case where $\{y_n\}$ is a white noise process). This biased estimator satisfies the following analysis of variance condition for all J and all sample sizes N_y :

$$\sum_{j=0}^J \hat{\sigma}_{y^*,\max}^2(2^j) + \tilde{\eta}_{y^*,\max}^2(2^{J+1}) = 2\hat{\sigma}_y^2, \quad \text{where } \tilde{\eta}_{y^*,\max}^2(2^{J+1}) \equiv \frac{2}{N_y} \|\tilde{w}_J^*\|^2 - 2\bar{y}^2.$$

Finally we note that there is a very simple relationship between $\hat{\sigma}_{y^*,\max}^2(2^j)$ and Totvar estimator (Greenhall, 1997, private communication):

$$\text{Totvar}(2^j, N_y, \tau_0) = \frac{N_y}{N_y - 1} \hat{\sigma}_{y^*,\max}^2(2^j),$$

where Totvar is defined as in Equation (4) of Howe and Greenhall [1].

5 SUMMARY AND COMMENTS

We have developed a relationship between the sample variance $\hat{\sigma}_y^2$ and the Totvar estimator $\text{Totvar}(m, N_y, \tau_0)$ of the Allan variance $\sigma_y^2(m)$, where m sets the averaging time $m\tau_0$, N_y is the number of τ_0 -average fractional frequency deviates $\{y_n\}$, and τ_0 is the basic sampling and averaging time of the observed deviates. For any sample size N_y and any positive integer J , we have demonstrated that

$$\frac{N_y - 1}{N_y} \sum_{j=0}^J \text{Totvar}(2^j, N_y, \tau_0) + \tilde{\eta}_{y^*,\max}^2(2^{J+1}) = 2\hat{\sigma}_y^2,$$

where $\hat{\eta}_{y,\max}^2(2^{J+1})$ can be interpreted in terms of variations in $\{y_n\}$ at all dyadic averaging times greater than 2^J . We have also shown that the Totvar estimator is related to a biased maximal overlap estimator of the Allan variance that is based upon $\{y_n^*\}$, which is a sequence of length $2N_y$ formed by tacking onto $\{y_n\}$ a reversed version of itself.

In closing, we make the following comments about our results, some of which will be expanded upon in future research.

- It can be shown that, if $\{y_n\}$ is a portion of a realization of a stationary or nonstationary process $\{Y_n\}$ for which the Allan variance is well-defined, then we have

$$\sum_{j=0}^{\infty} \sigma_y^2(2^j) = 2\sigma_y^2,$$

where σ_y^2 is the process variance of $\{Y_n\}$ (this is taken to be infinite if $\{Y_n\}$ is nonstationary). The $\hat{\sigma}_{y,\max}^2(2^j)$ estimator is the first "modern" estimator of the Allan variance to mimic this important property.

- Because higher order Daubechies wavelet filters also satisfy Equation (2), the above development extends trivially to higher order wavelet variances (the Allan variance is essentially twice the Haar wavelet variance). These higher order wavelet variances are suitable substitutes for some of the variations on the Allan variance that have been proposed and studied in the literature (an example is the modified Allan variance). For details, see [2].
- In addition to plotting $\hat{\sigma}_{y,\max}^2(2^j)$ versus $2^j\tau_0$ on a log-log scale, we suggest that $\hat{\eta}_{y,\max}^2(2^{J+1})$ be plotted (with a separate symbol) versus $2^{J+1}\tau_0$ – this will indicate how much of $2\hat{\sigma}_y^2$ has not been accounted for by estimates of the Allan variance.
- In theory J can be made as large as desired, but there will be serious biases in $\hat{\sigma}_{y,\max}^2(2^J)$ for any J such that $2^J > N_y$. Because of its close relationship to Totvar, the results of Howe and Greenhall [1] indicate that $\hat{\sigma}_{y,\max}^2(2^j)$ outperforms traditional estimators of the Allan variance for averaging times close to $\frac{N_y}{2}$.

References

- [1] D. A. Howe and C. A. Greenhall 1998, "Total Variance: a Progress Report on a New Frequency Stability Characterization," 29th PTTI Meeting, these Proceedings.
- [2] D. A. Howe and D. B. Percival 1995, "Wavelet Variance, Allan Variance, and Leakage," IEEE Trans. Instrum. Meas. IM-44, 94–97.
- [3] D. B. Percival 1991, "Characterization of Frequency Stability: Frequency-Domain Estimation of Stability Measures," Proc. IEEE 79, 961–972.
- [4] M. Vetterli and J. Kovačević 1995, Wavelets and Subband Coding (Englewood Cliffs, New Jersey: Prentice Hall).

NARROW-BAND SEARCHES FOR GRAVITATIONAL RADIATION WITH SPACECRAFT DOPPLER TRACKING

Massimo Tinto and J. W. Armstrong
Jet Propulsion Laboratory, California Institute of Technology
Pasadena, California 91109

Abstract

We discuss a filtering technique for reducing the two-way Doppler frequency fluctuations of noise sources localized in space (like the troposphere, or the master clock) that affect the sensitivity of spacecraft Doppler tracking searches for gravitational radiation. This method takes advantage of the sinusoidal behavior of the transfer function to the Doppler observable of these noise sources, which displays sharp nulls at selected Fourier components.

The non-zero gravitational wave signal remaining at these frequencies makes this Doppler tracking technique the equivalent of a series of narrow-band detectors of gravitational radiation^[1], distributed across the low-frequency band. Estimates for the sensitivities achievable with the future Cassini Doppler tracking experiments are presented in the context of broad-band gravitational wave bursts, monochromatic signals, and a stochastic background of gravitational radiation^[2].

INTRODUCTION

Doppler tracking of interplanetary spacecraft is the only existing technique that allows searches for gravitational radiation in the millihertz frequency region.^[3] The frequency fluctuations induced by the intervening media have severely limited the sensitivities of these experiments. Among all the propagation noise sources (ionosphere, troposphere, interplanetary plasma) observed at high radio frequencies, the troposphere is the largest and the hardest to calibrate to a reasonably low level. The frequency fluctuations due this noise source have been observed with water vapor radiometers to be a few parts in 10^{-14} at 1000 seconds integration time^[4].

Mechanical vibrations of the ground antenna also introduce frequency fluctuations in the Doppler data, and in some occasions represent the limits in the sensitivity of these gravitational wave experiments. Recent frequency stability measurements performed on the antenna of the Deep Space Network (DSN) that will track the Cassini spacecraft at Ka-Band

(32 GHz), indicate that the frequency fluctuations it introduces are as large as 3.0×10^{-15} at 1000 seconds integration time.^[5] This number is comparable to the requirement in frequency stability requested by the experimenters for the overall performance of the DSN during the Cassini gravitational wave experiments at Ka-Band. Although work is in progress to identify the causes of this performance, it might turn out to be intrinsically impossible to compensate or calibrate the mechanical vibrations of the antenna.

In order to minimize the effects of the troposphere, ionosphere, and of the ground antenna in the Doppler data, it was first pointed out by Estabrook^[6] that the explicit transfer function to the Doppler observable of, for example, tropospheric and antenna mechanical noise are sinusoidal, and therefore their magnitudes can be reduced at selected Fourier frequencies. In this paper we show how this modulation of the noise spectrum can be exploited in a very robust way when these noise sources are the limiting ones. As a specific example we will estimate the sensitivity to gravitational radiation that Doppler tracking data from Cassini will be able to identify by using this narrow-banding technique. Cassini will take advantage of a multilink radio system for removing the frequency fluctuations introduced by the interplanetary plasma in the Doppler data, and its Doppler sensitivity to gravitational radiation could be limited by the frequency fluctuations introduced by the ground antenna.

THE TWO-WAY DOPPLER RESPONSE

In the Doppler tracking technique, the Earth and an interplanetary spacecraft act as free test masses. The Doppler tracking system continuously measures their relative dimensionless velocity, $\Delta v/c = \Delta \nu/\nu_0$ (here Δv is the relative velocity, $\Delta \nu$ is the Doppler frequency fluctuation, and ν_0 is the nominal frequency of the microwave link). A gravitational wave of strain amplitude $h(t)$ incident on the system causes small perturbations in the Doppler time series of $\Delta \nu(t)/\nu_0$. These perturbations are of order h and are replicated three times in the tracking record with a characteristic pattern that depends on the source-Earth-spacecraft angle^[3]. These three events in the time series can be thought of as due to the gravitational wave buffeting the Earth, the spacecraft, and the original Earth buffeting event transponded back to the Earth at a time $2L/c$ later, where we have denoted with L the distance between the Earth and the spacecraft, and c is the speed of light. The sum of these three Doppler perturbations is zero. This overlap of the three events, and partial cancellation, occurs for gravitational wave pulses having widths larger than about L/c .

Detection of gravitational wave signals in this millihertz band is complicated by various noises. The principal noise sources are^[4,5,7]: ground electronics noise (including frequency standard and frequency distribution noise), antenna mechanical noise (unmodeled motion of the antenna), thermal noise (finite signal-to-noise ratio on the radio links), spacecraft noise (electronics and unmodeled motion of the spacecraft), and propagation noise (phase scintillation as the radio beams pass through irregularities in the troposphere, ionosphere,

and the solar wind). Electronic and thermal noises can be made very small, and propagation noises can be mitigated through use of higher or multiple radio frequencies to suppress or remove entirely charged particle scintillation, and by employing water vapor radiometers to measure tropospheric scintillation. Residual uncalibrated troposphere and antenna mechanical noise are expected to be leading noise sources in the future Cassini gravitational wave experiment^[9].

If we introduce a set of Cartesian orthogonal coordinates (X, Y, Z) in which the wave is propagating along the Z -axis and (X, Y) are two orthogonal axes in the plane of the wave, then the Doppler response at time t can be written in the following form^[1,3,4]

$$\begin{aligned} y(t) \equiv \left(\frac{\Delta\nu(t)}{\nu_0} \right) = & -\frac{(1-\mu)}{2} h(t) - \mu h(t - (1+\mu)L) + \frac{(1+\mu)}{2} h(t - 2L) \\ & + C(t-2L) - C(t) + 2B(t-L) + T(t-2L) + T(t) \\ & + A_E(t-2L) + A_{sc}(t-L) + TR(t-L) + EL(t) + P(t), \quad (1) \end{aligned}$$

where $h(t)$ is equal to

$$h(t) = h_+(t) \cos(2\phi) + h_x(t) \sin(2\phi). \quad (2)$$

Here $h_+(t)$, $h_x(t)$ are the wave's two amplitudes with respect to the (X, Y) axis, (θ, ϕ) are the polar angles describing the location of the spacecraft with respect to the (X, Y, Z) coordinates, μ is equal to $\cos \theta$, and L is the distance to the spacecraft (units in which the speed of light $c = 1$).

We have denoted by $C(t)$ the random process associated with the frequency fluctuations of the clock on the Earth, $B(t)$ the joint effect of the noise from buffeting of the probe by non-gravitational forces and from the antenna of the spacecraft, $T(t)$ the joint frequency fluctuations due to the troposphere, ionosphere and ground antenna, $A_E(t)$ the noise of the radio transmitter on the ground, $A_{sc}(t)$ the noise of the radio transmitter on board, $TR(t)$ the noise due to the spacecraft transponder, $EL(t)$ the noise from the electronics on the ground, and $P(t)$ the fluctuations due to the interplanetary plasma. Since the frequency fluctuations induced by the plasma are, to first order, inversely proportional to the square of the radio frequency, by using high frequency radio signals or by monitoring two different radio frequencies transmitted to the spacecraft and coherently transmitted back to Earth, this noise source can be suppressed to very low levels or entirely removed from the data respectively.^[10]

From Eq. (1) we deduce that gravitational wave pulses of duration longer than the round-trip light time $2L$ give a Doppler response $y(t)$ that, to first order, tends to zero. The tracking system essentially acts as a pass-band device, in which the low-frequency limit f_l is roughly equal to $(2L)^{-1}$ Hz, and the high-frequency limit f_H is set by the thermal noise in the receiver. Since the reference clock and some electronic components are most stable at integration times around 1000 seconds, Doppler tracking experiments are performed when the distance to the spacecraft is of the order of a few Astronomical Units. This sets the

value of f_l for a typical experiment to about 10^{-4} Hz, while the thermal noise gives an f_H of about 3×10^{-2} Hz.

It is important to note the characteristic time signatures of the clock noise $C(t)$, of the probe antenna and buffeting noise $B(t)$, of the troposphere, ionosphere, and ground antenna noise $T(t)$, and the transmitters $A_E(t)$, $A_{sc}(t)$. The time signature of the clock noise can be understood by observing that the frequency of the signal received at time t contains clock fluctuations transmitted $2L$ seconds earlier. By subtracting from the received frequency the frequency of the radio signal transmitted at time t , we also subtract clock frequency fluctuations^[1,3,4] with the net result shown in Eq. (1).

As far as the fluctuations due to the troposphere, ionosphere, and ground antenna are concerned, the frequency of the received signal is affected at the moment of reception, as well as $2L$ seconds earlier. Since the frequency of the signal generated at time t does not contain yet any of these fluctuations, we conclude that $T(t)$ is positive-correlated at the round trip light time $2L$ ^[1,4]. The time signature of the noises $B(t)$, $A_E(t)$, $A_{sc}(t)$, and $TR_{sc}(t)$ in Eq. (1) can be understood through similar considerations.

If we denote with $\tilde{y}(f)$ the Fourier transform of the Doppler response $y(t)$

$$\tilde{y}(f) = \int_{-\infty}^{\infty} y(t) e^{2\pi i f t} dt, \quad (3)$$

we can rewrite Eq. (1) in the Fourier domain as follows

$$\begin{aligned} \tilde{y}(f) = & \left[-\frac{(1-\mu)}{2} - \mu e^{2\pi i f(1+\mu)L} + \frac{(1+\mu)}{2} e^{4\pi i f L} \right] \tilde{h}(f) + \tilde{C}(f) [e^{4\pi i f L} - 1] \\ & + \tilde{T}(f) [e^{4\pi i f L} + 1] + 2\tilde{B}(f) e^{2\pi i f L} + [\tilde{A}_{sc}(f) + \tilde{TR}(f)] e^{2\pi i f L} \\ & + \tilde{A}_E(f) e^{4\pi i f L} + \tilde{EL}(f) + \tilde{P}(f). \end{aligned} \quad (4)$$

If the noise due to the troposphere, ionosphere, and mechanical vibrations, T , will dominate over the remaining noise sources, as it might be the case during the Cassini experiments, then the spectra of the noise will appear modulated, and will display minima at the following frequencies

$$f_k = \frac{(2k-1)}{4L}; \quad k = 1, 2, 3, \dots \quad (5)$$

At these frequencies Eq. (4) can be rewritten in the following approximate form^[1,2]

$$\begin{aligned} \tilde{y}(f_k) \approx & [-1 + i(-1)^k \mu e^{\frac{\pi}{2} i (2k-1) \mu}] \tilde{h}(f_k) - 2\tilde{C}(f_k) + \tilde{T}(f_k)(\pi i L \Delta f) + \\ & + i(-1)^{k+1} [2\tilde{B}(f_k) + \tilde{TR}(f_k) + \tilde{A}_{sc}(f_k)] - \tilde{A}_E(f_k) + \tilde{EL}(f_k) + \tilde{P}(f_k) \end{aligned} \quad (6)$$

where Δf is the frequency resolution in the Fourier domain.

For current generation precision Doppler experiments, utilizing approximately 8 GHz radio links, observations in the anti-solar hemisphere have significant contributions from tropospheric and extended solar wind scintillation, while ionospheric, frequency standard, and antenna mechanical noise are secondary disturbances in the Doppler link.^[4] As an example, in Figure 1 we show the temporal autocorrelation function of 10-second time resolution Mars Global Surveyor (*MGS*) data taken on April 17, 1997, when the two-way light time $2L/c$ was equal to 504 seconds. The clear positive correlation at time lag of 504 seconds indicates that tropospheric scintillation and fluctuations induced by mechanical vibrations of the ground antenna dominate the noise on this data set.

The inset plot in Figure 1 shows the power spectrum of the *MGS* data, with frequency scale marked in units of $1/2L$. No smoothing of the spectrum has been done and much of its spikiness is due to estimation error.^[11] The cosine-squared modulation is however evident, showing that there are nulls at odd multiples of $1/(4L)$. At these frequencies, fluctuations from other noise sources will dominate the power spectrum. If the spectral level of these secondary noises is low, there is a potentially large improvement in SNR for gravitational wave signals having Fourier power at the nulls of the troposphere/antenna mechanical transfer function. In its simplest form, filtering the data to pass a comb of narrow bands centered on the nulls of the cosine-squared transfer function blocks the troposphere/antenna mechanical noise while passing gravity wave power at these frequencies. This is robust, in that nothing needs to be known about the signal except that it (by hypothesis) has power at odd multiples of $1/(4L)$.

In Figure 2 we plot the estimated one-sided power spectrum of the noise that will affect the Cassini Doppler data in its frequency band of observation. The lower curve represents the configuration in which eighty percent of the noise due to the troposphere is calibrated out by means of water vapor radiometry, while the upper curve corresponds to the configuration without calibration of the troposphere. Note that the minima of both curves coincide at the nulls of the transfer function of the random process T .

We should point out that, in order to derive the Fourier transform of the Doppler response in Eq. (6), we have assumed the distance to the spacecraft to be constant during the duration of the experiment. In the case of the *MGS* experiment we have found that we could integrate coherently over a time scale equal to about eight hours, before the frequencies f_k would change by an amount larger than the frequency resolution Δf . For the Cassini trajectory instead the integration time can be extended to the entire duration (forty days) of the experiments. This can be seen by considering the time dependence of the ranging to Cassini, $L(t)$, during the gravitational wave experiments. For the three experiment opportunities, $L(t)$ can be represented quite accurately by a quadratic expression^[12]

$$\begin{aligned}
L(t) &= a + bt + ct^2 \\
a &= 2.9 \times 10^3 \text{ sec} \\
b &= -1.4 \times 10^{-5} \\
c &= 1.1 \times 10^{-11} \text{ Hz}
\end{aligned} \tag{7}$$

where the numerical values of the coefficients a, b, c correspond to the first Cassini gravitational wave experiment. Since the variation δf of the frequencies f_k is determined by the time derivative $\dot{L}(t)$, from Eq. (7) we find that

$$\dot{L}(\tau) = \frac{\delta f}{f_1} = 6.3 \times 10^{-5} < \frac{1}{(\tau f_1)} = \frac{\Delta f}{f_1} = 4.8 \times 10^{-3}, \tag{8}$$

where τ is the integration time, which we have assumed to be equal to about 14 days. We have calculated the right-hand side of Eq. (8) also for the remaining two Cassini oppositions and we have found that the maximum variation of the frequencies f_k due to the change of the spacecraft distance is smaller than the frequency resolution Δf .

SENSITIVITIES WITH CASSINI

From the plot given in Figure 2 of the estimated one-sided power spectral density of the noise affecting the Cassini Doppler data, we can calculate the root-mean-squared (r.m.s.) noise level $\sigma(f_k)$ of the frequency fluctuations in the bins of width Δf , around the frequencies f_k ($k = 1, 2, 3, \dots$). This is given by the following expression

$$\sigma(f_k) = [S_y(f_k) \Delta f]^{1/2}, \quad k = 1, 2, 3, \dots, \tag{9}$$

where $S_y(f_k)$ is the one-sided power spectral density of the noise sources in the Doppler response $y(t)$ at the frequency f_k as given in Figure 2.

This measure of the Doppler sensitivity is appropriate for sinusoidal or stochastic gravitational wave signals, while it probably overestimates the sensitivity to bursts. A detailed and quantitative analysis for various burst waveforms will be investigated in a forthcoming paper. Here we will rely on the quantitative results implied by the formula given in Eq. (9), keeping in mind the considerations made.

In Figure 3 we plot the sensitivity curve achievable with this technique when applied to the Cassini Doppler data during the first solar opposition, when the distance to the spacecraft is about $L = 5.5$ AU. The corresponding fundamental frequency f_0 is equal to 4.5×10^{-5} Hz. We also assume an integration time of about 14 days, since only one of the three DSN complexes will have the capability of supporting simultaneous transmission and reception of

X and K_a band signals. In the assumption of calibrating entirely the plasma noise with the use of dual frequencies, at $f_0 = 4.5 \times 10^{-5}$ we find a sensitivity equal to about 2.0×10^{-16} . The best sensitivity is however achieved at about 2.0×10^{-3} , at a level of about 5.0×10^{-17} .

CONCLUSIONS

The main result of our analysis shows that, during searches for gravitational radiation, it is possible to reduce the effects of the troposphere, ionosphere, and mechanical vibrations of the ground antenna at selected Fourier components of the power spectrum of two-way Doppler tracking data. A sensitivity equal to about 5.0×10^{-17} at a frequency of 2.0×10^{-3} has been estimated for the future Cassini gravitational wave experiments, which will first be performed in December 2001.

The experimental technique presented in this paper can be extended to a configuration with two spacecraft tracking each other through microwave or laser links. Future space-based laser interferometric detectors of gravitational waves^[13], for instance, could implement this technique as a backup option, if failure of some of their components would make the normal interferometric operation impossible.

ACKNOWLEDGEMENTS

This work was performed at the Jet Propulsion Laboratory, California Institute of Technology, under a contract with the National Aeronautics and Space Administration.

REFERENCES

- [1] M. Tinto, *Phys. Rev. D*, **53**, 5354 (1996).
- [2] M. Tinto and John W. Armstrong, *Phys. Rev. D*. In preparation.
- [3] F.B. Estabrook and H.D. Wahlquist, *Gen. Rel. Grav.* **6**, 439 (1975).
- [4] J.W. Armstrong In: *Gravitational Wave Data Analysis*, ed. B.F. Schutz (Dordrecht:Kluwer), (1989). See in particular S.J. Keihm, *TDA Progress Report*, **42-122**, 1 (1995).
- [5] M. Gatti, M. Tinto, G. Morris, R. Perez, S. Petty, P. Cramer, P. Kuhnle, M. Gudim, D. Rogstad, L. Riley, and M. Marina. *Cassini Radio Science Ground System Cost and Schedule Review* Pasadena, California, (unpublished) (1997).
- [6] F. B. Estabrook In: *A close-up to the Sun*, eds. M. Neugebauer and R.W. Davis, JPL Publication 78-70 (1978).
- [7] H.D. Wahlquist: *Search for Low-Frequency Gravitational Waves using the Cassini Radio Science System Facility*, Cassini Project, JPL (1990) (unpublished). See also H.D.

Wahlquist, J.D. Anderson, F.B. Estabrook, and K.S. Thorne. *Atti dei Convegni dei Lincei*, **34**, 335 (1977).

[8] F.B. Estabrook: *Proposal for Participation on Radio Science/Celestial Mechanics Team for an Investigation of Gravitational Radiation*, Galileo Project, JPL (1976) (unpublished). See also F.B. Estabrook, R.W. Hellings, H.D. Wahlquist, J.D. Anderson, and R.S. Wolff. In: *Sources of Gravitational Radiation*, ed. L. Smarr (Cambridge University Press, Cambridge, 1979).

[9] T.K. Peng, J.W. Armstrong, J.C. Breidenthal, F.F. Donovan, and N.C. Ham, *Acta Astronautica*, **17**, 321 (1988).

[10] B. Bertotti, G. Comoretto, and L. Iess, *Astron. Astrophys.*, **269**, 608 (1993).

[11] G.M. Jenkins and D.G. Watts, *Spectral Analysis and Its Applications*, (Holden-day, San Francisco) (1968).

[12] Cassini Mission Plan Document, JPL Publication D-5564, Rev. F Pasadena, California, April 1 (1995).

[13] LISA: *Laser Interferometer Space Antenna for the detection and observation of gravitational waves*, Pre-Phase A Report. Max-Planck-Institute für Quantenoptic, Garching bei München, MPQ 208 (1996).

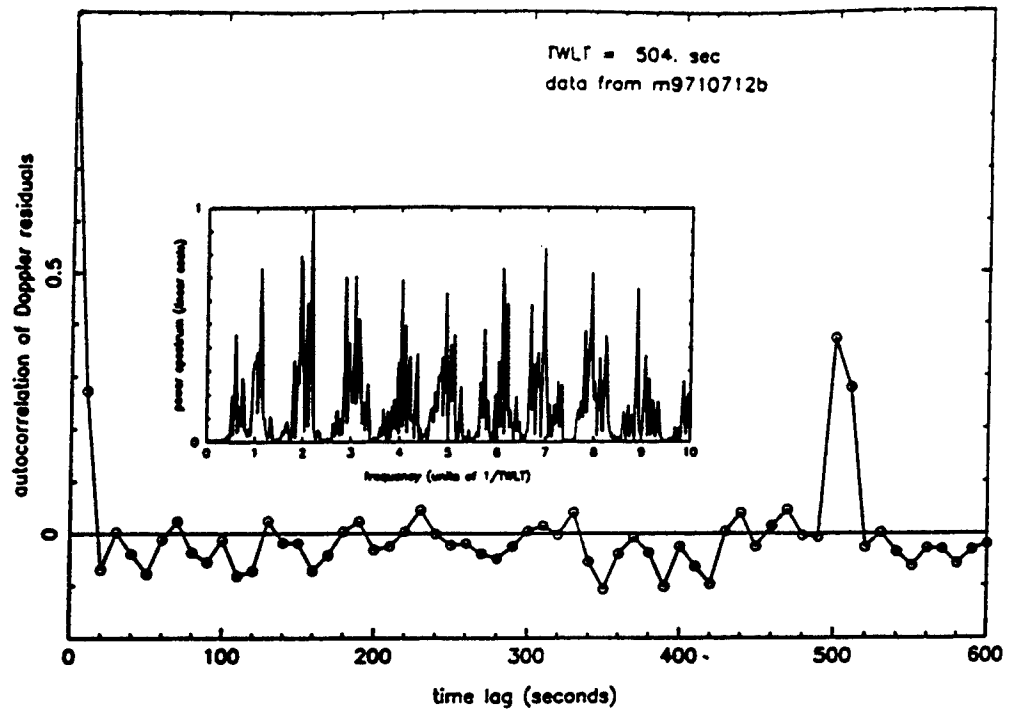


Figure 1: The temporal autocorrelation function of 10-second time resolution Mars Global Surveyor (MGS) data taken on April 17, 1997, when the two-way light time $2L/c$ was equal to 504 seconds. The inset plot shows the power spectrum, with frequency scale marked in units of $1/2L$.

Power Spectral Densities for the Noise in the Cassini Doppler Data

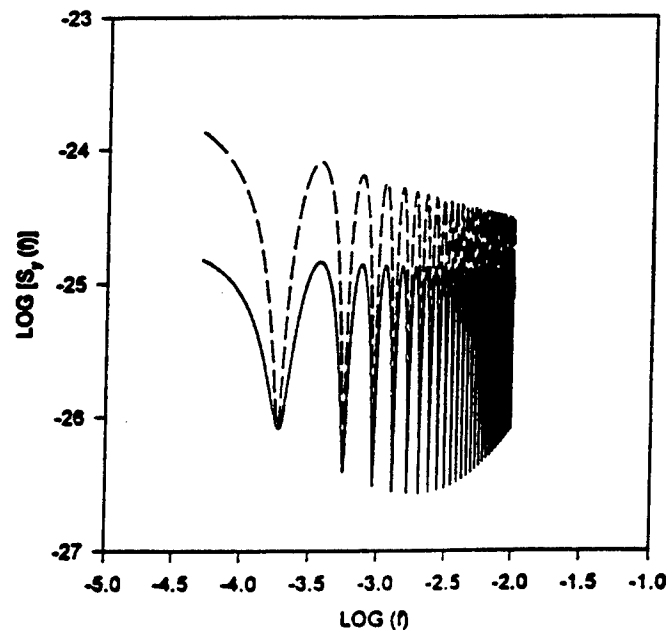


Figure 2: The estimated one-sided power spectrum of the noise that will affect the Cassini Doppler data in its frequency band of observation. The lower curve represents the configuration in which eighty percent of the noise due to the troposphere is calibrated out by means of water vapor radiometry. The upper curve corresponds to the configuration without calibration of the troposphere.

Cassini Sensitivity at the Frequencies f_k .

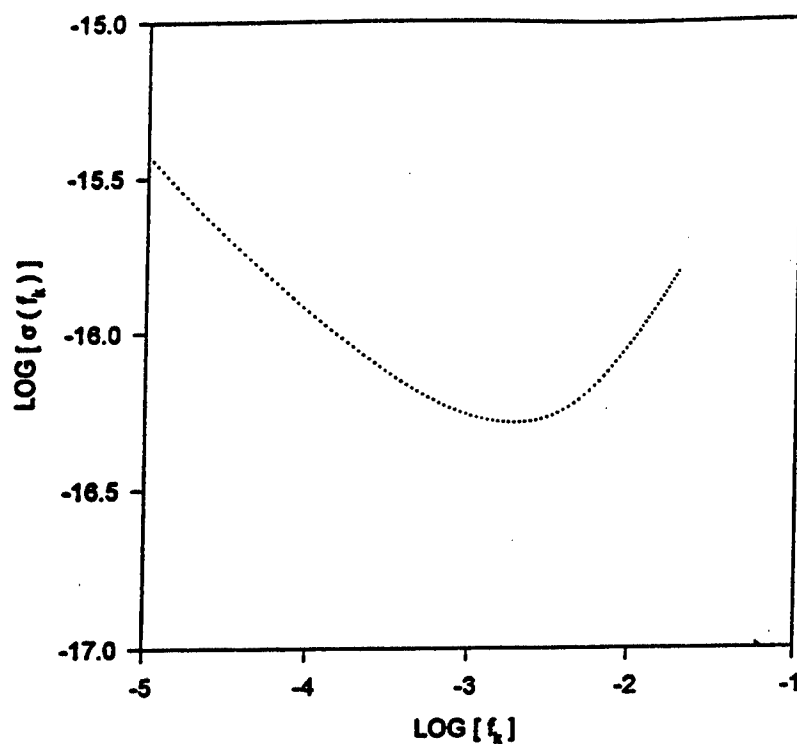


Figure 3: The sensitivity curve achievable with the Cassini Doppler data during the first solar opposition. The distance to the spacecraft is about $L = 5.5$ AU, and the corresponding fundamental frequency f_0 is equal to 4.5×10^{-5} Hz.

THE 2 SOPS EPHEMERIS ENHANCEMENT ENDEAVOR (EEE)

Capt Jeffrey D. Crum, USAF
2nd Space Operations Squadron
300 O'Malley Avenue, Suite 41
Falcon AFB, CO 80912-3041, USA

Steven T. Hutsell
United States Naval Observatory
Alternate Master Clock

Ronald T. Smetek Jr
Boeing North American
Space Operations Company

Abstract

Historically, one of the main goals of the 2d Space Operations Squadron (2 SOPS) in maintaining the GPS constellation has been to achieve the best possible system accuracy. The Master Control Station (MCS) Kalman filter plays a key role in meeting this goal. Through a process known as tuning, the database values that control the Kalman filter operation are optimized to provide the best possible estimation and prediction. Over the years, a series of in-house efforts have dramatically improved the accuracy, reliability, and integrity of the GPS signal. The latest iteration of these efforts is called the Ephemeris Enhancement Endeavor (EEE).

Air Force and contractor personnel have concentrated on two main areas as part of the EEE: Kalman filter tuning and deterministic models. Results of this effort demonstrate a 20% reduction in ranging errors and a 17% reduction in time transfer errors. The authors will present descriptions of each area investigated, explain how the new tuning parameters were derived, and provide detailed results of their efforts to date.

BACKGROUND

The mission of the 2d Space Operations Squadron (2 SOPS) is to provide highly accurate time transfer and navigation data to properly equipped military and civilian users. In the process of accomplishing this mission, the 2 SOPS has established several goals. Among these goals is to continuously improve operations and to exceed customer expectations. The 2 SOPS actively participates in routine interaction and feedback sessions with all GPS users. One of the most effective forums for this feedback is the Performance Analysis Working Group (PAWG).

The 1996 PAWG, held in August at Peterson Air Force Base, identified unprecedented levels of GPS timing and position accuracy. Several presentations highlighted and lauded the work of the men and women of the 2 SOPS in constellation operations. There were, however, also several presentations that identified periodic errors affecting GPS performance. The identification and resolution of these errors is the topic of this paper. Prior to elaborating on this project, we must first establish some additional background about how the Master Control Station (MCS) Kalman filter operates.

MCS KALMAN FILTER Q s AND TUNING

The MCS Kalman filter process is controlled by several database parameters maintained by the 2 SOPS. These parameters collectively serve to optimize or *tune* filter performance. In practice, tuning the Kalman filter is not an easy task. However, it can be safely said that the majority of this task is accomplished through a set of values known as *filter qs*. These values are maintained in a database file, called the *KKS file*, for each satellite.[1]

There are essentially two types of *qs* in the MCS Kalman filter: measurement *qs*, which model noise inherent in the measurement-taking process (such as monitor station receiver noise), and system *qs*, which model the random processes in the actual GPS system. These system *qs* can be further broken down into clock, ephemeris, and solar pressure *qs*.

Until 1994, the *qs* in the Kalman filter had remained mostly unchanged since the inception of GPS. That is, those values that were derived prior to the first Block II/IIA launch were never recalculated from actual on-orbit data once vehicles were launched. In 1994, the 2 SOPS undertook an effort to recalculate these values for the satellite vehicle atomic frequency standards. Using clock stability analysis data from the Naval Research Laboratory (NRL), 2 SOPS showed that empirical performance could be related to optimal choices for clock *qs*. Subsequently new, larger *qs* were calculated. Once implemented, GPS navigation and time transfer efforts improved significantly, a result supported by several outside agencies.[2]

RESULTS OF PAWG-96

One of the first presentations made at PAWG-96 solidified the need for 2 SOPS to revisit the tuning process, this time for ephemeris and solar states. Mr. Steve Malys of the National Imagery and Mapping Agency (NIMA) presented his methods for comparing the broadcast navigation message to the NIMA precise ephemeris. He then represented these differences as a function of User Range Error (URE) and plotted the constellation average, as shown in Figure 1. The results indicated a 12-hour periodic with an amplitude of 2-3 meters.[3]

The Aerospace Corporation and the Naval Surface Warfare Center presented similar results. Mr. Everett Swift identified an excessively long "memory effect" in the MCS Kalman filter, implying that the filter seemed to respond sluggishly to changes in ephemeris or solar states. This conclusion was consistent with MCS experience, and suggested that the ephemeris and solar *qs* were set too low and/or the measurement *qs* were too large.[4]

Yet a third presentation placed a final twist on this issue. Results presented by Lockheed Martin demonstrated that performance errors can in part be related to the minimum Sun-Vehicle-Earth angle (beta angle) of the satellite in question. Figure 2 showed how URE increased with decreasing beta angle. The correlation of these errors to the satellite position in its orbit further suggested solar pressure mismodeling.[5]

Given the definitive results of PAWG-96, 2 SOPS/DOUAN decided it was time to revisit the ephemeris/solar state accuracy topic. Members of 2 SOPS/DOUAN, the United States Naval Observatory (USNO), Boeing North American, NIMA, Lockheed Martin, and Aerospace met in late August 1996 to discuss this issue.

EEE AREAS OF INVESTIGATION

The EEE team concentrated its initial investigation in two areas: deterministic errors and MCS Kalman filter tuning. Several elements of the MCS deterministic modeling process contain known or suspected deficiencies. They include:

1. **Solar Pressure States.** A 1995 study revealed that some deficiencies exist within the solar state model used by the MCS Satellite Vehicle Positioning (SVPOS) software.[6] This deterministic model, used to generate the solar component of the satellite reference trajectory, does not account for solar transients observed early in the life of each satellite. Further work by Mr. Henry Fliegel of the Aerospace Corporation showed several shortcomings in the solar model—namely the omission of vehicle plume shield and thermal radiation effects—that combine to cause a 7% to 10% error in solar force calculation.[7] Still other studies identify similar shortcomings in other deterministic models such as the Earth Albedo model and the solar panel alignment model.
2. **Solar Array Slewing/Misalignments.** These errors result from the inability of SVPOS to model effects of array pointing during eclipse season.
3. **Thruster Firings.** Five GPS satellites currently use thrusters to manage reaction wheel momentum. Over time, these thruster firings can perturb the MCS model of the satellite vehicle orbit.
4. **The SVPOS Integrator.** Evidence from four extended stationkeeping maneuvers (over 20 minutes) suggested that the SVPOS integrator may lack fidelity. Specifically, when comparisons are made between other models and SVPOS models for extended maneuvers, large offsets on the order of tens of kilometers typically result.
5. **Relativistic Effects.** Many presentations have been made debating the MCS Kalman filter model of relativity. Some argue the MCS does not properly compensate for these effects, while others argue the math is handled correctly. Recent work has shown that this error source is negligible or non-existent, and poses no immediate concern for future tuning work.[8]

Several qs affect the MCS Kalman filter processing of routine ephemeris and solar state behavior. They include:

1. **Gravitational Velocity Process Noise Variance.** This process noise compensates for random velocity changes resulting from irregularities in the Earth's gravitational field. They are broken into radial, along-track, and cross-track (RAC) components.
2. **Solar Pressure Process Noise Variance.** This process noise compensates for solar radiation acceleration on the satellite. It is broken into the familiar solar K_1 and K_2 components.

The EEE team decided that filter tuning would be the easiest and most logical place to start with these improvements; the entire process could be performed in-house at no additional cost to the government. The next section details how the new ephemeris and solar qs were derived.

THE NEW FILTER EPHEMERIS AND SOLAR Q_s

The EEE team used the previously accomplished clock tuning as the guide for this tuning analysis.[2] In the clock world, the task of estimating a clock's polynomial coefficients is made challenging by natural disturbances called *noise*. Besides measurement noise, precision oscillators exhibit what the MCS calls *process noise*. In particular, clock states have a tendency to somewhat randomly wander off as a function of time. The clock "random walks" that the MCS accounts for are *random walk PM* (or white FM), *random walk FM*, and *random run FM*.

In the Kalman filter, the MCS accounts for these effects by increasing the clock state covariances during each time update. The MCS q_s should ideally depend on the magnitude of the respective random walk effects. Clock q_s relate as follows: [9]

Q Value:	Accounts for random walk in:	Noise type:
q_1	phase (BIAS)	random walk PM (White FM)
q_2	frequency (DRIFT)	random walk FM
q_3	frequency drift (DRIFT RATE)	random run FM

Work done in 1995 showed that not only does the MCS model help to account for most of the observable atomic frequency standard noise, but that an equation exists to easily relate empirical performance towards optimal choices for clock q_s . [9]

For orbital states, the challenge becomes complicated. One could safely argue that GPS satellite orbits exhibit largely random walk behaviors in most of the classical orbital elements, such as eccentricity, inclination, and right ascension of the ascending node. However, the MCS does not explicitly treat these as random walk processes. Rather, the MCS uses three q values, for radial, along-track, and cross-track velocities. Though, over time, the "random" behavior of RAC values between 15-minute updates will propagate into changes in the classical orbital elements, RAC deviations themselves behave more as 12-hour periodics rather than as random walks. The problem further complicates with the addition (and coupling) of solar states, whose values (and changes) propagate into ephemeris states.

RAC Q_s

The approach to the first challenge was to examine the RAC component that behaves closest to a random walk process -- the along-track component. Though, over 12 hours, orbit perturbations will show a periodic in along-track, over 2-3 days, the effect will appear more like a random walk. And, for longer periods, the deviation will behave more as a random run, meaning not only is the position randomly walking off, but the rate or slope (velocity) at which the along-track is deviating also appears to randomly walk.

MCS along-track deviation plots were examined for all GPS satellites operational at the time (August 96), and it was possible to pinpoint Tau (time interval since the previous reference trajectory update) values that appeared to show a random walk in velocity (a random run in position).

For clock states, random walks in frequency translate into phase variance by the following equation:

$$\text{Variance}_{\text{phase}} = \frac{q_z \tau^3}{3} \quad (1)$$

Applying this equation to the analogy for along-track error:

$$\text{Error}_{\text{ATRK}}^2 = \frac{q_{va} \tau^3}{3} \quad (2)$$

where q_{va} is the MCS's along-track velocity q .

Using this equation, various observed Tau values and their corresponding along-track errors were tried, to backwards-derive satellite-specific q_{va} values. The EEE team concluded that the differences between satellites were more likely due to the limited sampling, as opposed to satellite- or orbit-specific uniqueness, therefore one q_{va} value was chosen that seemed to conservatively best represent the constellation as a whole.

The chosen value was: $q_{va} = 6.12 \text{ E-15 m}^2/\text{s}^3$ (Old value: $2.7 \text{ E-16 m}^2/\text{s}^3$)

Orbit perturbations over short intervals (such as 15 minutes) are arguably omnidirectional. Although the net effect results most apparently in along-track, the root cause of along-track error is usually a combination of both along-track and/or radial perturbations. For that reason, an equal q value for radial was chosen:

$$q_{vr} = 6.12 \text{ E-15 m}^2/\text{s}^3 \quad (\text{Old value: } 2.7 \text{ E-16 m}^2/\text{s}^3)$$

For cross-track, Mr. Ken Brown of IBM-published work discussing the fact that the cross-track q value has historically been kept higher. Simply, cross-track perturbations do not geometrically correlate into radial or along-track errors, and, for that matter, do not orbitally propagate into radial or along-track errors significantly.[10]

Additionally, cross-track errors do not directly translate into ranging errors, due to the orthogonality of cross-track with respect to the locational direction of GPS users. Because of this, 2 SOPS has been able to afford to keep the cross-track q high, since large uncertainty in cross-track estimates do not directly translate into large ranging uncertainties. For this reason, we use:

$$q_{vc} = 4.6 \text{ E-13 m}^2/\text{s}^3 \quad (\text{No change from old value})$$

Largely because of the relatively lesser effect of q_{vc} , the EEE team decided to keep it unchanged.

Solar Q s

Note that the RAC q derivations have essentially ignored the short-term effects of solar acceleration. Since acceleration is a higher order effect, random walks in acceleration should theoretically show up for Tau values higher than those for random walks in velocity. By assuming this Tau-separation, solar state q derivation would assume a simple approach. In a same-state random walk process, such as clock frequency drift, the state variance relates to the state q as follows:

$$\text{Frequency Drift Variance} = q_3 \times \text{Tau} \quad (3)$$

In the clock example, the square of the frequency drift error, due to random walk in frequency drift, is time proportional to the q_3 value. By examining MCS solar state estimates, and looking for Tau values exhibiting the appearance of a random walk, one can analogously apply the clock frequency drift equation to K_1 and K_2 :

$$\text{Error}_{K1}^2 = q_{K1} \tau \quad (4)$$

$$\text{Error}_{K2}^2 = q_{K2} \tau \quad (5)$$

Again, by examining all operational satellites, and choosing values conservatively representative of the constellation as a whole, the EEE team derived the following values:

$$\begin{array}{ll} q_{K1} = 1.15 \text{ E-11 } 1/\text{s} & (\text{Old value: } 3.0 \text{ E-12 } 1/\text{s}) \\ q_{K2} = 3.3 \text{ E-27 } \text{m}^2/\text{s}^5 & (\text{Old value: } 3.3 \text{ E-29 } \text{m}^2/\text{s}^5) \end{array}$$

For SVN23, since the arrays are manually slewed, an alternate set of solar q s was selected:

$$\begin{array}{ll} q_{K1} = 2.3 \text{ E-11 } 1/\text{s} & (\text{Old value: } 3.0 \text{ E-12 } 1/\text{s}) \\ q_{K2} = 3.3 \text{ E-27 } \text{m}^2/\text{s}^5 & (\text{Old value: } 3.3 \text{ E-29 } \text{m}^2/\text{s}^5) \end{array}$$

The above values, though derived using empirical data, seemed representative of the general experiences 2 SOPS had with ephemeris/solar state estimation. The periodic effect that several outside agencies identified was likely due to filter time constants that were too lengthy. This in turn implied the old q s were too tight. Though the proposed q s were increases of 1-2 orders of magnitude, the net effect on the degree of freedom in the Filter is a function of, roughly, the quartic (fourth) root of the change in q s. Meaning, a q increase by a factor of 16 should result in a two-fold increase in Filter freedom.

VALIDATION

The EEE team conducted several off-line tests of the new tuning numbers before implementing them in the mission environment. The first of these tests used the Experimental Navigation software package at the MCS. Seven days of mission L-band data were used in a "before and after" comparison; the first run used the old tuning numbers and the second run used the new tuning numbers. The EEE team concluded the new values did not adversely impact GPS performance, and in fact, reduced ranging errors toward the end of the test. With only 7 days of data, however, it was difficult to assess the degree of improvement the new numbers would achieve.

Lockheed Martin Federal Systems (LMFS) in Gaithersburg, MD provided an independent assessment of the q s. Mr. Bill Mathon performed a similar Experimental Navigation simulation using a different 7-day L-band data set. His results supported the 2 SOPS' conclusion and helped pave the way for operational implementation.

IMPLEMENTATION

The 2 SOPS chose to update the satellite-specific files incrementally over a period of several weeks to mitigate the remaining risk of altering these database parameters. The EEE team concluded the safest approach was to choose a single satellite for the first update. SVN30 (PRN30) was chosen based on two main characteristics: it was set unhealthy to the Auxiliary User and it did not contribute to the composite GPS time scale. Given this configuration, the 2 SOPS minimized exposure of the changes to users and allowed the EEE team to safely perform a final verification of the changes.

On January 30, 1997, the 2 SOPS updated the KKS file for SVN30. Over the course of the next four days, 2 SOPS, USNO, and NIMA closely observed the ranging error and timing performance of SVN30. The results were immediately encouraging. All available metrics indicated improved performance. Based on the positive feedback from NIMA and USNO, the EEE team proceeded to update the KKS files for all other satellites throughout the month of February, completing the process on February 28, 1997.

METRIC SELECTION

The 2 SOPS uses a variety of in-house metrics to validate GPS mission performance. Since these metrics were used in the assessment of EEE, they are briefly summarized here:

- **Estimated Range Deviation (ERD)** – Difference between the range determined from the current Kalman filter state estimates and the range determined from the navigation upload page valid for the same time. Measured in meters and calculated every 15 minutes for all satellites.
- **Observed Range Deviation (ORD)** – Difference between the ionospherically corrected smoothed pseudorange observed at a monitor station and the pseudorange constructed from the navigation upload page for the same time. Measured in meters and calculated every 15 minutes for every satellite-monitor station pair.
- **Zero Age of Data** – Ranging error due to steady state Kalman filter error. Measured in meters and calculated every 24 hours for all satellites.
- **Time Transfer RMS** – RMS of all the UTC(GPS) – UTC(USNO) time difference errors for the previous day. Measured in nanoseconds and calculated every 24 hours for the constellation.

RESULTS

Since the completion of the re-tuning, 2 SOPS and other outside agencies have documented improvements in all facets of GPS mission performance. This section will present data that show significant reduction in the periodic error, time transfer RMS error, and Zero Age of Data error. The results also document an improvement in the daily upload prediction quality and the extended navigation performance.

Figure 3 shows before and after results of GPS ranging errors with increasing age of data.^[11] The post-tuning change line illustrates the significant reduction to the periodic error initially identified at PAWG-96.^[3] One of the main goals of the EEE project was to remove this periodic error, and Figure 3

shows this goal was met. Further data provided by NIMA indicate a 20% reduction in broadcast ranging errors.[12]

Figure 4 shows the monthly Time Transfer RMS comparisons from 1996 to 1997. Without exception, every month since the tuning changes has had better time transfer performance than the previous year. To date, we have documented a 17.95% improvement from 1996 to 1997. Since 1 Mar 97, the daily time transfer RMS has exceeded 10 ns on only eight days, none since 5 Jun 97.

2 SOPS uses the ERD metric to assess the quality of the broadcast navigation message. As ERDs reach an operations-defined threshold, 2 SOPS chooses to perform an out-of-cycle update to the navigation and timing data on-board the satellite. The navigation uploads are called ERD contingency uploads, and do not count as one of the daily navigation message updates. Prior to the implementation of EEE, 2 SOPS operations crews were performing, on average, more than 5 ERD contingencies per day.

Figure 5 shows the average number of ERD contingencies per day for 1996 and 1997. Note that upon the completion of the re-tuning, the average number of extra uploads dropped to just over 1.2, an improvement of approximately 75%. This significant drop signaled an improvement in the quality of the navigation message prediction; the ranging errors remained below the established threshold for a longer period of time. Given this dramatic drop, 2 SOPS chose to lower the ERD contingency threshold even further on 29 May 97. The more stringent threshold resulted in about 3.2 ERD contingency navigation uploads per day, still well below the pre-tuning update level. Thus, at no extra cost to the operations crews, the 2 SOPS was able to provide even better navigation message accuracy to the user.

The 2 SOPS uses the Smooth Measurement Residual (SMRES) Tool to assess GPS Zero Age of Data performance. Two runs of this program are made every 24 hours. The first run is based on ranging data from NIMA monitor stations only. The second run is based on data from both NIMA and Air Force monitor stations. The tool tests the data against two limits: a 4.2-meter tolerance for individual satellites, and a 3.2-meter tolerance for the constellation RMS. Historically, GPS has performed well within these limits, but the EEE changes resulted in a noticeable improvement to the Zero Age of Data performance.

Figure 6 plots the SMRES data from 1 Jan 97 to 30 Sep 97 for both runs. Each shows an obvious improvement upon completion of the database updates. To date, we have documented a 30% reduction in the Zero Age of Data errors.

The EEE team was presented with a unique opportunity to validate extended navigation operations with the new tuning values. SVN28 (PRN28), an unhealthy but usable asset at the time, was used for this extended navigation test. On 19 Mar 97, 2 SOPS placed a navigation upload into SVN28 and then did not re-upload for approximately 21 days. GPS has a requirement for no more than 200 meters of single-satellite ranging error at 14 days age of data. Our results showed only 49.2 meters of error at 14 days. Although not an exhaustive test, these results indicate that no sacrifice was made to the extended navigation mission in order to achieve the results presented above.

FURTHER TUNING CHANGES

Based upon the early results of this effort, the EEE team began to explore updating other database parameters. The next most logical adjustment was the measurement noise increment. This value, also called σ_0 , is used to account for the white/flicker noise in pseudorange (PR) measurements. This

parameter was modified from 1.0 m^2 to 0.74 m^2 for all monitor stations in 1994 following satellite clock tuning.[2] The EEE team investigated the impacts of further lowering this value.

The methodology for the derivation of a new q_0 was similar to that used for the ephemeris and solar q_s . The EEE team examined an RMS of the PR residuals at each monitor station over a period of several days. The four non-CONUS sites were all near 0.59 m (0.35 m^2), and COSPM was near 0.72 m (0.52 m^2). The reasons for noisier measurements at COSPM are not clear, but several theories have been presented elsewhere and will not be discussed here.

Again, the EEE team used a 7-day set of L-band data on the Experimental Navigation software package to test these new values. Unfortunately, there was no significant improvement in the Zero Age of Data, and even a minor degradation in ERD performance. LMFS performed a second test in Gaithersburg and reached the same conclusion. As a result, the EEE team decided to leave the q_0 term unchanged at 0.74 m^2 for all monitor stations.

WHAT'S NEXT?

The results of the tuning changes have been overwhelmingly positive. The EEE team met—and exceeded—all of the initial goals with this project. There is, however, still some room for improvement. Some of the other areas we are currently investigating include: refinement of the current tuning numbers, orbit-season specific or satellite-specific q_s , and deterministic modeling errors.

Each of these areas requires additional on-orbit data before any conclusions can be made. The initial data indicates that all satellites experienced varying degrees of improvement. In a few rare cases, the “after” errors are slightly larger than the “before” errors. Without exception, however, these satellites had the smallest initial errors to begin with. It is the goal of the EEE team to choose tuning values to optimize the performance of all satellites. This project is an on-going effort, and will continue to evolve as the constellation changes. The 2 SOPS and its contractor support team are committed to providing the best possible navigation and timing signal to the GPS user community.

ACKNOWLEDGMENTS

The authors would like to thank the following people and agencies for their generous assistance with the Ephemeris Enhancement Endeavor and with this paper:

The men and women of the 2d Space Operations Squadron

C.H. Cook, Steve Malys, and Lisa McCormick, NIMA

William Mathon, LMFS

Richard Harris, SAIC

Jack Taylor, LMMS

Ben Huber, BNA

Tom Bahder, ARL

Marc Weiss, NIST

Jim DeYoung, G. Al Gifford, Mihran Miranian, Lara Schmidt, Francine Vannicola, USNO

REFERENCES

1. Scardera, Michael P.; Smetek, Ronald T. Jr; and Crum, Jeffrey D., *MCS Kalman Filter Mission Support Study Guide*, 3rd edition, 2 SOPS Internal Training Document, pp. 21-136, March 8, 1996.
2. Hutsell, Steven T., *Fine Tuning GPS Clock Estimation in the MCS*, Proceedings of the 26th annual Precise Time and Time Interval (PTTI) Applications and Planning Meeting, 6-8 December 1994, Reston, VA, USA (NASA CP-3302), pp. 63-74.
3. Malys, Steve, *Comparison of URE Characterization Methods*, Proceedings of PAWG-96, 21-22 August 1996, Peterson AFB, CO, USA.
4. Swift, Everett and Merrigan, Mike, *Expected Improvement in OCS Kalman Filter Estimates and Predictions Due to Adding DMA Stations and Using a Single Partition*, Proceedings of PAWG-96, 21-22 August 1996, Peterson AFB, CO, USA.
5. Frey, Chuck; McReynolds, Steve; Metzger, Tom; Moore, Jerry, *GPS MCS Filter Performance*, Proceedings of PAWG-96, 21-22 August 1996, Peterson AFB, CO, USA.
6. Smetek, Ronald T. Jr and Taylor IV, John V., *Between Sun and Earth: Solar Pressure State Estimation in the GPS Master Control Station*, Proceedings of ION-GPS-94, 20-23 September 1994, Salt Lake City, UT, USA, pp. 275-284.
7. Fliegel, Henry, *A Place in the Sun: Direct and Indirect Solar Effects on GPS Satellites*, The Aerospace Corporation, 8 April 1993.
8. Weiss, Marc and Ashby, Neil, *Comments on GPS and Relativity: An Engineering Overview*, National Institute of Standards and Technology Memo, 13 March 1997.
9. Hutsell, Steven T., *Relating the Hadamard Variance to MCS Kalman Filter Clock Estimation*, Proceedings of the 27th Annual Precise Time and Time Interval (PTTI) Applications and Planning Meeting, 29 November – 1 December 1995, San Diego, CA, USA, (NASA CP-3334), pp. 291-299.
10. Brown, Ken, *Characterizations of OCS Kalman Filter Errors*, Proceedings of ION-GPS-91, 11-13 September 1991, Albuquerque, NM, USA.
11. Lockheed Martin Federal Systems and Overlook Systems Technology, *GPS Performance Data Package*, 29 August 1997.
12. McCormick, Lisa, *Analysis of the 2 SOPS Ephemeris Enhancement Endeavor*, Proceedings of PAWG-97, 20-21 August 1997, Peterson AFB, CO, USA.

TOTAL URES - DAY 96016

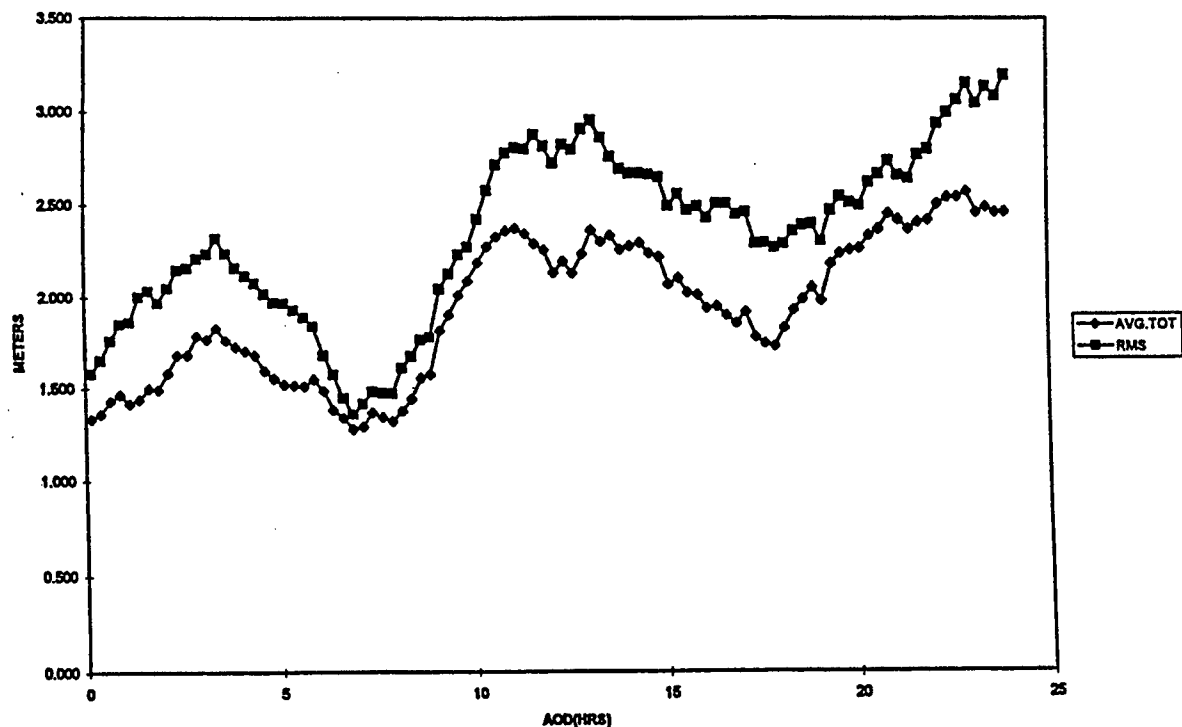
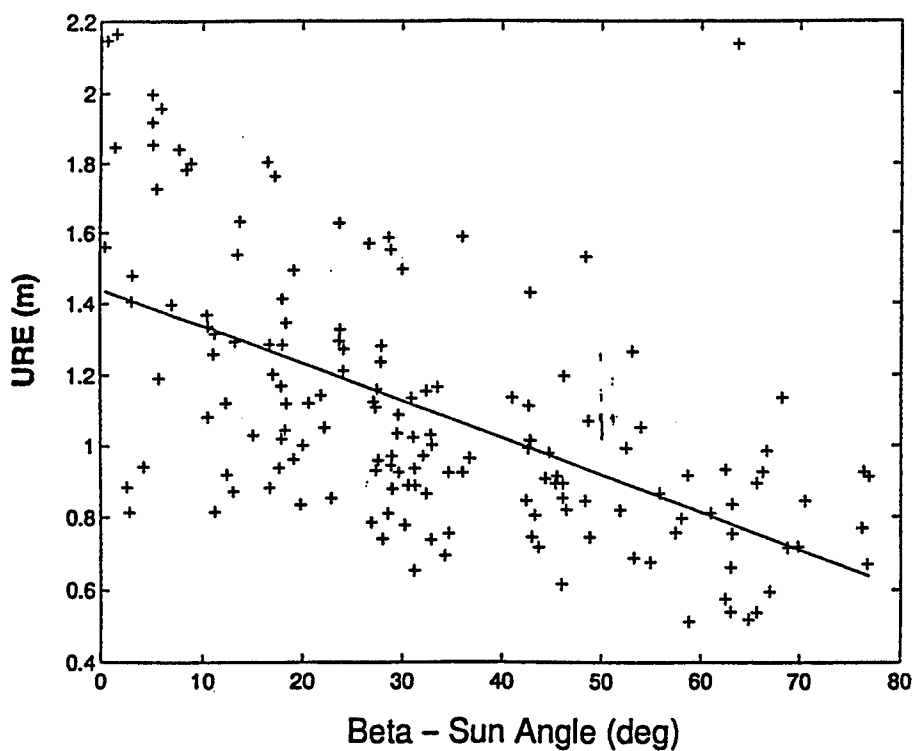


Figure 1. Total constellation composite showing the offset between broadcast navigation message and NIMA precise ephemeris. Originally presented by Stephen Malys.



*Note: each point represents the average for one GPS SV for 4 days
(days: 95 352, 96 003, 96 045, 96 073, 96 100, 96 129, 96 157, 96 185)

Figure 2. URE vs. Beta Angle. Originally presented by Tom Metzger.

RMS ORD as Function of Age of Data: 1996 versus 1997

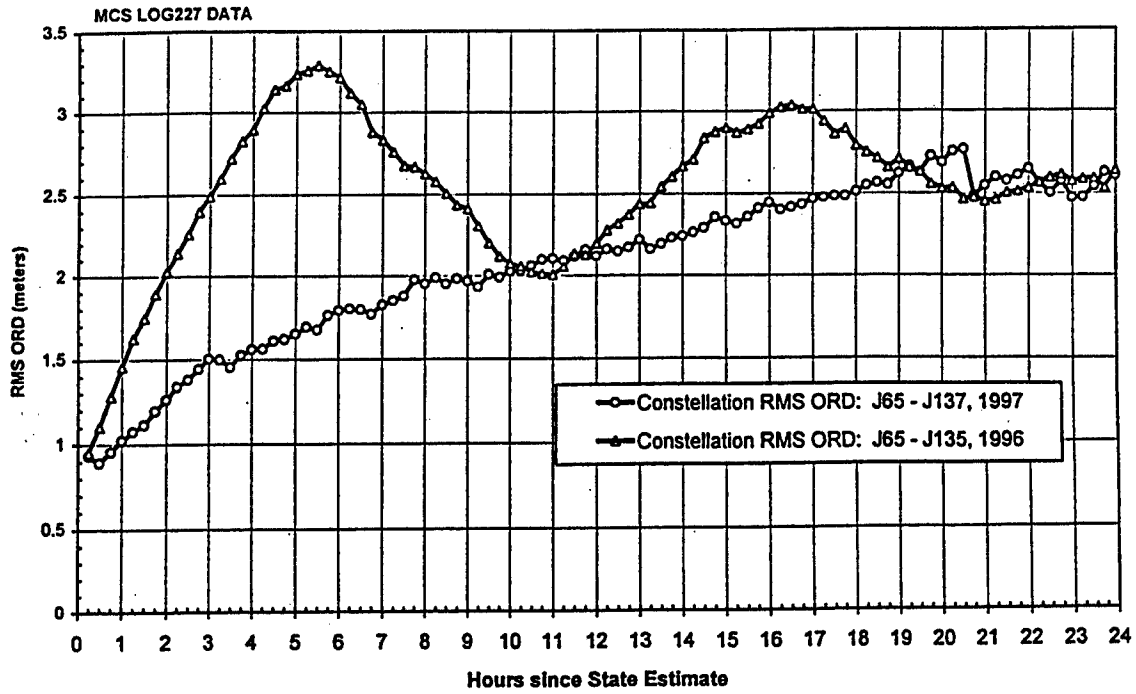


Figure 3. RMS ORD with Increasing Age of Data. Originally presented by LMFS and Overlook.

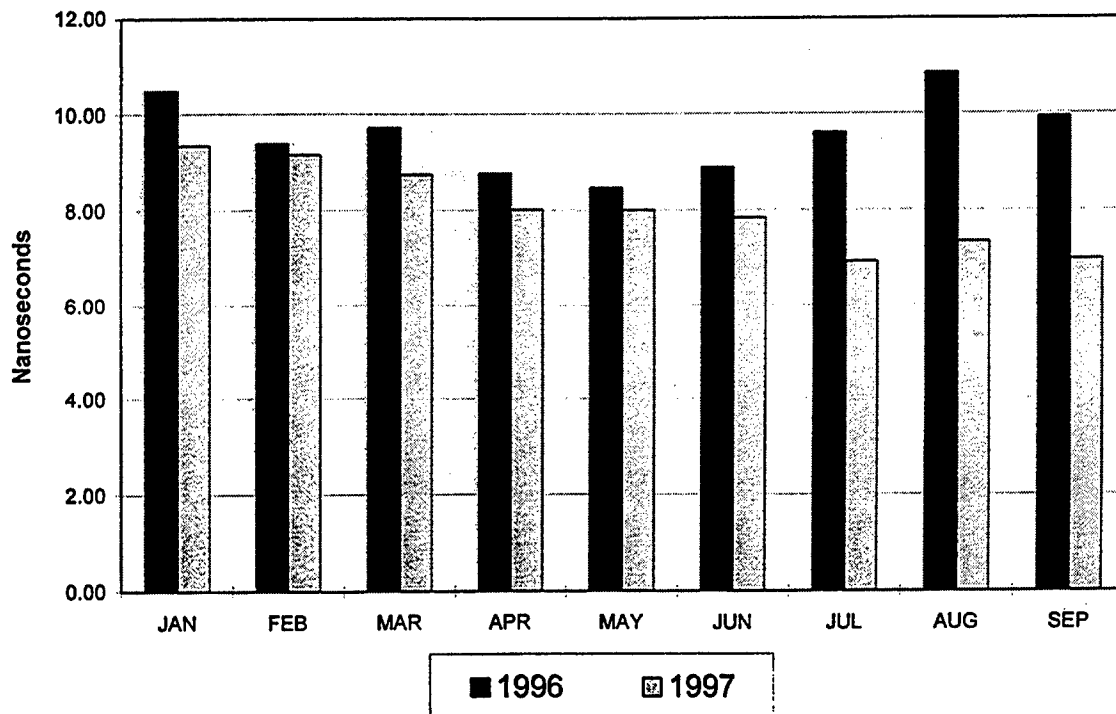


Figure 4. Time Transfer RMS Comparison.

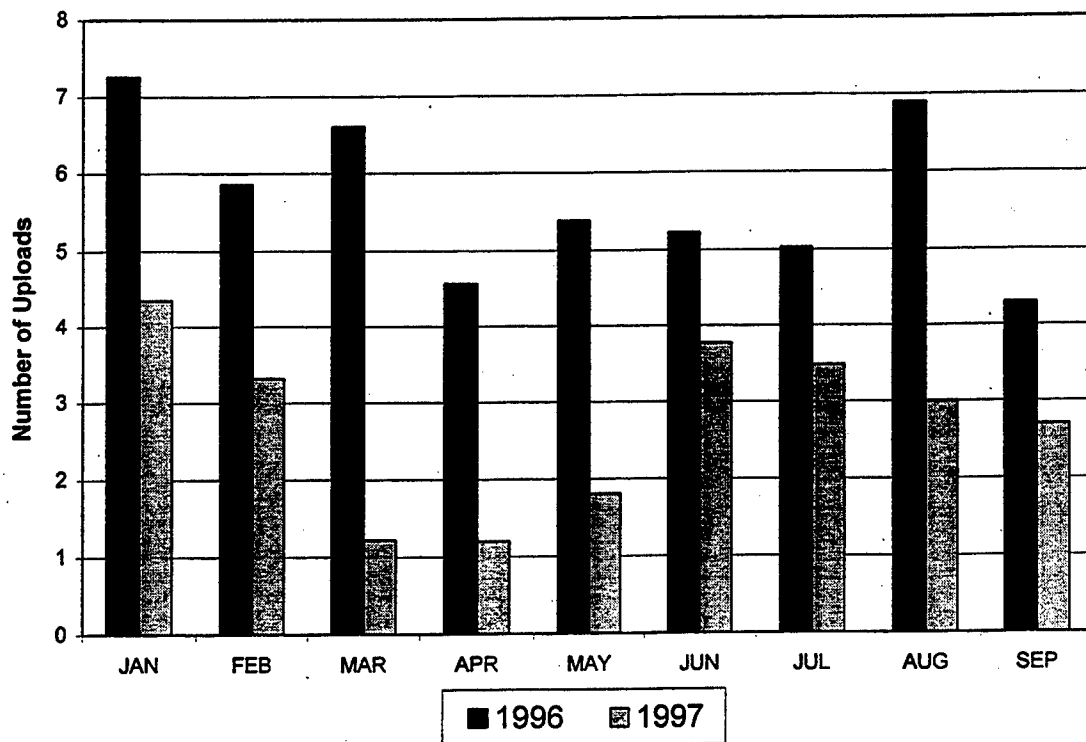


Figure 5. Average Number of Estimated Range Deviation (ERD) Contingency Navigation Uploads per Day.

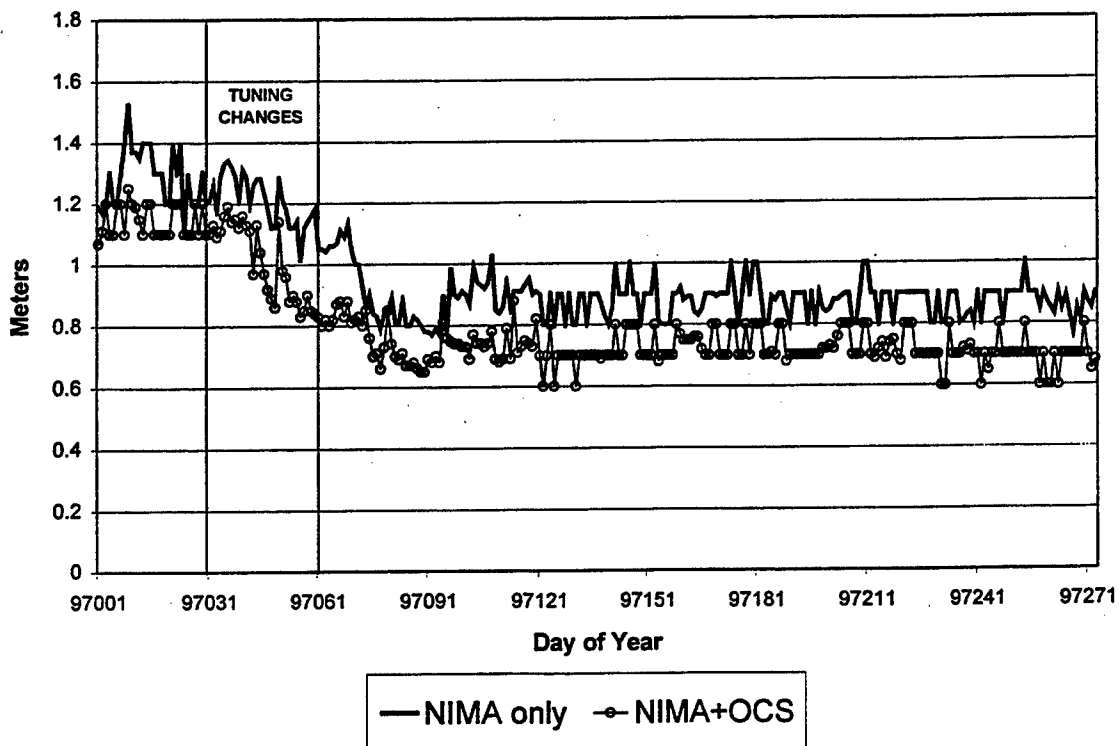


Figure 6. Smooth Measurement Residual (SMRES) Tool Results for 1997.

Questions and Answers

PHIL TALLEY (SFA/NRL): I remember in times past we used to have a parameter that was separated between clock and ephemeris errors. In the effort you are putting in now, does that still leave the clock errors approximately where they were and improve the ephemeris errors?

CAPTAIN JEFF CRUM (FALCON AFB): Are you speaking in addition to the tuning efforts that we are doing quarterly now or are you talking about another parameter?

PHIL TALLEY: I am unfortunately speaking from several years ago when we used to have the estimate of the precision divided between clock and ephemeris errors. Maybe you do not even do that anymore, and maybe I am the only one in the room that is concerned. But I just wondered if it did indicate that improvement was strictly on the ephemeris or if it did improve the appearance of the clock performance.

CAPTAIN JEFF CRUM: Yes, there was some leakage of ephemeris error into the clock states because the covariances were too tight for ephemeris and solar. The filter, in trying to do the best that it could was leaking some into the clock states. To some extent, at zero age of data, some of that error actually canceled out. For users that received Kalman filter estimates in near real time, it was not as big a problem; but for users that received the navigation message, that basically do not get updates much more often than once every 24 hours, it was causing a problem. Because, a lot of the times the clock states would be formulated at one of the peaks of the 12-hour or 24-hour humps, if you will; and when the prediction is based off of that, the prediction will be pretty much a straight line if it is a cesium. The frequency estimate will be a straight line over that 24-hour prediction. When it is corrupted like that, due to the periodic, it can and did cause a little bit of error, which this reduced.

REFINING MONITOR STATION WEIGHTING IN THE GPS COMPOSITE CLOCK

1st Lt H. Shawn Mobbs, USAF
2d Space Operations Squadron
300 O'Malley Avenue Suite 41
Falcon AFB, CO 80912-3041

Mr. Steven T. Hutsell,
USNO Alternate Master Clock

Abstract

The two closely linked missions of the Global Positioning System (GPS) are precise positioning for navigation accuracy and precise time transfer. Positioning has typically received the most attention; however, the ability to derive a precise position depends on having a stable and reliable time scale as a starting point. Throughout the history of GPS, its time scale has slowly evolved through many phases. The most significant change came with the introduction of the Composite Clock in 1990. Additionally, in recent years the 2^d Space Operations Squadron (2 SOPS) has tuned the Composite Clock to take better advantage of its contributing timing sources. In addition to reviewing the Composite Clock's tuning history, the authors will discuss the recent implementation of unique tuning for each of the GPS monitor station frequency standards.

As pointed out in a previous paper regarding satellite clock-unique tuning^[1], no two satellite frequency standards exhibit the same performance. This also holds true for monitor station frequency standards. However, other factors must be considered when deriving process noise values (tuning parameters) for ground system contributors to the Composite Clock. Mainly because the values chosen for each clock determine the size of its vote in contributing to GPS time, one must look not only at clock performance, but environmental factors as well. An excellent clock placed in an environment with significant temperature and humidity fluctuations can be very detrimental to GPS time if that clock is weighted heavily in the Composite.

This newly adopted concept of representing monitor station clocks based on individual performance and environmental history has significantly improved the stability and reliability of GPS Time. The authors discuss several examples that reveal the robustness of the new tuning as well as the current implicit long-term weighting given to each frequency standard that contributes to the Composite Clock.

INTRODUCTION

Throughout the history of the Global Positioning System (GPS) the 2d Space Operations Squadron (2 SOPS), Department of Defense (DoD) agencies, and contractors have been striving to improve the performance to users. Both position and time solutions produced by GPS have dramatically improved since its inception. As the system evolved and a greater understanding of the science of the control system of GPS became available, the system has undergone many refining stages. These enhancements are due to the

ingenuity of dedicated individuals using practical ideas and the flexibility (data base parameters) offered by the original system. The most popular improvements are those which enhance the position solutions for users. However, the heartbeat of the GPS service relies on the ability to produce and maintain a reliable and stable time scale. Since initial operational capability the GPS program has made several advancements in the area of establishing and maintaining its time scale. After several years of evolution and coordinated efforts amongst various agencies, the current GPS system has greatly matured.

EVOLUTION OF GPS TIME

The Master Clock

In the beginning years of the GPS program a single reference clock known as a master clock [not to be confused with the United States Naval Observatory (USNO) Master Clock] represented GPS time. This arrangement simply meant that one clock in the GPS control network was deemed as the closest to an ideal clock or "truth" source. All other clock offsets were then measured against this reference clock. The GPS master clock approach worked sufficiently as long as the one clock chosen as master performed well. Unfortunately, if this one clock failed or experienced instability then the GPS time scale suffered as well. Despite its drawbacks the GPS master clock served as a starting point in the development of GPS time.

The Composite Clock

Fortunately, in 1987, Mr. Ken Brown of IBM proposed using a majority of the estimated clocks in the GPS system as contributors into what is essentially a Kalman filter-based time scale. His idea of creating a "Composite Clock" came to fruition when employed operationally in 1990. The Composite Clock theory, described in detail in [2], provided the platform for GPS time as we know it today. In short, the Composite Clock is an implicit ensemble mean of corrected clocks residing within the Master Control Station (MCS) Kalman filter. In the Composite design, all clocks whose offsets are estimated within the Kalman filter can contribute to the GPS time scale. The amount that each clock contributes to the final Composite Clock is implicitly represented by the relative variances associated with that particular clock. In the initial employment of the Composite Clock all satellite and Monitor Station (MS) clocks had the same process noise values (or q_s). GPS time operated under this philosophy for several years.

The transition from a single master clock to a Composite Clock philosophy has probably been the single most valuable advancement in the evolution of GPS time. It provided a more stable time scale, in that with more clocks contributing, the failure or instability of a single clock has a much smaller impact to GPS time and thus to users, compared to the impact of problems with a single master clock. This impact due to the instability of a

single clock is roughly proportional to $1/n$, where n is the number of contributing clocks. Therefore, the more clocks allowed to contribute, the more robust the Composite time scale. Also, a system of n clocks should theoretically demonstrate stability roughly proportional to $n^{-1/2}$. Thus more clocks equate to greater stability. However, as with any new idea, there was still room for improvement in order to make the most of this new operational philosophy.

Tuning the Composite Clock

As previously mentioned, the original implementation of the Composite Clock theory used an approach that assumed all clocks exhibited similar stability performance. This assumption, of course, is not true and in fact all clocks do exhibit unique noise characteristics. To determine what qs best represent each clock's performance one must obtain empirical performance of the GPS clocks. Thankfully, agencies like the National Imagery and Mapping Agency (NIMA) and the Naval Research Lab (NRL) have developed the capabilities to monitor, track, and trend clock performance data for all vehicle and MS clocks within GPS. Their analyses provide the tools necessary to enhance the operational Composite Clock.

In 1994 2 SOPS began the initial effort to fine tune the Composite Clock. At first, 2 SOPS addressed the rubidium process noise values,^[3] and subsequently evaluated and modified the qs for the entire satellite clock constellation^[1]. This successful tuning effort brought the GPS time scale another step closer towards optimum utilization. The only other contributing timing sources to GPS time not optimally tuned until recently were those residing at the MSs.

RECENT EFFORTS IN MONITOR STATION TUNING

The remote MS clocks previously each contributed equal weights in long-term weighting to GPS time. For years the MS qs were representative of normal HP 5061 Frequency Standard (FS) performance in a stable environment. However, historically MS environmental problems have in many instances caused severe degradation to the stability of the GPS time scale.^[4] With most of the ground system clocks located in facilities susceptible to severe temperature, humidity, and mechanical disturbances, performance problems can occur. Also, much like orbiting clocks, no two ground FSs exhibit the same stability. Thus, having equal process noise values for all ground clocks did not make optimal use of their contributions to GPS time. For these reasons, in late 1996 2 SOPS began implementing monitor station-unique qs on a quarterly basis along with the satellite-unique qs .

Initial Derivation of the MS q s

Derivation of the MS q s follows nearly the same methodology as that used for deriving the satellite q s. By using the following equation^[1]

$$\text{Allan deviation } (\tau) = [(q_1/\tau) + (q_2*\tau)/3]^{1/2} \quad (1)$$

one can plot the theoretical Allan deviations from a predetermined set of process noise values (q_1 and q_2) for each MS clock. The resulting plots can then be compared to empirical plots produced by NRL similar to that in Figure 1^[5]. These plots are possible due to the analysis capability recently developed by NRL in Linked Common View Time Transfer (LCVTT)^[6]. MCS operators can adjust the noise parameters q_1 and q_2 to match empirical MS clock performance. This process is repeated for each monitor station clock to derive an initial set of q s.

Environmental Considerations

MS clocks operate in environments different from orbiting clocks as mentioned earlier, and therefore must be subjected to other considerations when deciding on the implementation of unique q s. For example, the MS frequency standards at Hawaii reside in a room that is usually occupied with people coming and going quite often. Contrary to that situation, the frequency source for the Colorado Springs MS is the USNO Alternate Master Clock (AMC), which is operated in a controlled environment. Additionally, the Colorado Springs timing source is much more stable than those at all other MSs, due primarily to the AMC's use of a hydrogen maser reference, which is steered via two-way satellite time transfer to the DoD Master Clock at USNO, Washington D.C.^[7] Given such inherent differences between MSs, using equal q values, and thus equal implicit weighting, is intuitively not the best choice.

Tuning the Backup MS FS

With two frequency standards located at each site, one must determine what q s to use for the backup, should the operational fail. The phase and frequency offsets and associated variances for the operational FSs at each site are estimated through the Kalman filter process, and therefore contribute to GPS time. Unfortunately, since the MCS only estimates the "site" phase and frequency offsets, one only has insight to the current operational FS. Because HP 5061 FSs have non-trivial environmental sensitivities^[8] the differences in noise characteristics, simply due to the physics of each clock being unique, are overshadowed by the noise characteristics due to environmental changes. For this reason one may assume that the long-term performance of two clocks in the exact same environment will be very similar. Based on this assumption, 2 SOPS currently uses the same q values for the operational and backup FSs at each remote site. The only exception to this practice is for the Colorado Springs MS. Though the primary timing source for

this site is the USNO AMC, the backup FS at this site is a single HP 5061, and therefore uses the process noise values more suited to its performance.

Operational Considerations

During planned maintenance periods, the 2 SOPS operators may evaluate and modify the process noise values to effectively de-weight MS clock contributions as necessary. During February of 1997, the Air Force physically relocated the Diego MS equipment into a newly constructed facility. During this move, the operational HP 5061 FS remained powered on but still experienced a period of environmental instability inherent to any construction project. Starting at the time of the move and for several months afterwards, the 2 SOPS operators chose to effectively de-weight the Diego MS clock's contribution to the GPS time scale by increasing the process noise values. With a different noise signature expected in the new facility, increasing the q values initially helped to protect the GPS time scale from potential corruption during the stabilization period. In this circumstance, 2 SOPS operators proactively modified MCS Kalman filter qs to help maintain a reliable and stable time source during a period of instability in the GPS system.

MCS Partitioning Considerations

Due to system processing limitations, the contributing clocks in GPS are dispersed throughout three separate estimating partitions. Each of these partitions contains the states of up to six different satellite clocks and all five MS clocks. Each partition is integrated into GPS time through a MCS process known as partition reconciliation. Because each partition contains its own estimate of each MS clock, the weight implicitly given to each ground clock in GPS time is effectively tripled. In order to compensate for this inherent weighting increase, 2 SOPS multiplies the q values derived from the NRL plots by a factor of three (or the current number of estimating partitions)^[9]. These modified values are then implemented by updating the operational database of the GPS control segment.

With the considerations discussed above, the current philosophy employed by the 2 SOPS for MS tuning is to examine the current and previous two to three quarterly reports provided by NRL, in order to analyze any MS-specific trends. Typically, the worst case deviation plot from all the available NRL plots for each MS is used to derive the tuning qs for each MS in question. Exceptions are taken when known maintenance or anomalies have occurred or are planned to occur in the future, as discussed earlier.

RELATIVE CLOCK WEIGHTING IN GPS TIME

Once the new q values are updated on the operational system, one can view the implicit long-term weighting given to each contributing clock towards GPS time. The long-term

weighting can be thought of as being inversely proportional to the long-term steady state frequency variances produced from the Kalman filter process for each of the clocks, taking into account the effective tripling of MS weighting. That is, the relative long-term weighting of clock x (W_x) with respect to an n -clock ensemble can be represented by:

$$W_x = \frac{1/\text{Var}_x}{1/\text{Var}_1 + 1/\text{Var}_2 + \dots + 1/\text{Var}_x + \dots + 1/\text{Var}_n} \quad (2)$$

where Var_x = the long-term variance of clock x

Following a settling out period after q changes, one can observe the steady state frequency variances from the operational display NPARCOV as shown in Figure 2. Examples of the various weightings in GPS time as described by the above equation are shown in Figures 3 and 4.

The weighting now applied to all the operational clocks within GPS, which represents each clock uniquely according to its actual historical behavior, serves to better optimize the true benefits of the Composite Clock. Clock-unique weighting allows excellent performing FSs to contribute more to GPS time, while allowing other FSs to still contribute. Our MS tuning efforts have contributed to the best ever synchronization and stability of GPS with respect to UTC as demonstrated in Figures 5 and 6 respectively.

Allowing more clocks to contribute increases the robustness of the system, as mentioned earlier. Currently, the MCS utilizes three estimating partitions with six vehicles and five estimating ground states each, resulting in a maximum of twenty-three GPS clocks that can contribute to GPS time at any instance. Typically, 2 SOPS maintains this configuration and only modifies the partitioning layout as necessary for maintenance or anomalous/troubleshooting periods.^[3]

FUTURE IMPROVEMENTS

The frequency of the tuning of MCS clock state estimation is currently limited by the data collection analysis and distribution processes required between NIMA, NRL, and 2 SOPS. Additionally, the overall system performance is limited by the environmental sensitivity of the HP 5061 FSs, which could be significantly alleviated with a simple upgrade to HP 5071 FSs at the Air Force remote MSs. This would significantly reduce the environmental sensitivity and add many more stable clocks for higher weighting in the GPS time scale. The stability difference between the two frequency standards is clearly visible by looking at the Allan deviation plots in NRL's quarterly reports. NIMA MS HP 5071 FSs demonstrate an average stability of 3×10^{-14} at one day, which is better than typical HP 5061 FS performance at the Air Force MSs, which can be as poor as 1×10^{-13} at one day.^[5]

Several system changes planned for the near future should also serve to improve the performance of the GPS time scale. For example, under the new Architecture Evolution Plan (AEP), the control segment will have the capability to operate with all satellite vehicles in a single estimating partition. This capability will alleviate the need for artificially multiplying the process noise due to the multiple partitioning used in today's system, but it will also permit better flexibility to allow more satellite clocks to contribute to GPS time. Also, the Accuracy Improvement Initiative (AII) will allow the addition of more ground system clocks to contribute to GPS time by incorporating the NIMA MSs into the control segment of GPS. As mentioned earlier, the HP 5071s at the NIMA sites already demonstrate excellent stability characteristics. Both the AEP and AII projects are currently funded and scheduled to be operational by late 1999 to mid 2000. Lastly, very encouraging initial on-orbit performance of recently activated Block IIR rubidium FSs paints an optimistic picture in terms of the quality of future on-orbit clocks contributing to GPS time.

CONCLUSION

The most significant step in the evolution of GPS time came with the implementation of the Composite Clock in 1990. Following this new idea, 2 SOPS, alongside other DoD agencies, has worked to accurately tune the system to optimize the robustness and stability offered by a Composite Clock. The authors have described the most recent step in this process, MS clock unique tuning, and have shown the resulting implicit long-term weighting for all the clocks currently contributing to GPS time. To complement the quarterly tuning philosophy adopted by 2 SOPS, plans for further improvements mentioned in this paper should also contribute to better performance of the GPS time scale for the user community.

ACKNOWLEDGEMENTS

The authors wish to thank the following people and agencies for their generous assistance with both our timing improvements and this paper:

Ronald L. Beard, NRL
Kenneth R. Brown, LMFS
Jim A. Buisson, SFA
Thomas B. McCaskill, NRL
O. Jay Oaks, NRL
Wilson G. Reid, NRL
Hugh E. Warren, SFA
The members of 2 SOPS

REFERENCES

- [1] S. T. Hutsell, 1995, *Fine Tuning GPS Clock Estimation in the MCS*, Proceedings of the 26th Annual Precise Time and Time Interval (PTTI) Meeting, 6-8 December 1994, pp. 63-74.
- [2] K. R. Brown, 1992, *The Theory of the GPS Composite Clock*, Proceedings of ION GPS-91, 11-13 September 1991, pp. 223-242.
- [3] S. T. Hutsell, 1995, *Recent MCS Improvements to GPS Timing*, Proceedings of ION GPS-94, 20-23 September 1994, pp. 261-273.
- [4] S. T. Hutsell, 1996, *Ideas for Future GPS Timing Improvements*, Proceedings of the 27th Annual Precise Time and Time Interval (PTTI) Meeting, 29 November – 1 December 1995, pp. 63-73.
- [5] W. G. Reid, and J. A. Buisson, NRL Analysis Updates No. 96-1 through 97-2.
- [6] W. G. Reid, T. B. McCaskill, and O.J. Oaks, J. A. Bussion, and H. E. Warren, 1996, *Common View Time Transfer Using Worldwide GPS and DMA Monitor Stations*, Proceedings of the 27th Annual Precise Time and Time Interval (PTTI) Meeting, 29 November – 1 December 1995, pp. 145–155.
- [7] W. V. Bollwerk, 1997, *The Alternate Master Clock and Precise Time Requirements; Why an Alternate Master Clock?*, Proceedings of the 28th Annual Precise Time and Time Interval (PTTI) Meeting, 3-5 December 1996, pp. 141-145.
- [8] R. L. Sydnor, T. K. Tucker, C. A. Greenhall, W. A. Diener, and L. Maleki, 1990, *Environmental Tests of Cesium Beam Frequency Standards at the Frequency Standards Laboratory of the Jet Propulsion Laboratory*, Proceedings of the 21st Annual Precise Time and Time Interval (PTTI) Meeting, 28-30 November 1989, pp. 409-420.
- [9] K. R. Brown, private communications, March 1994.

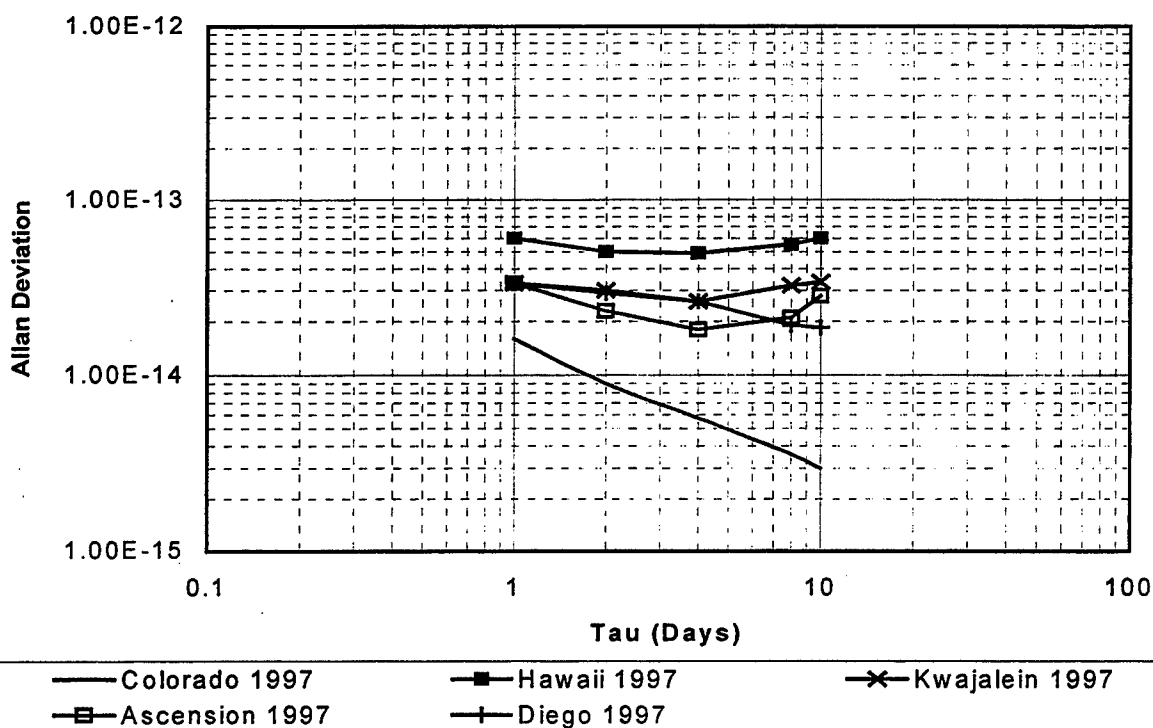


Figure 1. Air Force MS HP 5061 FS Allan Deviation Plots Produced by NRL

PARTITION	COVARIANCE	PARTID: 1				TIME:	230/01:15:00
SVID	B4/35	E2/21	B3/13	A1/39	D4/34	A2/25	
EPH EPOCH TIME	203/00:00:00	203/00:00:00	203/00:00:00	203/00:00:00	203/00:00:00	203/00:00:00	
X-REF (m2)	8.93E+04	5.46E+03	7.85E+03	2.37E+05	1.13E+04	2.31E+04	
Y-REF (m2)	2.23E+03	1.90E+05	2.37E+05	3.14E+04	1.16E+05	1.45E+05	
Z-REF (m2)	1.72E+05	5.85E+03	1.51E+04	2.25E+04	1.11E+05	1.18E+05	
VX-REF (m2/s2)	2.58E-05	1.29E-03	1.73E-03	9.58E-07	3.81E-03	4.59E-03	
VY-REF (m2/s2)	5.56E-03	2.18E-04	4.51E-04	2.59E-03	1.89E-04	6.07E-05	
VZ-REF (m2/s2)	2.96E-05	2.78E-03	3.27E-03	3.63E-03	1.09E-03	1.39E-03	
K1-RES	6.89E-06	4.68E-06	6.38E-06	8.36E-06	5.48E-06	8.02E-06	
K2-RES (m2/s4)	5.57E-21	8.17E-21	5.52E-21	4.97E-21	6.11E-21	5.00E-21	
B-RES (s2)	1.59E-17	1.21E-17	1.37E-17	1.27E-17	1.32E-17	1.21E-17	
D-RES (s2/s2)	5.81E-27	2.85E-27	3.09E-27	2.97E-27	1.34E-27	1.32E-27	
DR-RES (s2/s4)	0.00E+00	0.00E+00	0.00E+00	0.00E+00	0.00E+00	0.00E+00	
MS STATES	--ASCNM--	--DIEGOM--	--KWAJM--	--HAWAIM--	--COSPM--		
B-RES (s2)	1.19E-17	1.33E-17	1.38E-17	1.57E-17	1.06E-17		
D-RES (s2/s2)	2.91E-27	1.56E-26	3.00E-27	1.58E-26	1.12E-27		
TROPO RES (m2)	0.00E+00	0.00E+00	0.00E+00	0.00E+00	0.00E+00		

Figure 2. NPARCOVDisplay from Partition One

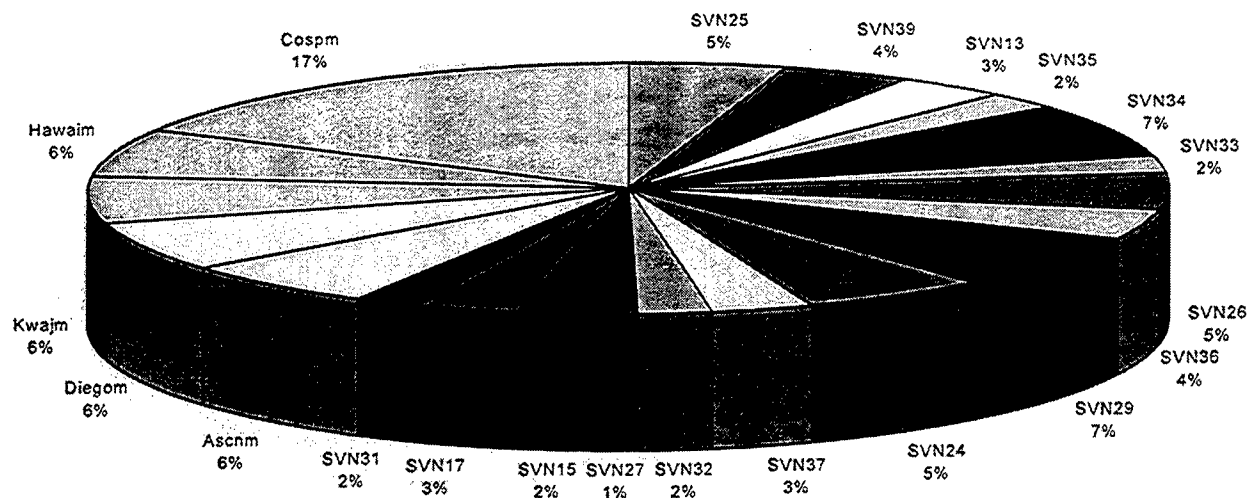


Figure 3. Implicit Long Term Weighting of GPS Time 1 December 1996

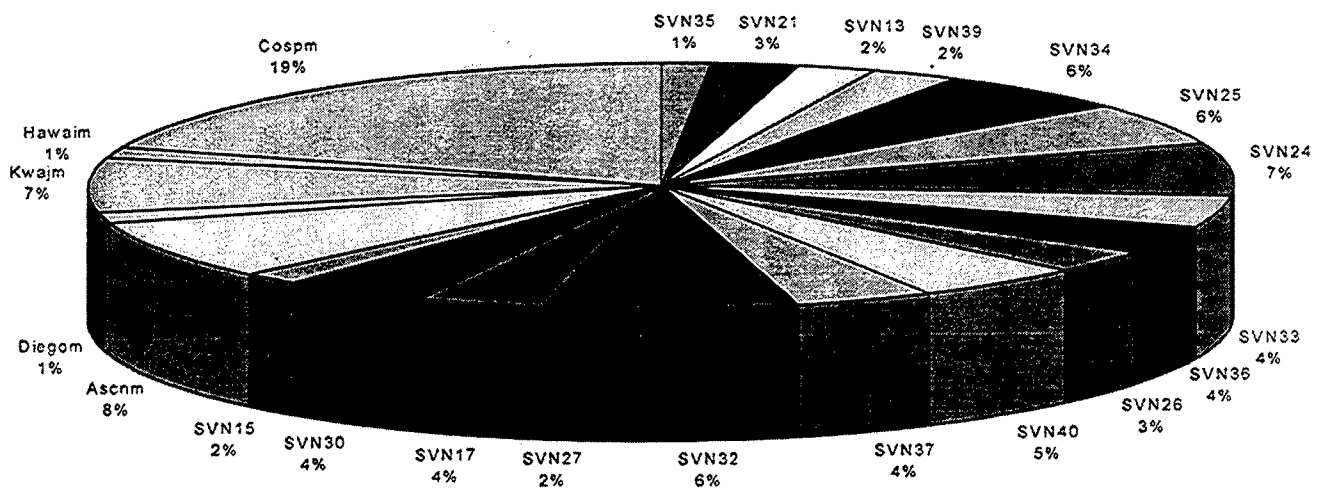


Figure 4. Implicit Long Term Weighting of GPS Time 18 August 1997

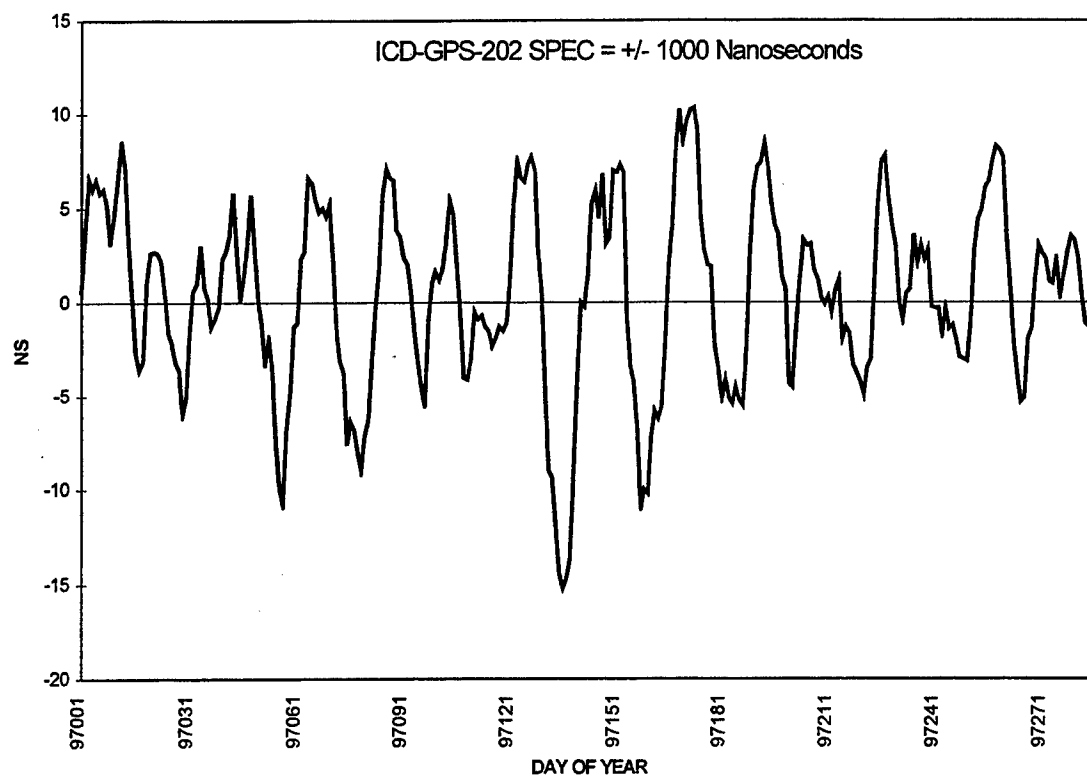


Figure 5. 1997 Daily GPS - UTC(USNO)

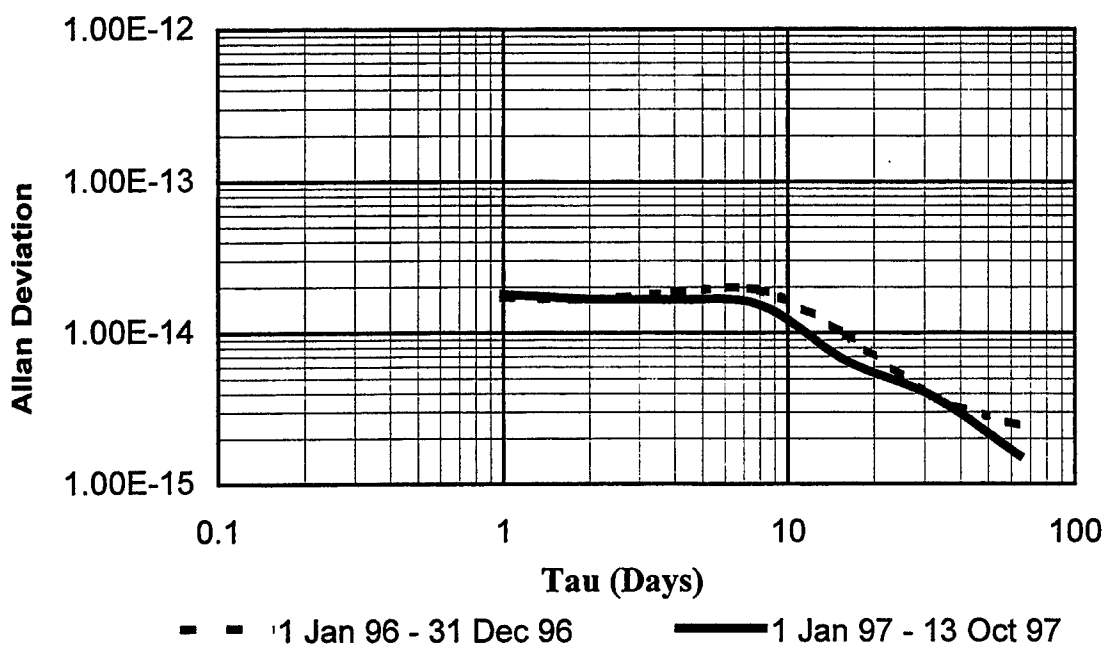


Figure 6. GPS-UTC(USNO) Stability for 1996 and 1997

A NEW APPROACH TO IONOSPHERIC DELAY CORRECTIONS IN SINGLE FREQUENCY GPS RECEIVERS

G. Mirenni (*), V. Pettiti, F. Cordara
Istituto Elettrotecnico Nazionale Galileo Ferraris (IEN)
Strada delle Cacce, 91 - 10135 Torino, Italy
Tel.+39 11 3919 239, Fax +39 11 346 384, e-mail cordara@tf.ien.it
(*) guest researcher

L. Ciraolo
CNR - Istituto di Ricerca sulle Onde Elettromagnetiche "Nello Carrara" (IROE)
Via Panciatichi, 64 - 50127 Firenze, Italy

Abstract

The IEN Time and Frequency Laboratory is equipped with single frequency GPS receivers to relate the Italian time scale to UTC and to give the traceability to the reference clocks of secondary laboratories. The synchronization data obtainable from the GPS system, in spite of its high performances, are affected by various error sources, one of the most important being the ionospheric corrections applied inside the receivers according to a model.

To evaluate the influence of these corrections on the common-view synchronization results, some investigations have been performed at IEN, using measurement from an ionosonde to test some ionospheric models, and the data supplied by two dual-frequency GPS receivers located at or nearby time and frequency laboratories. For each geodetic receiver and satellite tracked, the differential hardware delay was computed using an original approach developed at IROE.

The computed ionospheric delay corrections have subsequently been used to post-process a set of GPS common-view synchronization results between IEN-Italy and ROA-Spain and the uncertainty of the comparisons evaluated.

INTRODUCTION

The comparisons between the reference clocks maintained in timekeeping laboratories are based worldwide on the GPS signals reception using the common-view technique according to the BIPM schedule. The increased accuracy and stability of the new commercial cesium clocks and of the primary frequency standards require an improvement in the uncertainty of the synchronization links.

One of the most limiting factors in achieving this goal with the equipment actually in use is related to the ionospheric correction model adopted in the one-channel, single frequency GPS receivers, normally operated in the timing centers.

In this way it is difficult in fact to have a correct estimate of the delay affecting the GPS signals crossing the ionized part of the atmosphere, i.e. the ionosphere (about 100 to 1000 km in height) and the plasmasphere (beyond 1000 km).

A single-frequency GPS receiver is being used at IEN to synchronize the atomic clocks with those of other laboratories when a GPS satellite is visible in common-view. Measuring clock differences versus GPS time, a slight residual error of the order of nanoseconds, mostly due to the ionospheric time-delay, can be present.

Having the capability to access a data base of RINEX (Receiver INdependent EXchange) files, where the pseudorange, carrier phase data and navigation messages provided by dual-frequency GPS receivers of the Italian Geodetic Network, located in Torino and Rome, and by the Royal Observatory of San Fernando (Spain) are available, the following topics have been investigated and operations performed:

- some existing models for the computation of the *TEC* (Total Electron Content), in the direction of the satellites tracked, using the data obtained by an ionosonde and by a dual frequency geodetic receiver, both located at the ING (Istituto Nazionale di Geofisica) in Roma, have been compared;
- a computer program has been developed to get the ionospheric delay from the geodetic receivers data, requiring that the hardware delay only be supplied by an external source;
- the differential hardware delays of the satellites L1 and L2 carrier frequencies and of the dual-frequency GPS receivers, used to measure the ionospheric propagation delays (in Torino and San Fernando), to be substituted in the common-view differences, have been computed at IROE with a software that will be described in the followings;
- the improvement achievable, substituting the ionospheric corrections obtained from the previous technique over a ten days sample of GPS data files supplied by the single frequency receivers of IEN and ROA, have been checked versus the time scale differences computed using the standard common-view data.

MEASURING THE IONOSPHERIC DELAYS WITH GPS

The computer program realized, aiming to reduce the uncertainty contribution of the ionosphere on the GPS synchronization data as described later on, has allowed to compare the ionospheric delay measurements coming from a dual-frequency GPS receiver with those obtained from three ionospheric models. These models are the IRI-90 [1], the DGR (Di Giovanni, Radicella) [2] and a third model obtained by reconstructing the ionospheric electron density profile on the basis of a virtual profile from ionograms, provided by an ionosonde, for lower ionosphere, and from the DGR model for the topside of the ionosphere [3].

The DGR model is based on few particular points, critical frequencies and corresponding heights, in the ionogram that become fixed points for some mathematical functions approximating the electron density profile. This model was chosen because developed for the geographical site of the ionosonde (Rome).

The IRI-90 (International Reference Ionosphere) is the most common model describing the ionosphere for geomagnetically quiet conditions. This model uses the longest series of data that is the basis for electron density profile computations. The input parameters for the three models have been obtained from ionograms given every five minutes by one of the ING ionosondes.

The three models provide an evaluation of the vertical *TEC* (Total Electron Content), measured in *TEC* units (10^{16} electrons/meter²). This evaluation has been slanted in the direction towards GPS satellites.

The ionospheric time-delay for a signal at frequency f is bound to *TEC* along the signal path as follows:

$$\Delta t_{ion} = \frac{40.3}{c \cdot f^2} \cdot TEC \quad [s] \quad (1)$$

For the GPS L1 carrier (1.57442 GHz), 1 *TEC* unit corresponds to 0.54 ns of ionospheric time delay. In any case, all the three models provide an evaluation of the real ionospheric *TEC* and they don't consider the plasmasphere. In accordance with the results obtained by Ciralo and Spalla at IROE [4], it has been assumed that the plasmaspheric contribution is (3 ± 1) *TEC* units without either daily or seasonal perceptible variability. Therefore 3 *TEC* units have been added to the evaluations of *TEC* obtained by the three models in order to include plasmasphere.

In Fig.1 data are shown regarding satellites PRN03 and PRN15, observed in Rome on 23 June 1996. The solid curve is provided by the geodetic receiver of ING, the dashed one represents DGR data, the dash-dot one IRI-90 data and the dotted one is relative to the third model.

Taking into account the azimuth of the satellites, it can be observed that satellites to the north and mostly to the northwest direction show almost always overestimated measurements of ionospheric time delay according to the three models with respect to GPS measurements. On the contrary, satellites to the south usually show subestimated measurements of the ionospheric delay. Satellites to the west and especially to the east show minimal differences between models and GPS measurements.

To have an idea about the magnitude of the differences between the GPS and models results, the mean $\bar{\epsilon}$ of the absolute value of these differences and the standard deviation σ_e have been computed both for the daily values and for the whole period of observation and are shown in Table 1.

Date	DGR		IRI-90		Third model	
	$\bar{\epsilon}$	σ_e	$\bar{\epsilon}$	σ_e	$\bar{\epsilon}$	σ_e
1996/06/19	16	11	14	10	24	16
1996/06/20	14	10	13	9	26	17
1996/06/22	13	13	12	11	21	16
1996/06/23	13	10	12	8	23	15
Global	14	11	13	10	24	17

Table 1 - Differences of GPS dual frequency data versus ionospheric models in *TEC* units

Evaluations performed with the ionospheric models are not satisfactory because of several approximations passing from vertical to slant *TEC*, and of the presence of a persistent E sporadic layer not allowing for a precise acquisition of input data for models.

Due to the dispersive features in frequency of the ionosphere, using the L1 and L2 GPS carriers, one can evaluate the ionospheric delay. For both carriers (L1=1.57442 GHz and L2=1.22760 GHz) the GPS receivers measure, usually every 30 seconds, pseudoranges R_1 , R_2 and carrier phases ϕ_1 , ϕ_2 . Pseudoranges are very noisy measurements both because of their nature and of the intentional errors in GPS (Selective Availability and Anti Spoofing [3]). The problem with carrier phase measurements is the carrier cycle ambiguity; that is the number of full cycles along the line of sight between the satellite and receiver is initially unknown.

Pseudoranges R_i for Li ($i=1$ or 2) carrier can be modelled as:

$$R_i = \rho + c\Delta\delta + \Delta R_{i,ion} + \Delta R_{tro} \quad [\text{m}] \quad (2)$$

where ρ is the true distance receiver-satellite, c is the light speed, $\Delta\delta$ is the bias between satellite atomic clock and the receiver clock, $\Delta R_{i,ion}$ is the ionospheric delay in range units, and ΔR_{tro} is the tropospheric delay.

Carrier phases ϕ_i can be modelled in range units also as:

$$\lambda_i \Phi_i = \rho + \lambda_i N_i + c\Delta\delta - \Delta R_{i,ion} + \Delta R_{tro} \quad [\text{m}] \quad (3)$$

where λ_i is the carrier wavelength and N_i is the carrier cycle ambiguity. The minus sign in the ionospheric delay is due to the different sign in the ionospheric group or phase refractive index.

In pseudorange measurements, $\Delta R_{i,ion}$ is the only term depending on the signal frequency; so one can write:

$$\begin{aligned} \rho &= R_1 - \Delta_{1,ion} \\ \rho &= R_2 - \Delta_{2,ion} \end{aligned} \quad (4)$$

and using (1) it is easy to deduce:

$$\Delta R_{i,ion} = \frac{R_1 - R_2}{1 - f_1^2 / f_2^2} \quad [\text{m}] \quad (5)$$

Following a similar procedure for the carrier phase we obtain:

$$\Delta \Phi_{1,ion} = \frac{f_2^2}{f_2^2 - f_1^2} \left[\Phi_1 - N_1 - \frac{f_1}{f_2} (\Phi_2 - N_2) \right] \quad [\text{cycles}] \quad (6)$$

where the problem is that N_1 and N_2 are unknown.

But if N_1 and N_2 are neglected and the values obtained by (6) are subtracted from the first good datum, an extremely precise measurement of ionospheric delay variability is obtained. The first good datum is the one acquired when the satellite is for the first time above 30° minimum elevation. Subtracting this variability from (5), the data obtained are constant except for the noise which is presumably at null average value. So working out the average of theses data, its noise is removed and

the "ionospheric offset" is obtained. Finally, the variability worked out using carrier phase is added to this offset.

For PRN03 satellite received in Roma on 23 of June 1996, one can see in Fig. 2 the difference in measurement precision of the ionospheric time-delay in *TEC* units using only the pseudoranges (segmented line) or the algorithm described above.

As a matter of fact many problems have to be solved in order to reach the most demanding levels of uncertainty needed by timing centers. The most relevant items are the cycle slips, that can occur when the GPS signal is lost for sometime and then tracked back again, and the hardware differential delays. As regards to the cycle slips, an automatic procedure for detecting and correcting the results, based on data taken before the occurrence of phase steps, has been developed and tested successfully [5].

HARDWARE DELAY EVALUATION

The problem of the hardware differential delays or biases, due to the fact that the coded signals passing through different satellite and receiver hardware are subject to different delays for the two carriers, has been solved making the following assumptions:

- the observed DGD (Differential Group Delay), equivalent to the differential pseudorange (5) but expressed in *TEC* units, is written in terms of the slant *TEC* from the station to the satellite and the hardware bias β as:

$$DGD = TEC + \beta \quad (7)$$

- the ionosphere is an infinitesimally thick spherical slab, concentric to the Earth, located at an height of 400 km. The intersection point between the ionosphere and the satellite to station ray path is defined as the ionospheric point P as shown in Fig.3.

- given the vertical electron content *VEC* in P, *TEC* is written as:

$$TEC = VEC \cdot \sec \chi \quad (8)$$

where χ is the angle between the ray path and the vertical in P.

Each observation to the *s*-th satellite, referring to a specific ionospheric point P of known latitude Φ_s and longitude Λ_s , at a station time *t*, becomes:

$$DGD_s(t) = VEC(t, \Lambda_s, \Phi_s) \cdot \sec \chi_s(t) + \beta_s \quad (9)$$

Assumption of a model able to map $VEC(t, \Lambda_s, \Phi_s)$ as a function of a set of coefficients makes it possible to write a set of equations of observation in terms of the unknown model coefficients and the biases β .

Several methods have been proposed to perform this, from the global multistation approach [6] to the simple single-station one used in this work, which is a development of the technique presented in [7]. In this approach it is assumed that the dependence of *VEC* versus latitude is linear, while time-longitude dependence occurs only through the local time $LT=t+\Lambda$ (in coherent units). *VEC* around the station, at a given time t_s^* , can be written, introducing the latitudinal slope of *VEC*, $m(t)$, as:

$$VEC(t_s^*, \Lambda_s, \Phi_s) = VEC(t) + m(t) \cdot (\Phi_s - \Phi_{sta}) \quad (10)$$

where $VEC(t)$ is the vertical TEC at the station taken at a time t to which the same local time of the ionospheric point: $t_s^* + \Lambda_s = t + \Lambda_{sta}$.

Using (9) and (10), one can write VEC relative to the station at some time t :

$$VEC(t, \Lambda_{sta}, \Phi_{sta}) = [DGD_s(t_s^*) - \beta_s] \cos \chi_s(t_s^*) - m[\Phi_s(t_s^*) - \Phi_{sta}] \quad (11)$$

Due to the global performance of GPS, the presence at any time t of at least four satellites (generally up to 7-8) over the horizon of the station, provides a corresponding number of DGD observations, not only at time t , but also at t_s^* . This enables comparison through (11) the estimations of the same $VEC(t, \Lambda_{sta}, \Phi_{sta})$ inferred by satellite s and r , namely:

$$[DGD_s(t_s^*) - \beta_s] \cos \chi_s(t_s^*) - m(t_s^*)[\Phi_s(t_s^*) - \Phi_{sta}] = [DGD_r(t_r^*) - \beta_r] \cos \chi_r(t_r^*) - m(t_r^*)[\Phi_r(t_r^*) - \Phi_{sta}] \quad (12)$$

For each epoch of observation, all the possible pairs of (12) are written. Moving the terms containing the unknowns on the left and the known terms on the right provides a set of linear equations of condition in the unknown β_s and the latitudinal slopes $m(t)$, which in matrix form is written as:

$$\mathbf{B}\hat{\beta} + \mathbf{M}\hat{\mu} = \hat{\varepsilon} \quad (13)$$

where $\hat{\beta}$ is the vector of the unknown satellite plus receiver biases, and $\hat{\mu}$ the one of unknown latitudinal slope; vector $\hat{\varepsilon}$ accounts for errors (noise, multipath) and model inadequacy. \mathbf{B} and \mathbf{M} are the coefficients of the unknowns as computed by (11).

The steps needed for the solution are described in the followings:

- differential phase and group delays are computed from the RINEX observation file smoothing the differential data over 10 minutes;
- navigation files containing the orbital data of GPS satellites are used to compute the satellite position, from which the ionospheric point and all the geometrical quantities involved can be obtained;
- according to (11), observations relative to the ionospheric points having the same local time are paired to build up the system (13).

The Least Squares solution is performed through successive approximations starting from null latitudinal slopes. No elevation mask is a priori used: low elevation points are automatically rejected, if needed, during the process of discarding the outliers. The internal consistency of the method results in better than one TEC unit; the accuracy is limited to 2-3 TEC units by the dynamics of the ionosphere and, sometimes more severely, by the effects of multipath.

POSTPROCESSING OF GPS COMMON-VIEW DATA

With the computer programs described before, the ionospheric corrections for two sites, Torino and San Fernando, where the national time scales of Italy and Spain are maintained and both single-frequency and dual-frequency GPS receivers are operated, have been determined. The geodetic receivers available were namely a Trimble 4000 SSI at the Politecnico di Torino (45°03'48" N,

07°39'41" E, 311 m height) and a Trimble 4000 SSE at the Real Instituto y Observatorio de la Armada in San Fernando (36°27'52" N, 06°12'20" W, 86 m height). The single-frequency receivers used for the measurements in common-view at IEN and ROA are an NBS/GPS and an AOA TTR6 respectively.

For eleven days, starting from 13 February 1997, for each satellite tracked by the geodetic receivers and included in the BIPM common-view schedule, the ionospheric corrections have been computed using the information in RINEX files, and the results have been used to correct the synchronization results obtained from the straight use of the single frequency receiver output data.

The curves for the two cases, reported in Fig.4, were obtained computing a daily mean value at 0h UTC of the difference between the two time scales by means of a linear regression over about 25 common-view data, after having applied a 3σ filtering. The standard deviation of the residuals computed for the link, in the case of the improved ionospheric corrections is slightly smaller (10%) than the customary one (2.5 ns).

The differences between the ionospheric delay corrections computed from the geodetic receiver data and those supplied by the timing receivers, for the same period, are better seen in Fig.5 which shows a peak-to-peak excursion of 2.1 ns and an average bias of -0.5 ns with a standard deviation of 0.6 ns. These results suggest that a further processing of the standard common-view synchronization data does not improve significantly the uncertainty of the comparisons but, from the detailed representation of one day of the two ensemble of ionospheric corrections data for each satellite used (Fig.6), it can be seen that the "modelled" one exhibits an overestimate of the correction (2 to 9 ns) at both sites, with maximum values around local noon. In Fig.7 the same information is reported for the whole period of the time comparisons. As only the satellite passages for which results from the two kind of receivers were available both in Torino and in San Fernando have been used for this investigation, the average number of data was 25, about 40% lower than the customary one utilized in time scale comparisons with GPS.

From what seen above, in the case of a user not operating its receiver in the common-view mode, the correction technique described in this paper can improve significantly the synchronization results. It must also be taken into account that this experiment has taken place in a period close to the minimum of solar activity and therefore some of the effects seen before can be even of more significance in the years to come.

CONCLUSIONS

An investigation on the improvement obtainable in time scales comparisons, performed with the common-view technique and the standard timing receivers, using ionospheric corrections computed from phases and pseudorange measurements of dual-frequency GPS receivers, has been performed at IEN using the data available in RINEX files and relative to two Italian geodetic stations and the Observatory of San Fernando in Spain.

Both for the determination of the ionospheric corrections and the evaluation of the differential hardware delays, a new approach for which computer programs have been developed and tested experimentally at IEN and IROE has been adopted.

While the comparisons with the common-view technique between the time scales of IEN and ROA do not show to gain significantly from the use of the ionospheric corrections applied, at least in this period of small solar activity, it is evident that in the case of a one-way user, the experimented technique can bring an improvement over the synchronization data as given by the standard GPS receivers.

ACKNOWLEDGMENTS

The authors wish to thank the following people and institutions for their helpful cooperation: E. Zuccheretti and F. Riguzzi (ING - Rome), A. Cina and A. Manzino (Politecnico di Torino - Dipartimento di Georisorse e Territorio) and J. Palacio Rodriguez (ROA - San Fernando, Spain).

REFERENCES

- [1] D. Bilitza: "*International Reference Ionosphere 1990*". NSSDC 90-92, World Data Center A Rockets & Satellites, Greenbelt, U.S.A. 1990.
- [2] S.M. Radicella, "*The improved DGR analytical model of electron density height profile and total electron content in the ionosphere*" *Annali di Geofisica*, Vol. XXXVIII, n. 1, March 1995, pp. 35-41.
- [3] G. Miredda: "*Ionospheric corrections for the GPS system*". Thesis in Telecommunications Engineering, Politecnico di Torino, 1996.
- [4] L. Ciralo, P. Spalla: "*Comparison of TEC evaluation from NNSS and GPS*". *Radio Science*, Vol. 32, (3), pp. 1071-1080, May - June 1997.
- [5] G. Miredda, F. Riguzzi, E. Zuccheretti: "*Measurements of ionospheric TEC in the direction of GPS satellites and comparisons with three ionospheric models*". To be published on *Annali di Geofisica*, 1997.
- [6] G.E. Lanyi, T. Roth: "*A comparison of mapped and measured total ionospheric electron content using Global Positioning System and beacon satellite observations*". *Radio Science*, Vol. 23 (4), pp. 483 - 492, 1988.
- [7] L. Ciralo: "*Evaluation of GPS L2-L1 biases and related daily TEC profiles*". Proc. Workshop on Modelling the Ionosphere for GPS Applications, Neustrelitz, 29-30 September 1993.

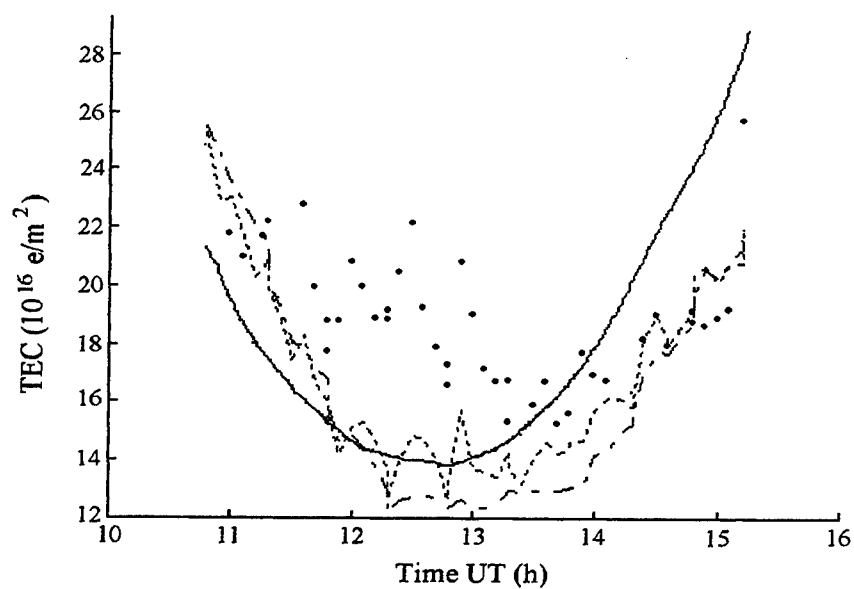


Fig. 1.a - Comparison between the data supplied by a dual-frequency GPS receiver and models for ionospheric corrections (PRN03, 1996-06-23).

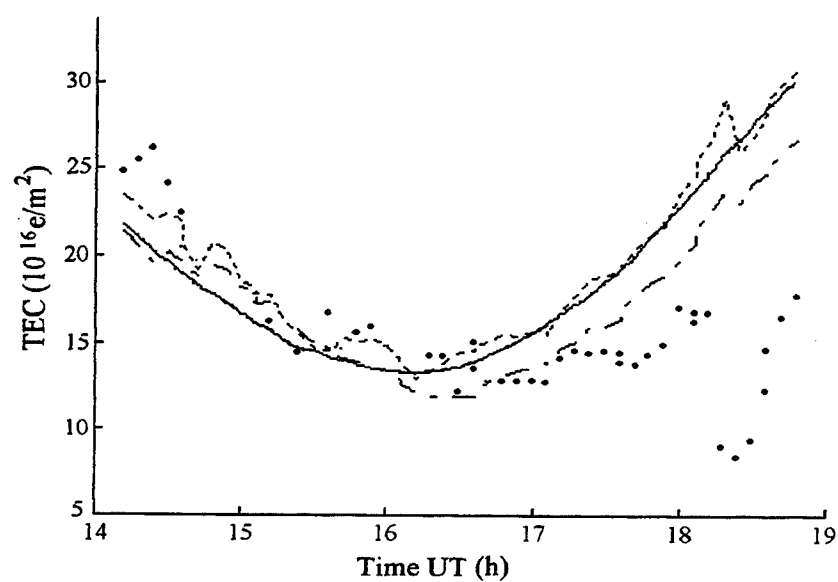


Fig. 1.b - Comparison between the data supplied by a dual-frequency GPS receiver and models for ionospheric corrections (PRN15, 1996-06-23).

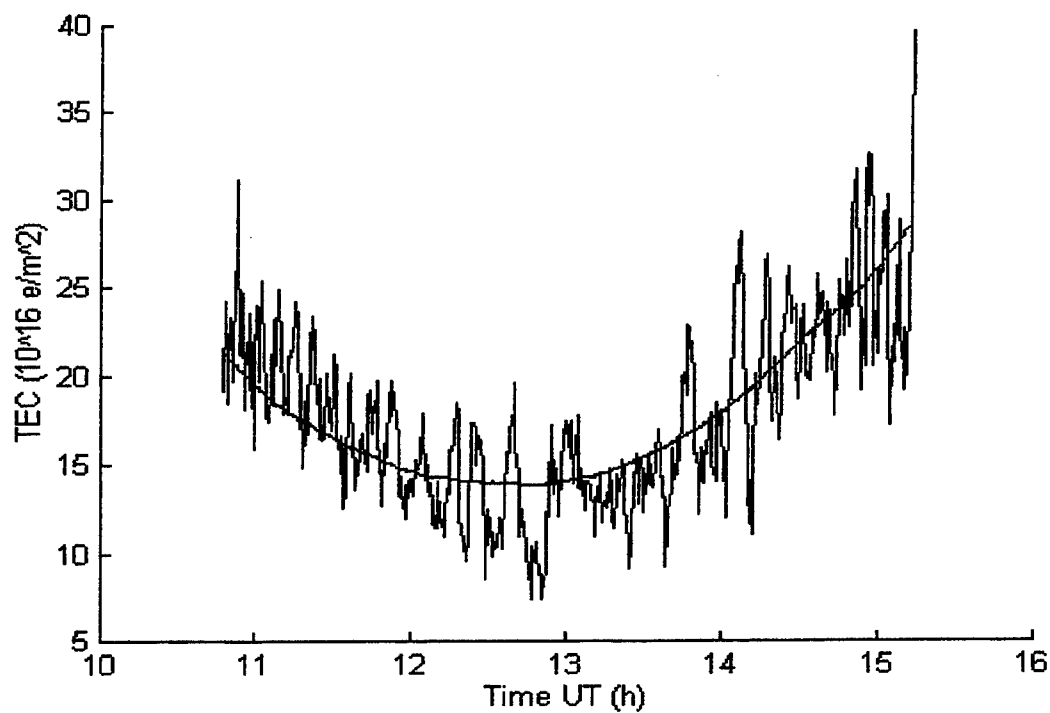


Fig. 2 - Ionospheric time delay (in TEC units) obtained from pseudoranges (segmented line) or computed at IEN.

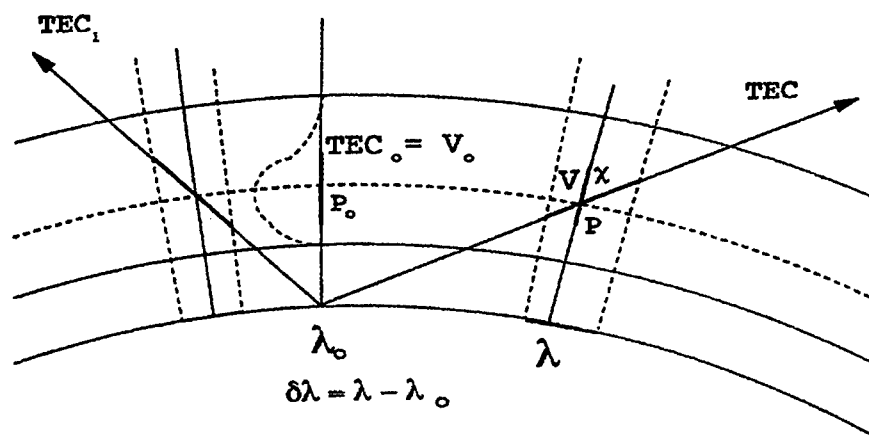


Fig. 3 -Representation of the relationship between the TEC in the satellite direction (slant) and the vertical one.

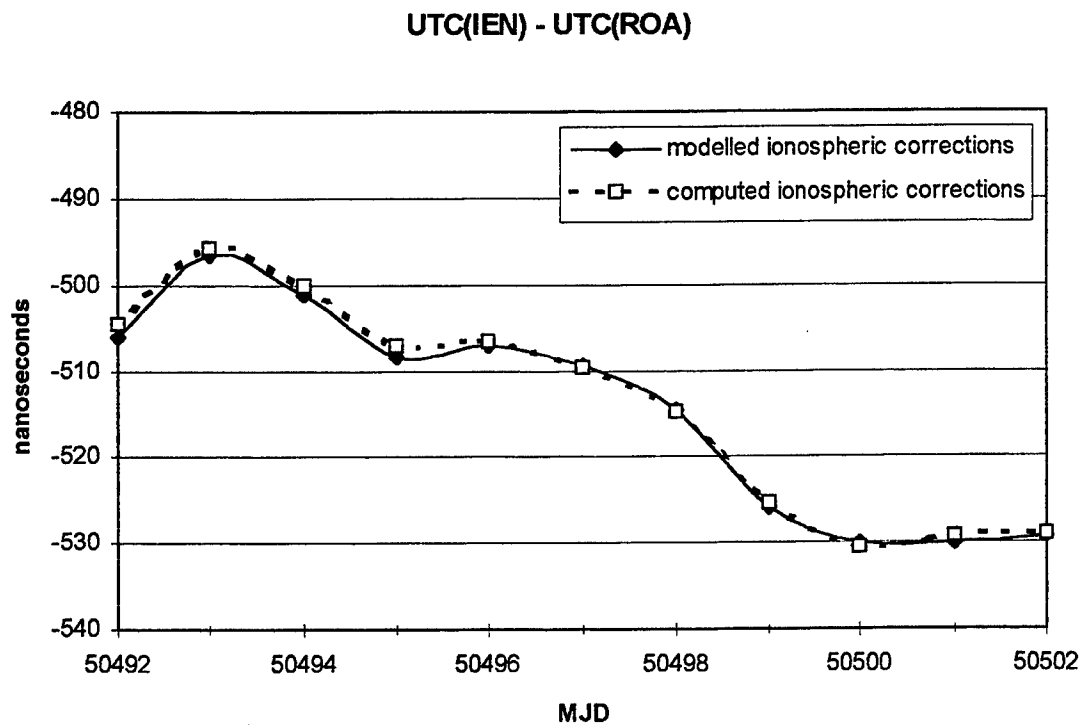


Fig. 4 - Time scales comparison using standard receiver output data or correcting for the ionospheric time delays.

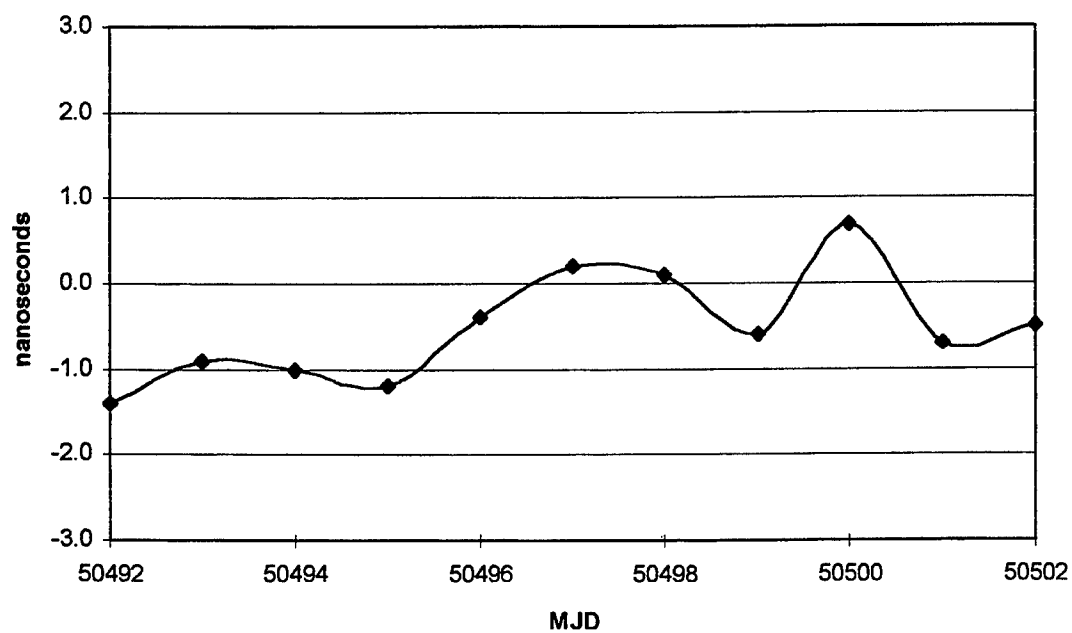


Fig. 5 - Differences between modelled and measured ionospheric corrections.

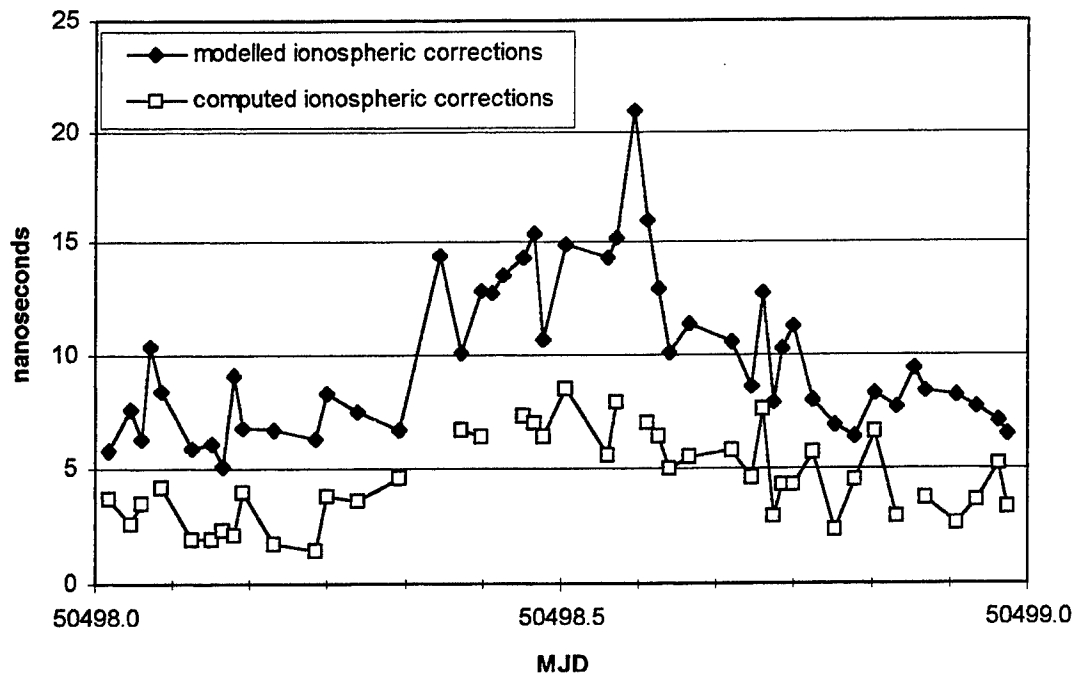


Fig. 6 - Modelled and measured ionospheric corrections for IEN-Torino (1997-02-19).

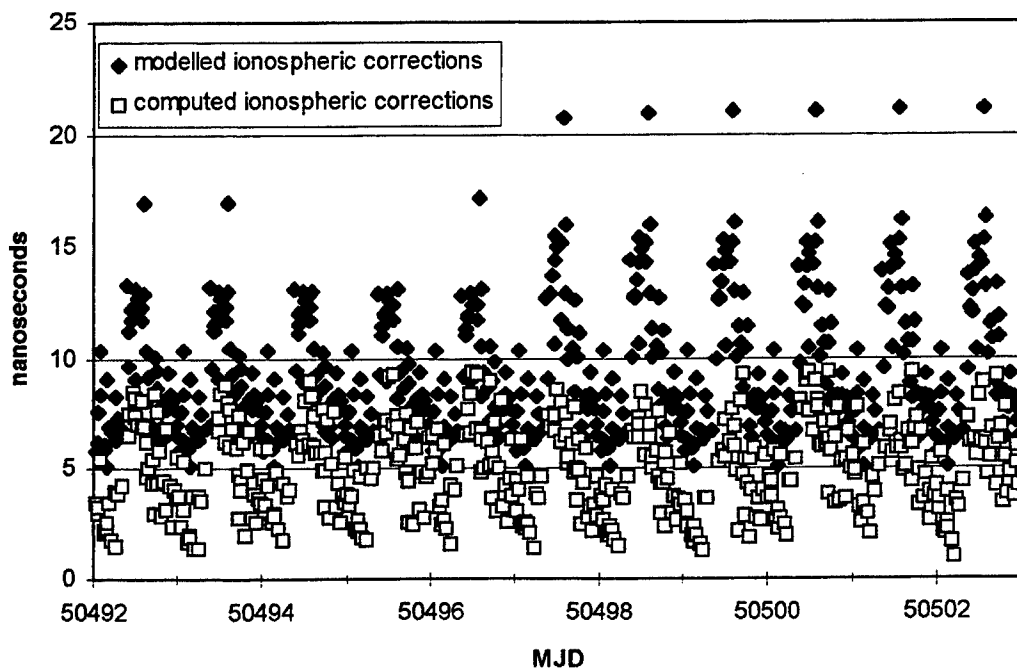


Fig. 7 - Modelled and measured ionospheric corrections for IEN-Torino (1997-02-13 to 1997-02-23).

Performance of the Kalman Filter of the Global Positioning System Operational Control Segment During January - March 1997*

Marc Weiss, Audrey Zarr
National Institute of Standards and Technology
Time and Frequency Division
325 Broadway, Boulder, CO 80303

Abstract

We characterize the errors in the broadcast estimates of the Global Positioning System's satellite ephemeris and clock states made by the Operational Control Segment's (OCS) Kalman filter over the period when the system ephemeris Q's were changed. This change was called the Ephemeris Enhancement Endeavor (EEE).

We report on the accuracy, stability, and periodic variations of the GPS Kalman filter's estimates of satellite clocks and ephemerides, particularly how they changed with EEE. Root-sum-squared (RSS) ephemeris error variations decreased by a factor of 1.7. The amplitude of the 2 cycle/d component decreased by a factor of 2.2. While the 2 cycle/d periodic effects dropped from 0.65 to 0.49 of the RSS ephemeris error, they still seem to be a major component. Radial ephemeris errors appear to be negatively biased by about 1 m. This bias is unchanged by EEE. Error deviations are generally no more than SV clock stabilities — the Kalman filter Q's are generally good. Clock estimate errors are worse than ephemeris errors — there may still be some room for improvement. Broadcast ephemeris errors add diurnal variations to the GPS time offset from the U. S. Naval Observatory Master Clock (USNO MC). GPS - USNO MC variations for averaging times near 1 d are consistent with White PM, averaging down to 1.5 ns at 1 d with 48 points/d. GPS - USNO MC appears to have periodic variations with periodicity spread approximately over periods from 16 to 24 d and a total amplitude of up to 4.5 ns.

INTRODUCTION

This report characterizes the performance of the ephemeris and clock parameters as broadcast from the Global Positioning System satellite vehicles (SVs) [1] during the first three months of 1997. During this period a change was made to refine the way these parameters are estimated by the Operational Control Segment's

* Contribution of U.S. Government, not subject to copyright.

(OCS) Kalman filter. This change was called the Ephemeris Enhancement Endeavor (EEE). EEE changed the estimated stochastic noise levels for the variations in the satellite ephemerides, the so-called ephemeris Q's of the Kalman filter for each satellite. These changes were made in the operational filter for each satellite at a specific time. Hence, it is possible to study the steady-state performance of the broadcast parameters from each satellite before and after the EEE changes were introduced. The precise ephemeris of the National Imagery and Mapping Agency (NIMA) [2] was used as the reference. Besides studying the broadcast ephemeris errors we also characterized the steering of GPS time to the U. S. Naval Observatory Master Clock (USNO MC), and the broadcast estimates of SV clock against GPS time.

BROADCAST EPHEMERIS ERRORS

To study the broadcast ephemeris errors, we compared the broadcast ephemerides to the NIMA precise ephemerides. We obtained the broadcast ephemerides from the Crustal Dynamics Data Information System (CDDIS) web site [3,4]. This is a NASA data bank on the Internet which, among other things, serves as a global data center for the International GPS Service for Geodynamics (IGS). We obtained the precise ephemerides directly from NIMA. The precise ephemerides gives x -, y -, and z -coordinates for each SV every 15 minutes. We evaluated the broadcast ephemerides for these 15-minute points and subtracted the position vectors from the precise ephemerides. The results were the ephemeris error vectors. We then projected these errors into radial, in-track, and cross-track components. In this way we produced three time series for each SV for the 90 d period, 1 point every 15 minutes, representing the SV's ephemeris errors.

BLIND SEARCH FOR EEE CHANGES

We looked for a change in the amplitude of the 2 cycle/d Fourier component. To search for a change, we broke the 90 d, 1 point every 15 minutes data into 256-point segments. This created data sets $2\frac{2}{3}$ d long. We computed the 2 cycle/d Fourier component for each of these segments, and looked for a significant drop in value. In some satellites, there was a clear drop, while in others the change was less clear.

The ratio of the 2 cycle/d component to the RSS of all Fourier components seemed to have no significant drop in much of the data. This suggests that the EEE changes improved the stability of the ephemerides in general, though they did not particularly reduce the 2 cycle/d periodic effects. As we shall see in later results, these are still about 0.5 times the total ephemeris error. The results of the blind search generally agreed within a few days of the actual change. The cases where the agreement is less good are those for which the drop was less obvious.

ANALYSIS OF EEE CHANGES

Using the actual dates for the EEE changes, we broke the data into two segments for each satellite. We then computed an estimate of the spectrum and the time variance, TDEV [5,6], for each satellite and for each of the vector error components: radial, in-track, and cross-track. There are two topics of particular interest from these studies: the 2 cycle/d periodic variations and the TDEV variations at 1 d. We discuss the 2 cycle/d periodic variations and the TDEV variations in this section, leaving the discussion of 1 d performance to go along with the discussion of SV clock estimate errors.

The periodic variations of ephemeris error are summarized in Table I. We use here the accepted formula for projecting error vectors on the earth by weighting radial, in-track, and cross-track terms as follows [7,8]:

$$\text{Projected Error} = \sqrt{\text{Radial}^2 + \frac{\text{In-Track}^2 + \text{Cross-Track}^2}{49}}. \quad (1)$$

For each segment and for each SV we report the projected values for the 2 cycle/d Fourier amplitude, the RSS of all Fourier components, and the $\frac{1}{4}$ d TDEV value. The RSS of all Fourier components equals the standard deviation. A periodic term affects the TDEV values, providing a maximum at half the period. Hence, the 2 cycle/d component appears in TDEV at the $\frac{1}{4}$ d averaging time. We also give the ratios of the 2 cycle/d Fourier amplitudes to the RSS of all Fourier components in Table II. This allows us to quantify how the EEE changes affected the noise level of the ephemeris error as a whole versus the 2 cycle/d periodic term. The RMS of this ratio over all SV's yields 0.65 before the changes and 0.49 after. Although there is significant reduction in the dominance of this periodic effect, it is still a major source of error.

GPS TIME VERSUS USNO MC

Measurements of GPS time against USNO MC were provided by USNO. These data had no selective availability (SA) effects and, after January 28, were corrected for measured ionospheric delays. Each data point is the average of 13 minutes of measurements of GPS time against USNO MC using one satellite. We graphed received data (Figure 1a). We corrected the data for the ephemeris error, using the NIMA precise ephemeris as "truth" (Figure 1b). We used a low-pass filter to remove white phase modulation (Figure 1c).

For each of the three time series, we interpolated the data to an even spacing of 48 points per day, then computed TDEV to estimate the spectrum. The TDEV graphs are displayed in Figures 2a, 2b, and 2c. (GPS - USNO MC) variations for averaging times near 1 d are consistent with white PM, averaging down to 1.5 ns at 1 d with 48 points/d. (GPS - USNO MC) appears to have periodic variations with periodicity spread approximately over periods from 16 to 24 d and a total amplitude of up to 4.5 ns. This periodicity was best seen in the TDEV plots. The periodic terms are so spread out that the spectral estimate gives a poor indication of the individual periodic components. A modulating frequency f_m with amplitude A , small compared to the high-frequency cut-off of the measurement system, affects TDEV according to [5,6]

$$TDEV(\tau) = A \sqrt{\frac{8}{3}} \cdot \left| \frac{\sin^3(\pi \tau f_m)}{\pi \tau f_m} \right|. \quad (2)$$

TDEV(τ) reaches its first maximum when $\tau f_m = \frac{1}{2}$, or $\tau = \tau_p$, where τ_p is the period. In that case, $TDEV_{\max} \approx A \cdot 1.04$. Hence, $TDEV_{\max}$ is approximately the amplitude of the modulating periodic effect. If we consider that the TDEV of 4.5 ns at 10 d is the RSS of an effect due to periodicity and white PM of about 0.5 ns, that implies an amplitude of about 4.5 ns.

BROADCAST CLOCK CORRECTION ERRORS

We estimated the clock correction errors for each SV. We obtained the values of (GPS - USNO MC) for each SV from the data that USNO provided. We removed the ephemeris errors from these data, giving an estimate of (GPS - USNO MC) via that satellite. We then subtracted our filtered estimate of (GPS - USNO MC) from

these data. The residuals are an estimate of the error in the broadcast value used to correct that SV clock for GPS time. We computed TDEV and a spectral estimate for these data for each SV. Since the SV clock stability determines its predictability, the clock correction error should be no worse than the clock stability at 1 d. Similarly, since the clock is the reference used to determine the satellite ephemeris, the 1 d TDEV of the ephemeris error should be less than the clock stability. Table III gives the 1 d TDEV values for the SV clocks, the ephemerides, and the clock correction errors. The instabilities of the ephemeris errors are all smaller than the clock instabilities. Values where the clock correction error instabilities are larger than the SV clock instabilities are in bold.

Finally, we looked at the mean and standard deviation values for the error terms. We computed these for the projected ephemeris errors for each satellite for both segments 1 and 2. We also compute these values for the clock correction errors for each satellite for both segments 1 and 2. We found that the mean ephemeris error terms are always negative. This is because the radial errors all have a negative bias of order 1 m, both before and after EEE. The overall RMS of the standard deviations is 1.8 m before EEE and 1.1 m after EEE. The clock errors appear unbiased, and their RMS standard deviations appear unaffected by EEE.

CONCLUSIONS

EEE significantly reduced the GPS satellite broadcast ephemeris error deviations, reducing the RSS ephemeris errors by a factor of 1.7 and the amplitude of the 2 cycle/day Fourier component decreased by a factor of 2.2. The 2 cycle/d periodic component remains a major part of the error. Radial ephemeris errors appear to be negatively biased by about 1 m. The reason for this is unknown. The Kalman filter Q's are generally good, though there may still be some room for improvement in the clock Q's. Broadcast ephemeris errors add diurnal variations to (GPS - USNO MC). (GPS - USNO MC) variations for averaging times near 1 d are consistent with white PM, averaging down to 1.5 ns at 1 d with 48 points/d. (GPS - USNO MC) appears to have periodic variations spread over 16 to 24 d with a total amplitude of up to 4.5 ns.

REFERENCES

- [1] "Navstar GPS Space Segment/Navigation User Interfaces," ICD-GPS-200, Revision C, 15 Dec 1994, ARINC Research Corporation, 4055 Hancock Street, San Diego, CA 92110.
- [2] Malys, S., and J. Slater, "Maintenance and Enhancement of the World Geodetic System 1984," Proc. ION-GPS-94, Salt Lake City, Sept. 20-23, 1994, pp 17-24 (1994).
- [3] Flow, Archiving, and Distribution of Global GPS Data and Products for the IGS and the Role of the Crustal Dynamics Data Information System (CDDIS), Proc. of the Workshop on Improving the DGPS Infrastructure for Earth and Atmospheric Science Applications, March 1996, available from the CDDIS Internet web site.
- [4] The Internet address for the CDDIS is <http://cddis.gsfc.nasa.gov/cddis.html>
- [5] ANSI Telecommunication Standard T1.101.
- [6] D.W. Allan, M.A. Weiss, J.L. Jespersen, "A Frequency-Domain View of Time-Domain

Characterization of Clocks and Time and Frequency Distribution Systems," Proc. 45th Frequency Control Symposium, 1991.

- [7] W. Fees, M. Menn, and Zeitzew, "OCS Performance Analysis," Proc. of the 1996 Performance Analysis Working Group (PAWG), Peterson Air Force Base, Colorado.
- [8] C. Chuck, S. McReynolds, T. Metzger, and J. Moore, "GPS MCS Kalman filter performance," Proc. of the 1996 Performance Analysis Working Group (PAWG), Peterson Air Force Base, Colorado.

Table I: Broadcast Ephemeris Error, Periodic Behavior from Spectrum and TDEV values in meters, component projected toward earth

SV	PR	Segment 1			Segment 2		
		2 Cycle/d	Total FFT	TDEV (¼ d)	2 Cycle/d	Total FFT	TDEV (¼ d)
13	02	1.2	1.7	1.6	0.4	0.9	0.6
14	14	0.9	2.9	1.4	0.5	1.6	1.1
15	15	1.2	1.7	1.8	0.5	1.0	0.8
16	16	1.0	2.8	1.8	0.2	1.0	0.6
17	17	1.3	1.8	1.8	0.5	0.9	0.8
18	18	0.4	1.3	1.1	0.3	1.1	1.1
19	19	0.5	1.0	0.8	0.3	1.3	0.8
21	21	1.4	2.3	2.1	0.4	0.8	0.6
22	22	1.6	2.0	2.0	0.7	1.2	1.1
23	23	1.0	1.9	1.9	0.9	1.9	1.5
24	24	1.1	1.5	1.4	0.4	0.7	0.6
25	25	0.7	1.1	1.0	0.4	0.9	0.7
26	26	0.7	1.0	1.0	0.1	0.9	0.6
27	27	0.8	1.2	1.1	0.6	1.1	0.9
29	29	0.6	0.9	0.9	0.7	1.0	1.0
30	30	2.0	2.5	2.4	0.2	0.8	0.5
31	31	0.9	1.4	1.6	0.5	0.8	0.8
32	01	1.1	1.5	1.8	0.6	1.0	1.1
33	03	1.6	2.2	2.2	0.6	1.2	1.1
34	04	0.7	1.1	1.0	0.3	0.7	0.5
35	05	1.3	1.9	1.8	0.2	0.6	0.4
36	06	1.8	2.4	2.6	1.3	1.7	1.8
37	07	1.5	2.1	2.4	0.6	0.9	1.1
39	09	0.4	0.7	0.7	0.4	0.8	0.6
40	10	1.8	2.8	2.5	0.3	0.9	0.7
RSS		5.93	9.28	8.60	2.69	5.37	4.57

Table II
FFT Ratios: 2 Cycle/d Amplitude
RSS of all Spectral Components

SVN	PRN	Segment 1 Ratios	Segment 2 Ratios
13	02	0.71	0.44
14	14	0.31	0.31
15	15	0.71	0.50
16	16	0.36	0.20
17	17	0.72	0.56
18	18	0.31	0.27
19	19	0.50	0.23
21	21	0.61	0.50
22	22	0.80	0.58
23	23	0.53	0.47
24	24	0.73	0.57
25	25	0.64	0.44
26	26	0.70	0.11
27	27	0.67	0.55
29	29	0.67	0.70
30	30	0.80	0.25
31	31	0.64	0.63
32	01	0.73	0.60
33	03	0.73	0.50
34	04	0.64	0.43
35	05	0.68	0.33
36	06	0.75	0.76
37	07	0.71	0.67
39	09	0.57	0.50
40	10	0.64	0.33
RMS over all SV's:		0.65	0.49

Table III
One Day TDEV values
(in meters)

SVN #	PRN #	SV Clock	Segment 1		Segment 2	
			Ephemeris Error	Clock Correction Error	Ephemeris Error	Clock Correction Error
13	02	1.2	0.1	1.0	0.3	1.0
14	14	1.8	0.9	1.8	0.7	1.6
15	15	1.9	0.1	1.2	0.3	1.1
16	16	1.1	0.9	1.3	0.7	1.0
17	17	1.3	0.1	1.4	0.2	0.7
18	18	1.7	0.5	1.3	0.7	1.2
19	19	1.5	0.3	0.6	0.6	0.6
21	21	1.4	0.1	1.3	0.2	1.3
22	22	1.6	0.2	1.7	0.3	1.2
23	23	1.7	0.3	0.9	0.4	1.2
24	24	3.0	0.1	0.6	0.2	0.9
25	25	0.9	0.1	1.0	0.3	1.1
26	26	0.9	0.1	0.9	0.2	0.9
27	27	2.3	0.1	1.0	0.3	1.0
29	29	0.9	0.2	1.1	0.3	0.4
30	30	1.3	0.1	1.0	0.3	0.8
31	31	1.4	0.1	0.9	0.1	1.1
32	01	1.2	0.1	1.1	0.2	1.2
33	03	0.8	0.1	0.9	0.3	0.9
34	04	0.7	0.1	0.8	0.3	1.1
35	05	1.1	0.1	1.1	0.2	0.9
36	06	1.1	0.2	1.0	0.3	1.3
37	07	0.8	0.1	0.9	0.2	0.5
39	09	1.0	0.1	0.8	0.2	1.1
40	10	1.0	0.3	1.1	0.2	1.1

Figure 2a

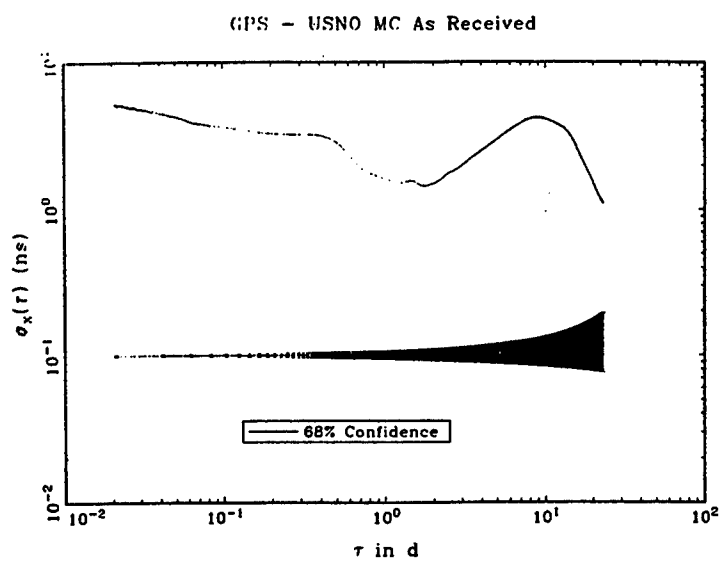


Figure 2b

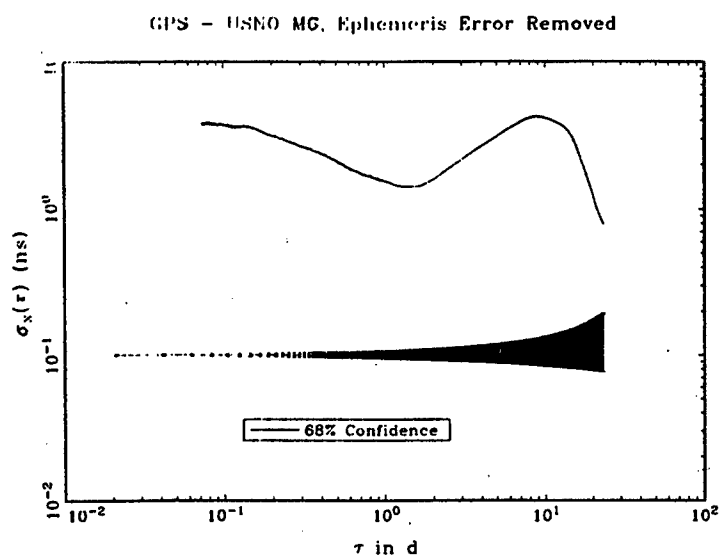


Figure 2c

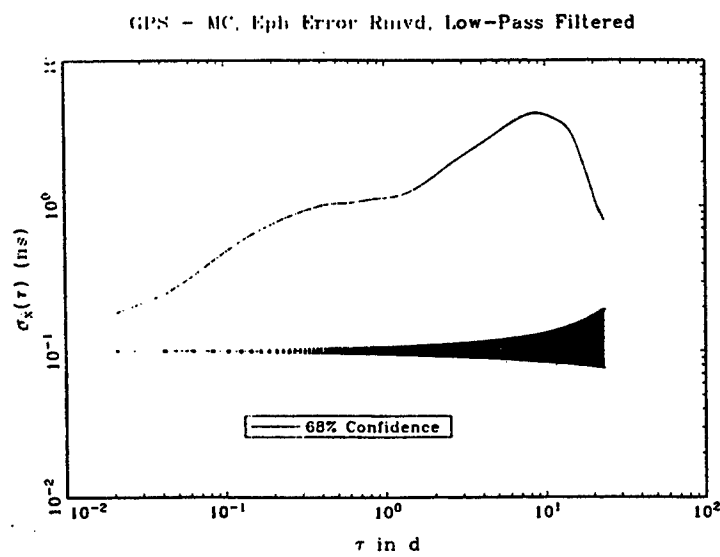


Figure 1a

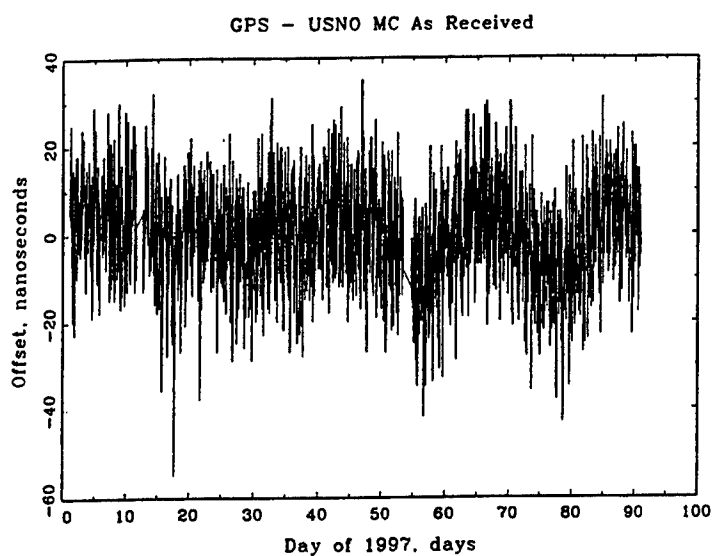


Figure 1b

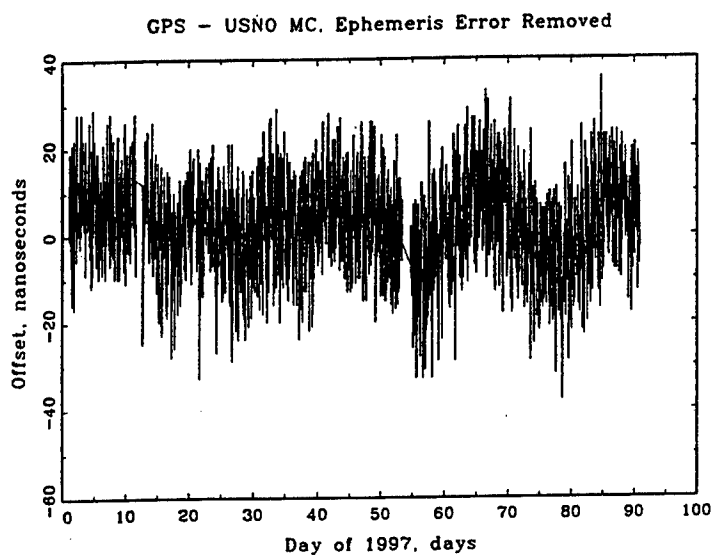
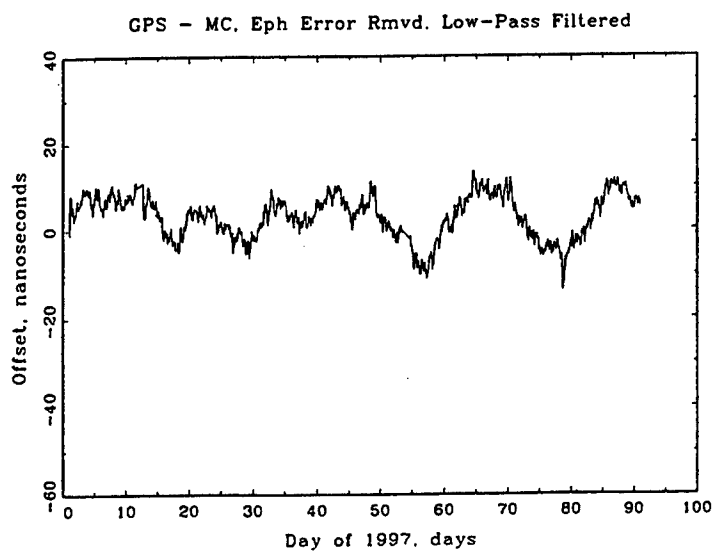


Figure 1c



Long-Term Evaluation of GPS Timing Receiver Failures

DIETER HÖCHTL, ULRICH SCHMID

Technische Universität Wien
Department of Automation
Treitlstraße 1, A-1040 Vienna, Austria
Email: {hoechtl, s}@auto.tuwien.ac.at

Abstract

This paper provides an overview of the results of a continuous, 2-month experimental evaluation of all timing data provided by several GPS receivers. The primary purpose of this experiment was to provide measurement data facilitating fault modeling in our project SynUTC¹, which aims at external clock synchronization in fault-tolerant distributed real-time systems. As expected, the GPS receivers under test exhibited a wide variety of failures, ranging from transient omissions up to considerable deviations of the timing signals provided. Whereas those findings justify the appropriateness of our basic failure assumptions, it became nevertheless apparent that rerunning the experiment for a longer duration and with new brands/models of GPS receivers is advisable.

Keywords: experimental evaluation, GPS timing receivers, integrity, availability, reliability, faults, external clock synchronization, fault-tolerant distributed real-time systems.

1 Introduction

A rapidly increasing number of users rely upon GPS as the primary/sole means for acquiring highly accurate positioning and timing information, see [Dan97] for an overview. In fact, the introduction of the GPS caused a revolution in such different areas as navigation, land surveying, and time transfer, and provides enabling technology for many diverse applications in those areas. Despite of the unrivaled accuracy and reliability of GPS, however, applications eventually emerged that caused searching questions of what quality of service can actually be expected from the GPS.

Primarily driven by the stringent safety requirements of civil aviation [Dur90], integrity of the timing/positioning data provided by GPS receivers became a primary issue in GPS research. Several receiver autonomous monitoring (RAIM, see e.g. [BSK89],

[Mic95]) and failure detection and isolation (FDI, see e.g. [DL95], [BD94]) schemes were developed, which try to identify/remove apparently erroneous data. In the meantime, such techniques are pretty standard and incorporated in low-cost GPS receivers [GKKT95] as well.

Although RAIM/FDI techniques considerably increase the reliability of the positioning/timing output of a GPS receiver, there are nevertheless inherent limitations. As a remedy, augmentations of the GPS have been proposed, which distribute information from external monitoring of the GPS satellites via dedicated *GPS Integrity Channels* (GIC); see e.g. [BC94], [VMLE94]. Related standardization efforts like the *Wide Area Integrity Broadcast* (WIB) [DE94]; however, primarily target FAA's *GPS Wide-Area Augmentation System* (WAAS) and are, hence, not likely to be incorporated in commercial (low-cost) GPS receivers.

Whether RAIM/FDI/GIC is employed or not, however, there is the problem of assessing, i.e., determining, GPS integrity. In fact, any appropriate experimental evaluation is difficult since GPS failures are rare events —although manufacturers of GPS receivers are well aware of their occurrence, see [Dan97], [GKKT95]— that are not easy to observe and to trace back [Gol90] in practice. Comprehensive fault modelling is also difficult due to the fact that GPS is a complex system, with many potential sources of errors: Faults leading to an erroneous positioning/timing output of a GPS receiver may occur in the quite advanced receiver electronics [Die95], as well as in the GPS space and/or control segment. Note that it is even non-trivial to characterize the “normal” (fault-free) operation of GPS; see [Con93].

Most existing attempts to assess GPS integrity hence consider faults in the space segment (“satellite outages”) only. Relying on an *a posteriori* analysis of observational data, fault models like the ones of [DC90], [DC91], [PPP94] assume satellite failure probabilities of about 10^{-4} per hour. Simulation is the primary evaluation tool in the vast majority of related work [DL95], [BSK89], [GKKT95], [PPP94], [VMLE94]; we only know of a few papers [BD94], [Dyk92], [DBS93], [NT93] that deal with experimental evaluation as well.

Given those limitations, it is not too surprising that usual assessments of integrity are not particularly

¹This research is part of our project SynUTC, which has been supported by the Austrian Science Foundation (FWF) under grant no. P10244-OMA and is now continued under the START programme Y41-MAT.

meaningful for even more demanding GPS applications. For example, when GPS receivers are used as the sole means for establishing a common notion of time in fault-tolerant distributed real-time systems, not even a single erroneous timing datum should occur or escape detection. By contrast, typical integrity-dependent applications like civil aviation usually only require one “certified” positioning/timing datum within a certain time interval. Reasoning about (or, as in our case, arguing against²) such “naive” GPS applications, however, requires knowledge of the erroneous behavior of any timing datum provided by a GPS receiver — something that cannot be inferred from existing integrity reports.

Therefore, when we started our work on external clock synchronization in fault-tolerant distributed real-time systems [Sch94], we decided to conduct some experiments of our own to justify our undertaking and to facilitate the task of fault modeling. A continuous experimental evaluation of six commercially available GPS timing receivers was eventually performed from December 12, 1995 to February 15, 1996, which is comprehensively documented in [Hoe96].

This paper provides an overview of the most important results obtained from the analysis of the 778 MB of sampled data. It is organized as follows: In Section 2, we provide some information on fault-tolerant distributed real-time systems that will further motivate our study. Section 3 contains an overview of our measurement setup, Section 4 elaborates on the generation of the reference time scale. The actual results of our experimental evaluation are presented in Section 5, along with a number of graphs and charts contained in the appendix. Some conclusions and directions of further work provided in Section 6 eventually complete our paper.

2 Fault-Tolerant Real-Time Applications

It is well-known that designing distributed real-time systems is considerably simplified when local clocks displaying a common (global) notion of time are available at all computing nodes. Temporally ordered events are in fact beneficial for a wide variety of tasks, ranging from relating sensor data gathered at different nodes up to fully-fledged distributed algorithms, see [Lis93] for some examples. A synchronization tightness in the ms-range is usually sufficient here, although there are applications like [Mar96] that call for a μ s-range precision. To achieve this goal, it is common practice in industry to equip each node of the distributed system with a modular GPS timing receiver.

This solution, however, is not feasible when stringent fault-tolerance requirements are to be met. For example, it was noted in [GKKT95] that a prototype

²We are of course aware of the fact that any experimental evaluation can only provide a “snapshot” of possible failures, which is not sufficient for *confirming* a certain failure assumption. However, the outcome of an experiment can *invalidate* one, thereby increasing the *verisimilitude* (truthlikeness, see [Pop89, Chap. 10]) of the “surviving” assumptions, and this is why experiments are nevertheless appropriate.

TDMA communications system at Motorola eventually broke down due to a certain GPS failure. Similarly, real-time systems architectures like the one of [HW97] that simply phase-lock an internal clock to the 1 pps (1 pulse-per-second) output of a GPS timing receiver are bound to assign incorrect timestamps — taken arbitrarily in a one-second interval — if there is just a single incorrect 1 pps pulse. Obviously, to assess the overall reliability of such systems, the erroneous behavior of all timing data provided by a GPS receiver must be known.

To satisfy increased reliability requirements, fault-tolerant external clock synchronization techniques have been developed; see [Sch97] for the current status of research. Among these is our *interval-based clock validation* approach introduced in [Sch94] and further developed in a number of papers [SS97], [Scho97], [SSHL97], [HSS97], etc., which solves the external clock synchronization problem for large-scale, fault-tolerant distributed real-time systems. It is based on the idea of verifying whether the highly accurate, but possibly faulty, “authoritative time” supplied, e.g. by a GPS receiver, is consistent with some less accurate but reliable “validation time” backed up by all the nodes’ local (quartz) clocks. If so, the distinguished time is accepted; otherwise, it is discarded and the nodes rely on the validation time instead. In essence, our clock validation technique simultaneously increases the fault-tolerance degree and decreases the total number of GPS receivers required in the distributed system. Consequently, it does not suffer from the “forest” of GPS antennas that would be required for a large (LAN-based) distributed system with dedicated GPS receivers. Still, information on all possible failures of GPS receivers is mandatory here as well for proper fault modeling.

From the above considerations, it is apparent that one should know as much as possible about those (rare) events where a GPS timing receiver provides erroneous data. Getting this information, however, is difficult enough under “ideal” operating conditions, and in fact made worse by the requirement of covering issues like receiver (software) errors as well as suboptimal reception and interfacing conditions. After all, circumstances like a 250 μ s timing bias (as exhibited by our first NavSymm receiver) cannot be detected without external verification, which will usually never take place in real applications: Commonly, an off-the-shelf GPS receiver is connected to an interface, undergoes some configuring (without knowing the antenna’s exact 3D-position) — and is then assumed to provide correct time.

Hence, we argue that a meaningful experimental evaluation need not care about “fairness” and “nominal test conditions” and similar things that are likely to be violated in practice. Consequently, we did not run our experiment with multiple instances of the same receiver, and did not bother too much with optimizing antenna positions (w.r.t., e.g., multipath problems) or detecting presumed signaling noise across the interface. We are convinced, though, that our results are more meaningful for practical purposes than those obtained

under "artificial" test conditions. Bear in mind, however, that our evaluation does not impose a legitimate ranking of the evaluated receivers' *potential* capabilities.

3 Experimental Setup

Having decided on the general issues, our first task (Dec. 1994 – Jan. 1995) was selection and purchase of "representative" GPS receivers. Constrained by our limited budget, we were looking for an affordable collection of timing receivers that reasonably covers the available spectrum. Based on a market survey guided by [GPS94] and [GPS95], we eventually chose the models listed in Table 1.

The market survey was also used to decide the question of what kind of GPS interface our custom clock synchronization hardware, namely, the *Network Time Interface* (NTI) M-Module [HSS97] resp. its pivotal UTC-SU-ASIC [SSHL97], should provide. Since it turned out that all timing receivers support

- a digital (usually TTL-level) 1 pps signal that accurately indicates the beginning of a second,
- a serial interface utilizing some (proprietary) protocol to supply the current *time tag* (minute, hour, day, year) as well as additional status information,

whereas a few high-end receivers also provide

- an additional digital *status signal* to indicate health of the 1 pps pulse,
- a 10 MHz *frequency output*,

we decided to support both the 1 pps and a status signal. Moreover, our NTI can optionally be paced with an externally supplied 10 MHz frequency.

The next step was to conceive questions that were to be answered by our experimental evaluation. With $x(t)$ denoting the deviation of a receiver's view of time and a suitable reference time (ideally, t) at the occurrence time t of the appropriate 1 pps pulse, the most important ones can be stated as follows:

- (1) How does the distribution function of the deviations $x(t)$ look like?
- (2) How does the distribution function of $\Delta x(\tau) = x(t + \tau) - x(t)$ for some fixed τ , i.e., the difference between deviations lying τ seconds apart, look like?
- (3) Same as above for an "artificial" 1 pps pulse obtained by dividing the 10 MHz frequency output (if provided) by 10^7 .
- (4) Are there missing or faulty 1 pps pulses and how does $x(t)$ behave in such cases?
- (5) Is there wrong information (time tag, health status) provided via the serial interface?

We will justify the appropriateness of the above questions in Section 5, where we discuss our results.

For data acquisition, answering those questions implies collection of the one-second timing information of

all GPS receivers for the full period of measurement. This means that each 1 pps pulse (including the artificial ones derived from the 10 MHz outputs) of each GPS receiver must be "timestamped" according to a reference clock and stored for later processing. In addition, the information provided via the receivers' serial interfaces must be correctly associated and saved with those timestamps.

In reality, this problem becomes difficult due to the fact that one has to do this simultaneously for several 1 pps signals and with a few ns resolution. Of course, there are manufacturers offering highly sophisticated equipment for measuring phase differences of a single input against a reference signal. Our limited budget, however, did not allow us to replicate such expensive equipment.

The eventually chosen experimental setup shown in Figure 1 thus incorporates the following standard components only:

- On top of the figure, there are the *GPS Receivers* under test (see Table 1), along with the $10^7 : 1$ prescalers for the 10 MHz outputs provided by the Stellar and the NavSymm receiver.
 - The 10 MHz output of the *Reference Clock* (Ball Efratom FRS-C rubidium clock in a climatic housing) is divided by 10^5 resp. 10^7 to generate a 100 pps resp. 1 pps reference signal. In addition, another prescaler $8 : 1$ is responsible for providing a symmetric trigger signal with period 8 s used for alternation control (see below).
 - At the heart of our setup are two *Logic Analyzers* LA1 and LA2 (HP 16500B) used for sampling the 1 pps pulses with 8 ns resolution. Note that we utilized the analyzers' event trigger mode, where a timestamp of the internal LA clock is sampled into memory upon occurrence of a pulse at any input channel.
- Both logic analyzers alternately perform data acquisition and memory transfer to the Measurement PC via a HP-IB interface. More specifically, the leading edge of the 8 s trigger signal mentioned above initiates sampling at LA1 and causes LA2 to be read out, whereas the falling edge triggers sampling at LA2 and read out of LA1. This way, continuous measurement is accomplished.
- Apart from being responsible for reading out the memory of the logic analyzers via the HP-IB interface, the *Measurement PC* also provides the serial interfaces required for getting time tag and status information from the GPS receivers. It associates the 1 pps data from the LA with the additional information and computes a full reference timestamp by combining the LA clock timestamps with the sampled 100 pps rubidium pulses. Complete records, including "spurious pulse" data, are eventually sent to the Server PC via a RS-232 interface.

- Finally, the *Server PC* is responsible for storing the data sent by the Measurement PC on disk, one separate file for each hour of measurement. It is connected to the campus network for easy access and backup purposes.

4 Reference Time

In the course of our experimental evaluation, all 1 pps pulses from the GPS receivers were timestamped according to a free-running *reference clock*. As outlined in the previous section, this is basically a rubidium atomic clock augmented by the logic analyzers' high-resolution internal clocks. In view of the long measurement period vs. the relatively low stability of the rubidium clock, however, we cannot simply use those reference clock readings as a reference time. We need to establish an "artificial" *reference time* instead, which approximates real-time³ as accurately as possible. For this purpose, we take advantage of the fact that a great deal of the stochastic fluctuations of the 1 pps pulses of a high-quality GPS receiver vary not too slowly, so that they can be averaged out even by our low performance reference clock.

More formally, with $T(\text{clock}, t)$ denoting the time value some specified *clock* displays at real time t , the offset $x(t)$ of the best of our GPS receivers (Stellar) from the reference clock, observed at any time t when a 1 pps pulse from the Stellar occurs, can be written as

$$x(t) \equiv T(\text{Stellar}, t) - T(\text{Refclock}, t). \quad (1)$$

The offset $x(t)$ is impaired by both systematic (deterministic) deviations and stochastic, zero-mean noise originating in either the Stellar's 1 pps pulses or the reference clock. Apart from constant time and frequency offsets (irrelevant for our purposes), the sampled data reveal a systematic frequency drift $D_0 \approx 5 \cdot 10^{-18} \text{ s}^{-1}$, which is, however, small enough to be ignored. To analyze the stochastic part, we employ the well-known device of power spectral analysis (see [Ste85] for an overview and e.g. [Car86] for a thorough introduction): By means of Fourier analysis techniques, the (*one-sided*) *power spectral density* $S_x(f)$ depicted in Figure 2 can be computed from the sampled data $x(t)$, which gives the "signal power" per unit frequency at the particular center frequency f . Therefore, the area under $S_x(f)$ in a range $f_1 \leq f \leq f_2$ gives the proportion of the total signal power of $x(t)$ caused by its frequency contributions lying in $[f_1, f_2]$.

We should add that $S_x(f)$ was actually computed from the power spectral density $S_y(f)$ of the first differences of $x(t)$, which satisfy a well-known relation. The required $S_y(f)$ was obtained by applying a Fast Fourier Transform to the entire, properly Hanning-windowed data sample. As elaborated in [WP189], this produces

³We actually used GPST (the inherent system time of the GPS) instead of UTC as our notion of real-time. Apart from an integer number of leap seconds, GPST is almost equivalent to UTC, since it is steered to follow the MasterClock of the United States Naval Observatory UTC(USNO, MC) with high accuracy.

a basically unbiased estimate of the spectrum at "reasonable" frequencies, since the Hanning window removes the distorting effect of spectral leakage. However, it introduces gross errors at the lowest frequencies, which can be corrected by exploiting the well-known fact [All87] that there should be a dominating random walk behavior originating in the rubidium clock. Note that the particular noise level was determined by some additional measurements of our rubidium clock against a cesium normal, which were conducted for verification purposes.

Figure 2 reveals a number of interesting facts about the noise actually present in $x(t)$:

- For frequencies up to 10^{-2} Hz (period of 100 s), we are primarily concerned with white phase noise caused by the granularity of our reference clock.
- For lower frequencies down to approximately 10^{-5} Hz (period of 100000 s), white phase noise originating from the 1 pps output dominates. It is primarily caused by the GPS' Selective Availability (SA), a deliberate distortion of orbital and clock data of the satellites, which has been implemented to reduce the accuracy available to civilian GPS users. Taking into account that the Stellar averages over 5 different satellites, we find the level of noise in accordance with observation of others [Tho93].
- There are also two interesting peaks in the spectrum: The first one appears at a frequency corresponding to a period of one day and is probably caused by the daily variations of ionospheric and tropospheric conditions. The second peak at a period of half a day is presumably a consequence of the second harmonic of the first peak and the 12-hour periodicity of the GPS satellite constellation, which can produce such variations in case of imperfectly known antenna positions.
- At even lower frequencies (with a period longer than a day), the random walk frequency noise of the rubidium clock dominates. Note that it hides any slowly varying noise of the 1 pps pulses.

This information on the noise of $x(t)$ can be exploited to establish a less noisy reference time, which will be developed subsequently. Our approach rests upon a good approximation of the offsets x_{GPST} an ideal GPS receiver (continuously displaying perfect GPST) would provide w.r.t. our reference clock, at arbitrary real-times t :

$$x_{\text{GPST}}(t) \equiv \underbrace{T(\text{GPST}, t)}_{=t} - T(\text{Refclock}, t), \quad (2)$$

recall that we chose GPST as our measure of real-time, hence $T(\text{GPST}, t) = t$. Since the actually sought offsets $z_{\text{any}}(t)$ of any GPS receiver and GPST can be obtained

via

$$z_{\text{any}}(t) \equiv T(\text{any}, t) - \underbrace{T(\text{GPST}, t)}_{=t} = x_{\text{any}}(t) - x_{\text{GPST}}(t), \quad (3)$$

where of course

$$x_{\text{any}}(t) \equiv T(\text{any}, t) - T(\text{Refclock}, t), \quad (4)$$

we only need a good approximation of $x_{\text{GPST}}(t)$ to compute a good approximation of $z_{\text{any}}(t)$. Note carefully that (3) is totally independent of the reference clock.

To be able to use our knowledge of the noise properties of the 1 pps pulses of the Stellar, we define

$$z_S(t) \equiv T(\text{Stellar}, t) - \underbrace{T(\text{GPST}, t)}_{=t} = z_S^0(t) + \zeta_S(t), \quad (5)$$

taken at any occurrence time t of a 1 pps pulse. Herein, $\zeta_S(t)$ is meant to cover only known stochastic deviations (white phase noise from SA), whereas $z_S^0(t)$ contains the unknown rest, i.e., systematic deviations and slowly varying stochastic deviations (hidden by the rubidium clock's random walk noise).

Similarly, we split the time deviations

$$z_R(t) \equiv T(\text{rb clock}, t) - \underbrace{T(\text{GPST}, t)}_{=t} = z_R^0(t) + \zeta_R(t) \quad (6)$$

of the rubidium clock in a stochastic part $\zeta_R(t)$ and a systematic part $z_R^0(t)$, which can be described around a certain moment in time t_r by a quadratic polynomial

$$z_R^0(t) = z_0(t_r) + y_0(t_r) \cdot (t - t_r) + \frac{D_0(t_r)}{2} (t - t_r)^2. \quad (7)$$

With the foregoing definitions, the measured offset $x(t)$ can of course be rewritten as

$$x(t) = z_S(t) - z_R(t). \quad (8)$$

With $\overline{f(t)}$ denoting the result of applying any linear averaging operation—to be fully specified later—to $f(t)$, we hence obtain

$$\overline{x(t)} = \overline{z_S(t)} - \overline{z_R(t)}. \quad (9)$$

Combining this with $x_{\text{GPST}}(t) = -z_R(t)$, which is apparent from comparing (2) and (6), we find

$$\overline{x(t)} = x_{\text{GPST}}(t) + \overline{z_S(t)} + (z_R(t) - \overline{z_R(t)}). \quad (10)$$

If the second and third term on the right hand side of (10) are small, we have found a good approximation of GPST. To compare this with the situation without averaging, we observe e.g. from (1) and (2) that

$$x(t) = x_{\text{GPST}}(t) + z_S(t). \quad (11)$$

Averaging thus yields a reduction of $z_S(t) \rightarrow \overline{z_S(t)}$, but introduces new contributions from the reference clock

$z_R(t) - \overline{z_R(t)}$. Hence, our goal must be to choose an averaging operation that provides a suitable tradeoff. For that purpose, we introduce the linear averaging operation

$$\overline{x(t)} \equiv \int_{-\infty}^{\infty} h(\tau) x(t - \tau) d\tau. \quad (12)$$

along with two reasonable constraints on the weighting function $h(\tau)$, namely

$$\int_{-\infty}^{\infty} h(\tau) d\tau = 1, \quad \text{and} \quad h(\tau) = h(-\tau). \quad (13)$$

Splitting $z_S(t)$ resp. $z_R(t)$ into their corresponding systematic and stochastic parts according to (5) resp. (6), we can express (10) as

$$\overline{x(t)} = x_{\text{GPST}}(t) + \underbrace{\overline{z_S^0(t)} + (z_R^0(t) - \overline{z_R^0(t)})}_{\text{systematic}} + \underbrace{(\zeta_S(t) + (\zeta_R(t) - \overline{\zeta_R(t)}))}_{\text{stochastic}}. \quad (14)$$

Since $z_S^0(t)$ was assumed to consist of the systematic errors and slowly varying stochastic components, we can reasonably infer that $\overline{z_S^0(t)} = z_S^0(t)$, provided that the weighting function $h(\tau)$ is such that it puts (almost) zero weight to large τ . For determining $z_R^0(t)$, we apply the averaging operation (12) to (7) to obtain

$$\begin{aligned} \overline{z_R^0(t)} &= z_0(t_r) + y_0(t_r) \cdot (t - t_r) \\ &+ \frac{D_0(t_r)}{2} \left((t - t_r)^2 + \int_{-\infty}^{\infty} h(\tau) \tau^2 d\tau \right). \end{aligned} \quad (15)$$

Deriving this result, we used the fact that the required even symmetry of $h(\tau)$ implies $\int_{-\infty}^{\infty} \tau h(\tau) d\tau = 0$.

Subtracting (15) from (7), we arrive at

$$z_R^0(t) - \overline{z_R^0(t)} = -\frac{D_0(t_r)}{2} \int_{-\infty}^{\infty} h(\tau) \tau^2 d\tau. \quad (16)$$

Choosing the reference point $t_r = t$, (14) can eventually be written as

$$\begin{aligned} \overline{x(t)} &= x_{\text{GPST}}(t) + z_S^0(t) - \frac{D_0(t)}{2} \int_{-\infty}^{\infty} h(\tau) \tau^2 d\tau \\ &+ \overline{\zeta_S(t)} + (\zeta_R(t) - \overline{\zeta_R(t)}). \end{aligned} \quad (17)$$

Note that the systematic frequency drift $D_0(t)$ was determined to be about $D_0 \approx 5 \cdot 10^{-18} \text{ s}^{-1}$, independently of t , which yields a negligible contribution in (17).

Having settled the systematic parts in (17), we now turn our attention to the stochastic ones abbreviated by $\zeta(t) = \zeta_S(t) + (\zeta_R(t) - \zeta_R(t))$. Our purpose is still to fix the weighting function $h(\tau)$ to be used in the averaging operation. This is done by extracting the individual power spectral densities $S_S(f)$ of $\zeta_S(t)$ and $S_R(f)$ of $\zeta_R(t)$ from Figure 2, and choosing a function $h(\tau)$ that minimizes the spectral density $S_\zeta(f)$ of $\zeta(t)$, i.e., the (known) stochastic noise present in (10). Note that once $h(\tau)$ is determined, the sought approximation $\bar{x}(t)$ of $x_{\text{GPST}}(t)$ can be computed numerically from the sampled data without difficulties.

The power spectral density of the sole reference clock was modelled by

$$S_R(f) = \frac{10^{-30} \text{ Hz}^3}{f^4} + \frac{10^{-22} \text{ Hz}}{f^2}, \quad (18)$$

where the first term reflects the —deliberately overestimated (at minimum 6 dB higher)— random walk of our rubidium clock, cf. the lowest frequencies in Figure 2. The second term accounts for the rubidium clock's white frequency noise, which was found in our measurements against the cesium normal at frequencies higher than 10^{-4} Hz.

To characterize the noise properties of the sole 1 pps pulses of the Stellar, we simply assume that the white phase noise apparent in Figure 2 extends to frequencies lower than $f = 10^{-5}$ Hz as well. Hence, we simply cut off the random walk part to arrive at $S_S(f)$ depicted in Figure 3 below. After all, the reference clock's random walk noise dominates at the lowest frequencies, so that we cannot extract further information out of $S_x(f)$. Any overlooked noise remains in the term $z_S^0(t)$, cf. (5). Note that this is also true for the two peaks in Figure 2, which fully survive the averaging process.

With those preparations, we can eventually attack the problem of choosing $h(\tau)$: Since all contributions to $\zeta(t)$ are reasonably assumed to be zero-mean, stationary power signals and $\zeta_S(t)$ and $\zeta_R(t)$ are obviously statistically independent, the usual superposition and filtering properties [Car86, p. 166ff] for power spectral densities apply. The filter function involved in $\overline{\zeta_S(t)}$ is just $h(\tau)$, the one in $\zeta_R(t) - \overline{\zeta_R(t)}$ reads $\delta(\tau) - h(\tau)$ with $\delta(\tau)$ denoting Dirac's delta-function, so that immediately

$$S_\zeta(f) = S_S(f)H(f)^2 + S_R(f)(1 - H(f))^2,$$

where $H(f)$ is the Fourier transform of $h(\tau)$; note that, because of the requested even symmetry of $h(\tau)$, we have $H(f) = H^*(f)$, i.e., a real-valued function.

Differentiating equation (19) and equating it to zero, we obtain the optimal (minimizing) choice of $H(f)$ as

$$H(f) = \frac{S_R(f)}{S_R(f) + S_S(f)}. \quad (19)$$

Essentially, it says —what intuitively seems clear— that whenever $S_S(f)$ dominates over $S_R(f)$, the function $H(f)$ should be close to zero, and when the opposite is

true, close to one. Hence, a computationally feasible $h(\tau)$ should be chosen, whose power transfer function $H(f)^2$ changes rapidly from one to zero at a certain corner frequency. We decided to use a two-sided exponential function

$$h(\tau) = \frac{1}{2T} e^{-|\tau|/T} \leftrightarrow H(f) = \frac{1}{1 + (2\pi fT)^2}, \quad (20)$$

for this purpose. Figure 4 shows the power transfer function $H(f)^2$ for this weighting function, which decays as f^{-4} for f large enough.

The only remaining problem was to fix the parameter T , which was done by computing $S_\zeta(f)$ for various values of T and choosing the one with the lowest root-mean-square value of $\zeta(t)$ (which can be calculated simply by integrating the spectrum). The eventually chosen value was

$$T = 3450 \text{ s} \quad \text{resulting in} \quad \sigma_\zeta = 6.5 \text{ ns}. \quad (21)$$

Table 3 finally provides the results of applying this averaging function to the sampled data according to (10). For comparison, we provide the findings for the non-averaged case (11) as well.

In both cases, we are confronted with a term of unknown value $z_S^0(t)$ resp. $z_S^0(t)$, which barely differ for the chosen value of T . As mentioned earlier, it covers both unknown systematic errors like imperfectly known antenna position and deterministic delays in the receiver, as well as slowly varying stochastic errors originating in SA and variations of the tropospheric/ionospheric delays. Unfortunately, there is no other way of resolving this uncertainty but to establish a more accurate access to GPST, e.g., by means of common-view techniques.

5 Results

In this section, we survey the results of the analysis of the 778 MB of sampled data in order to answer the questions of Section 3. Additional information and further details may be found in [Hoe96].

5.1 Accuracy-related Quantities

According to item (1) of the list of questions in Section 3, we have to consider the difference $x(t)$ of a receiver's view of GPS time and our⁴ reference time observed at the occurrence of the 1 pps pulse. The sought distribution of $x(t)$ is in fact the quantity of primary interest in most evaluation reports on GPS receivers, cf. [KMB94]. In our clock validation framework, it is primarily required for deciding what maximum time uncertainty must be granted for a correct GPS receiver.

⁴Refer to Section 4 for the expected accuracy of our reference time, that is, its deviation from real-time t . Note that the appropriateness of our method of computing the reference time is also confirmed by the fact that the distribution of $x(t)$ for the Motorola GPS receiver in Figure 7 is in accordance with the results obtained in [KMB94].

Figure 7 in the appendix shows the distribution of $x(t)$ for all of our GPS receivers. Only correct 1 pps pulses were considered here, and any known systematic bias (e.g. resulting from the antenna cable delay) was removed beforehand. Moreover, the respective mean value \bar{x} was subtracted in the plots to make direct comparison easier. Table 2 summarizes the characteristic values of those distributions, namely, mean \bar{x} , standard deviation (root mean square) σ_x , and minimum and maximum offset ϵ_- and ϵ_+ taken relatively to \bar{x} .

Next, we turn our attention to questions (2) and (3) in the list of Section 3, which are devoted to the frequency stability of a GPS receiver for short averaging times $\tau \in [10 \text{ s} \dots 100 \text{ s}]$. The sought distribution of the differences $\Delta x(\tau) = x(t + \tau) - x(t)$ between the time deviation of a GPS receiver's 1 pps pulses lying (integer) τ seconds apart is particularly important for rate synchronization purposes: Our clock validation approach targets 1 μs synchronization tightness [HSS97], which makes it inevitable to synchronize not only clock states but also clock rates. In [Scho97], a suitable rate synchronization algorithm was introduced that requires periodic initiation with period $P_R \in [10 \text{ s} \dots 100 \text{ s}]$. For good performance, however, the intervals between any two initiation events should be as regular as possible.

Figure 8 and 9 in the appendix show⁵ the distributions of $\Delta x(\tau)$, $\tau \in \{30 \text{ s}, 100 \text{ s}\}$, for all the 1 pps and 10 MHz-derived outputs of our GPS receivers. Similarly as before, only correct pulses were considered here. Table 4 summarizes the characteristic values of those (zero-mean) distributions, namely, standard deviation σ_x , maximum value $\epsilon(\tau) = \max|\Delta x(\tau)|$, and corresponding maximum mean frequency deviation (stability) $\nu(\tau) = \epsilon(\tau)/\tau$.

Relating the results for the 1 pps outputs vs. the "artificial" 1 pps pulses derived from 10 MHz frequency outputs answers the question whether rate synchronization could benefit from GPS receivers with frequency output. However, it turns out that the additional effort is not worthwhile, at least for GPS receivers like the Stellar or the NavSymm: The ordinary 1 pps signal does not provide a significantly worse behavior.

5.2 Faulty Behavior

The issues of primary interest for fault tolerance are of course items (4) and (5) in the list of questions in Section 3. Owing to the fact that the receivers of Table 1 performed quite differently in this respect, we briefly report on the observed failures of each receiver separately.

Stellar GPS 100A

This GPS receiver produced no failures except 12 "spurious" 1 pps pulses, which appeared —partly in bursts—

⁵Note that the results in Figure 8 resp. 9 and Table 4 are considerably spoiled by the quantization noise caused by the relatively coarse granularity (8 ns) of our measurement setup. The vertical "stripes" appearing in the distributions are a visible sign of this problem, which obviously becomes less serious when τ is increased.

arbitrarily in between regular ones. We suppose that interfacing problems (possibly caused by ground loops) are responsible for this problem.

NavSymm NTRF-S

The 1 pps pulses of the originally shipped NavSymm receiver exhibited a constant bias of 250 μs ahead of UTC, which went completely unnoticed up to our first measurement epoch. It turned out that this problem was the result of a known(!) firmware bug, which was fixed in a replacement unit eventually used for actual evaluation.

The collected 1 pps data from the NavSymm receiver revealed 8 pulse jumps similar to the one shown in Figure 5: Initially, the so-called ACC-TIME value in the SFM-Message (indicating the 2σ -accuracy) jumped to zero, which means unacceptable accuracy. A few seconds later, the time offset $x(t)$ increased to several milliseconds and persisted in that gross error for about 1 minute. In addition, a few 1 pps pulses were occasionally lost during that period as well. Even worse, ACC-TIME returned to normal values of about 200–300 ns shortly after the pulse jump, although the 1 pps pulses were still extremely offset from UTC. Eventually, $x(t)$ instantaneously decreased to about 30 μs , from where it slowly approached normal values (within another minute).

Moreover, the NavSymm receiver also produced 6 pulse ramps like the one shown in Figure 6: The whole phenomenon lasted more than 1 minute and started with a change of ACC-TIME to zero, after which the offset $x(t)$ gradually grew to magnitudes around 1 μs . While the pulse was still offlying, ACC-TIME resumed displaying normal values, which were eventually also reached by $x(t)$.

Note that both kinds of failure forced us to exclude certain 1 pps pulses when computing the statistics of the NavSymm receiver in Section 5.1. More specifically, we discarded all pulses that occurred within 150 s after ACC-TIME became zero.

There was another, unexpected failure in the RS232-supplied time tag accompanying 2–3 consecutive 1 pps pulses at the beginning of certain days: The indicated day was too small. For example, the receiver said 1995 Dec 14 00:00:00, while it should have said 1995 Dec 15 00:00:00.

Motorola VP-Oncore

There were no failures except of ten omitted 1 pps pulses, which were lost along with their time tags.

Trimble SVeeSix-CM2

There were no failures in the 1 pps pulses, but several incorrect time tags during leap second insertion: The Trimble receiver outputs the time tag via its RS232 interface both in UTC and GPST. It happened that a leap second insertion was announced for the end of 1995, which changed the difference GPST-UTC from 10 s to

11 s. The Trimble receiver inserted the leap second incorrectly on 1996 Jan 01 00:00:00 GPST (=1995 Dec 31 23:59:50 UTC) instead of 1996 Jan 01 00:00:00 UTC. Therefore, the UTC second information was incorrect for ten seconds.

Magellan Brain

During 0.3 % of our evaluation period, the Magellan receiver was in the so-called *coasting*-mode, where too few satellites are tracked to obtain correct measurements. The linearly growing offset $x(t)$ indicates that the receiver derives its 1 pps pulse directly from its local clock in this case. Due to its low quality, this implies large time deviations at the end of long coasting periods (the longest one lasted 994 seconds!), which are instantaneously corrected upon the transition to normal operation.

Apart from coasting, the receiver also showed very irregular behavior during times of bad accuracy, which are indicated by the supplied TFOM value (time figure of merit, giving the expected time error of the 1 pps pulse). For about 10 % of the measurement period, this value indicated time errors greater than 1 μ s. The actual behavior of $x(t)$, however, was much worse: Apart from ramp errors, sudden jumps of 10 μ s and 1 ms occurred quite frequently. Note that such jumps were also observed for TFOM values less than 1 μ s. As in case of the NavSymm receiver, those frequent failures forced us to discard erroneous pulses from the statistical analysis in Section 5.1. More specifically, we discarded all pulses with TFOM > 1 μ s, as well as all remaining ones with offset $x(t)$ > 1 μ s.

In addition, one out of thousand of the time tags transmitted via RS232 were found to be incorrect (usually off by one second). This usually appears for whole "blocks" of consecutive seconds, primarily in conjunction with erroneous 1 pps pulses. The maximum observed block length was 993 s.

Rockwell Microtracker

The 1 pps pulse data of this receiver revealed a bad accuracy ($x(t)$ in the 10 μ s-range, cf. Figure 7), which made it impossible to separate normal behavior and failures.

6 Conclusions and Future Work

Our results, as limited as they are due to their snapshot-like nature, reveal a number of interesting facts about the issues touched in Section 2. First of all, our findings confirm that trusting blindly in all timing data provided by a GPS receiver is definitely inappropriate for fault-tolerant applications. Moreover, since failures like systematic bias cannot be locally detected, redundant verification information is mandatory — and this is exactly the basic assumption underlying our interval-based clock validation scheme.

In addition, the following facts deserve attention:

- Transient omissions of 1 pps pulses are relatively frequent.
- One cannot always rely upon the health status provided by a GPS receiver, in particular after a non-health situation.
- The time tag can be wrong, making some kind of agreement mandatory.

On the other hand, we do not have enough information on erroneous 1 pps pulses for quantitative modelling, in the sense that we are unable to give meaningful failure probabilities. We can only infer that the probability of any transient failure is about 10^{-6} , without significant correlations between different receivers. Our data reveal actually three different classes of transient failures, namely

- "obviously" erroneous (spurious) pulses,
- "step" pulses, characterized by a sudden deviation from the correct time,
- "ramp" pulses, which drift away from correct time gradually (and usually slowly).

Clock validation can eliminate the former two but not the latter one, which are hence those failures where we actually need more information. Note that our observations correspond nicely to findings in integrity research; recall Section 1, where one distinguishes *step* and *ramp errors*: It is well-known that the latter failures are more difficult to iron out by RAIM/FDI than the former ones; see, e.g., [Mic95], [GKKT95], [BSK89].

In order to get meaningful information on failure probabilities, it is inevitable to extend the 2-month period of experimental evaluation considerably. Rerunning our evaluation is also required for keeping track with the rapidly maturing GPS receiver technology, which renders our 1993–1995 receivers partly as out-of-date models. The improved reliability of state-of-the-art brands/models of GPS receivers, however, calls for an even much longer period of data acquisition in order to get hold of failures.

To support longer evaluation periods, several deficiencies and limitations of our experimental setup must be removed:

- The reliability of the measuring equipment — involving numerous components — needs improvement, since 42 of the more than 10^6 readouts of LA memory failed. Although this does of course not invalidate our results (the resulting probability of overlooking an erroneous behavior is only about 10^{-10}), something should be done about it.
- Noise induced by ground loops seems to be a major source of problems, which might even affect the interfaces to the GPS receivers.
- Size and lacking robustness of the experimental setup prohibit an easy change of location, which is desirable both for varying reception conditions and "calibration" purposes (see next item).
- It turned out that the stability of our (relatively low cost) rubidium atomic clock is not exciting

and should be somewhat improved. Incorporating common-view techniques or moving the whole experimental setup to an institution with a cesium atomic clock, preferably one that contributes to UTC, would of course be a more appealing alternative.

- Some countermeasures against long-lasting disruptions due to unnoticed power failures should also be considered.

An appropriately improved and extended experimental evaluation will be incorporated in the comprehensive evaluation of our interval-based clock validation architecture [HSS97]. It will utilize a completely different data acquisition system based on a custom timestamping unit in conjunction with robust industrial VME-bus components, which is currently under development.

Acknowledgements

We gratefully acknowledge the efforts of our "hosts" Dietmar Loy and Martin Horauer, who helped us to cope with several problems arising in the design and implementation of the experimental setup.

References

- [All87] D.W. Allan. *Time and Frequency (Time-Domain) Characterization, Estimation, and Predication of Precision Clocks and Oscillators*, IEEE Trans. on Ultrasonics, Ferroelectrics, and Frequency Control, UFFC-34(6), November 1987.
- [BC94] S. Basker, I. Casewell. *Time and Clock Issues in WADGPS*, Proc. 7th International Technical Meeting of the Satellite Division of the Institute of Navigation (ION GPS-94), Alexandria, 1994, vol. 2, p. 1509-1518.
- [BD94] P. Brown, F. van Diggelen. *Experiences with RAIM, altitude-aided RAIM, and FDI: risks and benefits*, Proc. 3rd International Conference on Differential Satellite Navigation Systems (DSNS 94), London, 1994, vol. 2, p. 1-7.
- [BSK89] J.M. Brown, H. Schwartz, D. Kolody. *RAIM-an implementation study*, Proc. 2nd International Technical Meeting of the Satellite Division of the Institute of Navigation (ION GPS-89), Colorado Springs, 1989, p. 379-388.
- [Car86] A.B. Carlson. *Communication Systems*, 3rd. ed., McGraw Hill, 1986.
- [Con93] R. Conley. *GPS performance: what is normal?*, Navigation, 40(3), 1993, p. 261-281.
- [Dan97] P.H. Dana. *Global Positioning System (GPS) Time Dissemination for Real-Time Applications*, Journal of Real-Time Systems 12(1), January 1997.
- [DBS93] F. van Diggelen, A. Brown, J. Spalding. *Test results of a new DGPS RAIM software package*, Proc. 49th Annual Meeting of the Institute of Navigation, Alexandria, 1993, p. 641-646.
- [DC90] J.-M. Durand, A. Caseau. *GPS availability II. Evaluation of state probabilities for 21 satellite and 24 satellite constellations*, Navigation, 37(3), 1993, p. 285-296.
- [DC91] J.-M. Durand, T.M. Carlier. *GPS Continuity: Initial Findings*, Proc. 4th International Technical Meeting of the Satellite Division of the Institute of Navigation (ION GPS-91), 1991, p. 971-980.
- [DE94] A.J. Van Dierendonck, P. Enge. *RTCA SC-159 Wide Area Integrity Broadcast/Wide Area Differential GPS Status*, Proc. IEEE Position Location and Navigation Symposium, Las Vegas, 1994, p. 733-738.
- [Die95] A.J. Van Dierendonck. *Understanding GPS Receiver Terminology: A Tutorial*, GPS World, January 1995.
- [DL95] Ren Da, Ching-Fang Lin. *Failure Detection and Isolation Structure for Global Positioning System Autonomous Integrity Monitoring*, Journal of Guidance, Control, and Dynamics, 18(2), March-April 1995, p. 291-297.
- [Dur90] J.-M. Durand. *GPS inadequacies: comparative study into solutions for civil aviation*, Journal of Navigation, 43(1), 1990, p. 8-17.
- [Dyk92] K.L. Van Dyke. *RAIM availability for supplemental GPS navigation*, Navigation, 39(4), 1992/93, p. 429-443.
- [GKKT95] G.J. Geier, T.M. King, H.L. Kennedy, R.D. Thomas. *Prediction of the time accuracy and integrity of GPS timing*, Proc. 49th IEEE International Frequency Control Symposium, San Francisco, 1995, p. 266-274.
- [Gol90] K.L. Gold. *Ghost busting. The return from the dead of PRN 8 causes pseudo-range transients*, Proc. 3rd International Technical Meeting of the Satellite Division of the Institute of Navigation (ION GPS-90), Colorado Springs, 1990, p. 569-575.
- [GPS94] *GPS World Receiver Survey*, GPS World, January 1994, p. 38-56.

- [GPS95] *GPS World Receiver Survey*, GPS World, January 1995, p. 46–56.
- [Hoe96] D. Höchtel, *Fehlverhalten von GPS-Satellitenempfängern im Hinblick auf ihren Einsatz im Forschungsprojekt SynUTC* (in German), Master Thesis Dept. of Automation, Technische Universität Wien, 1996.
- [HSS97] M. Horauer, U. Schmid, K. Schossmaier. *NTI: A Network Time Interface M-Module for High-Accuracy Clock Synchronization*, submitted, 1997.
- [HW97] W.A. Halang, M. Wannemacher. *High Accuracy Concurrent Event Processing in Hard Real-Time Systems*, J. Real-Time Systems, 12(1), 1997.
- [KMB94] M. King, M. Miranian, D. Busch. *Test Results and Analysis of a Low Cost Core GPS Receiver for Time Transfer Applications*, Proc. National Technical Meeting of the Institute of Navigation, January 1994.
- [Lis93] B. Liskov. *Practical uses of synchronized clocks in distributed systems*, Distributed Computing, 6, p. 211–219, 1993.
- [Mar96] K.E. Martin. *Powerful Connections: High-Energy Transmission with High-Precision GPS Time*, GPS World, March 1996, p. 20–36.
- [Mic95] W.R. Michalson. *Ensuring GPS Navigation Integrity using Receiver Autonomous Integrity Monitoring*, IEEE Aerospace and Electronic Systems Magazine, 10, Oct. 1995, p. 31–34.
- [NT93] D.A. Nethropp, B. Tanju. *Test and evaluation of embedded GPS systems*, Proc. National Technical Meeting of the Institute of Navigation, Alexandria, 1993, p. 295–304.
- [Pop89] K. R. Popper. *Conjectures and Refutations*. 5th ed., Routledge, London.
- [PPP94] S.P. Pullen, B.S. Pervan, B.W. Parkinson. *A new approach to GPS integrity monitoring using prior probability models and optimal threshold search*, Proc. IEEE Position Location and Navigation Symposium, Las Vegas, 1994, p. 739–746.
- [Sch94] U. Schmid. *Synchronized UTC for Distributed Real-Time Systems*, Proc. IFAC WRTTP'94, Lake Constance, Germany, p. 101–107.
- [Sch95] U. Schmid. *Synchronized Universal Time Coordinated for Distributed Real-Time Systems*, Control Engineering Practice 3(6), p. 877–884, 1995. (Reprinted from [Sch94]).
- [Sch97] U. Schmid (ed.). Special Issue J. Real-Time Systems on *The Challenge of Global Time in Large-Scale Distributed Real-Time Systems*, Journal of Real-Time Systems, 12(1–3), 1997.
- [Scho97] K. Schossmaier. *An Interval-Based Framework for Clock Rate Synchronization*, to appear in Proc. ACM Symp. on Principles of Distributed Computing (PODC'97), 1997.
- [SS97] U. Schmid, K. Schossmaier. *Interval-based Clock Synchronization*, J. Real-Time Systems, 12(2), 1997, p. 173–228.
- [SSHL97] K. Schossmaier, U. Schmid, M. Horauer, D. Loy. *Specification and Implementation of the Universal Time Coordinated Synchronization Unit (UTCSU)*, Journal of Real-Time Systems, 12(3), May 1997.
- [Ste85] S.R. Stein. *Frequency and Time — Their Measurement and Characterization*, in E.A. Gerber, A. Ballato (eds.): Precision Frequency Control, Vol. 2, Academic Press, New York, 1985.
- [Tho93] C. Thomas. *Real-Time Restitution of GPS time*, 7th European Frequency and Time Forum, Neuchâtel, March 1993.
- [VMLE94] V.G. Virball, W.R. Michalson, P.L. Levin, P.K. Enge. *A GPS integrity channel based fault detection and exclusion algorithm using maximum solution separation*, Proc. IEEE Position Location and Navigation Symposium, Las Vegas, 1994, p. 747–754.
- [WPI89] F.L. Walls, D.B. Percival, W.R. Ireland. *Biases and Variances of several FFT Spectral Estimators as a Function of Noise Type and Number of Samples*, Proceedings of the 43rd Annual Symposium of Frequency Control, 1989.

Model	#Chn.	Year/Vers.	US \$
Stellar 100 GPS Clock	5	1995	4.500,-
NavSymm NTFR-S	6	1995/2.9	3.500,-
Motorola VP Oncore	6	1994/6.x	300,-
Trimble SVeeSix-CM2	6	1994	750,-
Magellan Brain	5	1993	600,-
Rockwell Microtracker	5	1993	350,-

Table 1: GPS receivers used for evaluation

Signal	\bar{x}/ns	σ_x/ns	ϵ_-/ns	ϵ_+/ns
Stellar 1 pps	0	37	-188	191
NavSymm 1 pps ^a	244	46	-263	361
Motorola 1 pps	108	46	-246	253
Trimble 1 pps	310	309	-1308	1346
Magellan 1 pps	60	155	-1602	1677
Rockwell 1 pps ^b	7.933	2.380	-5434	4518

Table 2: Characteristic values for the 1 pps pulses vs. reference time

^aNote that those characteristic values —in particular, the mean \bar{x} — are not fully compatible with the corresponding ones of the other receivers due to the fact that the NavSymm cannot output GPST on its 1 pps signal, but only UTC.

^bThe 1 pps pulse provided by the Rockwell receiver is not phase-locked to GPST but rather free-running. An offset value supplied via RS232 must be used to compute a "software 1 pps pulse".

	Contribution	Amount	Origin/Reason for chosen value
without	$z_S^0(t)$	unknown	Systematic and slowly varying 1 pps noise
average	$\zeta_S(t)$	$\sigma = 38.0 \text{ ns}$	SA and quantization noise
	$z_S^0(t)$	$\approx z_S^0(t)$	Averaged $z_S^0(t)$
with	$\zeta_S(t)$	$\sigma = 5.7 \text{ ns}$	Averaged $\zeta_S(t)$
average	$z_R^0(t) - z_R^0(t)$	$\approx 0 \text{ s}$	No significant drift in data
	$\zeta_R(t) - \zeta_R(t)$	$\sigma = 3.2 \text{ ns}$	Introduced noise of rubidium clock

Table 3: Error contributions for non-averaged and averaged 1 pps pulses of Stellar receiver

Receiver	τ	$\sigma_{\Delta x}(\tau)/\text{ns}$	$\epsilon(\tau)/\text{ns}$	$\nu(\tau)$
Stellar	30 s	10.9	80	$2.7 \cdot 10^{-9}$
Stellar	100 s	27.2	196	$2.0 \cdot 10^{-9}$
Stellar 10 MHz	30 s	10.2	84	$2.8 \cdot 10^{-9}$
Stellar 10 MHz	100 s	27.0	200	$2.0 \cdot 10^{-9}$
NavSymm	30 s	27.1	201	$6.7 \cdot 10^{-9}$
NavSymm	100 s	47.5	399	$4.0 \cdot 10^{-9}$
NavSymm 10 MHz	30 s	29.7	224	$7.5 \cdot 10^{-9}$
NavSymm 10 MHz	100 s	49.2	394	$3.9 \cdot 10^{-9}$
Motorola	30 s	44.8	252	$8.4 \cdot 10^{-9}$
Motorola	100 s	51.7	290	$2.9 \cdot 10^{-9}$
Trimble	30 s	383.5	1688	$5.6 \cdot 10^{-8}$
Trimble	100 s	413.6	1715	$1.7 \cdot 10^{-8}$
Magellan	30 s	70.6	1896	$6.3 \cdot 10^{-8}$
Magellan	100 s	139.1	1865	$1.9 \cdot 10^{-8}$
Rockwell	30 s	210.4	6685	$2.2 \cdot 10^{-7}$
Rockwell	100 s	251.6	6997	$7.0 \cdot 10^{-8}$

Table 4: Characteristical values for pulses lying τ seconds apart

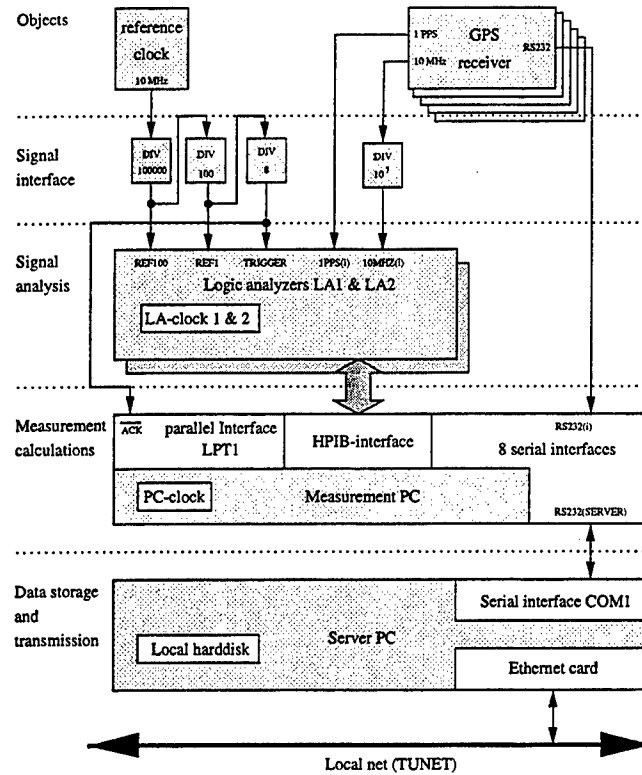


Figure 1: Schematics of experimental setup

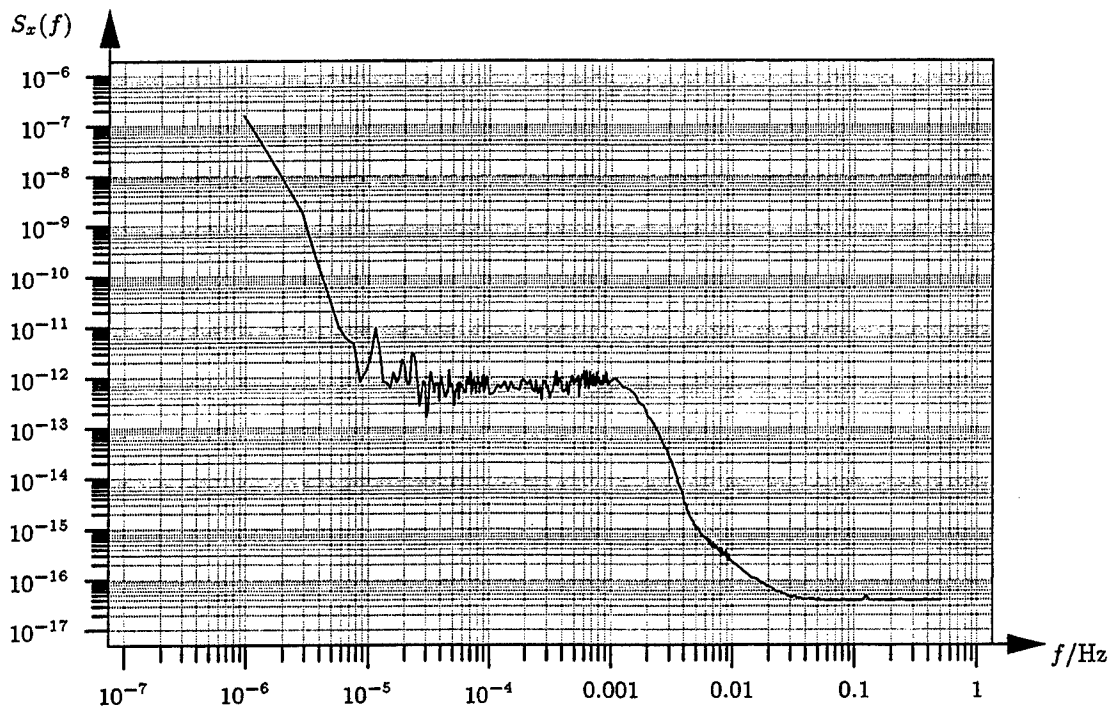


Figure 2: Power spectral density for the Stellar's 1 pps pulses vs. reference clock

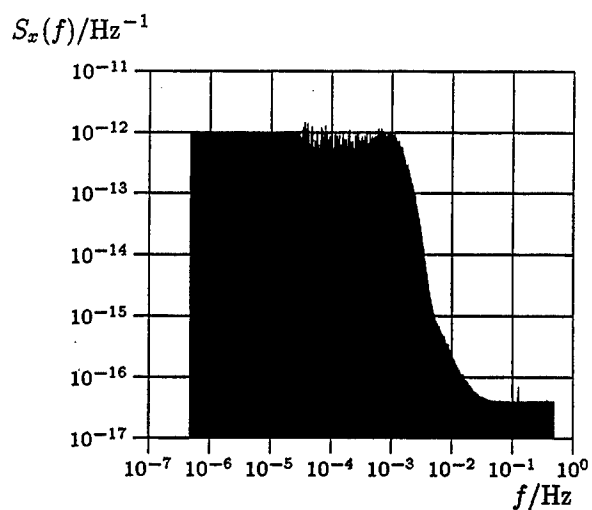


Figure 3: Power spectral density for 1 pps pulse cleaned from rb clock random walk noise

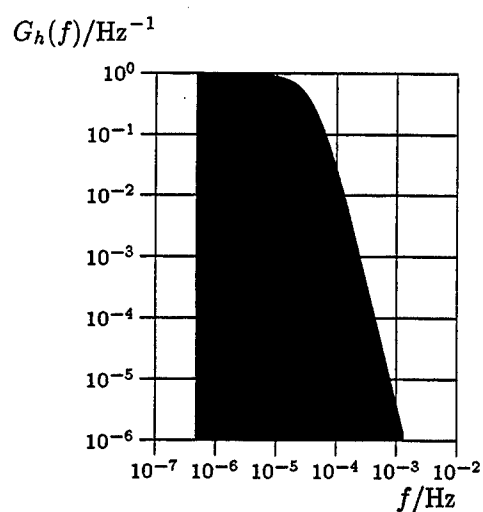


Figure 4: Power transfer function for a weighting function $h(\tau) = 1/2T e^{-|\tau|/T}$, $T = 3450$ s

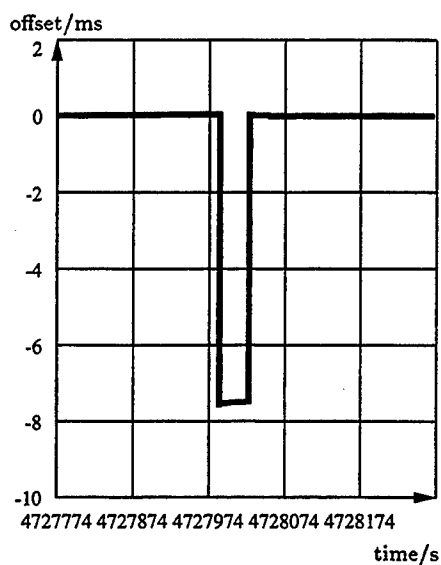


Figure 5: Pulse jumps of the NavSym receiver

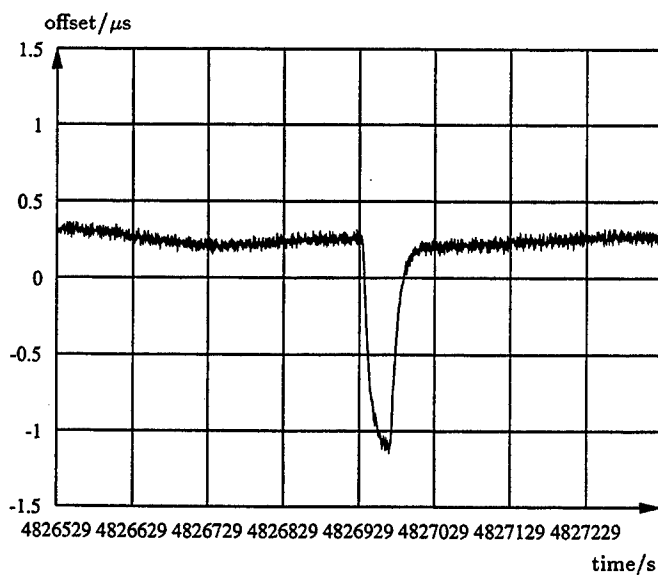


Figure 6: Pulse ramps of the NavSym receiver

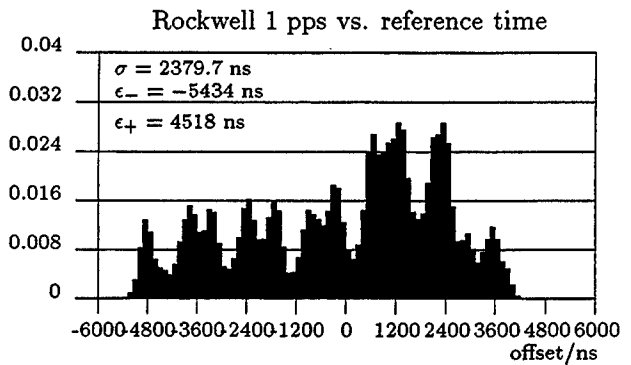
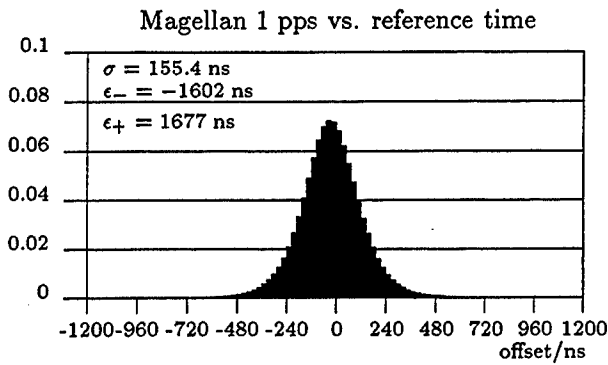
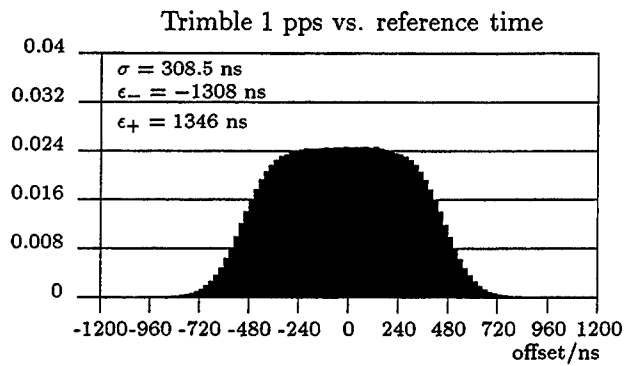
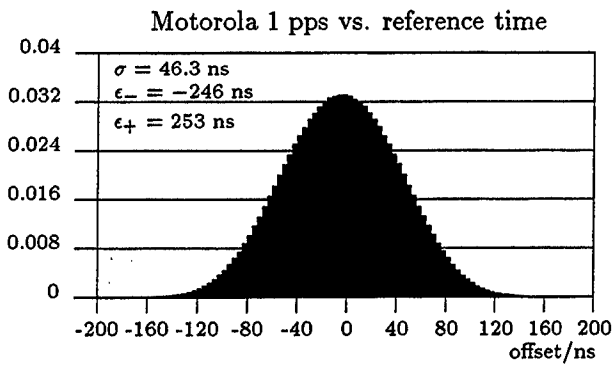
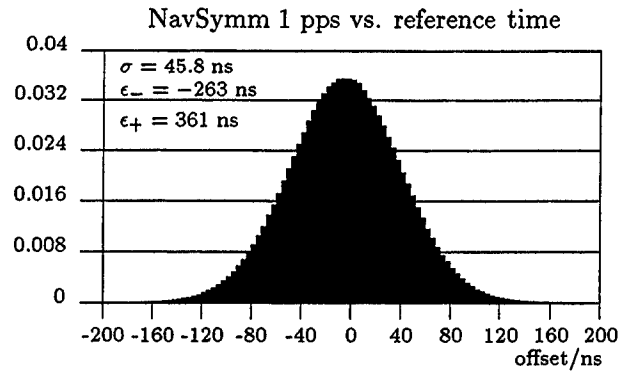
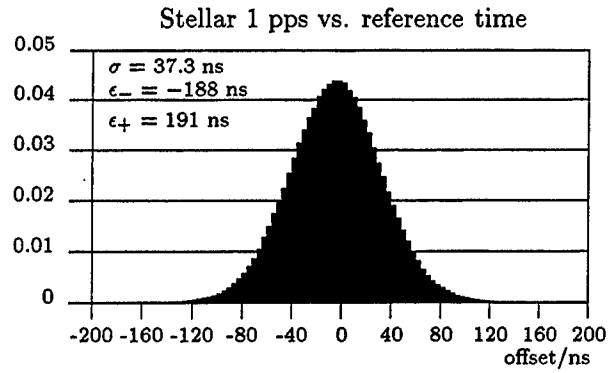


Figure 7: Distribution functions for 1 pps pulses of all 6 receivers against the reference time (the means were eliminated)

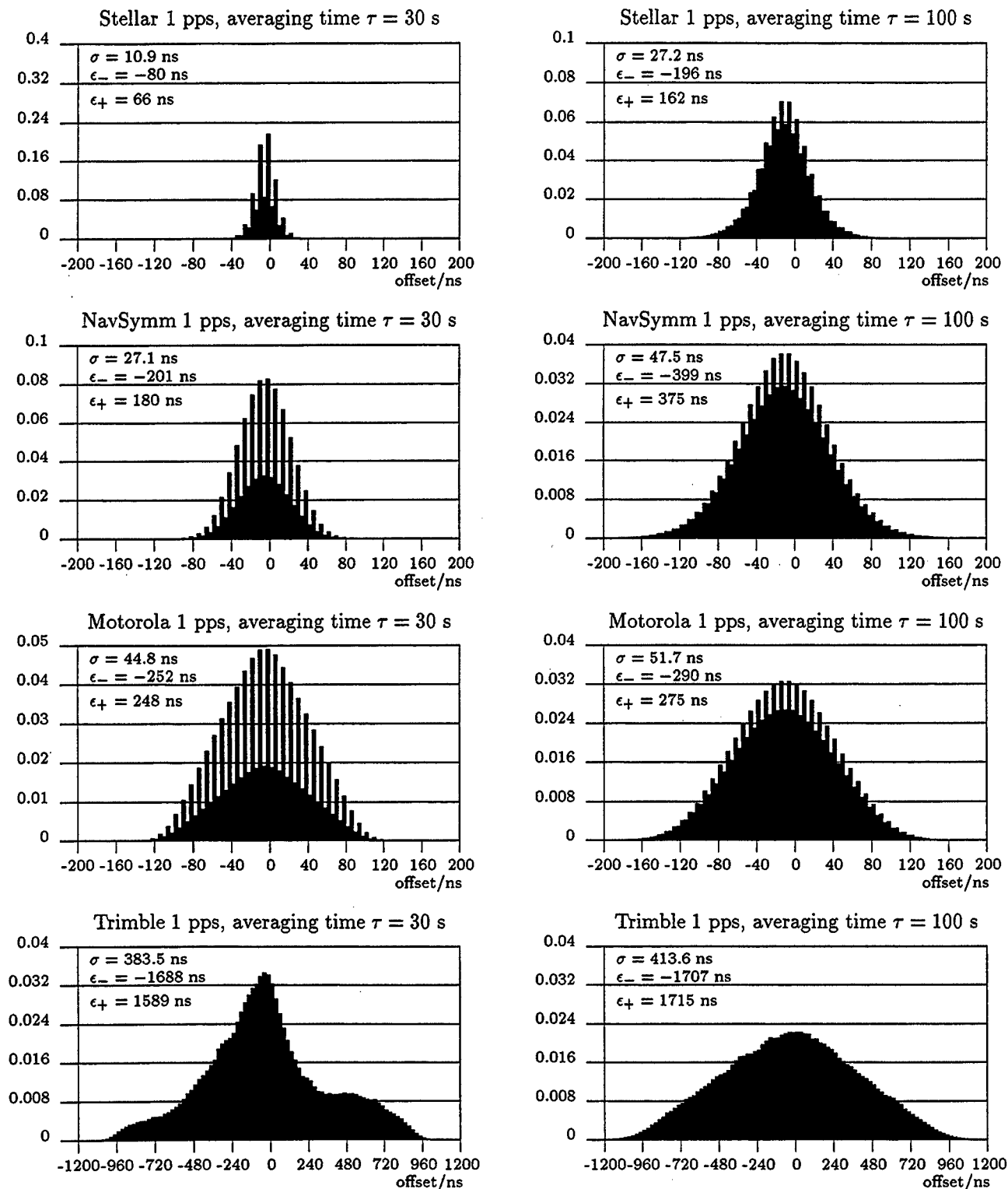


Figure 8: Distribution functions for $x(t + \tau) - x(t)$ for all 6 receivers for $\tau = 30, 100$ s

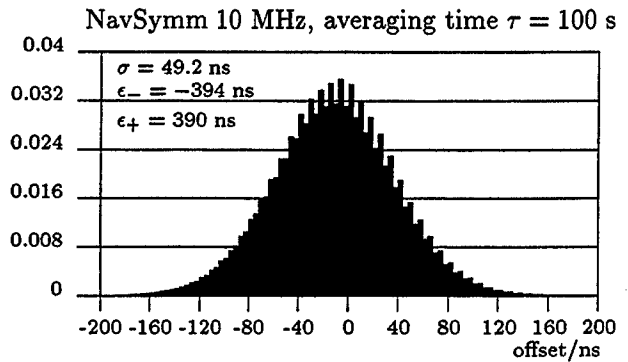
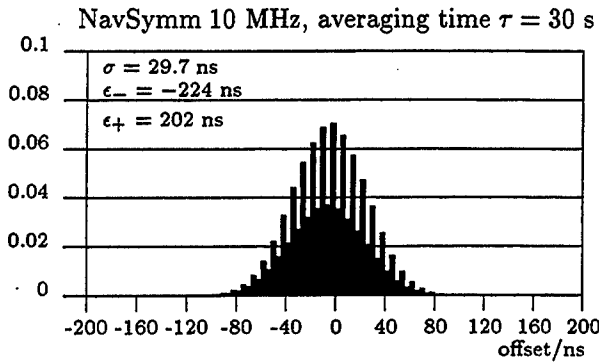
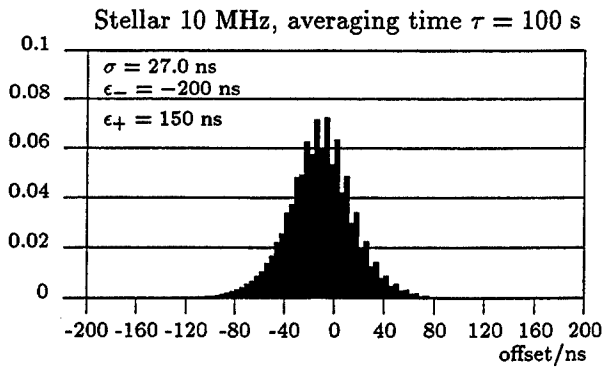
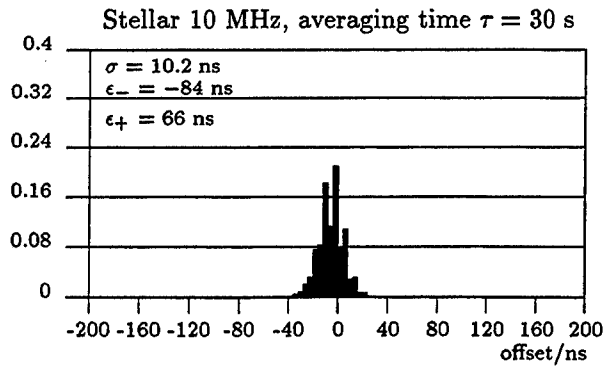
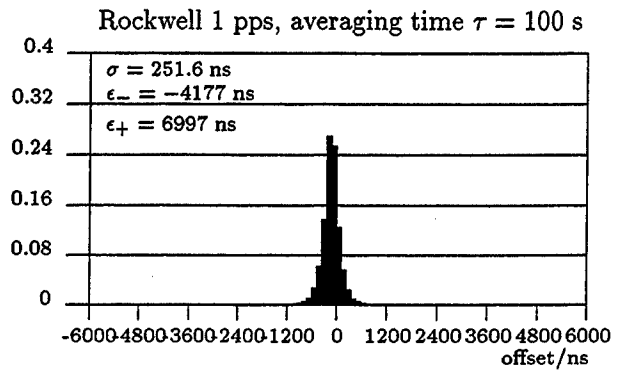
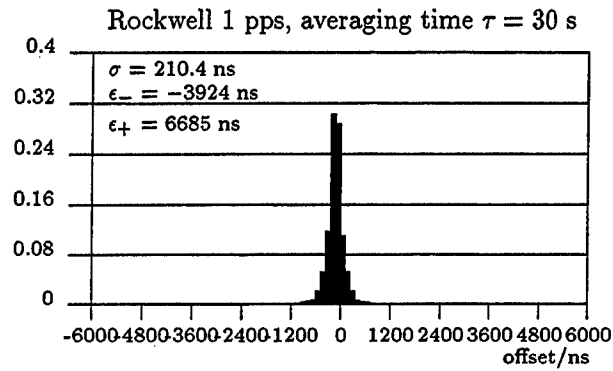
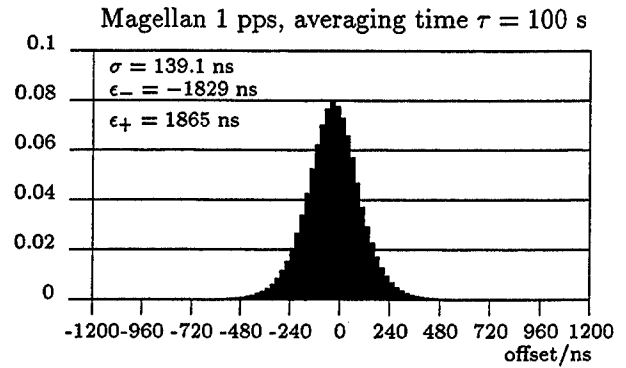
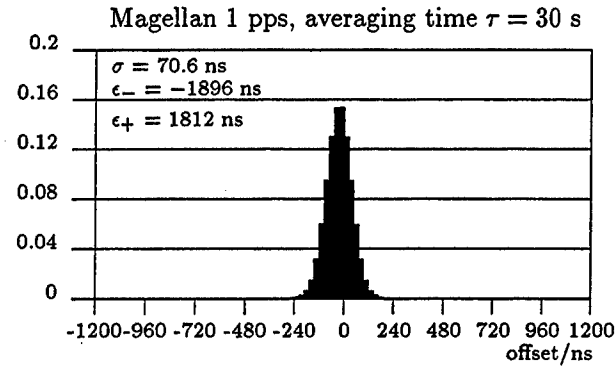


Figure 9: Distribution functions for $x(t + \tau) - x(t)$ for all 6 receivers for $\tau = 30, 100$ s

SVN 20 End-Of-Life Frequency Standard Test Results

1Lt Reeves E. Bower
U.S. Air Force, 2 SOPS/ DOUAN
300 O' MALLEY AVE. STE 41
FALCON AFB, CO 80912-3041

Gary L. Dieter
NAVSTAR GPS OPERATIONS
BOEING NORTH AMERICAN SPACE OPERATIONS COMPANY
FALCON AFB, CO 80912-4438

M.J. Van Melle
NAVSTAR GPS OPERATIONS
BOEING NORTH AMERICAN SPACE OPERATIONS COMPANY
FALCON AFB, CO 80912-4438

Abstract

In early 1989 the first Block II Global Positioning System (GPS) satellites were launched, marking the beginning of the second phase of the GPS program. The satellites were designed for a seven-and-one-half year lifespan and a six-year mean mission duration. Launched in March of 1990, SVN 20 was the seventh of the Block II GPS satellites. On 11 May 1996, SVN 20 was set permanently unhealthy to users after being operational for just over six years. Due to degradation of the Attitude Velocity and Control Subsystem (AVCS), SVN 20 was no longer capable of maintaining the stable, earth-pointing platform necessary to perform the GPS navigation mission. However, through intensive maintenance by personnel at the Master Control Station (MCS) at Falcon Air Force Base, it was possible to stabilize the vehicle long enough to perform extensive end-of-life testing on the four on-board atomic frequency standards. These tests on both the cesium and rubidium frequency standards varied in duration and complexity.

Of the four frequency standards, one had been operational for five months, two had been used previously but were since off-line for two years and four years, respectively, and one had never been initialized. Areas of interest for the rubidium clocks included the determination of the temperature coefficient, voltage-controlled crystal oscillator (VCXO) open-loop operations, and measurement of the C-field and VCXO tune ranges. For the cesium frequency standards, the tests focused on Ramsey pattern generation, gain determination through loop time constant measurement, and C-field and VCXO performance degradation.

All four clocks were still operational at various levels of performance and accuracy. The results of these tests were encouraging in that they supported conclusions made during the SVN 9 and SVN 10 (Block I) end-of-life testing. It is hoped these results will be useful to the GPS clock community as observations of performance characteristics of space-based atomic frequency standards.

I. INTRODUCTION

On 11 May 1996, SVN 20 became the first Block II satellite to leave operational service. Due to problems with the vehicle's Attitude, Velocity and Control Subsystem (AVCS), the satellite could not provide a reliable, three-axis stabilized platform. Since a stable platform is essential to the navigation mission, the satellite was no longer useful as an operational asset. However, the vehicle could still provide valuable information about the performance of atomic frequency standards in a space environment.

Because of SVN 20's unusual configuration at the time of testing, there were unique challenges to overcome. With the satellite spinning about its yaw axis (≈ 25 rpm) without its L-band assembly consistently fixed on the earth, the Master Control Station (MCS) could only gather approximately 1.5 hours of navigation data per 12-hour orbit. The reliability of the MCS Kalman filter state estimates normally decreases with smaller than normal amounts of data. However, Boeing and Air Force studies proved that the filter's convergence in the case of SVN 20 would have been operationally acceptable, if necessary. Additionally, the testing had to be accomplished in a limited time frame (16 September 1996 through 26 November 1996) due to other vehicle considerations. The clock tests performed were the Temperature Coefficient Determination, the Voltage-Controlled Crystal Oscillator (VCXO) Open-Loop Test, Ramsey Pattern Generation, and Loop Time Constant Determination. Additionally, Rubidium Frequency Standard (RFS) #1 was initialized for the first time, and Cesium Frequency Standard (CFS) #3 and CFS#4 were re-initialized. Many interesting results were obtained, which will prove useful to those interested in space-based frequency standard performance.

II. TEMPERATURE COEFFICIENT DETERMINATION

The effects of temperature changes play a large role in determining the final frequency stability of GPS clocks. Rubidium frequency standards are more temperature-dependent than cesiums, and this is reflected in the GPS Block II program specifications for temperature coefficient. According to these specifications, Block II cesium standards must have a temperature coefficient of less than 2 parts in 10^{-13} parts per degree Celsius.^[1] Rubidium standard specifications require a coefficient of less than 2 parts in 10^{-12} parts per degree Celsius.^[2] Because of this order of magnitude difference, rubidium standards are equipped with Active Baseplate Temperature Control Units (ABTCUs). These heaters were designed to maintain clock temperature within $\pm 0.1^\circ\text{C}$ on one of four commandable settings. These settings are: "A" = 26.8°C , "B" = 29.9°C , "C" = 33.4°C , "D" = 37.0°C .^[3]

Method

The temperature coefficient of a rubidium standard can be measured by recording the MCS Kalman filter's estimate of frequency offset, in the units of s/s, at ABTCU setting "D," along with the clock's exact temperature at that point. The ABTCU is then commanded to setting "C." Once the clock's temperature stabilizes at the lower value, the Kalman filter's estimate of frequency offset is again recorded (approximately 24 hours later), along with clock temperature. This process is repeated for every lower ABTCU setting that can provide a stable temperature above the cyclic operating temperature of the rest of the payload. The standard's temperature coefficient is obtained by calculating the ratio of frequency change to temperature change. RFS#1 and RFS#2 were tested on SVN 20. By comparing the current temperature coefficients to

coefficients obtained during pre-launch testing, approximately 10 years earlier, the effects of prolonged exposure to the space environment could be determined. We expected the temperature coefficients to degrade slightly over time, but not enough to create any mission impact.

Test Results

The clock temperature on RFS#1 changed from 37.26° to 34.36° when the ABTCU was commanded to setting "C" from setting "D". After approximately 72 hours, the Kalman estimate of frequency offset changed from +5.34e-12 to +1.22e-11. This change in frequency yielded a temperature coefficient of -23.66 10e-13 $\Delta f/f$ per degree Celsius. Ground testing accomplished in July 1987 measured the temperature coefficient as -2.7 10e-13 $\Delta f/f$ per degree Celsius.

RFS#2's ABTCU was commanded to setting "C" from setting "D". After approximately 12 hours of ABTCU temperature observation, the final resting temperature of RFS#2 was about 2°C higher than that of ABTCU setting "C". Because of this, the ABTCU was unable to properly regulate the clock temperature at setting "C" and MCS operators were unable to obtain temperature coefficient data on RFS#2.

Conclusions

The results of this test show the temperature coefficient of RFS#1 worsened by a factor of 8.76 from July 1987 to September 1996. It appears prolonged exposure to the space environment (over 6 years) and a period of over 3 years spent on the ground had an effect on the temperature coefficient of RFS#1. The extent of this effect on the navigation mission is directly related to the ability of the ABTCU to regulate temperature to within its designed range of ± 0.1 °C. Obviously, any degradation of the ability of the ABTCU to regulate temperature is more severe with a larger temperature coefficient. It is important operators realize ground test values of temperature coefficients will degrade over time, and should properly account for this change when analyzing clock and ABTCU performance.

III. VCXO OPEN-LOOP RUN TEST

The nominal configuration of a GPS frequency standard involves locking the VCXO to the stabilizing effects of the physics package loop. In the event the physics package becomes unstable, it may be necessary to use the VCXO in an open-loop configuration. We used this test to determine the feasibility of operating in the open-loop configuration. We expected the open-loop configuration would not prove to be acceptable for operations due to very large ranging errors and inconsistent run-offs.

Method

In separate tests, RFS#1 and RFS#2 were commanded into the open atomic loop configuration, disconnecting the VCXO from the rubidium physics package. The VCXOs were then tuned to a nominal value and the satellite's ranging errors were observed, once every 15-minute K-point, for several visibility periods. These measurements informed MCS operators of the consistency and magnitude of the open loop run-off.

Test Results

Tables 1, 2, and 3 show the ranging errors recorded with RFS#1, RFS#2, and CFS#3 in an open-loop configuration.

Conclusions

The rates of run-off for all three open-loop tests seem to be fairly consistent from visibility period to visibility period. These run-off rates are directly related to how accurately MCS operators could tune each VCXO after opening the loop. It is clear the average frequency residuals for RFS#2 & CFS#3 were orders of magnitude smaller than that of RFS#1. This is because RFS#1 was tuned to 50% and RFS#2 and CFS#3 were tuned to match their loop control voltages with their previous closed-loop values. Even the most accurately tuned VCXO achieved an average frequency residual of 4.9×10^{-10} s/s. This is more than an order of magnitude larger than a normal closed-loop clock.

Due to the large magnitude of the ranging errors and timing discrepancies, it is unrealistic to expect a standard to operate in the open-loop configuration without abnormal MCS intervention. The necessary Kalman maintenance, frequent uploads, and timing adjusts would burden the operations crews to a more than acceptable level.

IV. RAMSEY PATTERN GENERATION

The Ramsey pattern of a GPS cesium frequency standard shows the condition of the beam tube, such as where the center and side lobe frequencies of the standard are located with respect to the clock's VCXO tuning range. It also provides insight into the gain of the tube and the symmetry of the RF inserted into the tube. Based on SVN 10's end-of-life test results, it was expected the Ramsey patterns of SVN 20's cesium standards would show some degradation over time.^[4]

Method

An operational frequency standard normally operates with the atomic loop closed and the center frequency located somewhere near the VCXO's 50% tune value. It is possible to plot the Ramsey pattern of a GPS cesium frequency standard by opening the atomic loop and commanding the VCXO to incremental tune values. In this case, increments of 5 and 10% were used. At each tuning value, the beam current (proportional to the gain of the system) is recorded and plotted versus the tune percentage. The resulting plot shows peaks and valleys, with the peaks being either the center or side lobe frequencies.

Test Results

Once the beam current is plotted versus the VCXO tune percentage, one can see where the center frequency may lie, depending on how much the VCXO has aged. Data for CFS#3 from 6 Aug 94 and 7 Nov 96 are shown in Figures A and B. Data for CFS#4 from 21 Nov 96 are seen in Figure C.

Conclusions

The data indicate the Ramsey pattern of SVN 20's cesium standards degraded with age. When comparing the Ramsey pattern of CFS#3 recorded in 1994 with that recorded in 1996, one can see, as the gain of the system degraded, the definition of the Ramsey pattern also degraded. This could be a contributing factor to the instability of CFS#3 when it was deactivated in 1994. When observing the Ramsey pattern of CFS#4, it is apparent the side lobes are not clearly defined. This may be due to the gain of this standard degrading and the noise level increasing. It also indicates that frequency standards degrade in space even when not powered on. Because there are no pre-launch Ramsey patterns to compare our results with, it is unclear exactly how much CFS#4's Ramsey pattern changed over time.

V. LOOP TIME CONSTANT DETERMINATION

The atomic loop of a cesium standard detects a change in the frequency of the VCXO and makes appropriate changes to return the frequency to its nominal value. The correction for any given frequency change takes a greater amount of time as the frequency standard ages. This amount of time is known as the loop time constant (LTC). An average value of LTC for a new cesium standard is about 10-15 seconds. It was expected the LTCs of SVN 20's standards would show some degradation over time, because the LTC is a function of the gain of the system. This test was devised to determine to what extent the LTCs of SVN 20's cesium clocks have degraded with age.

Method

It is possible to determine the LTC of a cesium frequency standard by commanding the VCXO to a value about 4% (or 0.2 Hz) greater than its nominal tune and recording the time the close loop command was accepted. At this point the VCXO will begin correcting for the induced frequency change. The time it takes for the VCXO to recover 63% of the induced frequency error is the LTC. This process can also be repeated for a tune value about 4% lower than the VCXO's nominal tune value to observe the symmetry of the Ramsey pattern.

Test Results

CFS#3 LTC when moved up in frequency about 4%:	142 seconds
CFS#3 LTC when moved down in frequency about 4%:	127 seconds
CFS#4 LTC when moved up in frequency about 4%:	104 seconds
CFS#4 LTC when moved down in frequency about 4%:	80 seconds

Conclusions

Six years of exposure to the space environment affected the LTCs of SVN 20's cesium standards. CFS#3's LTC degraded (equivalent to a loss of gain) by a factor of 9 and CFS#4's LTC degraded by a factor of 6. A large degradation factor was expected for CFS#3 because it was powered on for over 4 years. CFS#4 showed a rather large degradation factor for being powered on for only 4 months. It should be noted that both cesium standards started out with the same beam current value of 18 nanoamperes. It is apparent time spent on the ground and in space degrades the LTC of cesium standards, even when not powered on. This may be a

consideration when determining which clock to swap to (Rb vs. Cs) in future operational situations.

VI. NEW CLOCK INITIALIZATION (RFS#1)

Due to the low reliability of atomic frequency standards (0.64 for cesium and .76 for rubidium) with respect to other satellite components, each GPS satellite carries four atomic clocks into orbit. When an operational clock fails, a standby clock is powered up and brought on line. SVN 20 was launched in March of 1990. The first clock, CFS#3, operated for more than 4 years and was turned off in August 1994. RFS#2 was subsequently powered up and was in operation until January 1996. CFS#4 was then turned on and remained in service until the end of SVN20's operational lifetime due to AVCS problems in May 1996. RFS#1 was never powered on during SVN 20's operational lifetime. This test was designed to initialize RFS#1 after over 6 years of cold storage in orbit. Because of the harsh space environment, there was a definite chance the standby clock would not function properly after so many years of cold storage ($\sim 10^{\circ}\text{C}$). Based on previous end-of-life test results, it was expected SVN 20's RFS#1 would power on nominally and perform at nominal operational levels.^[4,5]

Method

The test followed standard clock initialization procedures. The new clock was powered up and allowed to stabilize (approximately a two-hour process). A C-field tune was accomplished to minimize the frequency offset. As soon as the C-field tune was complete, SVN 20 was provided with a routine navigation upload. Since it was unhealthy, the vehicle was usually uploaded once a day regardless of the size of the ranging errors. NRL observed the clock's one-day stability through the use of the Hadamard deviation.

Test Results

The performance characteristics test of RFS#1 started on 22 July 1996 and lasted until 26 September 1996. The clock was powered up on 1 July 1996. The tests recorded Kalman data as the clock warmed up. The Kalman estimate of the A_1 (frequency offset) state at the end of the test is shown in Table 4. Also shown is the NRL estimates of the clock stability based on the Hadamard deviation.

Conclusions

RFS#1 behaved normally for a newly initialized Block II Rubidium standard. Its clock frequency state estimate was certainly within operational limits. In the realm of stability, RFS#1 met one-day stability program specifications ($5.0 \text{ e-}13$) and was easily acceptable for operational use.^[2] Based on drift plots for the last three days of the characteristics observation, it was observed that RFS#1 had assumed a negative drift rate. This is expected of a nominally performing rubidium frequency standard after 2 to 3 months of activation.

The results of this test are encouraging. Based on the performance of RFS#1 after over 6 years of cold storage, it seems this clock would have behaved acceptably were it necessary to utilize it as an operational asset. This bodes well for the chances of other clocks in the constellation which have been stored for similar periods of time.

VII. OLD CLOCK RE-INITIALIZATION (RFS#2, CFS#3)

This test was designed to re-initialize RFS#2 and CFS#3 after being deactivated on 16 Jan 96 and 6 Aug 94, respectively. Upon re-initialization, each clock's performance characteristics were recorded and analyzed. Our expectation was that RFS#2 would perform relatively well. It was deactivated due to suspect performance, with these end-of-life data points providing some additional insight into its instability when deactivated in Jan 1996. We expected CFS#3 to perform at a less than adequate level. It was in operation for over 4 years, and its gain (beam current) was relatively low when deactivated.

Method

Clock stability was recorded by Naval Research Laboratory (NRL), and the MCS Kalman filter estimated clock states.

Test Results

RFS#2 was powered back up on 17 October 96. Data were received from 17 October 96 - 4 November 96. Table 5 describes RFS#2's performance characteristics during that time period. The one-day stability data were obtained from Naval Research Laboratory's (NRL) Navstar Analysis Update No. 20-12. The clock state estimates were obtained from the MCS Kalman filter. CFS#3 was powered back up on 6 November 96. Data were received from 8 November 96 - 20 November 96. Table 6 describes CFS#3's performance characteristics during that time period. The clock state estimates were obtained from the MCS Kalman filter.

Conclusions

The results obtained from observing RFS#2 did not produce any discouraging conclusions. RFS#2's Kalman clock states were all within operational limits, and looked very normal for a rubidium frequency standard that had been earlier labeled "suspect". Its one-day stability was well within the system specification of 5×10^{-13} .^[2] CFS#3's clock states were nominal for the short period of time they were monitored by the MCS. It is expected that its stability, however, would have been questionable due to its low beam current (gain) value of about 1.6 na.

VIII. CONCLUSION

Despite its unique configuration and other obstacles, a great deal was learned from SVN 20's end-of-life frequency standard testing. One of the greatest benefits was confirmation of test results obtained from SVN 9 and SVN 10 during their end-of-life testing. Even with the Block IIR satellites entering the constellation, the Block II/IIA constellation will remain the majority for many years. Information gained from these types of tests will help the MCS operators sustain the aging constellation more effectively and ensure continued support to navigation and time-transfer users worldwide well into the 21st century.

IX. ACKNOWLEDGMENTS

The authors gratefully thank the following individuals and their agencies for assistance and encouragement:

Mr. James A. Buisson, Antoine Enterprises, Inc./ SFA, Inc.
SrA Shawn E. Feeney, 2d Space Operations Squadron
Mr. Wilson G. Reid, United States Naval Research Laboratory
The Men and Women of the 2nd Space Operations Squadron
The Men and Women of Boeing North American Space Operations Company, Falcon AFB, CO

X. REFERENCES

- [1] "Cesium Standard Procurement Specification," MC474-0031, Rev. A, Sec. 05, 26 October 1981 (Rockwell International, Inc.).
- [2] "Rubidium Standard Procurement Specification," MC474-0030, Rev. F, Sec. 05, 5 May 1988 (Rockwell International, Inc.).
- [3] "Block II GPS Orbital Operations Handbook," Vol. I, Sec. 2.6, "Thermal Control Subsystem Description."
- [4] G.L Dieter and M.J. Van Melle 1996, "The End of an Era: SVN 10 End-Of-Life Frequency Standard Testing," Proceedings of the 28th Annual Precise Time and Time Interval (PTTI) Applications and Planning Meeting, 3-5 December 1996, Reston, Virginia, USA, pp. 429-439.
- [5] G.E. Hatten 1995, "SVN 9 End-Of-Life Testing," Proceedings of the 26th Annual Precise Time and Time Interval (PTTI) Applications and Planning Meeting, 6-8 December 1994, Reston, Virginia, USA (NASA CP-3302), pp. 405-414.

XI. TABLES & FIGURES

2 Oct 96/1253z Atomic Loop Opened & VCXO tuned to 50%.		
<u>Time</u>	<u>SV Clock Bias (s)</u>	<u>Ranging Error (m)</u>
2 Oct 96/2330z	3.05581401e-3	-916121
3 Oct 96/0000z	3.19976221e-3	-959276
average run-off 2 Oct 96/2330z - 3 Oct 96/0000z:		21577 meters/15 minutes
3 Oct 96/1045z	6.29589865e-3	-1887486
3 Oct 96/1100z	6.36795353e-3	-1909088
3 Oct 96/1115z	6.43995129e-3	-1930673
3 Oct 96/1130z	6.51195057e-3	-1952258
3 Oct 96/1145z	6.58394624e-3	-1973842
3 Oct 96/1200z	6.65594929e-3	-1995427
average run-off 3 Oct 96/1045z - 3 Oct 96/1200z:		21588 meters/15 minutes
RFS#1 Average Frequency Residual: 8.0 e-8 s/s		

Table 1. RFS#1 Open Loop Data.

7 Nov 96/1548z Atomic Loop Opened & VCXO tuned so that loop control voltage would match where it was when the clock was at GPS frequency.		
<u>Time</u>	<u>SV Clock Bias (s)</u>	<u>Ranging Error (m)</u>
7 Nov 96/2015z	4.52181102e-5	-13556
7 Nov 96/2030z	4.73212038e-5	-14187
7 Nov 96/2045z	4.95378854e-5	-14851
7 Nov 96/2100z	5.16745958e-5	-15492
average run-off 310/2015 - 310/2100:		645 meters/15 minutes
8 Nov 96/0815z	1.46054578e-4	-43787
8 Nov 96/0830z	1.48107409e-4	-44402
8 Nov 96/0845z	1.50157346e-4	-45017
8 Nov 96/0900z	1.52200032e-4	-45629
8 Nov 96/0915z	1.54237559e-4	-46240
8 Nov 96/0930z	1.56278328e-4	-46852
average run-off 311/0815 - 311/0930:		613 meters/15 minutes
RFS#2 Average Frequency Residual: 2.3 e-9 s/s		

Table 2. RFS#2 Open Loop Data.

20 Nov 96/1939z Atomic Loop Opened & VCXO tuned so that loop control voltage would match where it was when the clock was at GPS frequency.

Time	SV Clock Bias (s)	Ranging Error (m)
20 Nov 96/2045z	2.61563055e-6	-784
20 Nov 96/2100z	2.13284330e-6	-639
average run-off 20 Nov 96/2045z - 20 Nov 96/2100z: 145 meters/15 minutes		

21 Nov 96/0745z	-1.85124471e-5	5550
21 Nov 96/0800z	-1.89520962e-5	5681
21 Nov 96/0815z	-1.94207469e-5	5822
21 Nov 96/0830z	-1.98724160e-5	5958
21 Nov 96/0845z	-2.03418410e-5	6098
average run-off 21 Nov 96/0745z - 21 Nov 96/0845z: 137 meters/15 minutes		

21 Nov 96/1930z	-3.95204347e-5	11848
21 Nov 96/1945z	-3.99226219e-5	11969
21 Nov 96/2000z	-4.03524382e-5	12098
21 Nov 96/2015z	-4.07672579e-5	12222
21 Nov 96/2030z	-4.13194989e-5	12387
21 Nov 96/2045z	-4.16899654e-5	12498
21 Nov 96/2100z	-4.21059977e-5	12623
average run-off 21 Nov 96/1930z - 21 Nov 96/2100z: 129 meters/15 minutes		

22 Nov 96/0730z	-5.94009503e-5	17808
22 Nov 96/0745z	-5.97828011e-5	17923
22 Nov 96/0800z	-6.01886173e-5	18044
22 Nov 96/0815z	-6.05825976e-5	18162
22 Nov 96/0830z	-6.09610576e-5	18276
22 Nov 96/0845z	-6.13661593e-5	18397
average run-off 22 Nov 96/0730z - 22 Nov 96/0845z: 118 meters/15 minutes		

CFS#3 average frequency residual: 4.9 e-10 s/s

Table 3. CFS#3 Open Loop Data.

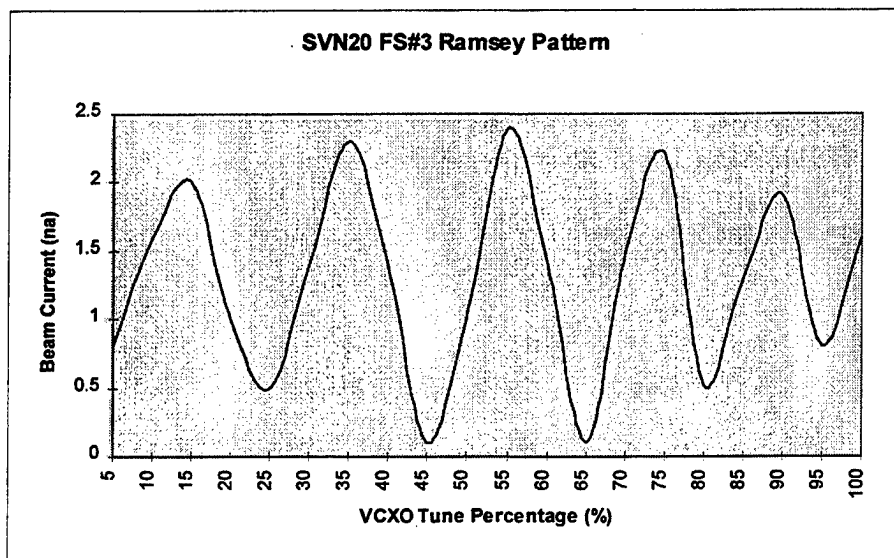


Figure A. CFS#3 Ramsey Pattern (6 Aug 94).

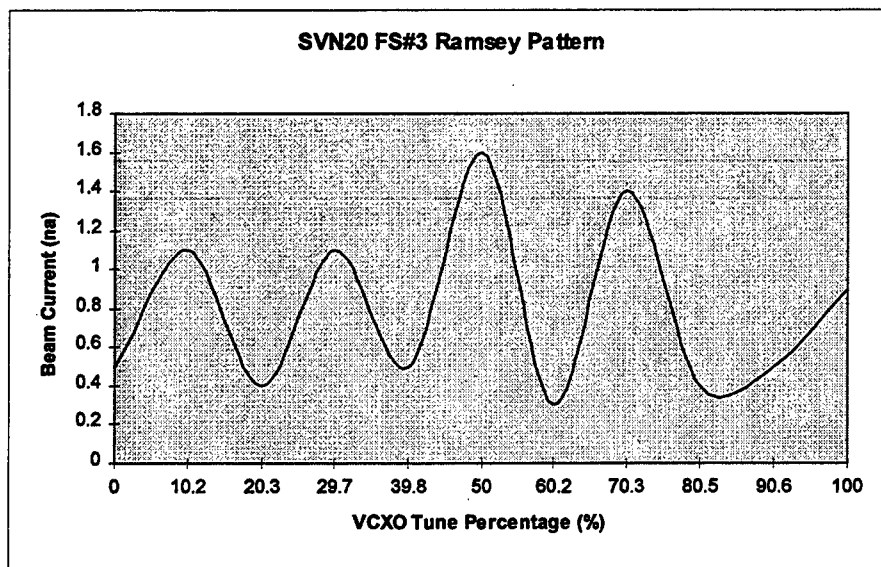


Figure B. CFS#3 Ramsey Pattern (7 Nov 96).

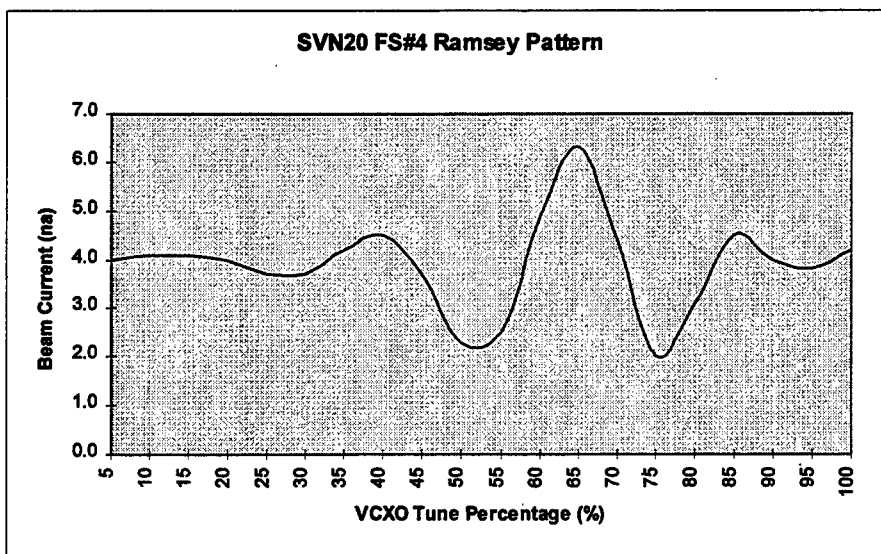


Figure C. CFS#4 Ramsey Pattern (21 Nov 96).

Clock State	FS #1
Clock Frequency (A_1)	$5.34 \text{ e-}12 \text{ (s/s)}$
Stability ($\tau = \text{one-day}$) (data from NRL)	$1.5 \text{ e-}13 \text{ (Hadamard Deviation)}$

Table 4. RFS#1 Initialization Data.

Clock State	FS #2
Clock Phase (A_0)	$-2.60 \text{ e-}5 \text{ (s)}$
Clock Frequency (A_1)	$-1.76 \text{ e-}11 \text{ (s/s)}$
Clock Frequency Drift (A_2)	$-3.32 \text{ e-}18 \text{ (s/s}^2\text{)}$
Stability ($\tau = \text{one day}$) (data from NRL)	$1.9 \text{ e-}13 \text{ (aging correction} = 1.3 \text{ e-}13 \text{ per day)}$

Table 5. RFS#2 Initialization Data.

Clock State	FS #3
Clock Phase (A_0)	$7.73 \text{ e-}5 \text{ (s)}$
Clock Frequency (A_1)	$-4.54 \text{ e-}13 \text{ (s/s)}$

Table 6. CFS#3 Initialization Data.

ABSOLUTE TIME ERROR CALIBRATION OF GPS RECEIVERS USING ADVANCED GPS SIMULATORS

E.D. Powers and M. Miranian
United States Naval Observatory
3450 Massachusetts Ave., NW
Washington DC 20392-5420 USA
Tel 202-762-1451 fax 202-762-1511
E-mail powers@drake.usno.navy.mil

J.D. White and J. Brad
United States Naval Research Laboratory
4555 Overlook Ave. SW, Code 8151
Washington DC 20375 USA

Abstract

Precise time transfer experiments using GPS with time stability's under ten nanoseconds are commonly being reported within the time transfer community. Relative calibrations are done by measuring the time error of one GPS receiver versus a "known master reference receiver." This relative calibration can produce very stable results, but this begs the question of "how does one calibrate the master reference GPS receiver."

In this paper we will discuss the use of advanced GPS simulators to measure the absolute time error of GPS receivers. This method has the advantage of calibrating a GPS receiver independent of any GPS system biases. The use of a GPS simulator also allows testing of special conditions of the GPS system, such as year 2000 rollover and the 1024 week epoch rollover.

INTRODUCTION

With the advent of the Global Positioning System (GPS), the Precise Time and Time Interval (PTTI) community has seen great advances in the ability to compare time and frequency at great distances. In practice, relative time transfer between two timing laboratories has achieved stabilities of a few nanoseconds with averaging times of only a few days [1]. Absolute time transfer between two timing laboratories is achieved by comparing one master timing GPS receiver to a secondary receiver over a period of time at a common location. Then the secondary timing GPS receiver is relocated to a remote timing laboratory to conduct the time transfer experiment. It is assumed that this hardware delay calibration of the secondary receiver will remain fixed.

The hardware delay in the GPS receiving equipment is one of the major sources of uncertainty and instability for these types of time transfer experiments. By using advanced GPS satellite simulators to characterize GPS timing receivers, the uncertainties could be reduced to less than one nanosecond.

Multi-channel GPS simulators that can be used as ideal signal sources for GPS timing receiver calibration are now being produced by many companies. Advanced GPS satellite simulators can produce the same RF conditions that are received from a live GPS satellite, but in a controlled and repeatable manner. In addition, these GPS simulators can be used to characterize a GPS receiver's performance under a wide variety of conditions. Troposphere, ionosphere, multi-path, and selective availability errors can be controlled or set to zero. Any date and time can be simulated to determine whether a GPS receiver can cross-critical date/time boundary conditions such as the coming GPS 1023 epoch rollover. A GPS simulator scenario can be repeated many times to judge the repeatability of the GPS timing receiver. This may be done over a wide variety of environmental conditions to characterize the receiver's stability.

SIMULATOR HARDWARE CALIBRATION

The first step in achieving a highly accurate GPS receiver timing calibration is to calibrate the calibration equipment. To calibrate the GPS simulator, the relationship of the one pulse-per-second (1 PPS) reference signal from the simulator and the code phase of the generated GPS signal must be measured. The bi-phase modulated GPS signal code transition occurs in a finite bandwidth and is modulated by timing pulses with rise times of several nanoseconds. Figure 1 shows a high-speed digital oscilloscope plot of an amplified GPS L1 carrier modulated with CA code near the time of the reference one pulse per second. The effect of C/A code modulation (with the navigation data turned off) is that the amplitude of the carrier at the actual time of the reference pulse goes nearly to zero. The ability to properly interpret this code transition is the major limiting factor in this calibration technique.

After calibration, some simulators such as the STel 7200 have the ability to adjust the reference timing pulse output phase to reduce this error to zero. The Northern Telecom model STR2760 simulator precise timing output cannot be adjusted, but this difference can be carried as a paper calibration adjustment to be removed from the final receiver calibration value.

For the purpose of this paper, three ten-channel/satellite Northern Telecom model STR2760 (NT2760) GPS simulators were used. Experience with the NT 2760 simulator has shown that from a cold start, and without running the internal self-calibration recommended by the manufacturer, there can be 10's of nanoseconds of total delay variation and comparable code phase differences between the L1 and L2 signals. Using the NT internal self-calibration procedure before the start of each simulation will reduce the total delay variations to a few nanoseconds and the L1 to L2 variations to about one nanosecond. Table 1 shows the results of our external simulator calibration after the internal calibration has been run for NT simulator serial number 147 over a period of several years. These results show that NT simulator has very repeatable delays when the internal calibration is used.

GPS RECEIVER HARDWARE CALIBRATION

Once the simulator has been calibrated, the GPS receiver is connected as shown in Figure 2. The use of cables with identical delays in the RF and reference lines simplifies calibration by matching delays in the test and reference paths. A standard GPS simulator scenario is created with a fixed position and nominal

ionosphere and troposphere. These factors are included since the modeled ionosphere and troposphere corrections in many receivers cannot be turned off. A standard GPS constellation is used with no errors in satellite positions or satellite clocks.

Date	L1 Delay (nsec)	L2 Delay (nsec)
2/23/95	99.7	100.9
3/3/95	98.8	100.3
6/18/97	96.8	97.9
10/4/97	98.4	99.2
10/7/97	99.6	99.6
10/14/97	100.0	100.0

Table 1. Simulator Calibration Data, C/A codes.

The next step in the calibration process is to determine the average measured time difference between the calibrated GPS simulator and the timing GPS receiver outputs. The final step is to apply the appropriate bookkeeping delay corrections for the simulator bias, test cables delays, and the delays for the antenna and antenna cable.

STANFORD TELECOM SIMULATOR CALIBRATION METHOD

Stanford Telecom has their own version of this simulator calibration method and has used it successfully to calibrate the masters USNO GPS/UTC monitor receivers [2]. The USNO master GPS/UTC monitor receiver has a built-in calibration mode that is compatible with a calibration function of the STel 7200 GPS signal simulator. This allows for a more precise calibration than would normally be possible.

SIMULATOR CALIBRATION TEST RESULTS OF AOA TTR-4P

Several attempts to calibrate the Allen Osborne Associate (AOA) Model TTR-4P have been performed since 1995. The calibration data show a run-to-run variation that is significantly larger than the standard deviations of the individual tests. These variations could be as large as 20 or more nanoseconds. Initially some of the changes were thought to have been correlated with temperature changes in the laboratory. To isolate temperature effects, the AOA TTR-4P receiver was placed in a thermal chamber and re-tested at several temperatures. No clear temperature effect was identified, although some of the data pointed to coefficients as large as 1 nanosecond per degree Celsius. In late 1995 it was concluded that more detailed testing was needed to document what temperature effects exist and whether or not they are unique to this particular receiver or whether they are generic to the TTR-4P design.

The simulator did not appear to be the cause of the shifts, since its calibration number had remained constant over time and a variety of laboratory conditions. However, to increase confidence in it, another experiment was done using a STel 5401C receiver. The scenario length was increased to one day to increase the chance of seeing any irregularity in the simulator signal. The room temperature was changed

from 21°C to 27°C for several hours and then back to 21°C during the run. Within the noise limits of the STel receiver (less than 5 nanoseconds), no changes in the simulator were seen.

In 1996 USNO reported an error in the AOA TTR-4P resulting from the phase relationship between the external 5 MHz provided to the AOA TTR-4P and the measured local 1 PPS signal. It was thought that the relationships of the external 5 MHz signal and 1 PPS must be held fixed and have no bias to produce consistent time transfer results. This would later be proved only partially correct.

In June of 1997 AOA TTR-4P serial number 164 was made available for further simulator calibration testing. A series of detailed experiments were conducted investigating the relationship of the external 5 MHz and 1 PPS signals. The externally provided 5 MHz was offset by 1 mHz to study in detail this USNO reported phase effect. It was discovered that there was indeed a large error resulting from the phase relationship of the externally provided 5 MHz and 1 PPS. Figure 3 shows a time series plot of the measured 1 PPS signal output from the TTR-4P and the internally derived measurements. An obvious measurement error can be seen in these data of up to 24.4 nanoseconds. The period of each cycle shift is not 1000 seconds as might be expected, because the external 5 MHz is multiplied inside the receiver to a frequency of 20.456 MHz. All measurements within the AOA TTR-4P are based on this 20.456 MHz internal clock. The 24.4 nanosecond amplitude of the time error results from a 0 – 180 degree phase shift in this 20.456 MHz signal.

Next, the externally provided 5 MHz reference frequency offset was set to zero and its phase relationship was set to match the externally provided 1 PPS signal to less than 100 picoseconds. The receiver was then reset many times and allowed to acquire the simulated GPS signal. Table 2 shows the results of this experiment. There were many times when the receiver came back to within a few nanoseconds of its previous value; then there were other times the receiver jumped ten or more nanoseconds to a new calibration value. The receiver seems only able to be calibrated to within a 24.4 nanosecond window of uncertainty.

Time	AOA TTR-4P Delay in (nsec)
11:30	-162
11:39	-158
11:41	-160
11:43	-154
11:45	-152
11:49	-149
11:53	-170

Table 2. AOA TTR-4P Simulator Calibration Data

To confirm these simulator experiments two AOA TTR-4P receivers were run on live GPS satellites for several months and common-view data collected. Several times during this experiment, one of the TTR-4P's was reset and the time bias changed in a way similar to the simulator calibration results. Figure 4 shows one of the resulting time bias changes in the receiver after a reset.

GPS BOUNDARY CONDITION TESTING

The NAVSTAR GPS Joint Program Office (JPO) funds a consortium of DOD agencies called the Joint Test Agency Test Group (JTAWG). The Satellite Simulator Control Working Group (SSCWG) sub-panel of the JTAWG was charged with creating a satellite simulator validation test plan and GPS receiver validation test plan for specific time boundary rollover conditions. The SSCWG members tasked with creating and accomplishing these test plans were the 746th Test Squadron (TS), Naval Research and Development (NRaD) San Diego, Naval Research Laboratory (NRL), and Electronic Proving Ground (EPG).

Listed below are the boundaries and navigation variables, which are being tested.

1. GPS epoch rollover from GPS epoch 0, week 1023, 21 Aug 1999 to GPS epoch 1, week 0, 22 Aug 1999.
2. GPS year 2000 rollover from December 31, 1999 to January 1, 2000.
3. GPS leap year rollover from February 28 to 29, 2000.
4. GPS Almanac Week boundaries

GPS 1024 WEEK EPOCH PROBLEM

The GPS week number is contained within the GPS NAV message in the form of a ten-bit binary number with a maximum decimal value of 1023, base epoch 0 or (11 1111 1111). This 1024-week period is commonly referred to as the GPS epoch. Rollover of this GPS week number may cause anomalous date determination within GPS receivers. The GPS Z-count has no provisions for determining which epoch is current. Week 0 of the first GPS epoch was defined as beginning 0000 hours January 6, 1980 the first crossover from week 1023-to-0 will occur 19.7 years later at 0000 on August 22, 1999. The GPS data structure does not contain information that would allow a GPS receiver to resolve which GPS epoch it is in. In GPS ICD-200 it states that "At the expiration of GPS week 1023, the GPS week number will rollover to zero (0). Users must account for the previous 1024 weeks." [3, 4]

GPS 1023 WEEK EPOCH TESTING

GPS simulators are the only testing tools available that can be used to determine if a GPS receiver will perform properly before, during and after this upcoming GPS 1023-week epoch crossover. Several timing GPS receivers were tested to determine if they would operate properly crossing this GPS 1023-week epoch crossover. We found that almost all timing GPS receivers with firmware older than 1995 would not fully function properly crossing this 1023-week boundary. The most common problem was that the date would jump back to Jan 6, 1980. Another problem observed was that a receiver might not be able to find any satellites visible because it tries to propagate the GPS almanac backward 19.7 years. One receiver appeared to function crossing the boundary, but the UTC (USNO) to GPS time correction was computed incorrectly because of the 1024 week jump causing a 74-microsecond time error

FUTURE WORK

The simulator calibration technique is still under going further refinement. We plan to begin using a calibrated anechoic chamber to directly couple the simulated GPS signal directly into the GPS antenna.

This will remove the uncertainty in the calibration of the GPS antenna and greatly improve our error budget. We will be testing several new GPS receivers such as the Motorola encore, AOA TTR6 and the DOD Precision Light Weight GPS receiver (PLGR).

CONCLUSION

Calibrations of GPS timing receivers using advanced GPS simulators have the potential to achieve nanosecond level absolute time calibration accuracies. The major limiting factor from a simulator perspective is the measurement of the absolute delay between the modulated GPS signal and the simulator precise timing output. The overall limiting factor is stability of the GPS timing receiver under test. GPS simulators also can be used to test for special boundary conditions coming in the GPS system such as the 1024-week rollover and the year 2000 rollover.

[1] W. Lewandowski 1994, "GPS Common-view Time Transfer" in Proceedings of the 25th Annual Precise Time and Time Applications and Planning Meeting (NASA Conference Publication 3267), pp. 133-148.

[2] J. Brad, E. Powers, J. White, and P. Landis 1996, "Receiver Time Delay Calibration Using a GPS Signal Simulator" PLANS Guidance Symposium, Jan 1996.

[3] GPS Standard Positioning Service System Specification, June 1995, second edition, GPS Joint Program Office.

[4] ICD-GPS-200 Navstar GPS Space Segment/Navigation User Interfaces, Rev C, IRN-201-001, Oct 1995.

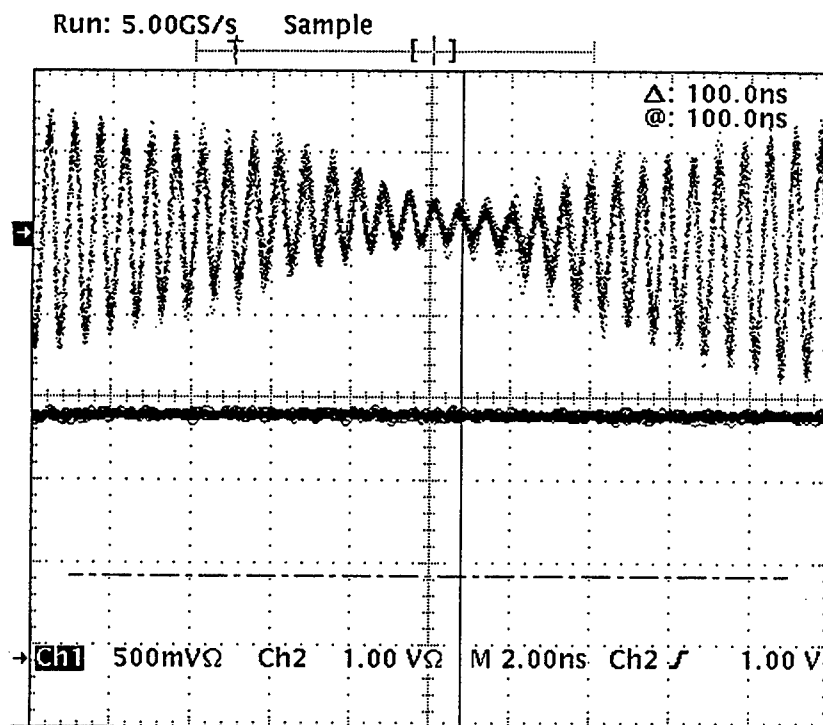


Figure 1. CA-code modulated GPS signal at L1 frequencies.

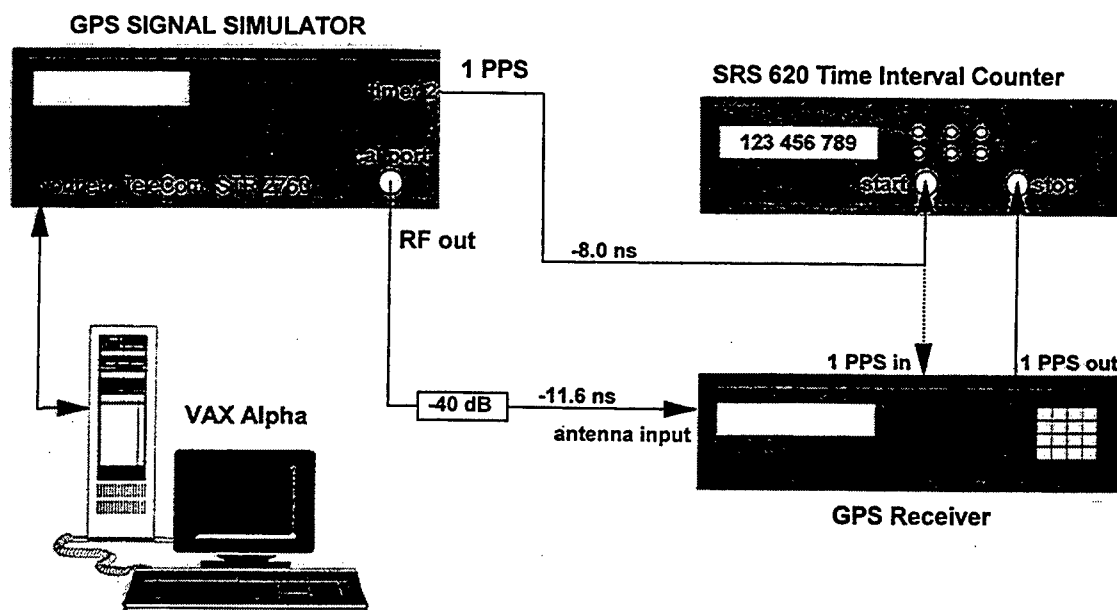


Figure 2. Timing GPS receiver calibration test setup.

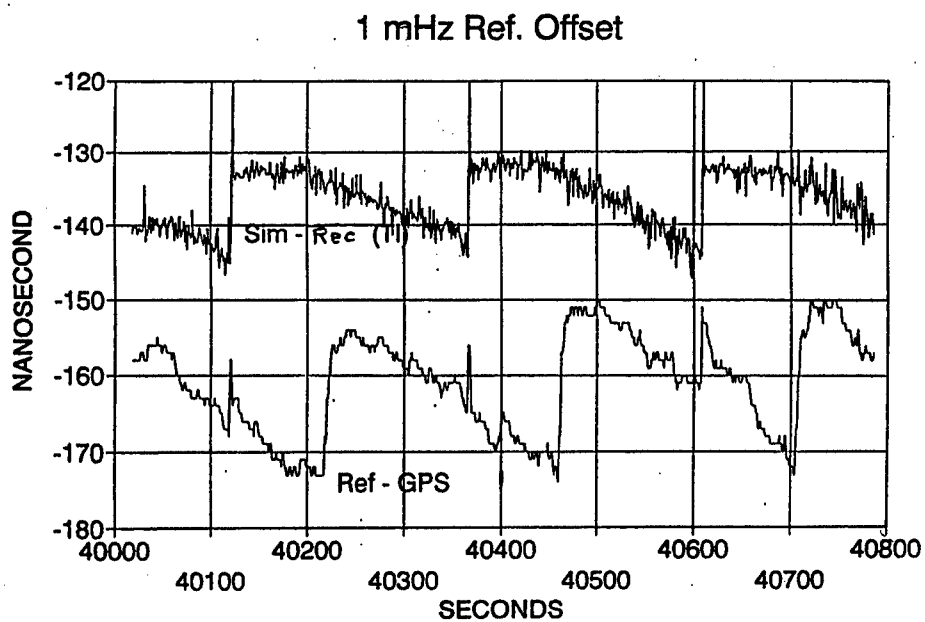


Figure 3. AOA TTR-4P external offset frequency reference problem.

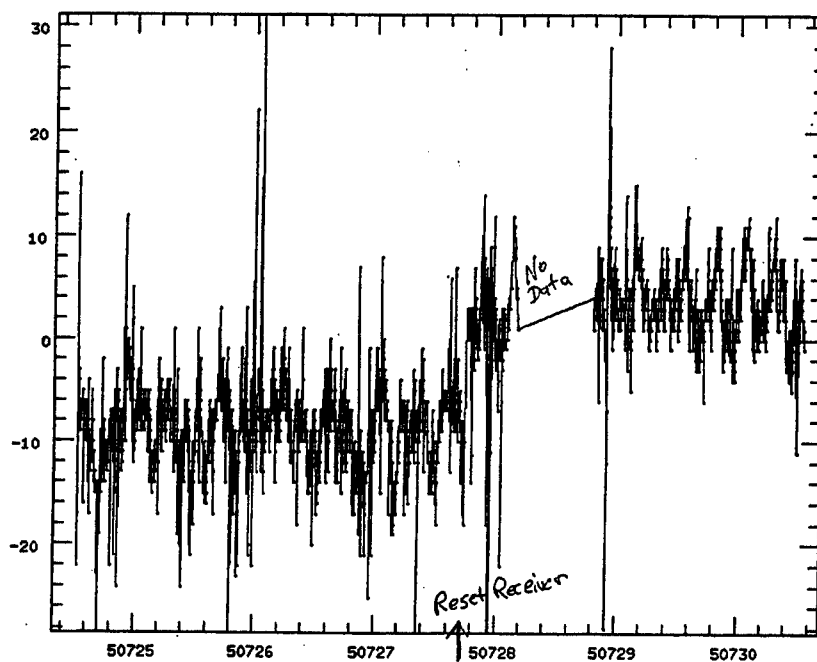


Figure 4. AOA TTR-4P abrupt calibration change at MJD 50728.

ATOMIC FREQUENCY STANDARDS FOR THE GPS IIF SATELLITES

Willem Emmer, Boeing

Eric Watts, Boeing

Abstract

The GPS IIF block of satellites will carry Cs beam and Rb vapor cell atomic frequency standards. This paper presents a description of the two frequency standards and reviews their expected performance. The performance of the two technologies is also assessed within the context of the orbital environment. User range error, a measure of accuracy, is calculated based on projected performance of the IIF frequency standards. Potential system performance improvements, possible with two future clock technologies, are also considered.

INTRODUCTION

Atomic frequency standards and the ultra-stable signal they provide enable the present GPS constellation and future GPS satellites to broadcast highly accurate navigation signals. The GPS IIF satellites will take advantage of recent advancements in frequency standard technology to improve upon the performance of the GPS Constellation. The current configuration of the GPS IIF satellites provides two cesium frequency standards (CFS) and two rubidium frequency standards (RFS) in response to the Government's system requirement for two frequency standard technologies to be provided on each satellite.

The GPS IIF Navigation Payload utilizes the same architecture as the successful GPS Block II/IIA Space vehicles. The Navigation Payload is comprised of four atomic frequency standards (AFSs), a frequency synthesizer & distribution unit (FSDU), the cross-link transponder & data unit (CTDU), and the navigation data unit (NDU). Each frequency standard outputs an ultra-stable 10.23MHz signal to the FSDU. The FSDU modifies that signal as required to support selective availability and distributes the signal to the NDU and other signal users. The NDU uses the 10.23MHz signal to generate the pseudo-random noise ranging codes (C/A & P(Y)), build the navigation message, and combine these two signals for modulation on the L-band carriers.

GPS IIF ATOMIC FREQUENCY STANDARDS

The cesium-beam frequency standards will be produced by Frequency and Time Systems (F&TS), a division of Datum Inc. The rubidium gas cell standards will be produced by EG&G's Electro-optics Division.

CESIUM ATOMIC FREQUENCY STANDARD

Frequency and Time Systems, which designed and built the cesium frequency standards for the GPS I and II/IIA satellites, was selected to develop and produce the cesium standards for the GPS-IIF program. F&TS's new cesium frequency standard design, designated the Model FTS 4410, will space-qualify microprocessor control technology for the frequency standard. The new design follows from F&TS developmental work sponsored by the Naval Research Laboratory (NRL).

The heart of the design is the cesium beam tube (CBT) which provides a suitable environment in which a beam of cesium atoms may be interrogated by a microwave field at 9.192... GHz. The Model FTS 7610 CBT used in the 4410 has its design heritage in the Cs beam tubes (CBTs) used in the GPS I and II/IIA clocks. For use in GPS IIF, the 7610 was enhanced to provide longer life, increased accuracy and frequency stability. Of particular concern in a CBT is the trade-off between short-term stability and lifetime. An increase in cesium beam intensity results in an improvement in short-term frequency stability at the expense of CBT lifetime. The 7610 is designed to meet the frequency stability requirements of GPS IIF, while supporting a 10-year operating life requirement. The CBT design must also withstand the mechanical rigors of satellite launch. Comprehensive vibration testing (to the GPS IIF qualification levels) of the FTS 7610 during the development phase has demonstrated that the design can survive and perform after exposure to the launch environment.

The enabling technology for the 4410 operation and performance is an embedded microprocessor. The microprocessor and its software algorithms perform several important tasks which include: lock acquisition at start-up; operation of the primary frequency-lock loop; operation of several "background" servos which stabilize the atomic interrogation process; and comprehensive monitoring of system operation to provide a robust indicator of clock state-of-health. Multiple software servos operate in the 4410 to continuously optimize its performance. The 4410 employs a servo architecture which "time shares" the atomic interrogation process among several tasks. The primary servo serves to frequency-lock the oven controlled quartz oscillator (OCXO) to the atomic resonance, thereby providing a clock output signal with the frequency accuracy and stability of the cesium atomic beam. Periodically, a "stolen cycle" is used to acquire information for one of several background servos; these servos control signal gains, interrogating microwave power, as well as the magnetic field within the cesium beam tube, to negate the effects of external magnetic fields. The time-sharing technique has the advantage that the primary servo is uncontaminated by the activity of the background servos. The multiple servos do not occupy the full processing capability of the microprocessor. The otherwise spare processor time is used to monitor numerous internal clock parameters to provide a robust and comprehensive evaluation of clock state-of-health. Twenty-eight internal parameters are monitored and reported over a satellite telemetry data channel.

The synthesizer is another important element in the atomic frequency standard. The synthesizer translates the clock output frequency (10.23 MHz in the case of GPS IIF clocks) to the atomic resonance frequency (9192631770 Hz for cesium). There are several requirements for this synthesizer: the signal at the atomic resonance frequency must be free of significant spurious responses which may cause "frequency pulling", a shift of the atomic resonance. The synthesizer must be able to generate interrogating signals at various frequencies within the cesium atomic resonance structure. The output power of the synthesizer must be controllable. Additionally, operation of the primary frequency lock loop servo requires a square wave frequency modulation of the interrogating signal. The OCXO at 10.23 MHz is the starting point. Frequency multipliers translate the frequency to the GHz realm. A surface acoustic wave (SAW) oscillator running at 9.192 GHz is controlled in an offset phase-lock loop to provide a "clean", spurious-free microwave signal for interrogation of the cesium atoms. The reference for the offset PLL is generated in a direct digital synthesizer (DDS) under control of the microprocessor. Microprocessor commands sent to

the DDS are translated to the SAW output frequency, thereby providing an ability to interrogate features of the atomic resonance.

The interrogating signal microwave power may change with time as a result of temperature, aging, or radiation effects upon the electronics. These changes in microwave power levels can, in turn, cause frequency instabilities in the clock. The microwave power servo modulates the microwave power, providing information which is used to optimize the microwave power level without contamination of the primary frequency lock loop performance.

The Model 9400-520 OCXO used in the 4410 CFS was developed specifically for use in space and contains a third overtone SC-cut resonator at 5.115 MHz. A doubler within the oscillator provides an output at 10.23 MHz. It has been used in numerous satellite applications.

RUBIDIUM ATOMIC FREQUENCY STANDARD

The Rubidium Frequency Standard (RFS) design evolved directly from a previously space-qualified design and employs classical rubidium gas cell principles. A voltage-controlled crystal oscillator at 10.23 MHz, synthesized from the Rb hyperfine resonant frequency, provides the output via an amplifier and crystal filter. Another crystal oscillator, resonant at approximately 13.4 MHz, excites the Rb physics package via a phase modulator and frequency multiplier chain. This produces a discriminator signal which is processed by a servo amplifier to lock that crystal to the Rb atomic resonance.

The classical rubidium gas cell principles used in the design of the frequency standard give the highest available performance consistent with program constraints. The discrete isotropic filter cell gives zero light shift over a range of light intensity and high signal-to-noise (S/N) ratio. This permits operation at a relatively low light level, thus reducing temperature and RF power dependencies.

The RF multiplier chain consists of a 13.4MHz voltage-controlled crystal oscillator (VCXO), a phase modulator, a diode tripler, a push-push doubler, and a x85 step recovery diode (SRD) multiplier. The low noise of the Rb reference permits a tight lock loop that allows the use of the low-complexity, non-ovenized crystal oscillator. An automatic level control loop is used to maintain constant drive to the SRD multiplier and a high-Q helical resonator RF bandpass filter is used ahead of the SRD multiplier. This approach provides high stability and spectral purity. A clean modulation waveform is generated by passive integration of a precision squarewave, and highly linear phase modulation is obtained by applying small excursions to a varactor diode.

The RFS synthesizer consists of a phase-lock loop employing two divider chains and a 10.23MHz VCXO. The 13.4MHz signal is divided by 3051 and the 10.23MHz signal is divided by 2329. These divider circuits provide frequencies of 4.39kHz to a phase detector. The phase detector in turn drives loop compensation amplifiers which steer the varactor tuning of the 10.23MHz VCXO.

The output amplifier provides a +18dBm low-distortion output and maintains a phase-continuous output under transient radiation. This "flywheel" effect is provided by a LC output tank and crystal bandpass filter.

The IIF RFS includes a built-in baseplate temperature controller. This controller maintains the baseplate of the RFS electronics at $+45^{\circ}\text{C} \pm 0.1^{\circ}\text{C}$, thus essentially eliminating the effects of space vehicle temperature variations.

NAVIGATION TIMING ERROR ANALYSIS

Timing of the navigation message is critical to GPS system performance where timing and positional accuracy are intimately tied via the speed of light. A one-nanosecond timing error yields a 0.3-meter range error. The frequency standards are allocated a timing requirement in term of User Range Error (URE) measured in meters. The bar chart of Figure 1 illustrates the GPS-IIF URE allocations including that of the frequency standards at an "age of data" (AOD) equal to 24 hours. Behind the control segment the frequency standards' performance is the major driver in the positional accuracy of the GPS Constellation. Age of data refers to the elapsed time since synchronization of a given space vehicle to GPS-time as defined by the **Control Segment**. Synchronization occurs at least once every 24 hours, but as often as every 15 minutes, as a means to limit a space vehicle's phase offset from system time and, hence, its range error. Error growth over the specified 24-hour period is of primary concern from the frequency standard design standpoint, since the frequency standard must perform over this time interval with prescribed stability.

The frequency stability of the GPS-IIF standards, as characterized by Allan deviation, is shown in Figure 2 along with measurements of the IIF CFS & RFS prototype stabilities. This random noise instability results in the largest contribution to URE. The required on-orbit performance of the GPS IIF frequency standards demands that both units have minimal environmental sensitivities. Thermal and magnetic environment fluctuations degrade the AFS's performance. An analysis was performed to estimate these effects and the results are presented below.

Random noise processes in frequency standards contribute to timing errors, and so called "optimum predictor" methods for estimating these contributions have been developed⁽¹¹⁾. The method employed in this analysis accounts for the various noise processes that are used to model observed instabilities^(9, 10). Based on the measured prototype performance, noise processes of the GPS frequency standards were estimated and used to calculate timing error growth over age of data, as shown in Figure 3. The analysis assumes perfect control segment modeling; the actual timing error, at zero age of data, will be small, but non zero.

The space vehicle will see a periodic thermal environment resulting in $\pm 3^\circ\text{C}$ changes at the frequency standards' baseplates. Since the RFS utilizes an integral baseplate temperature control unit to actively eliminate thermal variations, these fluctuations are of no consequence. The cesium standard, however, is affected. The temperature variation induces a sinusoidal frequency shift that is directly proportional to the measured thermal sensitivity of $\sim 3 \times 10^{-14} \Delta f/f/^\circ\text{C}$. Time integration of the frequency offset yields the timing error which is also sinusoidal with a peak-to-peak magnitude of 1.24 nanoseconds. This timing error is deterministic, but since control segment uplinks are not correlated with the thermal environment, the error cannot be fully removed. The Kalman filter of the **Control Segment** will partially compensate for this error, resulting in a cyclic temperature-induced timing error of zero mean and of the same magnitude of 1.24 nanoseconds. For system analysis for all ages of data, a value for the thermal timing error of one standard deviation is used, equal to 0.88 nanoseconds.

The frequency standards are also subject to external magnetic fields which will induce frequency shifts. The magnetic field of most concern is generated by three "torque-rod" electro-magnets in the Attitude, Determination & Control System (ADCS). The magnetic field at the location of each frequency standard depends upon the distance to each electro-magnet and its polarity. Preliminary calculations show that the cesium frequency standards will see a field as large as 1.64 gauss and the RFS a 0.88-gauss field. The electro-magnet duty cycle and polarity varies, with the minimum on time for each magnet being 100 seconds.

The GPS-IIF CFS utilizes a background servo to compensate for changes in magnetic field seen at the beam tube. This background servo effectively eliminates the effects of the external magnetic field by compensating for it, resulting in an insignificant contribution to phase error.

The GPS IIF RFS will exhibit an induced frequency shift and resulting phase error growth due to the presence of an external magnetic field. The prototype RFS exhibited a magnetic field sensitivity of approximately $\pm 0.33 \times 10^{-12} \Delta f/f$ per gauss, depending on polarity, for magnetic fields aligned with the RFS physics package axis. Computer simulation of GPS-IIF satellite momentum dumping over an orbit was used to generate timing profiles of the three electro-magnets. Using the RFS prototype magnetic sensitivity and the strength of the magnetic field aligned with the RFS physics package, the RFS magnetic timing error contribution was calculated. The cumulative timing error is reduced by magnetic fields of opposite polarity which induce frequency shifts of differing signs. The single-orbit time profiles of the electro-magnets are not periodic and the resulting phase error exhibits a component of linear drift over the period of the modeled orbit. The Kalman filter of the Control Segment will model and remove the linear phase drift component of this timing error. The resulting "compensated" phase error is shown in Figure 4, calculated as the difference between the magnetic field-induced phase shift and Kalman filter-modeled drift. As in the case of the temperature-induced timing error, for system analysis, a "reasonable" value for magnetic field-induced timing error has been assigned for all ages of data, equal to 0.14 nanoseconds. This value is one standard deviation of the predicted error (Figure 4).

Power variation measurements were made on both AFS prototypes. Applied variations in supplied power yielded no measurable frequency variations at either the output of the CFS or the RFS. No timing impact is predicted due to space vehicle power variations.

Total RFS and CFS contributions to the system URE are shown in Figure 5 as a function of age of data. Three- and twenty-four hour values are shown explicitly. The RFS contribution to URE is a function of the random noise instability and magnetic field phase errors. The CFS contribution to URE is a function of the random noise instability and thermal phase errors. The errors due to random noise instability, thermal and magnetic environment fluctuations are independent and are combined via the root-sum-square. System user range error requirements are based on vehicle performance over the period of operation, hence URE values are calculated as root-mean-square values over time. The combined contributions indicate both the IIF CFS and RFS will easily beat the URE allocation assigned to the frequency standards for all ages of data.

FUTURE FREQUENCY STANDARDS

The field of high performance frequency standards is rich with proposed and existing devices of ultra-high stability and accuracy^(1,2). However, when considering the need to qualify the frequency standards for space, the number of these standards is significantly reduced. Fundamental stability calculations have shown that 2-3 orders of magnitude improvement is possible from diode laser-pumped rubidium⁽³⁾ and cesium^(4,5) atomic frequency standards. However, since space-qualified diode lasers are not foreseen in the near future, introduction of such laser-pumped standards to the GPS Space Segment must wait.

Frequency standards based on advanced rubidium⁽⁶⁾ and linear ion-trap^(7,8) technologies promise significant near-term increased performance, while maintaining size, weight and power acceptable for satellite use.

LINEAR ION TRAP STANDARD

Linear Ion Trap standards are based on confinement of ions in small RF traps, where electromagnetic fields replace the physical walls required to confine the particles in conventional atomic standards. The ions, thus, remain unperturbed by de-phasing collisions with confining walls, eliminating a major source of frequency instability. Ion trap standards are also highly immune to environmental perturbations since, unlike masers or beam devices, they operate without resonant cavities. Proper choice of the atomic element for the ion standard reduces sensitivity to ambient electric or magnetic fields even further. (The fractional sensitivity of the mercury ion is nearly 1000 times smaller than the corresponding sensitivity of the hydrogen atom in the hydrogen maser) The sum of these characteristics make the stability of trapped ion devices orders of magnitude better than currently available atomic standards.

The Time and Frequency Systems Research group at NASA's Jet Propulsion Laboratory has been developing a trapped mercury ion frequency standard for ground-based applications over the past eight years. More recently, the JPL group has addressed the development of space flight frequency standards, and has produced a working prototype based on a novel "extended" linear electrode trap design⁽⁸⁾. This prototype is called the Linear Ion Trap-Extended, or LITE standard. The LITE traps Hg ions between four linear electrodes in one region and "interrogates" the ions optically in another. The separation of trapping and interrogation regions allows for an elegantly simple design.

The LITE prototype physics package is operated in conjunction with rack-mounted electronics. Although the electronics and support hardware of this prototype have not been optimized for space flight, estimates of flight unit parameters are 20 pounds and 15 Watts. The system performs as an ultra-stable frequency standard, as characterized by the Allan deviation shown in Figure 6.

ADVANCED RUBIDIUM STANDARD

As the supplier of GPS rubidium frequency standards, EG&G has gained insight into potential improvements for their standards, but paradoxically, for programmatic reasons, has not pursued them. The development of an advanced rubidium frequency standard would offer improved reliability, producibility, and an order of magnitude improvement in frequency stability. But such development is always accompanied by programmatic risk. Conservative program managers have avoided this risk by maintaining the current EG&G design without these improvements, even though such modifications are projected to put the advanced rubidium's performance close to that of a mercury linear ion trap standard.

Development of an advanced rubidium frequency standard would involve modifications to many aspects of the existing design. Incorporation of digital signal processing will improve producibility and performance. Digital techniques would allow numerical notch filtering of the 2nd harmonic signal, as well as various bookkeeping functions such as frequency self-calibration and tuning. Digital signal processing will also improve producibility by reducing the number of select in test components. Half of the RFS frequency instability is attributed to phase noise, much of which originates in the RF chain circuitry. The proposed use of a dielectric resonant oscillator in the high end of the RF chain and a numerically controlled oscillator in the low end can eliminate much of the phase noise. These techniques have already been successfully implemented in cesium-beam standards. Microwave cavity modifications can improve upon the limited utilization of the vapor cell volume for signal generation, increasing the signal-to-noise ratio. Cavity design can also improve the uniformity of magnetic field. These improvements involve well-established techniques and don't require the addition of any new, high-risk technologies.

CONCLUSION

Future implementation of ultra-precision frequency standards can improve the accuracy of the GPS system by nearly eliminating the AFS noise contribution to URE for all ages of data. However, the GPS "System" performance in the IIF timeframe will be principally determined by short-term AFS performance with age of data of 3 hours or less because of the unique GPS-IIF "crosslink update mode" and operational approaches. Figure 7 shows the projected random noise contribution to user range error for the advanced rubidium and linear ion-trap-based standards. The random noise error can be reduced to a few centimeters at 24 hours, as compared to the ~1 meter-noise contribution of current standards.

REFERENCES

1. L. Maleki, Frequency Standards from Government Over the Next 25 Years, Proceedings of the 25th Meeting PTTI, 1994.
2. N. Ramsey, The Past, Present, and Future of Atomic Time and Frequency, Proceedings of the IEEE, Vol. 79, No. 7, 1991.
3. J. Compararo, R. Fruehholz, Fundamental Stability limits for the Diode-Laser Pumped Rubidium Atomic Frequency Standard, J. Applied Physics, Vol. 59, May 15, 1986.
4. R. Drullinger, Frequency Standards Based on Optically Pumped Cesium, Proceedings of the IEEE, Vol. 74, No. 1, Jan. 1986.
5. R. Drullinger et. al., The NIST Optically Pumped Cesium Frequency Standard, IEEE Transactions on Instrumentation and Measurement, Vol. 40, No. 2, April 1991.
6. William Riley, EG&G Electro-Optics Division, Private Communication, 1997.
7. J. Prestage et. al., Improved Linear Ion Trap Physics Package, Proceedings of the IEEE International Frequency Control Symposium, 1993.
8. J. Prestage and L. Maleki, Space Flyable Hg Frequency Standards, Proceedings of the IEEE International Frequency Control Symposium, 1994.
9. D. Allan and H. Hellwig, Time Deviation and Time Prediction Error for Clock Specification, Characterization and Application, Proc. Of Position, Location, and Navigation Symp., San Diego CA, Nov.7-9, 1978, pp29-36.
10. D. Allan, Addendum Paper to: Time Deviation and Time Prediction Error for Clock Specification, Characterization and Application (see ref. 9), March, 1981.
11. D. Allan, Time and Frequency (Time-Domain) Characterization, Estimation, and Prediction of Precision Cocks and Oscillators, IEEE Trans. on Ultrasonics, Ferroelectrics, and Frequency Control, Vol. UFFC-34, No. 6, Nov., 1986.
12. K. Ghassemi and S. Fisher, Performance Projections of GPS-IIF, Proceedings of the Institute of Navigation, 1997.

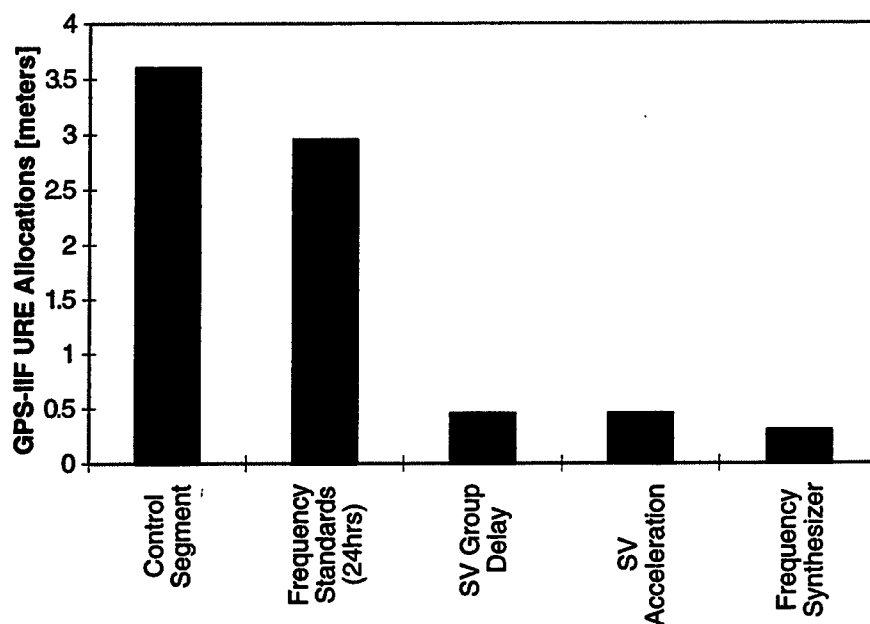


Figure 1. Significant allocated user range error contributions for the GPS-IIF satellites.

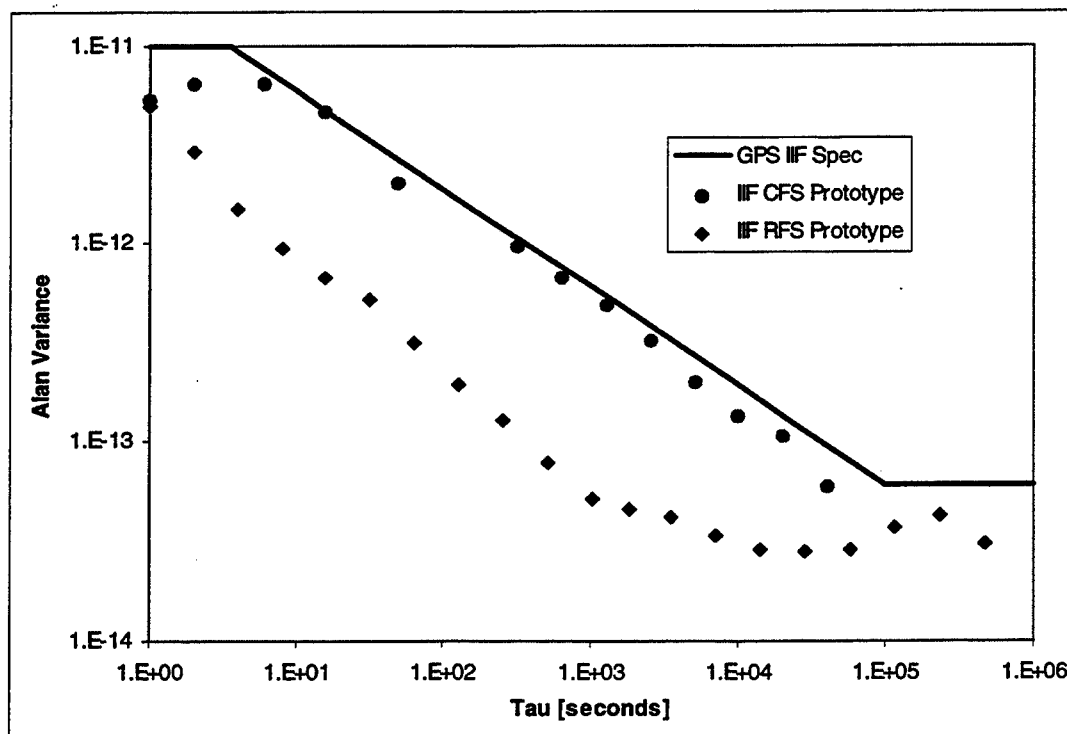


Figure 2. Preliminary AFS prototype stability data

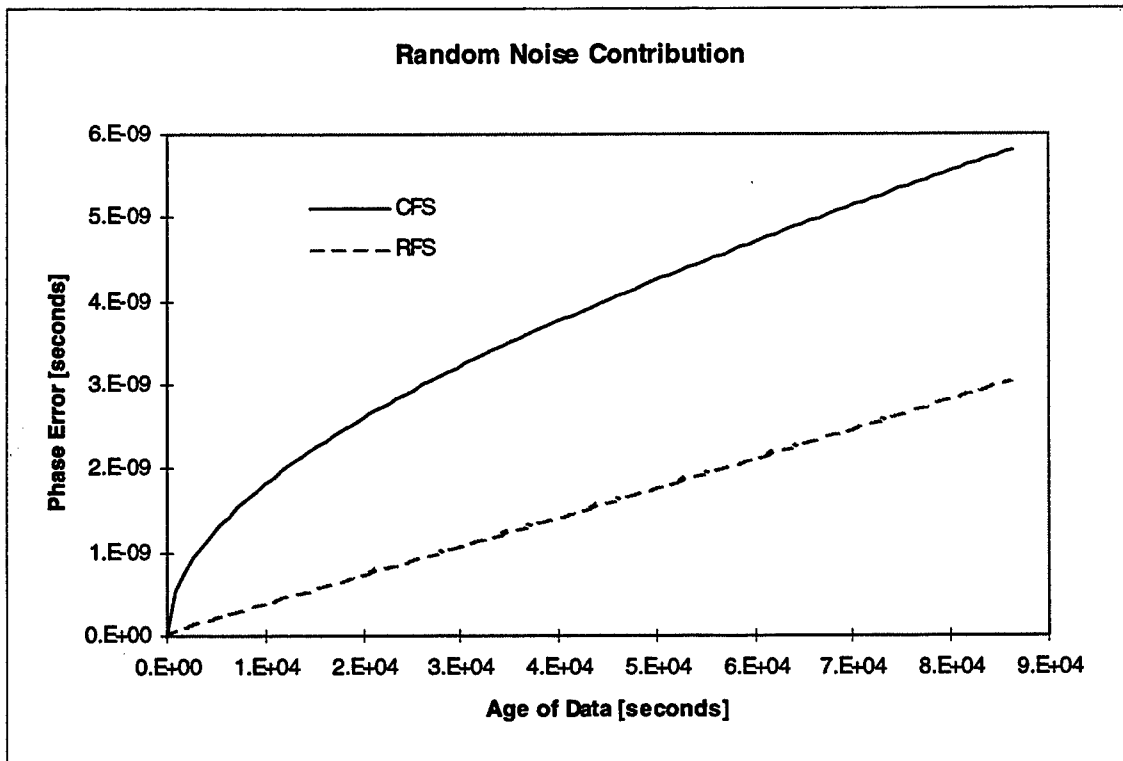


Figure 3. Random noise contribution to phase error

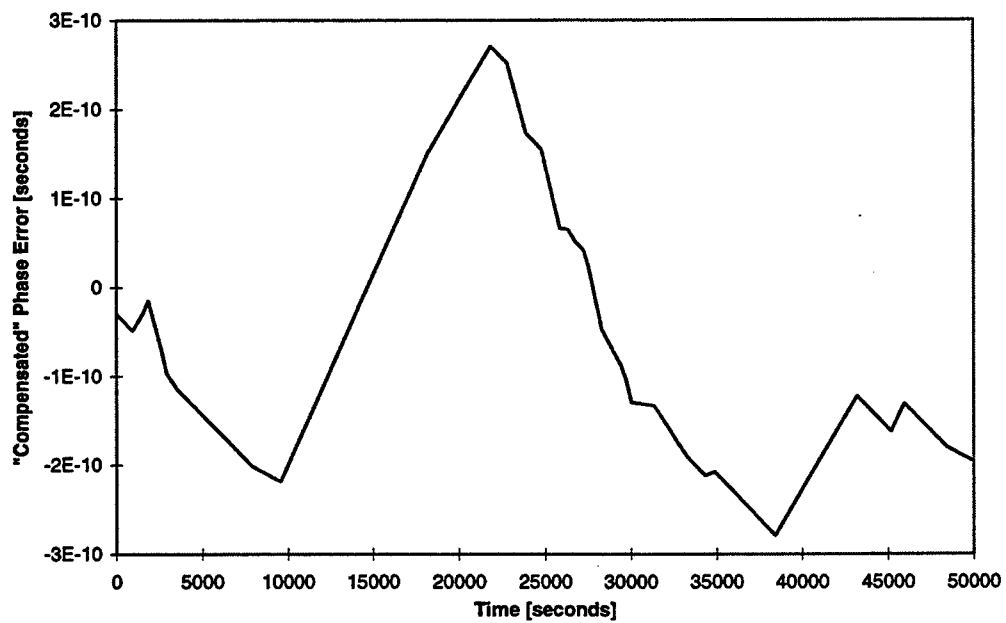


Figure 4. Control Segment compensated magnetic phase error

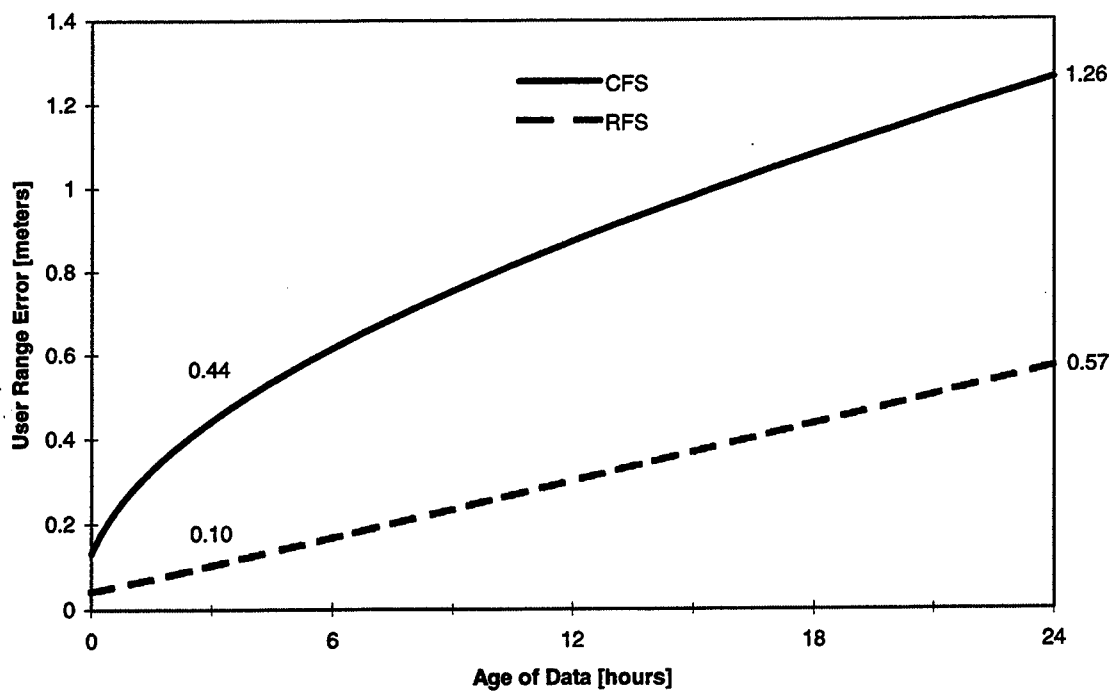


Figure 5. Frequency Standards Contribution to URE

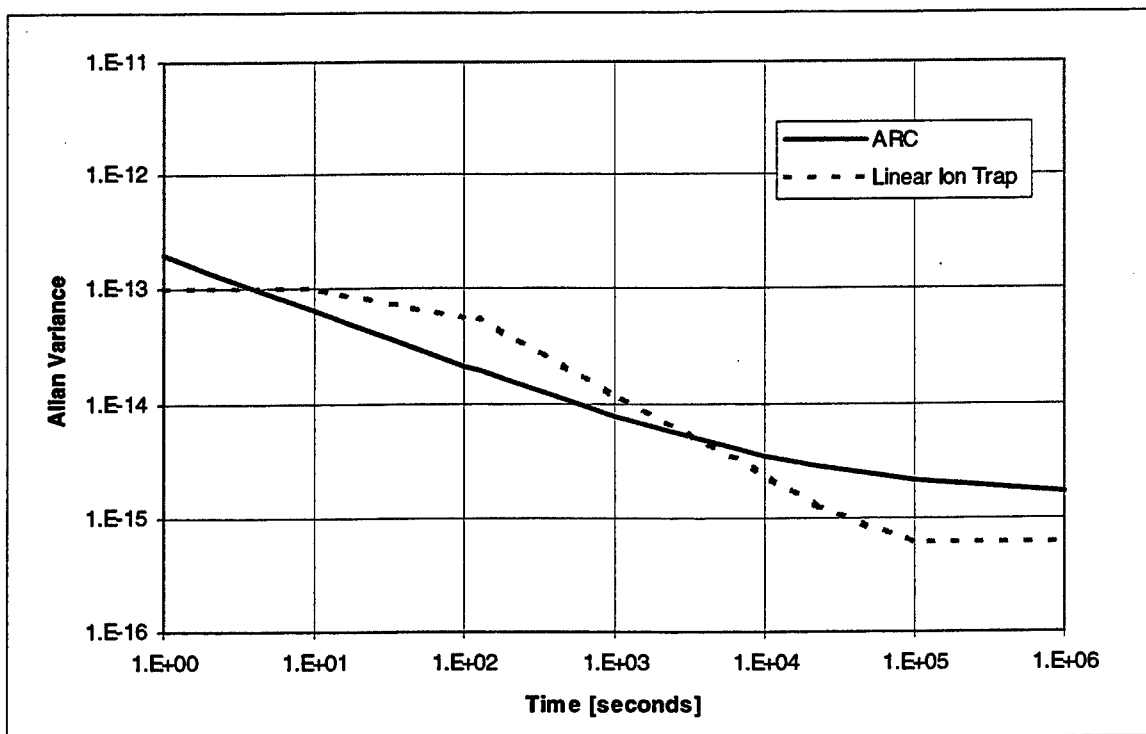


Figure 6. Frequency stability for proposed advanced space-qualified clocks

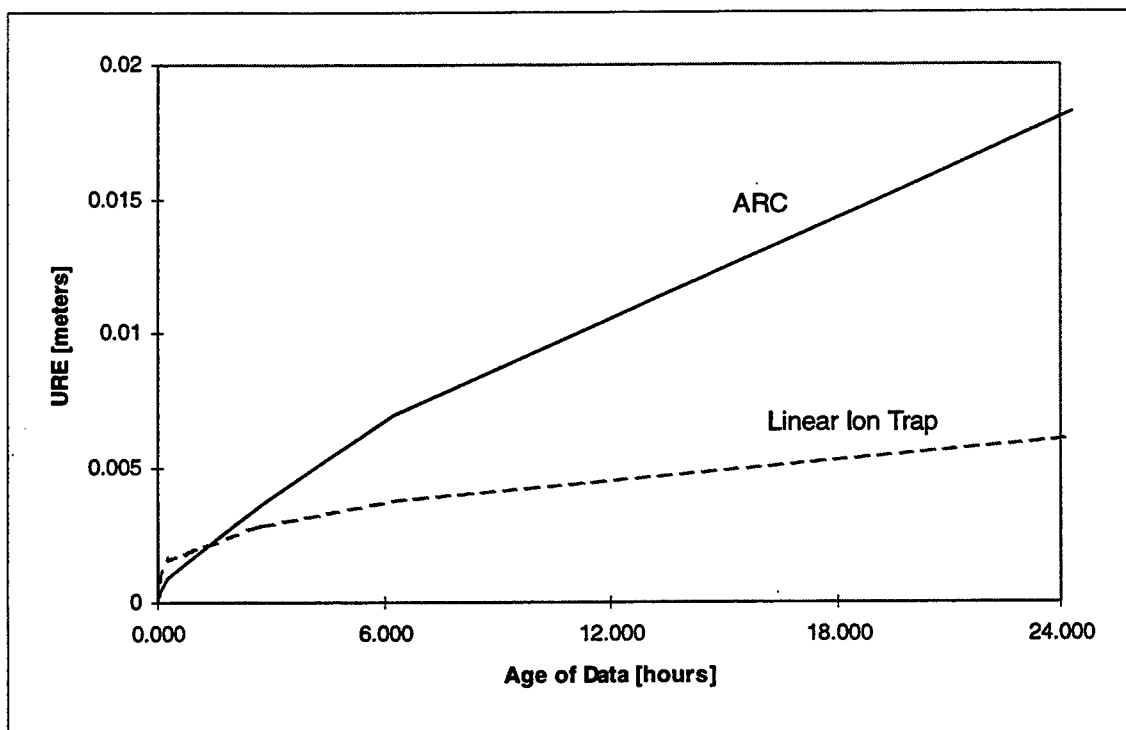


Figure 7. Proposed advanced clocks significantly reduce the user range error

EARLY IN-ORBIT PERFORMANCE OF GPS BLOCK IIR RUBIDIUM CLOCKS

W.J. Riley
EG&G Frequency Products
35 Congress Street
Salem, MA 01970 USA

Abstract

The first Block IIR GPS navigation satellite, placed in orbit on July 22, 1997, carried a new generation of rubidium clocks. Since then, two of these clocks have been activated, and both are performing well. This paper reports on those early results, and compares the in-orbit performance with ground acceptance test data.

EG&G has delivered about two-thirds of the 66 Rubidium Atomic Frequency Standards (RAFS) needed for the Block IIR GPS program. Composite frequency and time stability plots are presented for all delivered units, and more detailed acceptance test stability data are shown for the two RAFS that are operating on-board SVN43. In addition, similar life test data are shown for the two units that are undergoing life testing at NRL.

In-orbit stability and drift data are presented for RAFS S/N 005 and 006 using all available 15-minute precise ephemeris/clock data from the National Imagery and Mapping Agency (NIMA). RAFS S/N 006 was turned on 8/13/97 and was used as the active clock until 9/26/97. RAFS S/N 005 was turned on 8/22/97 and became the active clock on 9/26/97 at the beginning of a 2-month extended navigation test. Both are showing excellent stability and early drift stabilization.

INTRODUCTION

The first successfully launched Block IIR GPS navigation satellite was placed in orbit on July 22, 1997 carrying a new generation of rubidium clocks. Since then, two of these clocks have been activated, and both are performing well. This paper reports on those early results, and compares the in-orbit performance with ground acceptance test data.

RAFS PRODUCTION STATUS

EG&G has delivered about two-thirds of the 66 Rubidium Atomic Frequency Standards (RAFS) units needed for the Block IIR GPS program. Each of the 21 Block IIR space vehicles has three RAFS, two RAFS are undergoing ground life testing at the Naval Research Laboratory (NRL), and one unit is a spare. Composite Allan and time deviation plots showing the stability of all delivered units are shown in Figures 1 and 2. All units show negative drift with logarithmic stabilization that settles to below -1×10^{-13} /day in 1-2 months, and have a typical stability of $\sigma_y(\tau) = 2 \times 10^{-12} \tau^{-1/2} + 2 \times 10^{-14}$.

NRL LIFE TEST DATA

RAFS S/Ns 028 and 030 have been undergoing life testing under thermovac conditions at the Naval Research Laboratory since April, 1997. Both units are performing well and are displaying excellent stability and drift stabilization, as shown in the table below.^{[3], [4]} The stability value shown is the $\tau=1$ day Hadamard deviation (which removes the linear frequency drift).

RAFS S/N	Drift, pp10 ¹⁴ /day	Stability, pp10 ¹⁵
028	-8.1	5.6
030	-6.5	7.5

NIMA DATA

The National Imagery and Mapping Agency (NIMA) provides precise ephemeris and clock data for the GPS constellation at their Web site.^[5] These data are in the SP3 enhanced format and are organized into daily files by GPS week and day number (see on-line information). The early non-operational data for SVN43/PRN13 can be downloaded via ftp from special files.^[6] The NIMA precise ephemeris data are also used by NRL to generate reports regarding the in-orbit performance of GPS clocks.^[7]

RAFS S/N 006

Figure 3 shows about 39 days of $\tau=15$ minute NIMA frequency data for RAFS S/N 006 from 8/18/97 to 9/25/97, which covers the complete period from when these data became available to when tuning tests were conducted just prior to switching to RAFS S/N 005. The record shows the negative aging and logarithmic stabilization that is typical of all of these Rb clocks. A $y(t)=a \cdot \ln(bt+1)$ log fit to the frequency data allows the deterministic aging to be separated from the stochastic noise, and uses the entire record to determine the aging slope at the end, only -8.25×10^{-14} /day. A detailed inspection of the data shows a considerable amount of sharp phase noise and spikes, and some daily variations that are indicative of orbital effects.

Figure 4 shows the RAFS S/N 006 frequency residuals after the log fit is removed. The quality of the trend removal is excellent, and the residuals show the noise and diurnal variations more clearly. These residuals are then used to analyze the clock stability.

Figure 5 shows the RAFS S/N 006 frequency stability as measured during factory acceptance testing and by the NIMA in-orbit data for the complete SVN43 time keeping system (TKS). The order-of-magnitude increase in noise at short averaging times is due mainly to the coarse phase meter resolution, while the extra noise at intermediate averaging times is due mainly to VCXO noise and temperature sensitivity.^[1] It is also somewhat higher than measured during ITT acceptance testing^[2], perhaps because the actual orbital temperature variations are larger than predicted. The RAFS temperature sensitivity is negligible. The overall stability is near that of the RAFS itself at averaging times of 1 day and longer.

Figure 6 shows the RAFS S/N 006 time stability. The 1-day time deviation, $\sigma_x(\tau)$ or TDEV, is probably the single best indicator of clock performance in the GPS application. This value, 0.79 nsec or 0.24 meter, is excellent, and well within the 1.40 meter error budget allocation.^[2]

RAFS S/N 005

Figures 7-10 show similar data for RAFS S/N 005, which was turned on 8/22/97 and selected as the on-line clock on 9/26/97. NIMA tracking data for S/N 005 began on 9/27/97 and continued until 10/16/97, when it ended because of side effects of an extended navigation test that is expected to continue through 12/7/97. RAFS S/N 005 had a drift of -1.12×10^{-13} /day at the end of this record and a stability essentially identical to that of S/N 006. The 1-day TDEV for this clock was also similar, 0.59 nsec.

CONCLUSIONS

The first of a new generation of space-qualified rubidium clocks has been launched and their early performance is excellent.

ACKNOWLEDGEMENTS

The work on these high performance rubidium clocks has been underway for over 20 years, beginning at General Radio in 1975 and continuing at EG&G since 1980. Many persons and organizations have contributed to and supported this work, including the U.S. Air Force, Rockwell/Boeing, ITT, GE/Lockheed Martin, the Naval Research Laboratory and Aerospace Corporation.

REFERENCES

- [1] A. Wu, "Performance Evaluation of the GPS Block IIR Time Keeping System", Proceedings of the 28th Annual Precise Time and Time Interval (PTTI) Applications and Planning Meeting, December 3-5, 1996, pp. 441-453.
- [2] H. Rawicz and R. Smid, "GPS Block IIR Accuracy Verification", Proceedings of the ION GPS-97 Conference, pp. 377-385.
- [3] J.A. Buisson, "RAFS Life Test Analysis Update No. 28-29", Naval Research Laboratory, October 22, 1997.
- [4] J.A. Buisson, "RAFS Life Test Analysis Update No. 30-29", Naval Research Laboratory, October 22, 1997.
- [5] <http://164.214.2.59/geospatial/products/GandG/sathtml/>.
- [6] ftp://164.214.2.59/pub/sat_out/nimwwwwd.13, where www is the GPS week # and d is the day.
- [7] J.A. Buisson, "NAVSTAR Analysis Update No. 43-3", Naval Research Laboratory, October 14, 1997.

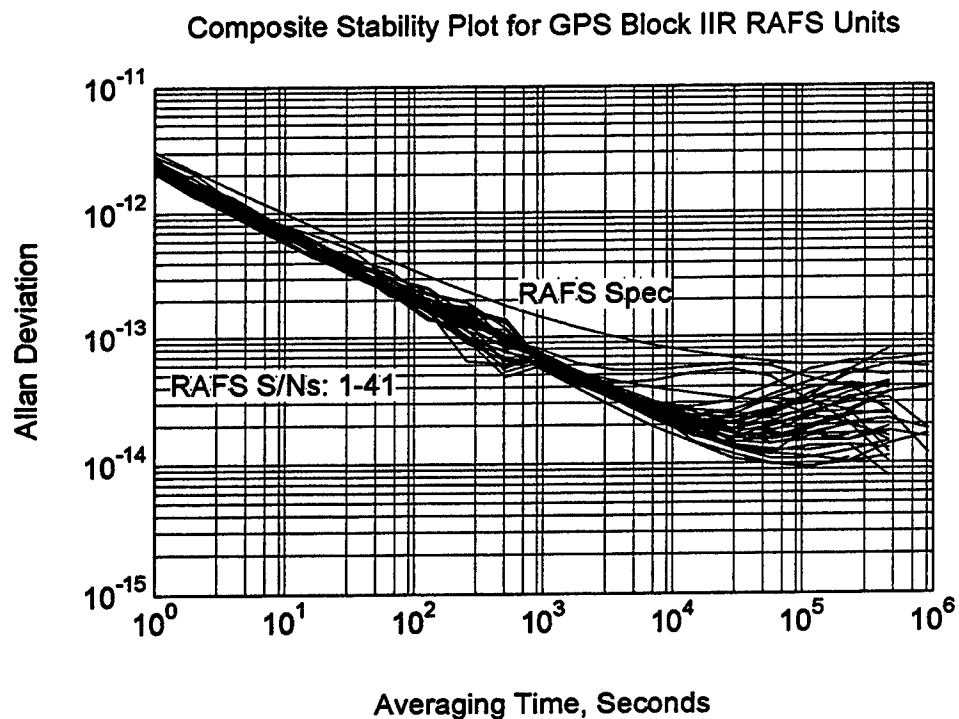


Figure 1 RAFS Composite Frequency Stability Plot

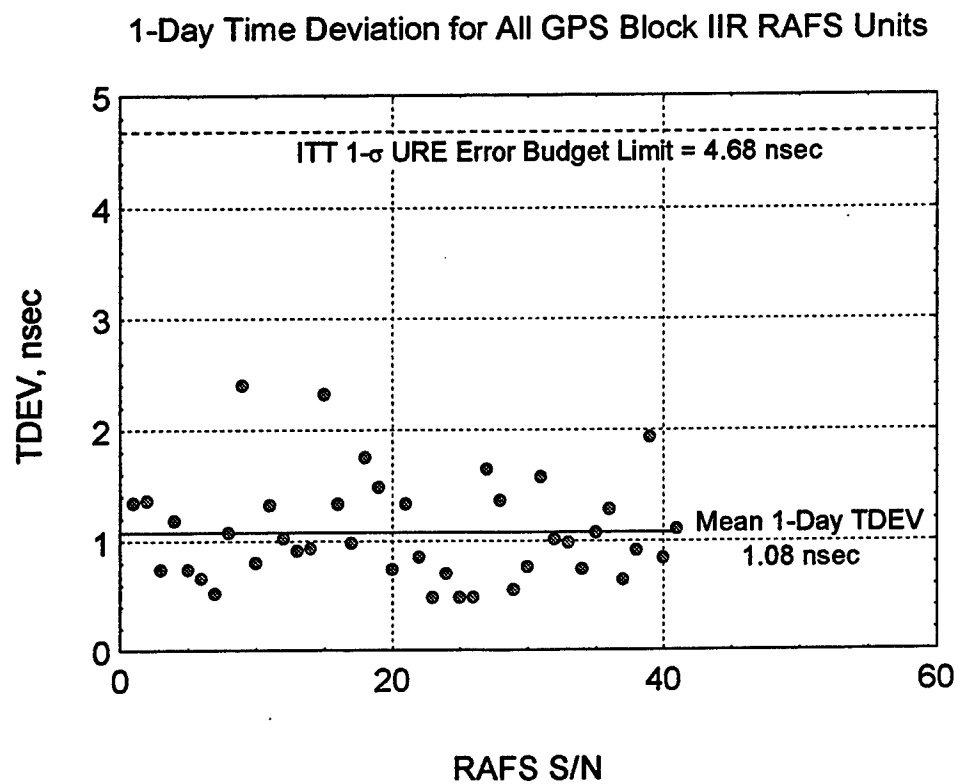


Figure 2 RAFS Composite Time Stability Plot

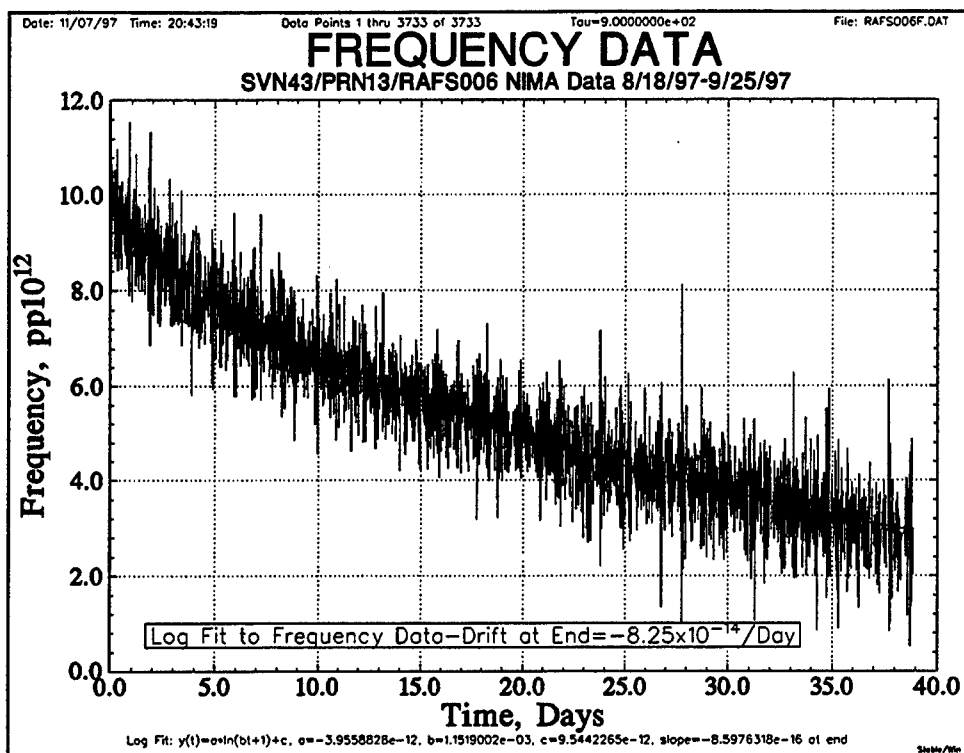


Figure 3 RAFS S/N 006 Frequency Data

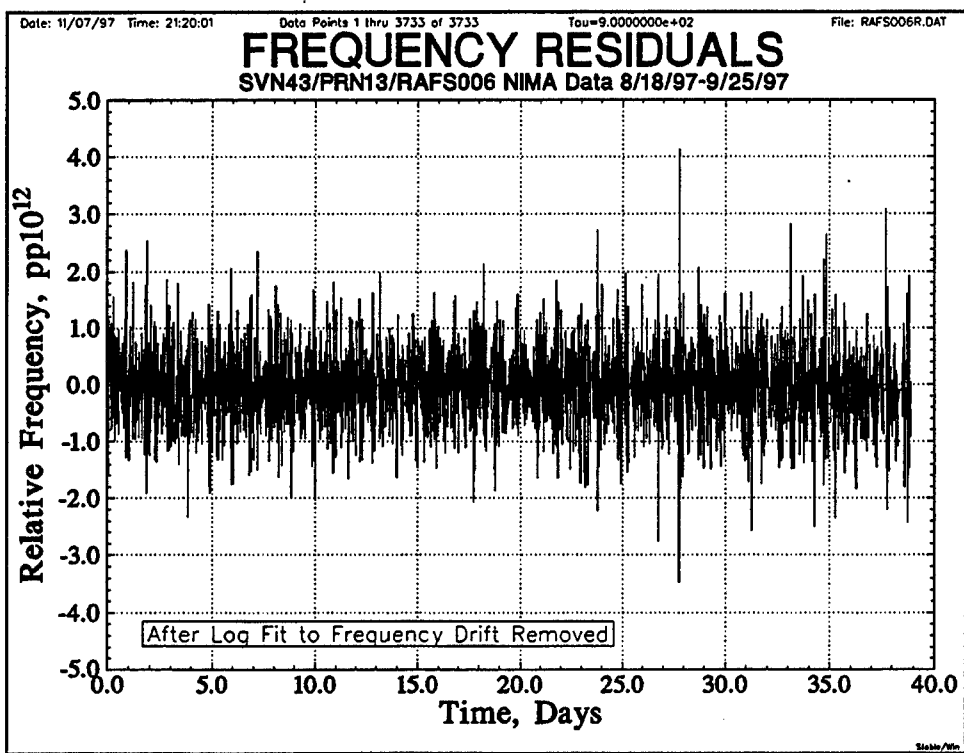


Figure 4 RAFS S/N 006 Frequency Residuals

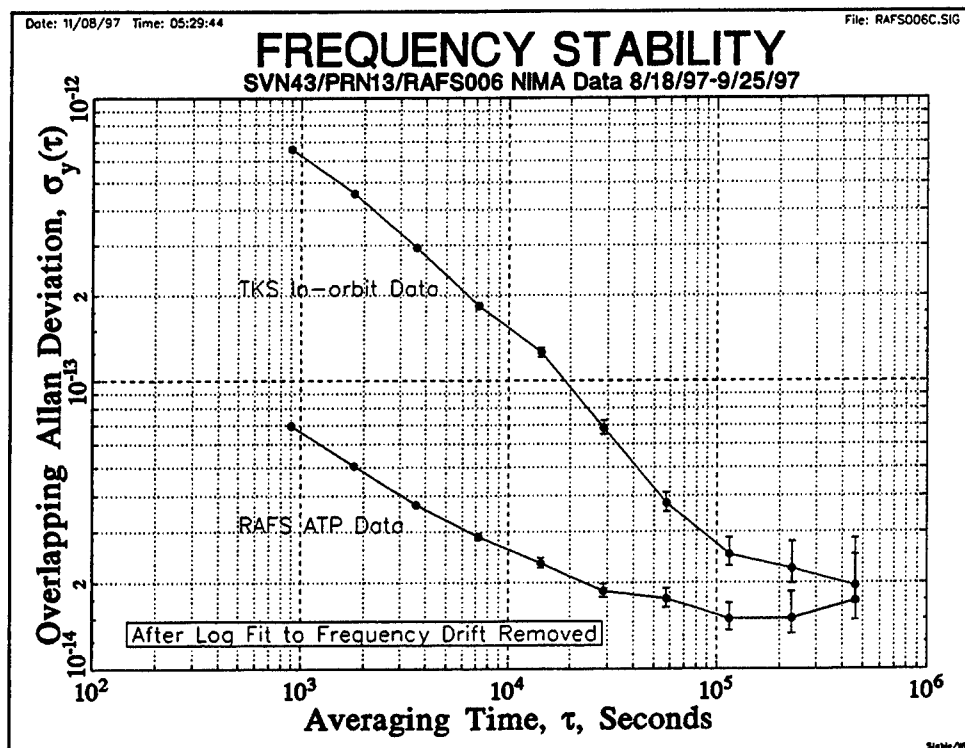


Figure 5 RAFS S/N 006 Frequency Stability

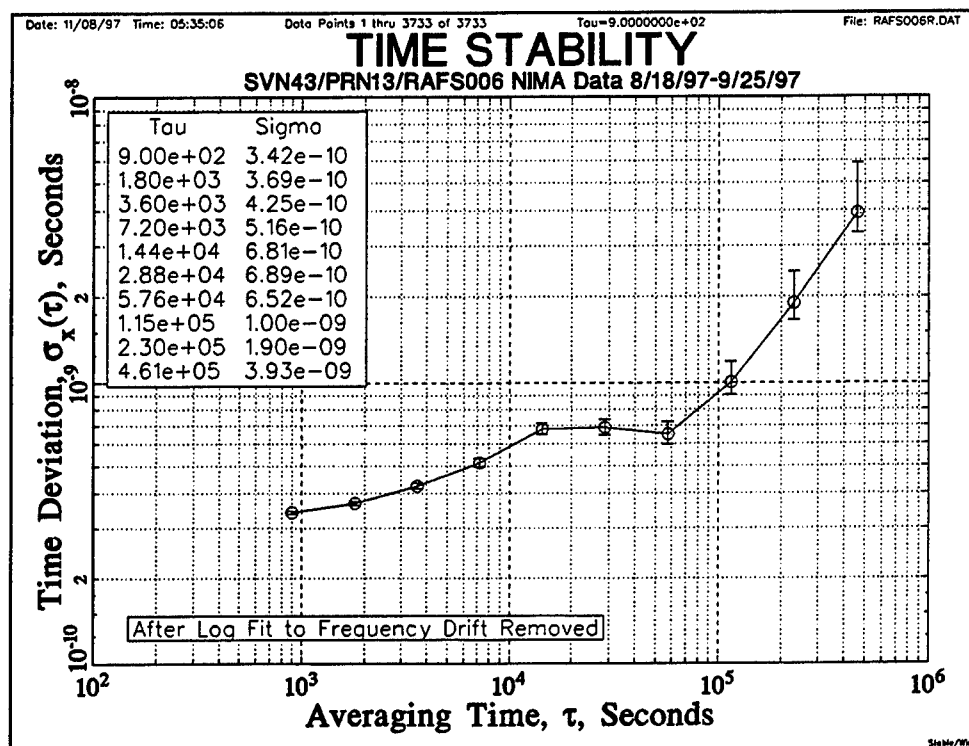


Figure 6 RAFS S/N 006 Time Stability

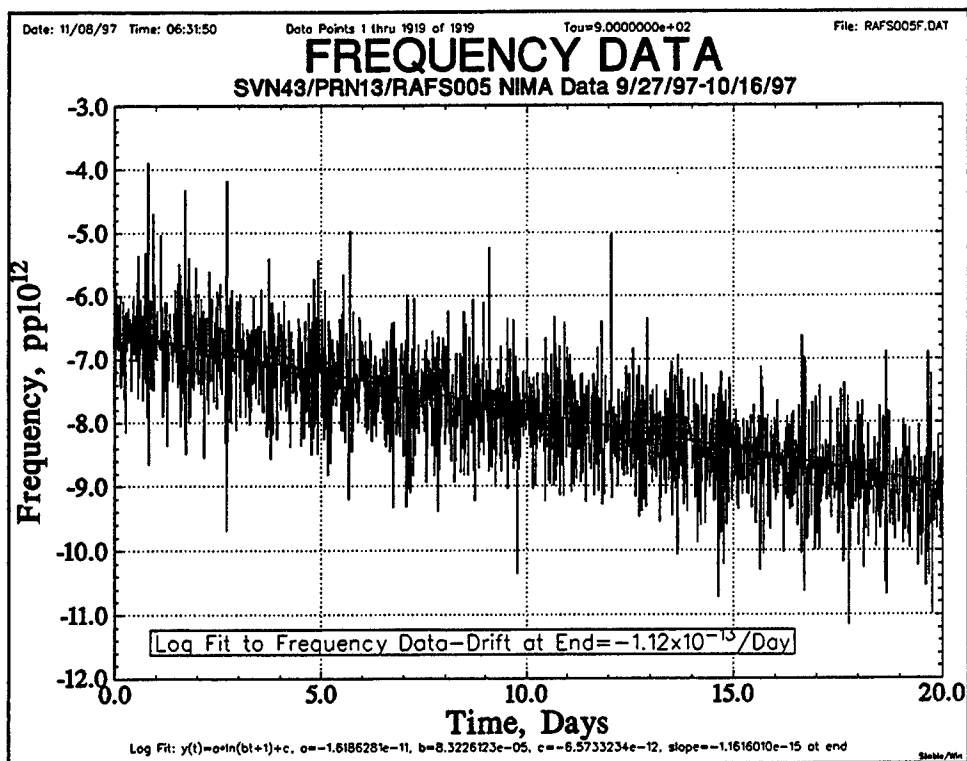


Figure 7 RAFS S/N 005 Frequency Data

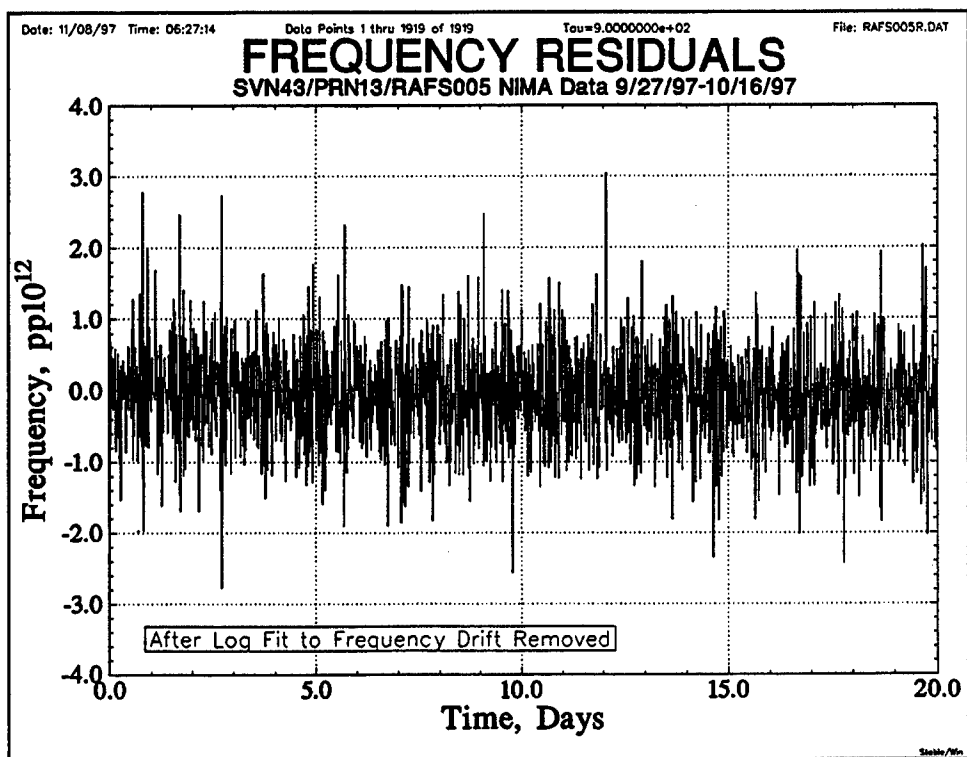


Figure 8 RAFS S/N 005 Frequency Residuals

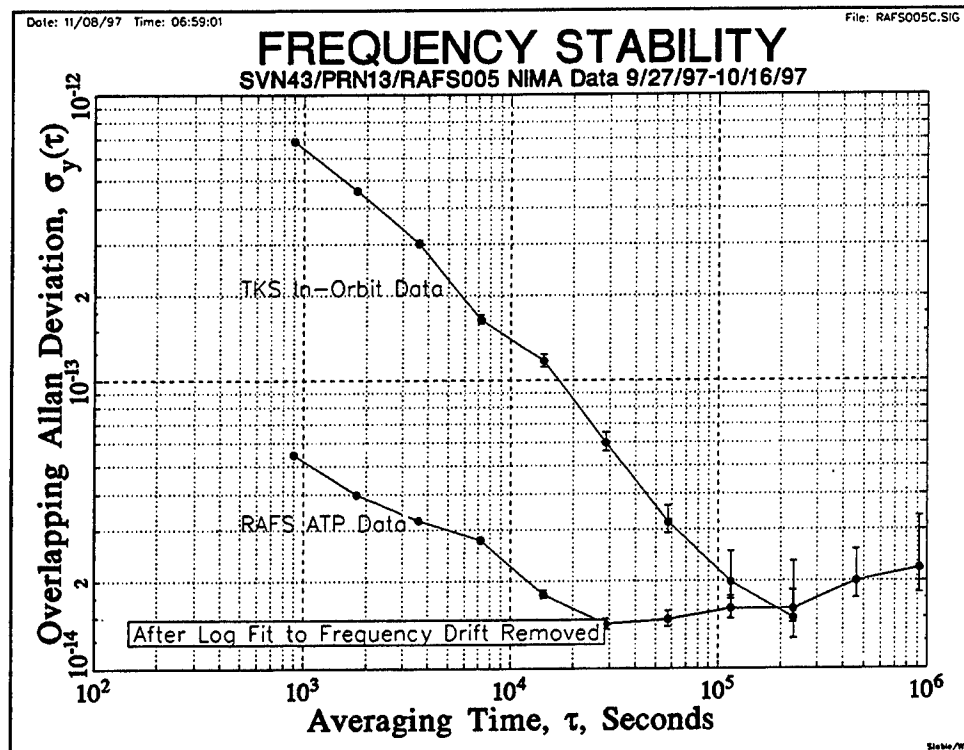


Figure 9 RAFS S/N 005 Frequency Stability

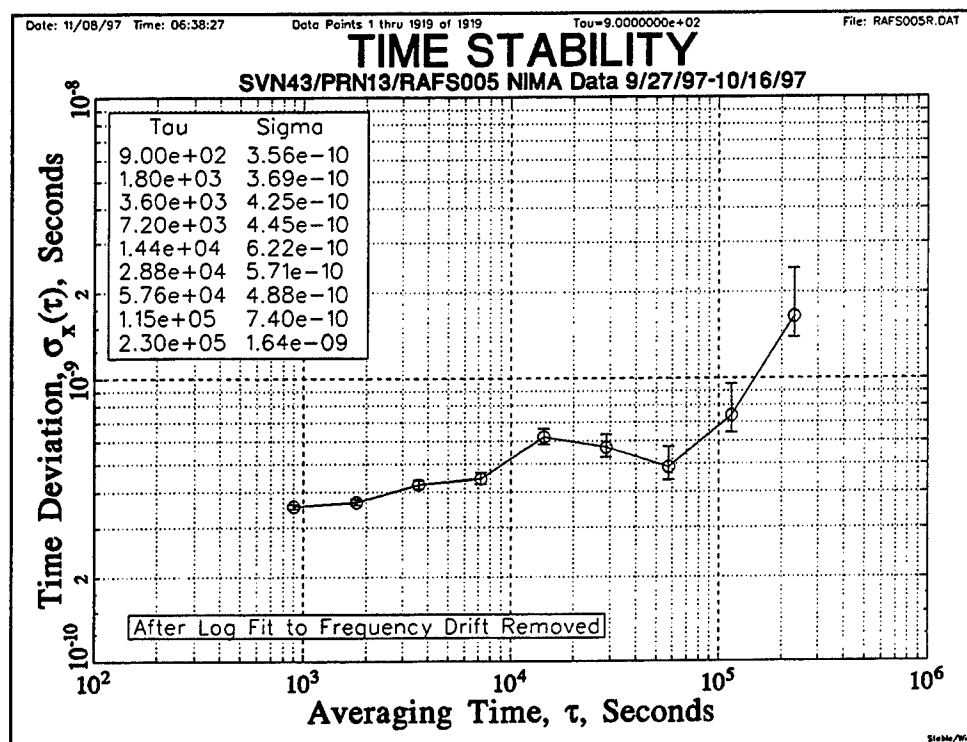


Figure 10 RAFS S/N 005 Time Stability

TIME TRANSFER USING GPS CARRIER PHASE METHODS

K. M. Larson
Department of Aerospace Engineering Sciences
University of Colorado, Boulder
Boulder, CO 80309
tel 303-492-6583 fax 303-492-7881
e-mail kristine.larson@colorado.edu

J. Levine
NIST Time and Frequency Division
JILA and Department of Physics
Boulder, CO 80309

Abstract

We have conducted several time-transfer experiments using the phase of the GPS carrier rather than the code, as is done in current GPS-based time transfer systems. We used data from geodetic quality "off-the-shelf" dual-frequency GPS receivers, where up to 8 satellites can be simultaneously observed.

We connected two GPS receivers to two different atomic clocks at NIST. The antennas connected to the receivers were separated by about 40 m. The time difference between the clocks connected to the GPS receivers was estimated using weighted least-squares methods and carrier phase data. These relative clock estimates were then compared with the NIST time-scale system. We find agreement between the two methods of 55-80 picoseconds over periods of a week.

INTRODUCTION

Soon after the Global Positioning System was developed, the geophysical community began to apply it to numerous scientific problems, including plate tectonics, post-glacial rebound, interseismic deformation, and volcano monitoring.^[1] The size of signals associated with these phenomena can be as small as 1 mm/yr. In order to address their science objectives, geophysicists have long been involved in research to improve the accuracy of GPS. When it became clear that their scientific goals required greater orbit accuracy, the geophysical community and their geodetic colleagues developed a global continuously operating GPS network. Data from this network are used to provide extremely accurate GPS ephemerides. Along with model improvements and careful reference frame definition, the accuracy of GPS position estimates now approaches one centimeter over averaging periods of a day.^[2] Sub-centimeter horizontal precisions are routinely reported for distances of several thousand kilometers.^[3] These achievements were made using the GPS carrier phase observable. The objective of this paper is to investigate the resolution of GPS carrier phase methods for time transfer.

ESTIMATION

The GPS carrier phase observable $\Delta\phi_r^s$ of wavelength λ can be written as:[4]

$$-\Delta\phi_r^s\lambda = \rho + c\delta^s - c\delta_r + N\lambda + \rho_t - \rho_i + \rho_m + \epsilon \quad (1)$$

where subscript r refers to the receiver and superscript s denotes the satellite. ρ is the geometric range, or $|\vec{X}^s - \vec{X}_r|$, where \vec{X}^s is the satellite position at the time of signal transmission and \vec{X}_r is the receiver position at reception time. Proper determination of ρ requires precise transformation parameters between the inertial and terrestrial reference frames, i.e. models of precession, nutation, polar motion, and UT1-UTC. ρ_t and ρ_i are the propagation delays due to the troposphere and ionosphere and ρ_m is the multipath error. ϵ represents unmodelled errors and receiver noise. Since the GPS receiver only tracks the fractional phase, an integer bias, N , must be introduced to the model equation. This bias is also known as the carrier phase ambiguity. δ^s and δ_r are the satellite and receiver clock errors. An equivalent model equation can be derived for the pseudorange or "code" observable with several important distinctions. Pseudorange is not biased and so N is not estimated. The magnitude of the ionospheric delay is the same, but opposite in sign. The most significant pseudorange limitation is that the ϵ term is nearly 100 times larger than for carrier phase.

The ionospheric delay can be effectively removed by combining the two GPS frequencies. The remaining parameters, δ^s , δ_r , \vec{X}^s , \vec{X}_r , ρ_t , and N must be estimated or known *a priori*. The model equation can be linearized and solved using weighted least squares. We used the GIPSY software to solve these equations.[5] Parameter estimation in GIPSY is carried out using a Square Root Information Filter (SRIF) algorithm described in [6]. Both satellite and receiver clocks are estimated at each data epoch relative to a reference receiver clock. The clock estimates are uncorrelated from epoch to epoch. The satellite coordinates \vec{X}^s are taken from the IGS service, with a radial accuracy of 5-10 cm.[7] The IGS analysis includes GPS data from 50 or more GPS receivers around the world. We estimate the wet tropospheric path delay at zenith as a time-dependent parameter with a random walk noise model.[8]

RESULTS

Over short baselines, most geodetic parameters, including clocks, are insensitive to orbit error. This is also true of atmospheric conditions, which are common to both antennas for a short baseline. The limiting error sources in this case are likely to be multipath and receiver noise.

Two geodetic quality GPS receivers were connected to NIST Clock 16 and NIST Clock 21. Clock 16 is a hydrogen maser and Clock 21 is a cesium standard. Each GPS antenna was mounted to the roof of the NIST facility. The distance between the antennas was approximately 40 meters. The receivers were operated continuously for 28 days at a data interval of 30 seconds. Parameter estimation over short distances includes the behavior of Clock 21, carrier phase ambiguities, and the coordinates of each antenna. The carrier phase ambiguity bias terms were resolved.[9] Clock 16 was treated as the reference clock and its time-varying behavior was not estimated. There was no direct connection between the GPS receivers. All GPS estimates of the clocks are based on a full analysis of the GPS carrier phase observables.

We have made independent measurements of Clock 16 and Clock 21 using a special hardware system that looks like a group of time interval counters (TIC). These data were acquired automatically every

12 minutes. The difference between Clock 16 and Clock 21 as measured by the TIC system is shown in Fig. 1.

Over the 28 days of this experiment, the GPS receiver connected to Clock 21 lost lock on all satellites 3 times. This resulted in minimal data loss (5-15 minutes), but did introduce a bias into our solutions. A geodetic GPS receiver is programmed by the manufacturer to "reset" its internal clock whenever the receiver loses lock on all satellites. The receiver sets its clock by the GPS constellation in view at that time. Because of selective ability this bias can be as large as 300 nsec. It is this internal clock that is used to define the carrier phase observable. With appropriate modifications to the receiver, this reset can be calibrated.

In Fig. 2 we demonstrate the advantage of using carrier phase data over pseudorange data. In each time series we have subtracted the TIC clock measurements as truth. Thus, we are showing the residual agreement for the measured difference between Clock 16 and Clock 21. In Fig. 2a we used only pseudorange data. The residuals show peak-to-peak scatter of 10 nsec, with a RMS agreement over the 7-day period of 2.3 nsec. The large daily signature in the pseudorange data is associated with multipath. Since a GPS satellite will appear 4 minutes earlier each day, we expect multipath to have a 23 hour 56 minute period. In Fig. 2b we used carrier phase data. The residual RMS agreement using carrier phase data is 55 picoseconds.

In Fig. 3 we summarize the results for our 28-day experiment. We have plotted the residual of the difference between the GPS estimates and the TIC values for the 4 separate sections of data. Each section is plotted against its own mean. The weighted RMS residuals for the 4 sections range from 55 to 81 picoseconds. At this scale we can see that carrier phase data are also affected by multipath.

CONCLUSIONS

We have demonstrated 55-81 picosecond accuracy for time transfer over short distances over periods of a week. The dominant error appears to be multipath. The effect of multipath can be reduced by careful site selection. To achieve 50 picosecond time transfer accuracy, geodetic quality dual frequency receivers with 8 or more channels must be used and ambiguity resolution is required.

ACKNOWLEDGEMENTS

We thank Ed Manzanares, Ulf Lindquister, Tom Meehan, Tom Yunck, Larry Young, Jim Ray, Demetrios Matsakis, and Ed Powers for lending us equipment and helpful discussions. We acknowledge computing facilities funded by NASA grant NAG1908. The GIPSY software was written by the Jet Propulsion Laboratory.

REFERENCES

- [1] P. Segall and J. Davis 1997, "GPS applications for geodynamics and earthquake studies," **IEEE Annual Reviews of Earth and Planetary Sciences**, 25, 310-336.
- [2] G. Blewitt, M. Heflin, W. Bertiger, F. Webb, U. Lindqwister, and R. Malla 1992, "Global coordinates with centimeter accuracy in the international terrestrial reference frame using the Global Positioning System," **Geophysical Research Letters**, 19, 853-856.
- [3] K. Larson, J. Freymueller, and S. Philipsen 1997, "Global plate motions from the Global Positioning System," **Journal of Geophysical Research**, 102, 9961-9981.

- [4] B. Hofmann-Wellenhof, H. Lichtenegger, and J. Collins 1994, **Global Positioning System Theory and Practice**, Springer-Verlag Wien, New York, New York, USA, p. 355.
- [5] S. Lichten and J. Border 1987, "*Strategies for high-precision Global Positioning System orbit determination*," **Journal of Geophysical Research**, **92**, 12,751-12,762.
- [6] G. Bierman 1977, **Factorization Methods for Discrete Sequential Estimation**, Academic, San Diego, Calif., USA.
- [7] G. Beutler, I.I. Mueller, and R.E. Neilan 1994, "*The International GPS Service for Geodynamics (IGS): Development and start of official service on January 1, 1994*," **Bulletin Geodesique**, **68**(1), 39-70.
- [8] D. Tralli, T. Dixon, and S. Stephens 1988, "*The effect of wet tropospheric delays on estimation of geodetic baselines in the Gulf of California using the Global Positioning System*," **Journal of Geophysical Research** **93**, 6545-6557.
- [9] G. Blewitt 1989, "*Carrier phase ambiguity resolution for the Global Positioning System applied to geodetic baselines up to 2000 km*", **Journal of Geophysical Research**, **94**, 10,187-10,282.

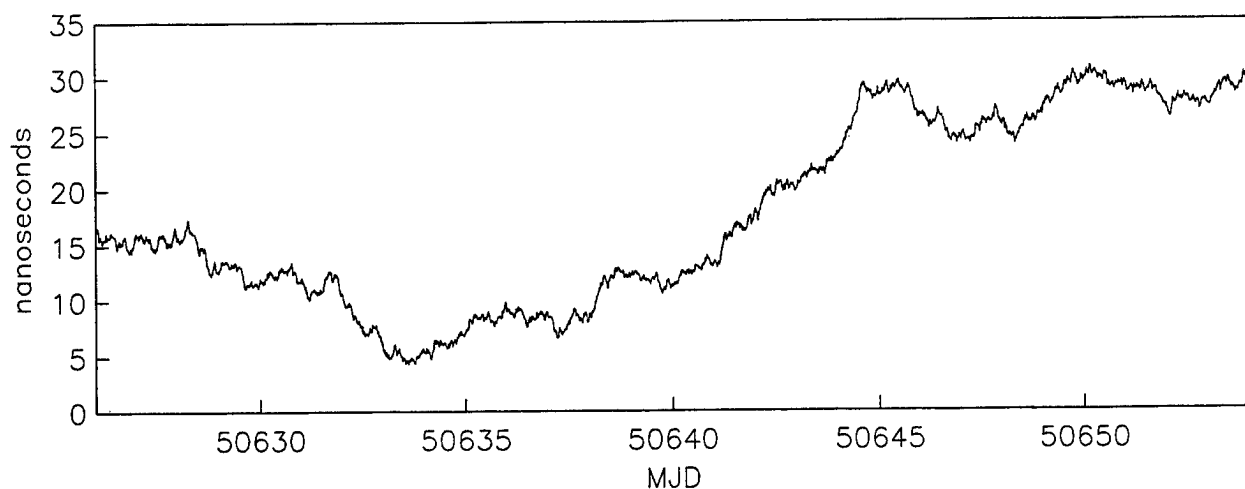


Fig. 1: Measured difference between NIST Clock 16 and NIST Clock 21 during GPS experiment using time interval counters.

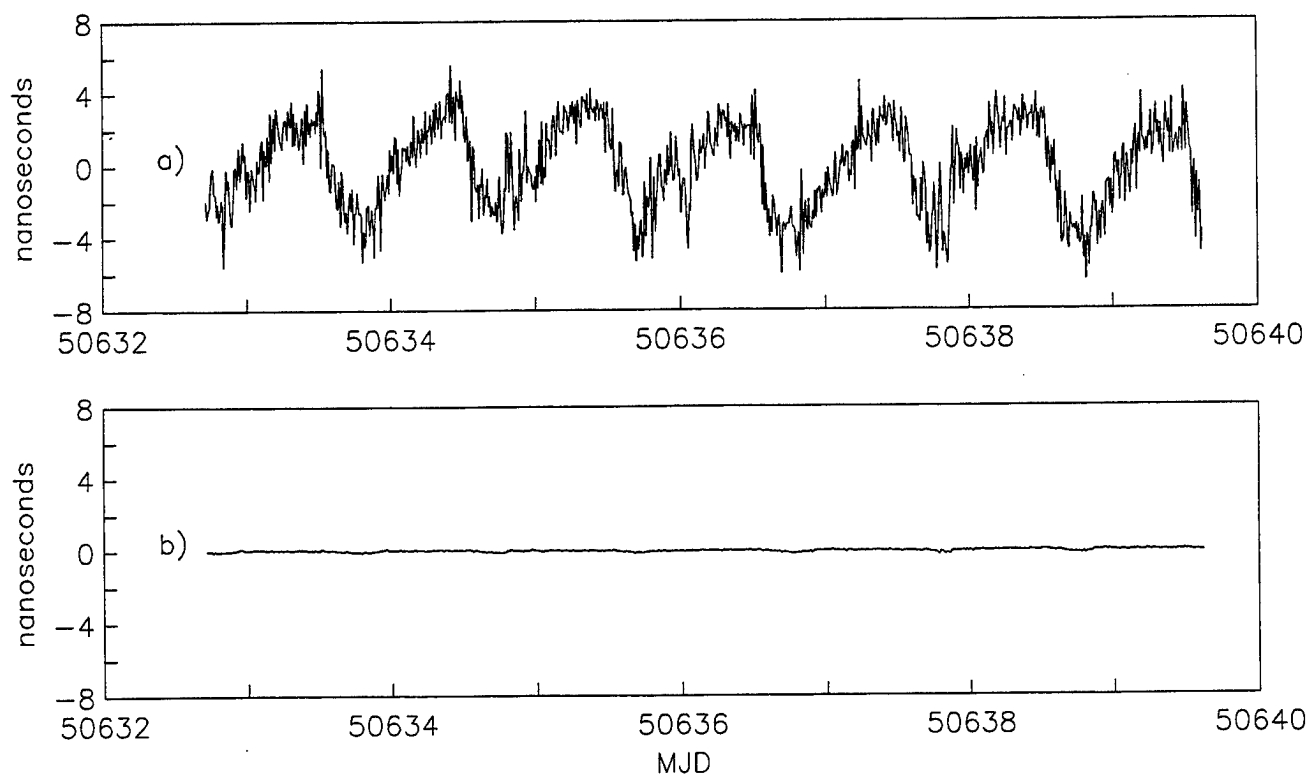


Fig. 2: The residuals between GPS estimates of the Clock 16-21 difference and the measured difference taken from Fig. 1 for a) pseudorange data and b) carrier phase data. The pseudorange RMS agreement is 2.38 nanoseconds. The carrier phase RMS agreement is 55 picoseconds.

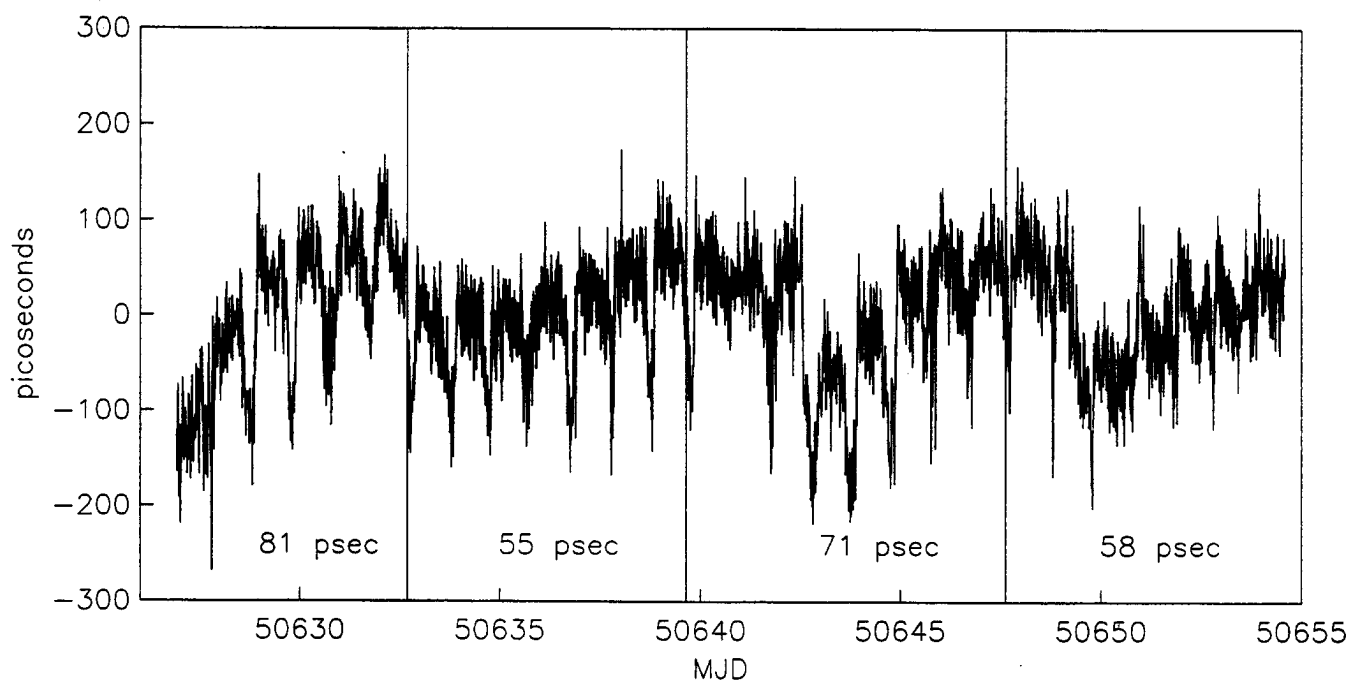


Fig. 3: The residuals between GPS estimates of the Clock 16-21 difference and the measured difference from Fig. 1 for 28-day period. Each vertical line represents independent analysis of data from the two GPS receivers. The RMS agreement for each data segment is shown below the data.

Questions and Answers

MARC WEISS (NIST): How do you know that those are diurnal effects or multi-path? Could they perhaps be ionosphere?

KRISTINE LARSON (UNIVERSITY OF COLORADO): No, they are not ionosphere. I am using a dual frequency correction for the ionosphere. These are geodetic quality, dual frequency geodetic receivers, and the ionospheric errors respectively reduce to a random error by doing that.

MARC WEISS: Do the satellites have biases that differ from one satellite to the other in the L1 - L2?

KRISTINE LARSON: Not the ionosphere. It is definitely not the ionosphere. There conceivably could be atmospheric effects, but it is not the ionosphere. You can check that by doing elevation cut-off tests and things like that. Multi-path will depend on those elevation cut-offs or how low you look in the sky; and so it is multi-path, but I did not demonstrate it here. I just said it was.

GERARD PETIT (BIPM): What about variations in the antenna delay and so on? You do not seem to experience such delays even in the long baseline experiments. In the short baseline, it is conceivable because the two sets of equipment are similar, should have similar variations. But the long baseline is also very –

KRISTINE LARSON: Delays in the antenna, temperature delays and things like that?

GERARD PETIT: Yes.

KRISTINE LARSON: Yes, I think that would be interesting to look at over a longer period of time. This was just a three-week experiment, and that is the next thing to look at. This looks very promising, and to do a proper comparison you have to look over a long enough period to see all the potential problems. I think that is a good thing to look at.

JOHN LUCK (ORRORAL GEODETIC OBSERVATORY): I understand that Ashtech are developing a system whereby the time is inserted from your local clock into the receiver. Would that get rid of the jumps that you were noticing?

KRISTINE LARSON: Right - Yes!

JOHN LUCK (ORRORAL GEODETIC OBSERVATORY): Do you know the status of the Ashtech development?

KRISTINE LARSON: I have heard that about Ashtech as well. In fact, I have heard they did it for the University of Bern. I think the TurboRogue folks could do it, too, if they wanted to; and in the meantime, I talked to the people at JPL, as most of you know, they helped develop the TurboRogue. They gave me a way to calibrate it without any change, but it would be easier if the manufacturer would just do it.

CLAUDINE THOMAS (BIPM): I can say that three of these new Ashtech's at 12-T, adapted to time, are now in operation; one at NPL in the UK, one at LPTF at the Paris Observatory, which is just beginning its work; and one at BIPM which arrived last Monday, and of course we do not have any data yet. But it will be in operation.

KRISTINE LARSON: These do not reset? Okay - Good!

GLONASS/GPS TIME TRANSFER AND THE PROBLEM OF THE DETERMINATION OF RECEIVER DELAYS

Gerrit de Jong
NMI van Swinden Laboratorium
P.O.Box 654
2600 AR, Delft
Netherlands

Włodzimierz Lewandowski
BIPM
Pavillon de Breteuil
F-92312 Sèvres Cedex
France

Abstract

GPS and recently also Glonass receivers are widely used for navigation. When these receivers are used for time and frequency transfer, then all the internal delays and their associated stability become very important. For accurate navigation they are in 'common mode' and only need to be constant during an integration period of less than about one minute. This nanosecond level problem is sometimes not understood by manufacturers and users of those GPS and Glonass timing receivers that were converted from navigation receivers. In the paper this problem is addressed and also the specific Glonass problem caused by the Frequency Division Multiplexing (FDM) used instead of Code Division Multiplexing (CDM) used in GPS. Some delay measurement results are presented. The calibration and characterization of these delays is important for the international atomic time scale.

INTRODUCTION

Since the introduction of the Global Positioning System (GPS), many manufacturers have developed and produced receivers for navigation or geodetic positioning. Those receivers consist of an antenna unit, a receiver with a correlator to lock to the coded bi-phase modulated satellite signals, a time reference (usually an internal quartz or rubidium clock), and a time interval counter (TIC) to measure the arrival time of the received signal from each satellite s with respect to the time reference (Fig. 1).

For each satellite s , the TIC reading $TI(s)$ is:

- the time offset of the satellite clock (1),
- + the propagation time (2) from satellite s to the antenna (including ionosphere delay, Sagnac effect and troposphere excess delays),
- + the signal delay in the antenna unit (3) (including delays in its filters and amplifiers),
- + the signal delay in the cable (4) from antenna unit to the receiver input,
- + the signal delay in the receiver (5) (filters, amplifiers, down converters),

- the time offset (6) of the reference clock (including the reference cable delay in case of the use of an external reference clock)

For each satellite the above delays 3, 4, 5 and 6 are equal, but delays 1 and 2 are different. The clock offset of each satellite clock is transmitted, so can be accounted for.

Navigation and positioning use the **propagation delay differences (2)** for their calculations, so the delays 3, 4, 5, 6 in Antenna, Cable, Receiver, Reference and Clock offset are **common** and should only not change within the (short) sequence time to measure 4 or more satellites. The propagation delays (2) are transformed into distances using the speed-of-light constant, these distances are the pseudo-ranges. From pseudo-ranges to 4 different satellites the position of the antenna is calculated.

Time Transfer uses known fixed antenna coordinates and calculates the local or internal **reference clock offset** from the **TI(s)**. Then the delays in Antenna(3), Cable (4), Receiver (5), reference cable (6) have to be known in absolute value: they should have been measured and, thus, been **calibrated**. Unknown changes due to changes in temperature, etc. in any of these delays become attributed to the calculated reference clock offset and are limiting the accuracy and precision of the time and frequency transfer.

The **necessity of knowing continuously** the values of hardware delays 3, 4, and 5 as well as the cable delay from delay 6 is often neglected when GPS and Glonass receivers developed firstly for positioning, are being transformed into timing receivers by changing only its software! This extra necessity is also the reason why geodesists have a problem to understand that, while they obtain centimeter position accuracy (equivalent to 30 ps time uncertainty), timing experts obtain for long-term (half day or longer) only about 3 ns time accuracy, which translates into meter position accuracy! This paper will further point to some sources of the (slow changing) delays (3), (4) and (5).

SOURCES OF SIGNAL OR GROUP DELAYS

The listing below shows a number of sources of signal delays.

Coaxial cables: typical 5 ns per meter for $Z = 50$ Ohm (with solid polyethylene insulator).
Amplifiers with transistors, resistors and (parasitic) capacitances, depending on bandwidth and frequency: wider bandwidth results in lower delay.

HF tuned L-C circuits, high, low and band pass filters, depending on bandwidth and frequency: wider bandwidth and higher frequency gives lower delay.

Surface Acoustic Wave (SAW) filters using ceramic or glass resonators: depending on excitation mode, propagation velocity in the material, bandwidth.

Optical fiber cables: see SAW filters.

FACTORS OF SIGNAL DELAY CHANGES

When these delays are known once, they may change due to sensitivity to some factors as given in the list below:

Temperature
Humidity

- Air Pressure
- Mechanical strain
- Aging
- Reflections in cables/fibers due to mismatch
- Supply Voltage
- Signal Power level in amplifiers, specially near the compression point

So all such factors should be examined to determine if they may result in significant changes of the delays for GPS, Glonass and Two-Way Satellite Time and Frequency Transfer [11, 12] equipment.

DELAYS IN GPS TIME TRANSFER RECEIVERS

In Fig. 2 and 3 the signal delay calibration curves of two different pre-correlation filters are shown for the GPS L1 frequency (1575.42 MHz). It is clearly seen that wide-band filters exhibit less delay than narrow-band filters. Also, when both filters would have the same percentage of temperature dependancy, the wide filter is more stable with temperature. Of course, the overall temperature coefficient depends on the temperature sensitivity of the used components [1, 3, 6, 7, 8, 9, 10, 11, 12]. For the P-code a ten times wider bandfilter is required compared to the C/A code. That is one reason why (geodetic) P-code receivers (mostly also dual-frequency) receivers generally could have smaller temperature sensitivities compared to C/A (mostly single-frequency) receivers.

Fig. 4 shows an example of a good characterization of a commercial filter, a linear group delay factor is given, as well as a parabolic and a ripple value.

DIFFERENTIAL DELAY IN DUAL-FREQUENCY L1 & L2 RECEIVERS

The excess delay due to the ionosphere cannot simply be determined. In receivers for the GPS L1 frequency (1575.42 MHz) using the C/A code, a model for the ionosphere and a parameter from the navigation message is used to calculate it. Fortunately, the ionosphere delay is frequency-dependant. So from pseudo-range measurements using the same signal from the same satellite (Fig. 5) but at a different frequency, the momentary ionosphere delay can be determined more accurately. The second frequency, L2, is 1227.6 MHz, and the delay in the receiver for this signal may differ from the L1 delay (see Fig. 9); this differential delay has to be calibrated in advance and should be subtracted from the measured L1-L2 pseudo-range difference to obtain the true ionosphere delay difference. Then the absolute ionospheric delay correction at L1 is calculated and used in the positioning and time transfer calculations.

SIGNAL DELAYS IN GLONASS (=MULTI-FREQUENCY) RECEIVERS

In the GPS all satellites transmit at the same nominal frequency for L1 and L2. The satellite signals are distinguishable because of the difference in their unique codes used for the bi-phase modulation. In the Glonass, the codes on all satellites are equal, but the transmit carrier

frequencies are different for each satellite; at L1: $(1602 + k \cdot 0.5625)$ MHz and at L2: $(1246 + k \cdot 0.4375)$ MHz, (where $k=0$ to 24), a difference of about 0.5 MHz between satellites. The L1 frequency range spans 13.5 MHz and L2 needs 10.5 MHz for the 24 satellites. The delay in antenna unit and receiver over these bands should be identical or its frequency dependency should be calibrated and corrected for (see an example in Fig. 9). This is necessary both for positioning and for time transfer, but is not easy to do at the 1 ns level or better.

A L1 & L2 Glonass receiver, thus, needs 24 L1 and 24 L2 differential calibration values, apart from one L1-L2 differential delay calibration for accurate positioning, and for time transfer at least one additional absolute calibration is needed. Due to the planned re-use of Glonass frequencies, now not all 24 calibrations are needed; in the future 12 will be enough. For Glonass receivers, delay stability with temperature is also a great necessity [2,3,4,5].

SIGNAL DELAYS IN MULTI-CHANNEL GPS AND GLONASS RECEIVERS

In single-channel receivers all measurements are using the same receiver channel. In multi-channel receivers (Fig. 7) there is a chance of differential delays between channels. These delays should be calibrated and corrected for in the software; or at least these differences should be smaller than a specified level, such as 1 ns.

SIGNAL DELAYS IN DIGITAL SIGNAL PROCESSORS (DSP'S)

Presently new GPS and Glonass receivers are using digital signal processors for the digitization, correlation, time interval and code-generation functions. The pseudo-ranges are determined using these very fast processors with the appropriate software. The processing in these DSP's take some time, which leads to an apparent receiver delay time, which is equivalent to the delay in filters and in digital circuitry. This delay will normally be identical for all tracked satellites and so will not normally be a problem with positioning applications, but are a big problem for time transfer. This delay has been reported to amount up to 2000 ns! This delay should be calibrated for time transfer applications. A better solution would be to minimize this DSP delay or even avoid it by optimizing the design of the hard and software of the DSP for time transfer.

CARRIER PHASE AND RECEIVER DELAYS

The use of carrier phase smoothed data for time transfer improves the short-term stability due to averaging more cycles in the same averaging time and less multipath, but the timing of the code sequence is still needed for initially identifying a carrier cycle. For the long term (a half day or longer), the phase of the carrier is also affected by the same filter and cable delay changes due to temperature, humidity, etc. as the coded bi-phase modulated carriers and these receivers need the same precautions to improve its long-term delay stability necessary for time transfer [8,9].

Table 1. Required Delay Calibrations

Receiver configuration	No. of bands	No. of frequencies per band	Total no. of frequencies	Navigation: no. of Calibrations	Time Transfer: no. of Calibrations
GPS C/A, single freq.	1	1	1	0	1 Absolute
GPS dual freq., P-code	2	1	2	1 Relative	2 Absolute = 1 Abs. + 1 Rel.
Glomass C/A, single band	1	24	24	24 Relative	24 Absolute = 1 Abs. + 23 Rel.
Glomass dual band, P-code	2	24	48	49 Relative	49 Absolute = 1 Abs. + 48 Rel.
Dual system GPS C/A & GLO C/A, Glomass dual band, P-code	3	1/24/24	49	50 Relative	50 Absolute = 1 Abs. + 49 Relative

RECOMMENDATION

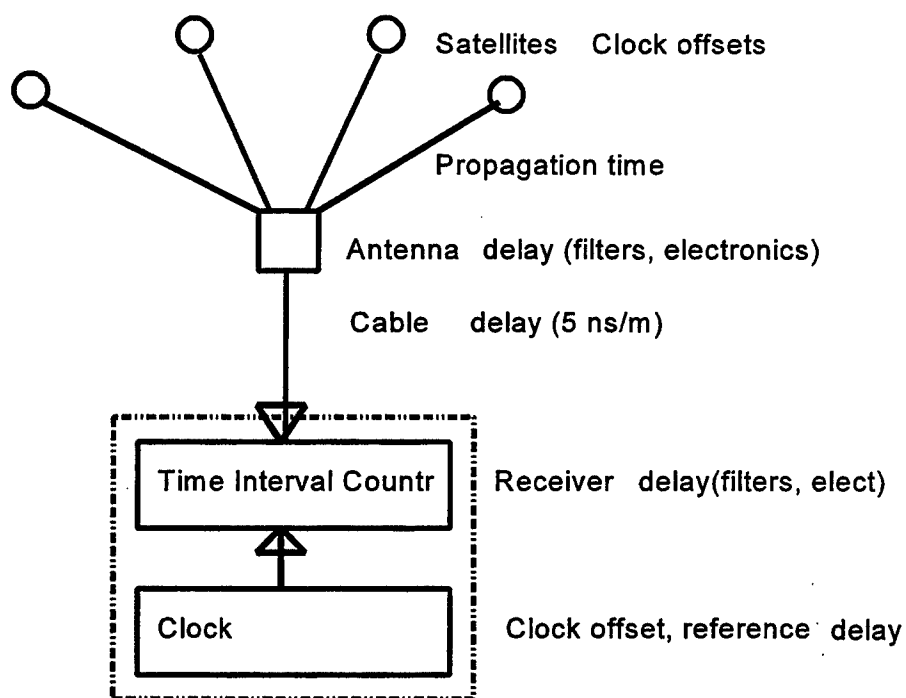
It is recommended that manufacturers of GPS and/or Glonass receivers for time transfer provide the values of the relative and absolute delays in each antenna and receiver unit on a calibration report or in a calibration data file; also that the receiver is prepared to use such a calibration file to correct the calculated time transfer data output.

Further research should be done to improve the long-term stability (specially temperature sensitivity) of GPS and Glonass receiver circuitry.

REFERENCES

- [1] G.de Jong 1985, "Measuring the propagation time of coaxial cables used with GPS receivers", Proceedings 17th Precise Time and Time Interval (PTTI) Applications and Planning Meeting, 3 - 5 December, Washington, D.C., USA, pp.223 - 232.
- [2] W. Lewandowski, P. Moussay, J. Danaher, R. Gerlach, E. Vasseur, 1997, "Temperature-protected antennas for Satellite Time Transfer Receivers", Proceedings 11th European Frequency and Time Forum (EFTF), 4 - 7 March 1997, Neuchâtel, Switzerland, pp. 498-503.

- [3] W. Lewandowski, J. Azoubib, M. Weiss, V. Zhang, V. Hanns, A.G. Gevorkyan, P.P. Bogdanov, N. Tutolmin, J. Danaher, G. de Jong, J. Hahn, M. Miranian 1997, "*Glonass Time transfer and its comparison with GPS*", Proceedings 11th European Frequency and Time Forum (EFTF), 4 - 7 March 1997, Neuchâtel, Switzerland, pp. 187-193.
- [4] W. Lewandowski, J. Azoubib, A.G. Gevorkyan, P.P. Bogdanov, J. Danaher, G. de Jong, J. Hahn, 1996, "*First results from Glonass common-view time comparisons realized according to the BIPM international schedule*", Proceedings 28th Precise Time and Time Interval (PTTI) Applications and Planning Meeting, 3 - 5 December, Reston, Virginia, USA, pp. 357 - 365.
- [5] [3] W. Lewandowski, J. Azoubib, M. Weiss, A.G. Gevorkyan, P.P. Bogdanov, W.J. Klepczynski, M. Miranian, J. Danaher, N.B. Koshelyaevsky, D.W. Allan 1996, "*A contribution to the standardization of GPS and Glonass time transfers*", Proceedings 28th Precise Time and Time Interval (PTTI) Applications and Planning Meeting, 3 - 5 December, Reston, Virginia, USA, pp. 367 - 386.
- [6] W. Lewandowski, P. Moussay, P. Guerin, F. Meyer, M. Vincent 1997, "*Testing Motorola Oncore GPS receiver and temperature-stabilized antennas for time metrology*", Proceedings 28th Precise Time and Time Interval (PTTI) Applications and Planning Meeting, 3 - 5 December, Reston, Virginia, USA, pp. 387 - 396.
- [7] W. Lewandowski, P. Tourde 1990, "*Sensitivity to the external temperature of some GPS time receivers*", Proceedings 22th Precise Time and Time Interval (PTTI) Applications and Planning Meeting, 4 - 6 December, Vienna, Virginia, USA, pp. 307 - 316.
- [8] P. Baeriswyl, T. Schildknecht, J. Utzinger, G. Beutler 1995, "*Frequency and time transfer with geodetic GPS receivers: first results*", Proceedings 9th European Frequency and Time Forum (EFTF), - March 1995, pp. 46-51.
- [9] F. Overney, L. Prost, U. Feller, T. Schildknecht, G. Beutler 1997, "*GPS time transfer using geodesic receivers: middle-term stability and temperature dependency of the signal delay*", Proceedings 11th European Frequency and Time Forum (EFTF), 4 - 7 March 1997, Neuchâtel, Switzerland, pp. 504-508.
- [10] R.J. Douglas, J. Popular 1994, "*PTTI applications at the limits of GPS*", Proceedings 26th Precise Time and Time Interval (PTTI) Applications and Planning Meeting, 6 - 8 December, Reston, Virginia, USA, pp. 141 - 151.
- [11] J.A. Davis, P.R. Pearce 1993, "*Characterization of the signal delays in a ground station designed for Two-Way Time Transfer*", Proceedings 7th European Frequency and Time Forum (EFTF), 16 - 18 March 1993, pp. 113-118.
- [12] G. de Jong 1997, "*Delay stability of the TWSTFT earth station at VSL*", Proceedings 29th Precise Time and Time Interval (PTTI) Applications and Planning Meeting, 2 - 4 December, Long Beach, California, USA. (this issue).



TIC reading = Sat. Offset + Prop.time + Ant delay + Cable dly + Rcvr dly - Ref. dly - Clk

Figure 1. GPS receiver principle with delays

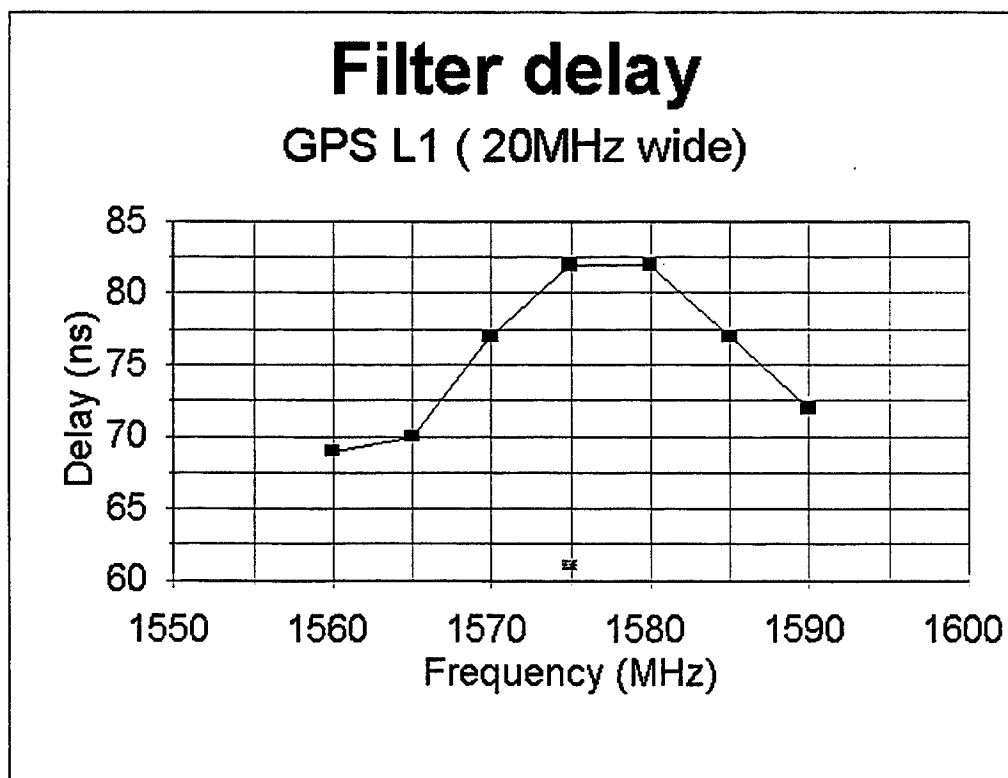


Figure 2. Delay versus frequency

Filter delay

GPS L1 (3MHz)

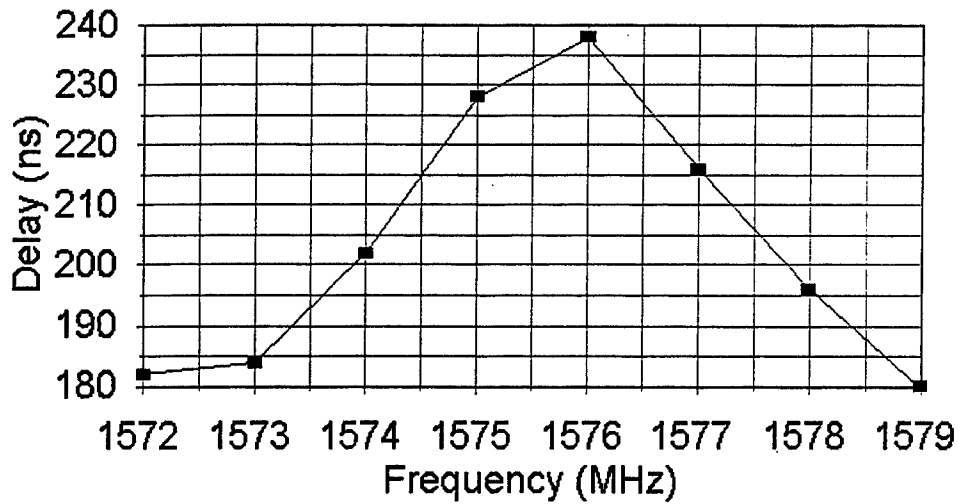
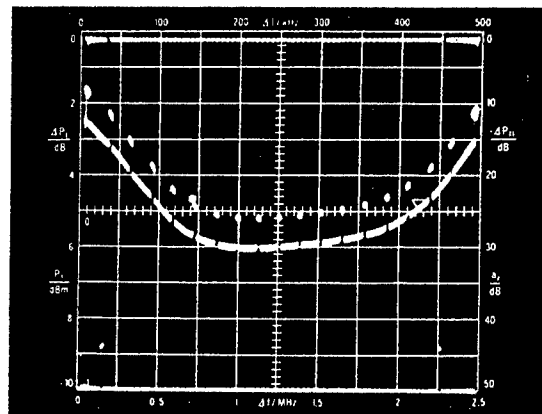


Figure 3. Delay versus frequency

Measured Group Delay Response, Low Band: 14.020 GHz

1 nsec/div
2 MHz markers



Measured Group Delay:

Linear: .01 ns/MHz

Parabolic: .01 ns/MHz²

Ripple: 6.3 ns peak-to-peak

Figure 4. Filter delay versus frequency (Y-axis top-down)

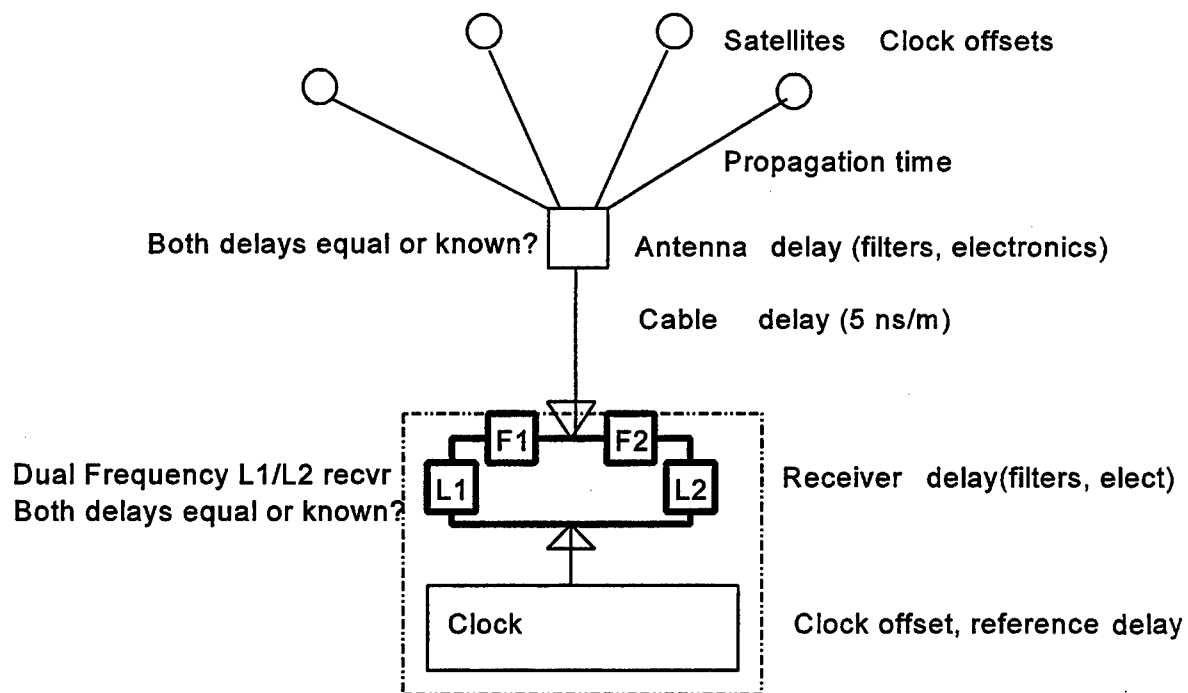


Figure 5, Dual-frequency receiver

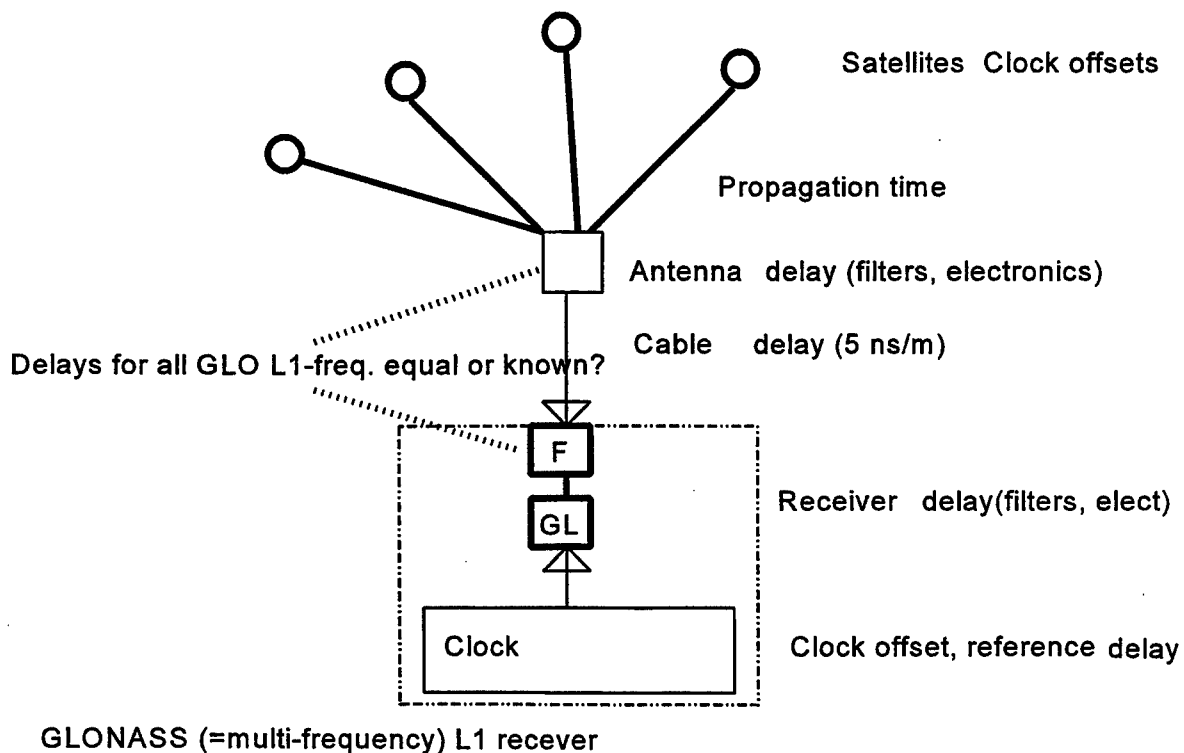


Figure 6. Glonass receiver

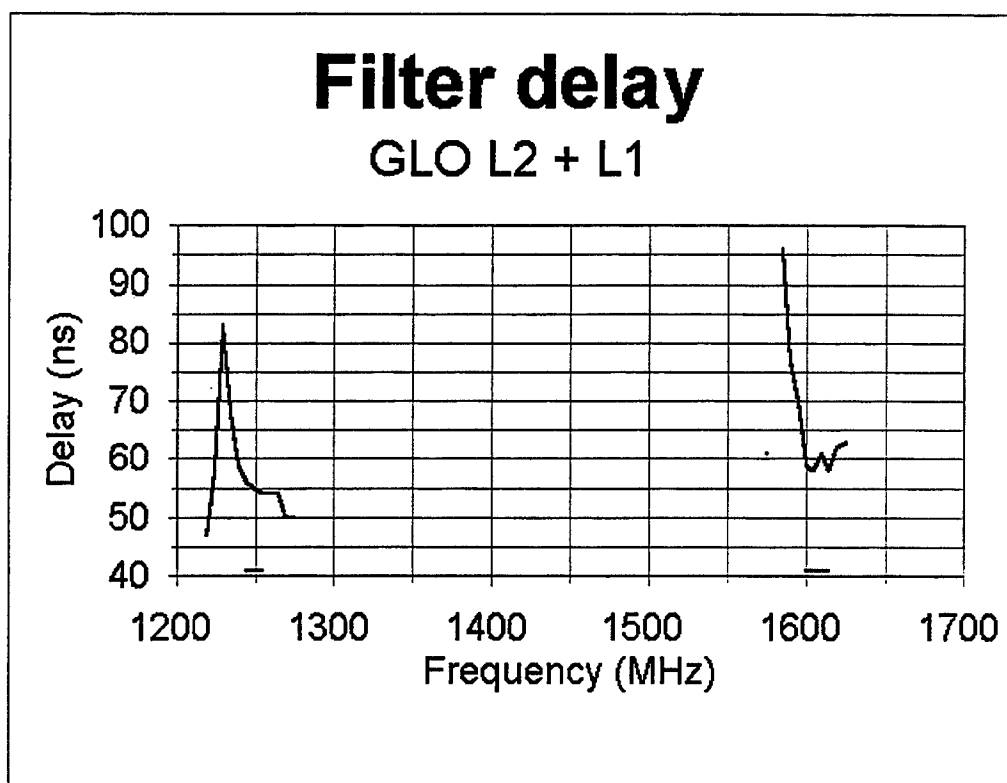


Figure 9. L2 & L1 filter delays

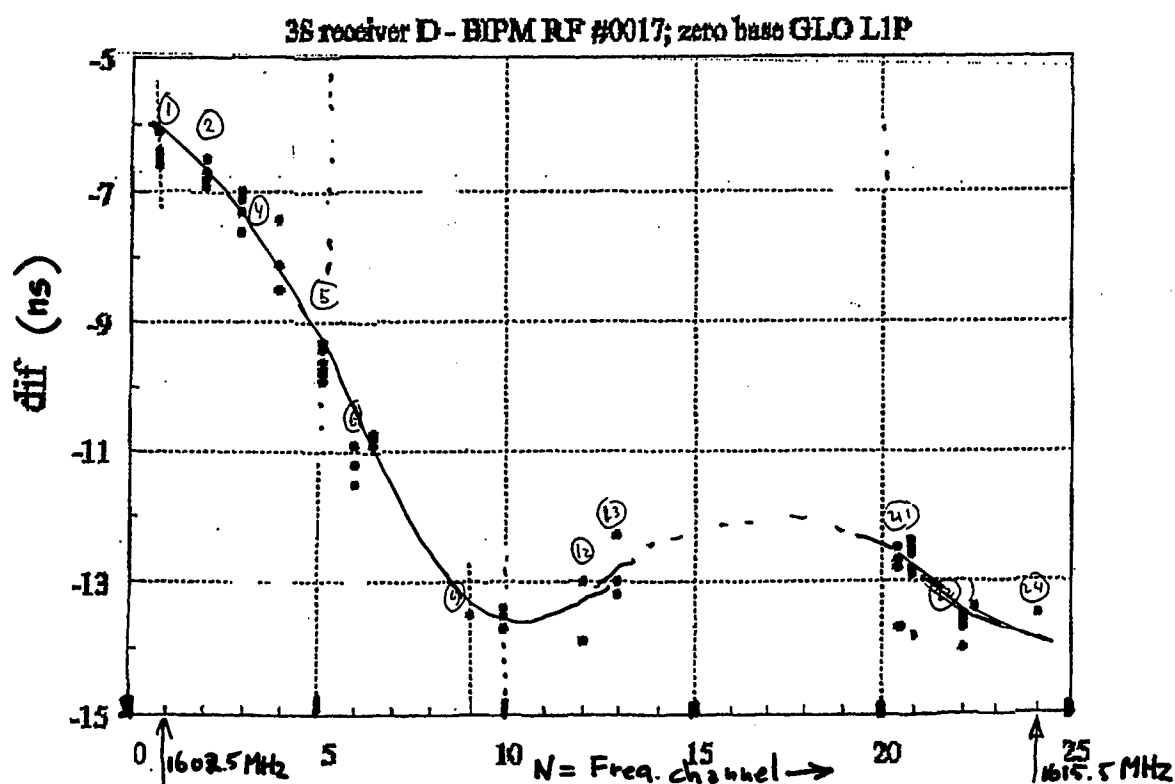


Figure 10. Delay difference of two Glonass receivers versus freq. channels 239/240

DELAY STABILITY OF THE TWSTFT EARTH STATION AT VSL

Gerrit de Jong
NMI Van Swinden Laboratorium
P.O. Box 654
2600 AR, Delft
Netherlands

Abstract

Frequency and time transfer methods rely on the stability of the propagation time of the signals through the systems involved. For TWSTFT the stability of the delays encountered in the earth station by the transmission of the local 1 PPS signal as well as that of the received remote 1 PPS signal, determines the uncertainty at sub-nanosecond level for such transfers. The characteristics of the TWSTFT earth station at NMI Van Swinden Laboratorium (VSL) based on data accumulated with its automated delay measurements system during about one year are presented and discussed in more detail. Delay stabilities TDEV of 100 ps for $\tau = 1$ h to 50 d are obtained, and frequency stabilities ADEV of 2.2×10^{-15} for $\tau = 1$ d.

INTRODUCTION

For the measurement of the difference of the delay in the transmit part (TX) and the delay in the receive part (RX) of the TWSTFT earth station at VSL, an automatic calibration system [3] has been developed, based on the use of a specially-at-VSL-developed satellite simulator SATSIM method [1,2]. The knowledge of this TX - RX delay is necessary if clocks at two remote sites are to be compared using the TWSTFT method; if both stations are equipped with such a system no additional visits [4] of other calibration equipment is necessary for absolute time comparisons. This paper shows what long-term performance can be expected from this TX-RX calibration. This method uses a calibrated reference cable, and this essential cable is also calibrated automatically in the automatic system. The main parts of the system used for the calibration are part of the TWSTFT equipment; only coaxial transfer switches are added, 70 MHz and 1425 MHz sine wave sources and the SATSIM, as shown in Fig.1a.

The cables and their delays are defined as follows (Fig. 1a+b):

- A is the cable from the Mitrex modem 70 MHz TX output to the up-converter Fup;
- B is the cable from the down-converter Fdn to the 70 MHz RX input of the Mitrex modem;
- C is the cable from the 70 MHz CW generator to the output of the amplifier;
- HL is the cable from amplifier output to the Sat. Simulator input;
- HL' is a cable equal to cable HL, and runs from the difference frequency generator DF to the other input of the Sat. Simulator; cable L is the sum of HL and HL';
- CL is the Reference cable being calibrated each time; it is the sum of C and HL;

RX is the Receive delay: the sum of the delay from the Sat. Simulator to the Feed, the delay from Feed to the output of the down-converter Fdn and cable B;

TX is the Transmit delay: the sum of the delay of cable A, from the input of the up-converter Fup to the Feed, from the Feed to the Sat. Simulator;

TX-RX is the value of interest for TWSTFT.

STABILITY OF THE REFERENCE CABLE DELAY CALIBRATION

Firstly, the delay of the reference cable CL is determined. Using a three-corner-hat method, the delay of C is determined from half of the sums of the delays of cables C+B and C+A minus the sum of cables A and B.

The stabilities of these three sums do not differ much; the structure of the variations (Fig. 2a and Fig. 3a) that can be seen, are originating in the MITREX modem itself, not in the cables. Also, a small slope during the year can be seen. Fig. 2a and 2b show the stability of A+B and 3a and 3b that of cable C+B. TDEV varies from 24 ps for $\tau = 1$ h to maximum 150 ps for $\tau = 1$ week. At MJD 50612 the original cable C has been replaced by a new cable with 70 ns less delay. The data taken after the replacement, which included the delay of cable C, have been corrected for this.

The delay of HL is determined by measuring C+B+L (Fig. 4a + b) and subtracting C+B and dividing the result by two. HL alone is determined with a very good long-term stability as shown in Fig. 5a and 5b, a TDEV of 10 ps at $\tau = 1$ h to 23 ps for $\tau = 50$ days! At MJD 50612 a residual step of 100 ps due to the replacement for cable C is visible and causes the rise of TDEV at τ of 20 d and 50 d.

Now the wanted delay of the reference cable CL is the sum of C and HL and its stability is shown to be 20 ps at $\tau = 1$ h to a maximum of 72 ps at $\tau = 1$ week in Fig. 6a and 6b.

STABILITY OF THE TOTAL TRANSMIT AND RECEIVE DELAY INCLUDING UP- AND DOWN CONVERTERS, HPA AND LNA

The next measurement is the sum of cables CL + RX which include the RF path from SATSIM to the receiver antenna and the down-converter and cable B. The total RX delay is calculated from CL + RX and subtraction of CL. Stability is shown in Figs. 7a+b, 8a+b; TDEV is constantly about 100 ps.

Then the sum of TX+RX is measured and the delay of TX (including the up-converter and RF path to the SATSIM) is calculated by subtraction of the RX delay determined before. Stability is shown in Figs. 9a+b, 10a+b, again a TDEV of about 100 ps for $\tau = 1$ h to 50 d.

STABILITY OF THE TRANSMIT - RECEIVE DELAY DIFFERENCE

Finally the TX-RX delay is calculated by subtraction of the RX delay from the TX delay; see Fig.11a and 11b for the stability. Now TDEV varies from 250 ps at $\tau = 1$ hr to 110 ps for $\tau = 50$ d. The associated frequency stability is showing mainly flicker phase noise and a modified Allan deviation of 2.2×10^{-15} is obtained at $\tau = 1$ day, 2.5×10^{-16} at 10 d and 4.5×10^{-17} at 50 d.

Fig 12a+b show the outside temperature and its stability. These figures help to see if correlations of delay stability with temperature exists. The 'TEMPDEV' shows a rise after 2 h and reaches a maximum as expected at a diurnal $\tau = 12$ h of 2.2 degrees C and drops to 1.2 at $\tau = 18$ h and 24 h. For TX-RX we also find a drop of TDEV from 150 ps at $\tau = 12$ h to 120 ps at $\tau = 18$ h and 110 ps at $\tau = 24$ h.

CONCLUSION

The TX-RX delay at the VSL earth station is stable to a TDEV of about 100 ps for τ of up to at least 50 days and the system is stable in frequency to 2×10^{-15} for $\tau = 1$ day. But while these delay changes are measured in near real time, they can be subtracted from actual Two-Way data, and enable the clock comparisons to an even much better level than the stability reported here. This could be demonstrated when two good H-masers were compared using TWSTFT stations equipped with such an automated delay measuring system and the TWSTFT data be corrected for the measured delay changes. So far, a best TDEV of 0.22 ns for $\tau = 1$ h to 0.18 ns for $\tau = 1$ d from hourly sessions of 300 s during 32 days using an "Atlantis" modem on a baseline of 2400 km has been reported [10].

The VSL full TX-RX stability results are up to two times better than the results reported by the Technical University Graz (TUG) [5, 7, 11, 12] when taking into account that the half TX-RX delay stability was reported; maybe this difference is because at VSL the up- and down-converter are mounted inside the building, just under the roof, while at TUG they are outside at the antenna.

RECOMMENDATIONS

Unfortunately the improvement of the performance of TWSTFT using delay measurements cannot be demonstrated further with good clocks now: the two laboratories equipped now with automated delay measuring systems (TUG and VSL) have no H-masers available and the labs that do have H-masers do not (yet) have an automated delay measuring system. This dilemma should be solved in the near future!

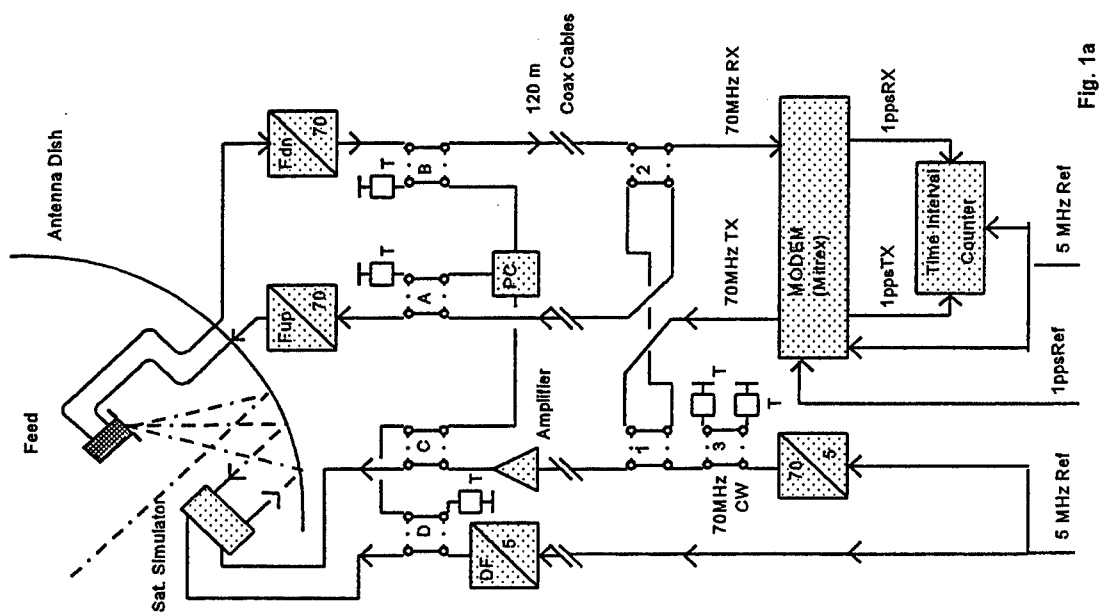
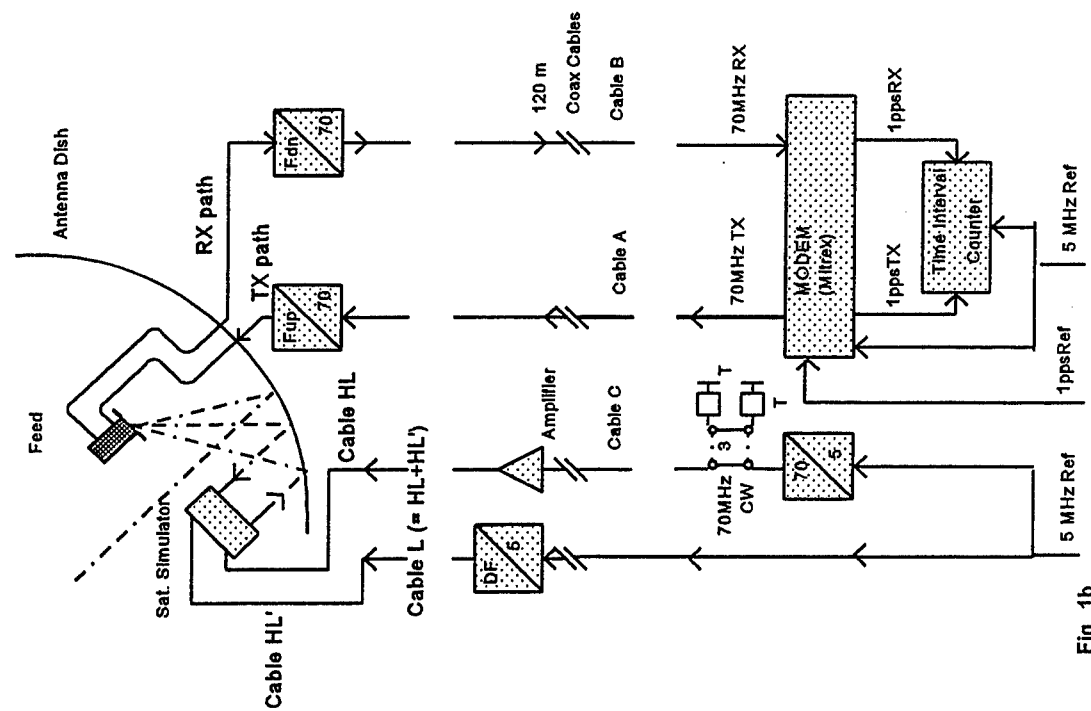
Another finding is that the used MITREX modem is sensitive to environmental factors for τ of 3 h to 10 d even when it was kept in a room at a temperature of 23 degrees centigrade controlled to about 0.3 degrees C and a relative humidity of 45% controlled to about 5 % RH. Also, it was noticed that the non-linearity of delays measured by the MITREX modem when

changing the length of the cable in known increments under circumstances is 100 ps or more. Some mismatch and / or cross-talk in the modem might be the cause of this. So modems still should be improved.

REFERENCES

- [1] G. de Jong 1989, "*Accurate delay calibration of satellite ground stations for Two-Way Time Transfer*", Proceedings of the 3rd European Frequency and Time Forum (EFTF), March 21-23, 1989, Besançon, France, pp. 198-203.
- [2] G. de Jong 1989, "*Accurate delay calibration for Two-Way Time Transfer earth stations*", Proceedings 21st Annual Precise Time and Time Interval (PTTI) Applications and Planning Meeting, November 28-30, 1989, Redondo Beach, CA, USA, pp. 107-116.
- [3] G. de Jong and M.C. Polderman 1994, "*Automated delay measurement system for an earth station for Two-Way Satellite Time and Frequency Transfer*", Proceedings 26th Annual Precise Time and Time Interval (PTTI) Applications and Planning Meeting, December 7-9, 1994, Reston, Virginia, USA, pp. 305-318.
- [4] G. de Jong, D. Kirchner, H. Ressler, P. Hetzel, J.A. Davis, P.R. Pearce, W. Powell, A. Davis McKinley, W. Klepczynski, J.A. DeYoung, C. Hackman, S.R. Jefferts, T.E. Parker 1995, "*Results of the calibration of the delays of earth stations for TWSTFT using the VSL Satellite Simulator method*", Proceedings 27th Annual Precise Time and Time Interval (PTTI) Applications and Planning Meeting, November 29 - December 1, 1995, San Diego, CA, USA, pp. 359 - 372.
- [5] D. Kirchner, H. Ressler, and R. Robnik 1995, "*An automated signal delay monitoring system for a Two-Way Satellite Time Transfer terminal*", Proceedings of the 9th European Frequency and Time Forum (EFTF), March 1995, Besançon, France, pp. 75-79.
- [6] C. Hackman, S.R. Jefferts, and T.E. Parker 1995, "*Common-clock Two-Way Satellite Time Transfer experiments*", Proceedings of the 1995 IEEE International Frequency Control Symposium, 31 May - 2 June 1995, San Francisco, California, USA, pp. 1169 - 1172.
- [7] D. Kirchner, H. Ressler, and R. Robnik 1995, "*Signal stability of a Ku-band Two-Way Satellite Time Transfer terminal*", Proceedings 27th Annual Precise Time and Time Interval (PTTI) Applications and Planning Meeting, November 29 - December 1, 1995, San Diego, CA, USA, pp. 303 - 311.
- [8] J.A. Davis 1996, "*Delay stability measurements made within a Two-Way Time Transfer system using satellite ranging from several locations*", Proceedings of the 10th European Frequency and Time Forum (EFTF), 5 - 7 March 1996, Brighton, UK, pp. 206-211.

- [9] F.G. Ascarrunz, S.R. Jefferts, and T.E. Parker 1996, *"Earth station errors in Two-Way Time transfer"*, Proceedings of the 1996 IEEE International Frequency Control Symposium, 5-7 June 1996, Honolulu, Hawaii, USA, IEEE Catalog No. 96CH35935, pp. 1169 - 1172.
- [10] J.A. DeYoung, F. Vannicola, and A. Davies McKinley 1996, *"A comparison of the highest precision commonly available Time Transfer methods: TWSTT and GPS CV"*, Proceedings 28th Annual Precise Time and Time Interval (PTTI) Applications and Planning Meeting, 3 - 5 December, 1996, Reston, Virginia, USA, pp. 349-355.
- [11] D. Kirchner, H. Ressler, and R. Robnik 1997, *"Recent work in the field of Two-Way Satellite Time Transfer carried out at the TUG"*, Proceedings of the 11th European Frequency and Time Forum (EFTF), 4 - 7 March 1997, Neuchâtel, Switzerland, pp. 205-208.
- [12] H. Ressler, D. Kirchner and R. Robnik 1997, *"Satellite earth stations for Two-Way Time Transfer at the Technical University Graz"*, Proceedings of the 11th European Frequency and Time Forum (EFTF), 4 - 7 March 1997, Neuchâtel, Switzerland, pp. 509-513.



Delay TWSTFT Earth Station

A&B-2347ns

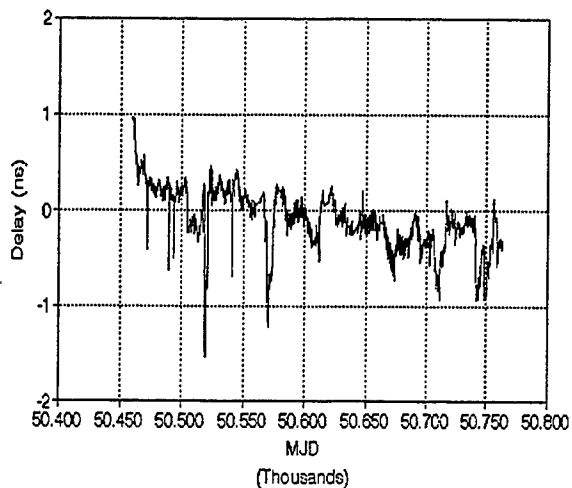


Fig. 2a

Stability of TW Earth Station Delay

A&B

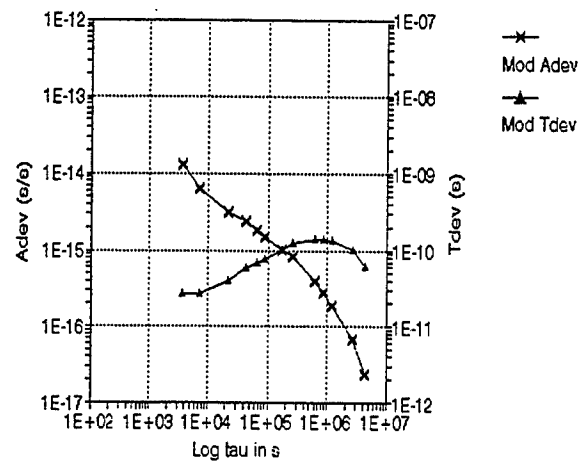


Fig. 2b

Delay TWSTFT Earth Station

C&B-2438 ns

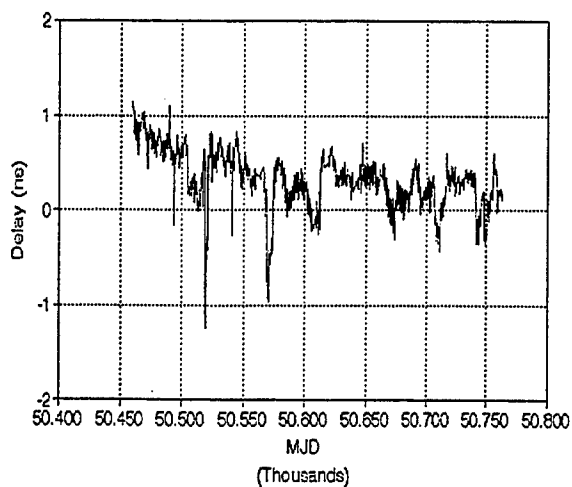


Fig. 3a

Stability of TW Earth Station Delay

C&B

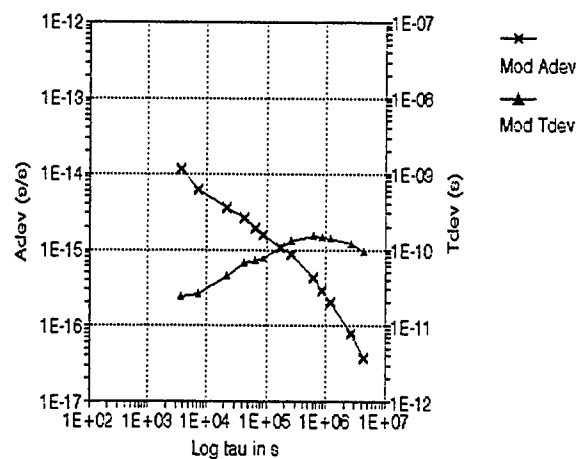


Fig. 3b

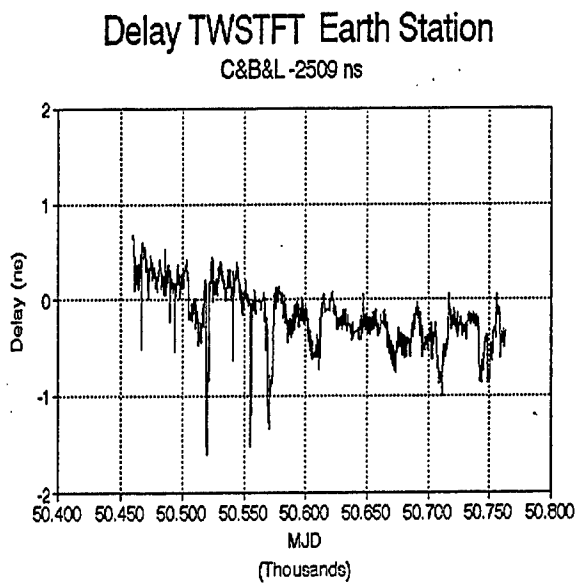


Fig. 4a

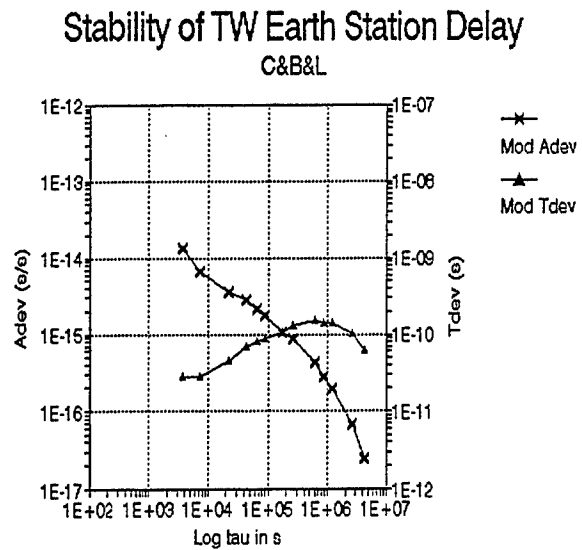


Fig. 4b

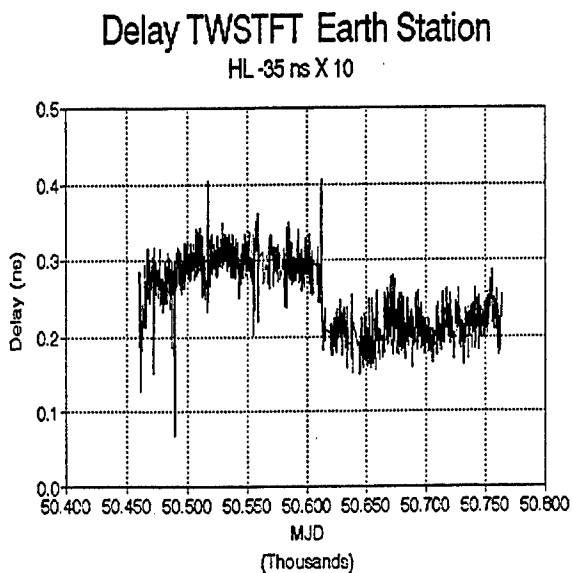


Fig. 5a

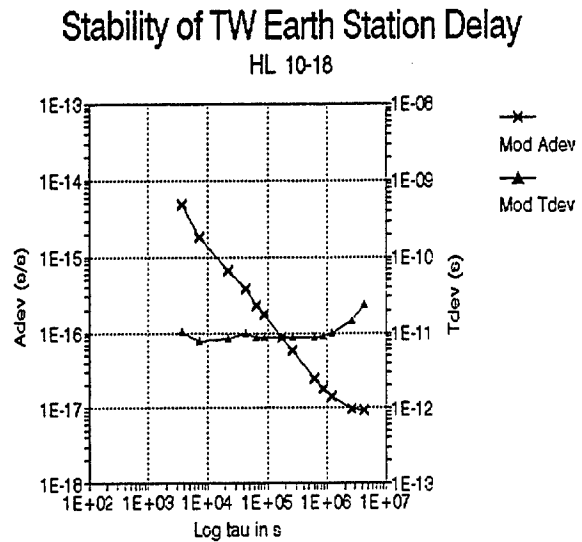


Fig. 5b

Delay TWSTFT Earth Station
CL-1310 ns

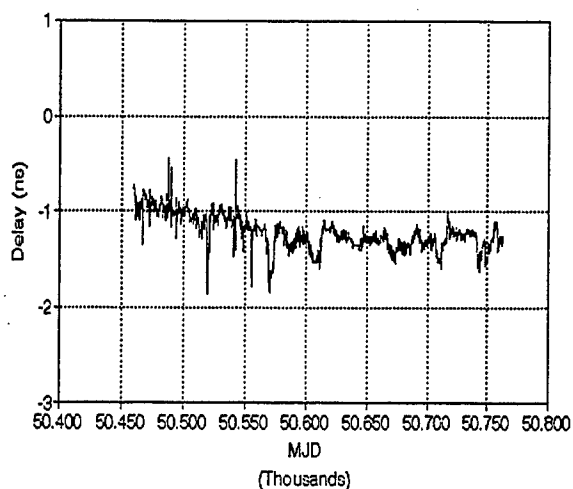


Fig. 6a

Stability of TW Earth Station Delay
CL

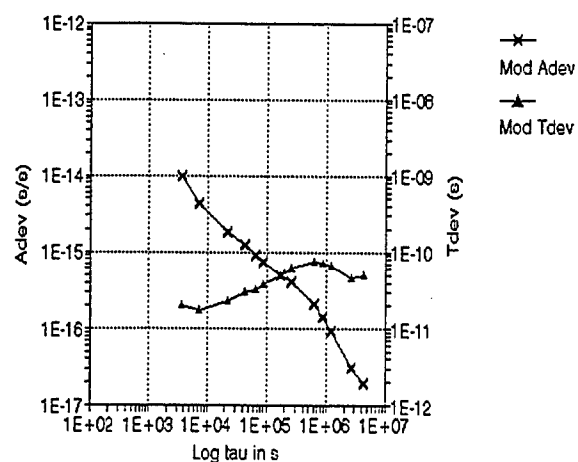


Fig. 6b

Delay TWSTFT Earth Station
CL&RX -2557 ns

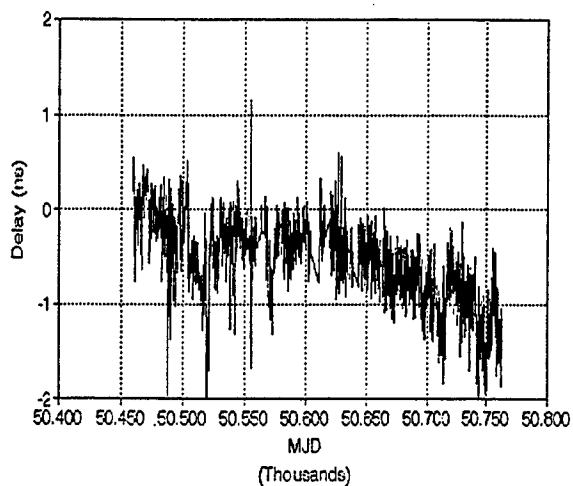


Fig. 7a

Stability of TW Earth Station Delay
CL&RX

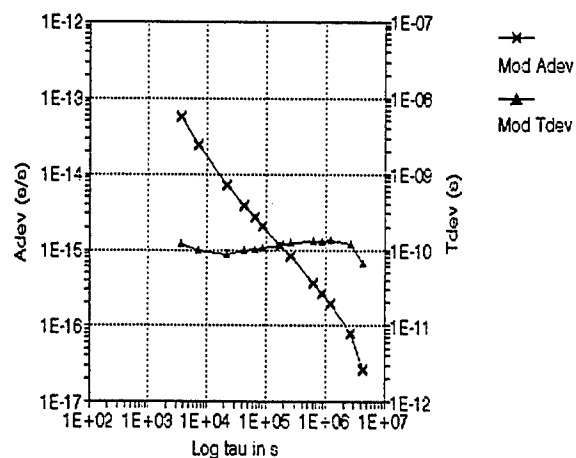


Fig. 7b

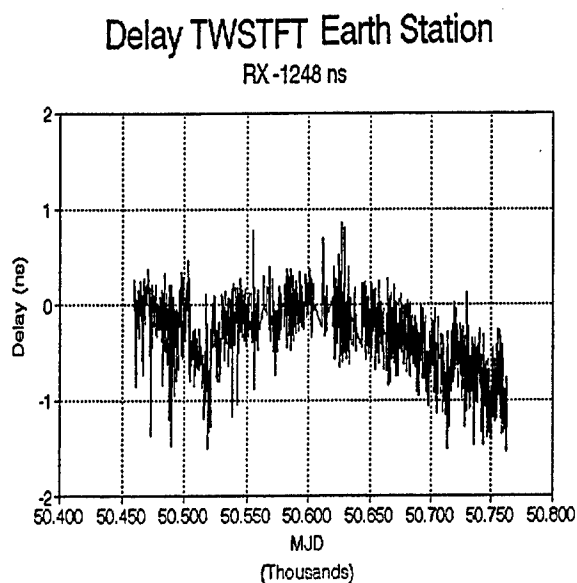


Fig. 8a

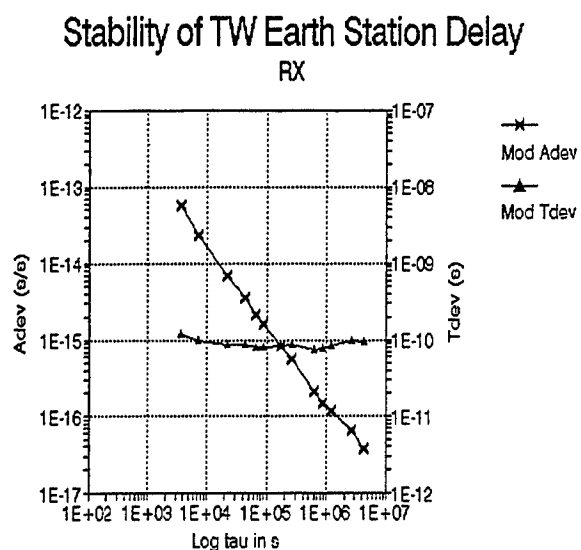


Fig 8b

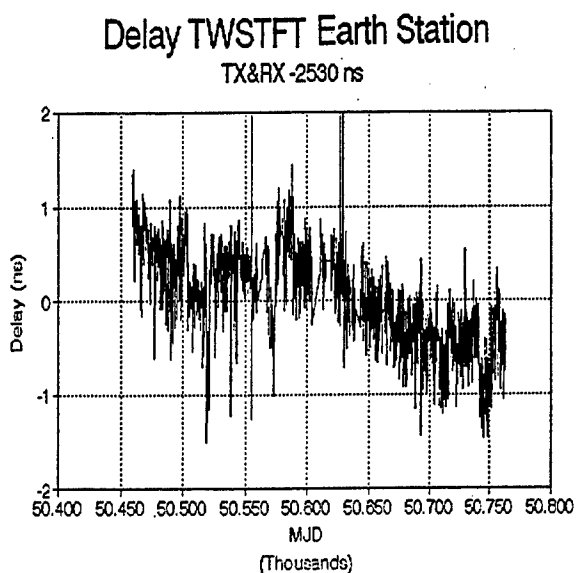


Fig. 9a

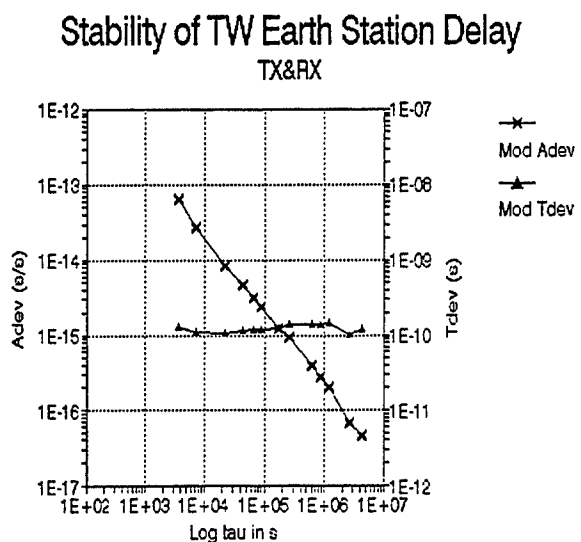


Fig. 9b

Delay TWSTFT Earth Station
TX-1283 ns

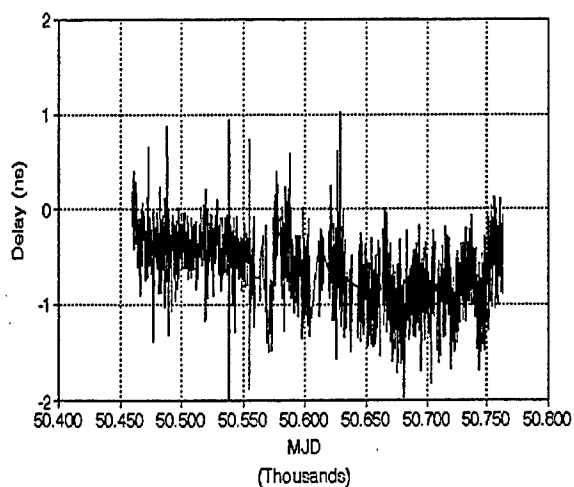


Fig. 10a

Stability of TW Earth Station Delay
TX

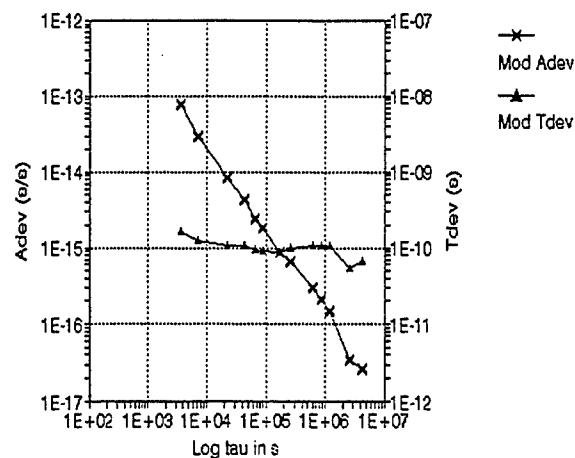


Fig. 10b

Delay TWSTFT Earth Station
TX-RX -35 ns

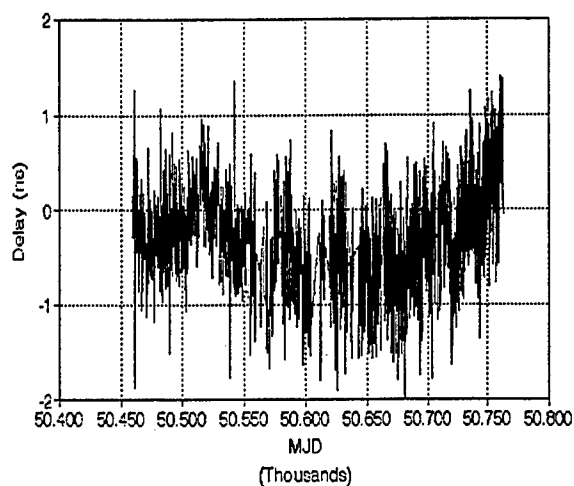


Fig. 11a

Stability of TW Earth Station Delay
TX-RX

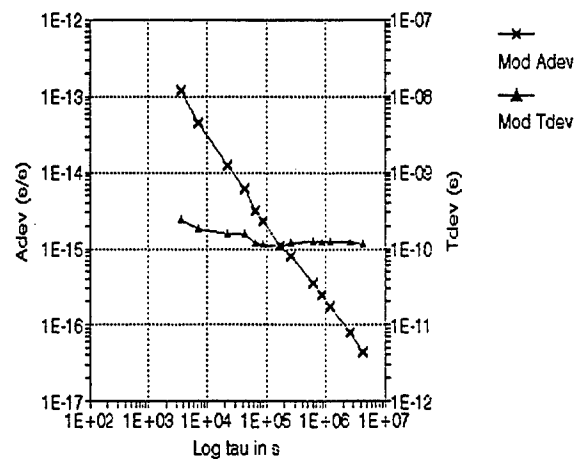


Fig. 11b

Delay TWSTFT Earth Station
Outside Temperature

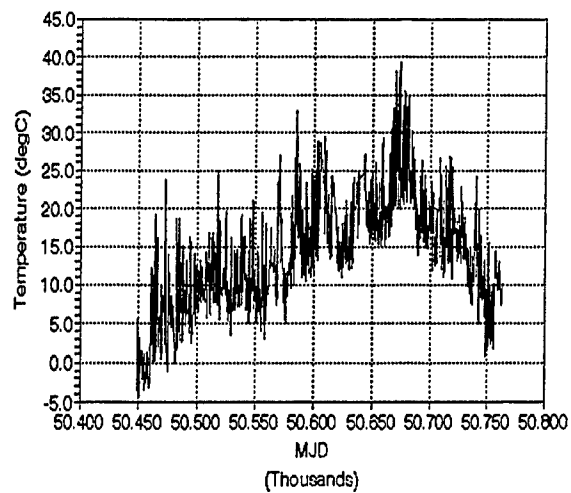


Fig. 12a

Stability of TW Earth Station Delay
Outside Temperature

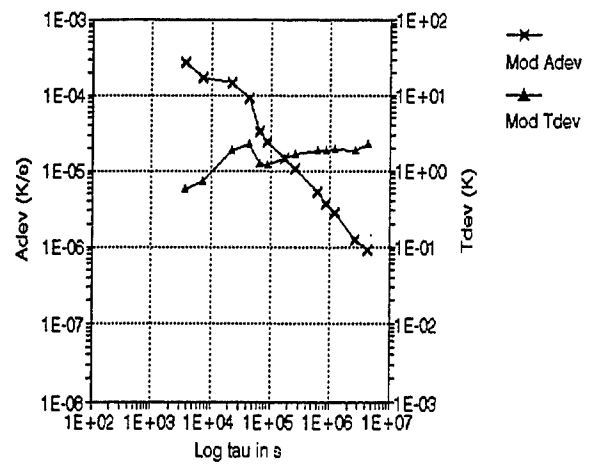


Fig. 12b

C-AND Ku-BAND TWO-WAY SATELLITE TIME TRANSFER COMPARISON EXPERIMENT

R. Beard, I. Galysh, J. Oaks, M. Largay, P. Landis, W. Reid
U.S. Naval Research Laboratory
Washington, DC

M. Ehnert and R. Eisenhauer
Space and Missile Systems Center, Detachment 8
Patrick AFB, FL

W. Hanson, L. Nelson, and A. Clements
National Institute of Standards and Technology
Boulder, CO

J. Durden and L. Brownhill
Comlink Inc.
Rockledge, FL

J. Wright and C. Duffy
Computer Sciences Raytheon
Patrick AFB, FL

J. Kasik
COMSAT
Washington, DC

J. Buisson
Antoine Enterprises Inc.
Alexandria, VA

Abstract

In the development of a new time dissemination capability for the U.S. Air Force Eastern Missile Test Range, the satcom channels to be used became an issue in terms of performance over different links and available coverage. A primary advantage of C band is that satellite coverage is more widely available in remote areas where Ku coverage is limited or not available at all. To investigate the performance issue, a Two-Way Satellite Time Transfer (TWSTT) experiment was performed to obtain comparative data over both C and Ku band. Time transfers between two sites using atomic frequency standard clocks were performed over both links to compare results in a controlled experiment. The objective of the experiment was to determine the relative precision of TWSTT over the frequency bands.

Time transfers were performed between a station located at Rockledge, Florida and the NIST facility at Ft. Collins, Colorado for a period of approximately ten days. GPS receivers were used in common-view mode referenced to the same clocks as an independent comparative measure. Tests were conducted over a wide range of temperature variations and weather conditions. Observations were obtained during snow, heavy rain and sun with temperatures from 8 to 90 degrees Fahrenheit at the two stations. Analysis of the resultant data shows that time transfer over the two links performed equally, with residual RMS results of approximately 5 nanoseconds.

INTRODUCTION

The U. S. Air Force Eastern Missile Test Range has a requirement for precise time synchronization of their remote tracking stations which stretch along the Atlantic Ocean from Cape Canaveral, FL to Ascension Island, UK. The current technology of Two-Way Satellite Time Transfer (TWSTT) can provide the accuracy required for the remote station synchronization. Most TWSTT applications have used Ku-band satellite links because of the lower cost of the earth station equipment. However, the Ku-band satellite coverage is limited to spot beams focused on the major continents and does not provide coverage in the Atlantic Ocean over Ascension Island. The C-band communications satellites have a global beam which covers an area of a hemisphere that includes all of the Eastern Missile Test Range remote sites. The purpose of this experiment was to compare the performance of Ku-band TWSTT to that of C-band and to establish the link equipment requirements for C-band.

TWO-WAY SATELLITE TIME TRANSFER (TWSTT)

TWSTT is a method for determining the precise time difference between two separated timing systems. The method uses Very Small Aperture Terminals (VSATs) and computer-controlled spread-spectrum modems to perform synchronization measurements via a geostationary satcom. The satcom contains a transponder with sufficient bandwidth to accommodate the 4 MHz two-way time transfer signal. Measurements are performed in sessions of five-minute measurement periods and each session takes 30 minutes or less to perform.

A basic TWSTT link is shown in Figure 1. The signal is transmitted between a Master and a Target site through the satcom satellite. The transmission between the two sites occurs simultaneously, which allows canceling of timing signal path delays when the measurements made at each site are differenced. The high accuracy of this technique is dependent upon these reciprocal delays canceling out in the comparison process. Operation as a Master or Target site is under software control, and an individual site may operate in either mode depending upon operator selection.

TWSTT ACCURACY AND ERRORS

The accuracy of the TWSTTs depends on several factors. These include the ionosphere, satellite movement, transponder delays, antenna hardware, cabling, and the quality of the clock source.

The ionosphere can cause delays in the signal path to and from the satellite. Since the uplink and downlink frequencies are separated by 2 GHz, the delays in the uplink and downlink can differ. The differential delays on C-band, which is at 6 GHz and 4 GHz, will vary more than at Ku band, which is at 14 GHz and 12 GHz. As the frequency increases, the effect from the ionosphere decreases. The errors are introduced when the ionosphere varies for each leg of the satcom link, leaving the two-way delay non-reciprocal.

Satellite movement may also affect the time transfer accuracy. If the satellite is not station kept, the path lengths can vary during the transfer operation and cause non-reciprocal errors. Depending on how much the satellite moves, a tracking antenna may also be required.

The properties of the satellite transponder can have a serious effect on the accuracy of the time transfer. The principal source of accuracy with this technique is common or reciprocal error that will cancel in a simultaneous two-way transmission. If the transponder uses the identical equipment in translation and retransmission of the signal, then the signal delays are identical and will cancel in the process. If, however, the equipment in changing frequencies between up and down links should also change antennas in the spacecraft, then the signals may not follow the same path and delays are not identical. Observed delays in some TWSTT applications have experienced large errors due to this effect.

Delays in the earth station antenna hardware may vary since it is exposed to the environment. Temperature variation will have the largest influence. Since the hardware used is sufficiently wide bandwidth, the hardware delay variations are less than two nanoseconds. Cables exposed to the environment, especially in long lengths, can have delay variations of multiple nanoseconds.

SATELLITE COVERAGE

The Ku-band continental spot beam coverage typical of satcoms is shown as the S2 footprint in Figure 2. This coverage is not adequate for the Eastern Missile Test Range application, which extends below the Equator into the South Atlantic Ocean. The C-band satcom coverage is represented by the outer concentric rings which include a hemisphere of the earth and all the remote sites of the test range. In fact, the area of interest in this application is located generally in the center of the C-band global beam coverage.

COMPARISON EXPERIMENT

A time transfer experiment was performed between a facility at COMLINK, Inc., Rockledge, FL and NIST, Fort Collins, CO. Each site had Ku-band and C-band earth station equipment with an NRL-designed TWSTT modem. The same modem was used for both Ku-band and C-band measurements. Each site used an HP 5061 cesium standard as a clock reference source. In addition, STEL 5401C GPS Time Transfer Receivers were used to perform independent common-view time transfer (CVTT) measurements during the experiment. Time transfer measurements were obtained over a period of six days during April, 1997. A comparison was made between the Ku-band and C-band TWSTT data to determine the difference in precision of the two measurement systems. The GPS CVTT data were also compared as an independent check of the time transfer results.

TWSTT RESULTS

The phase offset results from the Ku-band TWSTT are shown in Figure 3. The data show a phase offset of about 7.5 microseconds and a frequency offset of about $4 \text{ pp}10^{13}$. There are 31 sets of observations, and each observation represents five minutes of TWSTT measurements taken in groups of three about every twelve hours. Each five-minute measurement point is the result of averaging 300 one-second time interval measurements. The RMS ranges from 250 to 300 picoseconds. A plot of the residuals to a linear fit of the Ku-band data is shown in Figure 4. The scale is expanded in order to look at any signature in the data. The RMS of the residuals is eight nanoseconds. No particular interest was given to the variations in the data although some may be attributed to the behavior of the cesium reference at the Florida site due to a large temperature rise when the facility lost air conditioning. The objective was to determine how well C-band measurements would compare with those of Ku-band.

The C-band phase offset measurements are shown in Figure 5. There are 94 sets of observations shown here. Three or four sets of C-band measurements were taken before and after each Ku-band measurement session. The data show about the same phase offset and frequency difference as that of the Ku-band measurements. The residuals to a linear fit are shown in Figure 6. The RMS of the residuals is nine nanoseconds, which is comparable to the eight nanosecond RMS of the residuals of the Ku-band measurements.

GPS COMMON-VIEW TIME TRANSFER RESULTS

GPS common-view time transfer measurements were taken during the period of the TWSTT test as an independent comparison. Position of the receiver is a key parameter required for GPS time transfer and exact surveyed positions were not available. The STEL 5401C GPS receivers were used in a self-survey mode for about three days to determine positions of the two sites. The receivers were also operated in the GPS Standard Positioning Service (SPS) mode which results in noisy solutions and data due to the affects of GPS Selective Availability (SA). The GPS CVTT phase offset measurements are shown in Figure 7. The noise due to the effects of GPS SA are apparent in the spread with peak deviations of several hundred nanoseconds. The residuals of a linear fit are shown in Figure 8. The RMS of the residuals is 27 nanoseconds. It should be noted that an attempt was not made to achieve the best performance available from GPS, but rather to obtain an independent measurement for comparison to the TWSTT measurements.

COMPARISON RESULTS

A comparison of all the methods is summarized in Figure 9. The phase offset results of the Ku-band and C-band measurements are plotted on the same graph. The GPS CVTT measurements are also plotted for comparison. The TWSTT measurements track very closely and the GPS CVTT measurements show the same data trends with a bias. Since the interest was primarily in determining the difference in the Ku-band and C-band measurement systems, little attention was given to the absolute calibration of any of the time transfer measurement systems. For implementation in an actual time transfer application, significant

efforts are required to insure that each measurement system is calibrated and maintained in calibration.

CONCLUSIONS

The difference between the Ku-band and C-band results are shown in Figure 10. The RMS of the difference is 0.84 nanoseconds, which demonstrates comparable performance of the C-band TWSTT measurement system to that of Ku-band. The bias of 24 nanoseconds should be removed when both TWSTT measurement systems are calibrated. The C-band measurement system earth station requirements to achieve these results included a 5.5-meter antenna in Rockledge, FL and a 4.6-meter antenna in Ft. Collins, CO. The transmitted power was set at six to seven watts.

The results of this experimental comparison show that C-band TWSTT may be used in this application with comparable performance to Ku-band, and an adequate C-band earth station, would include approximately a five-meter antenna with a ten-watt RF transmitter.

REFERENCES

1. G. P. Landis, J. D. White, R. L. Beard, and J. A. Murray, "A New Two-way Time Transfer Modem," Twenty-first Annual Precise Time and Time Interval (PPTI) Applications and Planning Meeting, November 28 - November 30, 1989, pp. 131-137.
2. I. J. Galysh and G. P. Landis, "A New Two-way Time Transfer Modem," Twenty-second Annual Precise Time and Time Interval (PTTI) Applications and Planning Meeting, December 4 - December 6, 1990, pp. 345-348.
3. G. P. Landis, I. J. Galysh, A. Gifford, A. Osborne, "A New Two-way Time Transfer Modem," Twenty-third Annual Precise Time and Time Interval (PTTI) Applications and Planning Meeting, December 3-December 5, 1991.
4. G. P. Landis and I. J. Galysh, "NRL/USNO Two-way Time Transfer Modem Design and Test Results," Proceedings of the 1992 IEEE Frequency Control Symposium, May 27 - May 29, 1992, pp. 317-326.
5. I. J. Galysh and G. P. Landis, "Two-way Time Transfer Results at NRL and USNO," Twenty-fourth Annual Precise Time and Time Interval (PTTI) Applications and Planning Meeting, December 1 - December 3, 1992, pp. 231-242.

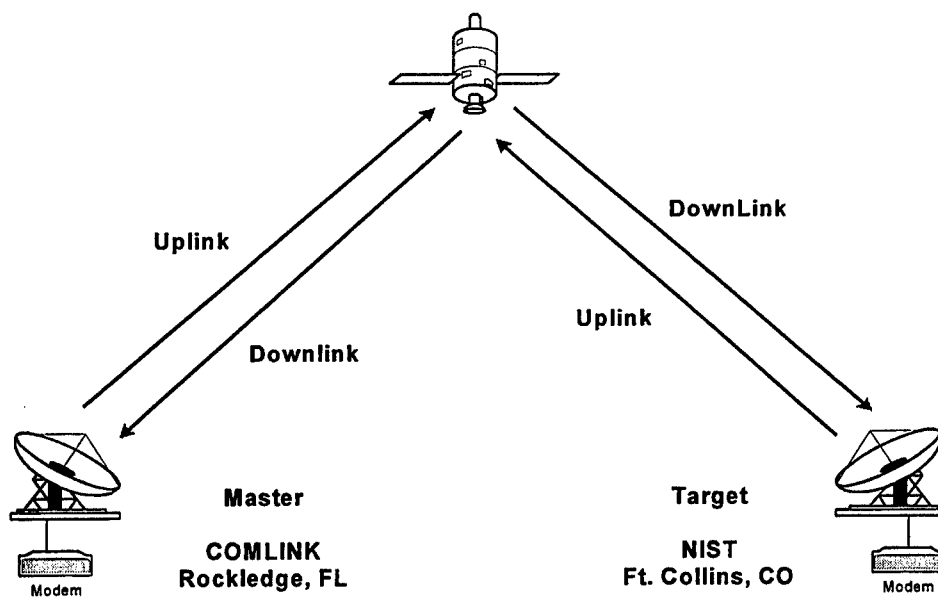


Figure 1. Basic Two-Way Satellite Time Transfer Link

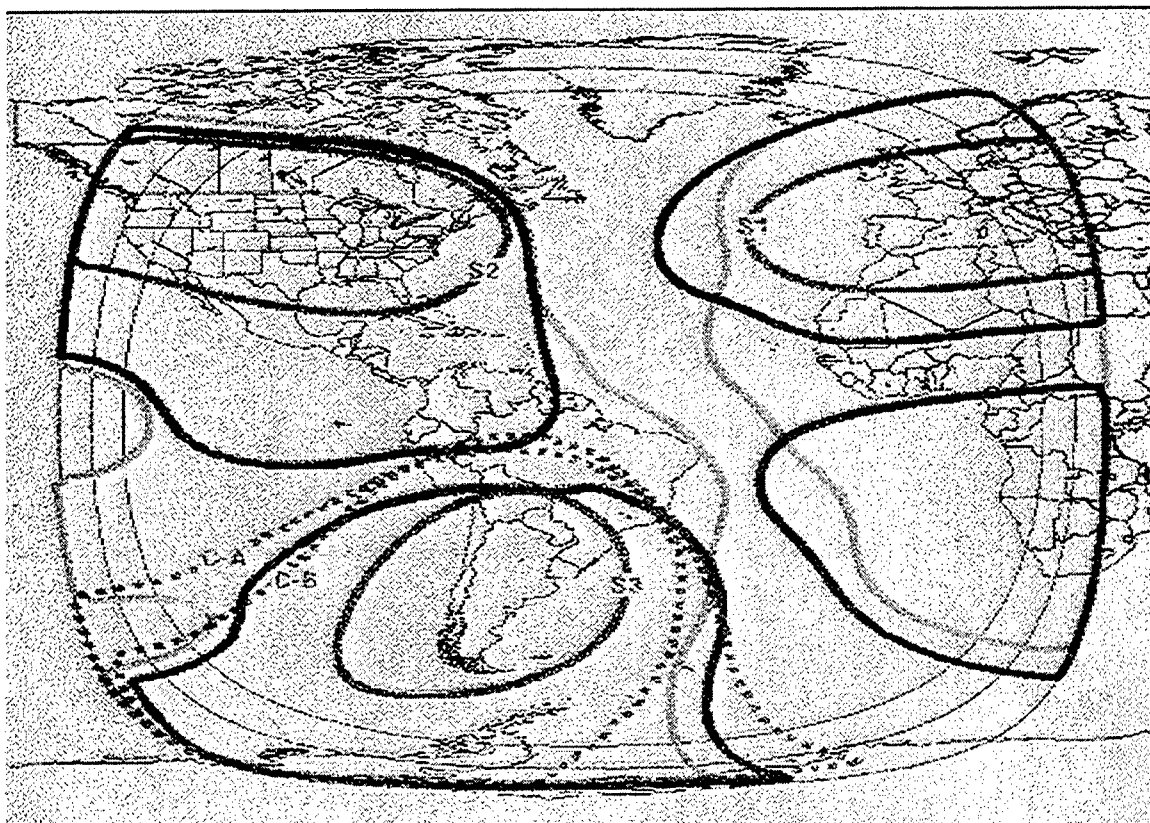


Figure 2. Satellite Footprint

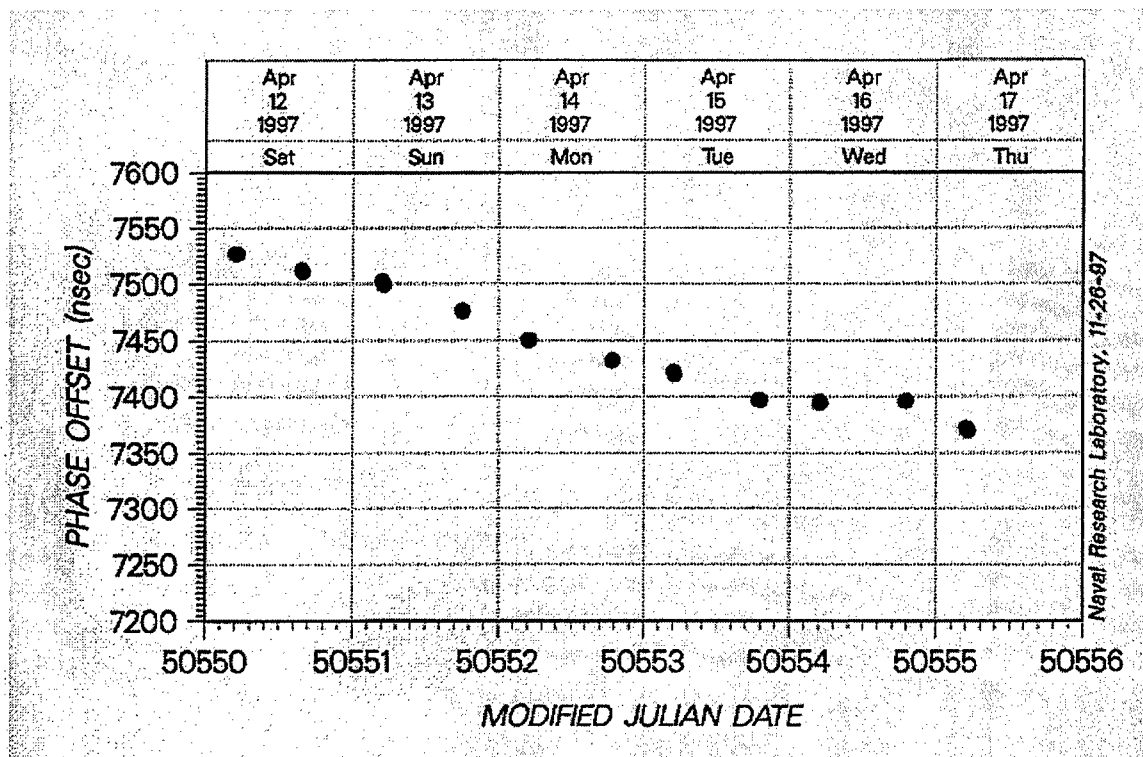


Figure 3. Rockledge, FL vs. Ft. Collins, CO Ku-band TWSTT

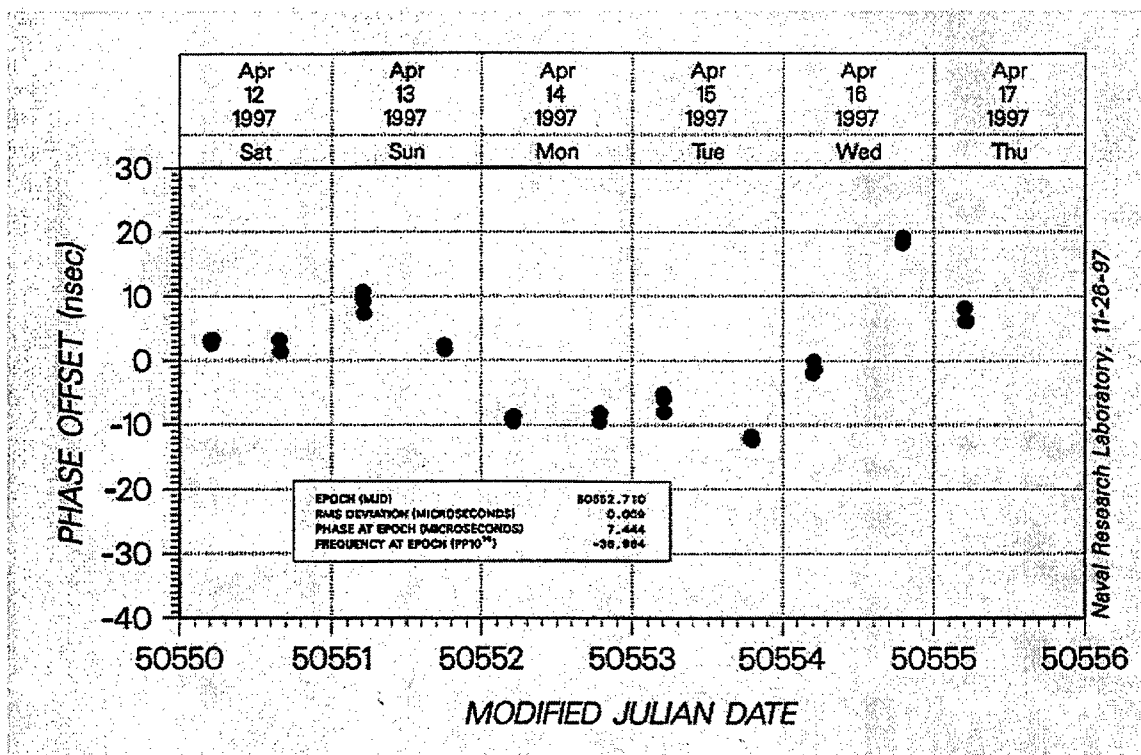


Figure 4. Rockledge, FL vs. Ft. Collins, CO Ku band TWSTT linear residuals

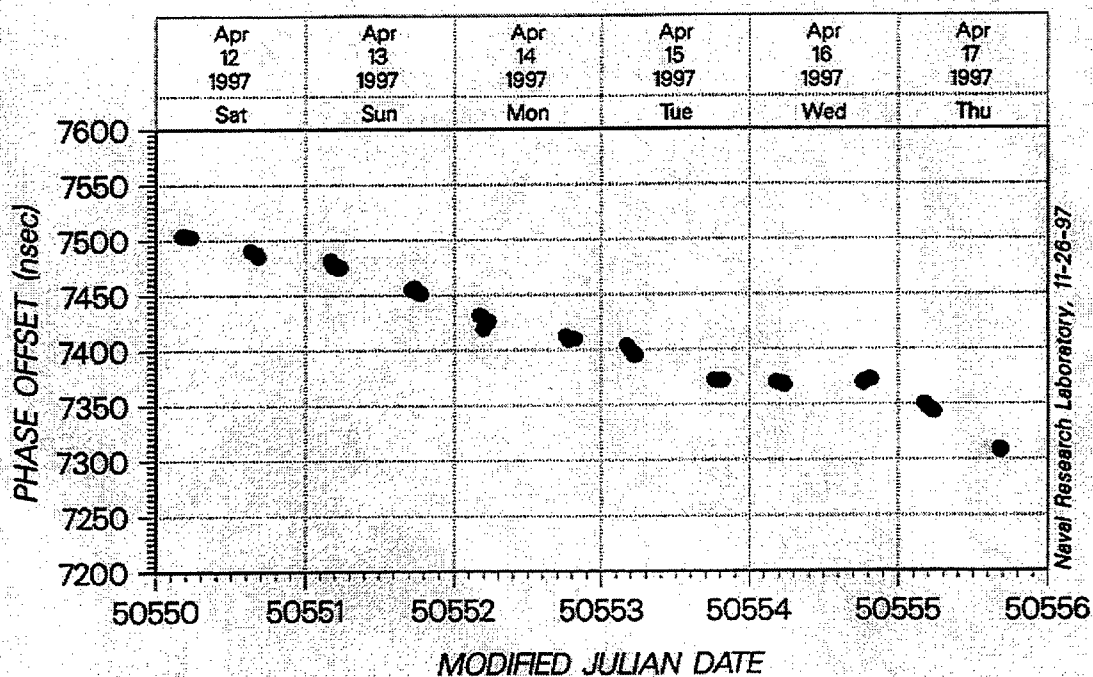


Figure 5. Rockledge, FL vs. Ft. Collins, CO C-band TWSTT

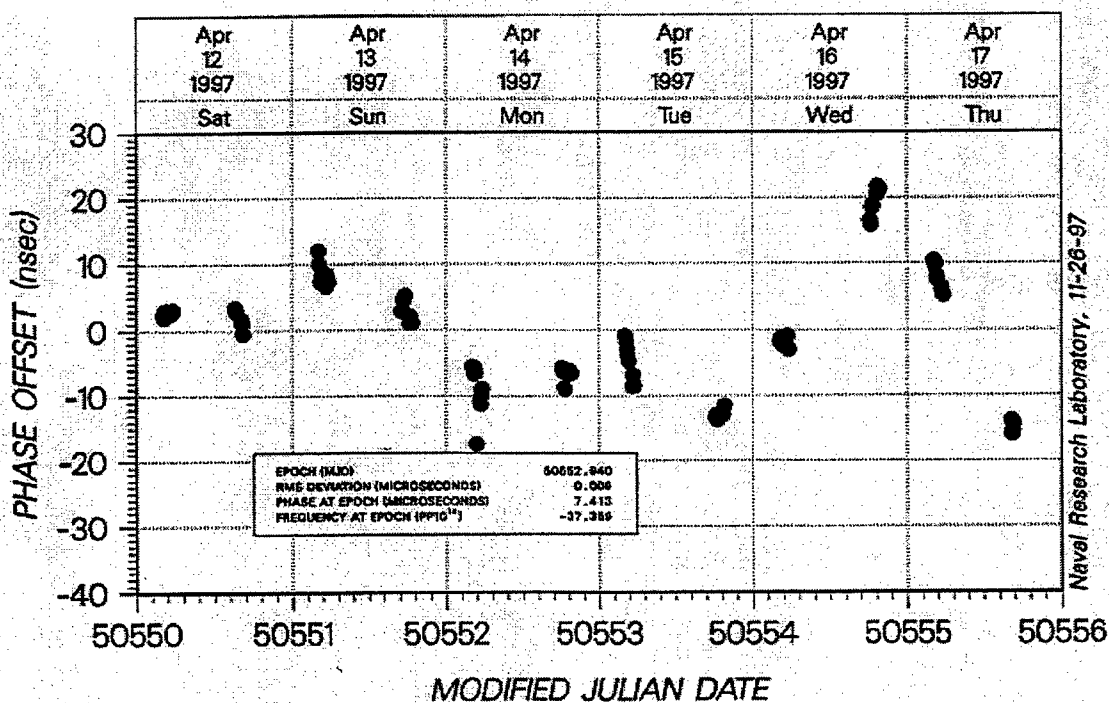


Figure 6. Rockledge, FL vs. Ft. Collins, CO C-band TWSTT linear residuals

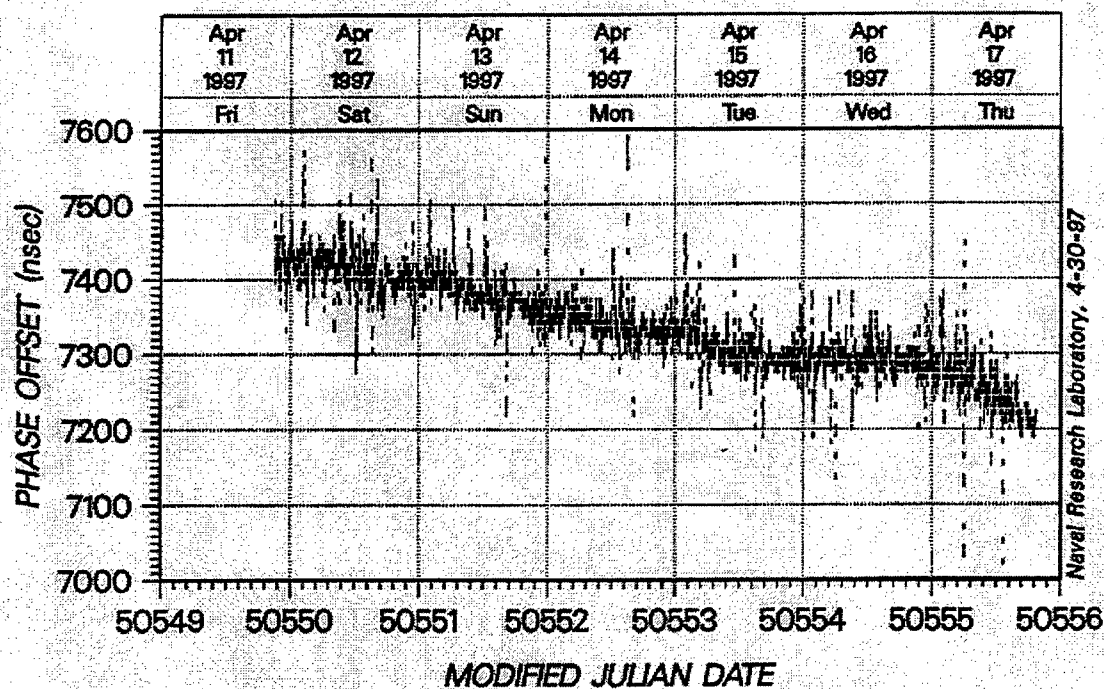


Figure 7. Rockledge, FL vs. Ft. Collins, CO GPS Common-View Time Transfer

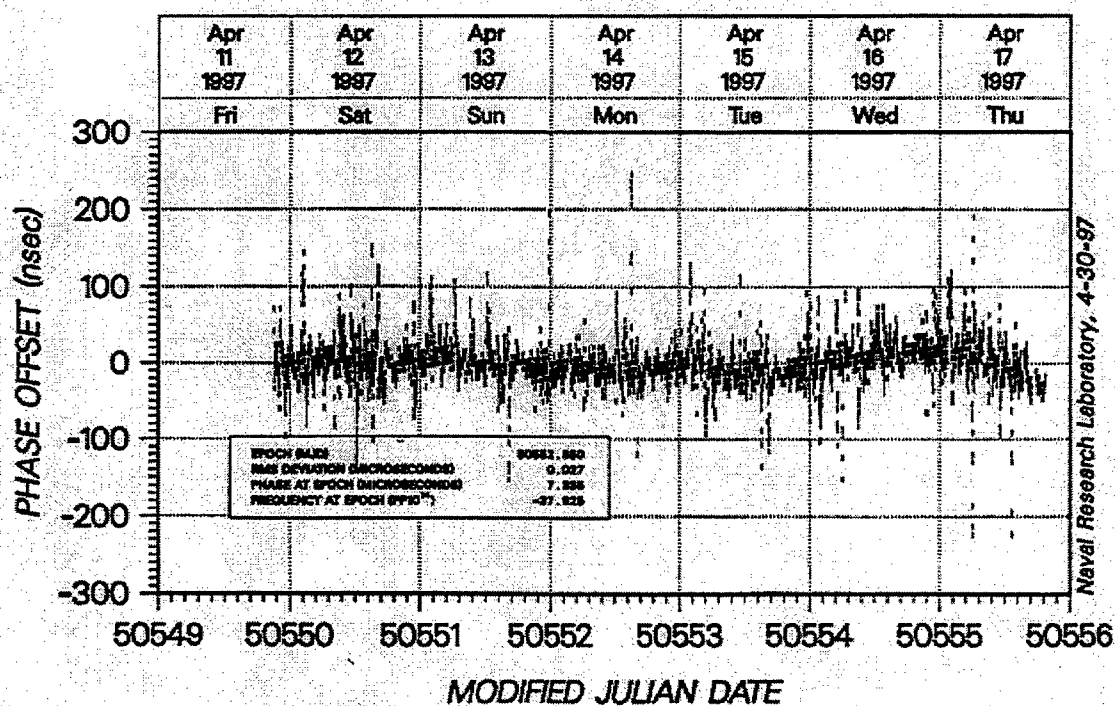


Figure 8. Rockledge, FL vs. Ft. Collins, CO GPS CVTT linear residuals

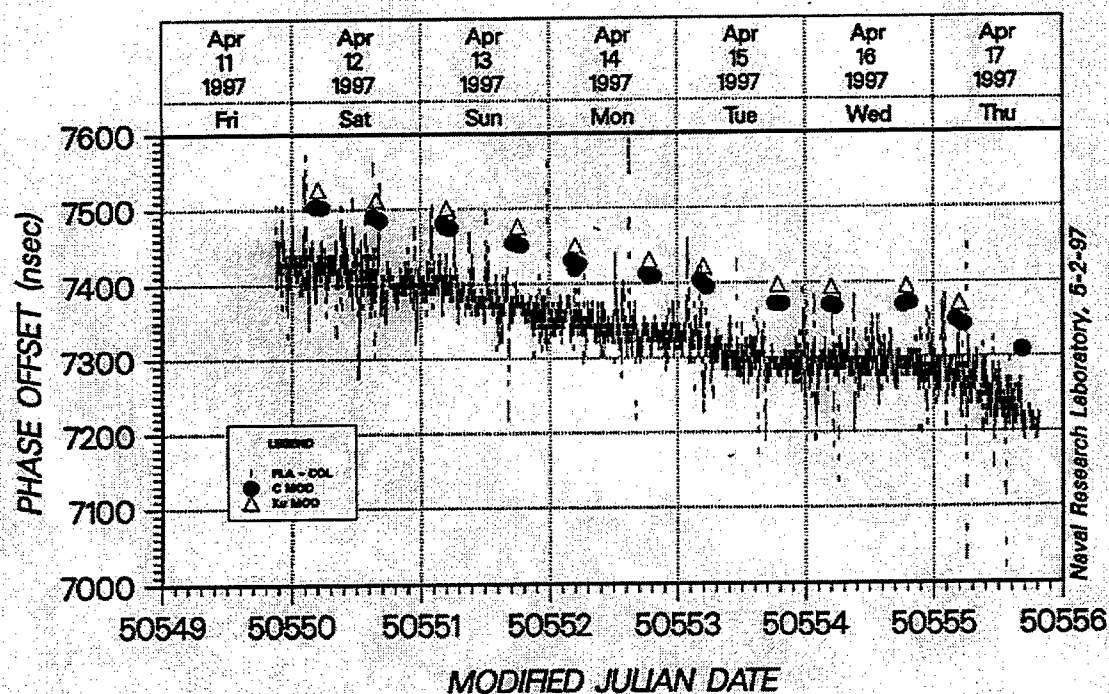


Figure 9. Rockledge, FL vs. Ft. Collins, CO Ku and C-band TWSTT, and GPS CVTT

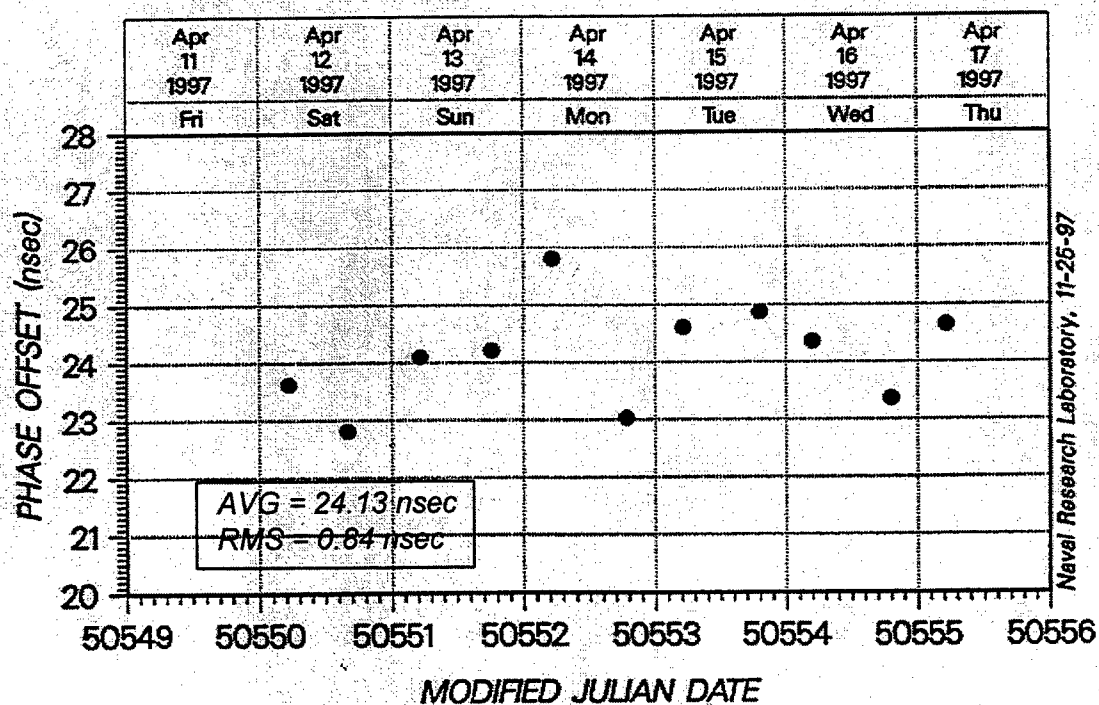


Figure 10. Ku-band and C-band TWSTT Difference

Questions and Answers

BOB WEAVER (UNIVERSITY OF SOUTHERN CALIFORNIA): What size C-band antenna did you use? You said you used 10 watts.

ORVILLE OAKS (NRL): The antenna was a five-and-a-half-meter antenna at the Florida site. NIST was 5.6, something like that.

AN OPERATIONAL TWSTT MONITORING SYSTEM

P. Mai and J. A. DeYoung

U.S. Naval Observatory
Time Service Department
3450 Massachusetts Avenue NW
Washington, DC 20392-5240 USA
phu@simon.usno.navy.mil
dey@herschel.usno.navy.mil

Abstract

The U.S. Naval Observatory (USNO) Time Service (TS) uses the AOA TWT-100 Atlantis Modem for its most important Two-Way Satellite Time Transfer (TWSTT) applications. A method was devised to measure delay changes due to hardware failures in an operational monitoring system. The VSAT on the Roof (VSR) of building 78 is a 1.8-meter dish using a SKYDATA RF unit and is used as the primary operational earth station for TWSTT with the USNO Alternate Master Clock (AMC) located at Falcon AFB, Colorado and for other stations. The Mobile Earth Station (MES) monitors the VSR performance by making six experiments per day. A second 1.8-meter VSat on the Other roof (VSO) is also used as a monitoring system. As long as the hardware remains in normal operating specifications, a constant time difference should result. The MES, VSR, and VSO are co-located with a common-clock reference, Master Clock 2 (MC2). Temperature measurements were taken using a thermocouple-based temperature measuring system. The thermocouple probes used to monitor the temperatures of each modem are located on top of the analog section. This paper presents the results of the estimation of time delay change with temperature difference between the modem in MES and a modem in the USNO TS earth station control room.

INTRODUCTION

A system of three Ku-band TWSTT stations has been developed to provide a routine operational

monitoring system looking for delay changes from hardware failure. The three TWSTT stations are known as the mobile earth station (MES), the VSat on the Roof (VSR) and the VSat on the Other roof (VSO). TWSTT experiments are taken routinely using a common-clock as reference, MC2. This allows for monitoring the stability of the time difference between the TWSTT. If the systems are performing well, the time-series of the measured time differences will remain at a constant value. However, if a hardware component fails, the measured time delay typically changes quite noticeably. With a three antenna system enough information is obtained to allow isolation of which individual TWSTT system has the failed component. The main goal of our TWSTT is to provide the most stable TWSTT reference to our remote users; see Figure 1 for a simple diagram of the system.

During normal operations the stability of the common-clock experiments are at the 300 picosecond level RMS. As a secondary effort, we decided it would be simple to install temperature probes on the modem to evaluate the time difference changes between MES and VSR. We installed temperature probes in the ceiling of the MES and the earth station control room (ESCR), as well as placing temperature probes on top of the analog section of each modem. This was done in order to try to gather data to allow evaluation of any temperature effects of the modems with time difference.

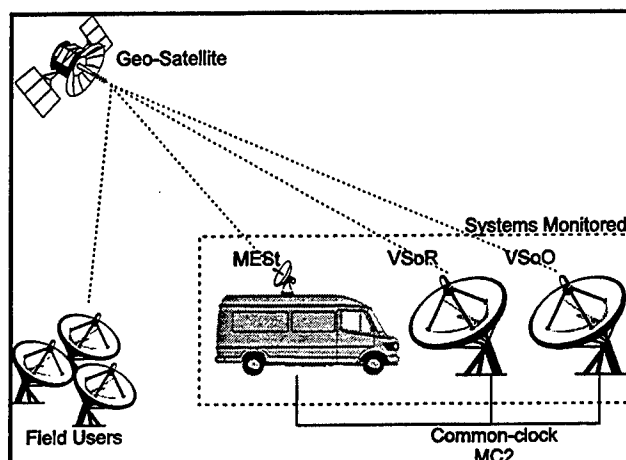


Figure 1

TEMPERATURE OF MODEMS AND TIME DELAY CHANGES

Not surprisingly there was a correlation with outside temperature and the van environment. The temperature as measured at the MES modem shows a diurnal variation locked to the outside temperature, but much reduced in amplitude. The ESCR shows little direct relationship to outside temperature. The data for temperature with respect to time difference are quite varied in the ESCR case! The behavior is very complex, depending on season, state of air conditioners and heating systems, whether rack doors were left open; etc., see Figure 2.

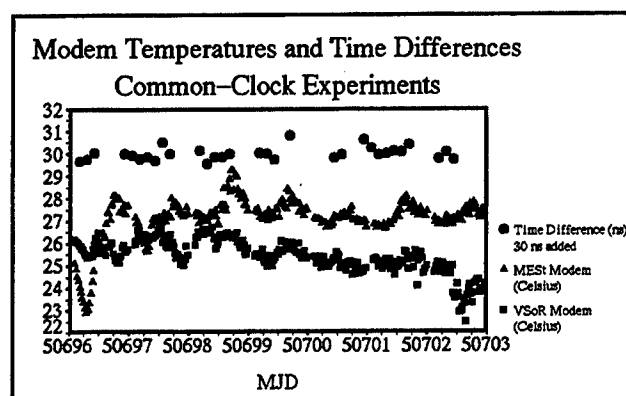


Figure 2

In order to have a small chance of making some sense of these data, we decided to select one week's worth of data (MJD 50696 to 50703) to

analyze in detail. Figure 2 shows the time difference VSR-MES (nanoseconds) and the temperature as measured on top of the analog section of the MES and VSR modems. A diurnal temperature variation in phase with outside temperature is evident, especially in the MES temperatures. The earth station control room modem temperatures are a bit more confusing. For the first two days the temperature measured at the modem in the ESCR are out of phase from those measured at the MES modem, then for a while they seem to be in phase, and later seem not related at all. It is clear, therefore, that any transfer function is very complex and variable with time. Since the time difference is measured as VSR-MES, it was decided that the appropriate thing to do was to compare the VSR(modem)-MES(modem) temperature difference with modem-induced delays in the time differences.

Figure 3 shows the time delays (275 ps RMS) with temperature difference between the two modems. A peak-to-peak variation of 6 degrees Celsius is evident between the two modems. Some evidence for short-term time difference structure correlated with temperature difference is visible. There seems to be only an extremely weak long-term relationship.

A linear least-squares fit to the temperature difference with time difference for the combination VSR-MES indicates a weak relationship of 85 picoseconds per degree Celsius; see Figure 4.

CONCLUSIONS

To minimize delay variations that will affect accuracy it is always important to consider the design of the complete system. Increasing the thermal stability of the systems through insulation, environmental control, etc. are easy to perform and will improve the stability. VSO can serve as a hot backup in case of failure of a critical component in the primary VSR system. A method of monitoring for long-term seasonal systematics would be a worthy, but difficult project, for future efforts.

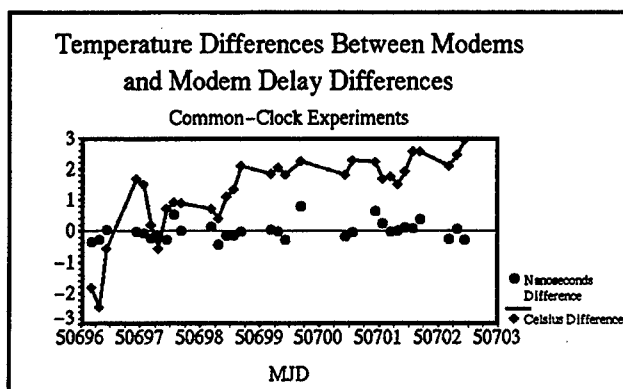


Figure 3

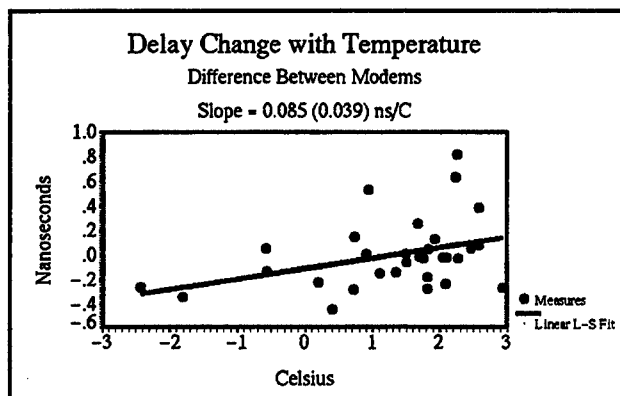


Figure 4

ACKNOWLEDGEMENTS

Thanks to to P. Wheeler, A. McKinley, J. Beish, and G. Luther for their yeoman work on TWSTT, and N. Jardine of USNO Time Service for her graphical layout of Figure 1.

COMMON-VIEW TIME TRANSFER USING MULTI-CHANNEL GPS RECEIVERS

Lara Schmidt, Mihran Miranian

U.S. Naval Observatory
3450 Massachusetts Ave., NW
Washington DC 20392 USA
phone (202)762-1452 fax (202)762-1511
lss@ramsey.usno.navy.mil mm@aitken.usno.navy.mil

Abstract

Common-View GPS has proven to be an accurate and reliable time transfer method capable of producing estimates of clock differences with a precision of 2-3 nanoseconds with averaging^[1]. The advent of multi-channel timing receivers promises enhanced coverage and increased precision due to the large number of common-view passes available between any two sites. This paper discusses the processing techniques used to reap the benefits of the multi-channel receivers, and compares common-view results with those achieved using standard single-channel receivers. The precision of multi-channel common-view is shown to be less than a nanosecond with averaging over one day for a 2400-km baseline.

INTRODUCTION

Multi-channel GPS timing receivers offer the opportunity to greatly increase the number of common-view passes between any two sites. The extent to which these additional passes enhance the precision of the common-view results can be deduced from the underlying statistical theory. For a random sample from a Gaussian distribution, the variation of the sample mean is inversely related to the sample size. Thus we might expect that the variance of the "average" common-view differences between two sites to decrease dramatically with increases in the sample size, i.e., the number of common-view passes. In order to validate this scenario, the USNO

conducted a three-month experiment comparing common-view results obtained via single-channel receivers with those obtained using multi-channel receivers.

HARDWARE AND SOFTWARE

TIME TRANSFER RECEIVERS

AOA TTR4P multi-channel receivers were used in the experiment. All receivers were upgraded to the 050 processor and were operating with version 3.0.34.3 software. This software version has two new features which are necessary for successful common-view time transfer, a new mode of operation called *Clock*, and the ability to apply ionospheric model corrections. When operating in *Clock* mode, the receiver will not try to automatically determine its position when it is reset, undergoes a power cycle, or loses lock on all satellites. Instead, the receiver maintains the position entered by the user. The ability to select the ionospheric model eliminates the problem of noisy ionospheric measurements for satellites below 30 degrees elevation, a characteristic of the TTR4P receiver. Furthermore, applying modeled ionospheric corrections maintains continuity with most common-view time transfer receivers in operation today.

MULTI-CHANNEL COMMON-VIEW SCHEDULES

In the traditional common-view (CV) algorithm, satellites are tracked according to a schedule issued by the BIPM twice annually. This schedule spaces the CV passes at least 15 minutes apart to allow for a two-minute acquisition period needed by many single-channel receivers. When using a multi-channel receiver in "all-in-view" mode, several satellites are tracked at once, potentially from horizon to horizon. Thus, the standard CV schedule is ineffective, both in terms of number and concentration of passes. To maximize the number of CV passes between the USNO and the USNO AMC, several different multi-channel common-view (MCV) schedules were tested.

The first schedule building technique identifies the time intervals when each satellite is in common-view between the two sites, and divides these time intervals into 13-minute MCV passes. In such a schedule, there are approximately 20 passes per satellite, as opposed to two or three passes in a traditional CV schedule. Like the traditional schedule, however, the MCV passes are slewed four minutes per day. Drawbacks to this schedule building technique include the following. (1) If common-view is to be done with a new site, a similar schedule must be constructed listing all passes in common between the USNO and the new site. This is undesirable if short-term MCV experiments occur with numerous sites. (2) The schedule must be "maintained," since satellite positions change over time. (3) There

is no guarantee that there will be *any* CV passes between receivers operating on this schedule and other time transfer receivers using the standard BIPM schedule.

The second schedule building technique reduces the time spent maintaining the schedules by disregarding the time intervals when each satellite is in common-view. Instead, MCV passes for every satellite are constructed by dividing the day into 110 thirteen-minute intervals. Thus, each 13-minute interval is a *potential* MCV pass for *all* satellites. In reality, of course, only approximately 20 of these will be tracked per satellite at both sites. While this does eliminate the need for constantly maintaining the schedule, it increases processing time since the raw data are searched for 110 passes per satellite, as opposed to 20 passes as in the first method. This technique is, however, flexible enough to be adapted to any new site, as it does not depend on location specific satellite view times.

A third technique was adopted after discussions with C. Thomas of the BIPM which allows all of the traditional CV passes to be included as a subset of the MCV passes. This is accomplished by dividing the day into 16-minute time intervals and setting the effective date of the MCV schedule to be the effective date of the most recent BIPM International CV Schedule. This technique not only allows CV comparisons with single-channel receivers, it is a convenient format that can be mutually agreed upon in order to exchange 13-minute data with any other lab. Data for exchange with other timing labs are formatted in accordance with the GGTTs guidelines.^[2]

MULTI-CHANNEL COMMON-VIEW PROCESSING

Using one of the above techniques to establish start and stop times of 13-minute passes for each satellite, the raw 10-second data are processed using a linear fit routine to produce 13-minute values which are referenced to the midpoint of the pass. Common-view differences are then identified in the standard way using a 20-degree elevation mask.^[3] The MCV differences are then filtered. Traditionally, a two-standard-deviation filter is used to remove outliers, but 5% upper- and lower-tail trimming were found to be more effective at removing systematic error sources from the common-view difference data between the USNO and the USNO AMC. The rationale for the trimming procedure will be discussed below. Next, linear fits are calculated using the filtered 13-minute differences from 1200 UT of one day to 1200 UT of the next day, and referenced to 0000 UT of the second day.^[4]

RESULTS

USNO - USNO AMC

Multi-channel common-view has been underway between the USNO in Washington, DC and the USNO AMC in Colorado Springs, Colorado since January 1997. Over

this 2400-kilometer baseline, approximately 360 MCV passes are observed daily. The receivers at each site are referenced to steered hydrogen masers which are generally kept within a few nanoseconds of each other via Two-Way Satellite Time Transfer (TWSTT).^[9] The results presented are for the time period 01 June 1997 through 05 September 1997, and include common-view passes for all healthy satellites except PRN02/SVN13.

During the experiment, the distribution of daily Reference-GPS measurements made by receivers at both sites was found to be approximately Gaussian when treating the Reference-GPS data as a random sample, not as a time series. The MCV difference data were thus expected to be Gaussian. In practice, however, it was found that the distribution of the MCV differences was heavy-tailed, indicating a systematic error source. Although this error source was not eliminated, the distribution was normalized by a 5% trimming of the upper and lower tails. Trimming the data as opposed to filtering based upon a two-standard-deviation limit was shown to reduce the scatter of the 13-minute differences by up to 0.5 nanoseconds with minimal loss of data.

Based upon one-day linear fits of the filtered 13-minute data, the average MCV difference between the two clocks was reported as -0.22 nanoseconds with an average one day RMS of 2.33 nanoseconds. The USNO also maintains STel 5401C single-channel, dual-frequency, P/Y code receivers which complete the same common-view link. During the same time period, the STel receivers reported an average RMS at one day of 4.38 nanoseconds using approximately 55 CV passes per day. It should be noted that the STel receivers apply a measured ionospheric correction which is quantized to nine nanoseconds, and undoubtedly contributes to the higher scatter of the 13-minute differences.

Receiver Type	Filtering Method	Precision at 13 Minutes	Number of CV Passes per Day	Precision at 1 Day
AOA TTR4P	$\bar{x} \pm 2s$	2.71 ns	377	0.72 ns
	5% trim	2.33 ns	358	0.71 ns
STel 5401C	$\bar{x} \pm 2s$	4.38 ns	55	1.05 ns

Estimates of the precision of the 1-day common-view differences were computed via the residuals of smoothed 13-minute MCV values. Figure 1 displays the smoothing

performed. A five-day moving average was utilized to remove longer-term effects such as clock rates and temperature effects. The variability of the residuals of the moving average was then used to estimate the precision of the MCV differences at one day. Due to the large number of MCV passes produced by the TTR4P receivers, the precision of the daily common-view estimates is smaller than that of the single-channel STel receivers. The estimated precision of the daily MCV values is 720 picoseconds, as shown in the table above.

By using a higher elevation mask when computing MCV differences, variation can be reduced at the price of fewer MCV passes. For example, using an elevation mask of 60 degrees lowers the RMS at one day to 2.15 ns, but the average number of MCV passes is reduced to 60 per day, which in turn reduces the precision over longer averaging times (see Figure 2).

USNO - BIPM

A short-lived MCV experiment between the USNO and the BIPM took place during 13 August 1997 to 18 August 1997 over a baseline of approximately 6000 kilometers. The BIPM TTR4P receiver was also running version 3.0.34.3 software, had a sample rate of one second, and was referenced to a HP5071A cesium clock.^[6] The scatter of the 13-minute differences was generally less than five nanoseconds, and the precision of the daily MCV estimates was approximately 630 picoseconds.

The link between the USNO and the BIPM is also made using AOA TTR6 single-channel receivers. Over the same time period, an average daily RMS of 3.2 nanoseconds was calculated for traditional CV between TTR6 receivers using approximately 16 passes daily, yielding an estimated precision of 1.30 nanoseconds.

Receiver Type	Filtering Method	Precision at 13 Minutes	Number of CV Passes Daily	Precision at 1 Day
AOA TTR4P	$\bar{x} \pm 2s$	4.68 ns	138	0.74 ns
	5% trim	4.50 ns	132	0.63 ns
AOA TTR6	$\bar{x} \pm 2s$	3.20 ns	16	1.30 ns

Once again, the use of multi-channel receivers increases the precision of the daily MCV estimates. In this case, the eight-channel receivers yield estimates of USNO-

BIPM that are approximately twice as precise as estimates obtained from the single-channel receiver.

RECEIVER CALIBRATION PROBLEM

During the experiment, a major problem with the time measurement hardware and software was discovered. A 24-nanosecond uncertainty in the absolute calibration of the TTR4P manifests itself each time the unit undergoes a power cycle or is reset. Therefore, once the unit has been powered on and the receiver bias has been set, the power must not be recycled. This was not a serious problem at either USNO site since all equipment is provided with an uninterrupted power supply. Additionally, to ensure the stability of the calibration of the receivers in Washington, common-view time transfer with a co-located AOA TTR6 receiver is continually performed to monitor the integrity of the receivers. AOA has acknowledged the 24-nanosecond uncertainty and has committed to resolving the problem. Figure 3 shows the results of several power cycles performed during testing at the USNO.

SUMMARY AND CONCLUSIONS

Aside from the standard common-view procedures utilized in this study, alternative data processing techniques should be investigated. Such techniques may include consolidating Reference - GPS measurements across several channels to produce 13-minute values which are averages of data from several satellites tracked concurrently at both sites. Estimates of clock differences formed in this fashion may prove to be more stable in the short term. However, using the standard common-view technique, it was shown that the increased number of common-view passes contributes to the increased precision of the estimates of clock differences. For the CV link between the USNO and the USNO AMC, the multi-channel receivers produced six times the number of CV passes as single-channel receivers, and enhanced the precision by a factor of 1.5 while showing little difference in the magnitude or variability of the raw measurements.

REFERENCES

- [1] W. Lewandowski, G. Petit, and C. Thomas 1993, "*Precision and Accuracy of GPS Time Transfer*," **IEEE Transactions on Instrumentation and Measurement**, 42, 474-479.
- [2] D.W. Allan, and C. Thomas 1994, "*Technical Directives for Standardization of GPS Time Receiver Software*," **Metrologia**, 31, 69-79.

[3] D.W. Allan, M. Weiss 1980, "*Accurate Time and Frequency Transfer during Common-View of a GPS Satellite*" in Proceedings of the 34th Annual Symposium on Frequency Control, pp. 334-346.

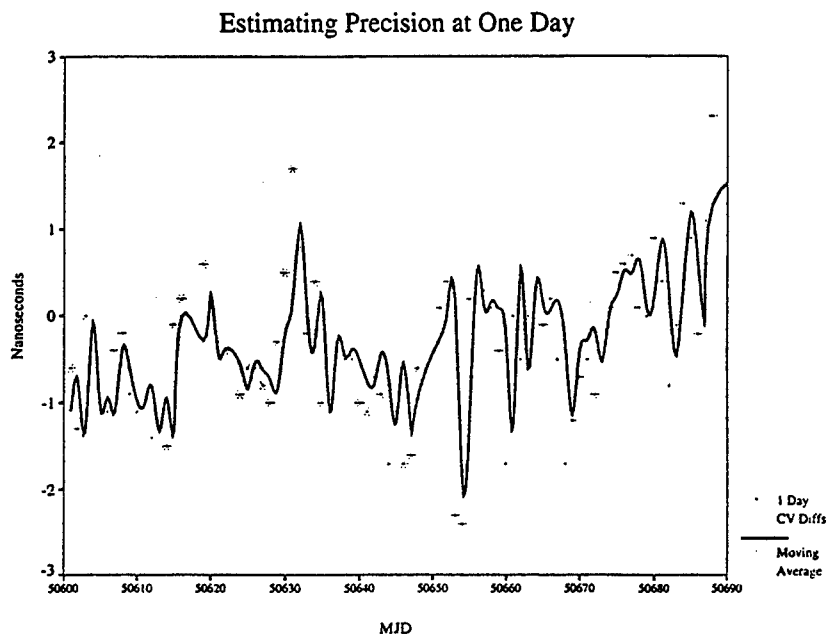
[4] M. Miranian, and W. Klepczynski 1991, "*Time Transfer via GPS at USNO*" in Proceedings of the Fourth International Technical Meeting of ION GPS-91, pp. 215-221.

[5] J. DeYoung, F. Vannicola, and A. McKinley 1996, "*A Comparison of the Highest Precision Commonly Available Time Transfer Methods: TWSTT and GPS CV*" in Proceedings of the 28th Annual PTTI Applications and Planning Meeting, pp. 349-355.

[6] P. Moussay, personal communication.

ACKNOWLEDGEMENTS

The authors would like to thank Claudine Thomas and Philippe Moussay of the BIPM for sharing GPS data, Jim DeYoung and Steven Hutsell of the USNO for contributing to the data analysis, and Francine Vannicola, Wendy King, and Ed Powers for contributing to hardware and software efforts.



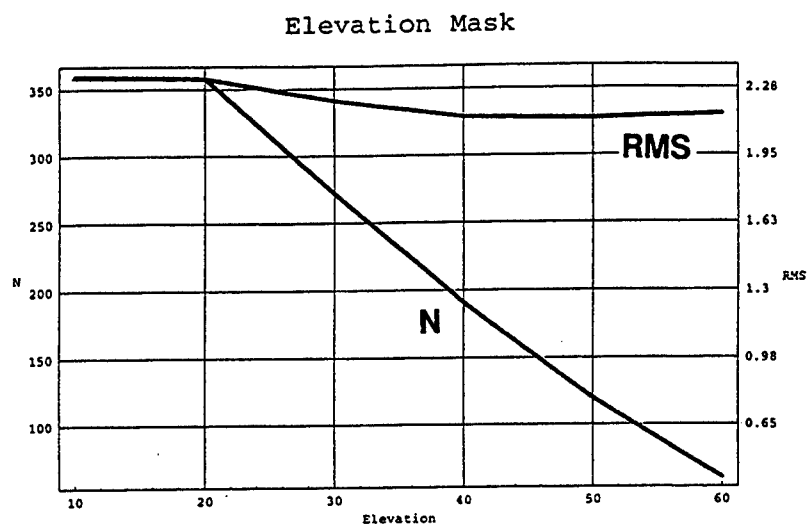


Figure 2.

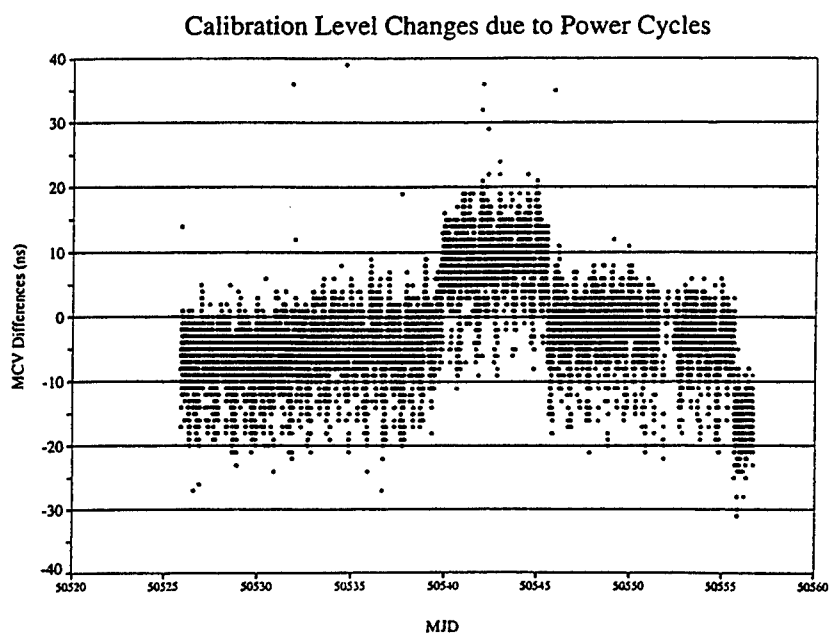


Figure 3.

MULTICHANNEL VS.COMMON-VIEW GPS FREQUENCY TRANSFER COMPARISON IN THE ASIA-PACIFIC REGION

P.T.H. Fisk, M. A. Lawn, S. Quigg, J.S. Thorn
National Measurement Laboratory
CSIRO Division of Telecommunications and Industrial Physics
PO Box 218, Lindfield NSW 2070
Sydney, Australia

T. Armstrong
Measurement Standards Laboratory of New Zealand
PO Box 31-310
Lower Hutt, New Zealand

J. McK. Luck, J. R. Woodger
Orroral Geodetic Observatory
Australian Surveying and Land Information Group
PO Box 2, Belconnen ACT 2616
Canberra, Australia

M. M. Ruiz
Industrial Technology Development Institute
DOST Complex, Gen. Santos Ave.
Bicutan Taguig, Metro Manila 1604
Philippines

Abstract

Global Positioning System timing receivers have made it possible for time and frequency to be realized conveniently for almost any application, with an accuracy previously achievable only with (far more expensive) cesium standards. Multichannel GPS receivers, which calculate a position and time solution using signals from six or more GPS satellites simultaneously, are now available from a number of manufacturers at very reasonable cost. These receivers are an attractive solution for high accuracy inter-laboratory frequency and time transfer where the cost of the more conventional "classical" GPS common-view receivers is not warranted. This paper presents results of several ongoing frequency/time transfer links over baselines of up to 6000 km, in the Asia-Pacific region.

INTRODUCTION

The performance and sophistication of multichannel GPS (MGPS) receivers, which calculate a position and time solution using signals from six or more GPS satellites simultaneously, have developed markedly over the past few years. For time and frequency transfer purposes, the potential performance of MGPS receivers has been shown^[1,2,3] to compare favorably with that of "classical" single channel common-view GPS time transfer units^[4], in some cases at significantly lower cost.

The work described in this paper is motivated primarily by the inconvenience and expense of shipping frequency standards belonging to Australian clients to the CSIRO National Measurement Laboratory (NML), located in Sydney, for calibration with respect to the Australian National Frequency Standard.

This procedure is particularly difficult when the owner of the frequency standard requires an accuracy which necessitates maintaining power to the instrument during transit. Within the Asia-Pacific region, the problem is compounded by the prohibition against carrying dangerous substances such as rubidium and cesium on commercial passenger-carrying aircraft. For most local clients, the cost of conventional "classical" GPS common-view (GPS-CV) time transfer receivers is not warranted, and in the Australasian region there is no suitable alternative means of high accuracy frequency transfer, such as WWV, DCF-77 or Loran-C.

It is necessary for NML to confirm the integrity of any method used for legally traceable frequency transfer in Australia. To this end, we have investigated the performance, as a frequency transfer device, not as a stand-alone frequency standard, of two implementations of MGPS receivers:

- A quartz oscillator which is frequency-steered by reference to the GPS system (a GPS-disciplined oscillator or GPSDO).
- A relatively low cost MGPS receiver programmed by an external computer to operate in a single-channel mode to emulate a classical GPS-CV receiver by making timing measurements on individual satellites according to a schedule. We denote the latter mode of operation MGPS-CV.

Both types of instrument are available from several manufacturers. The use of particular instruments in the present work should not be construed as a recommendation of these instruments in preference to the products of any other manufacturer.

The GPSDOs used in the present experiments operated in an "all-in-view" mode, so that up to 6 satellites contributed to their timing solution. The all-in-view and single-channel common-view methods of GPS frequency transfer differ fundamentally in that the all-in-view method is potentially vulnerable to clock errors in individual satellites if these errors are not recognized and rejected by the receiver's software. In contrast, because the single-channel common-view method uses timing signals from a single satellite as a frequency transfer medium, it is in principle unaffected by satellite clock errors.

The experiments used off-the-shelf hardware as far as possible. The data collection and processing software was also kept as simple (and consequently, cheap to maintain) as possible, since the purpose of the work was to demonstrate the performance of MGPS technology in straightforward frequency transfer applications as might be required by the majority of NML's clients. The data analysis presently considers only frequency stability and accuracy; analysis of receiver and antenna timing delays has not yet been carried out.

THE GPSDO "ALL-IN-VIEW" EXPERIMENT

This very simple demonstration experiment was conducted between NML in Sydney, Australia, and the Industrial Technology Development Institute (ITDI) in Manila, the Philippines. The distance between the two laboratories is approximately 6000 km.

The equipment used at NML and ITDI for this experiment was functionally identical, and the mode of operation was the same at each location. The installations consisted of a GPSDO (Hewlett-Packard HP58503A), a time-interval counter, a classical GPS-CV time-transfer receiver (Allen-Osborne TTR6), a data acquisition computer and a cesium frequency standard (Hewlett-Packard HP5071A). The classical GPS-CV receivers were programmed with the BIPM tracking schedule for the region. The antenna locations were determined using a GPS survey-receiver, and corrected for precise satellite ephemerides. The GPSDOs and classical common-view receivers were programmed with the coordinates obtained.

The phase of the 1 pulse/s output of the GPSDO with respect to the cesium standard was recorded once per minute for 41 days. The phase readings were averaged over 24 hours and are shown in fig. 1.

No outlying data points were removed from the GPSDO data. The modified Allan deviation for the NML-ITDI data is shown in fig. 2, and indicates a predominance of white phase noise for averaging times up to about 2 days. The modified Allan deviation for the data obtained concurrently using the classical GPS-CV receivers is also shown.

Due to the known frequency accuracy of the cesium standards used at both ends of the link, the data indicate that for frequency transfers averaged over 1 day, and over baselines of 6000 km or less, a 1σ uncertainty of less than one part in 10^{12} is achievable with this simple system.

The result of the present experiment is consistent with that of a previous (unpublished) study, which underpinned the decision to permit GPSDOs to be used, under certain circumstances, for legally traceable frequency transfer in Australia. Traceability of a remote GPSDO to NML is currently maintained by monitoring of GPS frequency in Sydney and will later be extended to other parts of Australia.

THE MGPS COMMON-VIEW EXPERIMENT

Equipment (fig. 3) for the MGPS-CV experiment was installed in three laboratories: NML, the Orroral Satellite Laser Ranging observatory (Orroral), 60 km south of Canberra, Australia, and the Measurement Standards Laboratory of New Zealand (MSL), Lower Hutt, 10 km north of Wellington, New Zealand. The inter-laboratory distances were : NML-Orroral 300 km, NML-MSL 2200 km. Classical GPS-CV receivers were also co-located with the MGPS equipment, but a series of unrelated hardware problems prevented any useful data being obtained from these units.

The MGPS receiver used for these experiments was the Motorola VP Oncore. The receivers were mounted on custom-built circuit boards which provided buffering for the timing and serial communications signals. Standard Motorola antennas were used, and antenna cable losses were kept within the limits specified in the Motorola manual; no external amplifiers were therefore necessary. The antenna locations were determined in the same way as for the GPSDO experiment and the receivers were programmed with the coordinates.

The receivers were programmed to track satellites for 13 minute periods, in single-channel mode, according to the BIPM schedule for the Australian region. All pseudo-range computations were performed by the MGPS receivers; the only corrections made to the measured epoch of the 1 pulse/s output of the MGPS receiver with respect to that of the local Cs standard were for the "sawtooth error" ^[5] of the timing pulse. The data files were transmitted, via the Internet or via the telephone system using a modem, to NML for processing.

The data from individual 13-minute satellite "tracks" were processed using the conventional procedure for GPS common-view data ^[6] and are shown in figs. 4 and 5. Modified Allan deviations calculated by averaging the data over 24-hour periods are shown in fig. 6. The effect of filtering out tracks for which the satellite elevation was below "mask angles" of 40° and 25° above the horizon is also shown. As in the case of the GPSDO time transfer experiment, the fluctuations in the data appear to be dominated by white phase noise up to averaging times of 2 days. In the case of the NML-Orroral link, over longer averaging times the fluctuations are close to those expected from the Cs frequency standards being intercompared.

The intrinsic timing noise in the MGPS receivers was investigated by conducting a zero-baseline experiment, where two systems as shown in fig. 3 were installed at NML and connected to a common time reference. The results are shown in fig. 7. The root-mean-square timing deviations from a straight line fit to the two data sets were 6.6 ns and 3.7 ns for 25° and 40° elevation mask angles respectively.

The noise level of the NML-NZ link (fig. 5) is markedly higher than that of the shorter baseline NML-Orroral link, and worsened noticeably after MJD 50740. The reason for this is not yet clear, and is under investigation. One possibility is that the MSL antenna, which is unavoidably located in a valley,

is receiving satellite signals reflected off nearby surfaces (multi-path effect), in addition to direct signals. The fact that the noise level increases as the elevation mask angle is reduced supports this hypothesis. We are not aware, however, of any changes in the antenna's environment which occurred around MJD 50740 which could account for an increase in multi-path signal levels after that date.

Substantial performance improvements could be obtained by making use of more than one channel of the receiver^[2,3]. However, this causes a substantial increase in software complexity, since many of the calculations performed by the MGPS receiver in the present system must be performed by the external computer's software in order to maintain independence of timing information obtained simultaneously from different satellites. Alternatively, a smaller performance improvement could be gained by optimizing the satellite tracking schedule for the distance between the receivers, which would provide more tracks of satellites at high elevation angles.

ANTENNA COORDINATES

Inaccurate values for the coordinates of the antenna have a substantial effect on the precision and accuracy of the results. The noise level in the NML-Orroral MGPS common-view link (fig. 8) shows a dramatic improvement when the coordinates of one antenna were corrected by 8 meters to bring them into conformity with ITRF-94 values obtained by precise geodetic surveying. (There is insignificant difference between ITRF and WGS-84 for these purposes.)

The inadequacy of self-surveying by time transfer units is clearly illustrated in fig. 9. For about 9 days, a "Totally Accurate Clock" ^[7], based on a Motorola VP Oncore engine was put in its default mode in which it continuously updates its position. In the periods before and after it was in this mode, the geodetic coordinates were held constant at their geodetically determined ITRF-94 values. It is often observed that the height component of coordinate solutions by GPS timing receivers varies by hundreds of meters from minute to minute; clearly, this effect is reflected to some extent in the stability of the timing solution.

Most countries now have accessible national geodetic networks accurately tied to the ITRF-94/WGS-84 to within a few centimeters. They are usually based on GPS carrier-phase observations and produce precise, post-processed orbits within 1-2 days after observation. It is strongly recommended that, in timing applications where short to medium-term stability, and/or accuracy are required, the coordinates used by the receiver be held constant at values determined by precise geodetic survey.

CONCLUSION

We plan to maintain the MGPS-CV link between NML, Orroral and MSL for at least another six months, and preferably longer. This will provide sufficient data to enable a more meaningful comparison with the performance of classical common-view receivers. Consequently, the conclusions presented in this paper must be regarded as preliminary.

We found that over the varied baselines covered by the experimental frequency transfer links described in this paper, both the GPSDO and MGPS-CV techniques proved capable of frequency transfer accuracy of better than 1 part in 10^{12} , averaged over 1 day. This performance is ample for maintaining a traceable frequency link between a rubidium standard located at a client's premises in Australia, and NML. The single-channel MGPS-CV technique appears particularly promising and cost-effective, showing excellent performance capability over a baseline of 300 km.

As expected, precise coordinates obtained from geodetic survey GPS receivers were necessary for optimum performance.

REFERENCES

- [1] W. Lewandowski, P. Moussay, P. Guerin, F. Meyer and M. Vincent 1997, "Testing Motorola Oncore GPS receiver for time metrology", Proc. 1997 European Frequency and Time Forum, in press

- [2] R.P. Giffard, L.S. Cutler, J.A. Kusters, M. Miranian and D.W. Allan 1996, "*Continuous, multi-channel common-view L1-GPS time-comparison over a 4000 km baseline*", Proc. 1996 IEEE Frequency Control Symposium, pp. 1198-1204
- [3] R.P. Giffard, L.S. Cutler, J.A. Kusters, M. Miranian and D.W. Allan 1996, "*Toward 10^{-15} and sub-nanosecond international frequency and time metrology*", Proc. 1996 European Frequency and Time Forum, pp. 528-533
- [4] W. Lewandowski and C. Thomas 1991, "*GPS time transfer*", Proc IEEE, 79, pp. 991-1000.
- [5] Motorola VP Oncore reference manual.
- [6] "*Technical directives for standardisation of GPS time receiver software*", International Bureau of Weights and Measures, Report BIPM-93/6
- [7] T. A. Clark 1997, ftp address: <ftp://aleph.gsfc.nasa.gov/GPS/totally.accurate.clock>

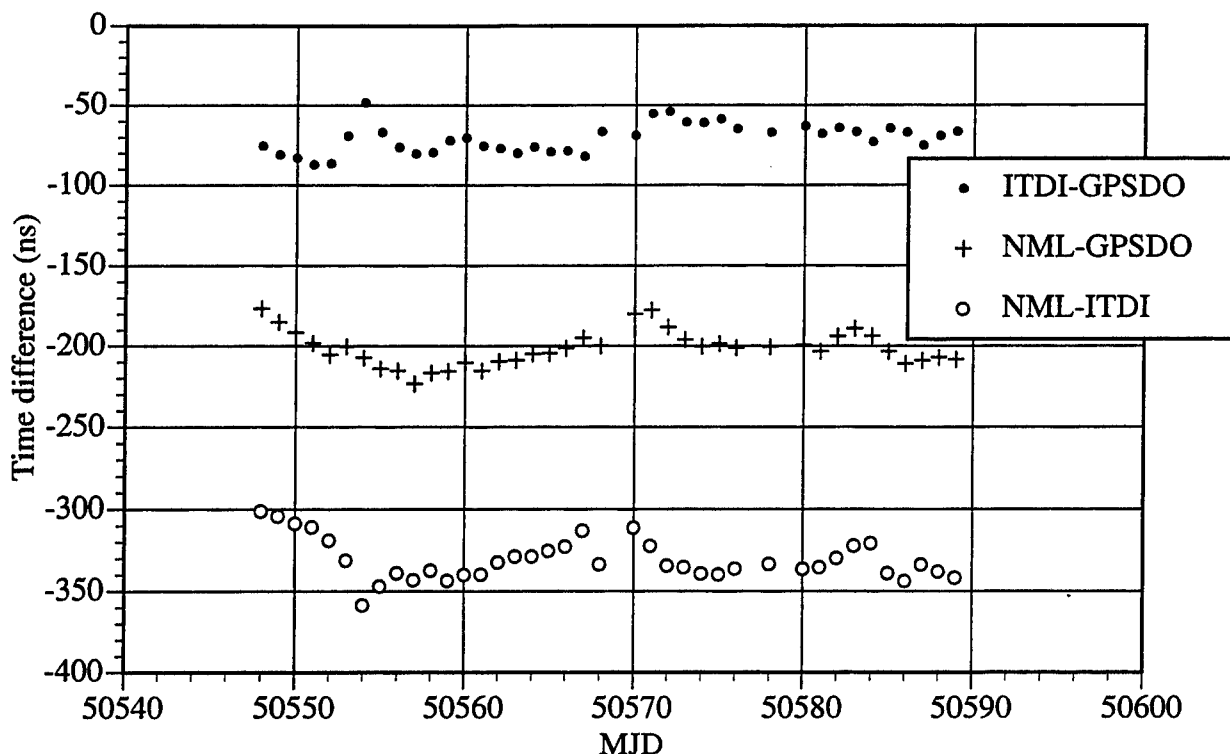


Figure 1: Time series data for the NML-ITDI experiment. Individual series are shifted vertically for clarity, thus introducing an arbitrary, constant time offset.

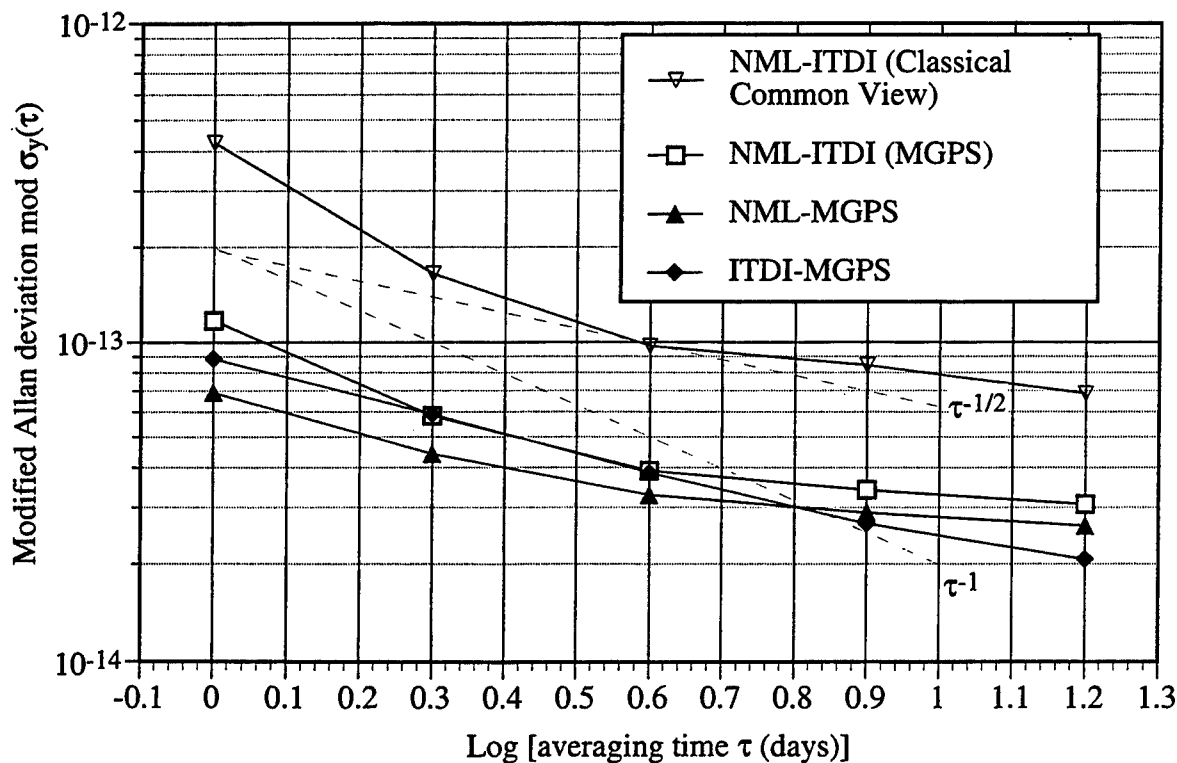


Figure 2: Frequency stability, as characterized by the modified Allan deviation, of the data shown in fig. 1.

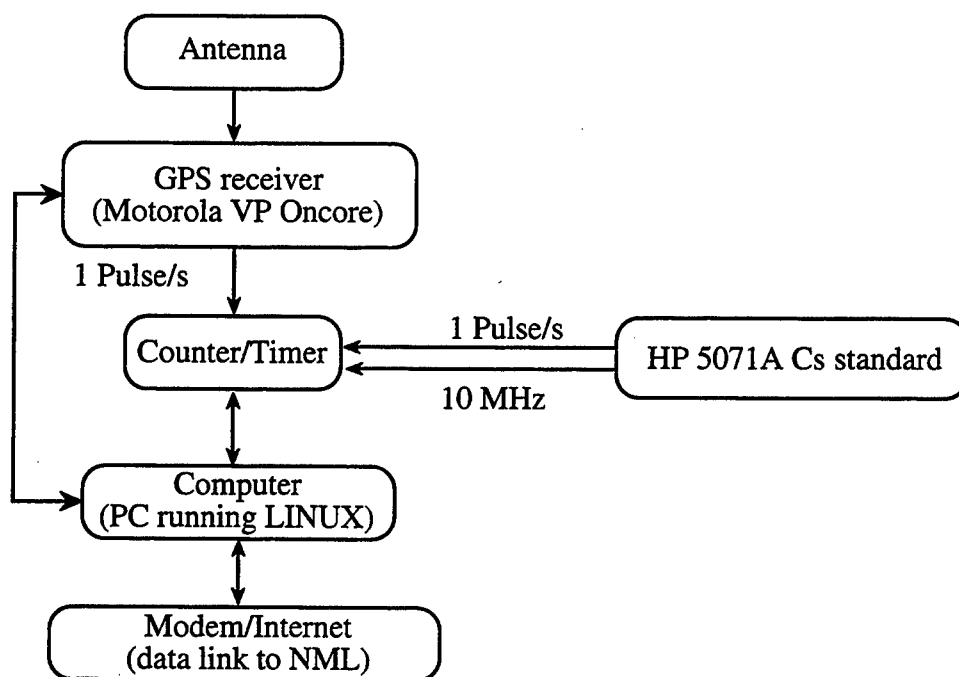


Figure 3: Schematic of MGPS common-view frequency transfer system, and interface to local frequency standard.

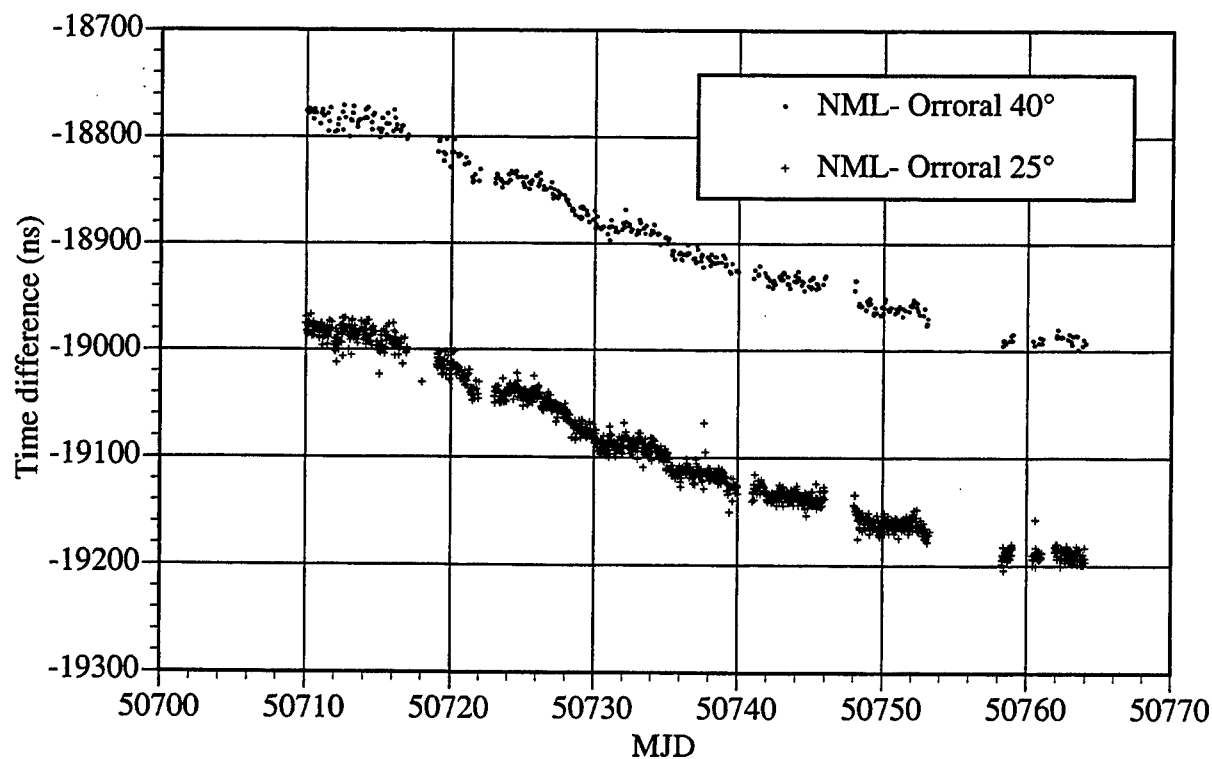


Figure 4: Time series data for the NML-Orroral MGPS-CV link, for elevation mask angles of 40° and 25°. Individual series are shifted vertically for clarity and 5 outlying points were removed.

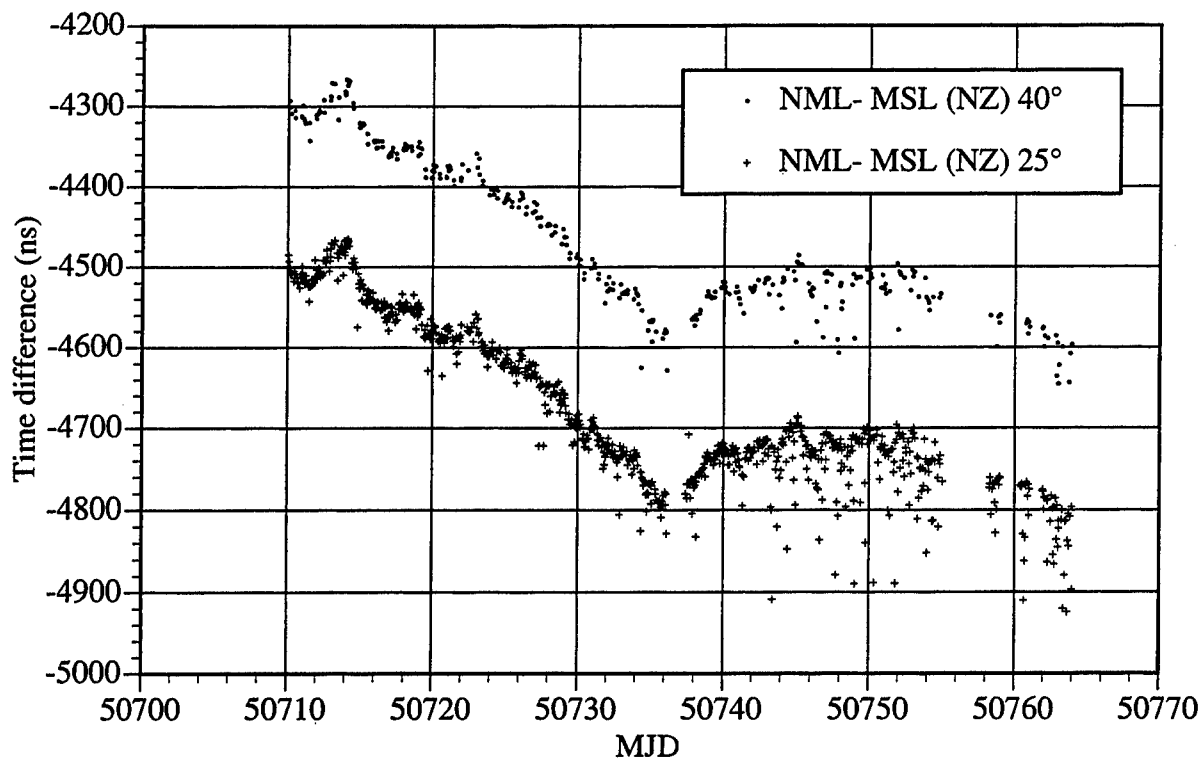


Figure 5: Time series data for the NML-Orroral MGPS-CV link, for elevation mask angles of 40° and 25°. Individual series are shifted vertically for clarity and 13 outlying points were removed.

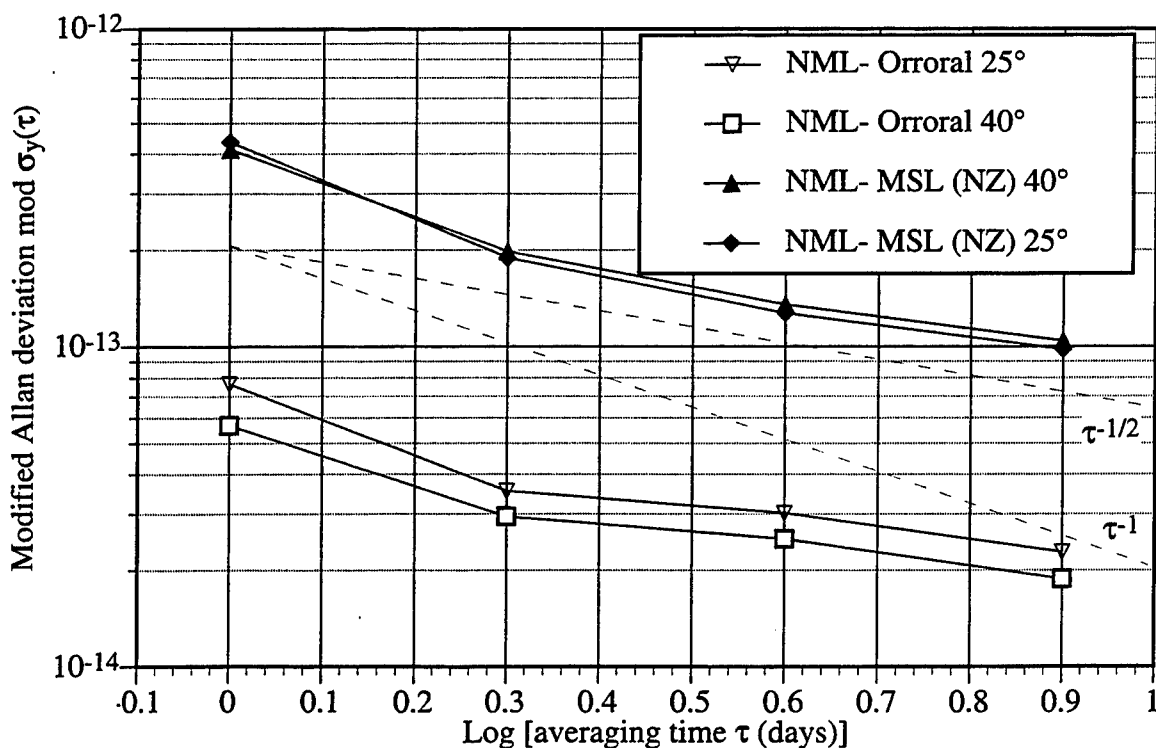


Figure 6: Frequency stability, as characterized by the modified Allan deviation, of the data (averaged over 24 hour intervals) shown in figs. 4 and 5.

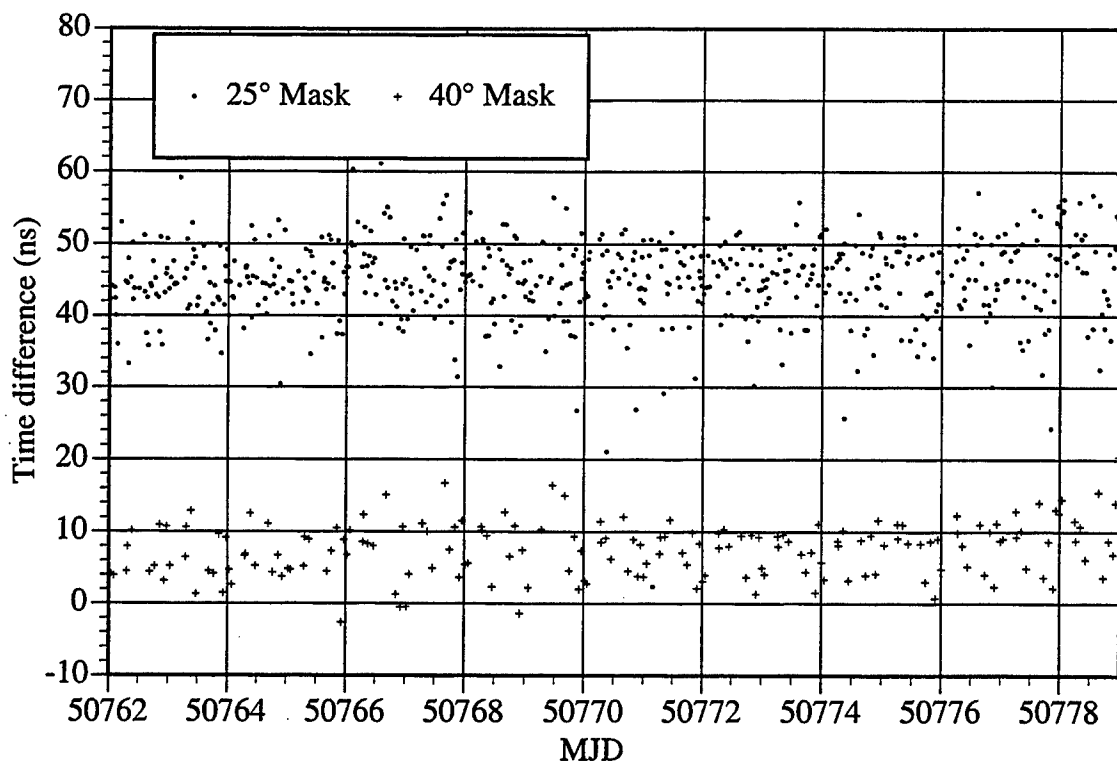


Figure 7: Time series data for the zero-baseline experiment. Individual series are shifted vertically for clarity. One outlying point was removed from the 25° data.

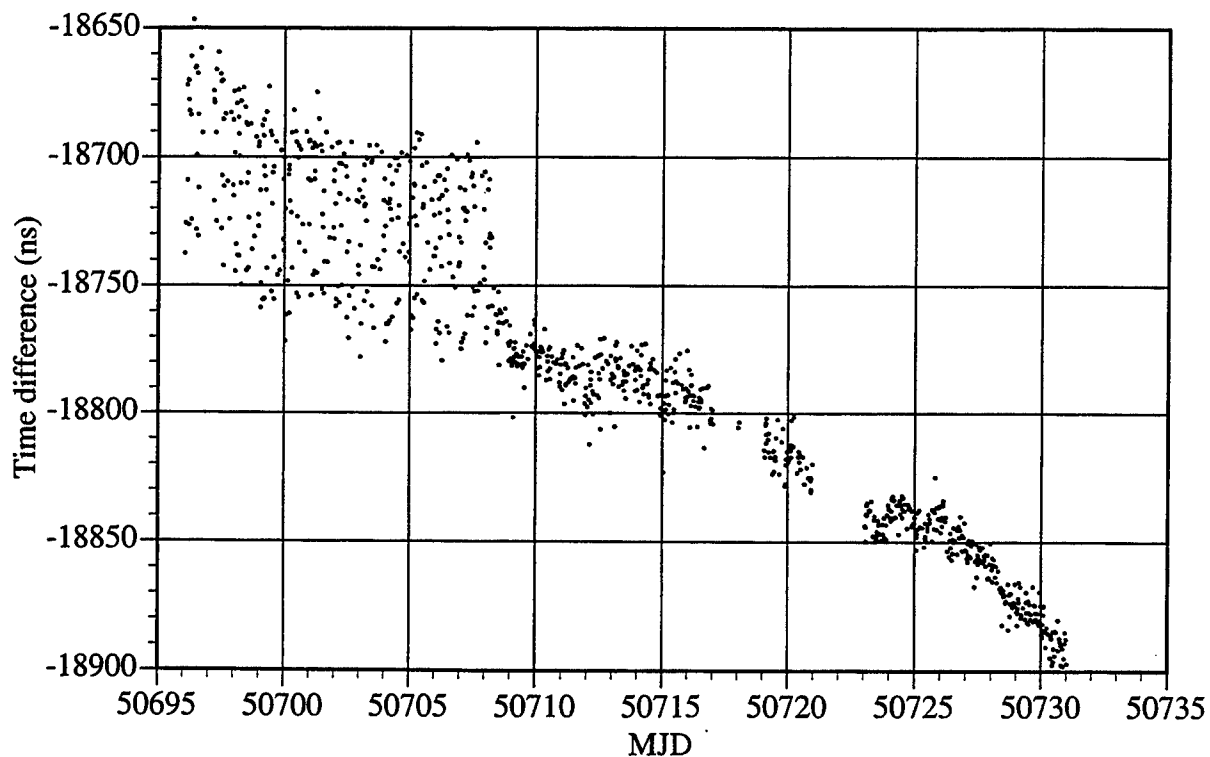


Figure 8: Time series data for the NML-MSL link, showing the effect of an 8 m horizontal error in the coordinates of the NML antenna. The error was corrected on MJD 50708. The elevation mask angle was 25°.

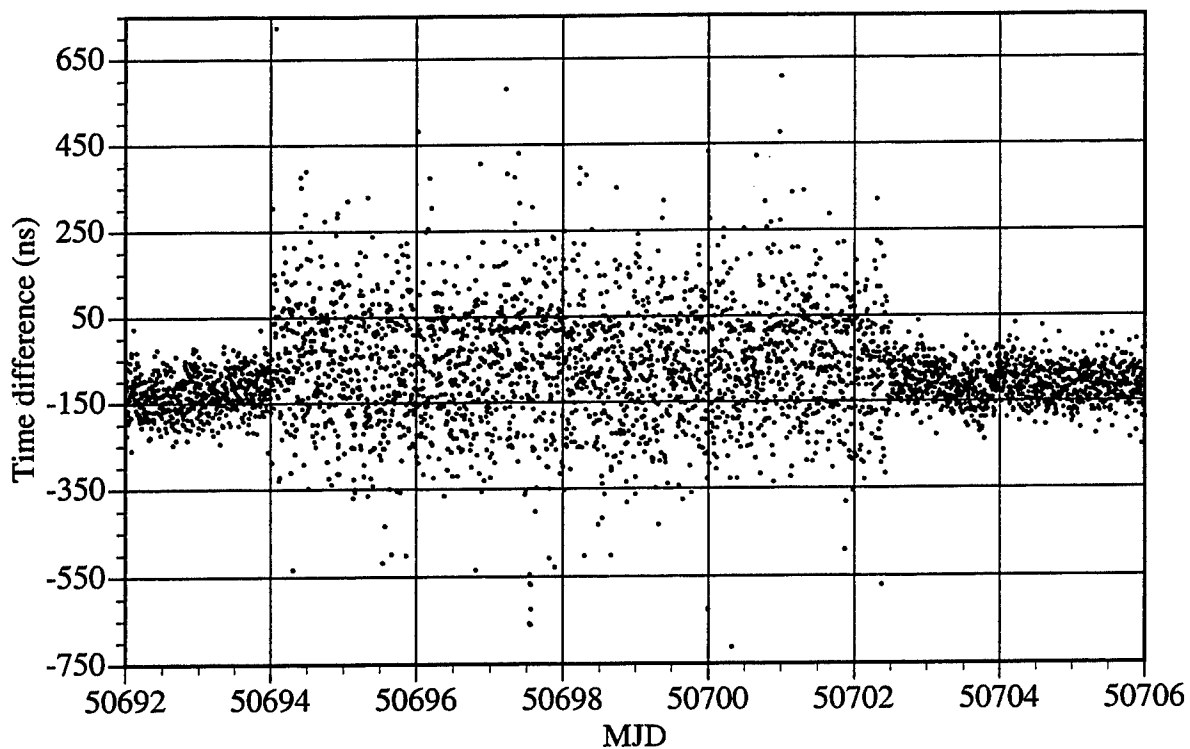


Figure 9: Time series data for the output of the “Totally Accurate Clock” (TAC) against UTC(Aus) at Orroral. The data points are separated by 5 minutes, and no averaging was performed. From MJD 50694 to 50702 the TAC was self-navigating, otherwise its internal coordinates were fixed at their ITRF-94 values.

ON IMPROVEMENTS OF AND SUGGESTIONS ABOUT GPS “COMMON VIEW” WITH MULTICHANNEL TIME RECEIVERS - FIRST RESULTS

J. Hahn and H. Nau

DLR, Institut für Hochfrequenztechnik
Postfach 1116, D-82230 Oberpfaffenhofen, Germany
joerg.hahn@dlr.de, hartmut.nau@dlr.de

P. Moussay

BIPM Section du temps
pavillon de Breteuil, F - 92312 Sèvres Cedex, France
pmoussay@bipm.fr

Abstract

At present time the international timing community has access to multichannel GPS and GLONASS time receivers. This new generation of time receivers offers a great potential to time users and timing labs can benefit from. One advantage is the continuous monitoring of the satellite clocks with the possibility for easy implementation of an international tracking schedule which need not be updated. Otherwise the user can perform study work in changing various processing parameters. If one uses high rate data (i.e. at one-second sample rate), investigations can be done in much more detail. This also leads into application of carrier phase observable if the receiver is capable for such measurements.

In this paper we give first results of "Common View" clock synchronization between DLR and BIPM using AOA TTR-4P GPS time receivers with GGTS data format version 1 output. Due to repeated problems with the BIPM receiver, NPL supported us with corresponding data files. C/A-code measurements have been analyzed and compared to data with usual one-channel receivers. Both results have been analyzed in view of precision and availability of synchronization data. Recommendations will be given for application of multichannel receivers for clock synchronization. It will be concluded that such receivers will certainly have a large impact for future clock synchronization, and far more investigation work is still required.

INTRODUCTION

The GPS "Common-View" method is the routine operation to make worldwide accurate clock synchronization successful. Also GLONASS offers such possibilities, and some labs are investigating this method to be established as a tool for the timing community [1].

The "Common View" method as implemented with conventional one-channel C/A time receivers, has some drawbacks which could be summarized here:

- A dedicated tracking schedule has to be implemented for each Earth's region;
- The need to update the tracking schedule twice per year (due to orbit satellite orbit changes /drifts);
- Only pseudo-range data are available (no carrier phase measurement);
- Ionospheric delay measurements are usually unavailable;
- Most of present receivers have a very limited memory (no real-time offload to a PC etc.) resulting in user made restrictions.

Now, new multichannel GPS time receivers and geodetic multichannel GPS receivers modified for time applications are available. The Allen Osborne Associates (AOA) TTR-4P GPS time receiver is one of them and will be studied in this work. This paper we will mainly refer to "Common View" and "stand-alone operation" application.

The TTR-4P is an enhancement of the Turbo Rogue GPS receiver architecture that was developed at the Jet Propulsion Laboratories (JPL) under the NASA Geodynamics Program [2]. The goal was to provide a field-worthy geodetic receiver with accuracy to suit the most demanding applications. The TTR-4P was jointly developed by AOA and JPL for missions requiring GPS data of very high precision and accuracy. Prospective applications included: geodesy, crustal dynamics, orbit determination for Earth satellites, time synchronization, ionospheric calibration for deep space navigation, atmospheric pressure and temperature modeling using atmospheric occultations and attitude determinations for dynamic platforms. The receiver tracks up to eight satellites simultaneously while measuring the pseudo-ranges and phase delays from L1-C/A, L1-P, and L2-P signals. The hardware and software employ unique signal processing techniques to extract accurate group delays which exhibit sub-centimeter level systematic errors (excluding antenna and multipath) when two or more satellites measurements are differenced. Phase measurements also provide a high degree (sub-millimeter) of accuracy and precision. A dual cross-band dipole antenna mounted to a choke ring backplane reduces multipath interference. It works with a 32 bit RISC processor.

As with the original Rogue, the TTR-4P can extract differential group-delay (P2-P1) and phase (L1-L2) with P-code encryption (A-S) on or off. Full P-code tracking provides highest precision phase and pseudo-range measurements and is the default tracking mode. Whenever the receiver discovers that a GPS satellite has encrypted its P-Code, P-codeless tracking is the automatic fall-back mode. This mode is not entirely codeless, since the receiver continues to track the C/A code normally. The receiver takes advantage of the fact that both L1 and L2 have the same P-code modulation / encryption. Because each carrier has identical modulation, the L1 signal can be cross-correlated with the L2 signal, resulting in both differential phase measurements (L1-L2) and group delay measurements (P1-P2). In P-codeless mode, L1-C/A code and carrier phase data as well as P-codeless data are output at a maximum rate of once per second.

The CCDS Sub-GROUP on GPS and GLONASS Time Transfer Standards (GGTTS) data format version 1 is a standardized format for both data format and data reduction procedure [3]. This format requires a specific output file for each observation channel. Some expectations of even available multichannel operation are:

- The only adjustment made to the GGTTS data format is that instead of putting the observations of each channel in individual files, all results of all channels are output in the same file;
- Thus, when using a common tracking reference date, all receivers world-wide track at the same time all visible satellites in their area. Therefore, any specific tracking schedule is included in the observations;
- Due to the multichannel output at one epoch the data can better match to different tracking schedule partitions for other regions of the Earth (increase of suitable data points);
- An improvement of accuracy for various applications is expected, even for a stand-alone application where noise due to SA-effect is reduced by the square root of the number of simultaneous observations (but there is a certain level where SA-noise cannot be further reduced !).

EXPERIMENTAL SETUP

The setup of the DLR Oberpfaffenhofen TTR-4P station in its branch Weilheim consists of the reference clock CH1-75 (1 pps & 5 MHz), an active H-maser (equal to UTC(DLR)) of the Russian company Kvarz. The antenna position had been determined during a PRARE campaign [4].

The setup looks similar at BIPM site (here Cs-clock Cs(BIPM)). At both sites also an one-channel GPS time receiver has been used, at DLR a TTR6, at BIPM a Sercel NRT1. Both are running with the common BIPM GPS tracking schedule. The overall setup is given in Fig. 1.

Due to some problems with the TTR-4P situated at BIPM another site was involved later: NPL (TTR-4P, TTR5A, Sigma Tau active H-maser - UTC(NPL)). This does not change the general procedure and we will refer to these data below.

SOFTWARE MATTERS

It should be pointed out here again, that we were studying the application point of TTR-4P for time transfer purposes as available presently. Concerning internal receiver details excellent work has been done by our BIPM colleagues [5].

Both DLR and BIPM used different software versions for TTR-4P. BIPM was operating with version 3.0.34.3 whereas DLR's receiver was delivered with the newer version 3.0.34.4 which outputs directly data in GGTTS format. This makes post-processing much more easier compared with the procedure for the older version. Also, the sample rate and other things are more standardized, which is a need even for a worldwide implementation in the timing community.

To the knowledge of the authors to date DLR seems to be the first company running TTR-4P with the new S/W version. This S/W is designed to operate the TTR-4P as a timing receiver [6]. It operates the system as a "stand-alone" unit or in the "Common-View" mode. The program formats data output into the GGTTS format and saves it on flash card from "Common-View" operation. It should also output timing information in real time for stand-alone operation.

In stand-alone operation an accuracy is specified by 60 ns and 10 ns with and without SA respectively. By using "Common-View" data, some systematic effects are removed and the accuracy is specified to be typically at 3 ns RMS with or without SA.

A special CLOCK mode is introduced for obtaining timing information from a known location. One can enter the position or determine it applying FIXED mode. In CLOCK mode the S/W tells the receiver to accept the position as completely accurate and change the times to match the pseudo-range from that location. From this also follows that if position is in error, it will not be possible to track satellites.

The default parameters in Tab. 1 are implemented in CLOCK mode (S/W 3.0.34.4), the same parameters were introduced in the receiver running the S/W 3.0.34.3.

Parameter	setting
Site type	CLOCK
Elevation Mask	20.0
Half Life	0.0 min
Nav Hlth	apply
Rf hlth	ignore
Ionosphere Mode	model
RAIM	on protect
Data bit checking	on

Tab. 1: Default parameters in CLOCK mode

The sample rate must be set to 1 sec to be compatible with GGTTS tracking mode. Ref-1pps delay can be set, also a antenna cable delay, receiver time delay (from manual), a 1 pps output delay. Some header information can be entered so as class, comm, frame, ims, lab, rcvr, ref. GGTTS data format can be logged by using the AUX port.

In CLOCK mode the receiver logs the data in one-second measurements. These data will be collected in 16 minute intervals from the entire 24 hour period. The collection takes place from minute 2 to minute 15 (780 sec), and there is a three-minute break before the next interval begins [6]. It is necessary to set the time to begin the process so that it will match data taken from other receivers. At the end of the 24-hour period, the start time will be automatically increased by 23 hours and 56 minutes. This makes the data collection keep pace with other BIPM data type units.

In the S/W all parameters can be changed too which allows a large flexibility at the application site, but it also offers some drawbacks as different sites may not measure in the same way what degrades or influences the results.

In this study only "standard GGTS data" were taken at DLR and BIPM site.

"SHIFTED COMMON VIEW"

A problem occurred later by starting to process additional NPL data. This should be explained here. While starting to process the data, a time shift of 18 sec between DLR and the NPL TTR-4P data blocks has been noticed. This 18-sec shift is due to the fact that NPL runs its TTR-4P in 30-sec sample rate. The first versions of TTR-4P software did not accept 1 sec as a sample rate: it had to be multiples of 10 sec. This means result lines are dated HH:MM:SS and HH:MM:30 GPS time and since there is a 12-sec difference between UTC and GPS presently the result lines are dated HH:MM:48 and HH:MM:18 UTC in the data file. Doing such a "Common-View" processing we have to speak about a "Shifted Common View". This is for sure an inconvenience at this point.

The same problem occurred processing BIPM data from the Sercel NRT1 receiver. The track times are 12 seconds apart from DLR (HH:MM:00) standard times because the receiver uses GPS time dates to start and stop tracking. This results also in a "Shifted Common-View" processing.

In preliminary discussion with USNO about long baseline comparisons the same feature could be observed. Their receiver has a sample rate of 10 sec and GGTS data format is spit out with HH:MM:08 data lines.

We can see here a problem for global clock comparisons in view of standardization which should be simply avoided in future !

OVERALL OBSERVATION PERIOD BETWEEN DLR AND BIPM WITH TTR-4P

First we want to give an overview of all data taken for comparison between DLR and BIPM. In Fig. 2 and Fig. 3 the recorded data block (local clock) - GPS is presented, whereas Fig. 4 gives the "Common-View" result. The result looks strange due to different problems at both sites. The reason will be explained here. Three phases could be identified after some analysis:

- I. from MJD 50699 till 50706.8: problems at DLR site with PRN15,
- II. from MJD 50707 till 50708.4: the only time a normal operation was achieved,
- III. after this period the BIPM receiver failed completely (problems with 4 receiver channels).

ABSOLUTE SYNCHRONIZATION WITH TTR-4P

We analyzed the capability of the TTR-4P to compare the local reference to a dedicated physical clock at a satellite and to GPS time. The result is presented in Fig. 5 till Fig. 7 for PRN22 with respect to DLR site, RMS values 45 ns and 44 ns for clock and GPS time monitoring respectively (linear regression). For GPS time monitoring the noise is mainly due to the SA. In Fig. 8 till Fig. 10 PRN15 is in analysis. It has

to be mentioned here, what has been noted during the processing, that as soon as the TTR-4P at DLR tracks PRN15 all measurements are degraded (cf. Fig. 4). This is supposed to be a S/W bug ! The RMS values are 31 ns (!) and 27 ns for clock and GPS time monitoring respectively (linear regression). After MJD 50707 PRN15 has been deselected in DLR to overcome this problem.

In Fig. 11 till Fig. 13 the BIPM site tracking for PRN15 is shown for comparison, RMS values 155 ns and 6 ns for clock and GPS time monitoring respectively (linear regression).

"MULTIPLE COMMON VIEW" WITH TTR-4P BETWEEN DLR AND BIPM

For this time period the "Common-View" result is shown in Fig. 14. Significant errors occur during periods of PRN15 visibility/reception at DLR site. From MJD 50707 PRN15 has been deselected at DLR's receiver, and the comparison as shown in Fig. 15 worked well: RMS 3.2 ns, rate 6.6 ns/d.

The "Shifted Common View" feature was not obtained in this case, because BIPM has modified its software to track in 1-sec sample rate.

CONVENTIONAL "COMMON VIEW" BETWEEN DLR AND BIPM

A "Shifted Common View" with one-channel receivers has been made between DLR and BIPM (TTR5, NRT1). The result for MJD 50692 till 50721 is given in Fig 16, RMS 4.4 ns, rate 8.4 ns/d. Partly problems occurred at DLR site (receiver lost/loses time?), and DLR only uses a partition of the international tracking schedule. Thus, the small number of data can be explained.

A discrepancy of about 30 ns can be obtained between multichannel and one-channel operation coming from calibration problems.

DATA FROM NPL

Due to the failure of BIPM receiver, we decided to ask our colleagues at NPL to support the analysis with NPL data (thanks John Davis). Thus, data have been sent to us and processed in a very similar way. GPS time monitoring at NPL site using PRN15 is given in Fig. 17, RMS 5 ns. It should be noted that the monitoring of PRN15 clock gave a RMS of 118 ns (BIPM 155 ns), and shows that the value of 31 ns at DLR was caused by a receiver error.

A "Shifted Common View" between DLR's and NPL's TTR-4P receivers is presented in Fig. 18 with a RMS of 4.1 ns, rate 9.4 ns/d. A systematic effect is clearly visible; maybe this comes from the "Shifted Common-View" mode or other uncertainties not compensated. Also, a conventional "Common View" has been made. This is shown in Fig. 19, RMS 7.4 ns, rate 9.7 ns/d. The rare data number is caused by the same problems as explained above. NPL told that the TTR-4P data are offset by "around" 39 μ s. Considering this approximate input, a calibration discrepancy of about 140 ns still remains, but the rates do agree well.

CONCLUSION: PROBLEMS AND RECOMMENDATIONS

Some problems are summarized here:

- The new S/W (3.0.34.4) has a bug in view of PRN15 reception which causes bad data for all other measurements during reception of this satellite;
- With the new S/W version (3.0.34.4) the receiver seemed to be not stable in long term. At DLR a need to touch the receiver's console from time to time has been discovered, otherwise the receiver hung up ("Tamagoshi"-like behavior);
- In the S/W 3.0.34.4, the RINEX observable data could not be downloaded neither in DLR or in BIPM where this version has been briefly tested. Thus, no frequency comparison using carrier phase can be done;
- In the new S/W (3.0.34.4) no mode guarantees a strict operation according to the Technical Directives [3]. For instance, the present CLOCK mode parameters can be modified by the user (i.e. sample rate, ionospheric model, etc.), with the consequence that similar operation at different sites are not assured;
- No ready manual is available; up to now the old document from S/W 3.0.34.3 has to be used, plus a very drafty version from the new S/W [6];
- The start-up procedure is not optimized. In (default) CLOCK mode the receiver did not track although accurate position data have been used. Thus, first the sample rate had to be increased to 10 sec, and the navigation parameters "position and clock" changed to be "close". After the receiver starts to track satellites and has been synchronized the sample rate must be set to 1 sec and "position and clock" to "good";
- In the new S/W (3.0.34.4) the start time is not attached to a particular date, so it is difficult to check if the start time introduced is the correct one;
- In the new S/W (3.0.34.4) some entries can only be made by means of a terminal (i.e. start time);
- In the S/W (3.0.34.3) the ionospheric model and measurements are not available simultaneously (only one or the other);
- According to the used sample rate, only "Shifted Common Views" may be possible.

This results in the following recommendations on the TTR-4P receiver:

- The S/W (3.0.34.4) is going in the right direction especially by making model and measured ionospheric measurements available at the same time. But its use cannot be recommended until the PRN 15 bug is corrected, the RINEX observable are downloadable, and a cold-start CLOCK procedure is possible;
- It would also be of interest to be able to input all settable parameters from the front panel, and to have an operational mode following strictly the recommendations expressed in the Technical Directives [3];

and the method:

- Use of a reference date to keep multichannel "Common-View" observations coherent with classical

"Common-View" schedules;

- Ensure 1-sec sample rate at all labs and "HH.MM:00 data lines" or any other recommended in the Technical Directives [3], and do not "shift" the "Common Views".

Multichannel "Common View" is a very promising technique, and more investigation work is needed, using reliable hardware and bug-free software for "Multiple Common View". The use of high rate data in form of carrier phase observable should bring an improvement in the accuracy of measurements.

REFERENCES

- [1] W. Lewandowski et al., GLONASS TIME TRANSFER AND ITS COMPARISON WITH GPS, proc. 11th EFTF, March 1997, pp. 187-193
- [2] User Manual TTR-4P GPS Receiver, March 1994, Allen Osborne Associates
- [3] D. W. Allan and C. Thomas, Technical Directives for Standardization of GPS Time Receiver Software, Metrologia, 1994, 31, pp. 69-79
- [4] Hahn, J., Bedrich S, "Common View" Clock Synchronization of Remote Atomic Clocks using GPS and PRARE onboard ERS-2, 10th European Frequency and Time Forum, Brighton, U.K., 5-7 Mar 96, Proc.: EFTF'96, Conf. Publ. 418, pp. 393 -398
- [5] G. Petit, Use of TTR4P data for sub-nanosecond time transfer, personal communication, October & September 1995
- [6] J. Holston, User Manual TTR-4P GPS Receiver, draft pages, Allen Osborne Associates, personal communication, 22 May 1997

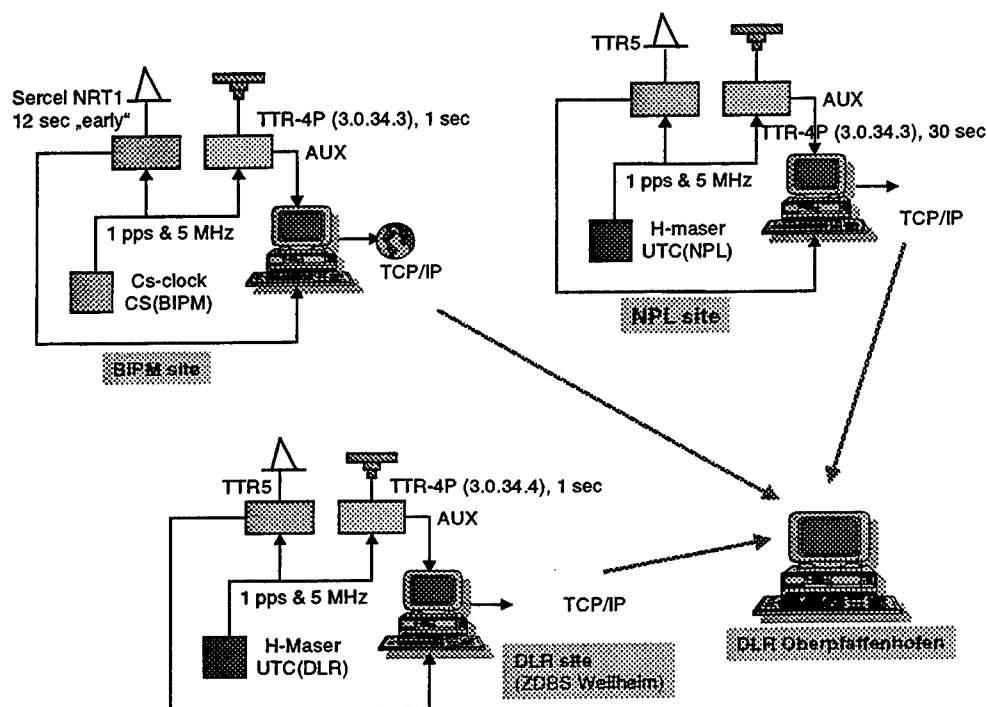


Fig. 1: Overall experimental setup

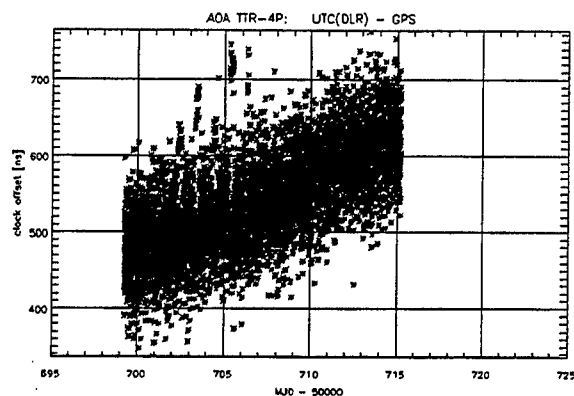


Fig. 2: GPS time reception at DLR site over all satellites with TTR-4P, RMS 47 ns

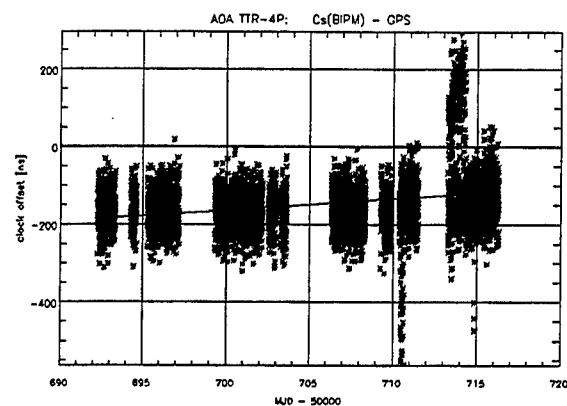


Fig. 3: GPS time reception at BIPM site over all satellites with TTR-4P

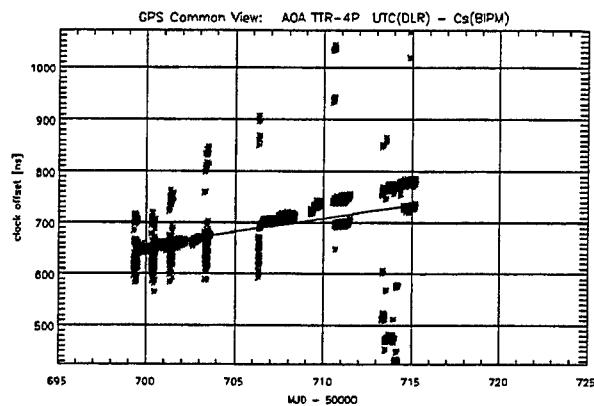


Fig. 4: GPS "Shifted Common View" between DLR and BIPM with TTR-4P over whole experimental period

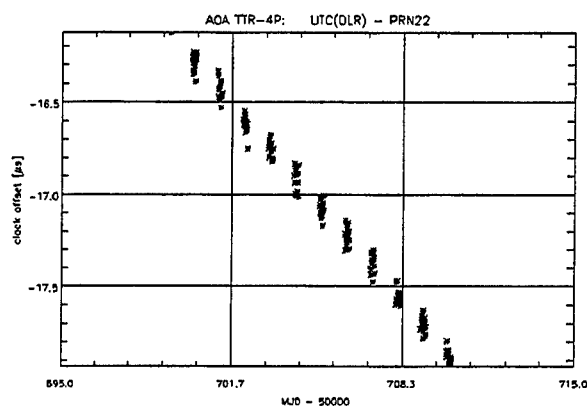


Fig. 5: PRN22 clock monitoring at DLR site with TTR-4P

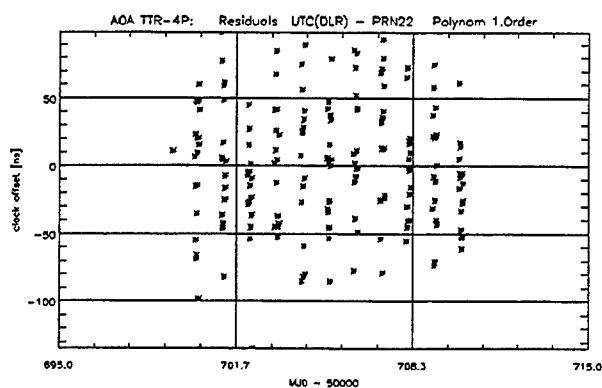


Fig. 6: Residuals of PRN22 clock monitoring at DLR site, RMS 45 ns

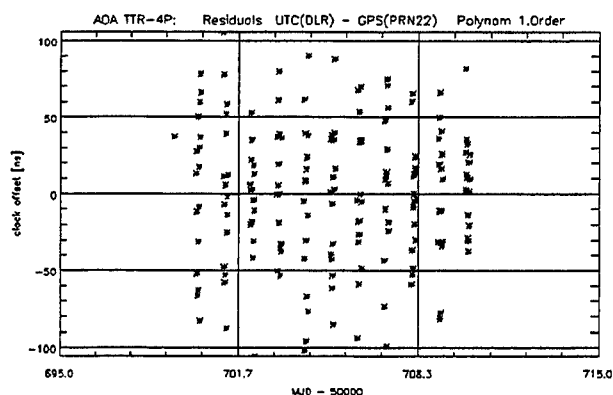


Fig. 7: Residuals of GPS time monitoring at DLR site using PRN22, RMS 44 ns

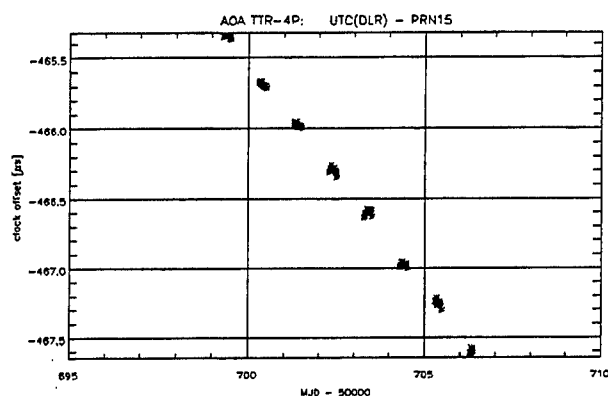


Fig. 8: PRN15 clock monitoring at DLR site with TTR-4P

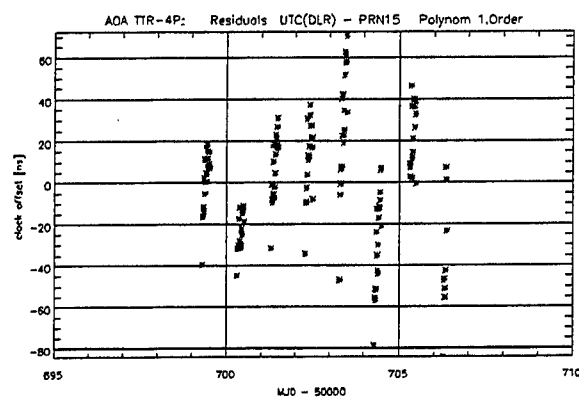


Fig. 9: Residuals of PRN15 clock monitoring at DLR site, RMS 31 ns

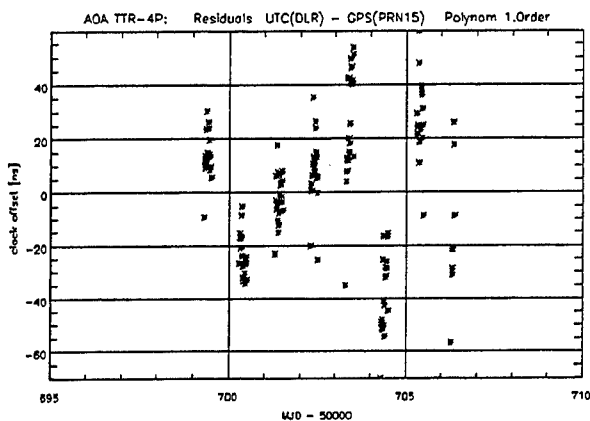


Fig. 10: Residuals of GPS time monitoring at DLR site using PRN15, RMS 27 ns

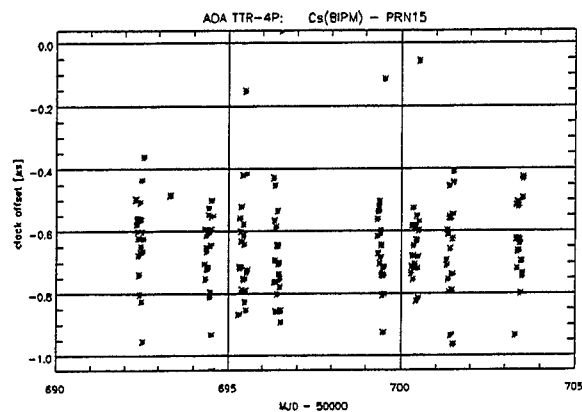


Fig. 11: PRN15 clock monitoring at BIPM site with TTR-4, RMS 155 ns

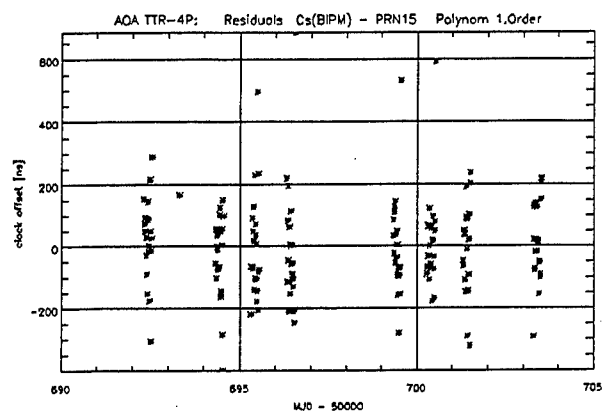


Fig. 12: Residuals of PRN15 clock monitoring at BIPM site, RMS 155 ns

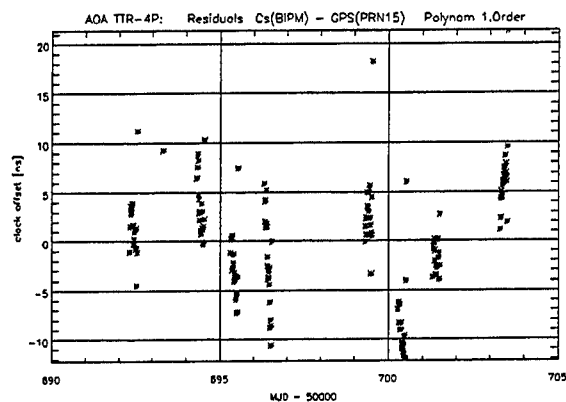


Fig. 13: Residuals of GPS time monitoring at BIPM site using PRN15, RMS 6 ns

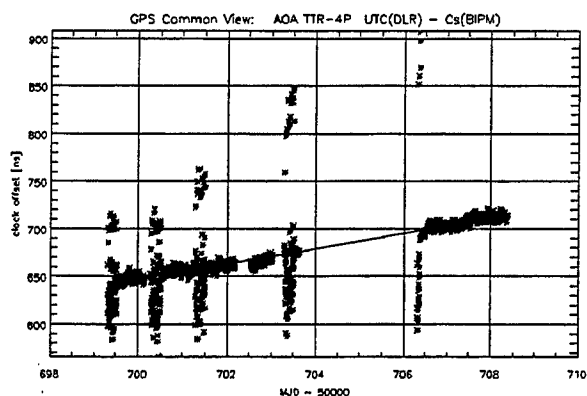


Fig. 14: GPS "Common View" between DLR and BIPM with TTR-4P over period with PRN15 problems at DLR site

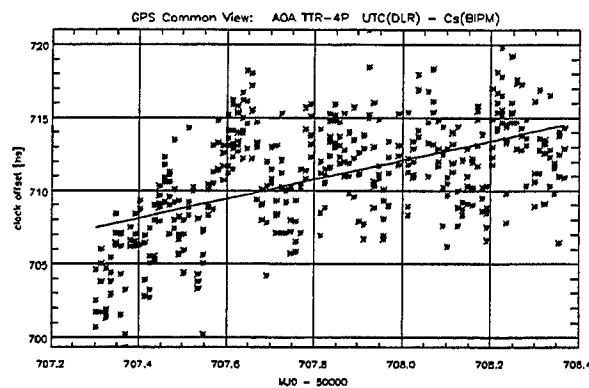


Fig. 15: GPS "Shifted Common View" between DLR and BIPM with TTR-4P over period with good data at both sites, RMS 3.2 ns

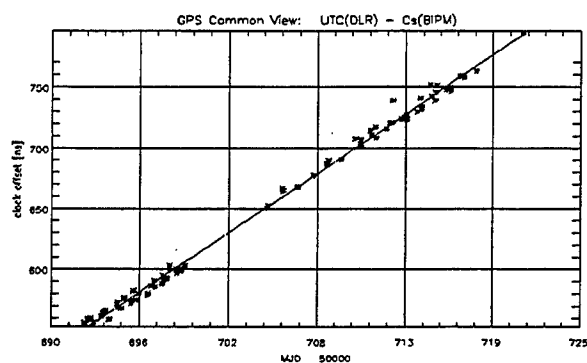


Fig. 16: Conventional GPS "Common View" (but also "Shifted" by 12 sec) between DLR and BIPM with one-channel receivers, RMS 4.4 ns

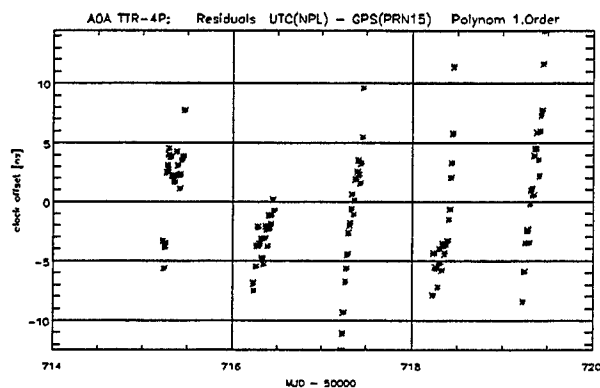


Fig. 17: Residuals of PRN15 clock monitoring at NPL site, RMS 5 ns

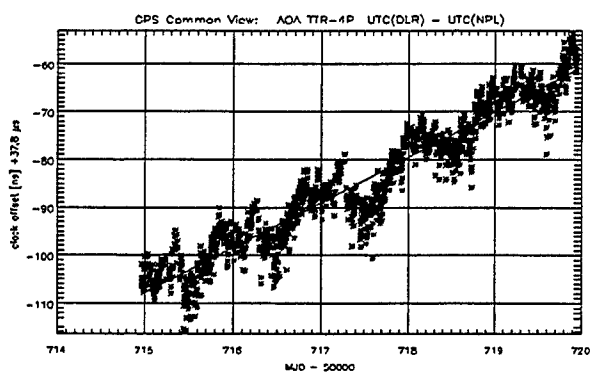


Fig. 18: GPS "Shifted Common View" between DLR and NPL with TTR-4P over period with good data at both sites, RMS 4.1 ns

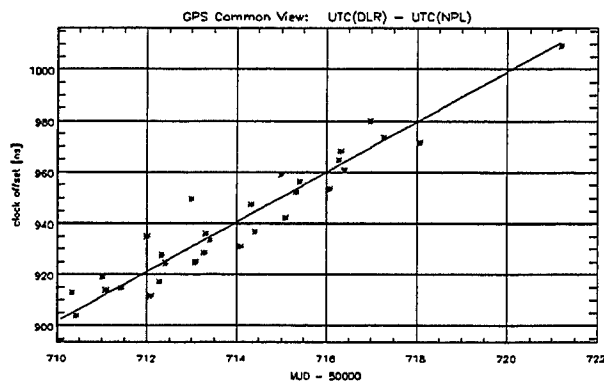


Fig. 19: Conventional CV between DLR and NPL, RMS 7.4 ns

Questions and Answers

ROB DOUGLAS (NATIONAL RESEARCH COUNCIL OF CANADA): There have to be questions after three papers like these, so I will try my hand at getting the flow going. One of the exciting things about a multi-channel receiver used in this mode is the very careful effort that manufacturers have put into having different channels calibrated, one with respect to the other. I am wondering if any of the three paper presenters has a comment on the use of these channels for timing calibration of the entire system by injecting a satellite simulator signal.

JOERG HAHN (DLR, INSTITUT für HOCHFREQUENZTECHNIK): My comment: What I have not shown here in this presentation, is the comparison of our results with a one-channel common-view operation, which is shown in the paper. We had some discrepancies in the order up to 120 nanoseconds compared to the conventional common views. But, of course, we need to consider what each channel has in calibration delays, and we are changing. In the meeting on Monday, we had the good proposal which could be done to track one satellite on several channels of the receiver. This could be a very good method of differential calibration between the receiver channels. But this is a matter for the software. Maybe Allen Osborne Associates could do something about this.

ROB DOUGLAS: Do the other two authors have a comment on calibrations?

MIHRAN MIRANIAN (USNO): I was going to say the same thing, that the simple way to do it would be to just track one satellite on all channels. Then you could immediately determine the inter-channel biases, if there are any, and correct for them.

ROB DOUGLAS: My perspective on this that I am going to inflict on you is that the calibration that I think is important is a calibration of all the filters and everything in the system. So absolute calibration, I think can be handled much better by multi-channel than by single-channel receivers. We are a long way from doing that, but maybe not as long a way as we think.

JUDAH LEVINE (NIST): I think, in many cases, a multi-channel receiver does not really have completely separate channels. So very often the many channels are implemented in the digital processing, whereas the analog system, the RF system is common. The result is that there are not eight filters to deal with, there is only one filter; the rest of it is just digital signal processing, and it is not quite as hard as you think.

The second thing is that there is a real difference between a receiver like the TTR-4P and a receiver like the Motorola Oncore because in the TTR-4P the same satellite will often come up in a different channel in a subsequent second. The result is that it is not true that if you are tracking Satellite Number 12, initially in the first channel it stays in the first channel for its entire time that you see it; sometimes it appears in another channel. You can keep track of that, but if you do not, you have lost it. Whereas, in a receiver like the Motorola Oncore, so far as we know, the satellite always stays in the same channel. Therefore, trying to do calibration, in a TTR-4P, is a very much more complicated business because of the fact that the satellites jump around among the channels.

JOERG HAHN: I have also solved this problem, it runs a display and quite rapidly.

JUDAH LEVINE: I do not think it is a problem. I think it is viewed as a feature.

JOERG HAHN: Maybe.

A NEW APPROACH TO COMMON-VIEW TIME TRANSFER USING 'ALL-IN-VIEW' MULTI-CHANNEL GPS AND GLONASS OBSERVATIONS

J. Azoubib¹, G. de Jong², J. Danaher³, W. Lewandowski¹

¹Bureau International des Poids et Mesures, Sèvres, France

²NMi Van Swinden Laboratorium, Delft, the Netherlands

³3S Navigation, Irvine, California

Abstract

The combined use of GPS and GLONASS for international time and frequency transfer is feasible despite differences between the two systems. The use of two systems in multichannel mode increases the number of observations by a factor of 20 in comparison to a one-channel one-system mode. This results in an improvement in frequency comparisons. Specially designed receivers for GPS + GLONASS multichannel time and frequency comparisons are described and some initial results are provided.

INTRODUCTION

For the past fifteen years international time transfer has been carried out using one-channel C/A-code GPS receivers and an international common-view schedule of standard 13-minute tracks [1]. Because older receivers have limited memory, no more than 48 tracks per day can be programmed; in practice, however, the useful number is even smaller. For regional time comparisons, within 1000 km, about 40 tracks are usually available, and for intercontinental distances about 10. At present, the estimated uncertainty of operational GPS time transfer is several nanoseconds for a single common-view observation and a few nanoseconds for a daily average, which corresponds to a few parts in 10^{14} in terms of frequency transfer. This performance is barely sufficient for the comparison of current atomic clocks and needs to be improved rapidly to meet the challenge of the clocks now being designed.

For this reason the timing community is engaged in the development of new approaches to remote clock comparison. Among them is the development of multichannel two-system C/A-code GPS and GLONASS receivers, and multichannel P-code GLONASS receivers.

The multichannel C/A-code receivers considered here observe all GPS and GLONASS satellites in view, 'all-in-view' operation, and use standard 13-minute tracks at the standard hours. At present, the standard hours are defined every six months by BIPM international common-view tracking schedules. Instruments which use the 'all-in-view' procedure necessarily observe the international schedule. This greatly simplifies

their parallel introduction into the present system of one-channel observations. In the future, a fixed reference date, adopted by convention, will set standard hours permanently.

Although, in theory, up to 12 GPS or GLONASS satellites can be observed simultaneously, only about five satellites are observed above 15° (and thus are of interest for time transfer) for each system at an average urban site. As there are 89 useful 16-minute periods in a day, 89 tracks may be observed in each channel. Using all available observations above 15° (about five per 16-minute period), we may therefore observe 445 tracks per day for each system, and 890 for two systems. All these tracks may be used for regional common-view links. For very large baselines, between continents, 160 to 200 common-view tracks for two systems may be available using a multichannel approach. The increase by a factor of twenty in the number of common views in the GPS + GLONASS multichannel approach relative to the one-channel-one-system mode, makes it possible to expect a consequent improvement in the quality of time transfer. Such observations, however, may be subject to systematic variations, mainly caused by environmental effects on the receivers.

In the trial comparison described in this paper, between the BIPM and the VSL and using 'all-in-view' GPS + GLONASS C/A-code measurements, we had about 605 useful observations per day. As the GLONASS constellation at the time of the experiment comprised 15 satellites instead of 24, this number is less than that quoted above, but still increased the number of tracks by a factor of about 15. A consequent improvement in the frequency comparison was expected.

Although GPS and GLONASS have some similarities, they also differ in many respects. We describe how these differences were overcome to allow the simultaneous use of the two systems for international time and frequency transfer.

TIME REFERENCES

One major difference between GPS and GLONASS is that they use different references for time. For its time reference, GPS relies on UTC(USNO), Coordinated Universal Time (UTC) as realized by the USNO. GLONASS relies on UTC(SU), UTC as realized by Russian Federation. The deviation of UTC(USNO) and GPS time (modulo 1 s) from UTC generally remains within a few tens of nanoseconds. This is not the case for Russian time scales (see Figure 1).

Following a recommendation on the coordination of satellite systems providing timing, adopted by the Comité International des Poids et Mesures (CIPM) at its 85th meeting held in September 1996 [2], the Russian Federation agreed to improve the synchronization of its time scales with UTC. On 27 November 1996 a time step of 9000 ns was applied to UTC(SU) in order to make it approach UTC. Next, on 10 January 1997, a frequency step was applied to GLONASS time to adjust its frequency to be close to that of UTC(SU). This was followed by a time step in GLONASS time of about 35300 ns on 1 July 1997. Following these changes, Russian time scales differ from UTC by a few hundred nanoseconds. As GLONASS time is linked to UTC(SU) with an accuracy of 200 ns, it is linked to UTC with the same accuracy. Further adjustments of these two time scales with respect to UTC are expected. This development is an important sign of goodwill and understanding.

Because GLONASS TIME receivers are not calibrated absolutely, we know [*UTC - GLONASS time*] to an accuracy no better than several hundreds of nanoseconds. GPS receivers are absolutely calibrated and [*UTC - GPS time*], after application of corrections for GPS precise ephemerides and ionospheric measurements, is known with an accuracy limited to about ten nanoseconds, mainly because of SA. It

follows that GLONASS provides an average user with world-wide real-time dissemination of UTC, as produced by the BIPM, to an uncertainty no better than several hundreds of nanoseconds after the recent improvement of the synchronization between UTC(SU) and UTC. GPS does the same with uncertainty of several tens of nanoseconds.

Summing up, we note that persisting differences between Russian time scales broadcast by GLONASS and UTC affect real-time dissemination of UTC through GLONASS, and to some extent complicate the dual GPS + GLONASS navigation solution. However, this discrepancy does not affect common-view time transfer, because readings of the satellite clock vanish in the difference. Also, the lack of absolutely calibrated GLONASS receivers is easily overcome for common-view time transfer by differential calibration of receivers [3].

REFERENCE FRAMES

The CIPM recommendation cited above also specifies a basis for harmonizing the reference frames of global satellite navigation systems by asking for adoption of the ITRF, the internationally recognized ultra-accurate terrestrial reference frame. The GPS almost fulfils this recommendation as WGS 84 its reference frame, since its most recent improvement differs from the ITRF by no more than one decimeter. This is not the case for GLONASS as its reference frame, PZ-90, can differ from the ITRF on the surface of the Earth by up to 20 m. In addition, access to PZ-90 is in most places limited to several meters. This presents a difficulty when using both GPS and GLONASS in the most demanding time and frequency transfers. One possible solution to this problem is the adoption by time laboratories of a common accurate reference frame for GPS and GLONASS ground antenna coordinates, and for post-processed satellite precise ephemerides. Obviously the preferred frame is the ITRF. Laboratories engaged in the accurate GPS time transfer agreed already several years ago to express ground-antenna coordinates with centimetric uncertainties in the ITRF. A proposal that the ITRF should also be used for GLONASS time transfer was submitted to CCTF Subgroup on GPS and GLONASS Time Transfer Standards (CGGTTS) [4] and adopted at its last meeting in December 1997. For baselines of up to a few thousands of kilometers, there is no need to correct the broadcast satellite ephemerides but, for longer baselines, the use of post-processed precise ephemerides expressed in the ITRF frame is necessary. For GPS, such ephemerides are provided by the International GPS Service for Geodynamics (IGS). This is not yet case for GLONASS but, at the 7th IGS Governing Board Meeting in September 1997 in Rio de Janeiro, it was decided that an experiment, the International GLONASS Experiment (IGEX), should be conducted in the second half of 1998, its goal being to provide GLONASS precise ephemerides expressed in terms of the ITRF. If successful, this project could become a permanent service.

BRIEF DESCRIPTION OF GPS + GLONASS MULTICHANNEL TIME RECEIVERS

Already several major timing centers around the globe observe GPS and GLONASS in multichannel mode. All receivers are of type R-100/30, manufactured by 3S Navigation. These take the form of a 12-channel GPS + GLONASS C/A-code card, and two or more cards with GLONASS P-code channels. The number of GLONASS P-code cards can be increased. Four to six satellites of each of the two systems are usually observed simultaneously on the 12-channel C/A-code part of the receiver. Only one antenna is used by each receiver. The receivers are controlled by a PC and use a standard format, developed for the GPS common-view technique by the CGGTTS [5], adapted to suit two-system two-code multichannel observations [4]. For the GLONASS part the receivers use the standard formulae and parameters adopted for GPS. These receivers have operated correctly over long periods of time and no bugs have been identified in the

software. Their metrological quality have been confirmed by comparison with other GPS time receivers [3]. 3S Navigation has recently introduced a new GPS + GLONASS time receiver, an 18-channel C/A-code GNSS-300T.

GPS AND GLONASS COMMON-VIEW SCHEDULES VERSUS 'ALL-IN-VIEW' OBSERVATIONS

The BIPM issues GPS and GLONASS international common-view schedules for international time and frequency comparisons twice a year. They indicate to receivers which satellites to observe at which time. Times of observations are redefined for each new schedule in order to start 13-min tracks at 00 h 02 UTC of the reference date and continue at 16-min intervals. These times are decremented by 4 minutes each day, to account for the sidereal orbits. This procedure means that we can use 89 of the 90 16-min intervals each day, the 90th being sacrificed to allow the 4-min correction.

The multichannel GPS + GLONASS time receivers considered here observe all the GPS and GLONASS satellites in view, in standard 13-min tracks every 16 minutes at scheduled standard times. Obviously there is no need to tell these receivers which satellites to observe, as is done for one-channel receivers, because such an ensemble of 'all-in-view' tracks necessarily includes the international schedules. This greatly simplifies the parallel introduction of GPS + GLONASS multichannel time receivers into the present system of scheduled GPS and GLONASS one-channel receivers. A further simplification will be the use of a permanent reference day for standard times adopted by the CGGTTS. In this case, multichannel receivers will not have to be updated for standard times when international schedules are changed for one-channel receivers.

TRIAL COMPARISON

The time link between the BIPM and the VSL considered in this trial comparison has a baseline of 400 km. Both laboratories are equipped with R-100/30 receivers and their ground-antenna coordinates are expressed in the ITRF with an uncertainty of 0.3 m. The same coordinates were used for GPS and GLONASS (see above paragraph on reference frames). At both laboratories, receivers were connected to HP5071A clocks. For this study we used data covering roughly 10 days. Both receivers were calibrated using a portable R-100/30 receiver [3]. We observed a constant bias of 6 ns between GPS and GLONASS links. After this correction was applied, the GPS and GLONASS data could be mixed and we computed [*BIPM clock* - *VSL clock*] using GPS + GLONASS. Figures 2 - 6 compare the two clocks over a common period of time using the same receivers to establish different time links. Table 1 shows the number of common views available for each link.

The level of noise for the above links is about 3 ns. The unusual level of noise of about 7 ns obtained for the same links during previous study [6] is now known to have been caused by an error of 2.5 m in the differential coordinates between the two laboratories: this has now been corrected. Our current interest is to point out the advantage obtained by increasing the number of daily common views from 38, for the one-channel GPS link, to the 605, for the multichannel GPS + GLONASS link. A theoretical gain in stability of $(605/38)^{1/2} = 4$ is expected in the regions where white phase noise is preponderant. This can be seen on the stability curves of Figure 7 for averaging times of less than 10^4 seconds. Additional systematic effects are observed for averaging times above 10^4 seconds. These are probably linked to the environmental sensitivity of the antennas or of receivers themselves. This problem has already been resolved, at least partially, by stabilizing ground-antenna temperature [7]. Following this study the two R-100/30 receivers operating at the BIPM were equipped with 3S Navigation Temperature-Stabilized Antennas (TSA). A preliminary

comparison shows the removal of the systematic effects observed on Figure 7, and a fractional frequency stability of a few parts in 10^{15} for averaging times of about one day.

CONCLUSIONS

- This study confirms the feasibility of GPS + GLONASS multichannel time transfer. The dual-system multichannel and multicode receivers operate smoothly and no bugs have been found in the software. They use standard software and format. Comparison with other GPS time receivers provides a test of their metrological quality.
- Increasing the number of daily common views from 38 for a one-channel GPS link to 605 for a multichannel GPS + GLONASS link greatly improves the reliability of time transfer.
- A stability gain of 4 was observed between a one-channel GPS link and a GPS + GLONASS multichannel link for averaging times less than 10^4 seconds.
- Additional systematic effects were observed for averaging times above 10^4 seconds. These are probably linked to the environmental sensitivity of the antennas or of receivers themselves. Once these systematic effects are removed by thermal protection of the receiving equipment, multichannel GPS and GLONASS code measurements can provide, for integration times of one day, the frequency differences between the remote atomic clocks at a level of few parts in 10^{15} . This performance approaches theoretical possibilities of phase measurements and Two-Way Satellite Time Transfer.

REFERENCES

- [1] Allan D., Weiss M., 1980, "Accurate Time and Frequency Transfer During Common-view of a GPS Satellite", Proc. 1980 Frequency Control Symposium, pp. 334-346.
- [2] Comité International des Poids et Mesures (CIPM), 1996, Recommendation 1 (CI-1996), Report of the 85th Meeting, Tome 64, p. 145.
- [3] Azoubib J., de Jong G., Lewandowski W., 1997, "Determination of differential time corrections for multichannel GPS and GLONASS time equipment located at 3S Navigation, BIPM and VSL", Rapport BIPM-97/6, Part 1.
- [4] Lewandowski W., Azoubib J., Gevorkyan, A.G., Bogdanov P.P., Klepczynski W.J., Miranian M., Danaher J., 1996, "A Contribution To the Standardization of GPS and GLONASS Time Transfers", Proc. 27th PTTI Meeting, pp. 367-383.
- [5] Allan D.W. and Thomas C., 1994, "Technical Directives for Standardization of GPS Time Receiver Software", Metrologia, 31, pp. 67-79.
- [6] Lewandowski W., Azoubib J., de Jong G., Nawrocki J., Danaher J., 1997, "A New Approach to International Satellite Time and Frequency Comparisons: 'All-in-View' Multichannel GPS+GLONASS Observations", Proc. ION GPS-97, pp. 1085-1091.
- [7] Lewandowski W., Moussay P., Danaher J., Gerlach R., LeVasseur E., 1997 "Temperature-Protected Antennas for Satellite Time Transfer Receivers", Proc. 11th EFTF, pp. 498-503.

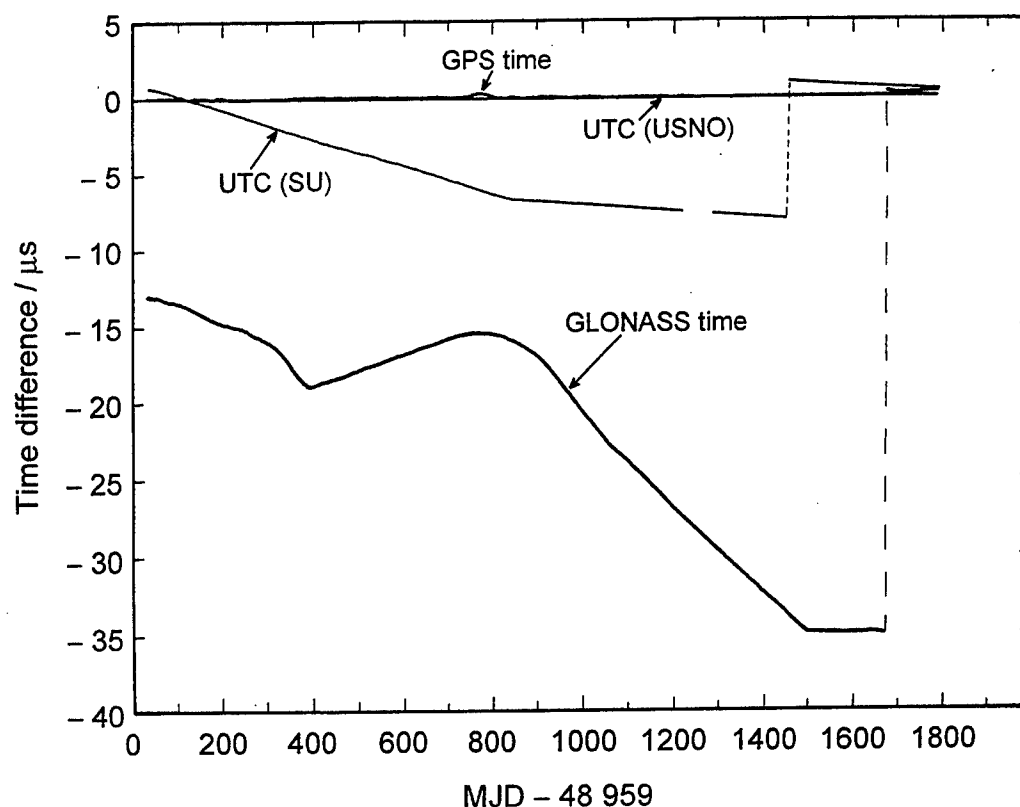


Figure 1: Deviation of UTC(USNO), UTC(SU), GPS time and GLONASS time from UTC from 3 December 1992 to 27 November 1997.

Table 1. Number of common views per day by different methods for [*BIPM clock - VSL clock*] comparison.

Method	Average number of common views per day	Average number of simultaneous common views
GPS one-channel	38	1
GLONASS one-channel	25	1
GPS multichannel	350	4.5
GLONASS multichannel	255	3.3
GPS+GLONASS multichannel	605	7.8

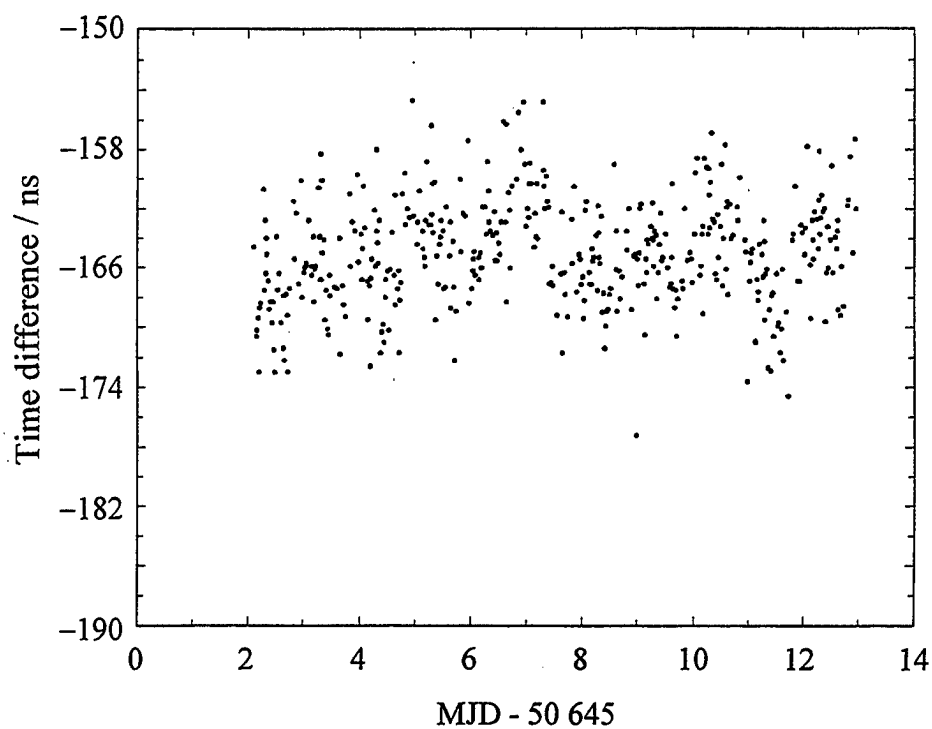


Figure 2. [*BIPM clock - VSL clock*] by one-channel GPS common views.

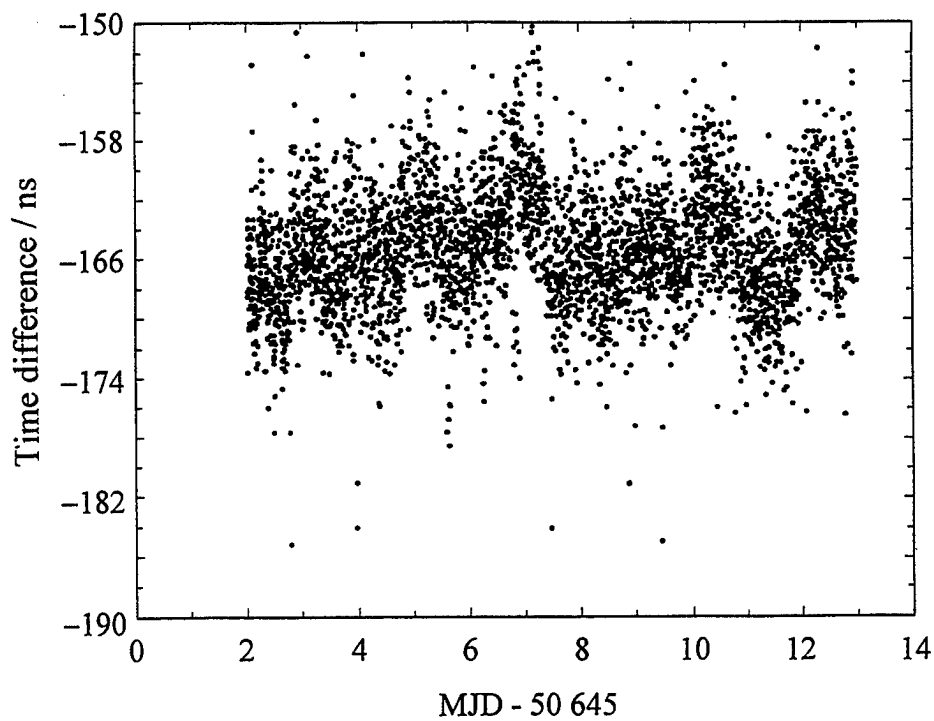


Figure 3. [*BIPM clock - VSL clock*] by GPS multichannel common views.

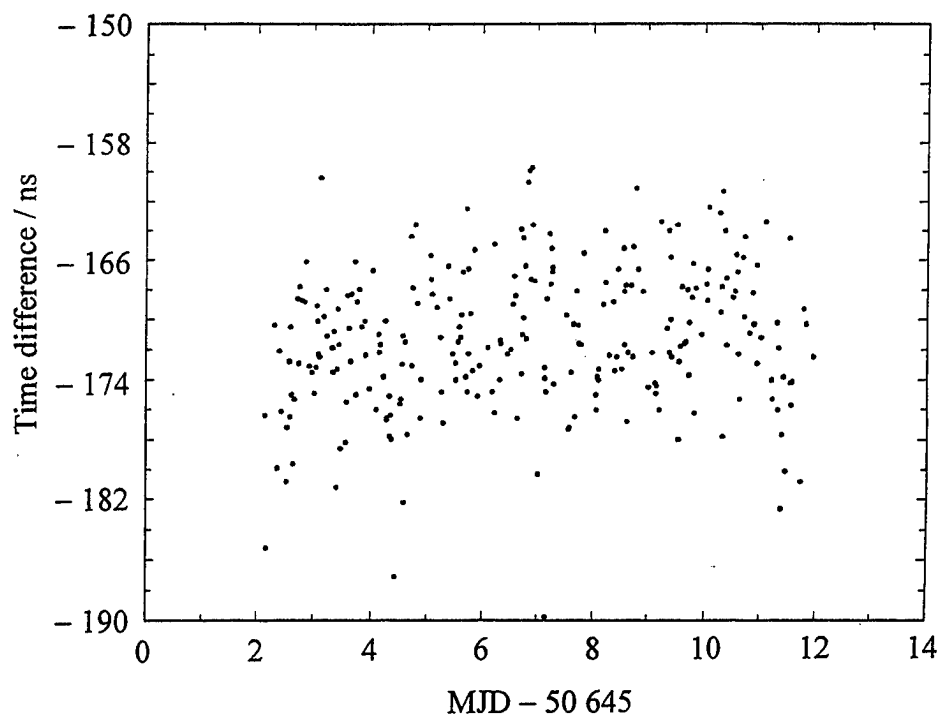


Figure 4. [*BIPM clock - VSL clock*] by GLONASS one-channel common views.

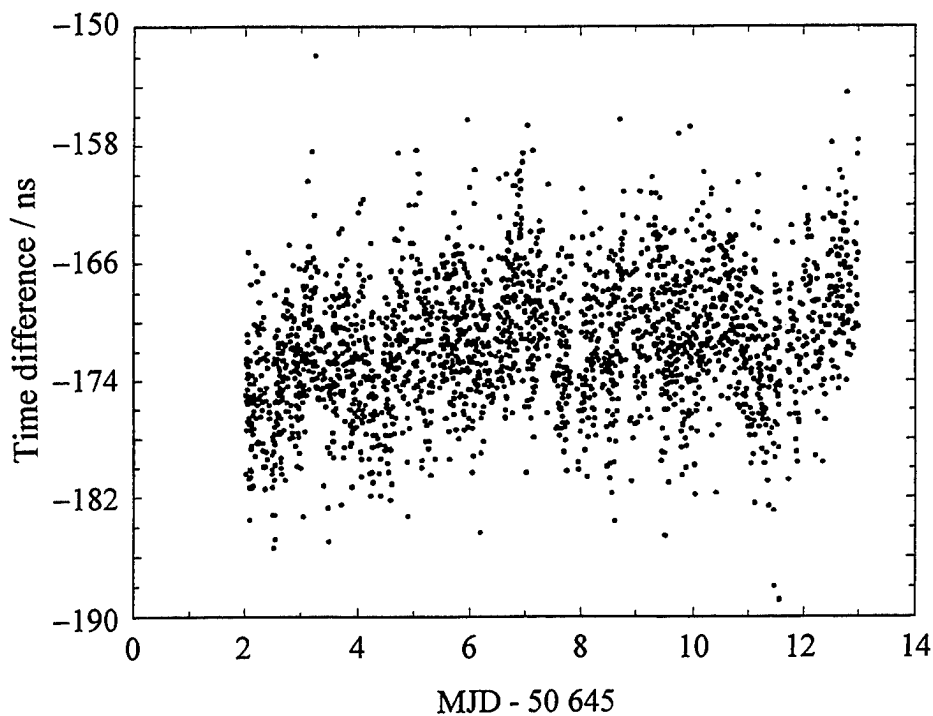


Figure 5. [*BIPM clock - VSL clock*] by GLONASS multichannel common views.

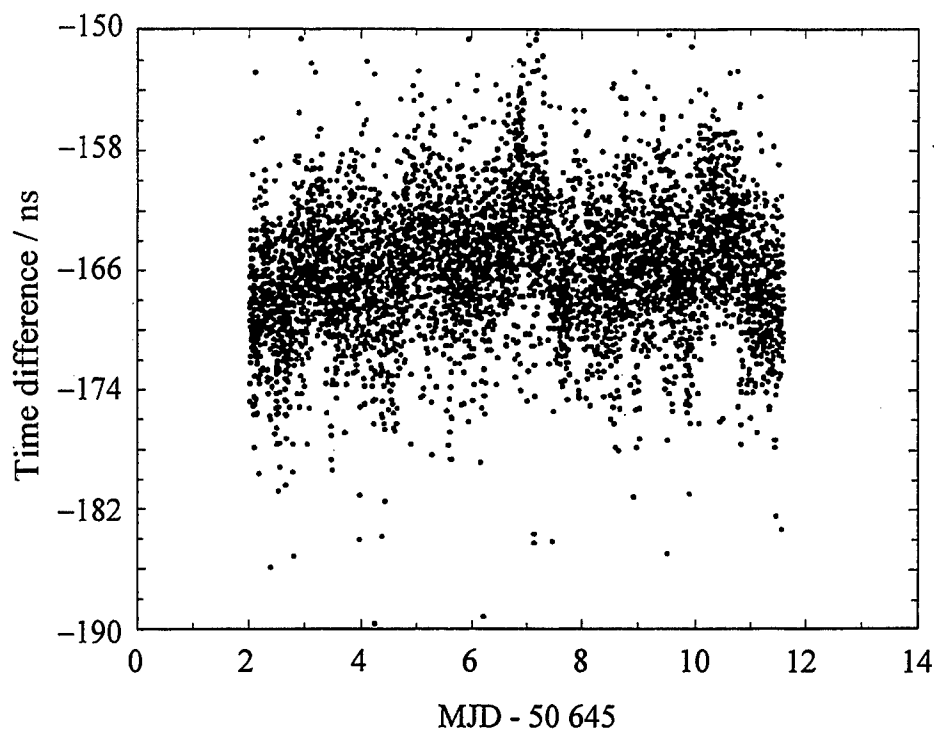


Figure 6. [*BIPM clock - VSL clock*] by GPS + GLONASS multichannel common views.

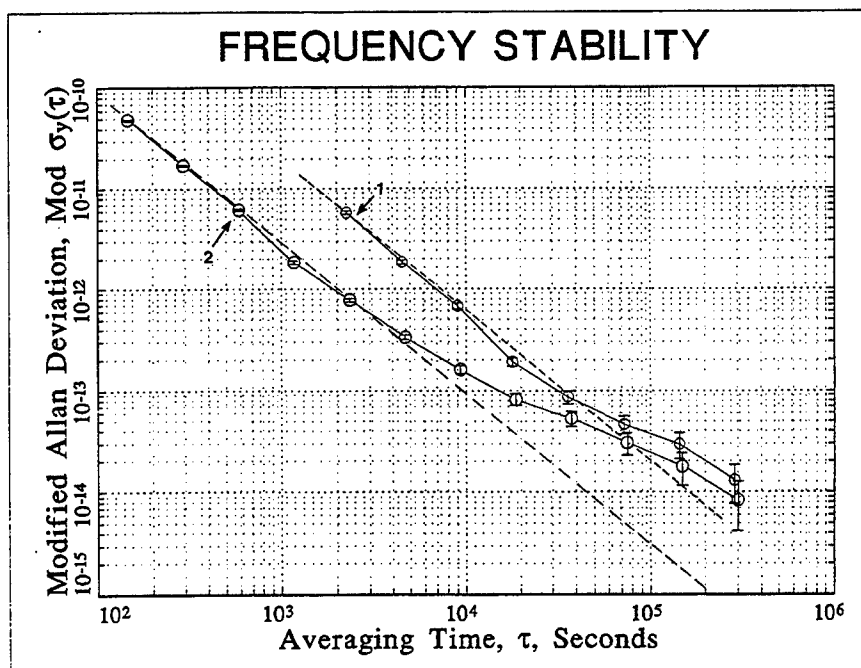


Figure 7. Modified Allan standard deviation of [*BIPM clock - VSL clock*] as given by one-channel GPS (1) and by multichannel GPS+GLONASS (2) observations.

Questions and Answers

ROBERT WEAVER (UNIVERSITY OF SOUTHERN CALIFORNIA): I did not quite understand your point about the multi-channel accuracy being improved by the use of an oven. Would not those temperature effects occur also for single-channel measures?

WLODZIMIERZ LEWANDOWSKI (BIPM): Of course, but we do not see this because the level of noise is higher; so we do not see this jump, this bump due to temperature.

ROBERT WEAVER: So you're saying that the single-channel performance is limited by the temperature drops.

WLODZIMIERZ LEWANDOWSKI: And other noises. What adds to multi-channels, many noise effects. The stability curves go down, and then we cross through the bump, which we cannot observe with one channel.

MULTI-CHANNEL GPS COMMON VIEW TIME TRANSFER EXPERIMENTS: FIRST RESULTS AND UNCERTAINTY STUDY

Gérard Petit, Claudine Thomas, Philippe Moussay
Bureau International des Poids et Mesures
92312 Sèvres Cedex, France

John A. Davis,
National Physical Laboratory,
Queens Road, Teddington Middlesex TW11 0LW, United Kingdom

Mihran Miranian
US Naval Observatory
3450 Massachussetts Ave NW, Washington DC 20392, USA

Juan Palacio
Real Instituto y Observatorio de la Armada
11 100 San Fernando, Spain

Abstract

For regular TAI computations, GPS time transfer is currently carried out using a number of common-view observations from single-channel single-frequency C/A code receivers operating in a scheduled mode. This mode of operation limits the accuracy of time transfer and serious problems of ageing of the current receivers are now being encountered. This paper considers all-in-view measurements from multi-channel dual-frequency GPS time receivers used to carry out time transfer between remote locations, taking into account all possible common-view observations for a given baseline.

We have used data from Allen Osborne Associates TTR-4P receivers operating at the BIPM, the NPL, the ROA and the USNO. Two approaches have been used. First we construct, for each station, standard 13-minute common-view observations of all available satellites and use these data to compute time differences for three baselines. We find that the results are better than those obtained with single-channel receivers, and are about in accord with what might be expected from the number of measurements. Second we use raw short-term data to compute time differences and compare the results with the standard approach for one baseline. We find that the raw data provide a better measurement of the time link than is possible using the standard approach. In all cases the equipment in use display large variations in the calibration delay that are likely to be induced by the environment and require a corrective action.

INTRODUCTION

For about fifteen years, remote clock comparisons have relied on GPS single-channel single-frequency time transfer receivers operated in the common-view mode [1]. Since a few years, progress in clock technology and ageing of the receivers have resulted in the fact that the time transfer technique itself is a limitation for averaging durations of up to a few days. One way to overcome this problem is to use the same basic technique but to expand it using multi-channel (possibly dual-frequency) GPS time receivers and all-in-view measurements so as to make use of all possible common-view observations. This is the subject of many studies [2, 3]. Here we apply this method to one of the available receivers, the Allen Osborne Associates TTR-4P, which provides eight channels with dual frequency.

In this paper we mainly focus on the stability of the time transfer technique. This is represented by the modified Allan deviation, or equivalently by the time deviation $\sigma_x(\tau)$. We do not treat the question of the absolute calibration of the link. We do note, however, that systematic variations in delays present a major problem in the data under study, and would render an exercise of absolute calibration of marginal utility. Methods to overcome these variations will, if successfully applied, result in a stable time link which is then suitable for absolute calibration.

One basic outcome of using multi-channel common-view observations affected by white phase noise, and more generally of using a number of independent measurement points larger by a factor of N , is an improvement in the fractional frequency stability, and therefore in the time deviation, by a factor of \sqrt{N} . In addition, the all-in-view approach has the potential to give access to smaller averaging durations than the standard 13-minute approach since the density of successful observations is likely to be larger.

STANDARD MULTI-CHANNEL COMMON VIEWS

The experiment described in this section was performed in August 1997, using TTR-4P units in operation at the National Physical Laboratory (NPL), Teddington, United Kingdom, the United States Naval Observatory (USNO), Washington DC, USA, and the Bureau International des Poids et Mesures (BIPM), Sèvres, France. Though the TTR-4P units operate in a dual-frequency mode, measured ionospheric delays are not generally available; rather the operator must choose to output values of either measured ionospheric delays or modelled ones using the GPS ionosphere model. For this experiment measured ionospheric delays were not available at the USNO, a circumstance which introduces a non-negligible level of noise to the two long distance links involving the USNO.

For each station, the available measurements are raw short-term time transfer data issued from the Block 100 output of the TTR-4P receivers. The sample rate for raw data is chosen by the operator: 10 s for the USNO and 30 s for the NPL and the BIPM. At each station these raw short-term data are processed in order to reconstruct standard common-view results. The treatment is basically the one which is described in the *Technical Directives* recommended by the Sub-Group of the Comité Consultatif pour le Temps et les Fréquences (CCTF, formerly the CCDS) dealing with GPS and GLONASS time transfer standards [4]. The standard common-view results obtained:

- are computed from a linear fit over 78 (10 s) or 26 (30 s) consecutive data and thus correspond to 13-minute averaging times,
- start at dates spaced by 16 minutes, and
- match the common-view grid described in the International GPS Common-View Tracking Schedule as issued by the BIPM.

Observations in which not all 78 or 26 data points were present were not used to avoid a contamination from the noise of Selective Availability.

Due to various factors, including a failure of the TTR-4P unit at the BIPM and gaps in the TTR-4P data at the NPL and the USNO, the data set presented here is somewhat limited. This does not imply that longer continuous intervals cannot be obtained, but is representative of operating problems that seem to appear systematically on some units. Here, 12 days of continuous data (from MJD 50668 to MJD 50679) have been used for the link NPL-USNO, and 6 days (from MJD 50673 to MJD 50679) for the two baselines involving the BIPM. To provide a basis for comparison, data from the single-channel single-frequency C/A code receivers that are regularly received at the BIPM for the computation of TAI have also been used. In addition, data outliers have been removed for all links under study.

For the transatlantic link NPL-USNO, the results can be summarized as follows:

- TTR-4P receivers on both sites, without removal of outliers,
 $\sigma_x(\tau_0 = 514 \text{ s}) = 5.7 \text{ ns.}$
- TTR-4P receivers on both sites, with removal of approximately 1% of the data
 $\sigma_x(\tau_0 = 521 \text{ s}) = 5.2 \text{ ns.}$
- Classical receivers, without removal of outliers,
 $\sigma_x(\tau_0 = 4760 \text{ s}) = 5.0 \text{ ns.}$
- Classical receivers, with removal of approximately 1% of the data,
 $\sigma_x(\tau_0 = 4820 \text{ s}) = 4.2 \text{ ns.}$

It seems that the deleted data correspond mainly to points with poor broadcast ephemerides, as no editing was required for data computed with precise ephemerides (see below). Curves showing the variation of σ_x with averaging time τ are shown in Fig. 1 for the two computations of the link NPL-USNO after deletion of outliers.

The observed improvement is by a factor of about 2.2 for an averaging duration of about 5000 seconds. As the number of measurements is larger by a factor of about 9, the improvement is less than expected from that effect alone (a factor of 3). One explanation may be that, in the larger data set of the multi-channel receiver, the proportion of data taken at low elevation is larger, and these observations have a larger measurement uncertainty. We note that for longer averaging durations (above 0.5 d) the two stability curves are similar (but slightly poorer for the multi-channel link). This is due to instabilities in the TTR-4P data, and is typical of diurnal signatures linked to environmental variations. It is likely that these instabilities have some effect even for an averaging duration around 5000 seconds, and could also explain why the improvement is only 2.2 for that averaging duration. Such instabilities may also be present in the data from single channel GPS receivers, but these are more difficult to detect because of the level of noise.

In addition, long-distance time links may be improved by using precise ephemerides and measured ionospheric delays. In this case the typical measurement uncertainty is about 3 ns as shown by the regular computation at the BIPM of the links between the Observatoire de Paris (OP), Paris, France, and the National Institute of Standards and Technology (NIST), Boulder, USA, or the Communications Research Laboratory (CRL), Tokyo, Japan [5]. Such an improvement could not be tested here because measured ionospheric delays were not available at the USNO. However, precise ephemerides from the International Geodynamics Service (IGS) have been used and have been shown to slightly improve the stability. For example over a 6-day interval of TTR-4P data, $\sigma_x = 4.4$ ns with precise ephemerides (without removal of outliers) and 5.7 ns with broadcast ephemerides ($\tau_0 = 506$ s).

Results for the link BIPM-USNO are similar, but are available over a period of 6 days only so they are not detailed here.

For the short-distance link BIPM-NPL, we find:

- TTR-4P receivers on both sites, without removal of outliers,
 $\sigma_x(\tau_0 = 259 \text{ s}) = 2.3 \text{ ns}.$

This number cannot be compared directly with that obtained from the classical measurements available from the NPL because the coordinates of the antenna of this particular receiver have an unusually large uncertainty. However, information can be gathered from many time links of similar distance which usually display a measurement noise of about 2 ns [6].

The complete stability curve for the link BIPM-NPL, using TTR-4P units on both sites, is shown in Fig. 2:

- For short averaging durations (up to 5000 seconds), data are affected by white phase noise and the improvement is simply that which corresponds to the increase in the number of measurements. This is a factor of about 3.6 with respect to the maximum number of observations obtainable from a single-channel receiver which tracks continuously (independently of the number of tracks recommended in the International GPS Tracking Schedule issued by the BIPM), and a factor of about 13 with respect to the usual implementation of the schedule, resulting in gains in stability of 1.8 and 3.6 respectively.
- For longer averaging durations, given the good short term stability, the instabilities present in the TTR-4P data are readily observed. They are again typical of large diurnal signatures linked to environmental variations.

SHORT-TERM COMMON VIEWS

This experiment was conducted during four days in October 1997 (from MJD 50724 to MJD 50728) when raw short-term (30 s) time transfer data were available from the TTR-4P units at the NPL and at the Real Instituto y Observatorio de la Armada (ROA), San Fernando, Spain. Unfortunately the set-up of the experiment was not optimal because the receiver at the ROA used measured ionospheric delays while that at the NPL used model ionospheric delays. Nevertheless this feature has little impact on the results of the present study. The data were used first to form time differences directly from the raw short-term data, then standard common-view measurements were reconstructed following the procedure described in the *Technical Directives* [4].

The main results are as follows:

- Short-term common views, with removal of the obvious outliers (about 0.2% of the data),
 $\sigma_x(\tau_0 = 5.9 \text{ s}) = 6.4 \text{ ns.}$
- Reconstructed common views, with removal of outliers,
 $\sigma_x(\tau_0 = 300 \text{ s}) = 3.8 \text{ ns.}$

The corresponding stability curves are shown in Fig. 3.

Using only observations at elevations greater than 25 degrees, we find:

- Short-term common views, with removal of the obvious outliers,
 $\sigma_x(\tau_0 = 8.0 \text{ s}) = 4.4 \text{ ns.}$
- Reconstructed common views, with removal of outliers,
 $\sigma_x(\tau_0 = 366 \text{ s}) = 3.4 \text{ ns.}$

When comparing the values of σ_x for several averaging durations (see Fig. 3), we observe that the improvement is by a factor of about 2.5 for 300 s, by a factor of about 2 for 1000 s, and that the values are similar for 5000 s and above. We have seen in the previous section that above 5000 s to 10000 s systematic instabilities begin to dominate and, in this particular case, additional noise is due to the fact that one station used measured ionospheric delays while the other one used a model. For shorter averaging durations, the improvement in using raw data is striking.

The improvement results, first from the increased number of data points. We observe that the reconstructed common-view approach results in using only about half the short-term data points. This factor of 2 can be decomposed in three parts. About 20% of the loss is due to the gap in the reconstruction scheme (3 minutes every 16 minutes), and about 30% is lost at each station due to micro-gaps in the data. Indeed, because of Selective Availability, the common-view observations must be reconstructed using all 26 raw data points and the loss of one single point at a single station prevents this reconstructed observation being used. Even though the observed percentage of missing raw data is less than 1 % at each station, the total effect on the number of reconstructed common views is large. In contrast, the number of usable raw time differences is 98.8% of the maximum possible number (not counting one larger gap of about two hours which is common to the two approaches).

A second point is that the detection of outliers is easier in the raw short-term data. Errors in raw data are usually very large and can be identified with very simple filters. This is a significant advantage though not a definitive one: in general, reconstructed common views containing one bad data point can also be identified, although the effect is less obvious.

These two factors can explain an improvement in stability by a factor of about 1.5, but cannot account for the actual 2.5 gain observed. This effect is even more important when an elevation cut-off of 25 degrees is used. Further investigation remain necessary to confirm this improvement and to explain it.

CONCLUSION

We studied data from multi-channel dual-frequency Allen Osborne Associates GPS time receivers of type TTR-4P, in terms of the stability of time transfer via common views on short and long baselines. We find that, for short averaging durations (up to 5000 seconds), data are affected by white phase noise and the increase in the number of measurements results in a better stability. An even better stability is achieved when using raw short-term measurements, rather than reconstructed standard common-view observations, to compute the time link.

For this particular equipment, the major limitation is systematic delay variations which dominate for averaging durations above 5000 s to 10000 s. Such variations are probably induced by environmental variations at the antenna and are being addressed by techniques such as the thermal stabilization of the complete antenna or of the first amplification stage [7].

Once this major limitation is removed, GPS code measurements are capable of providing a time deviation of less than one nanosecond for an averaging duration of 1000 s and therefore 0.1 ns for one day. The corresponding figures for the fractional frequency stability are about 1×10^{-12} and about 1×10^{-15} respectively. The stability for durations of one day and above is similar to what can be obtained by adding phase measurements [8], but this approach provides better stability for shorter averaging durations.

REFERENCES

- [1] W. Lewandowski, C. Thomas, 1991, *Proceedings of the IEEE*, 79, 7, 991-1000.
- [2] W. Lewandowski, J. Azoubib, G. de Jong, J. Nawrocki, J. Danaher, 1997, *Proc. ION GPS'97*, in press.
- [3] *In these proceedings:*
L. Schmidt, M. Miranian, pp. 269-276.
P. Fisk, S. Quigg, M. Ruiz, T. Armstrong, J. Luck, A.J. Woodger, pp. 277-286.
J. Hahn, H. Nau, P. Moussay, pp. 287-298.
J. Azoubib, G. de Jong, W. Lewandowski, pp. 299-308.
- [4] D. Allan, C. Thomas, *Metrologia*, 1994, 31, 69-79.
- [5] W. Lewandowski, G. Petit, C. Thomas, 1993, *IEEE Trans Instr. Meas.*, 42, 2, 474-479.
- [6] Annual Report of the BIPM Time Section, 1996, *BIPM Publication*, 9, 162 p.
- [7] W. Lewandowski, P. Moussay, J. Danaher, R. Gerlach, E. Levasseur, 1997, *Proc. 11th EFTF*, 498-503.
- [8] G. Petit, 1997, *Proc. 11th EFTF*, 336-340.

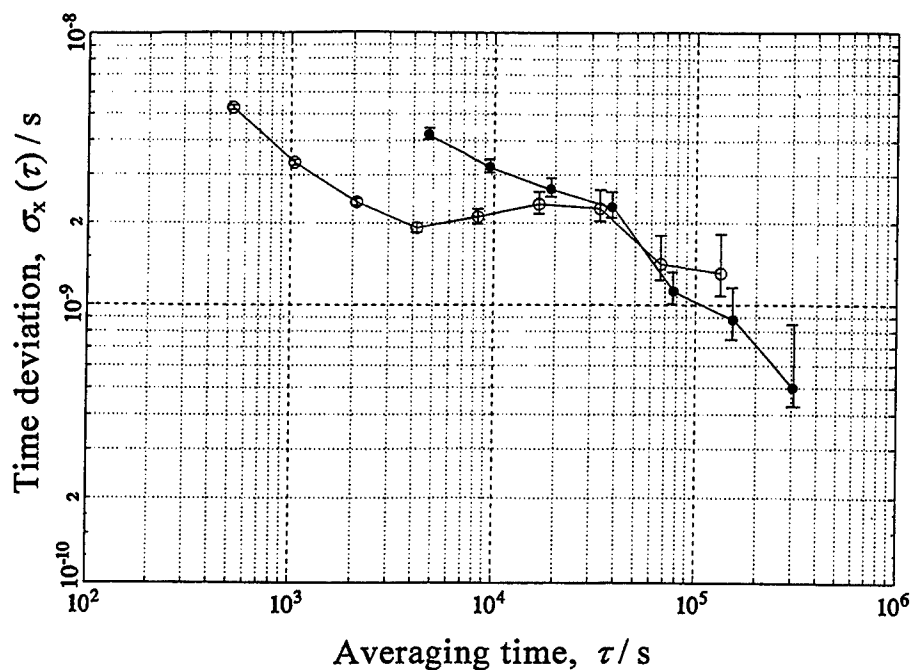


Fig. 1: Stability curves showing the variation of the time deviation σ_x versus the averaging time τ , for the time link NPL-USNO computed with standard common-view measurements provided by TTR-4P units (\circ) and classical receivers (\bullet) on both sites.

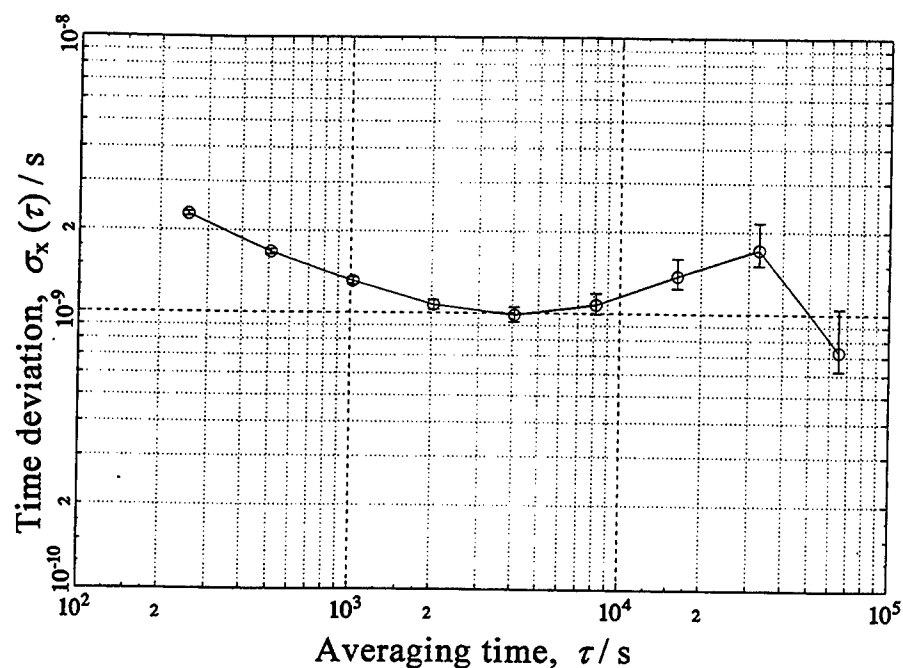


Fig. 2: Stability curve showing the variation of the time deviation σ_x versus the averaging time τ , for the time link BIPM-NPL computed with standard common-view measurements provided by TTR-4P units on both sites.

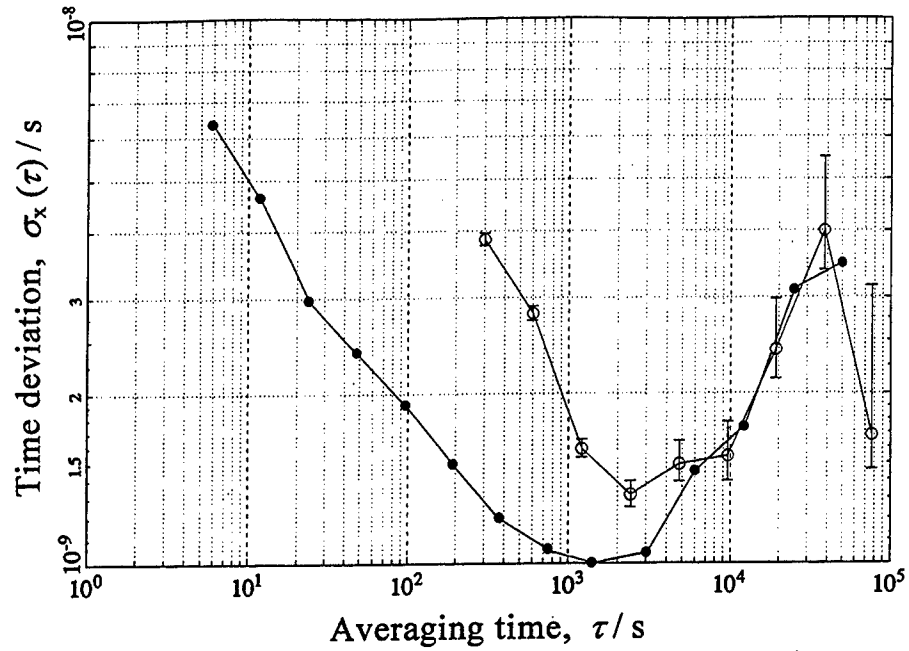


Fig. 3: Stability curves showing the variation of the time deviation σ_x versus the averaging time τ , for the time link ROA-NPL computed with short-term (30 s) common-view measurements (●) and reconstructed standard common-view measurements (○) provided by TTR-4P units on both sites.

Questions and Answers

JUDAH LEVINE (NIST): My comment is that the standard analysis method described in the BIPM documents requires one-second measurements. Once you do not have one-second measurements, you can reconstruct the common view, but it is not exactly the same. It averages the SA in a slightly different way because the BIPM method averages SA in a way that is different than the 26 thirty-second measurements. Now, that is not a problem if you compare the identical receivers using the identical method. But it does not necessarily mean that you can compare the new receivers with the old receivers because they are going to average the SA in a different way. That means that once you do not measure every second, I think there is no point reconstructing the BIPM method because you can not compare with the old receivers anyway. That is my bias, my preference; but you understand what I am saying, there is no point in going to 13-minute tracks because you can not compare with the old receivers anyway. Thank you.

GERARD PETIT (BIPM): Yes, you are right. But of course in this case it was similar receivers with similar setups.

JUDAH LEVINE: That is fine.

ROBERT WEAVER (UNIVERSITY OF SOUTHERN CALIFORNIA): I just wanted to share with you something, and with the other speakers who have brought out diurnal variations, probably due to temperature (perhaps other effects); and that relates to cable effects. I see that the use of an oven can take care of the temperature variations on antennas and the pre-amplifier perhaps. In my experience from a previous employment, we ran into cable phase variations that can amount on the order of .1 (point one) percent of the cable length, variations in delay of a cable. So if you have a cable that is 10 meters in length – I do not know what lengths you typically use – but that could perhaps amount to a fairly substantial variation that needs to be taken care of. That is my first point.

The second point is when you look at the effect of temperature on a cable, these effects that one would expect be reasonably linear or quadratic or something with the function of temperature are really not. Many materials that are used as the dielectric, in these cables, have sudden variations in temperature regions that correspond to the properties of the materials that are used as the dielectric. In our case, we were using Teflon dielectric that had a sudden variation around 20 degrees Celsius, or in that general vicinity; and you could have sudden jumps over an interval of perhaps 10 to 20 degrees Celsius where you would get this total variation of around .1 (point one) percent of the length of a cable.

I just want to bring that out as one possible area to look at for the systematic effects of temperature.

ROB DOUGLAS (NRC): That is a very helpful comment. Any other questions?

TOM PARKER (NIST): A comment about the cables. If you use a cable with a polyethylene dielectric, the stability is substantially better, and, in fact, you can get cables that are phase-stabilized and have a parabolic delay versus temperature dependence with a peak right around 20 degrees C.

ROB DOUGLAS: Not a lot of help from Canada these days. Are there other questions or comments? There are some other people in the audience who have multiple-channel timing experience.

WLODZIMIERZ LEWANDOWSKI (BIPM): A few comments about cables: Of course, we have been thinking about cables for a long time, but we have other problems not related to cables. We are now considering very strongly to make a build-up to protect cables from temperature variations and using cables of different materials. At BIPM, we are already considering putting our temperature-stabilized antennas just above the laboratory and build temperature protection for the cables. So, this is an obvious next step to do.

GERRIT de JONG (NMI VAN SWINDEN LABORATORIUM): I think cable is a secondary problem compared to the filters which are now included in the antenna path, in the active antenna especially, of course. It is mainly the filter, and also the amplifier contribution; but I think the first thing to do is to stabilize the temperature of the filter which is inside active antennas. Thank you.

GERARD PETIT: Yes, you are right. We have to treat the problems in the order in which they appear. It seems that now the antenna problem is being corrected, so cable is the next issue.

TIME TRANSFER WITH GPS MULTI-CHANNEL MOTOROLA ONCORE RECEIVER USING CCDS STANDARDS

J. Nawrocki*, W. Lewandowski**, J. Azoubib**

*Astrogeodynamical Observatory, Space Research Center, Polish Academy of
Sciences, Borowiec, Poland

**Bureau International des Poids et Mesures, Sèvres, France

Abstract

Most of the standard receivers used for the common-view time transfer are of the single-channel, single-frequency, Coarse/Acquisition code type. They all are built according to the "NBS standard" prototype from the early 1980's. The uncertainty of the common-view time comparisons varies between 2-3 ns RMS for the best of them. The new generation of the unexpensive, multi-channel C/A code receivers which are now available seems to make the old standard obsolete.

One of the interesting new solutions, proposed for the time transfer, is the 8-channel Motorola VP Oncore receiver combined with a time-interval counter and a microcomputer (Gifford et al., 1996), (Lewandowski et al., 1996).

Such a measurement system was tested for several months at the Time Section of the Bureau International des Poids et Mesures (BIPM) in Sèvres, yielding very interesting results (Lewandowski et al., 1997).

To maintain the compatibility with the old "NBS type" receivers, still in use at the majority of time laboratories, and to make use of the Motorola multi-channel capabilities, special software driving the receiver and the counter was developed at BIPM in 1997.

The results of tests in time transfer between BIPM in Sèvres and AOS in Borowiec (Astrogeodynamical Observatory in Borowiec, Poland) at the baseline of about 1200 km give the uncertainty of results in the range of 1-2 ns RMS when applying recommendations of CCDS (Allan, Thomas, 1993).

Introduction

The common-view method of GPS time transfer is one of the most precise and accurate methods for time comparison between remote clocks. The main aim of the method, proposed at the beginning of the '80s (Allan, Weiss, 1980) was to increase the accuracy of the comparisons into the range of a few nanoseconds. The method became especially important after the implementation of SA (selective availability). The observations of the same GPS satellite are carried on simultaneously at different laboratories according to the schedule published, usually twice a year, by the BIPM. Up to now, the common-view method is applied for single-frequency receivers which enable observation of up to 48 satellite passes per day.

New, inexpensive, multichannel receivers, enable observation of several satellites simultaneously. Motorola VP Oncore is especially interesting among them, because of the information available through the RS-232 communication port of the receiver. It is possible to relate the Motorola's 1 pps pulse with nanosecond accuracy to the internal time scale of the receiver. Full observed satellite information (raw satellite dispatch) and raw pseudorange measurements are also available.

It is possible to prepare the receiver independently of time comparisons, where all the computations are carried according to rules recommended by the CCDS (Comité Consultatif pour la Définition de la Seconde (Rapport BIPM-93/6). The essential advantage of such observations is the compatibility with old, single-channel, NBS-type receivers, still in use at the majority of time laboratories.

Setup of the equipment

The organization of the measurements is very similar to the setup applied at BIPM and Besançon in the experiment carried out in 1996 (Lewandowski et al., 1997). The Stanford SR-620 time-interval counter (Fig. 1) is started by the 1 pps pulse from the local UTC clock driven by the Oscilloquartz EUDICS 3020 cesium frequency standard. The counter is stopped by the 1 pps pulse from the Motorola Oncore VP receiver, working in the GPS synchronization mode. Both the counter and the receiver are controlled by the software installed on a PC computer. COM1 port is used for the communication with the counter: for sending commands and for gathering the readings 1PPS(local clock) - 1PPS(receiver). Serial COM2 port is used for the communication with Motorola. Set up of the experiment at BIPM in Sèvres is almost identical, the only difference is that Racal-Dana counter is controlled using HPIB interface instead of a serial one. The Racal-Dana counter is driven by the 5MHz frequency signal from HP5071Acesium time and frequency standard, also generating a laboratory 1pps pulse.

Software driving the measurements

The block diagram of the applied software is presented in Fig. 2. During the startup procedure the Motorola Oncore VP receiver is set up in the position-hold mode, with antenna coordinates known with cm accuracy in the ITRF reference frame. The 1pps signal output is formed by the internal GPS time scale of the receiver.

The reception of the measurement 1PPS(local clock)-1PPS(receiver) from the counter triggers the gathering of the following data from the Motorola:

- pseudoranges for each of the observed satellites,
- corrections connecting internal software GPS time scale of the receiver to its 1pps pulse.

Every 6 seconds the orbital data of the observed satellites (raw satellite frames) are also received. Satellite clock parameters, Keplerian elements of the orbit, and their reference time are decoded. The basic condition for the proper functioning of the software was to tie the internal time scale of the receiver to that generated by the receiver 1pps pulse. The work-out of the data during the pass is done exactly

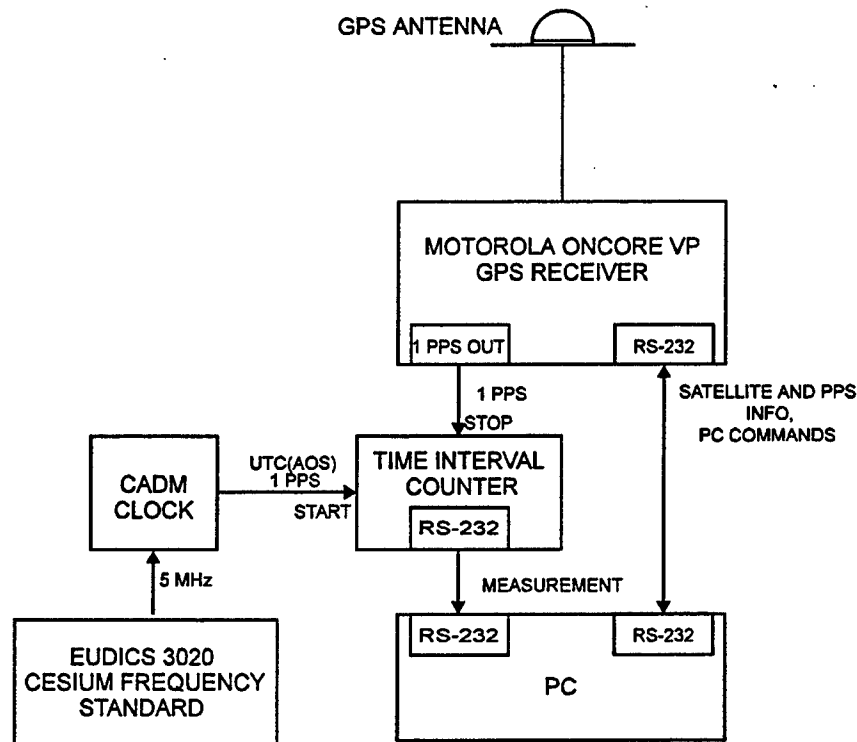


Fig. 1. Setup of the Experiment at Borowiec Observatory.

according to the recommendations of the CCDS (Rapport BIPM 1993/6). The 780 measurements carried in the period of time defined by the BIPM schedule are divided into 15 s intervals. The differences between the second of the local clock and i -th satellite time second are pseudoranges. The connection between Motorola internal second and the output 1pps pulse can be written as: $1\text{pps} + \Delta\tau$, where $\Delta\tau$ can be computed from the corrections transmitted one second before and one second after the 1pps pulse. The pseudorange for the i -th satellite can be thus written as:

$$\text{psd}_i = \text{UTC}(\text{loc}) - 1\text{pps}(\text{Motorola}) + 1\text{pps}(\text{Motorola}) - T(\text{sat}_i),$$

so:

$$\text{psd}_i = \text{UTC}(\text{loc}) - T(\text{sat}_i).$$

For each of the 15 s intervals, the pseudoranges are square fitted for the center of the interval. Satellite position, geometric delay as well as ionospheric, tropospheric, Sagnac, periodic relativistic, L1-L2 corrections are computed. Then the clock corrections for access to GPS time, using the broadcasted second-order polynomial are evaluated. The values obtained in this way are linear-fitted. The results for each satellite are stored in the standard format on the hard disk, ready for the transfer to the other laboratory participating in the experiment.

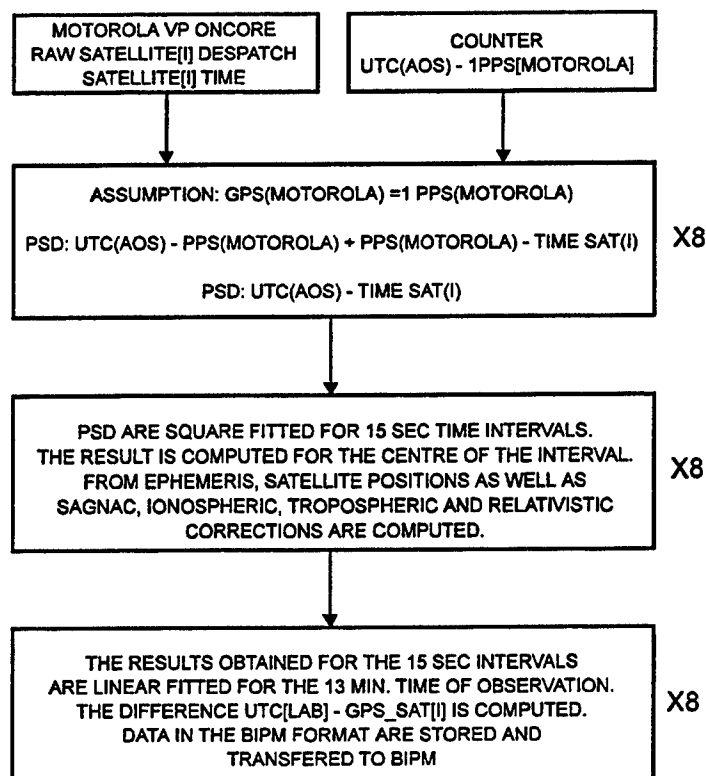


Fig. 2. General diagram of the software applied to the work-out of the Motorola VP Oncore data.

Common-view results of the experiment

In the experiment participated two Motorola Oncore VP receivers working simultaneously at BIPM (Sèvres, France) and AOS (Borowiec, Poland). The approximate baseline is about 1200 km. The results of the observations come from the period of MJD: 50679 - 50683 (19.08 - 23.08.1997) and present the time scales comparison between the BIPM and the AOS. The comparisons were obtained using both multi-channel and single-channel observations. Fig. 3 presents raw differences BIPM - AOS obtained for multi-channel observations between the two laboratories. One-channel comparisons are presented in Fig. 4. The results of the removal of slope are shown in Fig. 5 and Fig. 6 respectively. The period of observations is relatively short because of the quite significant drift of the clock at AOS. The EUDICS 3020 cesium frequency standard is at least by an order of magnitude less stable than the HP5071, equipped with high performance tube used at Sèvres.

Fig. 7 presents the modified Allan deviation computed for the BIPM - AOS multi-channel observations. Similar computations obtained for the one-channel observations are shown in the Fig. 8. The results of the time stability of the multi-channel and one-channel observations are analyzed in Fig. 9 and Fig. 10. The multi-channel results are more stable. The uncertainty of the comparisons (RMS) varies between 1.2 to 1.5 ns;

for one-channel observations it is by 1 ns worse. The certainty problem for all GPS receivers are the changes of internal receiver delay caused by the changes of external temperature (Lewandowski and Tourde, 1991). Fig. 11 presents the zero-baseline, one-channel comparisons between Motorola and Sercel receiver working at the BIPM time laboratory. The same 1pps pulse from local clock was used for the two receivers. The Sercel was equipped with the temperature-stabilized antenna; the Motorola was equipped with typical, unstabilized antenna. For the period of MJD: 50670 - 50721 the daily average of external temperature varied between 12° to 33° C. The changes in the difference Sercel - Motorola follow the pattern of the external temperature. The temperature coefficient is equal $\zeta = -0.27$ ns/deg.

Conclusions

The best single-channel, C/A code receivers built especially for timing purposes, e.g. Allen-Osborne TTR6, NBS TTR5, or Sercel, used for common-view observations for baselines 1000-2 000 km give the uncertainty of 2-3 ns. They observe up to 48, 13 min. satellite passes per day. The results obtained with the set of equipment consisting of an inexpensive, multi-channel Motorola VP Oncore receiver, a time counter with the 1 ns resolution, and the PC computer with especially prepared software are significantly better. As it was presented above, the obtained uncertainty is well below the 2 ns level. The Motorola at Borowiec observes about 650 satellite passes per day. Moreover, the results of the multi-channel satellite observations obtained with the software used at Sèvres and Borowiec are compatible with the old single-channel receivers widely used for timing purposes. The significant problem still concerns the relatively high dependence of Motorola observations on outside temperature, which can be resolved by thermal protection of its antenna.

References

1. D. W. Allan, A. M. Weiss, Accurate Time and Frequency Transfer During Common-View of GPS Satellite, Proc. 34th Ann. Symp. on Frequency Control, pp. 334 - 346, 1980.
2. The Group on GPS Time Transfer Standards, Technical Directives for Standardization of GPS Time Receiver Software, Rapport BIPM 1993/6.
3. W. Lewandowski, P. Moussay, P. Guerin, F. Meyer, M. Vincent, Testing Motorola Oncore GPS Receiver for Time Metrology, EFTF '97.
4. W. Lewandowski, R. Tourde, Sensitivity to the External Temperature of Some GPS Time Receivers, Proc. 22nd PTTI Meeting, pp. 307-316, 1990.

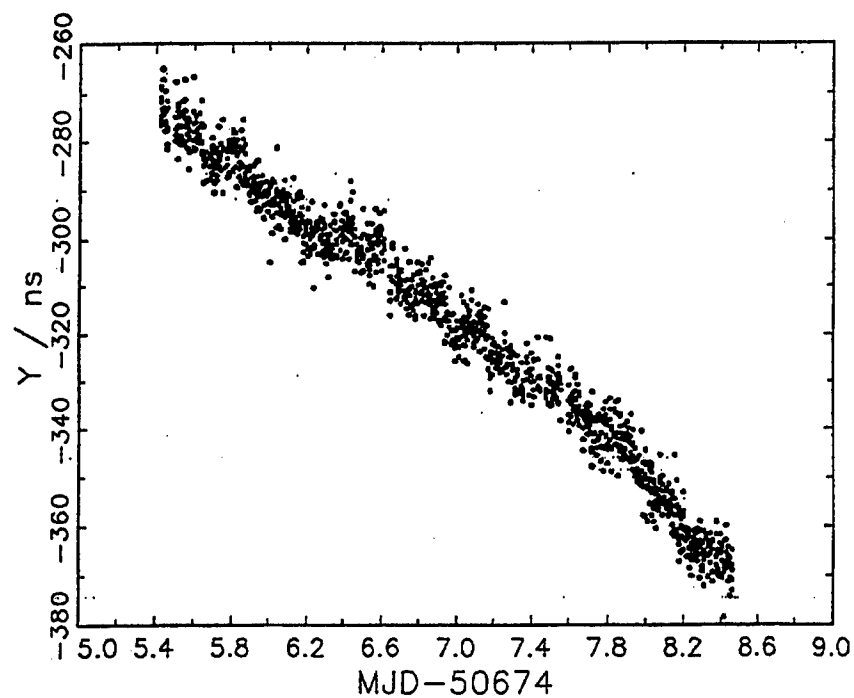


Fig. 3. Raw [BIPM clock - AOS clock] differences by Motorola multi-channel, common-view observations.

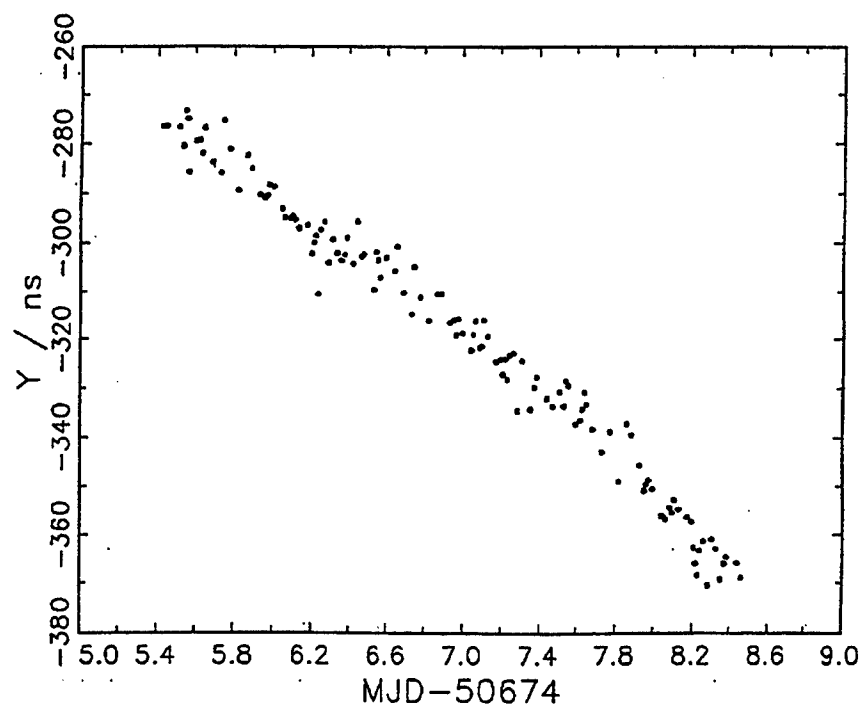


Fig. 4. Raw [BIPM clock - AOS clock] differences by Motorola one-channel observations.

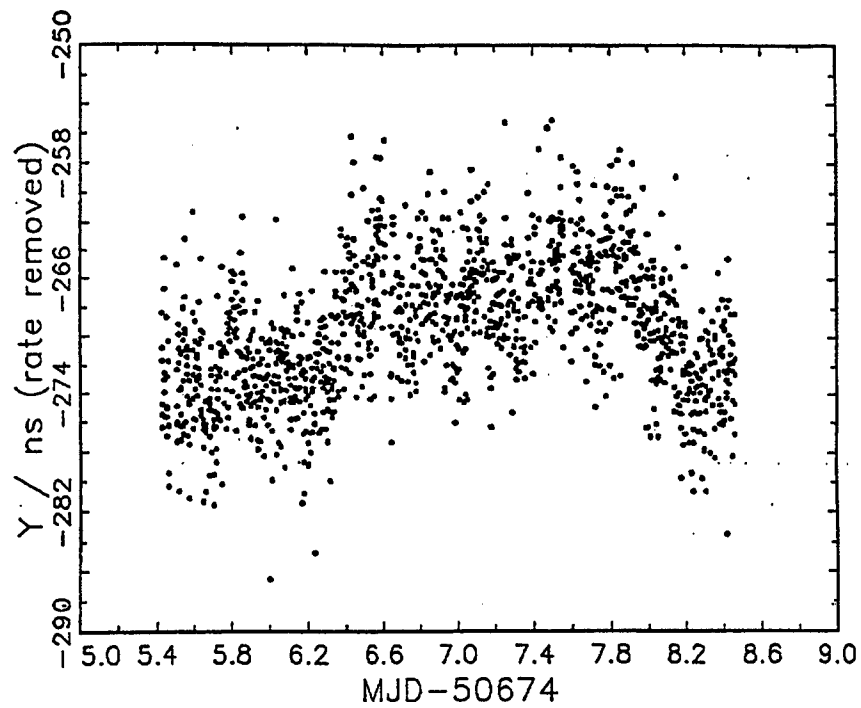


Fig. 5. Data of Fig. 3 after slope removal.

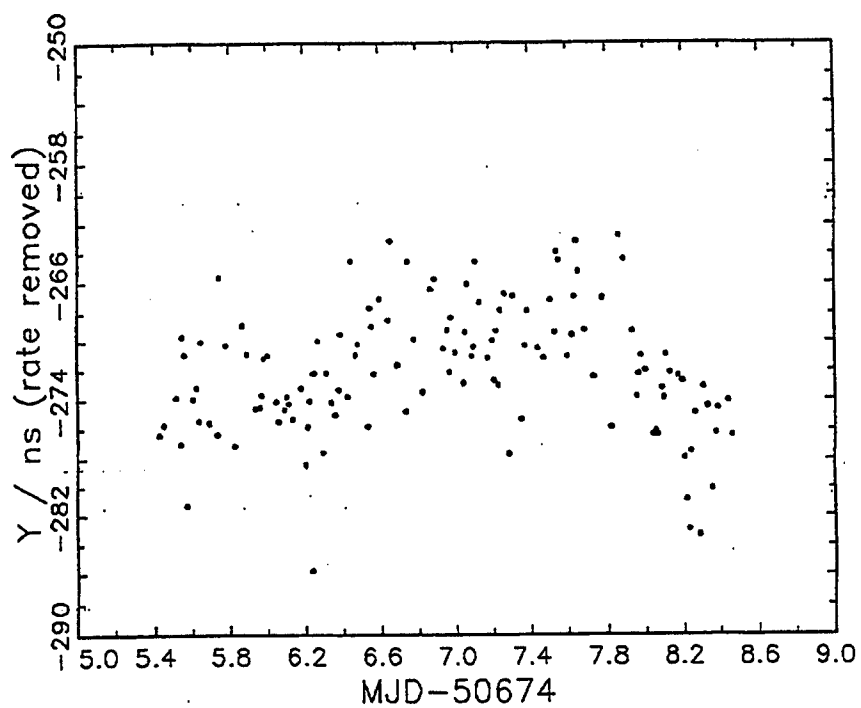


Fig. 6. Data of Fig. 4 after slope removal.

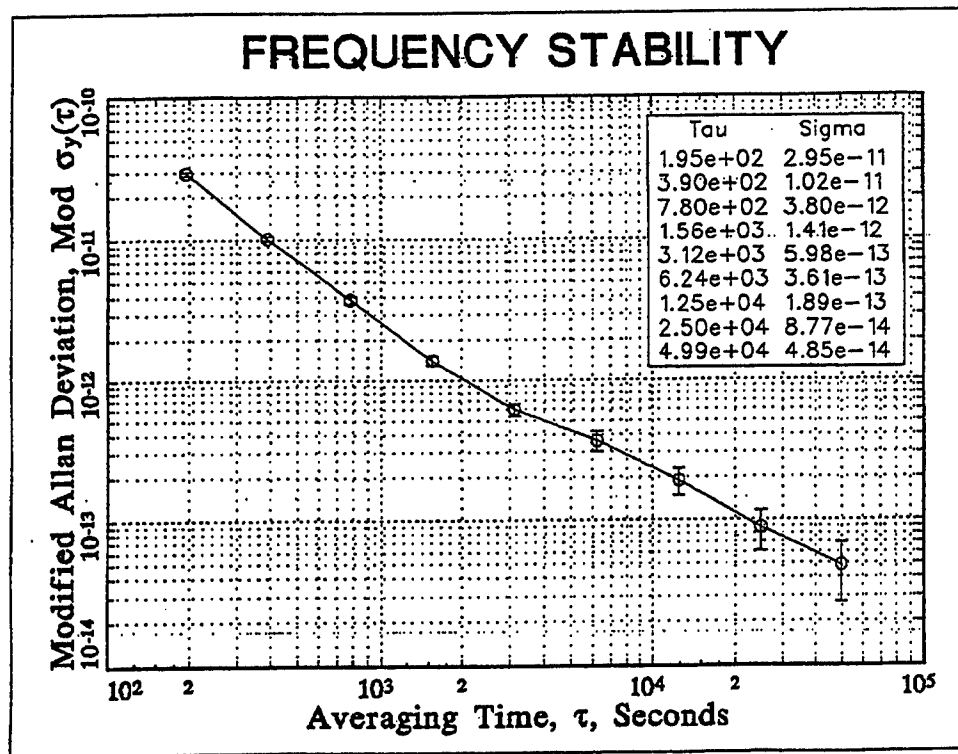


Fig. 7. Modified Allan Deviation of the [BIPM clock - AOS clock] differences from Motorola multi-channel observations.

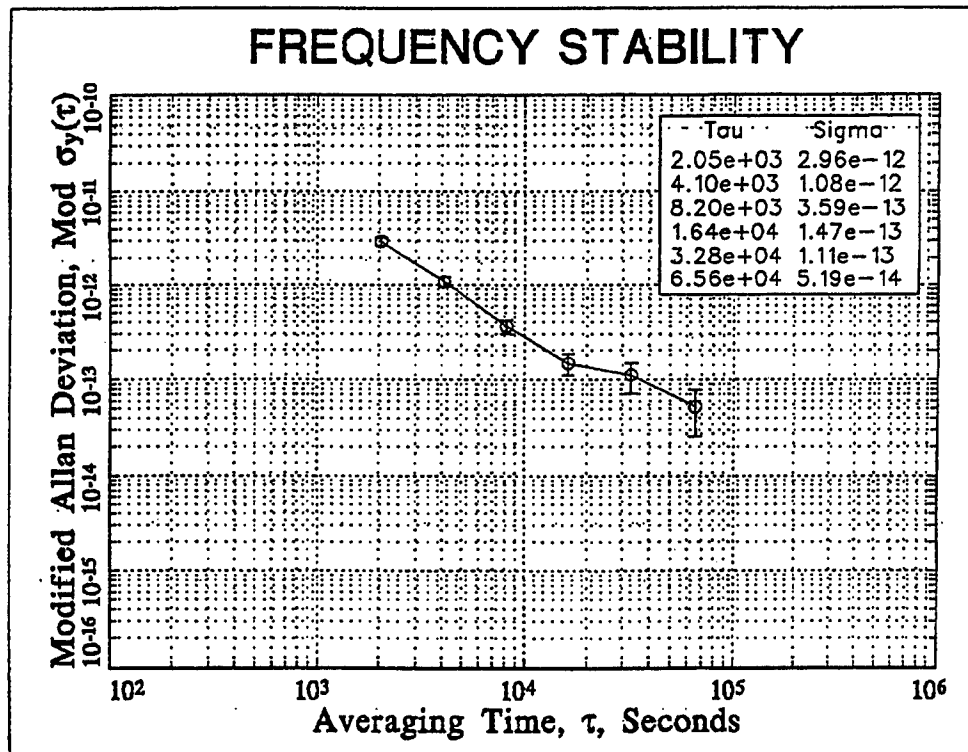


Fig. 8. Modified Allan Deviation of the [BIPM clock - AOS clock] differences from Motorola one-channel observations.

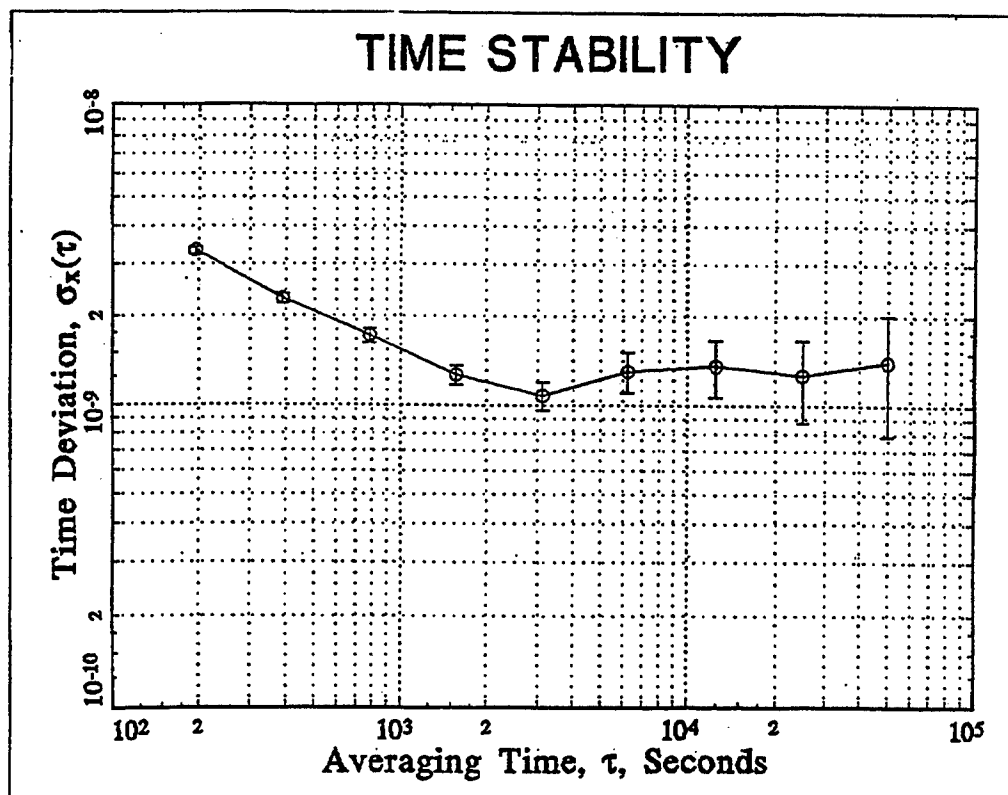


Fig. 9. Time deviation of the [BIPM clock - AOS clock] differences from Motorola multi-channel observations.

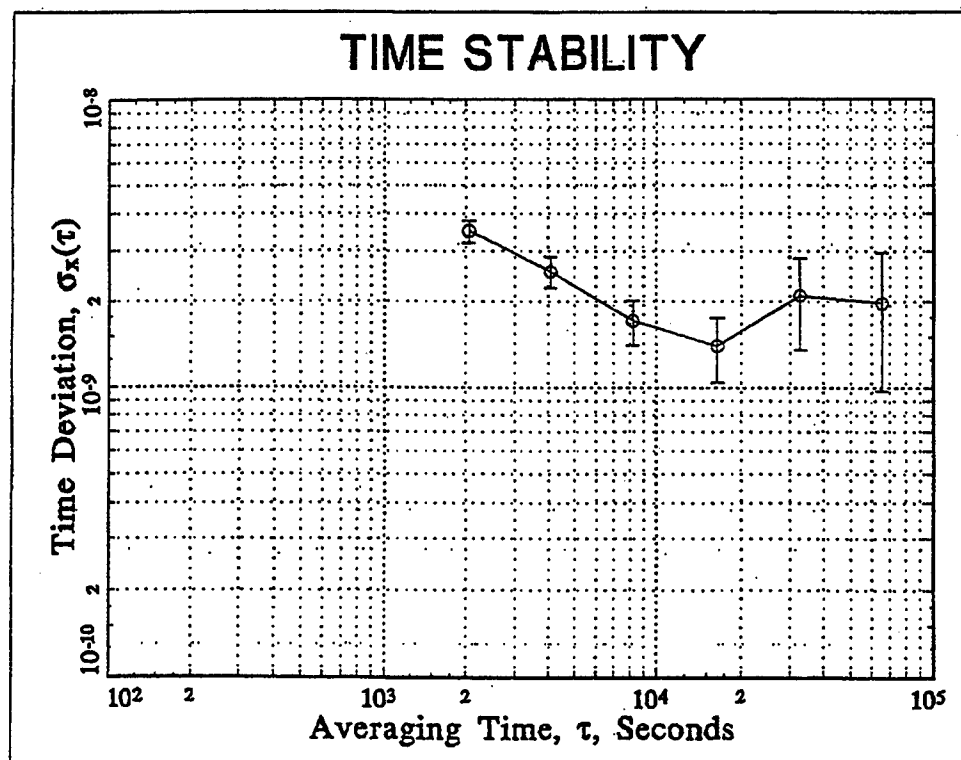


Fig. 10. Time deviation of the [BIPM clock - AOS clock] differences from Motorola one-channel observations.

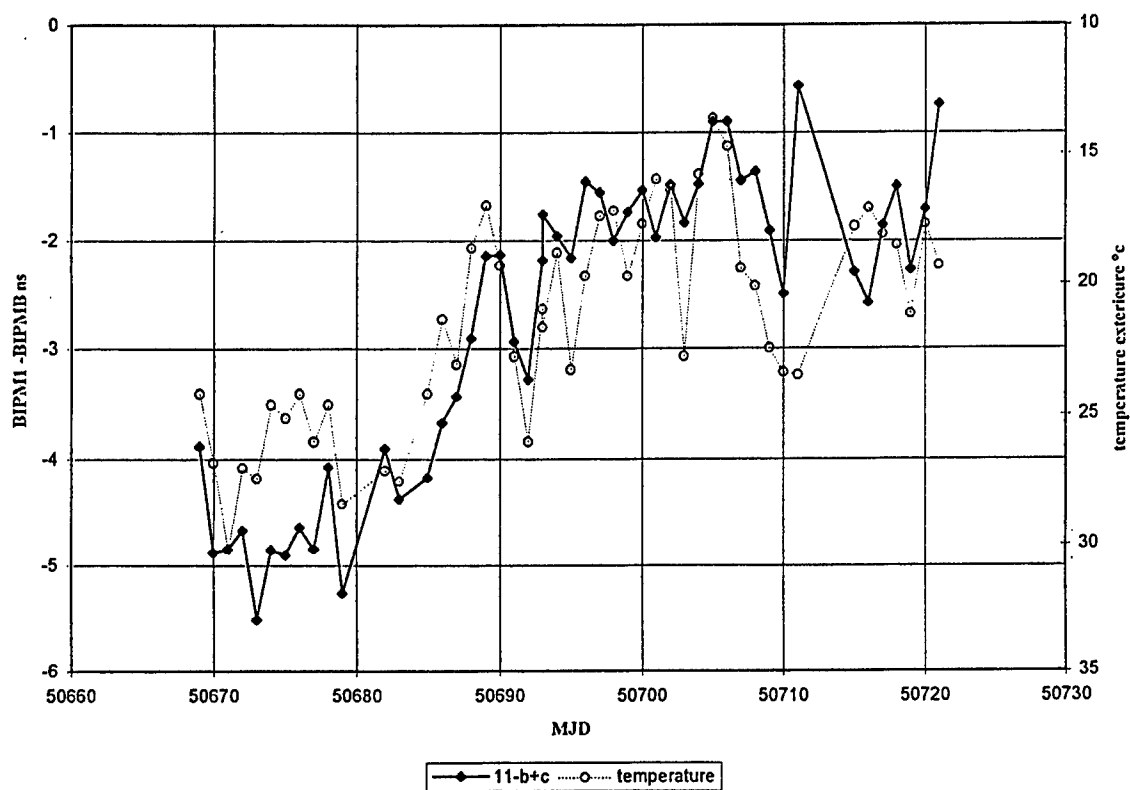


Fig. 11. Zero-baseline comparison between Sercel receiver (BIPM1) and Motorola receiver (BIPMB), and corresponding external temperature.

A STUDY EXAMINING THE POSSIBILITY OF OBTAINING TRACEABILITY TO UK NATIONAL STANDARDS OF TIME AND FREQUENCY USING GPS-DISCIPLINED OSCILLATORS

J.A.Davis and J.M.Furlong

Centre for Time Metrology,
National Physical Laboratory,
Queens Road, Teddington, Middlesex, TW11 0LW, UK

ABSTRACT

In the UK there is considerable interest in using GPS-Disciplined Oscillators (GPSDOs) as standards traceable to UTC(NPL). However, UK accreditation bodies are somewhat reluctant to accept GPSDOs as traceable standards, without a detailed study of the practical issues involved in establishing traceability. NPL has undertaken an extensive study, examining the performance of 15 GPSDOs loaned by 11 UK suppliers and manufacturers, to address this traceability issue. In this paper a detailed account is presented of the results obtained from the NPL study. A preliminary set of recommendations on the use of GPSDOs as standards traceable to UTC(NPL) have been produced. The progress made on implementing a mechanism enabling GPSDOs to be recognized as standards traceable to UTC(NPL) is outlined.

1) INTRODUCTION

GPS-Disciplined Oscillators (GPSDOs) are widely used in the United Kingdom as standards of time and frequency. GPSDOs combine the long-term stability of the timing signals available from the GPS with the short and medium-term frequency stability available from quartz or rubidium oscillators. The growth of the use of GPSDOs in calibration laboratories in the UK has been limited because GPSDOs have not been recognized as standards traceable to the UK national time scale UTC(NPL). GPSDOs offer many advantages over other time and frequency standards. The global nature of the GPS enables GPSDOs to be used anywhere in the world. The quality of the timing signals results in an improved accuracy over frequency standards disciplined by terrestrial standard frequency transmissions. GPSDOs do not require periodic recalibrations, they are not excessively expensive, costing typically between £2,000 and £12,000. GPSDOs have many applications world-wide, in particular within the telecommunications industry.

NPL has responded to the growing interest in using GPSDOs as traceable standards, by

undertaking an extensive study of the performance of GPSDOs in order to assess their suitability as time and frequency standards traceable to UTC(NPL) [1], [2], [3]. Fifteen GPSDOs have been examined at NPL for a period of three months. A detailed account of this study is presented in this paper.

The results of the study have been forwarded to the United Kingdom Accreditation Service (UKAS) who will ultimately decide on the suitability of GPSDOs. The future work between NPL and UKAS to establish GPSDOs as traceable standards within the UK is also outlined.

2) ELEMENTS OF THE GPSDO STUDY

To assess the suitability of GPSDOs as standards traceable to UTC(NPL), the following elements have been included in the GPSDO study:

- Measurement of the time and frequency characteristics of each GPSDO, by performing continuous comparisons of both phase and 1 pulse per second (1PPS) outputs against UTC(NPL) over a period of several weeks.
- Characterisation of the frequency output from the free-running oscillator within the GPSDO, by operating each GPSDO for several days in the absence of a GPS signal.
- Recording of all the available operating parameters of the GPSDOs obtained from their communications port, with the aim of correlating variations in the GPSDO's time and frequency characteristics with changes in these parameters.
- Investigating the integrity and status of each GPSDO under a selection of "non-ideal" operating conditions, for example by reducing the available satellite constellation, testing performance after a controlled mains power failure, operating the GPSDOs from erroneous antenna position coordinates, and removing all GPS satellite signals.
- Independently monitoring the accuracy and integrity of the GPS satellite constellation through the use of several multi-channel GPS receivers at NPL.
- Monitoring the local environment at NPL, eg, the air and surface temperature and the humidity, both within the laboratory, the outdoor air temperature and the temperature on the surface of the antenna.
- Performing of regular time transfer measurements between UTC(NPL) and UTC(USNO).
- Collating externally published information on the performance of the GPS during the period of the study, for example satellite outages and clock offsets.

- Produce a report now forwarded to UKAS [5], describing the findings of the study, which includes a series of recommendations on the operation of GPSDOs when used as traceable standards.

Measurements were performed between January 1997 and April 1997. Eleven organizations provided NPL with 15 GPSDOs. In addition three GPSDOs were monitored at other laboratories within the UK. The participants in the study were: Absolute Time, Datum, Efratom, Hewlett-Packard, Motorola, Navstar, Radiocode Clocks, Rapco Electronics, Quartzlock, Tekelek, Trak, and Truetime.

3) EXPERIMENTAL MEASUREMENTS

A 16-channel phase comparator (TimeTech model PComp 16-001/96) was used to compare the GPSDO's frequency output, against the standard frequency output from NPL's active hydrogen maser (Sigma Tau, model MHM 2010) generating UTC(NPL). The phase differences were recorded every second.

Four 1-nanosecond resolution counter timers (Racal Dana Universal Counter Timers, model 1991) were used to compare the 1PPS signal generated by each GPSDO against a 1PPS signal derived from UTC(NPL). Two double four-way switch boxes (Hewlett-Packard Model 59307A) were used to monitor the output from each GPSDO in turn. This switching arrangement resulted in a duty cycle of one minute on, three minutes off.

Status information on both the performance of each individual GPSDO and on the GPS constellation was obtained from the RS232 serial communications port. All available data sets were recorded once per minute during the duration of the study.

Three eight-channel GPS receivers were used to continuously monitor the GPS signals received at NPL during the study. These included one Allen Osborne Associates TTR-4P receiver and two Motorola VP Oncore receivers (with the Z option). The Motorola Oncore receivers were particularly valuable, being inexpensive C/A code receivers, similar to those used in most GPSDOs.

Both the local temperature and the humidity of the environment were recorded using three Grant Squirrel Logger Model No. 1200. Published information on the status of the GPS and on UTC(USNO) - GPS Time have been obtained from the USNO WWW site. Internal cable delays between UTC(NPL), the 1PPS logging system and each GPSDO 1PPS output were calculated using a portable cesium clock (Hewlett-Packard model 5071A, high performance option).

4) STUDY RESULTS

Examples of plots of the extended measurements of UTC(NPL) - GPSDO(1PPS), calculated

from both the 1PPS and phase outputs, are shown in Figures 1 and 2 respectively. Figure 1 shows the 1PPS output of a highly stable rubidium-based GPSDO, while Figure 2 shows the output of a less expensive quartz-based GPSDO. Several trends emerged:

- There were in most cases a strong correlation between the 1PPS and phase output of the GPSDOs.
- There was a wide variety in the mean value of UTC(NPL) - GPSDO(1PPS), suggesting that there were significant offsets in the calibrations of the GPSDOs against UTC.
- The standard deviation of the UTC(NPL) - GPSDO(1PPS) measurements ranged from 10 ns to 155 ns. In general, the rubidium-based GPSDOs were more stable than the quartz-based GPSDOs.

Standard time and frequency statistics have been applied to the data. Plots of $\text{Log}_{10}(\sigma_y)$ and $\text{Log}_{10}(\text{MOD } \sigma_y)$ and $\text{Log}_{10}(\text{Mean fractional frequency offset})$ against $\text{Log}_{10}(\tau)$ calculated from the phase data are shown in Figures 3, 4 and 5. Several trends emerged:

- The long-term ($\tau > 10,000$ s) and short-term ($\tau < 100$ s) frequency stability of the GPSDOs was in most cases very similar, with the long-term frequency variations being effectively disciplined by the GPS signals, and the short-term performance being limited by the local oscillators within the GPSDOs.
- The medium-term frequency stability was extremely varied with values of $\text{MOD } \sigma_y$ ($\tau = 1,000$ s) varying by over a factor of 100. In general, the rubidium-based GPSDOs were significantly more stable than the quartz-based GPSDOs. For averaging times of 1,000 s, the effects of the Selective Availability (SA) degrading the performance of the GPS signal will be at its most pronounced. At this averaging time the GPSDO will be relying on the internal local oscillator for its frequency stability. The differences in the performances of quartz and rubidium oscillators, which may be relatively large at $\tau = 1,000$ s, will then critically affect the performance of the GPSDOs.
- Plots of $\text{Log}_{10}(\text{fractional frequency stability})$ against $\text{Log}_{10}(\tau)$ calculated from the phase data were characterized by two regions. For short averaging times, the value of the fractional frequency offset remained constant. At longer averaging times, the disciplining effects of the GPS signal became effective and the graphs had gradients of -1. The change in gradient marked the averaging time when the disciplining process became effective and is related to the time constant of the disciplining algorithm.

The performance of the free-running oscillator within the GPSDO were studied by examining the GPSDOs in the absence of a GPS signal. Plots of $\text{Log}_{10}(\sigma_y)$ against $\text{Log}_{10}(\tau)$ are shown in Figure 6 and are compared against the performance of the GPSDOs. The example shown in the figure is from a medium-priced quartz-based GPSDO. Several trends emerged:

In almost all cases, the disciplining process improves the long-term performance of the GPSDO. However, this is at the cost of degrading the short/medium-term performance. This degradation is clearly observed in the example shown.

The averaging time (τ) at which the degradation of the GPSDO performance is at its worst depends both on the type of local oscillator and on the time constant of the disciplining algorithm. The performance degradation was generally worse with quartz-based GPSDOs and occurred at shorter averaging times.

Around 30% of the GPSDOs under study displayed time and frequency transients of amplitude greater than 100 ns. Examples of a typical transient are shown in Figures 7 and 8 showing both the changes in UTC(NPL) - GPSDO and changes in fractional frequency offsets. When transients occurred, they were observed in both the phase and 1PPS outputs of the GPSDOs. The majority of the transients followed the same pattern. There was a sudden change in the GPSDO frequency, possibly due to a sudden change in the DAC value. The "normal" disciplining process of the GPSDO will then restore the time and frequency outputs of the GPSDO to within their "normal" operating range. These transients may last for several hours and may seriously undermine the use of GPSDOs as traceable standards of time and frequency.

Correlation effects between GPSDO outputs have been investigated. Some strong correlations were observed. An example is shown in Figures 9 and 10; the sum and difference of the two UTC(NPL) - GPSDO outputs are plotted. These results were obtained from two quartz-based GPSDOs. The correlation effects were strongest for quartz-based GPSDOs where the time constants for the two disciplining algorithms were similar. The correlation effects are due to the reception of common GPS signals by the GPSDOs, the performance of both GPSDOs being limited by the presence of the same SA signal degradation.

The GPSDO antenna coordinate determination has been investigated and compared with the coordinates determined from site surveys undertaken at NPL. The GPSDO coordinate errors range from 1.6 m to 51 m, the mean coordinate error being 21 m. Most GPSDOs are operated under a "position hold" mode when the first 24 hours or longer of data collected are used to determine the antenna coordinates. These coordinates are then "fixed" and are used for time and frequency dissemination. A few GPSDOs operate using instantaneously determined positions; however, there was a noticeable increase in the scatter on the resulting time and frequency outputs of these GPSDOs. Some GPSDOs operate from coordinates determined from continuous extended averaging. The performance of these GPSDOs were equivalent to those operating using a position hold mode. Where there was a combination of an extremely stable GPSDO and poor antenna coordinate determination, then the determination of the antenna coordinates may limit the GPSDO performance.

Substantial monitoring took place of the GPS signals received at NPL. Peak-to-peak variations of several 100 ns were observed. This is at the limit of what would be expected from the effects of SA.

The performance characteristics of a number of GPSDOs were investigated when operating them under 'non-ideal' conditions. In particular, studies of trends and variations in the performance of these GPSDOs were made for a reduced satellite constellation, a change of antenna coordinates, a complete loss of GPS satellite signal and also for a temporary main power failure. Reducing the satellite constellation by 50% had very little effect on the GPSDO performance, as may be expected. This is due to satellite redundancy in the constellation, whilst the GPSDOs were operated in a position hold mode. Each GPSDO was typically tracking between 6 and 8 satellites continuously when operating at the NPL site.

Erroneous position coordinates were entered into the receivers, with antenna position offsets of 100 m along each coordinate axis (eg., latitude, longitude and height) in turn. The use of offset coordinates resulted in a diurnal cycle in the GPSDO timing outputs (Figure 11). This effect is highlighted by the case of the vertical position offset. Plots are shown in Figure 11 for two successive days showing a clearly repeating cycle in the measurement of the (Local Clock(1PPS) - GPSDO(1PPS)). The resulting frequency transfer performance of the GPSDOs is degraded by this effect.

The integrity of a GPSDO following the loss of all GPS satellite signals was examined by masking out the satellite transmissions to the antennas. The time-to-alarm, i.e., the time between the loss of the GPS signal and the reporting of this loss by the GPSDO was carefully monitored for each GPSDO under study. Results from our study showed that nearly all of the GPSDOs successfully recorded the absence of GPS signals (two were unavailable for testing). The loss of signal was indicated either on the front panel of the receiver or via commands through the RS232 connection.

The main power supply to the GPSDO units was switched off for a period of 30 s, and changes in both the 1PPS and phase output were measured when the power was returned. It was found that the phase characteristics for most GPSDOs were severely disrupted for a considerable length of time after the loss in power. The timing 1PPS output before and after the loss were not noticeably different for all but two of the GPSDOs tested.

5) DISCUSSION

The extent of the NPL GPSDO study has enabled substantial information to be obtained on the performance characteristics of GPSDOs. Many of the GPSDOs under examination showed no anomalous behavior during the course of the study, and will, therefore, perform well as both time and frequency standards traceable to UTC(NPL). However, a significant minority of the GPSDOs under examination did show anomalous behaviour that might undermine their performance as either traceable standards of time or frequency. Anomalous behavior that might affect the GPSDOs capability of acting as a traceable time standard includes offsets in the mean value of UTC(NPL)-GPSDO(1PPS) and drifts in the GPSDO instrumentation delays. Time and frequency transients may affect the GPSDOs' capability of acting as both a traceable standard of time or frequency. The accuracy level of the traceability is also important. If time dissemination

with an accuracy of only a few microseconds is required, then all of the GPSDOs under examination would be suitable. The performance of the GPSDOs under non-ideal operating conditions suggests that there is a high degree of integrity in the GPSDOs' performance. However, the behavior of GPSDOs has not been tested in the presence of highly erroneous GPS signals. The above issues have given careful consideration when formulating the recommendations outlined in Section 6.

6) TRACEABILITY RECOMMENDATIONS

NPL has produced a set of provisional recommendations on the use of GPSDOs as standards traceable to UTC(NPL). These recommendations may be revised in the light of future studies or after discussions with other interested parties within the UK. NPL recommends that:

- NPL should monitor the GPSDO constellation from its Teddington site, and publish to the UK time and frequency community information on any GPS system anomalies.
- Values of UTC(NPL) - UTC(USNO) should be regularly published by NPL.
- NPL should produce a sample error budget for a typical GPSDO based on the GPS user range errors and supported by empirical measurements. Error budgets of this type may then be used to set the accuracy levels of the traceability for individual models of GPSDOs.
- Each manufacturer's model of GPSDO should be characterized for both its time dissemination and frequency dissemination properties. The characterization of individual models of GPSDOs is sufficient if conservative error budgets are used in establishing traceability.
- To achieve traceability for the highest accuracy time dissemination, (uncertainties < 1,000 ns) each individual GPSDO should be calibrated against a primary time scale. Two co-located GPSDOs should be operated at each location, so as to check for systematic delay changes. When considering time dissemination traceability, there is a need to calibrate the GPSDO internal delays, as these can dominate the error budget.
- The frequency stability and accuracy of a GPSDO be specified at the averaging times appropriate to the measurement process, and that the specified performance is validated by measurement traceable to a primary time scale.
- Unless a model of GPSDO has been shown not to be vulnerable to transient effects, either two GPSDOs should be operated in parallel, or a single GPSDO should be operated alongside a highly stable local oscillator, so that transients may be identified.
- Sufficient sky should be visible for the GPSDO to continuously observe the number of

satellites required to maintain the GPSDO locked to the GPS system. Hence GPSDOs should be operated for several days at a new installation. During this time a record of the satellites observed should be recorded to check on the satellite visibility at that location.

- The GPSDOs should provide warning of any main power interrupt. The GPSDO should provide information on when the local oscillator has stabilized following a power interrupt. The duration of the interrupt should be recorded.
- The GPSDOs should provide warning of any loss of GPS lock, the method of implementation being at the discretion of the manufacturer.
- When considering both time and frequency traceability, there is a need to assess the magnitude of the local position errors, and to determine when these first become significant in the overall uncertainty budget. We note that where position errors are important, the cost of GPSDO installation could be reduced if appropriate self validation schemes are possible.

7) FUTURE WORK

There is still substantial analysis to be performed on the data collected from the NPL GPSDO study. In particular, it is important to attempt to understand the origins of some of the anomalous GPSDO behavior, in particular the occurrence of time and frequency transients.

Results from the GPSDO study have been forwarded to UKAS. The realization of a mechanism for achieving GPSDO traceability to UTC(NPL) is extremely important. The production of an uncertainty budget giving a worst case error analysis for operation of GPSDOs may be a key part of this process. This uncertainty budget may then be checked as part of a detailed characterization of various models of GPSDOs. The results from the present study may form part of the characterization process. To ensure the correct operation of GPSDOs at sites where they are to be used as traceable standards, a set of guidance documents may be developed outlining the installing and initial testing of the GPSDO.

8) CONCLUSIONS

NPL has undertaken an extensive study on the performance characteristics of GPSDO, which has enabled recommendations to be made on the possible use of GPSDOs as standards traceable to UTC(NPL).

ACKNOWLEDGEMENTS

The authors thank: Absolute Time, Datum, Efratom, Hewlett Packard, Motorola, Navstar,

Radiocode Clocks, Rapco Electronics, Quartzlock, Tekelek, Trak, and Truetime for their participation in the study. This work has been supported under the National Measurement System for Time and Frequency.

REFERENCES

- [1] R.J.Douglas, May 1996, "Frequency traceability using GPS signals: A Canadian (May 1996) perspective on procedures for worldwide acceptance", NCSA, Ottawa.
- [2] P. Fisk and S. Quigg, "Evaluation and comparison of GPS-disciplined oscillators for use in traceable frequency dissemination".
- [3] A. Bauch and P. Hetzel, "Traceability via GPS disciplined oscillators", contribution to the proposed Euromet Project, PTB, Brunswick, Germany.
- [4] J. A. Davis and J. M. Furlong, March 1997, "A study examining the possibility of obtaining traceability to UK national standards using GPS disciplined oscillators", . Proc. 11th EFTF-97, Neuchatel, Switzerland, 4-7th March 1997, pp.515-519.
- [5] J. A. Davis and J. M. Furlong, 1997, "Report on the study to determine the suitability of GPS disciplined oscillators as time and frequency standards traceable to the UK national time scale UTC(NPL)", NPL report No. CTM1.
- [6] J. M. Furlong and J. A. Davis, October 1997, "Suitability of using GPS disciplined oscillators as time and frequency standards traceable to the UK national time scale," BEMC conference proceedings.

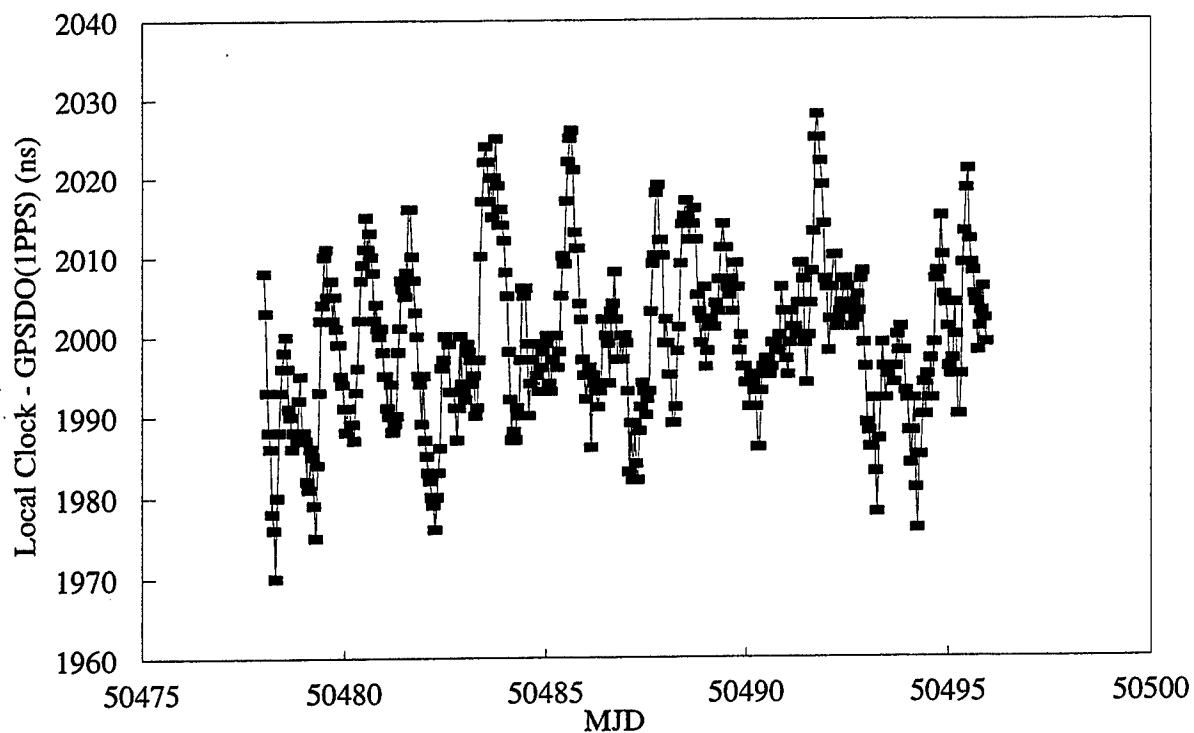


Figure 1: Graph of (Local clock - GPS(1pps)) calculated from an extended run of 1pps measurements

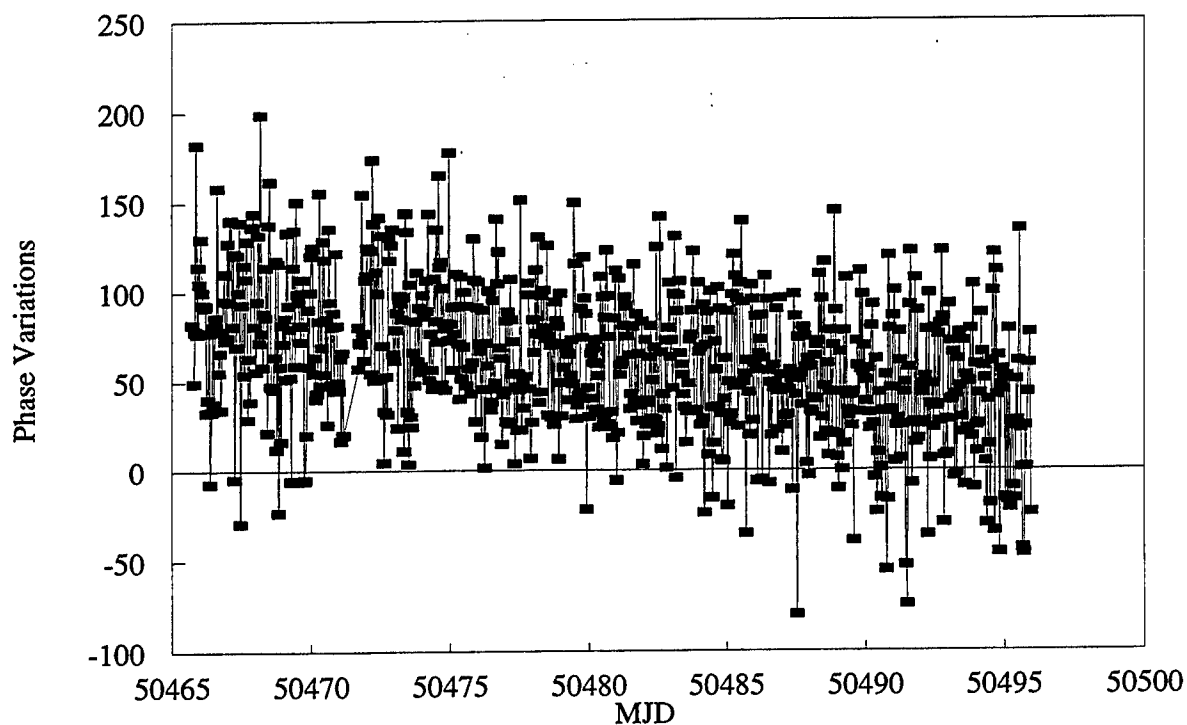


Figure 2: GPSDO phase variations calculated from extended measurements

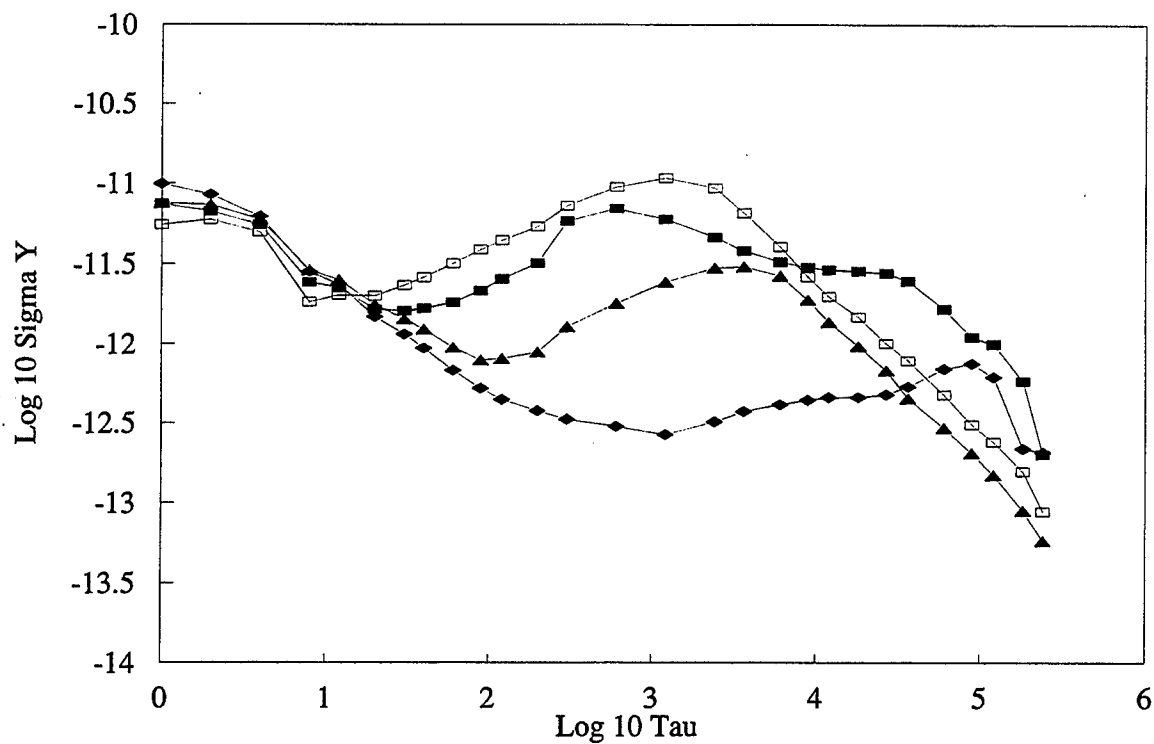


Figure 3: Graph of Log10 Sigma Y against Log 10 Tau - phase of GPSDO reference frequency

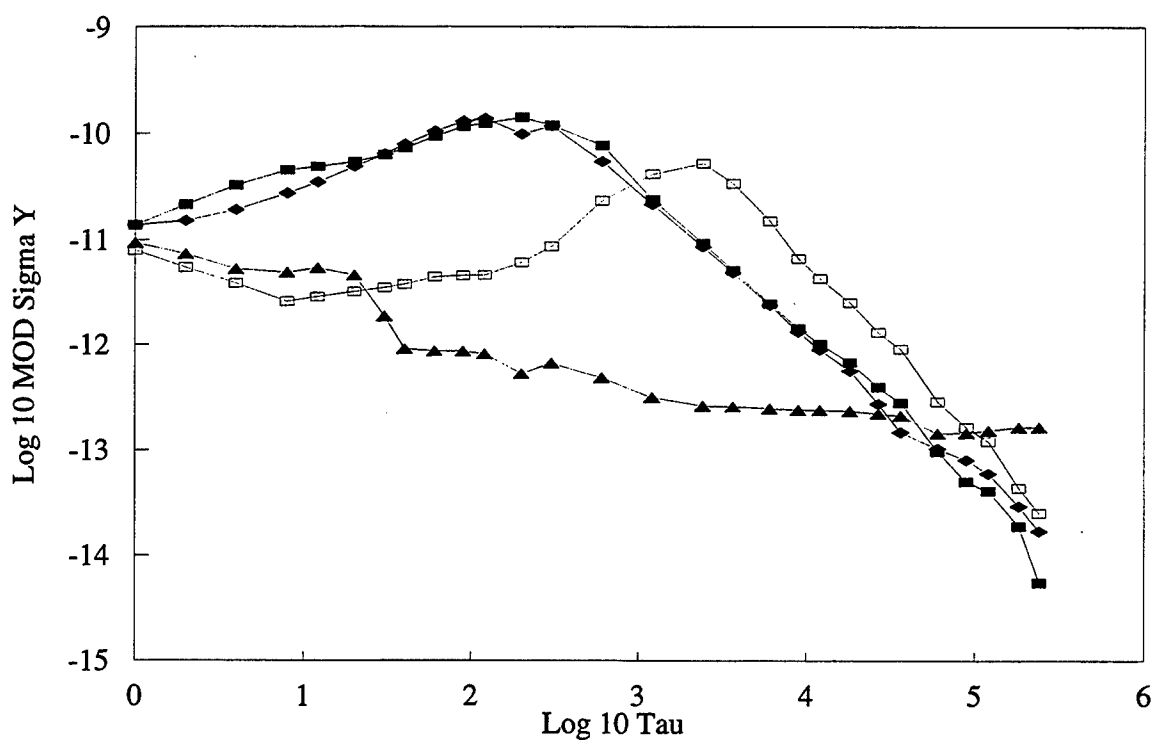


Figure 4: Graph of Log10 MOD Sigma Y against Log 10 Tau - phase of GPSDO reference frequency

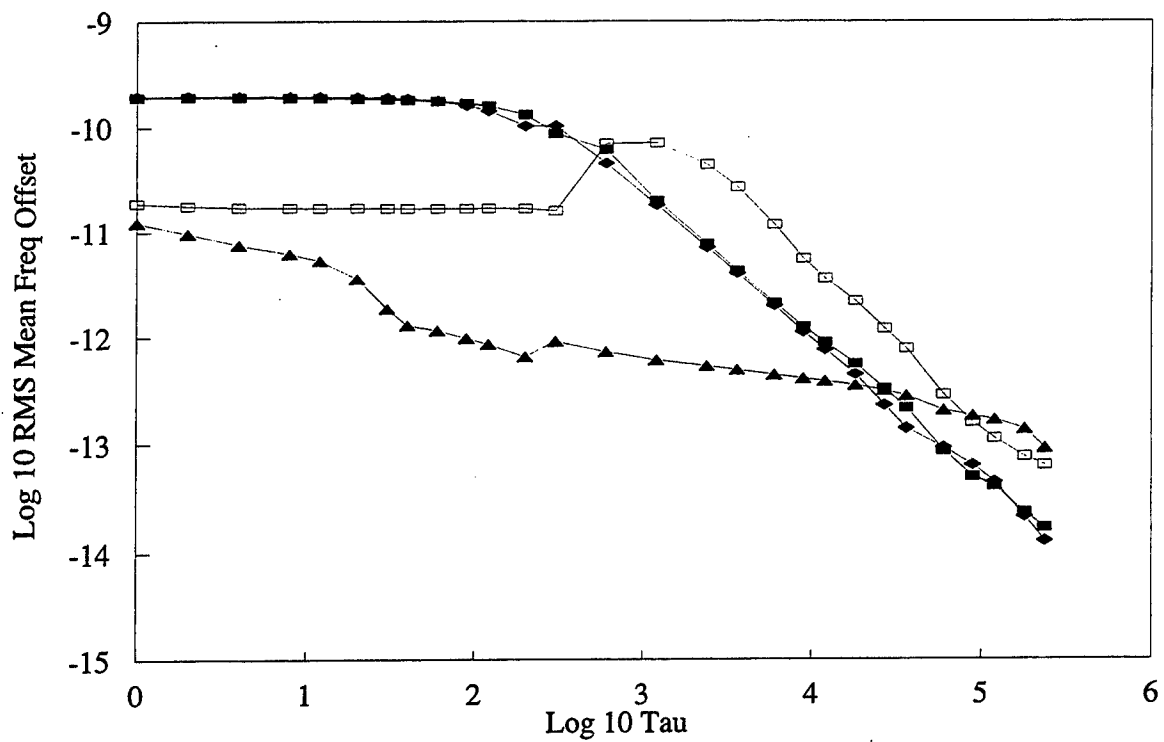


Figure 5: Graph of Log10 (Mean frequency Offset) against Log 10 Tau - phase of GPSDO reference frequency

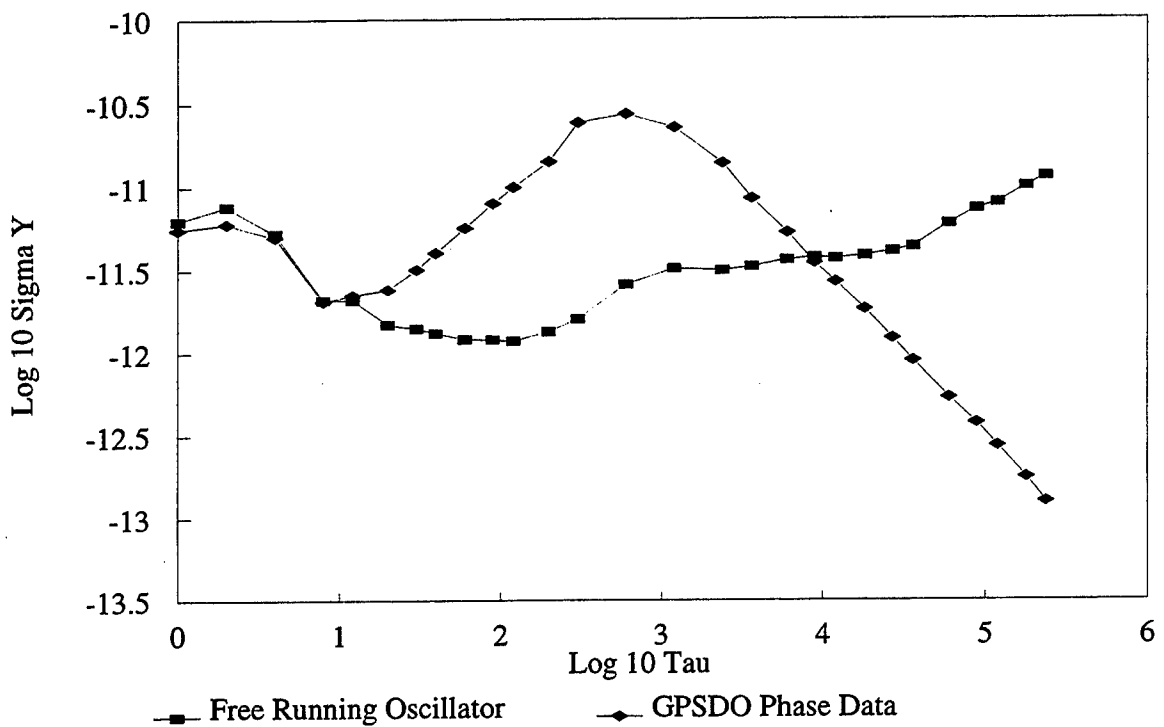


Figure 6: Comparison of disciplined and free-running local oscillators
Graph of Log 10 Sigma Y against Log 10 Tau

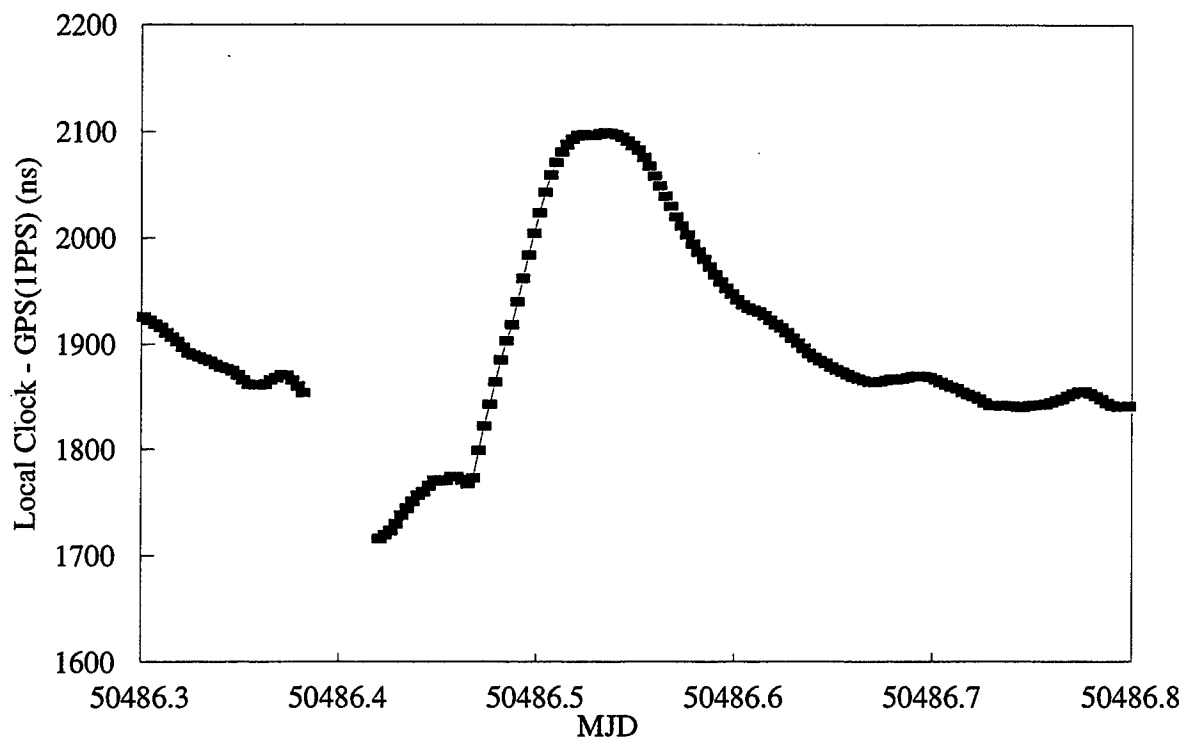


Figure 7: Time and frequency transient

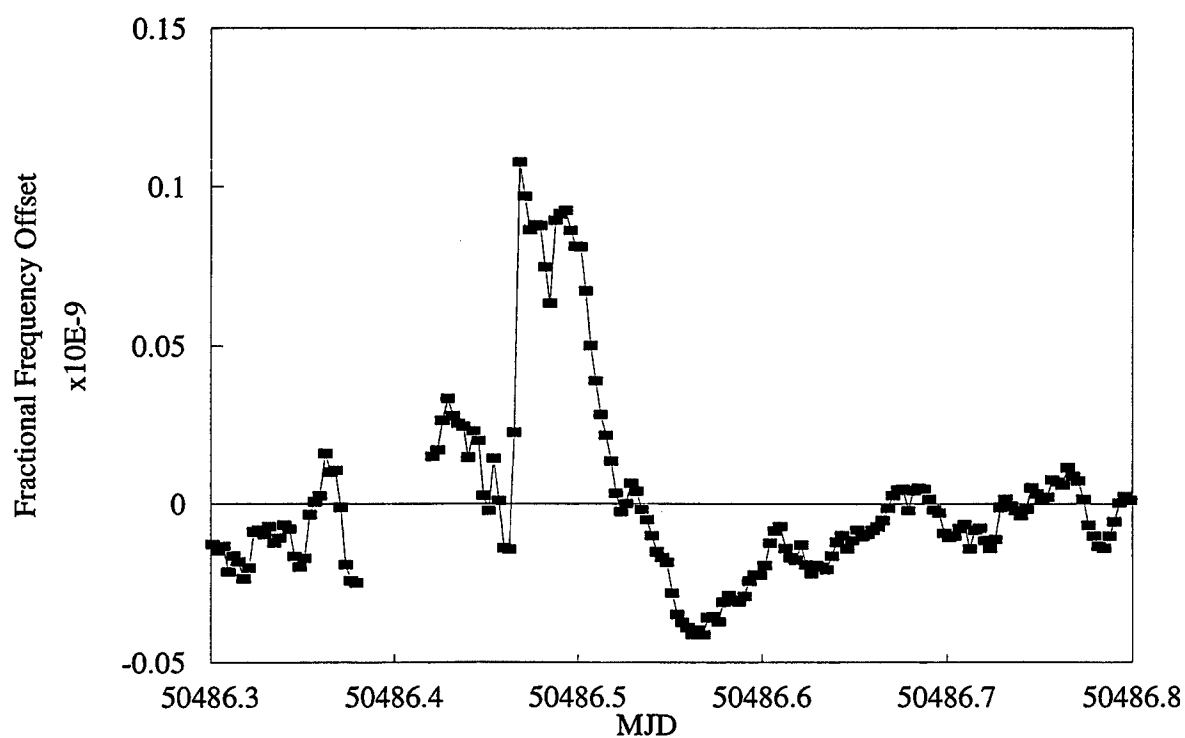


Figure 8: Time and frequency transient - fractional frequency offset

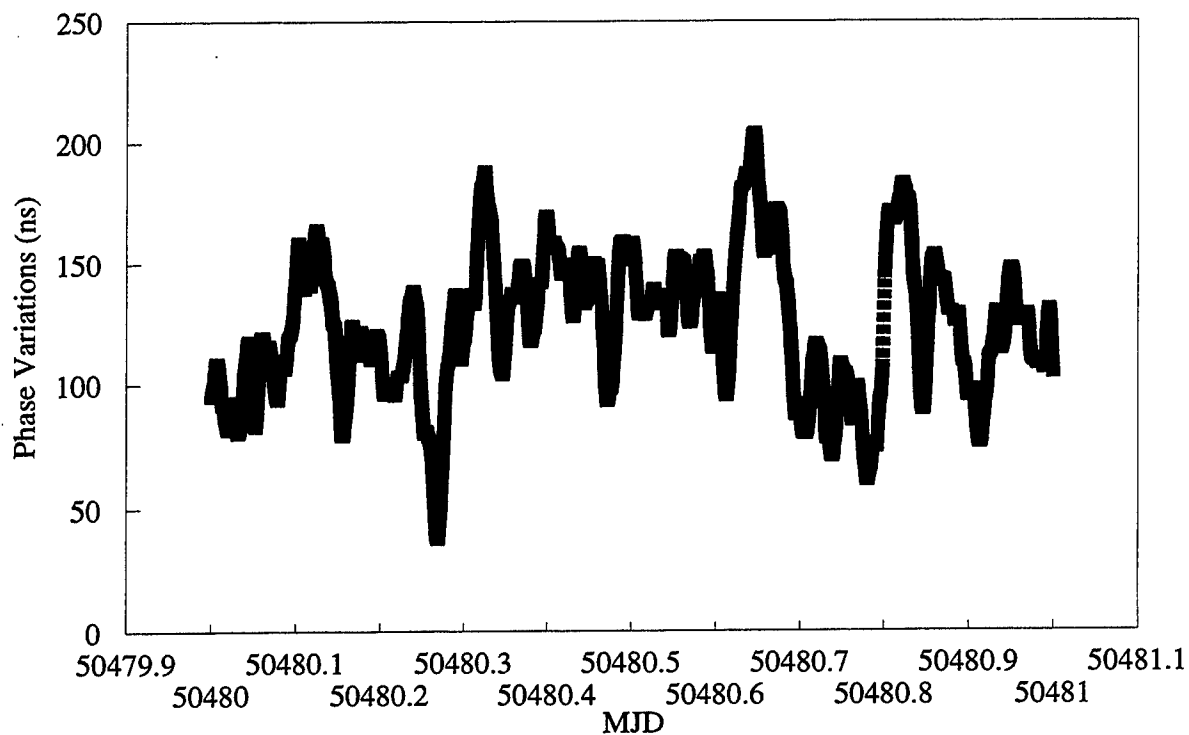


Figure 9: Phase variations of GPSDOs (sum)

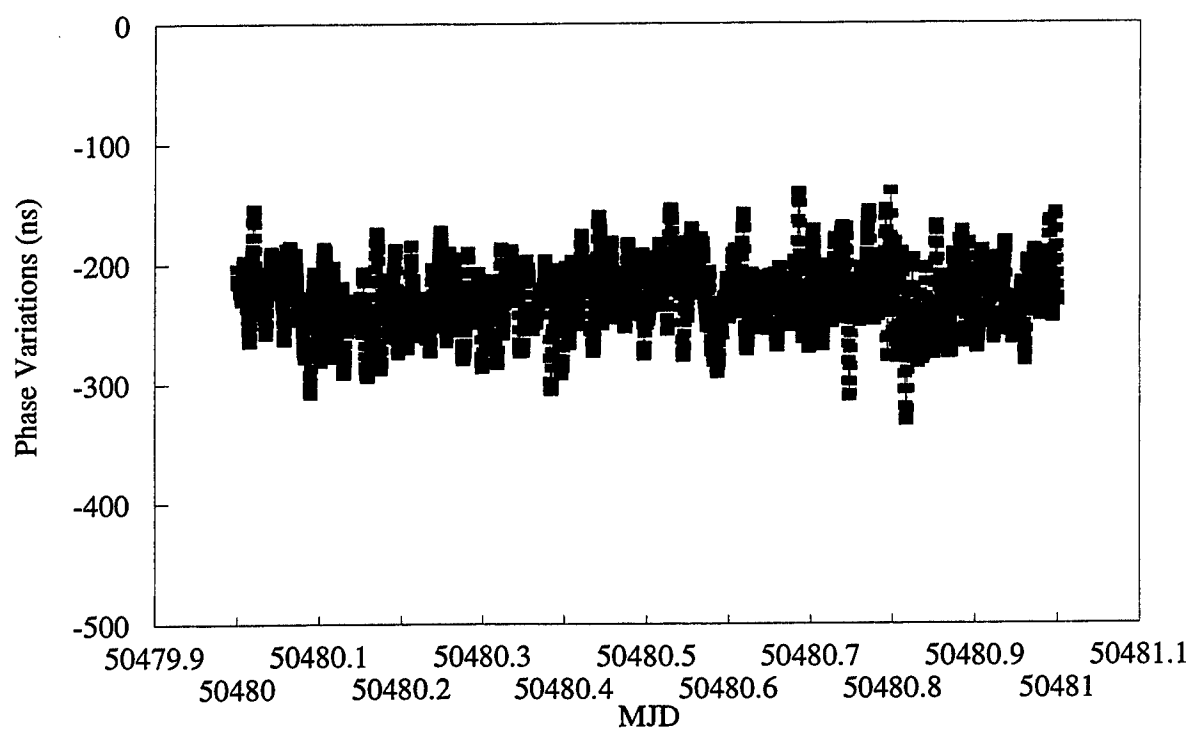


Figure 10: Phase variations of GPSDOs (difference)

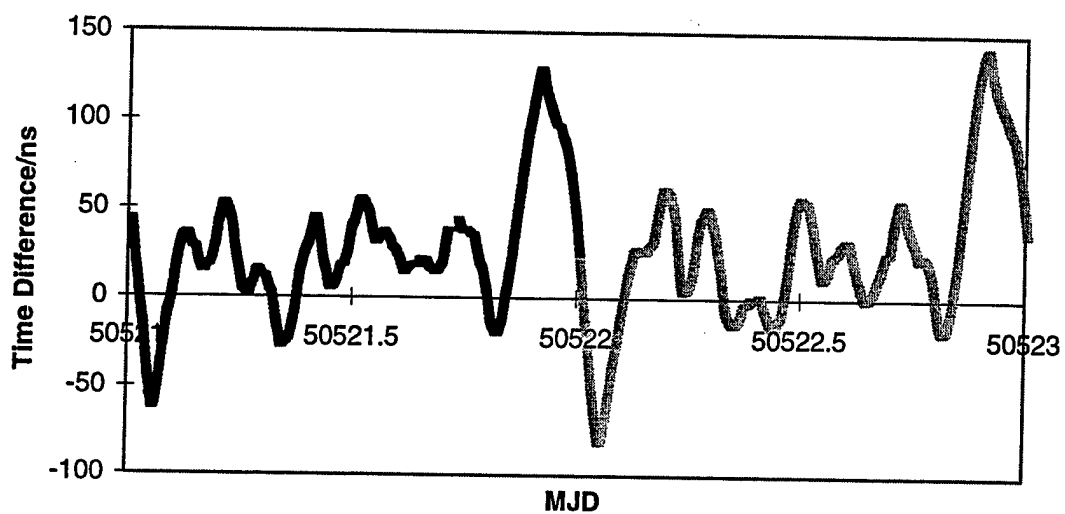


Figure 11: Phase output from a quartz GPSDO examined during the NPL study, after erroneous altitude coordinates have been entered into the unit. Note the repeating diurnal structure in the data.

Questions and Answers

DON MITCHELL (TRUETIME): We notice that some of the results you had were rather poor, in my opinion. Did you go back to the manufacturer and determine why those occurrences happened, - was there reasons?

JOHN DAVIS (NPL): We still do not do a lot of that. We have not as yet looked at the whole story because we have not had the chance to look in depth at the status information that was coming off the GPS Disciplined Oscillators (DO). So that is the first thing to do, and we will do that in the next few months. We have told all of the manufacturers, or at least they have seen the results for that particular disciplined oscillator; and some of the ones that are local to the UK. We have discussed what the situation is; and they have proposed some suggestions. They have just gone back to look at their GPS DO. There is still a lot of work to be done on that.

DON MITCHELL: I have a second question related to that as well. What is your end result that you are looking for from the manufacturers? Is it to certify receivers that are traceable to a certain level?

JOHN DAVIS: Yes, we want confidence in the receivers, that they will act as traceable standards to a certain level. So we are particularly worried that the transient effect for that model, that particular device, when a transient occurs that it will not be within the certified range.

DON MITCHELL: Are you discussing the results with NRC?

JOHN DAVIS: No, we have not as yet.

DON MITCHELL: I know that NIST is working on a similar thing, and Australia is working on something similar; so maybe you should try to get together an international consortium here to do this as a community effort.

ROB DOUGLAS (NRC): I should first of all say that the dialogue has begun. NPL is very kind in making available to us, and I think to many others in the timing community, a full copy of the report, which is a tome that is thick enough so you do not want to carry it around. My question, though, has to do with the concept of traceability when not all the elements are evaluated. Specifically, how do you envisage certifying a system as traceable when the multipath and positioning errors are not specifically known for a general site?

JOHN DAVIS: We are hoping that we can just, if you like, work on a worst-case basis, that at a given site the pass errors will not be greater than what we can put together for the worst-case estimate. I do not see any way we can go forward.

The other thing we would want to do is, we would actually not just certify the box, but we would actually certify the installation as well, so that we would actually look at the site; so we could actually check whether there were any large obstacles being placed next to the antenna.

ROB DOUGLAS: I think you are not quite as badly off as you claim. There is something that can be done for people who require it, and that is an on-site calibration of a GPS DO. This is where you would actually send an oscillator with known stability characteristics and a GPS receiver with known positioning characteristics and do a proper geodetic evaluation of the site and then a proper evaluation of the stability of the standard. From this you get an accuracy figure, with standard uncertainty versus averaging time.

Utilization of the Global Positioning System (GPS) for Timing Systems Under Range Standardization & Automation Phase-IIA Program

Ming C. Lee,

Lockheed Martin Space Mission Systems & Services

Abstract

Lockheed Martin was awarded a contract at the end of 1995 by the US Air Force to upgrade the space lift range infrastructure at Cape Canaveral Air Force Station in Florida and Vandenberg Air Force Base in California. The goal of the RSA Program is to reduce the total cost per launch while meeting the Range safety requirements. This will be accomplished on both coasts by adopting industry standards and replacing antiquated instruments with Commercial-off-the-Shelf (COTS) equipment. Furthermore, common operation and maintenance procedures will be developed for both ranges in order to reduce the total life cycle cost and subsequent operation and maintenance expenses at both ranges. The purpose of this paper is to present the overall system requirements and system architecture for the three timing product subsystems.

INTRODUCTION

Our Timing System consists of three product subsystems: GPS Timing, Range Countdown, and generation of Time of Vehicle First Motion (TVFM). These three product subsystems will directly or indirectly utilize the precise timing information broadcasted by the GPS satellites to generate accurate time, stable reference frequencies, countdown clock, and first motion time to support launch and launch related activities in both ranges.

GPS Timing Subsystem

Lockheed Martin proposed a GPS-based timing system to provide accurate time-of-day information, precise & stable reference frequencies, and clocks to synchronize communication network, computer workstations, and radar & telemetry instruments. The decision of implementing a GPS-based timing system is based on three significant factors. (1) The GPS Timing System has a significant lower initial procurement cost and subsequent operation and maintenance expenses compared against a primary

timing source, (2) The timing information broadcasted by the GPS satellites is available on a 24-hour basis, and (3) the accuracy of the GPS time is directly traceable to the DoD Master Clock (UTC-USNO) located at the U.S. Naval Observatory.

Requirements

Currently the stringent requirements imposed upon the GPS Timing Subsystem are that each timing station must have an accuracy within +/- one microsecond of UTC-USNO, the station-to-station accuracy must also be within +/- one microsecond, and all of the time codes generated by the GPS timing receivers must conform to Inter Range Instrumentation Group (IRIG) Standard 200-95, "IRIG Serial Time Code Formats". The accuracy and stability of timing product data are based on one sigma confidence level (68%).

The subsequent derived requirement requires that each timing station must be within +/- 500 nanoseconds of UTC-USNO, and the reference frequencies generated by each timing station shall be maintained at a Stratum Two level stability (1.6×10^{-8}). Based on a recent survey of commercial market, a typical Standard Positioning Service (SPS) GPS timing receiver will meet all of the timing requirements by maintaining an average of +/- 150 nanoseconds accuracy with respect to the DoD Master Clock. Furthermore, the reference frequencies generated by the GPS receivers will maintain a long-term Stratum One level (1×10^{-11}) of precision and stability. It has been determined that SPS receivers will meet and satisfy all of the requirements imposed by the Air Force.

Implementation

Each GPS timing station will either be a single receiver station or a redundant station. The GPS timing stations will be located throughout each range, including remote instrumentation sites. Refer to Figure 1, RSA-IIA GPS Timing System Overview.

Single Receiver Station

Each single GPS timing station will consist of a GPS-synchronized time and frequency receiver in a 3.5 inch chassis plus an antenna and pre-amplifier. Each timing receiver will have a basic IRIG-B and a One Pulse Per Second (1pps) output. In addition to the two basic outputs, each single station will have outputs for 1, 5, and 10 MHz reference frequencies and a multiple time code output module. The single receiver station will be strategically implemented throughout each range to allow timing users to receive time codes and reference frequencies from the nearest GPS timing station.

Redundant Receivers Station

Each redundant GPS timing station will consist of a redundant GPS synchronized time and frequency receiver in a distributed amplifier chassis with a fault-sensing switch unit (FSSU) embedded in the chassis. One of the GPS receivers will be designated as the Primary and the other one designated as Secondary (backup). Both the Primary and the Secondary receivers will generate the same seven time codes and reference frequencies (1 PPS, IRIG-B, 1, 5, and 10 MHz reference frequencies, plus two optional outputs). The same outputs from both receivers will be fed into the FSSU. Each FSSU module

will receive and monitor the time codes or reference frequencies from both GPS receivers. In the event of an anomaly in the time code or frequency module in the primary GPS receiver, the FSSU will automatically detect the interrupt of time code or reference frequency and switch the output from the Primary GPS receiver to the Secondary GPS receiver. The redundant receivers stations will be implemented at all Consolidated Instrumentation Facilities (CIF), because the CIF provides a significant role in tracking the vehicle flight and ensures safety of the civilian community surrounding the range. The redundant system will provide enhanced reliability in support of the operation of CIF.

Concept of Operation

Initialization & Cold Start

Each GPS receiver is designed to operate on a 24-hour basis. In the initiation stage, the geodetic information of each GPS receiver location will be programmed into the GPS receiver. In the case where the geodetic information is not available or the receiver is being used as a mobile unit, the GPS receiver will be initialized in the "AUTO" mode to allow the receiver to perform the long-term position averaging after it is stationary. It should take approximately 10 minutes to have the receiver lock on to the GPS constellation and download the new almanac data prior to performing a timing solution. Once the GPS receiver has been initialized, it will receive the GPS almanac information and determine the health of each GPS satellite. This will allow the receiver to only track the satellites that are healthy based on the almanac information provided by the GPS.

Generation of Time Codes and Reference Frequencies

In order to allow the GPS receiver to achieve its optimal performance, the receiver will be allowed to track as many healthy satellites as possible. Multiple satellites offer the strength of averaging and minimizing errors. The effect of Selective Availability (S/A, intentional degrading of accuracy) can be reduced by increasing the number of satellites being tracked. The antenna of the GPS receiver will be placed where an unobstructed and full view of the sky is available. Once the receiver has been initially setup, it will track the satellites that are available over the horizon. The propagation delay induced between the antenna and receiver will be compensated for by programming the cable delay at a rate of one nanosecond per foot based on the length of the cable from the antenna to the GPS receiver. All of the COTS GPS receivers we have looked at have modular design and are capable of generating accurate time codes and precise reference frequencies by implementing a time code module or a reference frequency module in the timing receiver hardware chassis.

Monitoring Health and Status of GPS Timing Receiver

This section describes some of the features in the GPS receiver that can be monitored by a Network Manager via the RS-232 interface of the GPS timing receiver. The following bullets describe the capabilities in some of the COTS GPS receivers that are currently available:

- **Acquire and Lock onto the GPS Satellites:** The GPS receiver will provide an indication whether the receiver has locked onto the GPS constellation.
- **Time Quality Check:** In a case of an anomaly in the GPS constellation or defective antenna, the GPS receiver will be unable to track the satellites. When an anomaly occurs, the internal oscillator will drive the time codes and reference frequency outputs. Since the oscillator is not perfect, each GPS receiver will have an average oscillator error rate programmed and will calculate the error that is being induced by the oscillator. There are different levels of error indication that can be obtained based on the rate of drift of the internal oscillator. Each level can be set up to provide an alarm and report the status to the Network Manager.
- **Satellite List:** A Network Manager will be able to retrieve information from the receiver via the RS-232 interface to see which satellite is currently being tracked.
- **Alarm Notification:** Health and status of the receiver will be provided to the Network Manager via the RS-232 interface. In case of an anomaly, an alarm notification will be generated for the Network Manager to initiate repair or maintenance action.

Reliability, Maintainability, and Availability (RMA) of GPS Timing Receiver

Based on the performance values supplied by some COTS GPS receiver manufacturers, a typical GPS receiver will have a Mean Time Between Failure (MTBF) of 78,000 hours, and Mean Time To Restore (MTTR) of 1 hour.

Distribution of Time Codes and Reference Frequencies

Since the proposed Timing System has a distributed architecture, instead of a centralized system, it is the intent that time codes and reference frequencies from each GPS timing station will only be distributed to local users. Conversely, each user shall obtain time codes and reference frequencies from the nearest GPS timing station. In order to maintain the required accuracy and precision of time codes and reference frequencies, time codes and reference frequencies will be transmitted using dedicated copper or coaxial cables. The error induced in the cable delay will be compensated for by the individual user.

Test & Evaluation

Accuracy of the GPS Timing Receiver

Each GPS timing receiver will be factory-certified and tested to guarantee its accuracy and confidence level. It is intended that the accuracy of each receiver will be re-evaluated during a scheduled or unscheduled maintenance by measuring the 1pps output against another 1pps generated by a primary time source or from another GPS receiver that has been calibrated by a standard laboratory.

The Stability of the Reference Frequency

The reference frequencies, generated by the GPS timing receiver, will be measured against a calibrated frequency counter or reference oscillator. The reference oscillator must be either a primary standard, if available, or another GPS disciplined frequency standard at least of equal stability to the unit under test. The stability of the reference frequency will be measured by an oscilloscope. All clocks and reference frequencies will be verified to ensure that the stability is maintained at a Stratum Two level (1.6×10^{-8}).

Maintenance Concept

All of the GPS timing receivers and associated equipment will have modular design using solid-state electronic components. All of the repair and scheduled and unscheduled maintenance will follow the prescribed maintenance procedures mandated by the manufacturer.

Summary of GPS Timing System

The overall system architecture is defined based on the requirements specified in the Space Lift Range System (SLRS) Specification. The goal of a modernized GPS-based timing system is to reduce the cost of operation and maintenance. We believe the employment of a GPS-based timing system will enable both ranges to achieve this goal.

Range Countdown Subsystem

The Countdown Subsystem provides a timeline for coordinating a multitude of tests and system validations between the Range and space vehicle operator in preparation for the launch of space vehicles. This is to ensure that the range and vehicle operator are operating on the same time scale with a common lift-off time.

Countdown System Requirements

The current requirements, specified in the Space Lift Range System Specification, indicate that the Countdown Subsystem shall provide eight simultaneous countdown signals. The accuracy of the countdown signal shall be within ± 100 milliseconds against the DoD Master Clock with a reference to a countdown script. The countdown format shall conform to the Inter Range Instrumentation Group (IRIG) 215-96 Standard. The Countdown Subsystem shall also provide the capability to allow authorized personnel to initiate, synchronize, suspend, resume, and terminate the countdown operation.

SLRS Countdown System Architecture Overview

This section describes the overall Countdown System Architecture. This includes how the countdown and lift-off signal will be generated and distributed to the Control and Display Segment (CDSEG), Instrumentation Segment (ISEG), and other internal and external SLRS users.

Countdown Data Format & Generation of Countdown Signal

There are four formats assigned under the IRIG 215-96: CS-511z, CS-522z, CS-513z, and CS-524z. There are two major determining factors why CS-524z was chosen. The first reason is that CS-524z allows the transport and display of countdown, vehicle first motion time, and lift-off indication as one data stream. The second factor is that the ASCII countdown data can be easily distributed using ATM/SONET transport medium. This is compatible with the proposed digital transport network that will be implemented under the RSA Program.

The CS-524z format consists of two elements. The first element is the countdown data, which consist of countdown information in days, hours, minutes, seconds, and tenth of seconds. The second element consists of the predicted or the actual lift-off time in days, hours, minutes, seconds, and milliseconds, and the launch information word. The launch information word provides the status of the launch vehicle. While the launch vehicle is still on the ground, the launch information word is represented with an ASCII "P" (predicted), which indicates that the launch vehicle is still on the launch pad, and the second element of the countdown data currently represents the predicted launch time. When the lift-off signal is received from the launch pad, the launch information word changes from an ASCII "P" to an ASCII "A" (actual), which indicates that the launch vehicle has lifted off from the launch pad and the second element of the countdown data represents the actual lift-off time.

The CS-524z countdown signal will be generated by a COTS countdown generator. The CS-524z will be outputted in an asynchronous ASCII format. It is intended to be transmitted at 9.6kbps with an RS-232 interface/connector. A total of eight (8) countdown generators will be procured to support the requirement of providing 8 simultaneous count signals. Each countdown generator will utilize an external IRIG time code with +/- 5 microseconds accuracy, generated by a GPS timing receiver, as the reference. The microprocessor, within the countdown generator, will be synchronized to the external IRIG time code and will generate the ASCII countdown data within +/- 100 milliseconds accuracy.

Distributing Countdown Signal to Control and Display Segment (CDSEG)

CDSEG provides a Local Area Network (LAN) connecting computer workstations to display operation data generated by various radar, telemetry, and optic instruments. The countdown data will be provided to the LAN server with an RS-232 physical connector and subsequently distributed to workstations via Distributed Computer System (DCS). Furthermore, an IRIG-B signal will be provided to the Network Timing Server (NTS) to allow all of the workstations on the LAN be synchronized to the same time.

Distributing Countdown Data to Instrumentation Segment (ISEG)

The ISEG provides tracking of vehicle flight utilizing telemetry receiving instrument, radars, and long-range and short-range optics instruments. The countdown signal will be distributed to these instruments via the Asynchronous Transfer Mode (ATM) network, digital microwave transmission system, or Synchronous Optical Network (SONET). The data format of countdown information will remain in ASCII throughout.

Distributing Countdown Data to External Range Users

The countdown data will be distributed to external Range users in the original ASCII format via the SONET/ATM transport medium. If the external user is located beyond the boundary of the Range campus, the countdown data will be delivered to a designated demarcation point. Subsequently, the data will be transported via another transport medium or carrier to the final user destination.

Concept of Operation

There are five functional capabilities that are required for the countdown subsystem, as specified in the Space Lift Range System Specification. These capabilities are: initiate, synchronize, suspend, resume, and terminate. All of these functional capabilities will be provided either via the keypad on the front panel or by an RS-232 interface from the countdown generator. Each functional capability is described below:

- **Initiate:** The countdown generator will be initiated by an authorized Range Operation personnel in order to perform the operation. Based on the operator input, the countdown generator could be programmed so the countdown can commence at a pre-determined time (UTC-USNO).
- **Synchronize:** The countdown generator could be adjusted to forward or retard the negative count based on the countdown script. An optional RS-232 interface will be available to receive the countdown clock generated by the vehicle user to allow Range operator to synchronize the range countdown to the user-generated countdown clock.
- **Suspend:** The countdown generator will provide the capability to allow authorized Range operator or Range user to suspend the countdown. The authorized personnel will be provided with the capability to suspend the count at a pre-determined time or instantaneously via an external interface to the countdown generator.
- **Resume:** The countdown generator will provide the capability to allow the authorized Range operator to resume the count from the termination of count suspend. The countdown generator will provide the capability to resume the count at a pre-determined time. This will allow the continuation of count for the operation.

- **Terminate:** The countdown generator will provide the capability to the authorized Range personnel to terminate the count upon completion of the operation.

Summary of Range Countdown System

The overall Countdown Subsystem architecture is entirely based on the requirements specified by the requirements stated in the Space Lift Range System Specification. The overall architecture will standardize the operational procedures and provide reduced cost of maintaining different hardware at both ranges. Furthermore, the new Countdown Subsystem will incorporate the features to integrate TVFM Subsystem in a common hardware chassis to enhance operation capability at both ranges.

Time of Vehicle First Motion (TVFM) Subsystem

The TVFM Subsystem generates the time and lift-off indication associated with the occurrence of the lift-off event. The first motion is primarily used as an event marker for the start of vehicle flight. The telemetry and metric-processing computers use the lift-off indication and time of first motion to compute the real-time position of the launch vehicle against the trajectory data to ensure the vehicle flight is nominal.

TVFM System Requirements

There are two requirements that are imposed upon the TVFM system. The first requirement is to time tag the lift-off event within +/- 10 microseconds after the lift-off signal is received. The second requirement is to distribute the TVFM and lift-off indication to internal and external Range users.

TVFM Subsystem Architecture Overview

Generation of TVFM

Since CS-524z countdown format has the provision of including the TVFM as part of the data stream, it is the intention to build the TVFM Subsystem as an integral part of the Countdown System. The vehicle user will be required to provide a 1 KHz sinewave to the range in order to generate the TVFM. While the launch vehicle is on the ground, a 1KHz sinewave is generated and distributed to the Range. Once the launch vehicle is lifted off from the launch pad, the 1 KHz sinewave is interrupted. The 1KHz sinewave will be transported, via a DS-0 voice channel off the SONET transport medium, to the countdown generator. When the countdown generator detects the interrupt of the 1KHz sinewave for a minimum of six milliseconds, the TVFM is generated. The generation of TVFM will take into consideration and compensate for the six milliseconds delay and the delay of distributing the 1KHz sinewave through the SONET transport system to ensure the TVFM data is accurate. (Refer to Figure 2, TVFM Subsystem Overview)

TVFM Hardware

Since the TVFM will be an integral part of the Countdown System, the TVFM subsystem will share the countdown generator hardware chassis with an implemented Event Capture Module. Once the TVFM is

generated, the time of vehicle first motion information will be provided to the Countdown Subsystem and the TVFM information (lift-off time and indication) will be included as part of the countdown data stream. The receipt of lift-off signal will also trigger the launch information word from an ASCII "P" to "A" which indicates that the lift-off event has occurred.

Transport of TVFM & Lift-Off Indication

The TVFM and lift-off indication will be distributed to CDSEG, ISEG, and other users as part of the countdown data stream. The TVFM and lift-off indication will be transported in the same manner as the countdown information.

Test of TVFM System

The TVFM will be verified against the IRIG time code generated by a GPS timing receiver. The accuracy of the TVFM is based on the receipt of the lift-off signal by the event capture module excluding the transmission delay. Since the TVFM is referenced to the IRIG time code input into the countdown generator, the accuracy of the TVFM will be that of the accuracy as the input reference IRIG time code.

Issue & Concern

The only issue that remains with the TVFM Subsystem is the requirement to time-tag the lift-off signal to within +/- 10 microseconds after the lift-off signal is received in the range. The concern is the delay variation of sending the lift-off signal through the SONET multiplexers and transport equipment, which may exceed 10 microseconds. This issue is currently being looked into to determine if the delay through the ATM or SONET can be minimized to within 10 microseconds.

Summary of TVFM System

The TVFM System will be an integral part of the Countdown Subsystem sharing the common hardware chassis. An integrated Countdown and TVFM System will relieve the Ranges from customized hardware and software systems and allow the government to realize subsequent savings in the areas of operation and maintenance.

Summary

The goal of the RSA program is to utilize COTS equipment with a standard management interface for ease of control, configuration, and management. The GPS Timing System, Countdown Subsystem, and Time of Vehicle First Motion Subsystem will utilize COTS equipment with the anticipation that subsequent operation and maintenance expenses can be minimized. The GPS Timing System and associated subsystems will be implemented beginning in August, 1998. Test and evaluation data from these subsystems will be collected to verify the requirements and performance imposed by the customer.

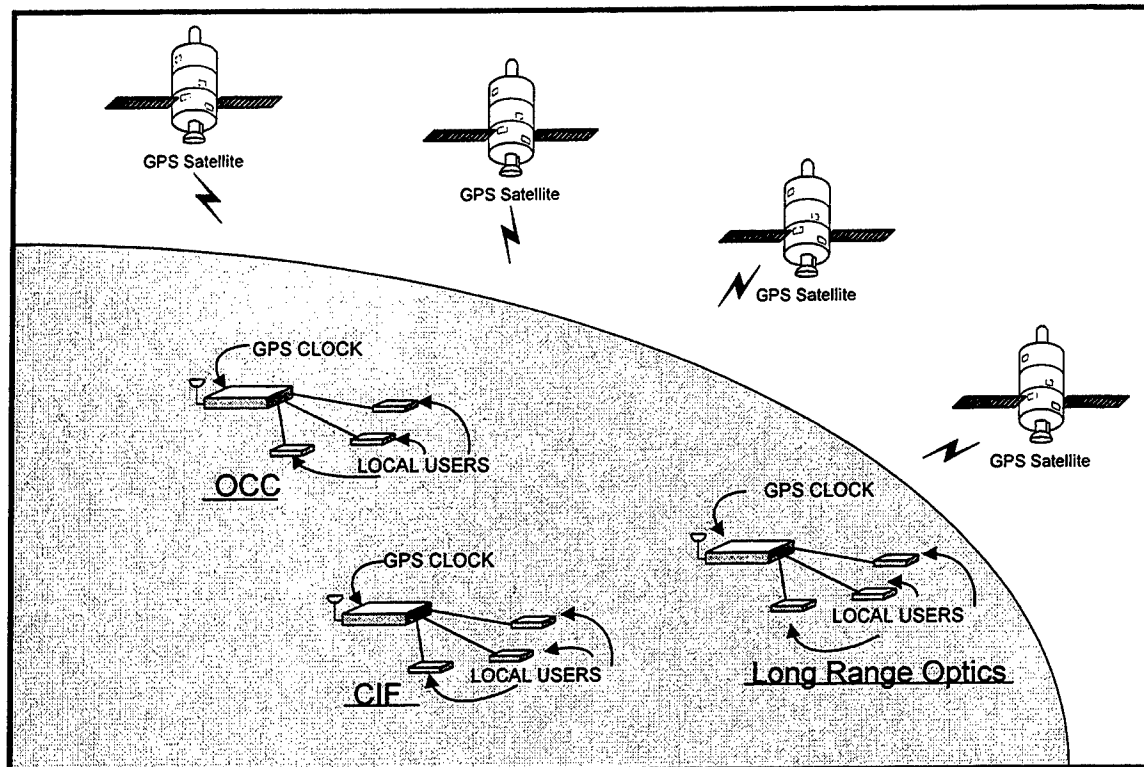


Figure 1 RSA-IIA GPS Timing System Overview

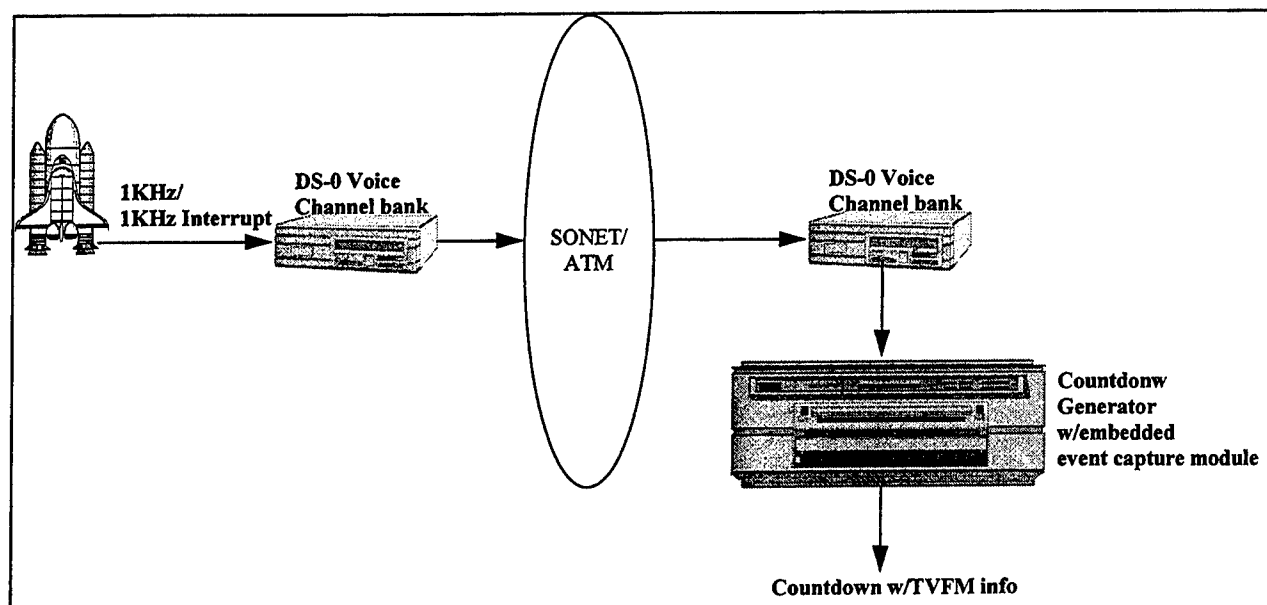


Figure 2 TVFM Subsystem Overview

Questions and Answers

JEFF INGOLD (ALLIED SIGNAL TECHNICAL SERVICES): Just wondering, you mentioned that you have not designed this yet. On the GPS segment, you said it was going to be CA Code. Have you picked if it is going to be a GPS-disciplined quartz oscillator or a rubidium?

MING LEE (LOCKHEED MARTIN): It is going to be a quartz oscillator.

HAROLD CHADSEY (USNO): We are currently controlling a cesium clock there via a micro-stepper. We are also doing the same thing at Vandenburg. Is this going to be an enhancement to that system and alternate to it, or how is it planned to be implemented?

MING LEE: I think my program will be totally separate from what is being done with a micro-stepper. I am not familiar with that part of the timing system in the Eastern range. As far as on the Western range, I believe that the company you are talking about is Precision Measurement Electronic Labs, so that is not part of the range. I do not think I will be dealing with that aspect of it. I am strictly dealing with the operation of the range.

THE WSMR TIMING SYSTEM: APPROACHING THE HORIZON

William A. Gilbert
White Sands Missile Range, New Mexico

Abstract

Over the past couple of years, WSMR has made significant strides in modernizing its Timing System. WSMR has purchased a new Master Timing Generation System (MTGS) to replace a thirty-five year old system. Specifications were written and requirements contracts were developed for Timing distribution equipment which includes Synchronized Time Code Generators (STGs), Versatile Timing Amplifiers (VTAs), and distribution units. This paper will explain why particular designs were chosen, the significance of the MTGS in the WSMR Timing System, and the difficulties associated with implementing a modernization plan.

Introduction

Significant modernization of the WSMR Timing System has not occurred for over twenty-five years. Yes, there have been improvements made, but most of them were from the modification of equipment and small purchases of hardware (mainly for programs with special needs). Over the last three years, however, Timing personnel have worked diligently to find ways to modernize. They developed and adopted a plan that clearly states the goals required for modernization and they established a mechanism to purchase new equipment when funds became available. In 1997, Timing reached one of their stated goals with the purchase and installation of a new Master Timing Generation System (MTGS). This new MTGS replaces a system that's been in service since 1962, which is only a few years older than some of the Synchronized Time Code Generators (STGs) used on the Range. Timing now has fifteen new STGs on hand and will need to purchase and install another three hundred and fifty before fulfilling the current needs.

Another activity that will improve the Timing System's effectiveness and reliability is the consolidation and reduction of Timing facilities. Timing has already started this process by installing the new MTGS at C-Station. C-Station is the current maintenance facility that will eventually house all of the clock, generation, and distribution equipment that resides at Uncle 2 (Present Master Timing Station). This will allow the Timing manager to more efficiently use the available personnel by drawing on the combined resources of both groups from one location. Additionally, Timing has closed several distribution stations and reduced the number of communication circuits required to carry Timing signals. These actions described above are all part of an ongoing process to try and improve the entire Timing System at WSMR. The following paragraphs will discuss in greater detail some of the changes that have occurred in the Timing System at WSMR, and how these changes have improved and provided the foundation for modernizing the Timing System.

Master Timing Generation System

There are three basic parts that make up the MTGS: a redundant Master Clock, the Time Code Generators (TCGs), and the distribution subsystem (See Figure 1). The Master Clock consists of a Global Positioning System (GPS) receiver and a set of cesium standards. The time code output from the GPS receiver initially synchronizes the TCGs and the frequency output from the selected cesium standard provides the time base. The three TCGs produce IRIG time codes A, B, E, and H in the modulated and DC level formats. These signals go to the Fault Sensing and Switching Unit (FSSU) for analysis, and the FSSU outputs the selected signals for distribution.

The WSMR MTGS produces InterRange Instrumentation Group (IRIG) time code signals. The time represented by these signals is the time of the WSMR Master Clock. To ensure the Master Clock remains within two hundred and fifty nanoseconds of UTC, the Correlator Switching Unit (CSU) constantly monitors and compares the selected standard's output to GPS. If an excessive amount of phase difference develops, the CSU will compare the backup Cesium with GPS and will switch it on line as long as it is within tolerance. By using GPS as a tool for the MTGS, the system has Coordinated Universal Time (UTC) traceability and has the capability to operate independently of the GPS source. This feature is very important since GPS is not always available on the Range.

Other important features of the MTGS are its ability to analyze the Time Code Generators (TCGs) outputs and the ability to switch TCG outputs when the MTGS determines there is a failure. The unit that performs this function is the FSSU. The FSSU uses a majority voting scheme to determine if the selected TCG's output time codes are valid. If the FSSU determines the phase offsets of the on-line TCG's output time codes are excessive when comparing them to the majority, the FSSU places the secondary TCG on line. This minimizes the possibility of time code errors and assures a continuous quality output.

As stated earlier, the new MTGS replaces a 1962 system. It is amazing how the fundamental design of the new MTGS mirrors that of the 1962 system. Yes, the new MTGS uses modern state-of-the-art components, but the fundamental design remains. Just as the fundamental use of the MTGS remains; which is to provide precise time and time interval information to WSMR facilities and to all Range customers. The purchase of the new MTGS assures that this service will continue in the future and provides the foundation upon which to build a modern Timing System.

Synchronized Time Code Generators

Time and time interval information provide a standard reference for all data collection, recording, display, and reduction systems at WSMR. WSMR uses GPS, VHF radio, and communication circuits (voice) to disseminate time signals. Most of the present systems at WSMR use a combination of equipment to obtain time at their sites. For instance, customers using the VHF system use a VHF receiver whose output synchronizes an STG and then its output goes to some other interface to get the time information in the proper format for use. The new STG specified for WSMR incorporates all these features in a single chassis. The new STG has modules available for synchronizing to time information from GPS, VHF, or communication circuits. Additionally, the STG can have more than one synchronizer installed at a time. The STG allows the user to

choose a primary and backup source for synchronization and will automatically switch to the backup synchronizer after the primary synchronizer has failed for a predetermined amount of time. During the period of time between primary failure and secondary switchover, the STG uses the internal oscillator at its last disciplined center frequency as the time base for time accumulation. In areas where a disruption of GPS service may occur, Timing personnel will configure these new STGs with a primary and backup sync source. This ensures quality service will continue under just about any circumstance.

During mission testing at WSMR, the amount of Timing equipment supporting a test can be in the hundreds. Most of the equipment is in the customers' systems, and Timing personnel have to configure it to meet that customer's specific requirements. The new STG will make the job of configuring Timing equipment much easier. The STG has modules that outputs most IRIG serial and parallel time codes, can generate both sinewaves and pulse rates at various frequencies, provides both digital and differential drivers, and has an IEEE interface, to name a few. The new STG has twelve slots to accommodate the different modules required. Essentially, Timing personnel can replace a half of rack of equipment with a single three-and-a-half inch chassis. In these days where space and time are at a premium, this makes a big difference.

Most of WSMR's Timing equipment requires Timing personnel to go out and check it to make sure it is working properly. This increases the amount of personnel and labor hours required to run the Timing system. The new STG will reduce this workload somewhat by having the capability of shipping pertinent information about it to monitor points. Some of the information the new STG can ship remotely includes: the types of modules installed, which slot the module resides in, fault status of each module, menu setup, time information, and oscillator performance. One of the primary goals set forth in the modernization plan by Timing personnel is to find ways to reduce the number of labor hours required to maintain the Timing system. Since there will be three hundred and fifty of these STGs throughout the Range, having a remote capable system sure will help reach that goal. Finally, one other goal that is very important that pertains to the new STG is ensuring its longevity. The STGs that are in use today have been in use for almost thirty years. There is no reason to believe that these new STGs won't have to perform the same feat. For this reason, Timing personnel placed great emphasis on the design and configuration of the new STG. The modular design of the STG, as well as the capability for easily upgrading the software, should aid in accomplishing this goal.

Versatile Timing Amplifiers

At WSMR, fixed (non-tracking) cameras provide a means of measuring the angular direction of an object by recording the object along with external and internal references on photographic film at successive instances in time. These sequences of photographs taken together with Timing data make it mathematically possible to determine a test object's trajectory. The device WSMR currently uses to place Timing on fixed camera film is the Camera Timing Amplifier (CTA). The CTA places precise pulses or Timing pips on film by energizing Light Emitting Diodes (LEDs). To energize these LEDs, the CTA uses each mark cycle of either serial time code format A or B. The code selection is based on the speed of the film and the Timing resolution required. The CTA normally receives its Timing signal via wireline, but the latest version of CTA can use a GPS module to transfer time and generate the required serial time code.

This modern CTA, called the Versatile Timing Amplifier (VTA), has many more uses than the designers envisioned. The VTA has a buffered output of the input signal that can be used to drive other CTAs or other time code equipment (daisy chaining). It's small and compact, weighing less than twelve pounds, and it comes with a battery that can last up to five hours before it requires recharging. This allows Timing personnel to go and set one of these units up in the middle of the desert without any other support and be ready for a test. The VTA also uses a quality oscillator that has a drift rate of less than two microseconds per hour for four hours after GPS has disciplined the oscillator for an hour. Hence, the VTA can exceed most Timing accuracy requirements at WSMR and is versatile enough that Timing personnel can use it most anywhere.

Distribution Units

The primary purpose of the Timing system is to provide time information in formats Range customers can use. This means Timing personnel must interface the Timing outputs from their Timing receivers with whatever equipment the customer has. One important piece of equipment that Timing uses to interface Timing signals with Range equipment is its Distribution Unit (DU). The DUs in use today are a little over twenty years old. They have worked wonderfully, but parts for them are scarce and new requirements exceed their capabilities. Timing has started fixing this problem by replacing them with new modern units. The new DU consists of a base chassis with a plug-in power supply and a variety of plug-in units available for demodulation, amplification, shaping, and distribution of Timing signals. The chassis fit into a standard nineteen-inch equipment rack and will accommodate up to thirteen modules. The two most popular modules scheduled for replacement are the dual-line amplifier and the demodulator amplifier. The dual-line amplifier distributes serial modulated time code formats over a frequency range of 30 hertz to 300 kilohertz (IRIG A,B,D,E,H). The amplifier can drive fifty and six hundred ohm loads with mark-to-space ratio ranging from two to one to six to one. The demodulator amplifier accepts serial modulated time codes as an input and reconstructs the DC level shift version of the time code. Its input to output delay is less than 45 degrees of the carrier frequency and the output is adjustable from 0 to 10 volts. This module typically drives strip chart recorders and FM multiplexing equipment. So far, Timing has twenty DUs and around one hundred and fifty modules, which is far short of what Timing requires to replace these aging units.

Remote Monitor System

Unmanned Timing stations at WSMR use a phase monitor and bit error detection system technique to alert Timing personnel when a discrepancy occurs between two compared signals. This technique compares the phase and time information generated from the sites STGs. Any differences between the time information or an excessive amount of phase will activate an alarm. Timing personnel monitor these alarms at the three customer service centers and take the appropriate corrective actions once an alarm has occurred. The new STGs have an RS-232 output that can provide health, status, and time information. For strategic sites on the Range, Timing personnel now monitor the following:

1. Time information to see if the STG is generating the correct second.

2. The difference between the STG's internal oscillator one Pulse Per Second (1 PPS) and the GPS 1 PPS.
3. The number of satellites the GPS receiver is tracking and the computed location of the receiver STG.

If any of these parameters are out of their normal bounds, immediate action is taken to minimize the effects and harm that it could cause during a test. Additionally, computers at the customer service centers store this information and Timing personnel can review it when required.

Conclusion

Present and proposed missile, satellite, and space research programs require the use of standardized and accurate time formats for the efficient interchange of test data among the various test Ranges, contractors, universities, and Government laboratories. The personnel in the WSMR Timing System are proud of the service they have provided these groups through the years, and want to ensure the service provided in the future is something they can be proud of as well. To ensure that quality service continues in the future or at least to minimize the losses of services that might occur in these times of downsizing, the architects of the Timing modernization program have taken great care in its design. The plan is flexible enough to adapt to changes in technology, funding, and personnel. It provides a means for the Timing System to become modern. All it will take is time, patience, and money as the WSMR Timing System Approaches its New Horizon.

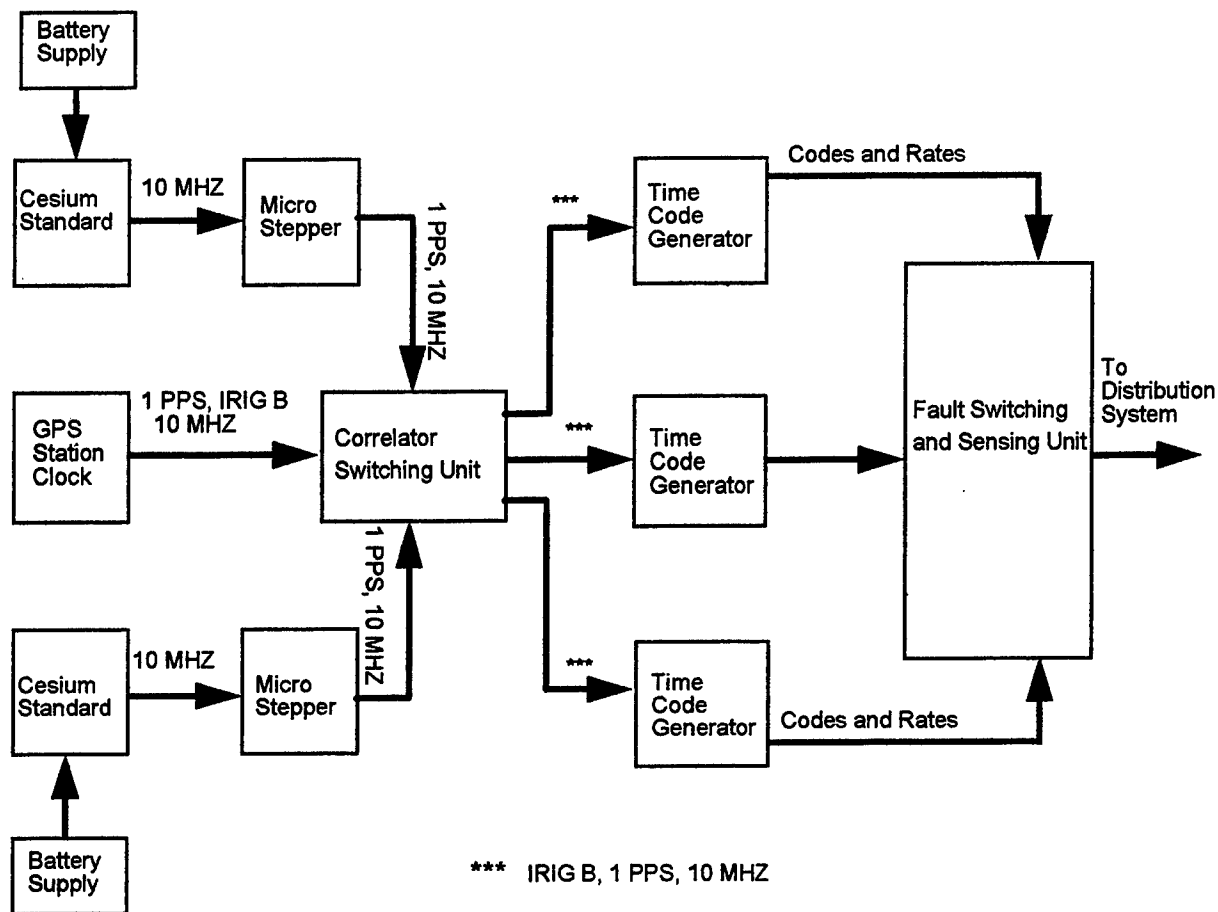


Figure 1 New Master Timing Generation System

Questions and Answers

DON MITCHELL (TRUETIME): What are you going to do with the old timing system?

BILL GILBERT (WSMR): Good question. What we are going to do is first knock down the wall, because when they put the system in, they had to take out a whole wall to get it in. But we are going to put part of it in the museum; and we are probably going to try to see if anybody else would like part of it, because at that time it was state of the art. For those history buffs, it really is "Whoops, oh no," but it is a good piece of equipment. If you have spare parts for it, you probably could fix it and make it work some more. But that is what we are going to do.

Internet Timekeeping Around the Globe¹

David L. Mills², Ajit Thyagarjan and Brian C. Huffman
Electrical and Computer Engineering Department
University of Delaware

Abstract

This paper describes a massive survey of Network Time Protocol (NTP) servers and clients in order to discover statistics of time and frequency errors, as well as determine the health and welfare of the NTP synchronization subnet operating in the global Internet. Among the conclusions of the survey are that most NTP clocks are within 21 ms of their synchronization sources and all are within 29 ms on average. However, additional errors up to one-half the roundtrip delay are possible, but relatively rare. There is, however, a disturbing incidence of improperly operating servers and misguided server configurations.

Keywords: computer time, network time, time synchronization

1. Introduction

Timekeeping via the Internet has become a ubiquitous service extending to well over 100,000 public servers and clients in many countries of the world. In addition, an uncounted number of private servers and clients lurk behind the firewalls of many large government and corporate networks. There have been several previous studies [1], [3], [4] which have compiled population and error statistics using time-dissemination protocols such as the Network Time Protocol (NTP) and others. However, only [4] considered reaching out to all hosts and routers in the global Internet. That study indexed the Domain Name System database of eight years ago and found about 21,000 hosts that returned time in one fashion or another. The newer studies used only a small population to evaluate protocol and algorithm improvements over the years since then.

Since the present day Internet has experienced an explosion of numbers, it is no longer acceptable or even possible to survey Internet hosts and routers by indexing a public directory service. However, it is possible to discover them for an organized subnetwork such as used by NTP. This paper presents a comprehensive survey of the NTP servers operating in the global Internet of today. While the search engine used in the survey could find only a fraction of all NTP outposts on the public Inter-

net, it did find 182,538 network paths used by 36,000 servers, 231 of these synchronized to UTC via radio, satellite or modem. Uncounted others, including large numbers of personal workstations operating as broadcast clients, escaped detection. The survey measured the time offsets of each client relative to its server, as well as related variables important to the health and welfare of the *NTP subnet* itself.

A comprehensive description of the NTP architecture, protocol and algorithms is beyond the scope of this paper, but can be found in [2] and citations found there. The NTP timekeeping network consists of a hierarchical tree of primary (stratum 1) time servers at the root. These provide synchronization to secondary servers at increasing stratum levels (hops) to the leaves of the tree. Figure 1 shows the functional organization of a NTP server. The server sends a message to one or more other *peer servers* and expects replies from each of them at some later time. From the four timestamps obtained upon departure and arrival of the request and response messages, the server calculates the clock offset and roundtrip delay relative to each peer. The clock filter algorithm selects the best measurements from each peer and the intersection and clustering algorithms the best combination of several *peers* operating simultaneously. The actual local clock oscillator (LCO) time and frequency are disciplined using an adaptive parameter, hybrid phase/frequency-lock loop.

1. Sponsored by: DARPA Information Technology Office Contract DABT 63-95-C-0046, NSF Division of Network and Communications Research and Infrastructure Grant NCR 93-01002, Northeastern Center for Electrical Engineering Education Contract A303 276-93, Army Research Laboratories Cooperative Agreement DAA L01-96-2-002, and Digital Equipment Corporation Research Agreement 1417.
2. Author's address: Electrical Engineering Department, University of Delaware, Newark, DE 19716; Internet mail: mills@udel.edu; URL: www.eecis.udel.edu/~mills.

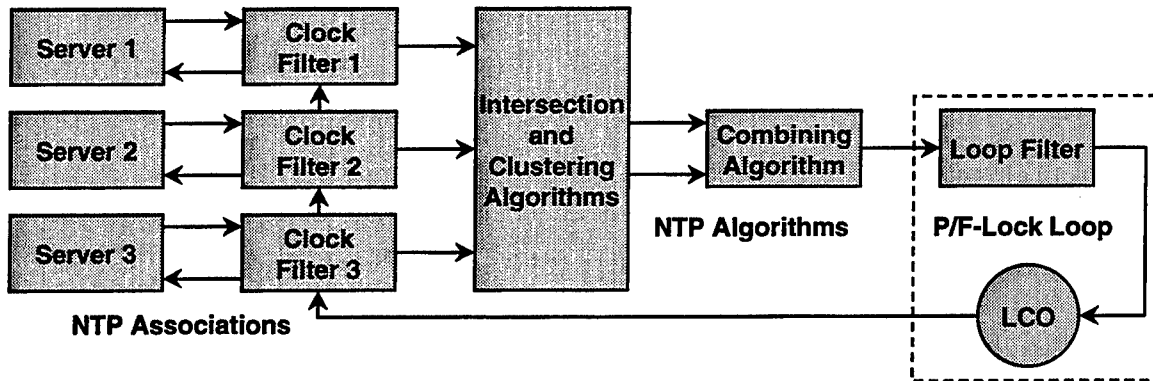


Figure 1. NTP Server Functional Organization

2. Survey Methodology

The survey which generated the bulk of the results presented in this paper was performed over some months in late 1995. The goal was to find as many NTP servers operating in the Internet as practical and determine their performance with respect to time and frequency errors, as well as the robustness and stability of the NTP subnet itself. The results serve as a baseline calibration of the subnet performance, as well as useful insights into subnet configuration and security management strategies.

The search engine used a variety of techniques, ranging from indexing available public databases to exploring the Internet NTP subnet in real time with available monitoring protocols and tools. In the following, *subnet* without the qualifier NTP means any subtree of the global NTP subnet tree. The strategy was to identify as many servers as possible from public lists, such as the database of public servers maintained at the NTP web page www.eecis.udel.edu/~ntp. There are currently 69 public primary (stratum 1) servers and 105 public secondary (stratum 2) servers listed in that database. In the initial round, these servers were queried using NTP monitoring and control protocols to identify their client servers. In the next round, those servers were queried to identify their client servers and so on. The survey continued for many rounds until no new servers could be found. Occasionally, the identity of a new server was discovered by other means and the survey continued for new rounds as necessary.

It was vital in the planning and execution of the survey to avoid network and server congestion due to the query messages themselves. Therefore, the intervals between messages were randomized over moderately long intervals in the order of minutes. Due to the volume of data involved, individual rounds required up to days to complete and the entire survey required many rounds.

The data for each server consist of a spreadsheet, where each line of the spreadsheet corresponds to a protocol instantiation, called an *association* between the server and its peer server, as shown in Figure 1. The peer is either another server or a primary reference clock, usually a GPS receiver. Typical server configurations include several associations, which run simultaneously in order to provide redundancy and diversity. The association data include the endpoint Internet addresses, stratum, mode, reachability status, relative clock offset, roundtrip delay and error estimate called *dispersion*.

Each association operates in a designated mode, depending on whether the server can synchronize the peer or whether the peer can synchronize the server. Symmetric modes are used when either peer can synchronize the other and where mutual backup is necessary in multiple-peer subnets. Client/server modes are used in subnets of modest size and where the highest accuracy is required. Broadcast modes are used in large subnets where the delays are small and the accuracy requirements not demanding.

The data analysis phase of the project considered 230,774 associations, but discarded 818 with misconfigured servers, 3,673 with broadcast servers, 25,640 with unreachable servers, 17,195 with invalid stratum and 1,293 duplicates, leaving 180,520 representing valid measurements of clock offset and roundtrip delay. In these, 36,478 distinct Internet addresses were found, each identifying a NTP server. It should be noted that these servers represent only a fraction of all servers in the NTP subnet. Clients operating in broadcast mode were not found, nor were many others on private networks or behind firewalls. Since these statistics were determined, a few additional valid associations were found, bringing the total to 182,538 associations and 38,722 servers.

Stratum	Servers	Associations	Maximum	Top Ten	Mean
1	220	11,223	652	421	51.0
2	4,438	49,164	356	276	11.1
3	6,591	106,825	558	377	16.2
4	2,254	14,221	398	262	6.3
5	317	9,90	68	25	3.1
6-14	60	115	na	na	na
Total	13,880	182,538	652	421	13.2

Figure 2. Association Population by Stratum

In the above totals, there were 3,673 servers operating in broadcast modes, or about one in ten. The number of clients of these servers is unknown, since broadcast clients ordinarily do not exchange messages with their servers. In fact, most broadcast servers have tens to hundreds of clients, so the actual client population is considerably underestimated. The 1,293 duplicates represent symmetric associations, where each of two peers agree to back up the other. Ordinarily, the offsets measured by symmetric peers have nearly the same magnitude, but opposite sign, and the delays are nearly the same, but this was not a factor in the analysis.

Figure 2 shows the number of associations by stratum. Among the 182,538 associations, there are 13,880 different servers with an overall average of 13.2 associations per server. The maximum number of associations per server is 652, but this understates the true value, since the maximum number the server monitoring cache can hold is near this number. From other data discussed later, higher values to 734 have been observed on one server which is certainly not the most heavily loaded. The fact that at most stratum levels the maximum and the top ten have about the same number of associations and the overall average is much lower suggests the population is dominated by a relatively small number of heavily loaded servers and the remainder relatively lightly loaded. About half the number of servers operate at stratum 3, which usually function as department servers dependent on redundant campus servers operating at stratum 2. The servers shown operating at stratum 6 and above are very likely broken or unstable.

3. Performance Indicators

The three most significant factors that affect timekeeping accuracy are network jitter, oscillator frequency stability and asymmetric network delays. The influence of these three factors varies widely in the NTP subnet, depending on the particular network path and particular oscillator implementation. The survey results allow each of these factors to be studied, evaluated and dis-

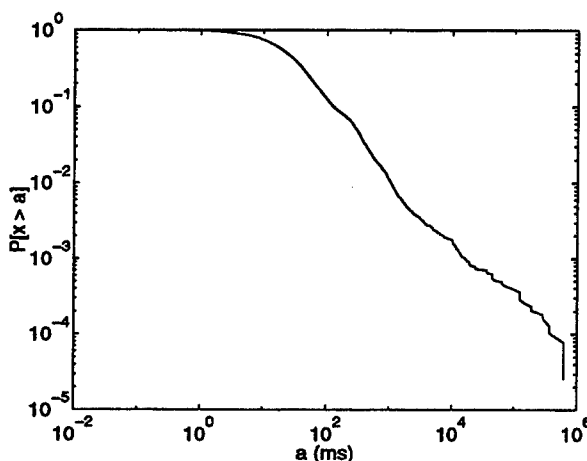


Figure 3. Time Offsets

played as graphs and tables and statistics derived from them. However, the survey was conducted over a period of months, where the particular network conditions were not completely stationary. For this reason, the results should be regarded as an approximation to a true snapshot.

3.1 Time Offsets

The most important indicator of timekeeping performance is the time offset measured by the server relative to the peer server for each association. Figure 3 shows the cumulative distribution function (CDF) of time offsets for 38,722 servers, where the median is 23.3 ms, mean 234 ms and maximum 686 ms. However, 3,833 servers with offsets greater than 128 ms were not synchronized by NTP at the time of the survey. When these servers are excluded, the median is 20.1 ms and mean 28.7 ms. Note that these results represent the global population at large, whereas clients on typical LANs have offsets generally less than a millisecond [3].

According to Figure 2, of the total population of 38,722 servers, 220 primary servers at the root of the NTP subnet tree provide synchronization to 13,660 secondary servers and these provide synchronization to the 24,842

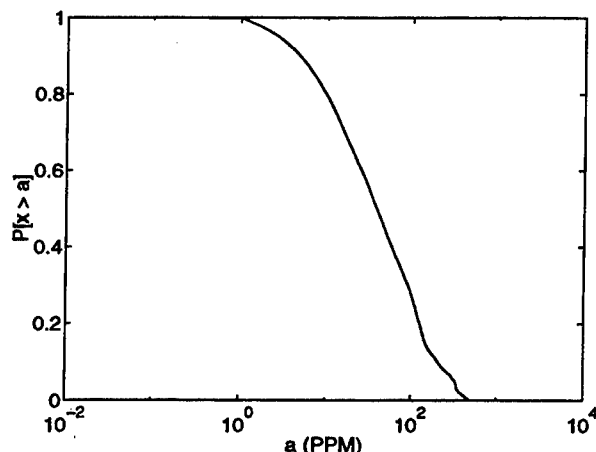


Figure 4. Systematic Frequency Offsets

remaining servers at the leaves of the tree. In the present NTP design, each server on the path from the leaves to the root independently disciplines its clock relative to the servers at the next lower stratum, in order to provide a stable, low-jitter reference for local applications. Thus, the figure shows the offset of a client relative to its server, not the offset relative to the primary servers at the root. In principle, the protocol could determine this by accumulating the offsets on each hop along the path to the primary servers. However, this statistic would result in large jitter and be unsuitable if used to discipline the system clock. In the interest of an economical packet header, it was not included in the NTP protocol design.

3.2 Clock Discipline Errors

The NTP clock discipline algorithm operates to minimize both phase and frequency errors. To the extent it makes good predictions based on measured time offsets produced by the protocol, phase errors due to systematic frequency offsets can be minimized. However, in order to provide millisecond accuracies with measurement intervals up to 1024 s, it is necessary to estimate the current frequency to less than one PPM, even when the systematic frequency offset is hundreds of PPM. The systematic frequency offsets and oscillator phase errors of 19,873 servers were determined from a special survey. Figure 4 shows the CDF for these servers less 593 outliers with offsets greater than 500 PPM, from which the median is 38.6 PPM and mean 78.1 PPM. Frequency offsets greater than 500 PPM are not credible, since that is the limit of the discipline loop capture range.

While most clock oscillators are moderately well behaved, there is a significant tail on the distribution. The results demonstrate that the NTP clock discipline must have a very large capture range and an adaptive time constant. In the present design, the capture range is

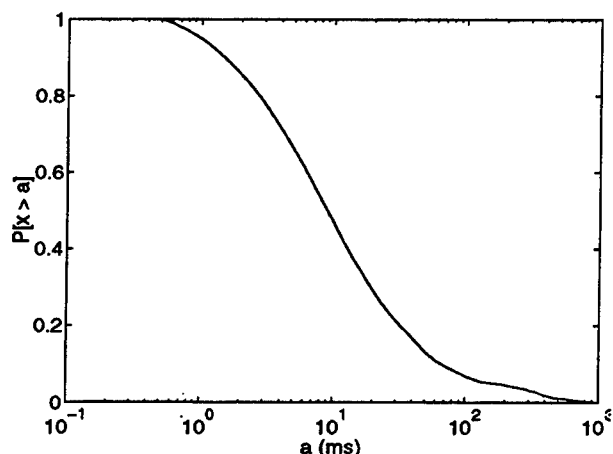


Figure 5. Oscillator Phase Errors

500 PPM and the time constant varies with the measurement interval from 64 s to 1024 s.

Oscillator phase errors are due both to frequency estimate errors and jitter in the network. Figure 5 shows the CDF for these errors for the 19,873 servers in the special survey, less 131 outliers with errors over 1 s, from which the median is 9.1 ms and mean 37.0 ms. Errors over 1 s can occur only if the peer is defective and the server is synchronized to another peer. Errors over 128 ms can occur only during initial synchronization after reboot or infrequently due to network or peer server disruptions. If these servers are excluded from the population, the median is 8.0 ms and mean 16.7 ms.

3.3 Asymmetric Delays

The NTP protocol design does not permit an absolute measurement of time difference between servers, unless an external common-view means is available, as in [1]. As a result, clock offset errors cannot be distinguished from asymmetric network delays. There is evidence to suggest that errors due this cause are not uncommon; however, by design the errors due to asymmetric delays are bounded by half the roundtrip delay [2], although errors this large are rare. Figure 6 shows the CDF for the delays measured between the 38,722 servers used in the time offset survey. The results show median delay 118 ms, mean 186 ms and maximum a whopping 1.9 s. As with other survey data analyzed, the tails on the distributions can be very long. From anecdotal evidence, the larger values due to the widely varying incidence of congestion in the Internet of modern times.

From anecdotal evidence and previously reported results [1], [3], the delay asymmetry is seldom more than one-tenth the roundtrip delay. For LANs with delays in the low milliseconds, the asymmetric errors are generally negligible. Even on long paths spanning the Atlantic

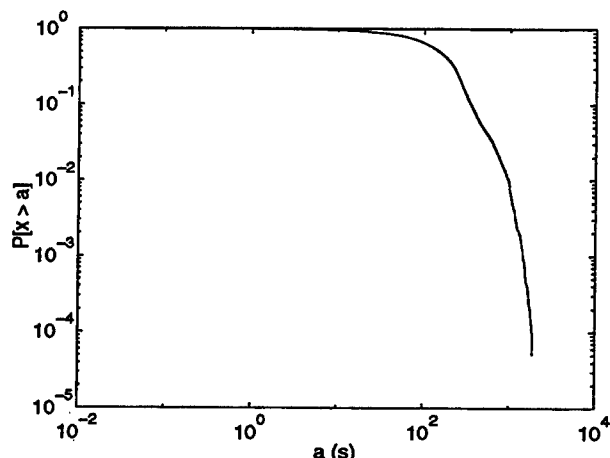


Figure 6. Roundtrip Delays

Count	Status
34,384	Selected for synchronization
319	Miscellaneous checks
60,105	Potential candidates
6,359	Rejected by clustering algorithm
68,966	Standby servers
1,854	Rejected by intersection algorithm
10,551	Peer unreachable
182,538	Total

Figure 7. Data Mitigation

where propagation delays dominate, the errors are small compared to those due to network jitter. However, in cases where one direction uses cable and the other satellite, for example, or where two peers are connected to different providers with very different network grids, the errors can be substantial.

3.4 Data Mitigation

A good idea of the general health of the NTP subnet can be determined from the status code maintained for each association. Figure 7 shows a breakdown of the 182,538 associations considered previously. The table is best interpreted starting from the bottom. At each step upward from the bottom, the indicated number of associations are discarded for the reason given on the same line. The line under the heading line shows the number of associations actually used to discipline the system clock. Since there is only one such association per server, this number represents the actual number of servers synchronized by NTP. Since there were 38,722 servers resulting from the time offset survey, the remaining 4,338 servers may be unsynchronized, about 11 percent of the total. Caution is advised when making such con-

Count	Service
47	satellite (GPS, GOES)
57	WWVB radio (US)
17	WWV radio (US)
63	DCF77 radio (Europe)
6	MSF radio (UK)
5	CHU radio (Canada)
7	modem (NIST, USNO, PTB, NPL)
25	other (cesium clock PPS, etc.)
231	Total

Figure 8. Primary Reference Clocks

clusions, since the survey errors due to changing network conditions could well account for the differences.

For the remaining lines of Figure 7, a few notes will clarify the operations involved. The intersection algorithm detects and discards associations which show a time interval outside the correct time interval determined for the majority of associations. Standby associations are those deemed correct, but not among the lowest ten in order of increasing synchronization distance. When more than ten associations are admitted to the clustering algorithm, excessive *clockhopping* can occur among the peers, which can result in excessive system clock jitter. The relatively high number of standby associations was traced to a provider using a very misguided configuration where each of about 100 NTP servers maintained associations with all of the others.

The clustering algorithm repeatedly discards outlier associations until either a minimum number of three remain or the residual sample variance cannot be reduced by further discards. The remaining population, including the top three lines in the table, represent candidate associations considered the pick of the litter. Selection among the candidates to determine the ones actually used to discipline the system clock is determined on the basis of synchronization distance. The combining algorithm computes the offset provided to the clock discipline as a average of the available candidates weighted by this distance. Thus, the average number of associations used to synchronize the system clock is 1.75.

3.5 Primary Servers

The accuracy and stability of the global NTP subnet depends on the reference clocks used to synchronize the primary servers. There are many different means used to do this, including radio, satellite, telephone modem and cesium clock ensemble. Figure 8 shows the population characteristics of the 231 primary reference clocks

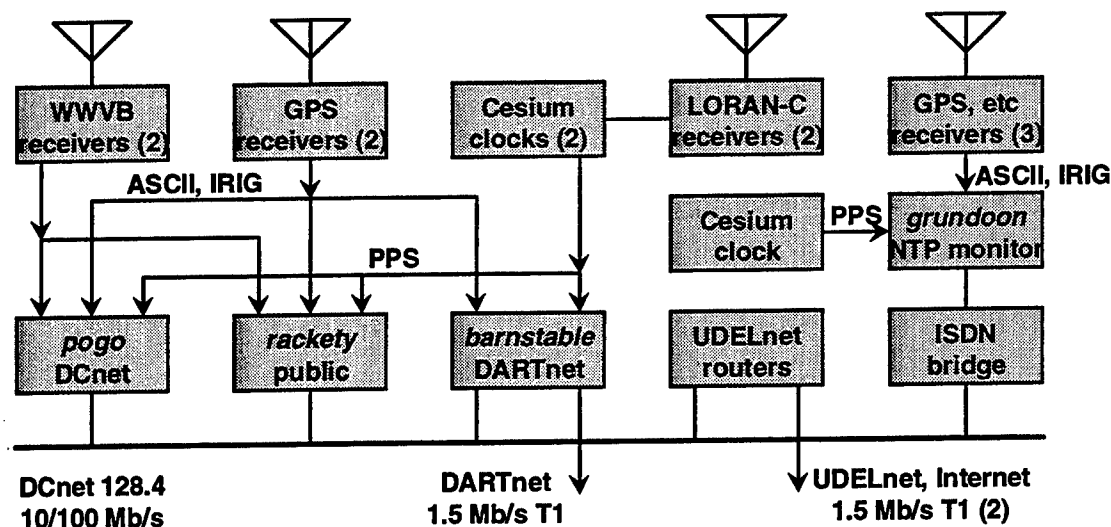


Figure 9. DCN Network Time Servers

found in the survey. Since this survey was completed, the national time dissemination services of France, Chile and Italy have become available and additional time servers operated by NIST and USNO have come online, making the total operating today significantly larger. The surprisingly large number of DCF77 reference clocks is undoubtedly due to the very inexpensive receivers available for this signal in Europe. In the interval since this survey was completed, and as inexpensive GPS receivers have come on the market, new servers are using GPS.

In addition to the 231 primary servers found, some 88 servers were found where the reference clock had either failed or had been misconfigured. In the NTP design, reference clocks are treated as ordinary peer servers, so many primary servers maintain associations for other servers as backup. When the radio fails, the other associations kick in and the server continues to operate at a higher stratum.

In some configurations, a special reference clock driver provides backup when all other sources fail. The driver simulates a reference clock operating at some higher stratum, usually 3. If all sources of lower stratum fail, the free-running server system clock becomes the NTP reference and the clients depending on the server synchronize to it. At the time of the survey, 1,502 servers were found to use this feature.

4. A Day in the Life of a Busy NTP Server

While some NTP servers are dedicated timekeepers, most serve other functions as well, including those of routers, file servers and ordinary workstations. It is of some concern to determine how much the resource

requirements of the timekeeping function impact on these other functions. Of principal concern are the processing and network overhead resulting from client requests to a busy time server.

Timekeeper *rackety*, one of the most experienced timekeepers in the business, is a well known primary time server with clients all over the world. The configuration of this server in the context of the other timekeeping gear in our laboratory is shown in Figure 9. Together with other timekeepers *pogo* and *barnstable*, this Sun Microsystems SPARCstation IPC functions as a file server, print server and router as well, although in this machine these functions have low demand. An Austron 2201A GPS receiver functions as the primary reference clock and a Spectracom WWVB receiver as backup. The operating system kernel is modified to use the pulse-per-second (PPS) signal from a Hewlett-Packard 5061A cesium oscillator to discipline the system clock, generally within a few tens of microseconds. While implemented expressly for the SunOS operating system, these kernel modifications are also in current Digital Unix and Sun Solaris operating systems.

In order to calibrate the resource demands of the timekeeping function, ordinary Unix commands were used to measure the CPU time consumed by the NTP daemon over about a day, which came to 1.54 percent. A network sniffer program captured all of the NTP packets for *rackety* that flew the DCnet wires during that day and saved them for later analysis. The 734 clients sent an average of 6.4 packets per second, which corresponds to a mean interarrival interval of 157 s for each client. This is curious, since after an initial training period, most NTP Version 3 clients should increase the poll interval in steps to 1024 s. The fact the interarrival inter-

val is so small suggests there are still a large number of previous versions in use.

Each input packet generated on average 0.64 output packets and required a total of 2.4 ms of CPU time for the request/response transaction. It is not known how many of the 734 clients were using cryptographic authentication; but, if so, the time to generate the request and response cryptosums on an IPC is about 300 μ s, but only about 30 μ s on an UltraSPARC 170.

Rackety is connected via a 10-Mb/s Ethernet, routers and 1.544 Mb/s T1 circuits to Internet backbone networks as shown in Figure 9. While the T1 circuits are not dedicated to NTP traffic, the other customers are few. Averaged over the day, the 76-octet NTP packet rate was measured at 10.5 packets per second. Exclusive of overhead bits, this is .064 percent of the Ethernet capacity and a maximum of 0.21 percent on each direction of the T1 capacity. The conclusion to be drawn here is that the resources required for NTP are minimal, even when hundreds of clients are involved and even with a slow processor.

5. Conclusions

The results of the survey demonstrate that most NTP clocks are within 21 ms of their servers and all are within 29 ms on average. The oscillator phase error may add a few milliseconds to these figures, but in most cases can be neglected. There may be additional errors due to asymmetrical paths, but this is bounded by one-half the roundtrip delay. While it is not possible using the NTP protocol itself to estimate the errors when multiple-hop paths are involved, a reasonable estimate may be the number of hops times these figures. It is clear from the graphs that the error distributions can have surprisingly large tails well above these figures, in some cases due to network congestion and in other cases due to improperly operating servers or misguided choice of servers.

The roundtrip delay statistic has proven very useful, not only to assess timekeeping performance, but in the general study of the worldwide Internet performance. The fact that NTP servers determine this statistic on a regular basis suggests the use of NTP as a network monitor with a coupling to the monitoring infrastructure using the Simple Network Monitoring Protocol (SNMP). In fact, this has been done on an experimental basis and described in a report now in preparation.

Perhaps the most disturbing results of the survey is the significant fraction of servers showing improper operating parameters or incorrectly configured servers. In many cases, this is due to benign neglect on the part of the operator, since timekeeping is not usually regarded as a revenue service, and providing NTP service to the community is a volunteer sport. This problem has been addressed in the design of the next version of the NTP protocol in the form of features to discover servers and configure the NTP subnet automatically and without the chance of operator error.

5.1 References

Note: The following publications are available in PostScript format at www.eecis.udel.edu/~mills.

1. Mills, D.L. The network computer as precision timekeeper. Proc. PTTI Meeting (December 1996).
2. Mills, D.L. Improved algorithms for synchronizing computer network clocks. *IEEE/ACM Trans. Networks* (June 1995).
3. Mills, D.L. Precision synchronization of computer network clocks. *ACM Computer Communications Review* (April, 1994).
4. Mills, D.L. On the accuracy and stability of clocks synchronized by the Network Time Protocol, *ACM Computer Communications Review* (January, 1990).

Questions and Answers

BILL KLEPCZYNSKI (INNOVATIVE SOLUTIONS INTERNATIONAL): You use the term "Stratum 1". Stratum 1 to the telecommunications people means a microsecond and a part of 10 to the 11th in frequency. Do you use that in the same sense or not, "Stratum 1"?

DAVID MILLS (UNIVERSITY OF DELAWARE): Of course not. You might say if we are talking about Stratum 1 being a part in 10 to the 12th, we are perhaps about nine orders of magnitude worse than that. I had not intended to poach on the nomenclature for the telecommunications industry, but I had to have something. So "Stratum 1" it is.

SIPRNET NETWORK TIME SERVICE

Richard E. Schmidt
Time Service Department
U.S. Naval Observatory
Washington, DC 20392

Abstract

SIPRNET, the Secret Internet Protocol Routing Network, is DoD's wide area network for encrypted hosts handling classified traffic. It is managed by the Defense Information Systems Agency. In 1997 the U.S. Naval Observatory established network time synchronization service on SIPRNET, with dedicated servers providing Network Time Protocol (NTP). These servers are synchronized to the USNO Master Clocks. An overview of time server design is presented, with details on expected accuracy and accessibility.

INTRODUCTION

At the 26th meeting of PTTI in December, 1993, USNO reported on the establishment of two Internet stratum 1 Network Time Protocol (NTP) servers. Synchronized to the USNO Master Clocks in Washington, DC, these servers were at that time handling 155,000 NTP packets per month^[1]. Today USNO operates 14 stratum 1 Internet NTP servers, currently handling 180 million packet requests per month. These servers, at the locations listed below, are *Hewlett-Packard 9000/747i* industrial workstations with embedded VME synchronized generators. The sync-gens (*TrueTime* GPS-VME, VME-SG and *Datum-Bancomm bc637vme*) are disciplined by Master Clock IRIG-B timecode and GPS. The NTP servers provide millisecond synchronization over TCP/IP networks. Time transfer is performed by exchange of local timestamps using User Datagram Packets detailed in the Internet Standard RFC-1305^[2].

USNO PUBLIC INTERNET NTP SERVERS 1997

LOCATION	IP ADDRESS	SYNC	CNAME
Time Service Dept., USNO, Washington, DC	192.5.41.40 192.5.41.41 192.5.41.209	IRIG	tick.usno.navy.mil tock.usno.navy.mil ntp2.usno.navy.mil
USNO AMC Falcon AFB, CO	204.34.198.40 204.34.198.41	IRIG	tick.usnogps.navy.mil tock.usnogps.navy.mil
Washington Univ., St. Louis, MO	128.252.19.1	GPS	ntp-wustl.usno.navy.mil
Digital Equipment Corp., Palo Alto, CA	204.123.2.72	GPS	ntp-dec.usno.navy.mil
MIT, Cambridge, MA	18.145.0.30	GPS	ntp-mit.usno.navy.mil
UCLA, Los Angeles, CA	164.67.62.194	GPS	ntp-ucla.usno.navy.mil
Univ. Houston, Houston, TX	129.7.1.66	GPS	ntp-uh.usno.navy.mil
Georgia Institute of Technology, Atlanta, GA	130.207.244.240	GPS	ntp- gatech.usno.navy.mil
Columbia University, New York, NY	128.59.39.48	GPS	ntp-cu.usno.navy.mil
Univ. Washington, Seattle, WA	140.142.16.34	GPS	ntp-uw.usno.navy.mil
Ohio State University, Columbus, OH	198.30.92.2	GPS	ntp-oar.usno.navy.mil

SIPRNET, the *Secret Internet Protocol Routing Network*, is a Department of Defense Internet for classified operations. The SIPRNET backbone is primarily T1 (1.54 Mb/s) with about 40 hub router sites in the U.S., a dozen sites in Europe, and about ten sites in Southeast Asia and the Pacific. SIPRNET is operated by the Defense Information Systems Agency (DISA).

In response to a number of requests from SIPRNET customers, including the Global Command and Communications System (GCCS), USNO has recently joined

with DISA in establishing NTP network time synchronization service on SIPRNET. DISA has extended SIPRNET hubs (128Kb fractional T1) to the USNO Master Clocks at the Alternate Master Clock Facility, Falcon, CO (November 97) and at the Time Service Department in Washington, DC (December 97). USNO has provided NTP servers which are steered to USNO Master Clocks.

USNO SIPRNET NTP SERVERS 1997

Location	IP Address	Sync	CNAME
AMC, Falcon	140.49.231.138	IRIG	ntp-amc.sipr.smil.mil
USNO Washington	140.49.183.70	IRIG	ntp-usno.sipr.smil.mil

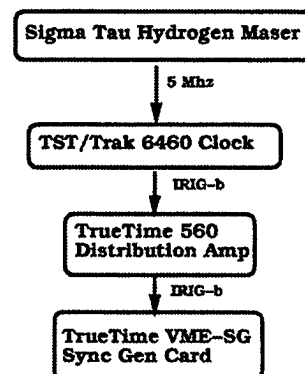
SIPRNET NTP SERVER DESIGN

The USNO SIPRNET NTP servers are dedicated UNIX workstations with dual embedded TrueTime VME-SG sync-gen cards. The *Hewlett-Packard 9000/747i* is an industrial VMEbus workstation running HP-UX 10.20. NTP release 3-5.90 was provided by David Mills, University of Delaware (web

address <http://www.eecis.udel.edu/~ntp/>). A C-language NTP refclock driver, developed by the Time Service Dept., USNO, provides a memory-mapped interface to VMEbus registers on the TrueTime VME-SG. From these,

BCD timecode can be read with essentially zero latency. Two sync-gen cards are installed in the NTP server. Each card is synchronized to one of USNO Master Clocks #1 or #2. Each Master Clock is a *Sigma Tau* Hydrogen Maser providing 5Mhz to *TST/Trak 6460* Clocks, which generate IRIG-B timecode that is distributed by *TrueTime 560* distribution amps with parallel output to multiple NTP server inputs.

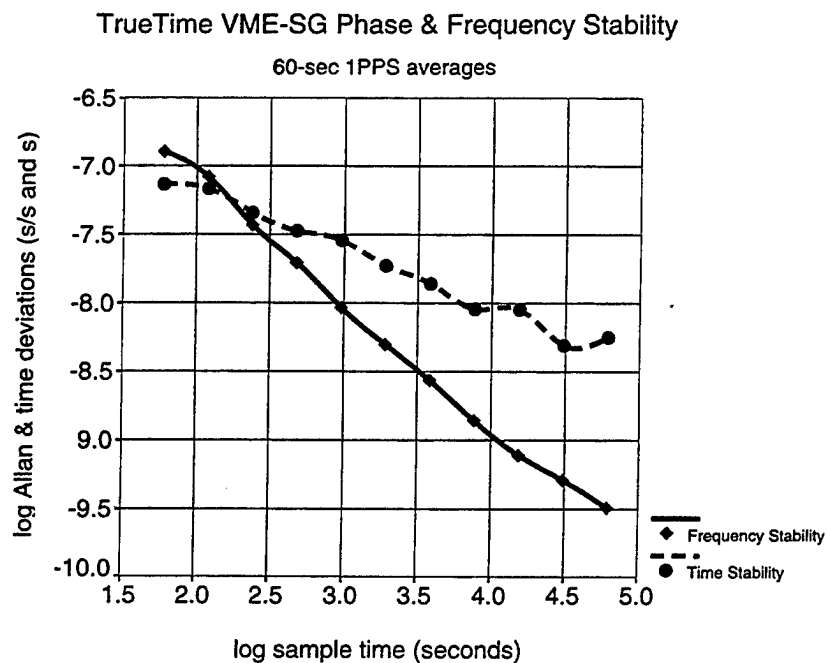
USNO MASTER CLOCK FEEDS



The NTP servers receive and transmit only unclassified data, but are located in a secure facilities. The Washington connection to SIPRNET uses a *Larscom* Access-t DSU/CSU and a *Cisco* AGS+ router. Between these units an *Allied Signal* KIV-7HS (KG-84) provides keyed encryption.

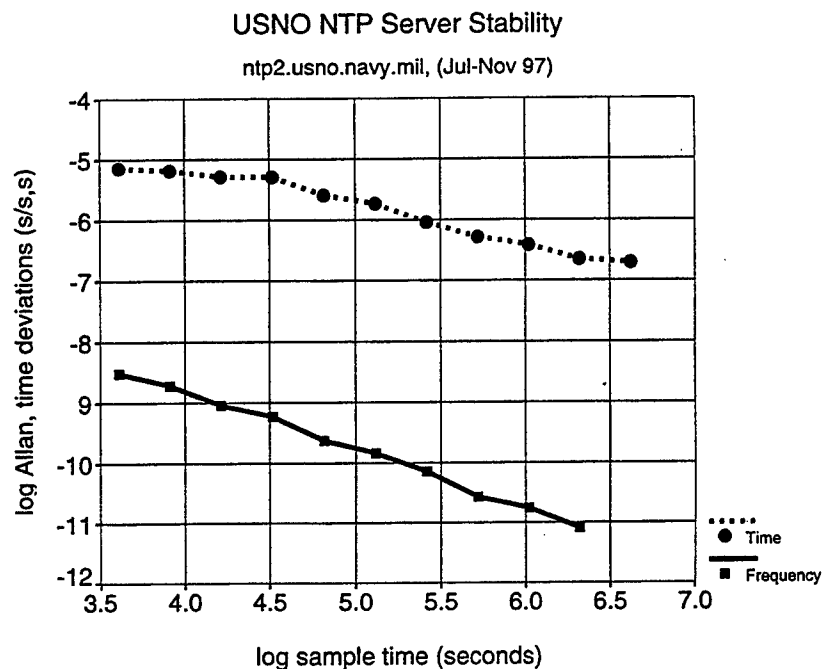
SERVER TIMING CHARACTERISTICS

The *TrueTime* VME-SG phase locks to IRIG-B in order to discipline its VCTCXO. Phase shifts are internally applied in 100 ns steps^[3]. Phase calibration was performed using a time-interval counter with 1PPS reference from a USNO Master Clock. A mean phase bias correction was then be programmed on the VME-SG. This oscillator is internally stable to about 200 ns. Allan and time deviation plots of the VME-SG frequency and phase stability are shown below. These are based on 60-second averages of 1pps phase comparisons with a USNO Master Clock.



NTP software is used to discipline the phase and frequency of the UNIX system clock, which alone is a poor oscillator, showing drifts as much as parts in 10^{-4} . The NTP driver software keeps the system clock frequency error to generally below 2 parts in 10^{-7} . Time is buffered through system calls to the UNIX system clock to provide readily accessible timestamps with a flywheel frequency in the event of loss of the sync-gens. In addition, the server peers with other NTP stratum 1 servers on the network and will maintain network synchronization with ~20 millisecond accuracy in the event of hardware clock failure.

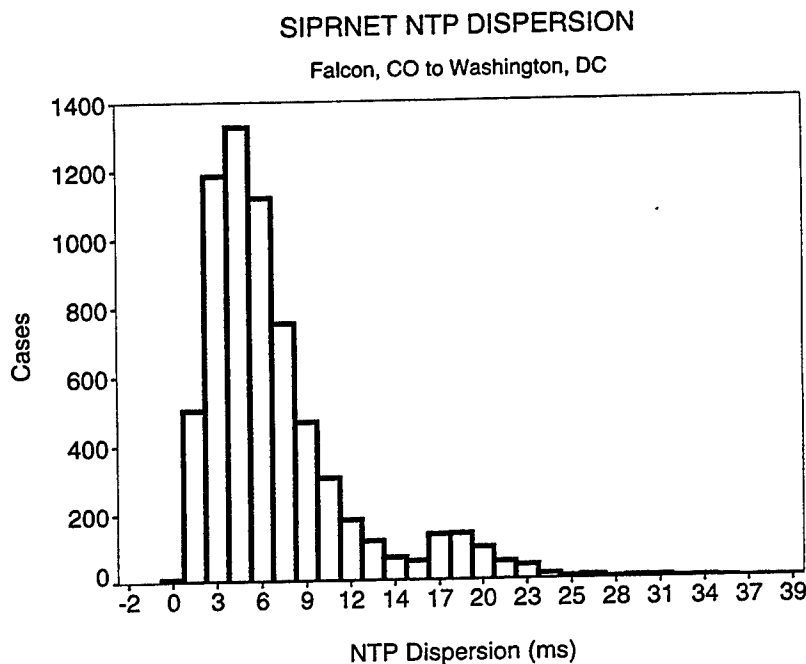
Internal frequency and time stability are shown in the Allan deviation and time deviation data shown below, which is based on five months of 16-second NTP phase comparisons of a server's system clock vs. the *TrueTime* VME-SG phase.



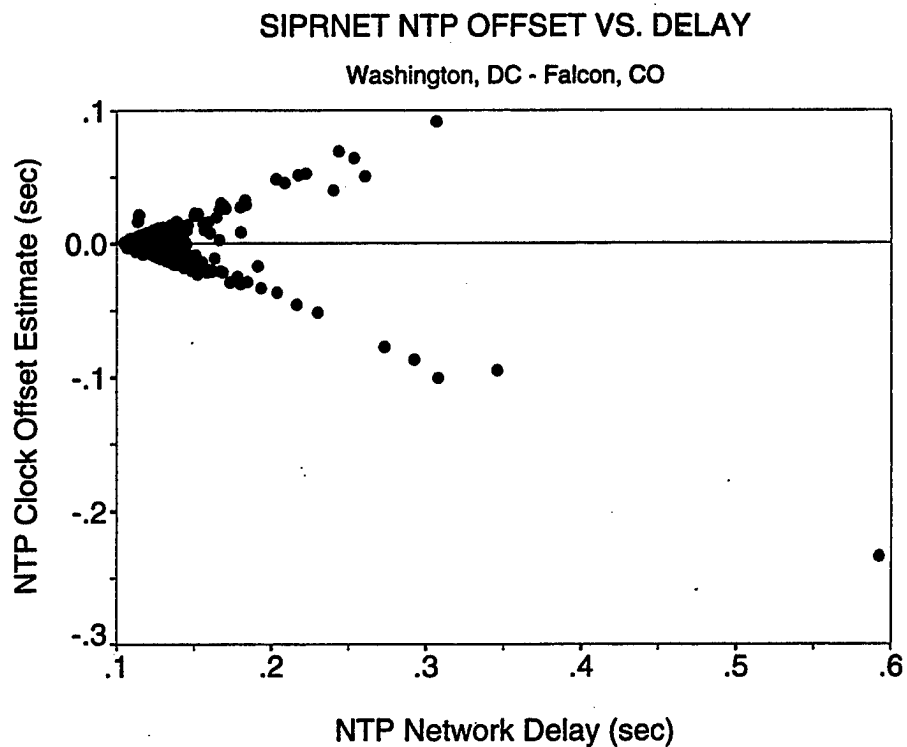
NETWORK TIMING ACCURACY

The accuracy of time transfer over a packet-switched Internet, will be considerably below the internal timekeeping ability of the server. NTP requires round-trip packet exchange between client and server. The inherent asymmetry of packet-switched network paths contributes most of the error in steering NTP clients to servers^[3]. NTP observes total round-trip network delay and computes a dispersion which provides an error bound for estimating clock offsets. With atomic or GPS NTP servers located at sites remote from USNO Washington, we can observe the interplay between the NTP values of network delay, dispersion, and clock offset, when the actual clock offset is zero. The standard deviation of Internet NTP clock offset estimations was 20 ms. In previous tests on a circuit-switched ISDN network (with no round-trip asymmetries), the corresponding standard deviation was below 1 ms^[4].

The expected accuracy of NTP over 3,000 km network paths is shown in the following histogram of NTP dispersion between the USNO Washington and Falcon, AFB, Colorado SIPRNET servers.



A look at NTP clock offset estimates vs. network delay produces an NTP "wedge plot," as seen below. Points along the edges of the wedge come from busy network routing queues, when round-trip network delay asymmetry dominates^[5]. Unfortunately, NTP attributes half of the delay asymmetry to clock offset. By dispersing NTP servers widely across the Internet, we strive to minimize this effect by shortening the total synchronization distance to any client.



REMOTE NTP SERVERS

DISA and USNO plan to extend SIPRNET NTP service to Europe and the Pacific in 1998. P/Y code GPS receivers will provide accurate and reliable timing. USNO's continual monitoring of GPS timing will assure that the performance of these GPS stratum 1 NTP servers will equal that of servers colocated at the Master Clock sites. Typical timing accuracies for NTP time service are summarized below.

Component	Accuracy (peak to peak)
TrueTime VME-SG	0.4 μ sec
NTP server UNIX system clock	50 μ sec
3000 km circuit-switched network	2 ms
3000 km packet-switched network	20 ms

REFERENCES

- [1] R. E. Schmidt, "Network Time Synchronization Servers at the U.S. Naval Observatory", Proceedings of the 26th Annual Precise Time and Time Interval (PTTI) Applications and Planning Meeting, pp.175-183, 1994.
- [2] D. L. Mills, *Network Time Protocol Version 3 specification, implementation, and analysis*", DARPA Network Working Group Report RFC-1305, University of Delaware, March 1992, 113 pp.
- [3] *TrueTime Model 560-5608 VME-SG [reference manual 560-5600.ONE]*, p 1-5, 1993.
- [4] R. E. Schmidt, "Introduction to Network Time Synchronization with NTP", presented at the International HP Workstation Users Group Conference, 1995.
- [5] G. D. Troxel, *Time surveying: Clock Synchronization over Packet Networks*", Ph.D. thesis, Department of Electrical Engineering and Computer Science, Massachusetts Institute of Technology, 1994.

THE APPLICATION OF NTP TO NAVY PLATFORMS

Karen F. O'Donoghue and David T. Marlow
Naval Surface Warfare Center Dahlgren Division
17320 Dahlgren Road, Dahlgren, Virginia 22448 USA
{kodonog|dmarlow}@nswc.navy.mil

Abstract

Navy platforms consist of many systems ranging from navigation and ship control to tactical analysis, sensors, and weapons. These systems, each composed possibly of multiple computing elements, are inherently time-dependent. In addition, modern surface ships are quickly adding additional COTS based computing elements and communication networks to address emerging requirements. Vital to making such a distributed system function in this environment is a stable robust time service. The Navy has been investigating various methods for the provision of a time service on shipboard platforms. This paper presents an overview of previous Navy efforts, a discussion of the metrics identified as applicable to the Navy environment, and a summary of the HiPer-D time synchronization subnet performance. In addition, this paper identifies ongoing and future work required to provide a stable robust time service in a shipboard environment.

INTRODUCTION

The modern-day surface ship is composed of a number of separately developed and maintained systems which together execute the functions needed to operate the entire platform. These systems work independently and collectively to perform the ship's mission. A key to making such a collection of systems work in this real-time environment is a common understanding of time. Time information must be represented accurately and consistently throughout all the systems of the platform and within the various components of the individual systems. This time information includes both time of day and time interval measurements. The end result is that Navy platforms require a stable robust time service.

The Navy has been investigating the requirements placed on a time service by Navy platforms and specific time service metrics applicable to these platforms. It has also been investigating various methods for the provision of a time service on shipboard platforms. The Network Time Protocol (NTP) has been identified as a technology with the potential to meet Navy shipboard time service needs. Various studies have been conducted to analyze the performance of NTP on particular computing elements, including modification of NTP parameters to better address specific Navy shipboard requirements.

The High Performance Distributed Computing Program (HiPer-D) is a joint effort between the Navy (the AEGIS Program Office) and the Defense Advanced Research Projects Agency (DARPA) to look at the use of distributed computing technologies. The Navy efforts in the area of time services were applied to the HiPer-D testbed. The HiPer-D testbed includes a heterogeneous computing base operating in a distributed fashion over multiple network technologies to provide actual AEGIS Combat System functionality. To support this testbed, a time synchronization subnet was designed and implemented using both NTP and GPS components. The long-term performance of the HiPer-D time synchronization subnet was measured and the results analyzed. Additional efforts including specific studies and experiments for future work were identified based on the metrics defined below and the experimental observations.

GENERIC TIME SERVICE MODEL

The provision of quality time information in a computer requires that a number of functions be carried out in a coordinated fashion. This collection of functions, related to computer clocks and the time information in a computer, is referred to as a *time service*. A generic time service model incorporates all of the components necessary to provide and manage quality time information in a system. A system is a collection of interconnected computers participating in related tasks. The foundation of this time service is the clock present in each computer. Three basic components that interact with these clocks are clock coordination, clock access, and time management. A *clock coordination service* synchronizes individual computer clocks to each other and to national and international time standards (e.g. UTC). A clock coordination service includes the mechanisms necessary to exchange time information between individual computer clocks and the algorithms required for processing this information in order to arrive at meaningful conclusions. The *clock access component* of a time service addresses the provision of time information to users. This time information may include both the current time value and the accuracy of that value. These users can be human operators, application processes, or the computer's operating system. The *time management service* component of a generic time service includes the functionality necessary to monitor and control both the various computers' clocks and the clock coordination service within a synchronization domain or system. One example of a clock management service is monitoring the accuracy achieved by the clock coordination service in a particular computer and modifying the operational parameters if the accuracy does not meet specified bounds.

TIME SERVICES FOR NAVY PLATFORMS

Navy ships are designed to perform a number of complex realtime tasks ranging from navigation and ship control to controlling complex sensors and weapon systems. This collection of applications places rather stringent requirements on the supporting computing and communication infrastructure, including the time service. First, to provide a stable and robust time service, clocks need to be synchronized in both phase and frequency to a defined standard (e.g. UTC). The Navy (via the Next Generation Computer Resources Program) has identified a basic phase accuracy requirement of 1 ms. [3]. Further analysis is necessary to look at the requirements of new and emerging applications.

There are a number of additional requirements for time services on Navy platforms, especially in light of the rapid evolution of shipboard platforms, tactical systems, and the technologies on which these are based. First, the time service needs to be fault-tolerant, surviving failures of both the time servers and the interconnecting communication links. Secondly, new platforms under development are demonstrating a trend to distribute processing to an increasing number of computers aboard a surface ship. As more processors are added, the time service must be scaled to meet new requirements. Experience has shown that techniques which adequately synchronize two computers are not necessarily sufficient for dozens or hundreds of computers. The time service must allow the incorporation of additional components requiring synchronization, with minimal impact to the existing time service and ship infrastructure. Finally, the time service needs to be cost-effective, utilizing the existing communication infrastructure and Commercial-Off-The-Shelf (COTS) components where possible. Concepts discussed here may have counterparts in commercial systems, particularly specialized applications such as air traffic control, but in general the requirements go beyond those found in non-military applications. Specific requirements of shipboard time services are discussed in detail in [3].

EXISTING TIME SERVICE APPROACHES

There are a number of existing approaches for clock synchronization on surface ships. The classic approach is the use of a single master clock chassis that distributes time information to a limited set of

computers via a set of point-to-point computer interface channels. More recent approaches have included the use of specialized clock interfaces located within computers and synchronized via a separate physical infrastructure using timecodes (e.g. IRIG-B). There is often a backup master clock or time source with a duplicate distribution network to support it. There are a number of common themes to these approaches to clock synchronization. These approaches strive to distribute time information to the computers rather than synchronize the computer's own clock resources. No attempt is made to coordinate the existing clock resource with the synchronization source. Secondly, these approaches utilize a special distribution network for time information. This involves a separate physical plant for the distribution of time information. Scalability issues arise with the time service as the number of computers increases.

APPLICABLE METRICS

Based on the needs of Navy platforms, time service metrics specifically applicable to these platforms have been identified. The first metric of interest is the most commonly recognized, *phase accuracy*. Clock phase represents the time value of the clock, and the accuracy associated with it is the difference between the phase of the clock of interest and the national or international reference standard. This is analyzed by measuring the clock offset between a clock and a reference source at any given instant in time. The second metric of interest is *frequency stability*. This represents the difference between the frequency of the clock of interest and the national or international standard. This is analyzed by observing the clock offsets between a clock and a reference source over a given interval of time. This is most commonly represented using the Allan variance. [4] The third metric of interest to the Navy is the *fault recovery time*. Navy platforms must adapt quickly to realtime conditions which may include failed communication links and time servers. In addition, the impact of these failures must be minimal. The time required to detect and recover from a fault condition is, therefore, defined as the fault recovery time. A final metric is *clock settling time*. This metric represents the time it takes the time service to reach a defined phase accuracy in an individual computing element after the machine begins initialization. These metrics help to characterize the time synchronization needs of Navy platforms. Engineering choices are made regarding resources consumed versus performance obtained. The trade-offs made by Navy platforms will be different than those of the global Internet.

THE NETWORK TIME PROTOCOL

The Network Time Protocol (NTP) [1] is a distributed clock synchronization protocol that provides for the coordination of interconnected computer clocks utilizing the existing communication infrastructure. NTP was developed by Dr. David Mills at the University of Delaware for use in the Internet community. NTP estimates the phase and frequency offset between two peer clocks and provides corrections for use by the local clock routines. NTP is a connectionless time information exchange protocol and an associated set of algorithms to process and act on the time information collected by the protocol. Some of the key features of NTP are highlighted here. First, NTP is based on a returnable time approach that reduces impact of communication path delays. The NTP synchronization subnet is a self-organizing hierarchy of time servers. Redundancy can be incorporated in the synchronization subnet using multiple servers and clock selection algorithms. NTP provides both phase and frequency corrections for the local clock. Finally, NTP operates in connectionless mode using the User Datagram Protocol (UDP) and the Internet Protocol (IP) in order to minimize latencies, simplify implementations, and provide ubiquitous internetworking.

NTP PARAMETER ANALYSIS

Initial experiments using NTP on small realtime networks produced peak clock phase offsets on the order of a few milliseconds using COTS equipment and default parameters for the public domain distribution of NTP available from the University of Delaware. The default parameters for NTP are tuned for operation

in the global Internet. As part of the Navy's analysis of NTP, it was determined that one promising path was the tuning of various NTP parameters to provide a responsiveness acceptable for a military system. Simulations and analysis indicated that the NTP client polling interval could be set to a shorter interval to provide faster synchronization, greater stability, and more rapid detection of any fault conditions. By default the NTP polling interval varies between a minimum of 64 seconds and a maximum of 1024 seconds depending on the perceived stability of the time synchronization subnet. The 1024-second default maximum polling interval is generally sufficient for the vast majority of applications. Only networked systems running applications that have strict clock synchronization requirements would have a need for a maximum polling interval smaller than 1024 seconds (i.e. a shipboard combat system). In such systems, shortening the maximum NTP polling interval may provide improvements in the quality of clock synchronization and the responsiveness of the synchronization subnet. There is a basic engineering tradeoff to be made between the amount of improvement in synchronization accuracy and the increase in network traffic and CPU processing required.

A number of experiments have been performed at the Shipboard Network Technology at the Naval Surface Warfare Center Dahlgren Division (NSWC-DD). Some of these experiments focused on the impact of lowering the maximum polling interval for NTP. The purpose of these experiments was to determine the effect of changing the maximum polling interval (from the default of 1024 seconds to 64 seconds) on the quality of clock synchronization between the NTP clients and the local time server. Several computer platforms were used in this experiment. The platforms were synchronized to a local time server using NTP with either the default (1024) or the modified (64) maximum polling intervals. The offsets were measured once a minute over a period of several hours. The results were examined to determine the amount of improvement in clock synchronization.

Examples of the results are shown in Figure 1. These plots show the offsets measured for both maximum polling intervals (1024 and 64 seconds) on a number of Sun workstations. Two separate data sets are overlaid to show the performance of the same platform utilizing either of the two polling intervals over several hours. The polling interval change has improved clock synchronization by about a factor of ten. Using the default polling interval settings, the clock offsets would wander as high as a few milliseconds. By shrinking the polling intervals to 64 seconds, the clock offsets are kept in the range of hundreds of microseconds. Additional experiments were done on polling intervals of 32 and 16 seconds with little appreciable improvement in clock synchronization accuracy. This analysis is specific to individual hardware and operating system combinations and may need to be revisited as systems evolve.

THE HIPER-D SYNCHRONIZATION SUBNET

The Department of Defense has directed the use of COTS components using commercial standards wherever possible. In addition to this general directive, there has been ongoing research into innovative distributed computing architectures for traditionally federated systems such as the AEGIS combat system. In this context, the High Performance Distributed Computing Program (HiPer-D) was conceived as a joint experiment, teaming the AEGIS Program Office with DARPA. The purpose of the HiPer-D experiment was to explore the feasibility of inserting DARPA-developed distributed computing technologies into the AEGIS combat system.

The HiPer-D experiment performs a significant number of the key functions of the AEGIS combat system, focusing on the Anti-Aircraft Warfare (AAW) problem space. The HiPer-D system is built using a fully distributed fault-tolerant architecture. The computing plant used for this system is a heterogeneous mix of systems from different vendors. In addition to the various hardware platforms and operating systems, four different network technologies are used, including Ethernet, FDDI, ATM, and Myrinet. Figure 2 illustrates the hardware and network configuration. Table 1 summarizes the platform and operating systems used.

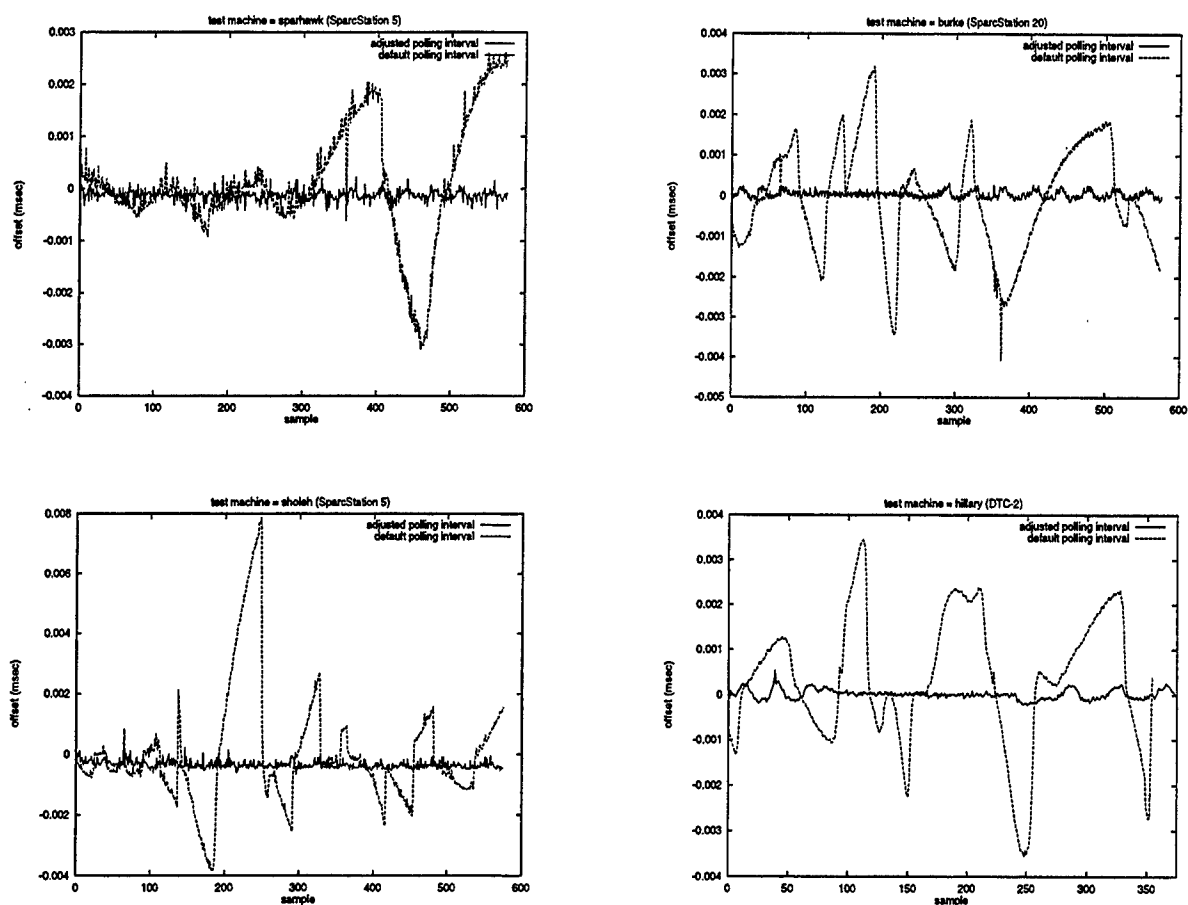


Figure 1: Sample Data from NTP Maximum Polling Interval Analysis

Table 1. HiPer-D Platform Configurations

Vendor	Hardware Platforms	Operating Systems
DEC	Alpha 200 4/233 Alpha 3000/600 Sable SMP 4	OSF/1.3.2
HP	HP 9000/770 (TAC-4)	HP-UX 9.07 HP-UX 10.10 OSF-RT PA
SGI	Origin 2	IRIX 6.3
SUN	SPARCstation 10 SPARCstation20 Ultra1 Ultra2 Sun 4/630	Sun Solaris 2.5.1
	Pentium PCs	OSF-RT

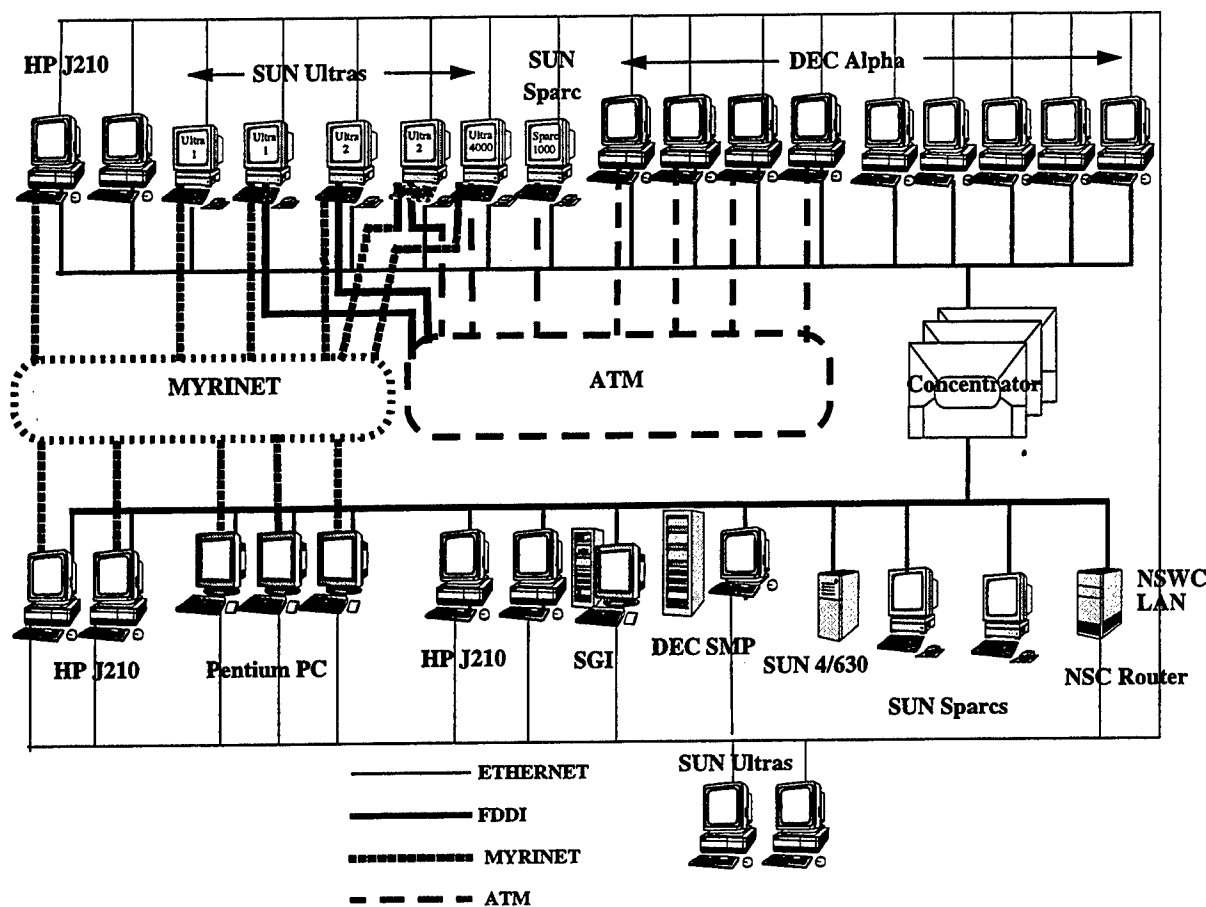


Figure 2: The HiPer-D Testbed Configuration

Based on initial experiments involving NTP in the Shipboard Network Technology Lab, the focus of the HiPer-D time service effort was incorporating improved time synchronization capability into the HiPer-D configuration. In the HiPer-D testbed many technology and operational prototypes are integrated together to study larger system-wide effects and capabilities. Here, the time service is one necessary component within the prototype shipboard system.

A time synchronization subnet was designed to meet the goals of the HiPer-D testbed. First, the synchronization subnet was to provide a stable time service for the HiPer-D experiment using the available COTS components. Second, the synchronization subnet was to require minimal modification of the available COTS products. Finally, due to the way the HiPer-D lab operates, the synchronization subnet was to operate with minimal operator intervention. The synchronization subnet was to be viewed as a component of the computing infrastructure. The goal was to determine the level of performance obtained based on the above objectives and constraints. Additionally, it was anticipated that the HiPer-D testbed could improve on the 1 millisecond requirement identified previously by Navy studies. The synchronization subnet designed is shown in Figure 3. There are four NTP client configurations. The primary time server is using GPS (via IRIG-B) and its own local clock as potential synchronization sources, with the understanding that the local clock will only be used in case the GPS interface fails. The backup servers each peer with the primary server and their own local clocks. All clients peer with the primary

server and the two secondary servers. It is expected that all machines will be using the primary time server as their synchronization source. This is not viewed as an optimal synchronization subnet, merely a sufficient one given the resources at hand. The polling interval is set to once every 64 seconds for all platforms. Most platforms had multiple network interfaces, and, in these cases, time information exchange is normally conducted using the default network interface.

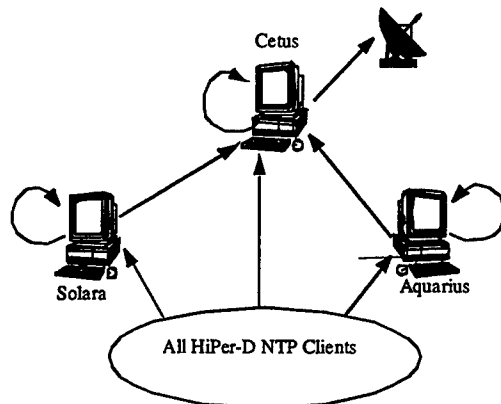


Figure 3: HiPer-D Synchronization Subnet Configuration

PERFORMANCE

The goal of this performance study was to analyze the long-term phase accuracy of the synchronization subnet, independent of any specific activity on the systems including CPU load and network load. Data were collected every fifteen minutes for a two-month period from September 3, 1997 to November 10, 1997. No limitations were placed on testbed activity during this timeframe. Table 2 shows data for each individual platform. Figure 4 illustrates the performance obtained for a few specific platforms. This performance shows that synchronization well below a millisecond was achieved on the vast majority of the platforms. There were some anomalies that require further investigation. The older DEC Alpha platforms performed much more poorly than newer Sun and HP platforms. This is to be expected given the rapid advances workstation vendors have made in the area of local clock hardware and software over the last few years. Note, this experiment only analyzed the first metric, phase accuracy. Additional data and analysis are required to examine the three remaining metrics.

SUMMARY AND CONCLUSIONS

Analysis of the data discussed above provides some initial conclusions. First, the synchronization subnet described performed quite well. Newer generations of machines demonstrated greater phase accuracy than older generations. Not surprisingly, classes of hardware running the same operating system demonstrated similar behavior. The reduction of the maximum polling interval proved to be one mechanism to improve the phase accuracy. Further investigations could reveal additional mechanisms. HiPer-D made an engineering trade-off that was acceptable for that particular environment. This trade-off may not be appropriate in more resource constrained systems.

Table 2. HiPer-D Synchronization Subnet Platform Specific Results ¹

Machine Name	Avg. Offset	Std. Dev.	% samples less than .1 (ms)	% samples between .1 and .5 (ms)	% samples between .5 and 1 (ms)	% samples between 1 and 5 (ms)	% samples greater than 5 (ms)
DEC²							
andromeda	1.154	0.847	5.459	23.883	19.805	50.853	0.000
aries	1.010	0.775	7.319	25.182	22.965	44.534	0.000
auriga	1.213	0.851	4.901	20.068	19.712	55.304	0.016
callisto	0.936	0.577	3.784	18.781	37.919	39.516	0.000
columbia	0.659	0.531	12.498	36.254	25.306	25.942	0.000
gemini	0.960	0.761	8.559	26.066	24.128	41.247	0.000
hydra	0.911	0.661	6.575	24.376	33.726	35.323	0.000
leo	0.671	0.535	12.704	34.388	26.105	26.803	0.000
taurus	0.669	0.739	12.390	35.432	25.880	26.283	0.016
titus	0.984	0.801	4.823	27.636	27.900	39.625	0.016
HP							
crux	0.116	0.421	84.210	12.399	1.149	2.129	0.113
hercules	0.071	0.132	85.802	12.804	0.737	0.658	0.000
jots1	0.292	0.242	38.413	25.917	35.554	0.116	0.000
jots28	0.068	0.111	80.290	19.157	0.252	0.300	0.000
myra	0.079	0.214	82.346	16.608	0.499	0.499	0.048
norma	0.056	0.099	89.556	9.885	0.341	0.217	0.000
vela	0.092	0.162	70.959	27.744	0.479	0.818	0.000
SGI							
capella	0.087	0.458	71.546	28.076	0.221	0.079	0.079
SUN							
aquarius	0.102	0.063	44.070	55.853	0.031	0.046	0.000
aquila	0.641	2.117	0.217	7.953	91.364	0.435	0.031
blofeld	0.604	0.123	0.248	7.881	91.219	0.652	0.000
carina	0.121	0.088	41.891	57.891	0.125	0.093	0.000
mercury	0.105	0.092	54.544	44.913	0.465	0.078	0.000
pavo	0.160	0.106	27.679	71.499	0.744	0.078	0.000
phoenix	0.610	0.089	0.016	4.746	94.960	0.279	0.000
saturn	0.473	0.091	0.140	62.872	36.864	0.124	0.000
solara	0.108	0.847	57.875	41.387	0.569	0.154	0.015
venus	0.090	0.106	65.545	33.432	0.807	0.217	0.000
PENTIUM PC							
ceres	0.451	0.263	8.364	50.083	41.289	0.265	0.000
luna	0.448	0.232	4.488	54.737	40.593	0.182	0.000
pallas	0.537	0.240	1.573	48.394	49.901	0.132	0.000
vesta	0.492	0.270	5.929	44.303	49.619	0.149	0.000

¹ Samples taken every fifteen minutes from 2200 on September 3, 1997 to 1515 on November 10, 1997.

² The DEC platforms are the oldest machines in the HiPer-D configuration representing an older generation of hardware and software. It is believed that newer generation hardware and software would perform on par with the other workstation vendors.

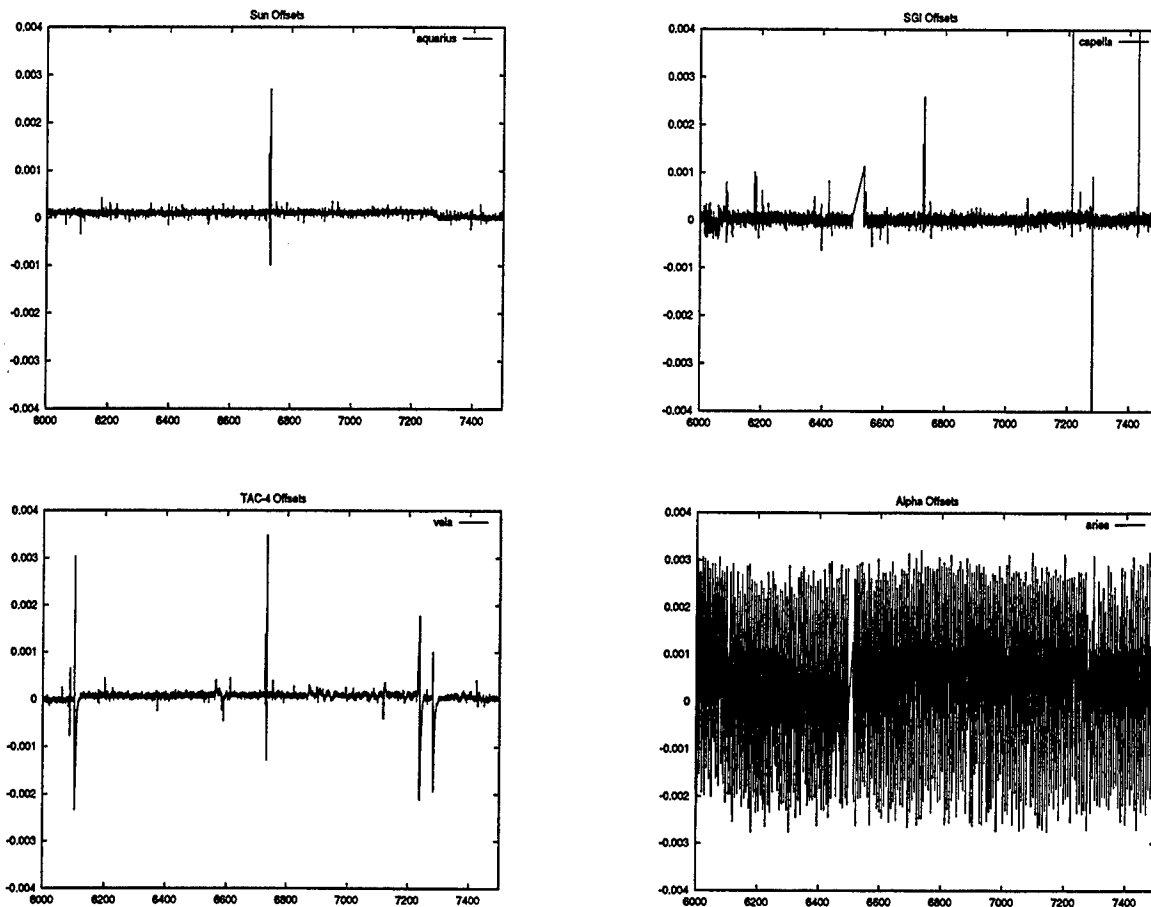


Figure 4: Sample HiPer-D Synchronization Subnet Platform Performance

A number of items have been identified as future work efforts. First, at least one and preferably two additional time servers need to be added to the HiPer-D testbed. A synchronization subnet that contains multiple time servers could provide greater fault tolerance. Performance analysis of multiple servers, especially in the case of server failure, is necessary. Second, although the quality of clocks in COTS workstations has improved over the past few years, new kernel modifications based on research by Dr. David Mills [2] are beginning to be delivered with commercial products. The Navy is depending on the COTS products to provide future generations of computing infrastructure for its platforms. Analysis of the workstation products being delivered in general and of the specific new kernel features in particular is necessary. Time service performance is tied closely to specific clock implementations provided by computer vendors. The Navy will need to test new generations of hardware and software to ensure that they provide the needed functionality. Finally, this study looked at the long-term phase accuracy of the HiPer-D synchronization subnet. Analysis of the frequency stability based on the collected data has not been completed at this time. In addition, no data were collected to study the fault recovery time or clock settling time metrics. Finally, focused analysis of the synchronization subnet under specific stress or fault scenarios (cpu load, network load, server failure, etc.) would be useful. All identified metrics need to be appropriately analyzed for the HiPer-D testbed.

The Navy has invested in the analysis of time services in general and NTP in particular. Results have shown that this technology, in conjunction with modern computing equipment, can provide a stable robust time service for Navy platforms.

ACKNOWLEDGEMENTS

A number of individuals contributed to the completion of this cycle of data collection and analysis. In particular, Barbara Davis assisted in the maintenance of the synchronization subnet, Timothy Plunkett conducted the NTP polling interval experiments and produced some of the analysis tools, and D. Wayne Mills provided review and oversight.

REFERENCES

- [1] D.L. Mills 1992, "Network Time Protocol (Version 3) specification, implementation and analysis," RFC 1305.
- [2] D.L. Mills 1996, "The Network Computer as Precision Timekeeper," 28th Annual Precise Time and Time Interval (PTTI) Applications and Planning Meeting, pp. 97-107.
- [3] K. F. O'Donoghue and D. T. Marlow, "Time Synchronization Services Aboard Surface Ships," Naval Engineers Journal, Vol. 108. No. 6., pp. 73-84.
- [4] D.W. Allan, Characterization of Clocks and Oscillators, ed. D.B. Sullivan, D.W. Allan, D.A. Howe, and F.L. Walls, NIST Note 1337, 1990, pp. TN121-TN128.

BENEFITS AND ISSUES ON THE INTEGRATION OF GPS WITH A WIRELESS COMMUNICATIONS LINK

Raymond DiEsposti, Steve Saks, Lubo Jocic
The Aerospace Corporation
Los Angeles CA 90009

Capt. Jordan Kayloe
Space and Missile Center
Los Angeles Air Force Base, CA 90009

Abstract

The NAVSTAR Global Positioning System (GPS) provides worldwide positioning service to 2-Dimensional, 95 percentile accuracies of 100 meters for the Standard Positioning Service (SPS) for civilians and about 15 meters for the Precise Positioning Service (PPS) available to authorized users only. In the past, GPS has been combined with other instruments, such as Inertial Navigation Systems (INS) and Doppler radars for navigation, and precise frequency standards for timing, to produce more robust and accurate integrated systems. Within the past few years, significant advances have been made in GPS receiver and wireless communication (comm) technologies. Handheld devices for GPS and Personal Communication Service (PCS) have decreased in size and cost, yet increased in capability and battery life. This paper analyzes the benefits and discusses conceptual design issues associated with a tight integration of GPS with a wireless communication link for both military and civilian users. In addition to providing a means for data and voice communication, the comm link can provide GPS initialization data that could significantly improve GPS acquisition and navigation (nav) performance, especially in stressed (interference prone) environments.

INTRODUCTION

Two technologies that have recently become prevalent in the private sector are wireless PCS (including cellular telephony and data messaging) and GPS. Many commercial applications require that the two technologies be merged. For example, fleet resource monitoring and emergency notification devices integrate both technologies. Since GPS and wireless PCS technologies are continuously shrinking in size and power consumption, it is reasonable to expect that the two can be effectively integrated into a single, practical handheld device in the near future. Also, the recent availability of low-cost GPS chip sets now allows a cost-effective way for vendors of PCS devices to integrate GPS into their products.

In a manner similar to GPS/INS integration, the two technologies of GPS and wireless communication can complement each other very well. In the GPS/INS union, the INS has good short-term stability, but poor long-term stability due to IMU drift. On the other hand, GPS accuracy is independent of elapsed time, but short-term errors on the order of several meters (PPS user) exist due to satellite switching (in the navigation solution), multipath, ionosphere, etc. Therefore, when combined, the GPS can be used to calibrate the long-term INS drift error, while the INS can be used to aid (steer) the GPS tracking loops and provide smoothing for GPS error fluctuations. A tight GPS/INS integration also enhances performance in stressed environments.

Now, consider the integration of GPS with wireless communication. Data supplied via a wireless comm link can greatly assist GPS initial signal acquisition. Without prior initialization data, a GPS "Cold Start" fix (acquisition without prior almanac, user location, or time data) may require several minutes or more. However, if initialization data can be supplied by a wireless comm link, GPS acquisition could be very fast, on the order of a few seconds. For GPS handsets operated in the quick fix mode, fast acquisition may have a large, positive impact on battery life. Accurate initialization data will allow a more effective GPS acquisition in the presence of interference and spoofing. Some of the other navigation benefits of a comm link are: (1) the ability to receive differential and ionospheric corrections for improved accuracy, (2) the ability to receive real-time GPS integrity information, (3) the ability of the user to report his location or intelligence data back to an emergency, central control, or monitoring center, and (4) the ability to assess positions of other users reporting their positions on a satcom-based mobile internet.

The addition of a comm link to a GPS user set provides the GPS user with obvious benefits, as discussed above. However, the benefits of adding GPS to assist the user whose primary function is communication, are also great -- In this case, the addition of GPS satisfies the needs of many commercial users to maintain accurate time and to report position to the resource control center for billing purposes. GPS further enables the following comm system features: (1) pre-synchronization interference with other comm links would be minimized in situations where GPS time is available to comm users prior to the uplink synchronization time-search, (2) control channel orderwire can be simplified if the user could report his position and time to the control center in the initial contact, and (3) a database of the mobile users' positions in the control center would improve resource allocation.

Most of the remainder of this paper further describes the ways in which a tightly coupled, wireless comm link could aid the primary function of navigation for a GPS user.

WIRELESS COMMUNICATION LINK AIDING GPS

Data received from an existing wireless comm link can benefit both GPS performance and security. Both speed of acquisition and anti-jam capability (increased Jammer/Signal (J/S) capability) for acquisition and track are possible. Navigation accuracy can be improved through the transmission of differential and ionospheric corrections. Security can be improved by using the comm link for transmission of electronic "black" keys for GPS encryption. Assuming that the comm link is tolerant to interference (stressed environment), it allows an efficient solution to the Direct-Y code acquisition problem. The direct

acquisition of GPS Y code, which has been advocated as a more reliable method of protecting the availability of GPS, requires prior knowledge of accurate time, rough user location, recent almanac, and cryptokey. The maintenance of this data when the GPS receiver is turned off for extended periods of time represents a logistics challenge, which can, however, be greatly simplified through the use of a wireless comm link.

Acquisition Time Enhancement

GPS acquisition speed is enhanced by the comm link's ability to provide the equivalent of the satellite's broadcast 50 Hz navigation message at a faster rate or at a much higher power level. The time and data maintenance requirement (necessity to maintain accurate time and recent nav message data) associated with the Direct-Y mode can be eliminated, since the comm link can provide the data at any time independent of the satellite signals. Faster acquisitions will result for both Normal Start (acquisition with satellite almanac, rough user location, and time) and Cold Start conditions (acquisition without prior almanac, user location, or time data). For both Cold Start and Normal Start initial conditions, the time required to read the entire 50 Hz nav message for almanac, ephemeris, and other data could be reduced from 12.5 minutes to a few seconds. Normal Start mode would then use the almanac or ephemeris nav message data along with resident user location and time. For Cold Start conditions, user location and time could be provided by the comm controller at the base station. Time accurate to a millisecond and position to 300 km are reasonable in theater. Repeated time pulses also allow synchronization of the receiver oscillator frequency. This further enhances acquisition by reducing the frequency offset search space.

Acquisition Anti-Jam (J/S) Enhancement

Whereas the GPS satellites are at an altitude of about 20,200 km, a terrestrial line-of-sight comm transmitter may be only a few 10's of kilometers away. Even at 100 km, the ratio of the $1/R$ squared path loss of a locally broadcast signal compared to a satellite signal amounts to over 40 dB. The GPS signal, as received at the Earth's surface, varies between -166 dBW (L2 P(Y)-code) and -160 dBW (L1 C/A-code), about 20-25 dB below ambient noise level. Through correlation despreading, the signal is amplified above the noise level to enable acquisition and tracking. Future satellites may employ spot beams which are capable of increasing power in a region by 20-25 dB. However, a local terrestrial comm link does not have the severe power constraints associated with the current GPS satellites, which derive their energy from solar power. Local comm signals, broadcast from a base station, can be several orders of magnitude stronger than the GPS signal.

The GPS C/A code acquisition threshold is 24 dB J/S. However, once the signal is acquired and the tracking loops have achieved lock on Y code, the J/S threshold to maintain Y code tracking/data demodulation exceeds 40 dB. Also, the J/S threshold to maintain code loop track can extend beyond 50 dB. Since the comm link can provide the GPS satellite message data, there is the possibility that GPS navigation can operate in the code only track mode. (GPS carrier track and data demodulation are no longer required, and code tracking can be extended by either data stripping the nav message data or squaring.) Accurate time and velocity aiding data may allow a direct handover from acquisition to code track without

achieving carrier lock. — Thus, with the addition of a higher power comm link, there is the potential of increasing the J/S capability of GPS operation by more than 20 dB.

Similarly, for a comm link provided via satellites, the satcom to omni receiver link has to be 20 to 30 dB higher than the GPS signal in order to enable more than 20 dB higher data rate (e.g., 4.8 kHz comm vs. 50 Hz GPS data rate). If the satellite is built for comm signal levels, it can also provide similar nav signal strength for acquisition.

Tracking Anti-Jam (J/S) Enhancement

High-power navigation signals compatible with satcom signal strength would increase the J/S capability for tracking by 20 dB to 30 dB. In addition, it may be possible to extend the J/S tracking threshold through the procedure of “data stripping”, in which the coherent integration time is extended beyond the 20 msec data bit interval by removing the known data bit from the signal stream. In this case, the GPS data bits can be provided through the comm link.

Security Enhancement

A wireless comm link capability in GPS receivers would greatly facilitate the planned implementation of electronic keying. The comm link provides a very efficient means for the distribution of “black” keys. In addition, more sophisticated encryption schemes can be developed when two-way comm is available. The integration of comm and nav terminals reduces the number of crypto systems for platforms that require both user terminals.

Logistics Enhancement

Direct-Y requires the maintenance of recent almanac or ephemeris data, rough user location, accurate time, and keying data [2]. When a receiver is turned on, these data can be kept current. However, when the receiver is turned off, time starts to drift based on the receiver oscillator instability. In general, increased oscillator stability requires increased power, which adversely impacts battery life, especially in handheld devices. A properly designed comm link can provide time to better than a millisecond accuracy. Also, as already discussed, the above data could be provided relatively quickly with a comm link having data rates of several kHz. Hence, the comm link can provide a enormous reduction in logistics burden associated with implementing Direct-Y code acquisition.

Accuracy Enhancement

The comm link can provide differential corrections, which can be applied to achieve accuracy on the order of a few meters, or even a few centimeters for cases when the carrier cycle ambiguities can be resolved.

Integrity Enhancement

The comm link can provide very timely integrity information related to satellite health and status, and the existence, characteristics, and location of any interference sources. If comm link data received by the user

to initialize the GPS function can be provided securely and reliably, then the risk of spoofing GPS during acquisition can be significantly reduced. -- Independent, precise timing data from the comm link may be used to detect erroneous signals. If carrier cycle ambiguity tracking can be applied, extremely reliable Receiver Autonomous Integrity Monitoring (RAIM) may be achievable, since a signal phase error of only a few centimeters is detectable.

INTEGRATION AND IMPLEMENTATION ISSUES

Some of the arguments discussed above relating the benefits of the merger of GPS and wireless comm link also apply to military users. However, many additional issues need to be considered by the military user that may be irrelevant to most civilian users.

Some conceptual design alternatives and other issues common to both are listed below:

- Two way vs. one way comm link. Significant benefit related to enhanced GPS performance requires only a one-way comm link, from the base station to the user. A one-way user set only requires a comm link receiver and not a transmitter. Thus, considerable cost and improved power consumption can be realized compared to a comm link needing a two-way capability. However, some electronic keying schemes require a two-way capability. Some military users need to remain "undetected". Thus, in some cases, a return path comm link may not be acceptable, unless a Low Probability of Detection (LPD) signal is employed.
- Partial GPS receiver integrated with a two-way comm link. An example of such a device is a translator, which takes in GPS signals, then rebroadcasts them to some central processing facility at a base station. The central processing station performs the tracking and navigation functions, adds in corrections, such as ionospheric, tropospheric, or differential, etc., then broadcasts the solution back to the user. However, in such a system, data latency or decorrelation of spatial corrections may be issues for the user that is located at a large distance from the base station. For a user moving at sufficiently high speeds, data latency may also effect navigation accuracy. Also, a partial receiver will not be able to operate as an independent, autonomous device -- that is, it will be useless when the comm link and central processing station is unavailable. Another advantage of this approach is that the user location is known by the central processing facility, which can then also be used as a resource management facility and command center. The ground and space-based cellular comm link infrastructure to support this type of capability is being rapidly developed in many parts of the world.
- Complete, autonomous GPS receiver is one that is able to operate with or without the comm link. This receiver has the capability to acquire and track the GPS satellites and compute the navigation solution when comm data are not available (in the same way that GPS user sets currently operate). However, when the comm link is present, the GPS performance, accuracy, and integrity can be greatly enhanced, as discussed above. The comm link can be used to provide accurate initialization data from the base station (such as almanac, ephemeris, accurate time and synchronization data, approximate user position,

and in the case of the military user, keying data). The availability of this data will allow very fast acquisition (even Direct-Y) and track of the GPS satellite signals, typically within a few seconds.

- Reporting information back to a central control facility. Both civilian and military users may benefit from this capability. Again, this requires that the user set include a comm link transmitter. Some commercial users may only need the transmit capability, in which case the user location (or measurements) is automatically sent back to the monitoring station. At the monitoring station, differential corrections can be applied for improved accuracy. In the case of military users, the ability to relay user location (and other intelligence information) to a central control facility is consistent with DoD plan to "digitize" the battlefield. Friendly and unfriendly forces could be digitized on a computer database and map. Information, such as location and description of friendly and unfriendly forces, provided through the receive comm link, would also be very useful to the user.
- Interference of comm link with GPS signal. Since a local comm link signal may be several orders of magnitude stronger than the global GPS signal, integrated systems need to be properly designed so that the stronger comm link signal does not jam nor cause degradation of the local GPS signal.

MILITARY UNIQUE ISSUES

- Implementation schedule. The cycle time associated with the acquisition, design, and launch of military satellites usually consists of 5 to 10 years (or more). On the other hand, cycle times for the acquisition of GPS user equipment are much shorter, 2 to 3 years. Since wireless comm technology is available today, there is the possibility of adding this enhancing technology within a much shorter time frame.
- Integration with a data bus. If the GPS and comm transceiver are integrated via a platform data bus, there is the issue of data latency. While latencies on the order of tens of milliseconds may be adequate for nav message data transfer, they may not be for time transfer to enable Direct-Y acquisition. Rewriting the data bus software to decrease latency may be very costly. We define a tight integration as one in which the GPS receiver and comm link transceiver are connected directly to each other, and to each respective antenna, bypassing the platform bus. -- In this case, latency errors are negligibly small.
- Comm link security. For military applications, there are several issues related to the security of the comm link. First of all is resistance of the comm link to jamming. The ability of the comm link to be spoofed, or provide misleading information to either the user, the GPS receiver, or the base station/control facility is also an important concern. For user sets that transmit and receive, there is also the concern of giving away the user's location and message. These concerns may require that a bursty comm link be designed using direct sequence spread-spectrum techniques with encrypted signals. With encrypted comm signals, there is the additional problem of key distribution.
- Comm link signal acquisition. Other issues related to military comm link usage are the speed of acquisition of the comm link signal and power levels. The comm signal can be designed so that acquiring the comm link signal is faster than typical GPS acquisition, while maintaining security. For a fixed data rate, the frequency hopping techniques can enable faster acquisition than direct sequence spread spectrum. Even if the signal is encrypted, this should be the case since the comm transmitter is not as severely power-limited as the GPS signal broadcast from current satellites. Higher comm link power levels (relative to GPS signal) can allow the increase of C/A code acquisition performance from the current J/S of 24 dB to the GPS data demodulation threshold of about 40 dB. In fact, with a comm

link providing the GPS nav message data, potential anti-jam performance may extend out to the Y code tracking threshold of about 50 dB for some cases.

- Comm link data rates. Also of issue is the comm link data rates. While the GPS data rate is 50 Hz, data rates approaching 5 kHz, typical of voice communication, are desirable for high speed transmission of GPS initialization data. The complete GPS data message is 37,500 bits long (12.5 minutes @ 50 Hz). The satellite constellation almanac data are spread out over 25 pages of length 30 sec each, whereas, the precise ephemeris data repeats every 30 sec. The almanac data assist acquisition by providing satellite position data to determine which satellites are in view. Almanac data are also used to reduce the time/frequency search space when combined with a priori user location/velocity and time. The ephemeris data are typically used for the navigation solution. Whereas almanac data several weeks old or more may provide sufficient accuracy for acquisition, in most cases, the ephemeris data must be read prior to computation of the navigation solution. Together with the overhead time associated with satellite C/A code acquisition, bit synch, frame synch, settling of tracking loops, etc., this limits the acquisition time to be no smaller than about 40 seconds, even for a warm receiver. However, assuming a comm link data rate of 5 kHz, all of the GPS nav message can be relayed in about 8 seconds, along with rough user location, and fairly accurate time. The GPS acquisition and navigation solution should then require no more than about 10 to 15 additional seconds, even for the case of a prior "Cold" receiver.
- GPS enhanced capability using comm link vs. advanced technology, such as precise clocks and advanced Digital Signal Processing (DSP) chips. Improved GPS performance (improved security and J/S) can also be realized without a comm link through the implementation of a near-autonomous form of Direct-Y employing advanced technologies. However, at this time, a robust form of Direct-Y is technically very difficult. Direct-Y is further complicated by the necessity of periodic operations needed to maintain current time and keying information. Direct-Y acquisition time can be greatly improved through the introduction of advanced, high accuracy, low-power time sources and DSP technologies. Then, if the keying methodology can be simplified, fast, reliable operation may be achieved without the use of a receive comm link to provide GPS initialization data. However, even with technology to provide "fast" acquisition, given the GPS signal structure, the fastest possible fix time for the general case, as discussed above (and without a comm link or direct data input via wireline), is about 40 sec. This constraint is not present with a high data rate comm link -- the ephemeris data could be quickly sent to the user in under a second.
- Global vs. local comm link. A global comm link using communications satellites would be widely available without the need to set up the infrastructure associated with terrestrial base stations. Also, dedicated military satellites could be more easily controlled and protected. Even though satellite signal power can be concentrated in spot beams, local base stations could have much larger power advantages than satellites, especially important in stressed environments. However, terrestrial stations often have significant range limitations associated with the line-of-sight constraint. In addition, they are very vulnerable to enemy or terrorist actions, when they transmit high-power signals above the ambient noise level. Improvement on these limitations is possible by placing the comm transmitter or relay station on a stand-off, high altitude platform.

- Integrated GPS/INS/comm link. Faster PPS fixes (when GPS is aided by the comm link), possibly even centimeter-level accuracies associated with carrier cycle ambiguity resolution, may greatly improve the speed and accuracy of INS calibration in integrated GPS/INS systems.

CONCLUSIONS

This paper provides a discussion of the benefits to GPS users of an integrated wireless communication data link. Recent technological advances in the field of wireless PCS make such a capability practical (size, battery life and cost considerations) even for GPS handheld user sets. The primary benefits of a receive comm link are: (1) very fast acquisition, even for the case of a "Cold" user set, without the need for advanced clock and digital signal processing technologies, (2) improved J/S capability during acquisition and possibly track, (3) if comm link is secure, reduced risk of spoofing GPS, (4) improved accuracy through the use of broadcast differential corrections, (5) improved integrity, (6) greatly reduced logistics burden associated with the Direct-Y acquisition mode of operation, and separate nav and comm crypto systems and user equipment, (7) reception of other sensitive data, such as location and description of friendly and unfriendly forces and commands, and (8) for handheld user sets, potential for greatly improved battery life. The main benefit of a transmit comm link would be to relay user location (and other intelligence data) and to communicate with a central control facility.

In some cases, it may be possible to implement a receive comm link through the use of a pseudolite type of local transmitter that broadcasts using a GPS-like signal, received through the GPS antenna and receiver, and that does not interfere with the satellite signals. In this case, the comm link receiver becomes an integral part of the GPS receiver.

REFERENCES

- [1] GPS Interface Control Document ICD-GPS-200, Revision C, 10 October 1993.
- [2] Direct-Y: Fast Acquisition of the GPS PPS Signal, O. M. Namoos, R. S. DiEsposti, Proceedings of the 27th Annual precise Time and Time Interval (PTTI) Applications and Planning Meeting, Nov 29 - Dec 1, 1995.

Panel Discussion on Time Rollover Events and Leap Seconds

Judah Levine
Time and Frequency Division
National Institute of Standards and Technology
Boulder, Colorado 80303

Abstract

The panel discussed the rollover in GPS time that will occur in 1999, the rollover in the civil date at the beginning of the year 2000 and the problems associated with leap seconds. We showed why these problems arise and we discussed various strategies for dealing with them. We also outlined difficulties that arise because of a lack of standardization in data formats and signaling standards. Judah Levine of NIST was the moderator; other members of the panel were David Mills, University of Delaware, Don Mitchell from TrueTime and Edward D. Powers from the US Naval Observatory.

THE CAUSES OF ROLLOVERS AND LEAP SECONDS

The Global Positioning System time is expressed using two parameters: the week number and the second of the week. Week number 0 began at 0000 UTC on 6 January 1980, and week number 1023 (the largest possible week number) will begin on 15 August 1999. The week number will wrap around to 0 at the start of the following week (22 August) and the cycle will then repeat. The GPS time message does not contain any indication of this rollover, so that all GPS times have an ambiguity of 1024 weeks.

Systems that use only two decimal digits to express the year will face a similar problem starting on 1 January 2000 -- the century associated with a year specified in this way will be ambiguous. In addition to these rollover problems, many databases use the year "99" as a flag meaning "forever." Dates such as 9/9/99 or 11/11/99 are often used for this purpose, since it is easy to enter them and they do not violate the 6-digit format expected by software that processes the date field.

The ambiguities produced by rollovers are a feature of all digital systems -- values are always represented in a finite-length field, and the maximum-possible value will be reached sooner or later. The value will wrap around to 0 after that and start over again, and there is generally no way of indicating this rollover in the time tag itself. The size of the field and, therefore, the interval between rollover events, is determined by a design trade-off: larger fields will have less frequent roll-overs, but the time tags will take up more space and will generally require more keystrokes to enter.

The need for leap seconds arises from fundamentally different considerations. The length of the UTC second is based on the defined frequency of a hyperfine transition in the ground state of the cesium atom (9 192 631 770 Hz). A day constructed using 86,400 of these seconds is somewhat shorter than an astronomical day based on the rotation rate of the earth, which is called UT1.

Clocks based on cesium frequency standards, therefore, run somewhat faster than a clock based on UT1. The difference is about 1 s/year on the average; it is removed by inserting "leap" seconds into the UTC time scale as necessary – in effect stopping the UTC-based clock so that the UT1 scale can catch up. When they are required, these additional seconds are added at the end of June or December. The difference UT1 - UTC therefore exhibits a sawtooth-like behavior – decreasing at a rate of somewhat less than 0.1 s/month for about a year, followed by a step increase of 1.0 s at the time of a leap second. The absolute value of this difference is kept less than 0.9s.

The rate difference UT1 – UTC has been negative since the current leap-second system was introduced in 1972. The magnitude of the rate difference will increase as the earth slows down, but this increase will be somewhat irregular, and it will not be possible to predict exactly when future leap seconds will be needed until a year or so before they are announced. Although "negative" leap seconds are also defined, the fact that the earth will probably continue to slow down (albeit irregularly) suggests that the rate difference between UT1 and UTC will not change sign, so that they will never be needed.

POSSIBLE SOLUTIONS TO THE ROLLOVER PROBLEM

One way to address the rollover problem is to define a sliding "window" in the software that processes the time-tag. Two-digit years less than or equal to 90, for example, could be assumed to refer to dates in the 21st century, while values of 91 or greater would be assumed to be in the 20th century. This window might be advanced with each revision of the software or whenever another rollover was imminent. The primary advantage of this method is that archived data files need not be changed, nor is any change required to the methods used to enter new records. We are, in effect, carrying part of the date in the time-tag itself and part in the software that interprets it. This method obviously fails for time intervals that span more than one rollover period or for time tags associated with events that are in the distant past or are far in the future. Since rollovers are relatively infrequent in all of the systems we are considering, we would hope that the number of time tags that are affected by these ambiguities would be pretty small. Events that would be affected in this way would be so precious that ancillary means will have to be provided for identifying the rollover value associated with them. If this is not the case, then one of the more general solutions discussed below will be needed.

Although data archives need not be changed, the sliding window solution *does* require a change to the software that processes the time tags, and identifying all of the programs that must be changed can be an enormously expensive and difficult job. If these costs are large enough, it may be worthwhile considering changing the formats of the time-tags themselves at the same time so as to realize a more permanent solution to the problem. One possibility is to change to a 4-digit year, but other solutions are possible that are almost as good and do not require more than the 6 digits currently used by the YYMMDD format. Changing to 3 digits for the year and 3 for the day of the year is one possibility; another would be to use a pure 6-digit day number – perhaps an expanded version of the Modified Julian Day number used by timing laboratories; still another would be to express the date in a base larger than base 10 (although this might break programs that expected only digits in the time-tag). A "shell" program would be needed in each of these cases to translate between the internal format and a more conventional one that was suitable for data entry and display.

The sliding window solution is not perfect, but, at least in the short run, it may be the cheapest one to implement, since most data records will not require modification. The rollover problem will return again near the end of the window period, of course, but the cost of dealing with a relatively infrequent rollover might be more than offset by the savings in file size or program complexity that can be realized in the interim. These savings were much more important in the past when computers had much less memory and much smaller disks. Nevertheless, pushing the cost of converting a large database into the future (when a more elegant solution might be available and when somebody else will pay the price for the conversion) is likely to remain an attractive possibility.

DEALING WITH LEAP SECONDS

There are two methods that are usually used to account for leap seconds when specifying a time-tag. In the first method, the clock always advances at a constant rate, and leap seconds are incorporated by a separate procedure that "knows" when each leap second has occurred (by means of a separate table, for example) and adjusts the time-tag as necessary. This procedure must intercept all requests for time-tags or time interval calculations and must do the "right thing" both for times in the past and those in the future. Alternatively, the clock itself is corrected for the leap second by applying a time or frequency step each time one occurs. The first method, which is also used to correct for daylight saving time in many systems, simplifies the clock hardware and software, while the second method is simpler to support since it does not require maintaining, distributing and verifying an ancillary table of the dates on which leap seconds have occurred. The second method has difficulties and ambiguities of its own, however, especially in a distributed environment, where different systems may realize the leap second time step in different ways and at slightly different times because they are not perfectly synchronized. Neither method is adequate for computing precise UTC-based time intervals very far in the future, since the times of future leap seconds cannot be accurately predicted. Time-tags of events in the past (before the current leap second system began) have additional ambiguities. These are especially confusing for precisely dating events between 1 January 1958 and 1 January 1972 because UTC was steered *both* in rate and in time during this period.

Leap seconds also introduce ambiguities into time intervals, and systems where time interval (or frequency) is the primary observable usually do not use a UTC-based scale for this reason. The most common contemporary example is GPS time, which keeps track of the number of leap seconds in a separate parameter that is not part of the clock reading itself. (GPS system time itself is not affected by a leap second – only the separate leap-second counters are changed when one occurs. Thus, the difference between GPS system time and UTC changes by 1s each time a leap second occurs. It is up to the receiver to deal with these flags and to include the correction in the output time message when a UTC-based time tag is requested.)

Leap seconds are added after 23:59:59 on the last day of June or December; the extra second is named 23:59:60, and it is followed by 00:00:00 of the next day. This nomenclature may be a problem in some situations. In the first place, a time tag with a value of 60 in the seconds field may be rejected as a format error by some applications. Furthermore, there is no natural way of incorporating leap seconds in formats that do not use hours, minutes and seconds to report the time. The Network Time Protocol falls into this category, as do many other formats that report the time as a number of seconds since some origin time.

There are two alternatives to reporting a time of 23:59:60 during a leap second: the first is to freeze the time at the format-specific equivalent of 23:59:59 for an extra second, and, optionally, to provide a separate flag to indicate that a leap second is in progress during the second of these seconds. This flag is extra baggage, of course, but it cannot be dropped because it is the only way of distinguishing between two physically distinct seconds that have the same time-tag. The second is to slow the frequency of the clock oscillator by a factor of 2 so that it takes two physical seconds to advance from 23:59:59 to 00:00:00. These two systems cannot be used together, of course, since they have very different notions of time-tags while the leap second is in progress: the leap second is identified as 23:59:59 with the ancillary flag set in the first realization and as 23:59:59.5 in the second version. Neither of them is consistent with the "standard" definition of 23:59:60 for the name of the leap second.

Even when the time is transmitted as HH:MM:SS, there are no standards either for how to provide advance notice that a leap second has been scheduled or for how to indicate that one is currently in progress. This notice is important for two reasons. In the first place, it can be used to signal the receiving software that a value of 60 for the seconds is a valid leap second and not a format error. In the second place it can be used to schedule a local procedure to incorporate the leap second into the local time scale in an orderly fashion in whatever way is deemed appropriate (i.e., using a frequency step, a time step or adding an entry to the leap-second table). The greatest ambiguities in how this notice is implemented arise in the IRIG codes, where different manufacturers use different control bits for the leap-second flag. The method used to specify the year in IRIG codes also varies from one implementation to another. Some industries have specified how these parameters shall be defined for the systems that they purchase, but these definitions are not universally recognized.

VERIFICATION AND TESTING

Whatever solution is adopted, rollovers and leap seconds are relatively rare events, and it is often difficult to verify that a particular system will handle them properly. This is especially serious for rollover events, since neither a century rollover nor a GPS week rollover has happened in the era of computers and digital systems. The performance of GPS receivers when the GPS week number rolls over to 0 can be evaluated using a simulator, and most of the newer receivers handle the rollover properly using some form of the sliding-window algorithm discussed above. Some older receivers may fail these tests, and it may be difficult or impossible to repair them. Some receivers will only fail in the immediate vicinity of the rollover because they will try to use a pre-rollover almanac to estimate the post-rollover positions of the satellites. Although the rollover ambiguity will mean that a conversion between GPS time and UTC always will be wrong by 1024 weeks following the rollover event, many of these older receivers will start tracking normally again after the rollover once a post-rollover almanac has been received. Although repairing software systems is possible in principle, the complexity of the programs and the inadequacy of the documentation may make this difficult (and therefore very expensive) in practice.

Radio and GPS receivers must also be tested to be sure that they recognize the flag giving advance notice of a leap second and that they respond properly during the event. This is not always a simple matter, since there may be a complicated interaction between the leap second logic and the "holdover" algorithm that controls the internal oscillator if the external time signal

is temporarily lost. (A similar ambiguity may arise when different GPS satellites are transmitting different values for the leap second flags.) In a worst-case approach, it may be prudent to ignore the time transmitted by a radio- or GPS-synchronized clock for some time after the leap second has occurred to give the receiver time to re-synchronize itself.

CONCLUSIONS

Rollover problems in digital time formats arise from engineering compromises between size, speed, time and money. While rollover events cannot be eliminated in a digital format, they can be pushed arbitrarily far into the future by making the time code longer or by using a shorter time code with ancillary flags to provide rollover information. This compromise cannot be the sole province of the system designer – the users must also play a role in formulating the balance between the savings that can be realized using a smaller time-tag and the costs of dealing with the more frequent rollovers that will result from this choice.

The problem of leap seconds is more complicated and the solutions are, therefore, more ambiguous. There is no simple way of simultaneously accommodating users who want an atomic-based time scale that is smooth and continuous and those who want one that closely approximates a time-scale based on astronomical observations. No single system can meet all of these requirements, and multiple systems will coexist for the foreseeable future as a result. Understanding how to convert among these systems will continue to be a guarantee of employment for some and a source of confusion for many others.

Finally, it would be useful to adopt standard methods for all aspects of a time code, including the relationship between the time-tag and the on-time marker and the method used to provide information about future and pending leap seconds.

LONG-TERM TIME TRANSFER STABILITY OF A FIBER OPTIC LINK

O. Buzek

Institute of Radio Engineering and Electronics
of the Czech Academy of Sciences
Chaberská 57, 182 51 Praha 8, Czech Republic
Phone +420 2 880144 Fax +420 2 880222
E-mail buzek@ure.cas.cz

Abstract

The paper is devoted to the study of the long-term stability of the propagation delay of a fiber-optic timing link under real environmental conditions. The temperature dependence of the light propagation delay on surrounding temperature changes has been found as dominant. An appropriate method has been developed to correct mathematically the thermal delay variations in the fiber. After the correction for this temperature effect, only subnanosecond residual variations have remained.

INTRODUCTION

To ensure subnanosecond time comparisons of the remote clocks over a long period of time (one year and more), an adequate transmission system must be used in addition to stable measurement and distribution systems. A time transfer link based on the optic fiber seems to fulfill the requirements for precise timing over a distance of several tens of kilometers. The electronic part of the optic transfer link can be basically well designed and maintained in closely controlled laboratory conditions. Also, the parameters of the electronics can be regularly checked to obtain good long-term time transfer stability. In contrast, the fiber, which spans the outer distances between the laboratories, is exposed to uncontrollable natural environment even if buried under ground, taking into account the insensitivity of the fiber to the electromagnetic perturbation, all other environmental factors like temperature, humidity, atmospheric pressure, etc. may have influence upon it. All these factors may cause the instability of the propagation delay of the optical signal in the fiber. The spurious fluctuations of the link propagation delay superimposed on true measured phase-time values could be mistakenly interpreted as the instability of the compared clocks unless special care (correction, compensation) is taken with respect to the measured data.

For this reason the investigation of time transfer parameters of fiber-optic links was one of the first tasks which arose just after the realization of the Czech National Time and Frequency Group Standard (CNTFGS) [1] in 1993. The CNTFGS is based on the HP 5071A cesium clocks operating in two remote laboratories in Prague. Fiber-optic links are used to provide the internal traceability of individual clocks. These transfer links (each of them consisting of an identical 1300 nm optical transmitter, approximately 10-km-long single-mode fiber buried underground, and an optical receiver followed by a 5 MHz PLL

filter) are used to transfer 5 MHz output signals of the clocks in both directions. The two-way configuration of the CNTFGS time transfer network permits use of the standard data obtained from the routine time scale comparisons for evaluation of the link transfer stability. This paper summarizes the results of nearly four-year study of the instability of the propagation delay of the fiber timing links. It has been found that the temperature of the soil surrounding the optic cable, which causes the thermal dilatation of the fiber, is dominant among all other environmental factors which also might affect the long-term propagation delay fluctuations of the whole link.

THE EXPERIMENT CONFIGURATION AND TIME RELATIONS

The basic configuration of the clocks and timing links is depicted in Figure 1. One cesium clock is located in laboratory A and two clocks in laboratory B. Identical automated measuring systems are used at both laboratories to provide simultaneous phase-time measurements. Two output signals transmitted from B at the time instants T_1 and T_2 using the links 1 and 2 are received at A at the time instants T_1^* and T_2^* , respectively. In the same way, the output signal transmitted from A at the time instant T_0 using the link 0 is received at B at T_0^* . Each transfer link is characterized by its total propagation delay which can be modeled as a sum of a constant and a variable parts. Only these variable components τ_i , ($i = 0, 1, 2$) will be of further interest. To make the remote clock comparisons, the differences $T_0 - T_1$ and $T_0 - T_2$ should be known. Apparently, they cannot be measured directly, but they can be evaluated from the differences measured at laboratory A:

$$\Delta T_{A1} = T_0 - T_1^* \quad (1a)$$

$$\Delta T_{A2} = T_0 - T_2^* \quad (1b)$$

$$\Delta T_{A12} = T_1^* - T_2^* \quad (1c)$$

and at laboratory B:

$$\Delta T_{B1} = T_0^* - T_1 \quad (2a)$$

$$\Delta T_{B2} = T_0^* - T_2 \quad (2b)$$

$$\Delta T_{B12} = T_1 - T_2 \quad (2c)$$

Since $T_i^* = T_i + \tau_i$, the desired phase-time differences

$$T_0 - T_1 = \Delta T_{A1} + \tau_1 = \Delta T_{B1} - \tau_0 \quad (3a)$$

$$T_0 - T_2 = \Delta T_{A2} + \tau_2 = \Delta T_{B2} - \tau_0 \quad (3a)$$

and the following relation can be derived from (1) and (2).

$$\Delta T_{B1} - \Delta T_{A1} = \Delta_1 = \tau_0 + \tau_1 \quad (4a)$$

$$\Delta T_{B2} - \Delta T_{A2} = \Delta_2 = \tau_0 + \tau_2 \quad (4b)$$

$$\Delta T_{B12} - \Delta T_{A12} = \delta = \tau_2 - \tau_1 \quad (4c)$$

$$\Delta T_{A1} + \Delta T_{B1} = 2(T_0 - T_1) + (\tau_0 - \tau_1) \quad (5a)$$

$$\Delta T_{A2} + \Delta T_{B2} = 2(T_0 - T_2) + (\tau_0 - \tau_2) \quad (5b)$$

Δ_1 and Δ_2 denote the summary delay of the loops 1 and 2 made up by the link 0 together with the links 1 and 2 respectively, and δ denotes the differential delay of the links 1 and 2.

ANALYSIS OF OBTAINED DATA

DELAY OF THE LOOPS 1 AND 2 AND ITS CORRECTION

The plots of daily values of Δ_1 and Δ_2 are displayed in Figure 2. One can see that the curves exhibit very similar seasonal variations with the peak-to-peak value being approximately 15 ns. The maximum frequency deviation is about $\pm 1.10^{-15}$. The third curve displayed in Figure 2 represents mean daily temperature T_{out} taken in Prague. The close correlation of the long-term propagation delay with the outdoor temperature is obvious. The detailed study shows that the correlation coefficient reaches its maximum value ($\rho \approx 0,85$) if the Δ_1 or Δ_2 functions are delayed by about 20 days with respect to T_{out} . Such a delay of the response to the outdoor temperature might be explained only by the slow propagation of heat in the soil. Therefore, it can be assumed that the underground temperature which has an influence on the fiber is the source of this type of fluctuations. To confirm this assumption, the underground temperature along the cable should be known. However, the direct measurement of this temperature is almost impossible. The fact is that the 9-km-long section of the optic cable traces the urban area and is buried in different depths varying from 0,5 m to 3 m (part of the cable is led in a cableduct; another part is laid in the soil). So the soil temperature was modeled under the following simplifying presumptions:

- the soil was presumed to be homogeneous,
- the mean daily temperature of the soil surface was supposed to be equal to the mean temperature of the air,
- there are no other sources of heat influencing the optic cable.

Under these conditions the soil temperature in different depths 0.25 m to 3 m was evaluated as described in [3]. The correlation of the Δ_1 and Δ_2 with the relative daily values of soil temperature in different depths was analyzed, yielding the results displayed in Figure 3. It is seen that the maximum correlation coefficients ($\rho_{\Delta_1, T(h)} \approx 0.93$ for Δ_1 and $\rho_{\Delta_2, T(h)} \approx 0.9$ for Δ_2) are obtained for the depth $h \approx 1.3$ m.

An attempt has been made to find a correlation of the Δ_1 and Δ_2 with other environmental factors (air pressure, indoor temperature of the laboratories A and B). None of the correlation coefficients have exceeded 0.05. This indicates that the temperature of the soil surrounding the optic cable has the dominating influence on the long-term stability of its propagation delay.

In order to make the optimal correction of the temperature changes of the link delay, the estimation method has been used. The temperature coefficient K_i [ns/km.°C] minimizing the value $A(h)$ for different values of the depth were chosen for the loop 1 and 2:

$$A(h) = \sum_{n=N_1}^{N_2} [\Delta_i(n) - K_i \cdot d \cdot T_h(n)]^2 \quad (6)$$

where $\Delta_i(n)$ - samples of daily values of the loop delay

$T_h(n)$ - samples of daily values of the soil temperature for the depth h

$N_1 = \text{MJD}_{\min}$

$N_2 = \text{MJD}_{\max}$.

$i = 1, 2$ denotes the number of loop
 d - length in km of the buried part of the cable ($d=9 + 9= 18$)

The minimum $A(h) \cong 1$ ns was found for $h = 1.3$ m . That is in a close agreement with the correlation result mentioned above. The values $K_1 = 0.046$ and $K_2 = 0.041$ obtained from (6) for this "effective" depth do not differ very much. This result is not surprising if we take into account that the individual fibers placed within one cable should exhibit very similar propagation delay variations under the same environmental conditions. That makes it possible to simplify the above relations by assuming

$$\tau_0 = \tau_1 = \tau_2 = \tau. \quad (7)$$

Under this assumption

$$\Delta = \Delta_1 = \Delta_2 = 2 \tau \quad (8)$$

holds and so the temperature-corrected loop delays Δ_{icorr} ($i = 1, 2$) can be evaluated as

$$\Delta_{icorr} = \Delta_i - K_i \cdot d \cdot T_h. \quad (9)$$

The plots of corrected time functions Δ_{1corr} and Δ_{2corr} are shown in Figure 4 . They have no long-term variations, but they show residual noise fluctuations as the curves Δ_1 and Δ_2 in Figure 3. Note that the records in Figure 3 and 4 consist of two different parts. The left-hand part (MJD 49379 to MJD 50299) has been obtained from the data measured by less accurate time interval counters, which provided uncertainty of $\sigma = 0.52$ ns. Since that uncertainty was too large, high resolution counters with $\sigma = 30$ ps were used later in the course of experiment (MJD 50300 to MJD 50687).

Among the measures used in the time domain, the time difference

$$TDEV(\tau) = \sqrt{\frac{1}{6} \langle (D^2 \bar{x})^2 \rangle} \quad (10)$$

seems to be optimal to describe the time stability of the uncorrected time transfer and to estimate the effect of temperature correction. TDEV ($1 \text{ day} \leq \tau \leq 240 \text{ days}$) was evaluated first for Δ_2 within the time interval MJD 49379 to 50299. The corresponding plot denoted as Δ_2 LRC is presented in Figure 5. It is seen that the TDEV(τ) is basically constant for $1 \text{ day} \leq \tau \leq 30 \text{ days}$. The value of TDEV ($\tau=1\text{day}$) = 0.94 ns . The TDEV(τ) is increasing for $\tau \geq 30$ days and it reaches its maximum for $\tau \cong 180$ days. This is the result of the seasonal fluctuations. Then the TDEV ($1 \leq t \leq 90 \text{ days}$) was evaluated for Δ_2 within the time interval MJD 50300 to MJD 50687. In this case the curve Δ_2 HRC representing TDEV(τ) characterizes the instability of the loop much better because of substantially higher resolution of the counters. The plot Δ_2 HRC starting from TDEV₂(1 day) = 0.4 ns is monotonously increasing and reaching the Δ_2 LRC for $\tau = 90$ days.

The corresponding TDEV(τ) plots (denoted by Δ_{2corr} LRC and Δ_{2corr} HRC) calculated for Δ_{2corr} in the above mentioned intervals of τ and MJD are displayed in Figure 6. We can see that the TDEV(τ) values characterizing the temperature-corrected loop propagation delay well correspond to the ones of uncorrected loop propagation delay within the interval $1 \text{ day} \leq \tau \leq 30 \text{ days}$. The correction effect is evident for $\tau > 30$ days.

CORRECTION OF MEASURED PHASE TIME DATA

Knowing the law of temperature dependence of the propagation delay, we can correct for the measured phase-time data in order to remove the long-term fluctuations due to the transmission link. For one-way time transfer the following formula ($i=1,2$) can be used:

$$T_o - T_i = \Delta T_{Ai} - K \cdot d \cdot T_h, \quad (11)$$

This correction needs the current soil temperature T_h to be evaluated from the mean daily outdoor temperature, as described in [3]. Let us mention that the outdoor temperature changes will exert an influence upon the fiber of the described system after a delay of 20 days.

Another way to correct the data is to take advantage of the two-way transmission. It is clear (if (7) and (8) are valid) that the desired time differences cleared of transmission link fluctuations can be obtained simply by using (5a, 5b) e.g.

$$T_o - T_i = \frac{\Delta T_{Ai} + \Delta T_{Bi}}{2} \quad (12)$$

even without the knowledge of the actual values of link propagation delay.

CONCLUSION

The obtained results demonstrate the possibility of stabilizing mathematically the propagation delay of the studied time transfer optic link within 1 ns or less (in the sense of $TDEV(\tau)$) for time intervals $\tau \geq 1$ day by correcting for the influence of the soil temperature variations upon the optic fiber buried underground. This correction reduces the long-term instability for time intervals longer than 30 days and permits us to reach 1 ns timing uncertainty within the group standard. In the course of almost four-year period of experiment, no significant systematic phase drifts (aging, etc.) have been observed.

Even after the temperature correction residual phase fluctuations for shorter time intervals, $\tau \leq 30$ days, remain. Their source is not yet fully known; however, from the data of the two sets of counters with different resolution we can conclude that at least a part of the fluctuations is due to the limited counter resolution.

REFERENCES

- [1] O. Buzek, J. Čermák, and B. Čemusová, "Czech National Time and Frequency Standard," in Proceedings of the 9th European Frequency and Time Forum (EFTF), March 1995, Besançon, France, pp. 400-403.
- [2] Czech Metrological Institute, "Monthly Meteorological Summaries from Observatory PRAHA - KARLOV," 1994-1995.

- [3] O. Buzek, "*Temperature Sensitivity of a Fibre Optic Timing Link*," in Proceedings of the 10th European Frequency and Time Forum (EFTF), March 1995, Brighton, UK, pp. 471-474.
- [4] H. Carslaw, J. Jaeger 1959, *Conduction of Heat in Solids*, Oxford, At the Clarenton Press, UK.
- [5] D. Allan, M. Weiss, and J. Jespersen, "*A Frequency-domain of the Time-domain Characterization of Clocks and Time and Frequency Distribution Systems*," in Tutorials of 1993 IEEE Frequency. Control Symposium, June 1993, Salt Lake City Marriott, USA

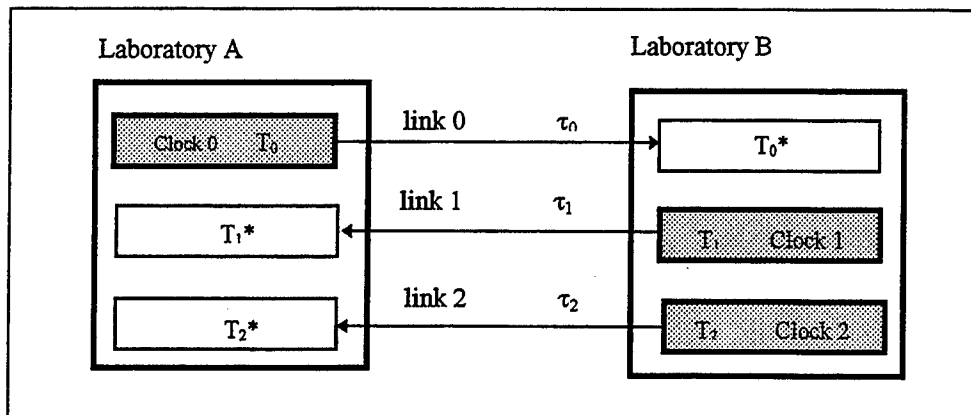


Fig.1 : Basic diagram of the time transfer system. One clock signal is transmitted from the laboratory A to the laboratory B and two clock signals are transmitted in a opposite direction using identical fiber-optic transfer links.

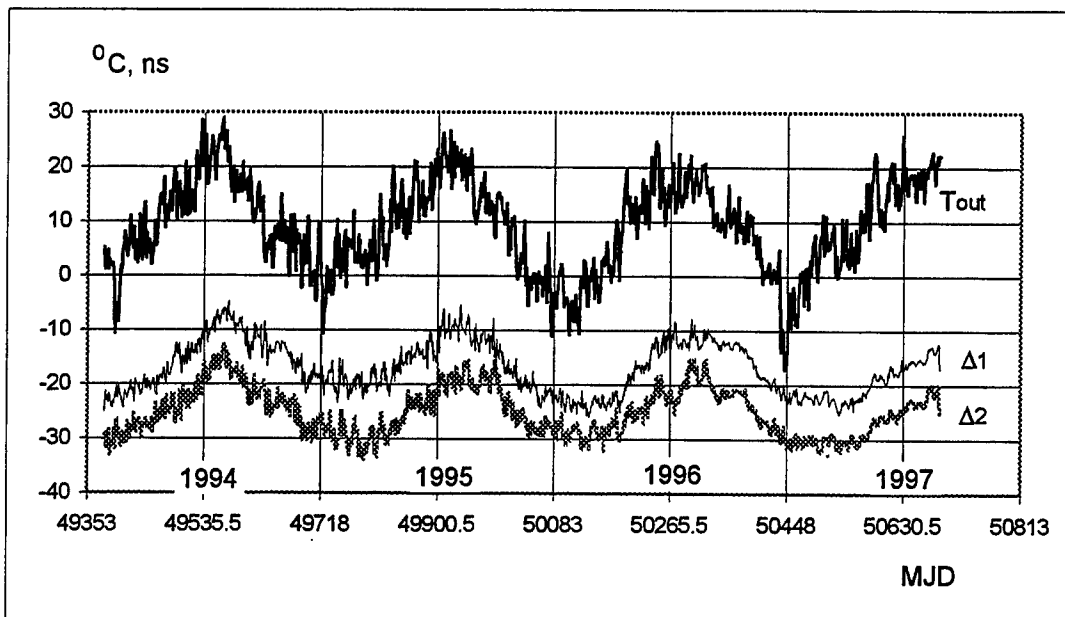


Fig.2 This figure shows the plots of relative summary propagation delay Δ_1 of the loop 1 created by links 0 and 1, and Δ_2 of the loop 2 created by links 0 and 2. The third plot displays the mean daily outdoor temperature T_{out} in Prague.

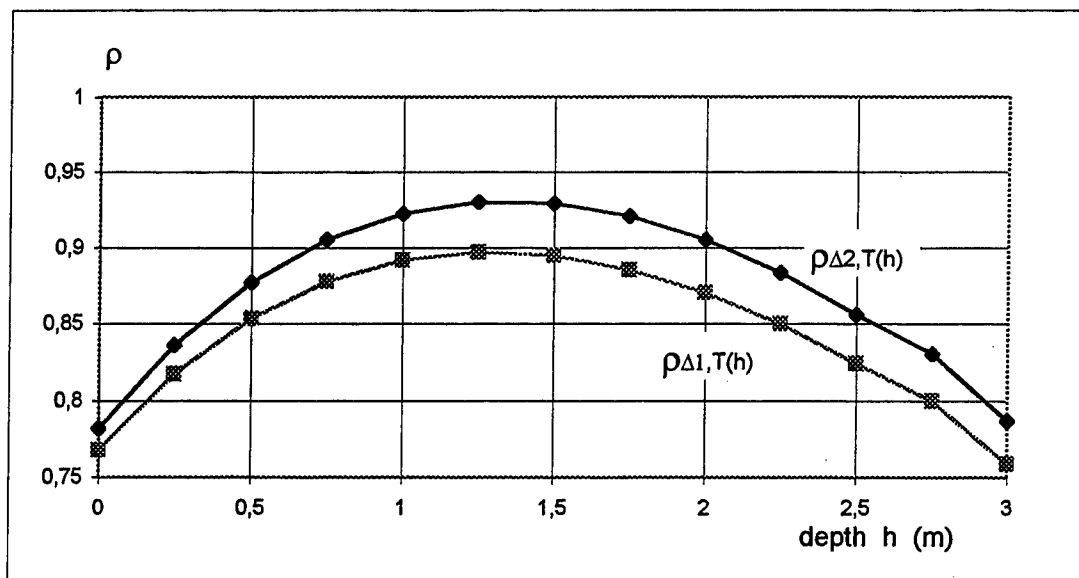


Fig.3 Correlation of loop delays with underground temperature in different depths. The correlation coefficient ρ reaches its maximum value for the depth $h \approx 1.3$ m.

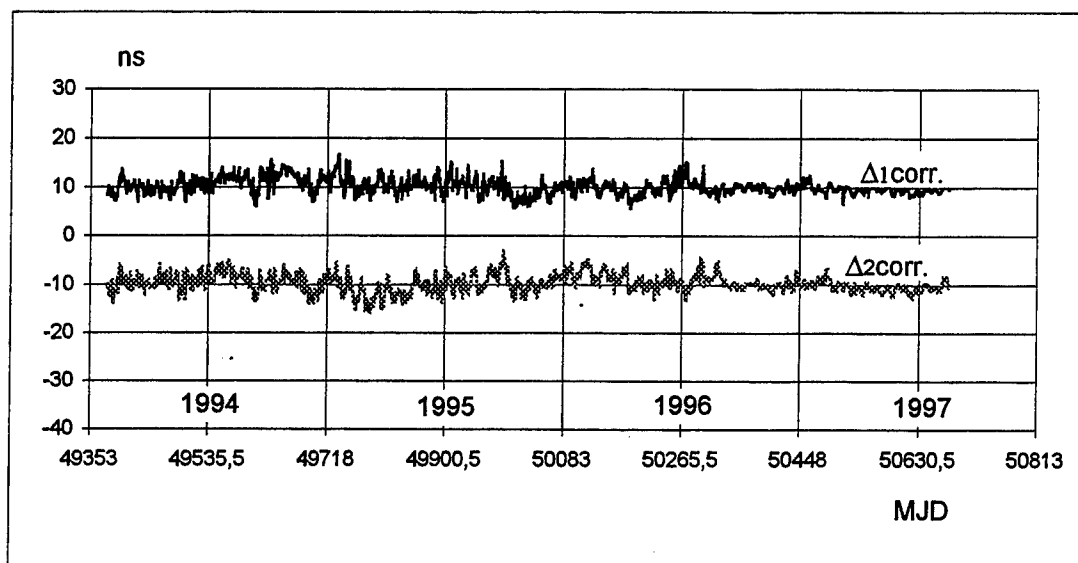


Fig.4 displays the plots of the relative propagation delays of the loops 1 and 2 after correction for the soil temperature in the depth $h = 1.3$ m

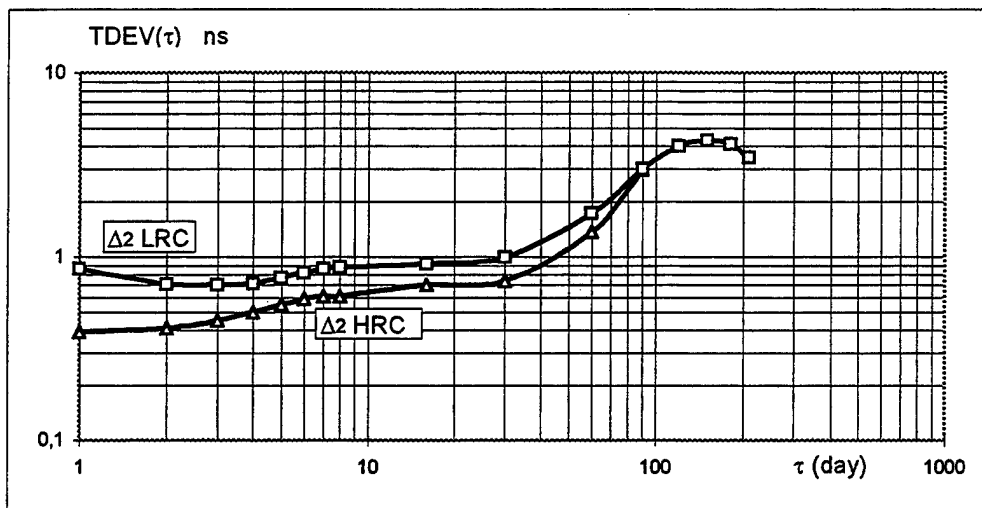


Fig. 5 displays the plots TDEV (τ) of uncorrected propagation delay of the loop 2 calculated from the data measured by low resolution counters (Δ_2 LRC) and by high resolution counters (Δ_2 HRC).

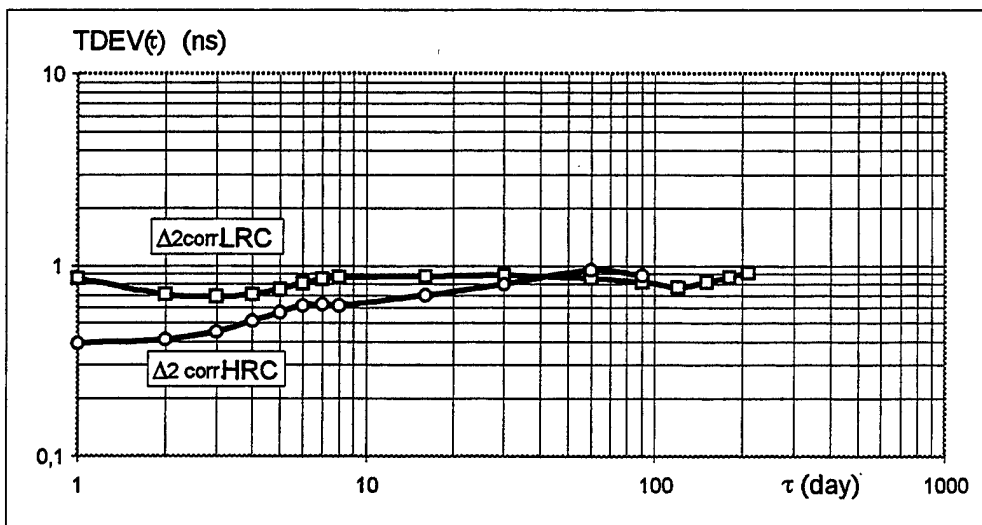


Fig. 6 displays the plots of TDEV (τ) of corrected propagation delay of the loop 2 calculated from the data measured by low resolution counters ($\Delta_{2\text{ corr.}}$ LRC) and by high resolution counters ($\Delta_{2\text{ corr.}}$ HRC).

Questions and Answers

ALBERT KIRK (JPL): You show a seasonal temperature plot and you also mention that the depth of the cable was between .5 (point 5) and three meters. At what depth did you measure the temperature?

OTOKAR BUZEK: The temperature measurement was not down under the ground. We used, as input data, the mean temperature of the air in Prague. It was supposed that this is the ground surface temperature. Then using the standard equations, the temperature underground was calculated. It was only calculated, because the soil is operating as a low-pass filter. Only the long wave of the heat is transported down and time delayed. So it was not measured, it was calculated.

ALBERT KIRK: Was most of the cable at the three-meter depth or between .5 (point 5) and three meters? Can you express that in a certain percentage, the relationship of depth for the 10 kilometers?

MALCOLM CALHOUN (JPL): May I answer that?

ALBERT KIRK: Yes, please.

MALCOLM CALHOUN: Eight hundred meters was at a half-meter depth. The rest of the link was at two to three meters. Unfortunately, the 800-meter at a half-meter depth would account for the biggest part of the cycling that we saw.

BOB WEAVER (UNIVERSITY OF SOUTHERN CALIFORNIA): What was the total extent of the temperature fluctuations in your graph? I could not quite read the graph.

MALCOLM CALHOUN: Minus 10 to plus 35 – yes, minus 10 C to plus 35 C.

OTOKAR BUZEK: These peaks are from approximately minus 18 to plus 30 degrees Celsius.

TWO-WAY TIME TRANSFER THROUGH 2.4 GBIT/S OPTICAL SDH SYSTEM

Masami Kihara and Atsushi Imaoka
NTT Optical Network Systems Laboratories, Japan
tel +81-468-59-3164 fax +81-468-55-1282
e-mail kihara@exa.onlab.ntt.co.jp

Michito Imae and Kuniyasu Imamura
Communications Research Laboratory (CRL), Japan
Ministry of Posts and Telecommunications

Abstract

An experiment to transfer time and frequency over 2.488 Gbit/s SDH (Synchronous Digital Hierarchy) systems using 175-km commercial optical fibers has been set up by CRL and NTT. We confirm that the frequency stability of the time comparison data is 10^{-12} /square root of tau at averaging times above 10 s. This equals that of the Cs frequency standard (HP5071A) used in this experiment. The time comparison resolution is of the order of 10^{-11} s (square root of time variance). The long-term stability of this system is expected to be better than 1 ns. The time comparison results of this experiment agree well the GPS common-view results.

INTRODUCTION

Terrestrial cable systems can be applied for time and frequency comparison and transfer as is possible with satellites[1][2]. While cable systems are disadvantaged in requiring repeaters to transmit information over long distances, they offer very stable communication links. Optical transmission systems based on SDH (Synchronous Digital Hierarchy) have been developed and deployed with bit rates of 600 Mb/s, 2.5 Gb/s, and 10 Gb/s. These bit rates enable highly stable frequency and time transfer.

We have been tackling transfer time and frequency over 2.488 Gbit/s SDH systems. The first goal was to ascertain the limitation of SDH systems in terms of frequency and time transfer capability. The second was to develop an accurate and stable standard signal distribution scheme over telecommunication networks. This paper describes the system configuration and initial results of the experiment.

EXPERIMENTAL SYSTEM

CRL in Koganei and NTT in Yokosuka were directly connected with a 2.488 Gbit/s SDH system as shown in Fig. 1; cross-connects were not used. The 175-km optical fiber cable contained 7 repeaters. The SDH termination equipment receives the reference signal generated by each standard, and transmits the reference signal using a data format based on SDH. Figure 2 shows the experimental system configuration. Reference second signals and measurement data are transmitted and received by time information transmitters and receivers that manipulate 2.488 Gbit/s SDH signals synchronized to a reference signal of 5 MHz. Measurement systems have functions of time interval counting and measurement data processing.

DATA PROCESSING

Measurement results at one site are immediately transmitted to the other site over the same SDH system as the time transfer experiment. This experiment system can thus achieve both conventional two-way time transfer and real-time data processing for frequency and time correction. The national standard of frequency and time generated in CRL can be continuously transferred to NTT.

The time difference (Δ) between two sites is determined from four data: the differences, measured in CRL, between the reference and transmitted second signals (t_1) and between the received and transmitted second signals (t_2), and the differences, measured in NTT, between the reference and transmitted second signals (t_3) and between the received and transmitted second signals (t_4). Time difference (Δ) is given by

$$\Delta = t_1 - t_3 + (t_2 - t_4) + (\tau_1 - \tau_2)/2$$

where t_1 and t_2 are the transmission delays from CRL to NTT and from NTT and CRL, respectively. Total transmission delay is

$$\tau_1 + \tau_2 = t_2 + t_4.$$

The asymmetry of transmission delay causes time error in Δ . While SDH signals are transmitted over different optical fibers, the two fibers are jacketed in the same cable. Transmission delay (t_1 and t_2) and delay variation are approximately the same. Time error factors are difference in wavelength between the two optical fibers, connector attaching processes in the ends of the optical fibers and circuit-delay difference in the repeaters (if used).

TIME TRANSFER FORMAT

Current digital transmission systems are based on Time Division Multiplex (TDM) and designate time slots for data transmission. We have to identify which time slot holds the reference second because the delay imposed by the transmitter is unpredictable. In this experiment, one bit of an undefined Section OverHead (SOH) byte is used to indicate carriage of the reference second. Measurement data are also transferred in other bits of the same SOH byte. Figure 3 shows SDH data format including SOH and the SOH byte used to transfer time. Time information is embedded in SOH bytes once per one frame period of 125 μ s. 8000 successively embedded SOH bytes construct one-second frame as shown in Fig.4.

FREQUENCY COMPARISON AND TIME TRANSFER

Figures 5 and 6 show the time comparison result and the total transmission delay between CRL and NTT, respectively. The constant time difference increase is caused by the frequency difference between CRL and NTT. Frequency deviation of the cesium standard in NTT is -1.27×10^{-13} compared to that in CRL. The total transmission delay is 1.7 ms, and the delay variation is approximately 200 ns over the period shown in Fig.6. The annual delay variation is expected to be around 300 ns based on the experimental results.

Figure 7 shows the short-term stability in Allan variance. This two-way time transfer system capability was measured in a room using a unique reference, and is plotted as 'system' in Fig.7. The experimental system can compare frequencies of 10^{-15} over a one day measurement period. The actual measurement result, plotted as 'CRL-NTT', basically follows the performance of the cesium standard used in NTT. If we use a hydrogen maser to generate the reference time, it is expected that the frequency comparison would show a flicker floor of 10^{-15} over the measurement period of more than 10^5 s.

Figure 8 shows time deviation as a function of averaging time. This two-way time transfer system can compare time at the order of 10^{-11} over measurement periods greater than 1 s. Time signals generated by an HP5071 cesium standard can be compared over measurement periods longer than

10 s. Figure 9 shows a comparison of this experimental system with GPS common view. Time difference increase due to frequency offset was removed before plotting these values. The time comparison of this experimental system agrees well the GPS common-view result. While these results do not show the time transfer capability in terms of long-term stability, since they include the time variation between the NTT standard and UTC(CRL), the long-term stability in this system is expected to be better than 1 ns.

CONCLUSION

We confirmed that the frequency stability of the time comparison is $10^{-12}/\text{square root of } \tau$ for the averaging time region, τ , greater than 10 s. This is equal to that of the Cs frequency standard (HP5071A) used in NTT. This result implies that two time scales based on Cs frequency standards can be compared using 2.488 Gbit/s SDH time transfer as if the two standards were standing alongside each other.

REFERENCES

- [1] M. Kihara, and A. Imaoka 1995, "SDH-based time and frequency transfer system", Proceedings of the 9th European Frequency and Time Forum.
- [2] M. A. Weiss, S. R. Jefferts, J. Levine, S. Dilla, T. E. Parker, and E. W. Bell 1996, "Two-way time and frequency transfer in SONET", Proceedings of the 1996 International Frequency Control Symposium, pp. 1163-1168.

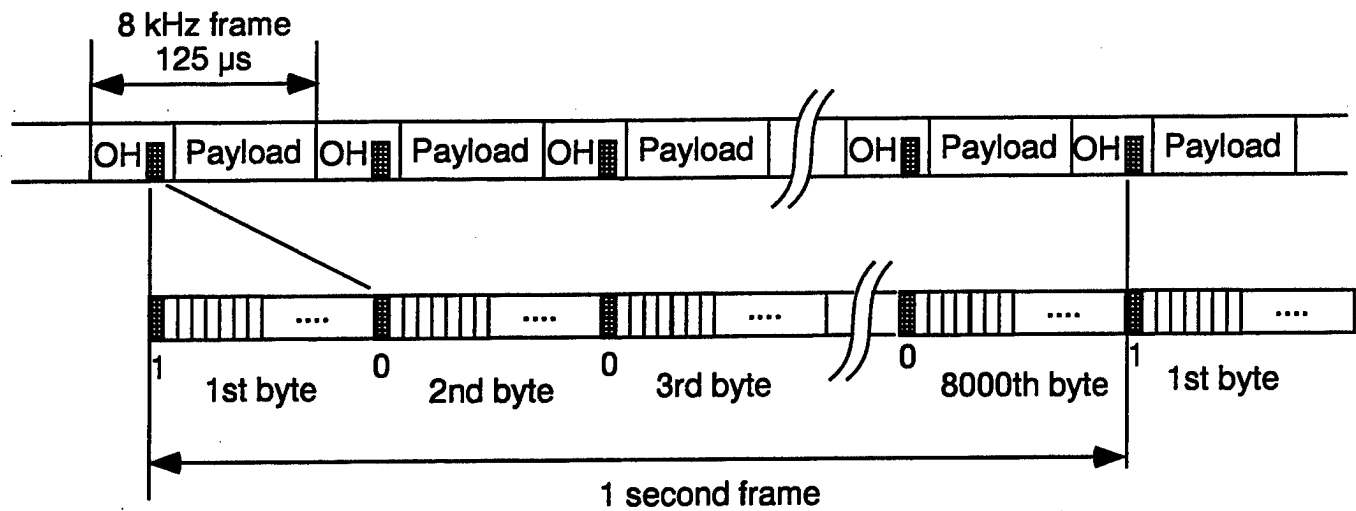


Figure 4 - SOH byte and one second frame

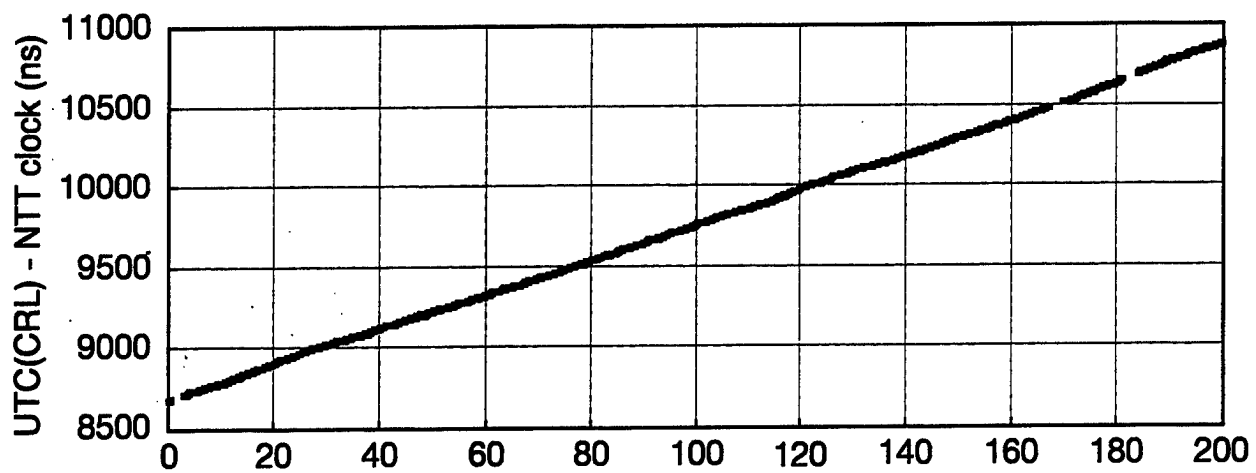


Figure 5 - Time comparison result

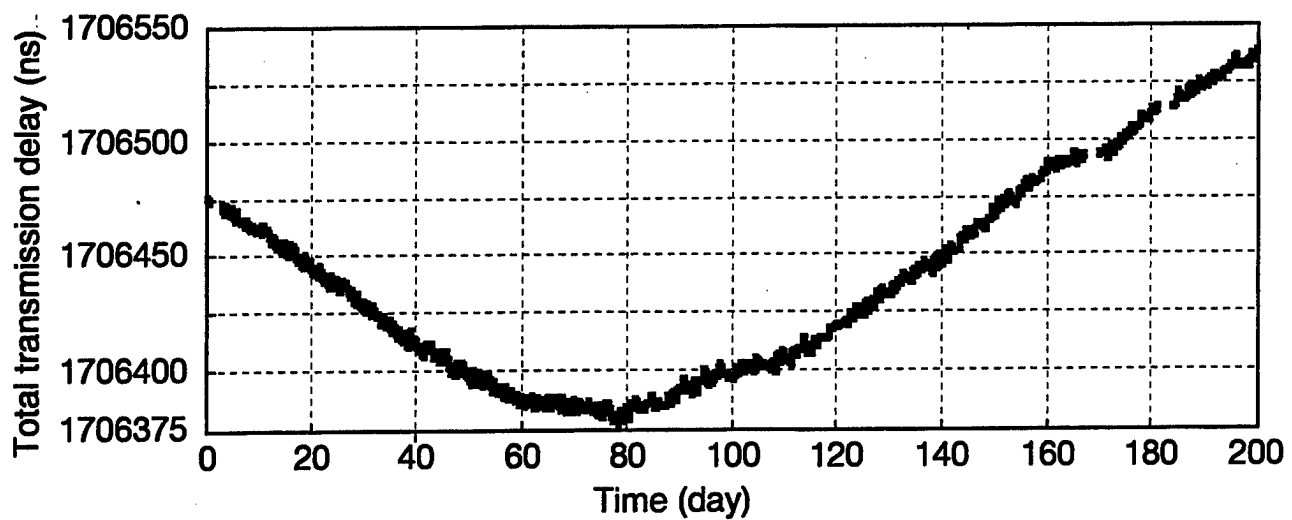


Figure 6 - Total transmission delay

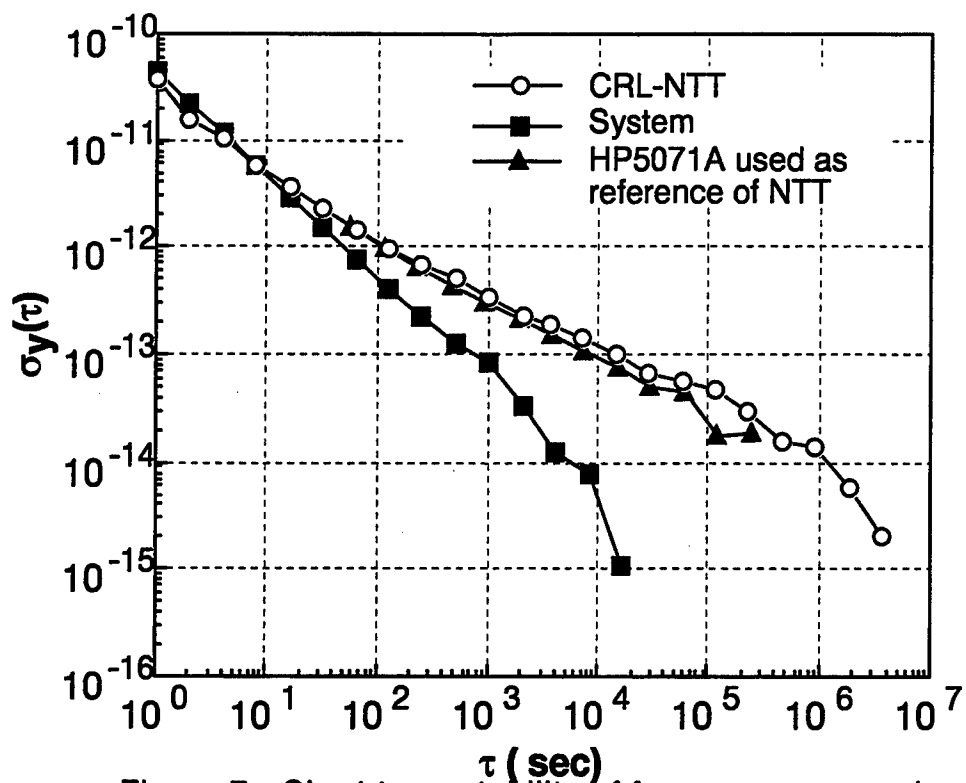


Figure 7 - Short-term stability of frequency comparison

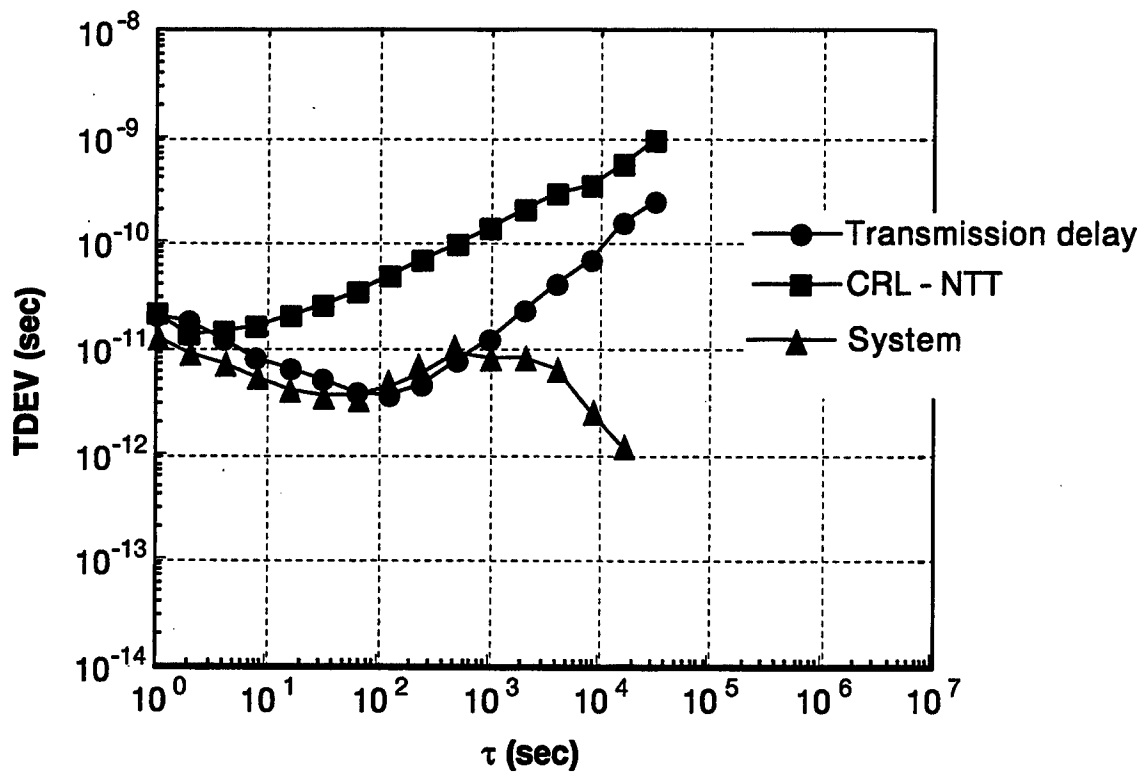


Figure 8 - Time deviation of time transfer

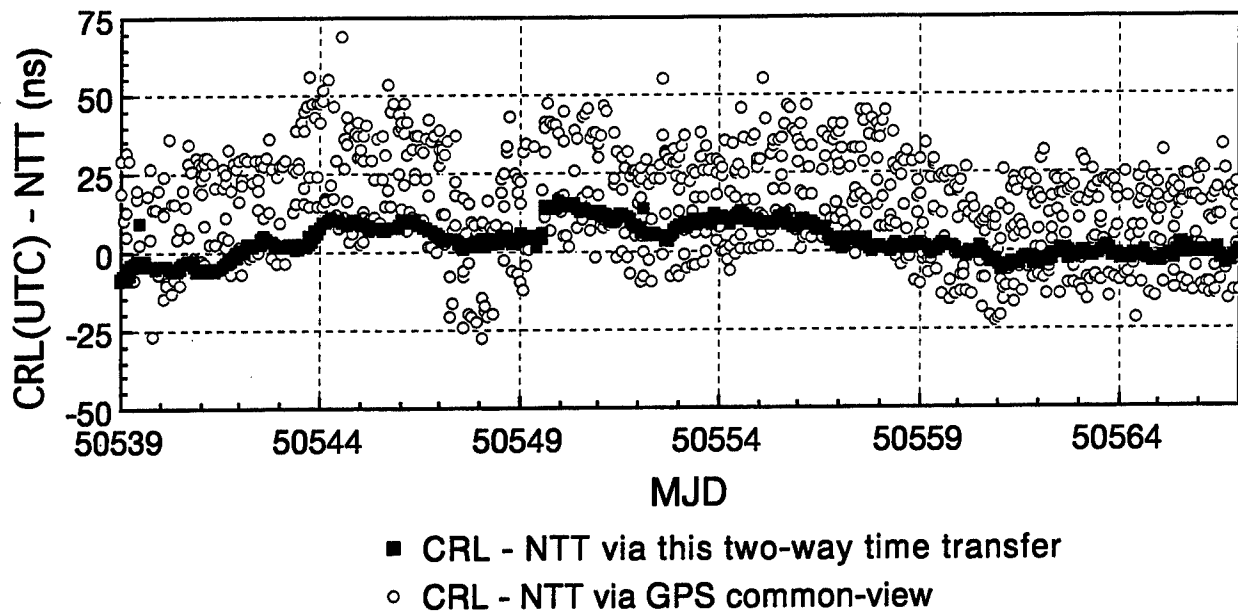


Figure 9 - Comparison of this two-way time transfer with GPS common-view

Results From Proof-Of-Concept Time-Based Communications Testing

T. P. Celano, Timing Solutions Corporation

S. R. Stein, Timing Solutions Corporation

G. A. Gifford, USNO

E. A. Swanson, MIT Lincoln Laboratory

B. R. Hemenway Jr., MIT Lincoln Laboratory

J. C. Carney, MIT Lincoln Laboratory

Time-based communications is a concept whereby the synchronous layer of a communications channel is used as a vehicle for two-way time transfer. The technology originated in 1995 (Ref 1) with prototype hardware designs for a self-calibrating optical two-way time transfer system. Point-to-point systems were built in 1996 and demonstrated synchronization error in a laboratory between a master clock and a recovered slave clock at the sub-nanosecond level over 10 km distribution distances using SONET. Since then, the communications payload capability has been added to the optical two-way system providing a true time-based communications channel with two-way time transfer functionality embedded in a OC-3 (155 Mb/s) data channel. In February 1997, two weeks of testing were performed at Lincoln Laboratory (MIT/LL) to collect an extensive data set on the timing and communications performance of the system. The test objectives included:

- A) Measure system performance with long-range (>10 km) cable runs in a laboratory environment.*
- B) Establish timing and communications performance in a laboratory environment with typical communications hardware in the fiber link.*
- C) Characterize system performance using "real-world" (outdoor) links exhibiting temperature dynamics that change the length of the fiber.*
- D) Determine the suitability for application in future wavelength division multiplexed (WDM) optical communications networks.*

This paper presents the results of the time-based communications testing performed at Lincoln Labs (MIT/LL) using an Optical Two-Way Time Transfer Communications System. A short explanation of system design and two-way time transfer implementation in a communications channel will be followed by a presentation of data sets from the Lincoln Laboratory testing. Time transfer measurement data will be presented from tests conducted from within the laboratory, as well as tests conducted over long-distance, outdoor links. The laboratory measurements to be presented include two-way time transfer results over fiber in a controlled (constant temperature) environment with typical communications hardware inserted in the link between clocks. The hardware used for laboratory measurements includes electro-optic repeaters and erbium-doped fiber-optic amplifiers. The outdoor fiber links (intended to represent real-world links) include a 75-km fiber run with OC-3 repeaters inserted at the midpoint, and 100-km with wave-division multiplexing equipment in the link.

Synchronization error measurement data are presented for each test configuration. Two-way delay data will be presented for the real world links to show the changes in fiber length induced by temperature variations in the outdoor environment.

1.0 BACKGROUND OF TIME-BASED COMMUNICATION

Time-Based Communications is a concept where continuous two-way time transfer information is embedded in an active communications channel (Ref. 1). The synchronous layer of the communications channel is exploited as a two-way vehicle. In the case of SONET (Synchronous Optical Network), the framing structure is used to provide an event to measure, and a byte in the administrative channel is used to provide a data channel between the ends of the link. Point-to-point SONET systems have been built and fielded by Timing Solutions Corporation (TSC) to provide sub-nanosecond time transfer capability in a controlled (indoor) environment for fiber links up to 10 km. Figure 1 shows the time transfer performance of the TSC system for the point-to-point case using the first generation equipment. These first generation systems were not capable of carrying data and only contained fiber between the two nodes (no repeaters or other communications equipment).

With the second generation hardware came the ability to transfer user data between nodes. The user data are not associated with the timing function and can be framed in any fashion that is applicable to the SONET frame. The TSC SONET Time Transfer System described in this paper utilizes a data payload which transfers 155 Mb/s of user data framed in ATM cells. This provides full use of the communications link for data transport with the two-way time transfer computation continuously running in the background.

2.0 OBJECTIVES OF PROTOTYPE TESTING

The primary objective of the testing was to extend the performance verification of the TSC SONET Time Transfer System past the point-to-point case. Since the desire is to field the system over a

typical communications network, the testing was aimed toward determining the feasibility of using the system over commercial links. The following areas were considered in determining the suitability of the TSC SONET Time Transfer System over commercial links:

- A) Long-range links: The first generation systems had a 10-km limit based on the power of the transceiver pair on either end of the fiber. Extending this limit to allow runs that are typical to the commercial communications environment was of interest. This includes the use of higher power transceivers, as well as amplification in the fiber links. Results presented in Sections 4 and 5 include high power transceivers and different methods of signal regeneration.
- B) Laboratory Testing of Communications Components: Fielding systems in a commercial environment requires a departure from the point-to-point case. Real-world links will likely contain regeneration equipment in order to maintain the required SNR over longer distances. Prior to fielding the equipment over real-world links, tests were run to establish timing and communications performance in a laboratory environment. Data were collected in the lab with typical communications hardware in the fiber link. Comparisons of the different data sets are presented in Section 4.0.
- C) Field-Testing of Communications Components: The MIT/LL test-bed includes links, which represent a "real-world" link. Fiber connections between MIT/LL in Lexington MA and the MIT campus in Cambridge were used to determine system performance in a dynamic environment. 12-24 hour tests were run to allow diurnal temperature effects to stress the system. Results from these tests are presented in Section 5.1.
- D) Future Networks: The MIT/LL test-bed also contains next generation communications hardware. This hardware includes All-Optical Network (AON) hardware, which utilizes wave division multiplexing to carry large amounts of data over a single fiber. Tests were run using the AON test-bed to determine the performance of the SONET Time Transfer System and the applicability of the technology to future communications systems. Results of the AON application are discussed in Section 5.2.

3.0 MIT/LL TEST-BED

The MIT/LL test-bed (Figure 2) provided an excellent environment in which to achieve the diverse test goals. The timing equipment was initially set up in a laboratory where links could be constructed to collect data against a specific goal or device. The timing configuration in the lab consisted of a TSC SONET Master and Slave, which were operated using two independent clocks. The SONET Master transferred time to the SONET slave where 5-MHz and 1-PPS signals were regenerated and steered to the clock source via optical two-way time transfer. The synchronization

error between the SONET Master and the SONET Slave was measured using the TSC 55000 Precision Time Measurement System. The TSC 55000 was used to measure the phase of a 5-MHz signal from the clock source and a 5-MHz signal from the slave and compute the time difference between the clock source and the slave signals. Once the system was calibrated, the time difference plot provided a direct measurement of the slave's ability to track the clock source.

The communications portion of the test set-up consisted of the data source and the link. The data source was a CERJACK ATM bit error rate tester, which provided data to the master and collected data from the slave. The unit provided a direct measurement of the number of bit errors over a period of time. The link for each test was constructed using the Lincoln Laboratory equipment either in the lab, in the field, or a combination of the two. The abundance of equipment in the lab allowed links to be constructed in an incremental fashion, beginning with short spans of fiber and culminating with an all-optical configuration with 100-km outdoor fiber spans containing optical routers and erbium amplifiers.

4.0 LABORATORY TESTS

In order to completely characterize the system performance in a commercial environment, it was necessary to get a "best case" baseline in the laboratory. The system was configured as seen in Figure 3 with the SONET master and SONET slave connected via a 90-km link with the component under test in the middle of each span. The following components were tested:

1. Optical Attenuator (baseline)
2. Electro/Optic Regenerator
3. Erbium Amplifier

The Optical Attenuator is of interest since it does not contain any active components and represents a negligible departure from the point-to-point case. It is used as the baseline data set to which to compare the other components. The Electro/Optic Regenerator converts the light signal to an electrical signal, where it is re-shaped and re-clocked before being converted back to the optical frequency. The Electro/Optic regenerator is used in many terrestrial links and is likely to be encountered in a commercial environment. The Erbium amplifier is an all-optical repeater where the signal is passed through a small section of erbium-doped fiber to increase the intensity. The erbium amplifier is used in transoceanic links and is of interest when considering optical time based communications between continents.

Each configuration was run overnight with measurements collected every 20 seconds using the TSC 55000. Comparison of the data sets collected (Figure 4) results in the conclusion that the addition of the components in the fiber path has a measurable but negligible effect on the synchronization error. By comparing the standard deviation of the data sets (72 ps for the Optical Attenuator, 103 ps for the Electro/Optic regenerator, and 152 ps for the Erbium Amplifier), it is noted that the erbium amplifier produced a factor of 2 increase in the noise level. This is still well within the acceptable operating range of the system. The main result gleaned from the laboratory tests is that the departure

from the point-to-point case is not significantly degraded by addition of (one stage of) regeneration equipment. This is a crucial test, as it allows the optical two-way time transfer technique to be considered for long-distance links.

5.0 FIELD TESTS

The field tests involve operating the SONET Time Transfer System in an environment that is typical for the target implementation, i.e. a typical commercial link. Two such links were considered using the MIT/LL test-bed: an implementation using technology encountered in today's commercial links, and an all-optical implementation using next generation technology. The goal of the field tests was to expose the system to a dynamic environment where the link is changing and the steering loops in the SONET slave must compensate appropriately. This differs from the lab case, where the fiber is held within a small temperature range by building climate control. In the field tests, the fiber used is exposed to the outdoor elements and, as a result, will experience temperature changes due to diurnal cycles and changing weather patterns. The tests detailed in the following sections present the SONET time transfer system performance over long links in a dynamic environment.

5.1 PERFORMANCE OVER CURRENT GENERATION LINKS

The test set-up using a link representing currently used commercial hardware is depicted in Figure 5. The optical signal (at 1310 nm) from the TSC SONET master (slave) was routed over a 37-km fiber to a remote facility where the signal was amplified using an Electro/Optic regenerator (regenerator had full clock recovery and data regeneration). The signal was then routed back (over a different fiber in the same fiber bundle) to MIT/LL, where the TSC SONET slave (master) received it. The system was run over a 24-hour period in order to experience one full diurnal temperature cycle.

System performance for the configuration in Figure 5 is plotted in Figure 6. Synchronization error is plotted, as well as the change in the round-trip delay. A round-trip delay measurement is provided by the SONET system as a by-product of the two-way process. The round-trip delay value includes the front-end electronics of the TSC SONET hardware and is of little interest as an absolute measurement. As a relative measurement (by subtracting the first value), the data provides a measurement of the change in the propagation delay of the link. Since propagation changes occur only for the part of the link exposed to temperature variation, this measurement provides an indication of the changes seen by the fiber between the nodes. The two plots contain data from the same measurement interval. Figure 6 shows that the SONET time transfer system demonstrated excellent performance in a dynamic environment over the 24-hour test period (standard deviation of 305 ps). With the exception of a 2-ns perturbation at the end of the data set (MJD 50501.4), the signals from the SONET slave remained within 1 ns of the master while the propagation delay in the fiber changed by over 100 ns (from -40 to +60). Correlation between the synchronization error and

the delay change is seen in Figure 6, but the system is able to remove the effects of the delay change and maintain the slave to within 1 ns of the master. The perturbation at MJD 50501.4 is caused by a change in the delay state in the front-end electronics of the SONET hardware (an effect which is being corrected in the third generation hardware).

5.2 TIME TRANSFER PERFORMANCE OVER NEXT GENERATION LINKS

The development of the time-based communication technology is geared toward application in future communications networks, as well as current generation networks. One example of a future communication network is the MIT/LL All-Optical Network, or AON (Ref 2), which utilizes wave division multiplexing to combine 20 channels of optical data (in the 1550 nm band) over a single fiber. Data sent over the AON are routed and amplified as optical signals, never needing conversion to electrical signals. This all-optical implementation is ideal for SONET time transfer, since the SONET frame, once created, remains intact from end to end (rather than going through electrical switching equipment, like in a typical SONET ADM or an ATM switch, where the SONET framing information is regenerated).

The equipment configuration for the AON test is seen in Figure 7. The optical signal from the SONET master is first routed through an optical terminal, which changes the wavelength from 1310 nm to 1556.6 nm. The link between the SONET master and slave contains three optical routers with erbium amplifiers, which have the ability to change the optical frequency of the signal as well as amplify the intensity. Prior to reception at the SONET slave, the wavelength must be converted back to 1310 nm. The total distance of the link between Lincoln Labs (MIT/LL) and MIT campus is 102 km.

System performance for a 12-hour test on the AON is plotted in Figure 8. With the exception of a small perturbation at the beginning of the data set, due to the same delay change effect discussed in Section 5.1, the system demonstrated sub-nanosecond performance (standard deviation of 657 ps). There was no degradation in system performance due to the wave division multiplexing equipment in the link. As in the current generation case, Section 5.2, the system was able to track a large temperature swing and maintain sub-nanosecond synchronization error.

6.0 CONCLUSIONS

The MIT/LL field-test has demonstrated the compatibility of two-way time transfer and commercial SONET equipment. Typical components such as repeaters and erbium amplifiers resulted in small, but acceptable, degradation of signal-to-noise ratio (for the number of repeaters tested). The field test also demonstrated that the two-way technique is able to compensate for delay changes encountered by fiber in typical outdoor installations, including long above-ground runs. Finally, the tests demonstrated that the All-Optical Network is an ideal platform for the integration of timing and communications, since the SONET signals are transmitted unaltered through all AON equipment.

7.0 REFERENCES

- [1] S.R. Stein, G.A. Gifford, T.P. Celano, *The Role of Time and Frequency in Future Systems*, Proceedings of the 27th Annual Precise Time and Time Interval Applications and Planning Meeting, November 29-December 1, 1995, pp. 51-58.

- [2] E.A. Swanson, I. P. Kaminow, C. Doerr, C. Dragone, T. Koch, U. Koren, A. A. M. Saleh, A. Kirby, C. Ozveren, B. Schofield, R. E. Thomas, R. A. Barry, D. M. Castagnozzi, V. W. S. Chan, B. R. Hemenway, D. Marquis, S. A. Parikh, M. L. Stevens, S. G. Finn, and R. G. Gallager, A Wideband All-Optical WDM Network, *Journal of Selected Areas in Communications*, 14, 780-799, June (1996). Invited Paper

8.0 FIGURES

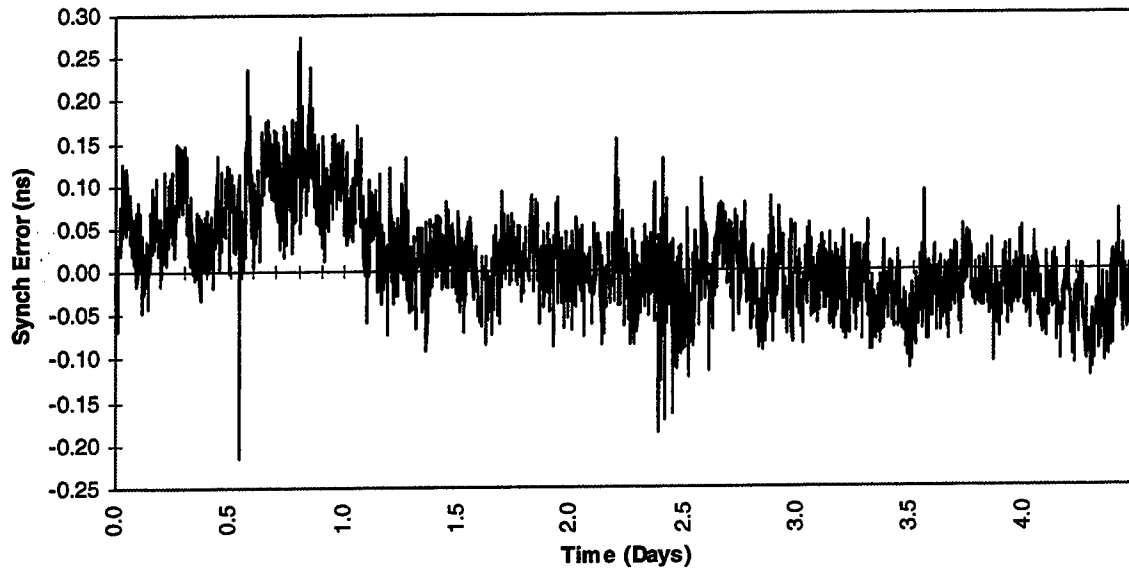


Figure 1: Point-to-Point Optical Time Transfer Performance

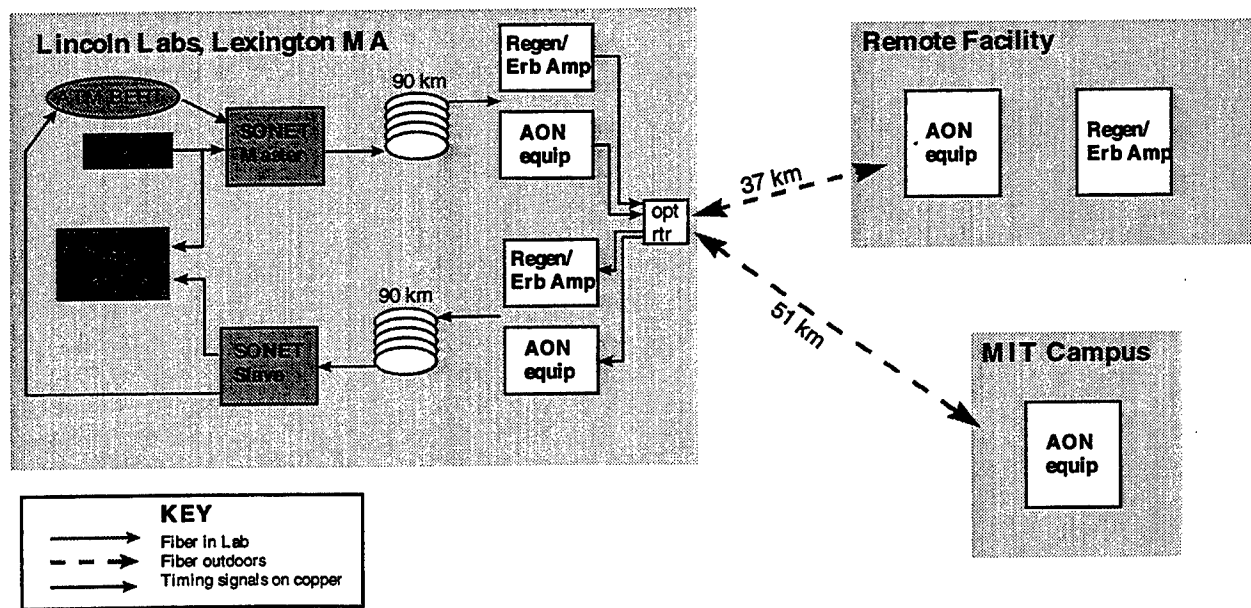


Figure 2: MIT/LL test-bed configuration

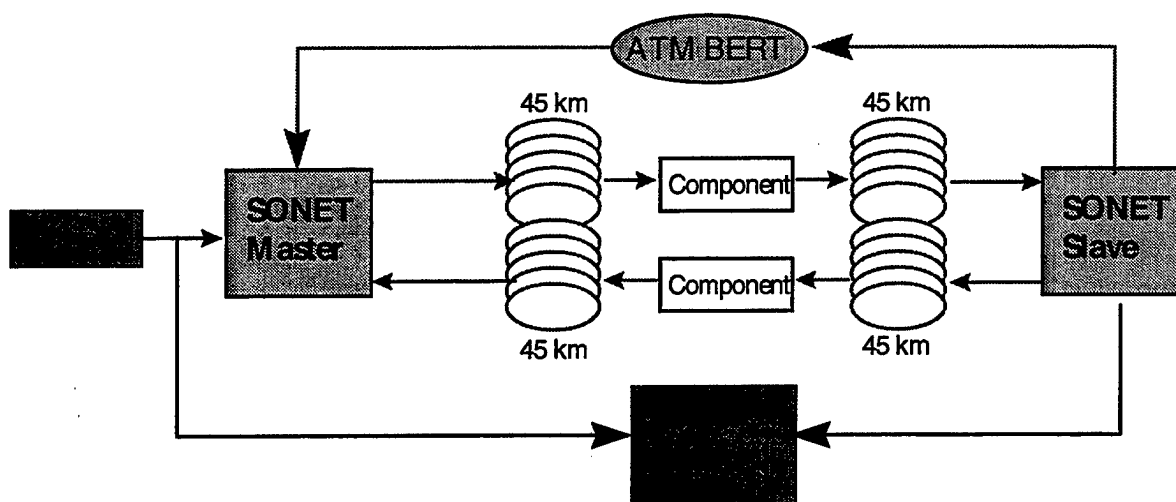


Figure 3: Laboratory configuration

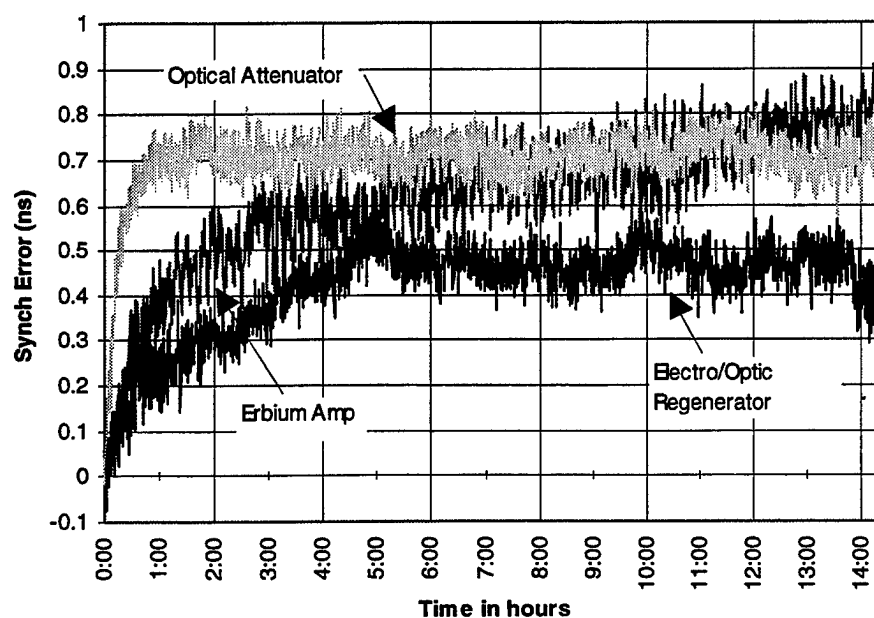


Figure 4: System Performance vs. various communications components in a lab environment

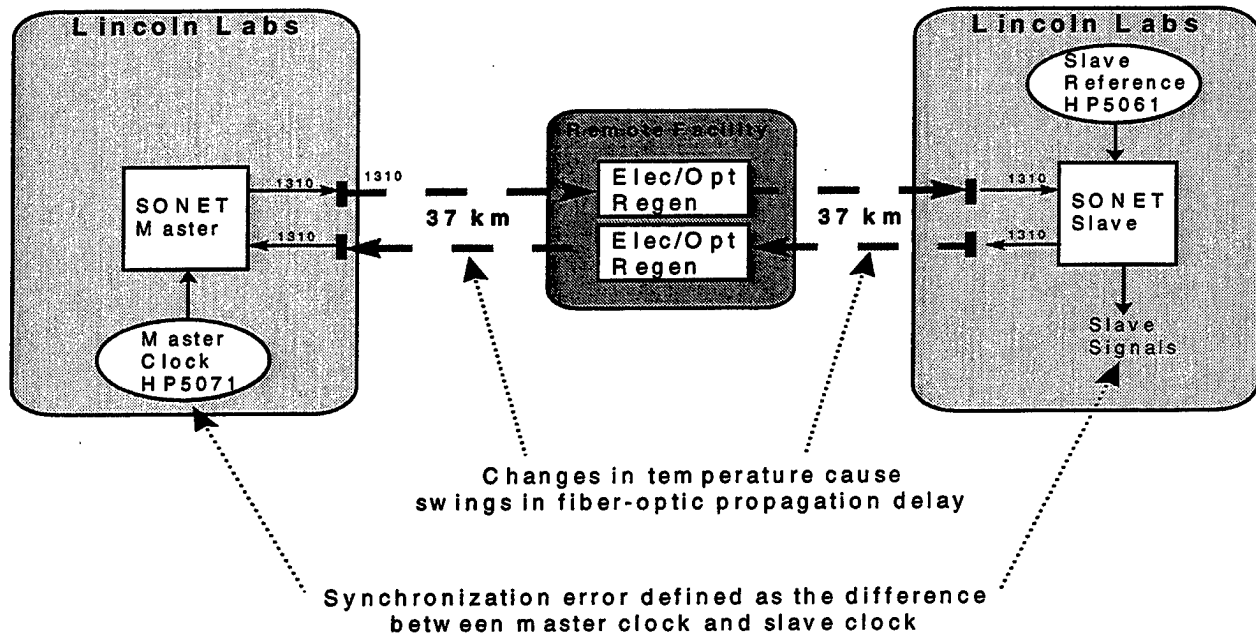


Figure 5: Equipment Configuration for Commercial Link Simulation

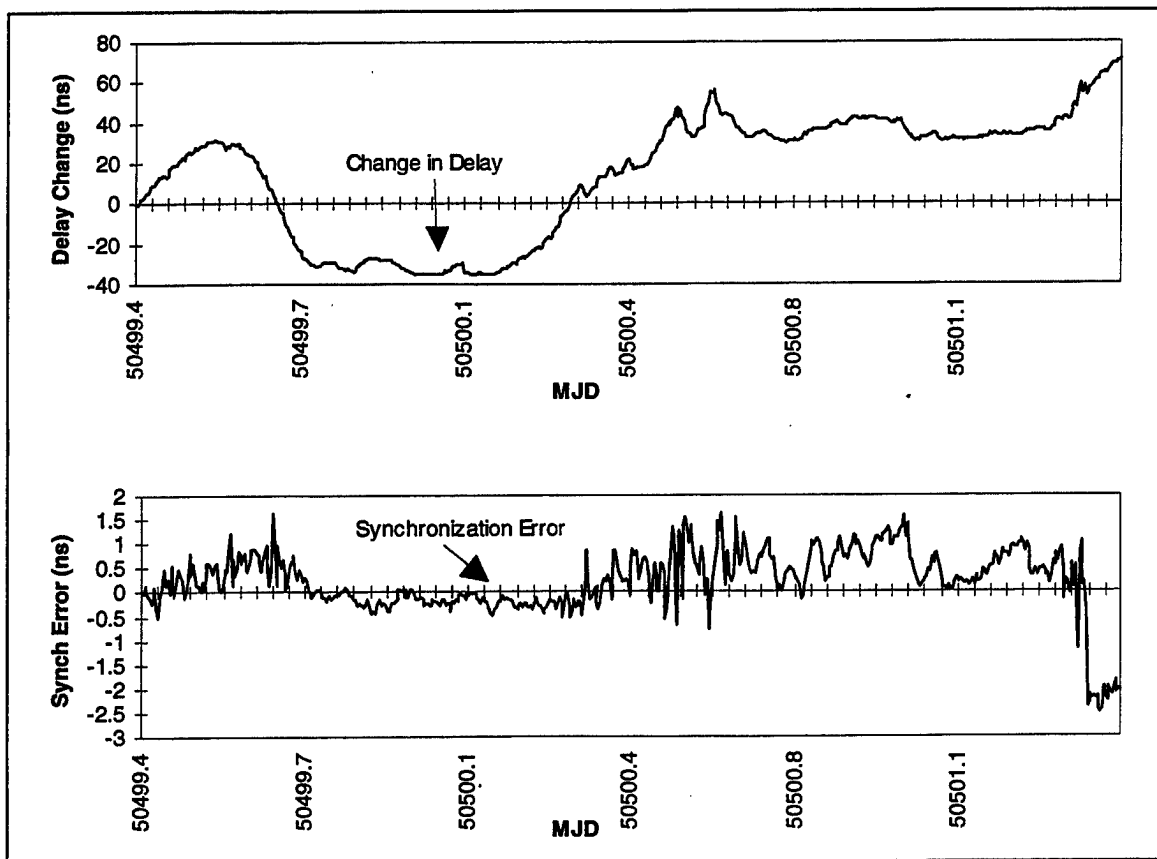


Figure 6: System Performance vs. Delay Change (74-km link)

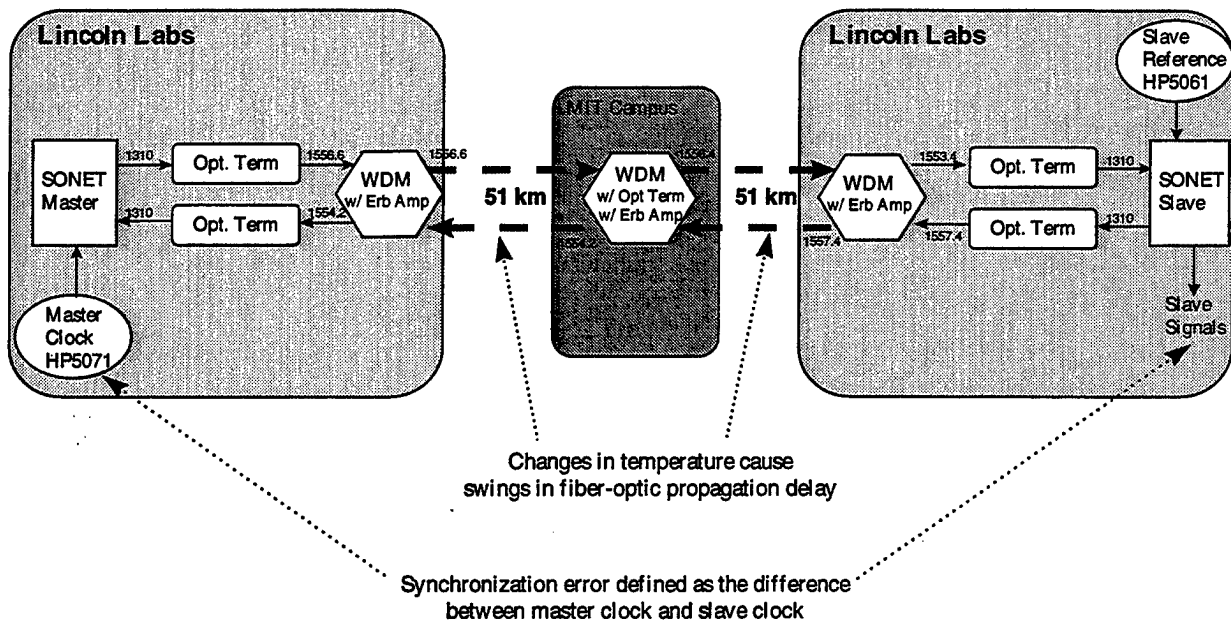


Figure 7: Hardware Configuration for All-Optical Link

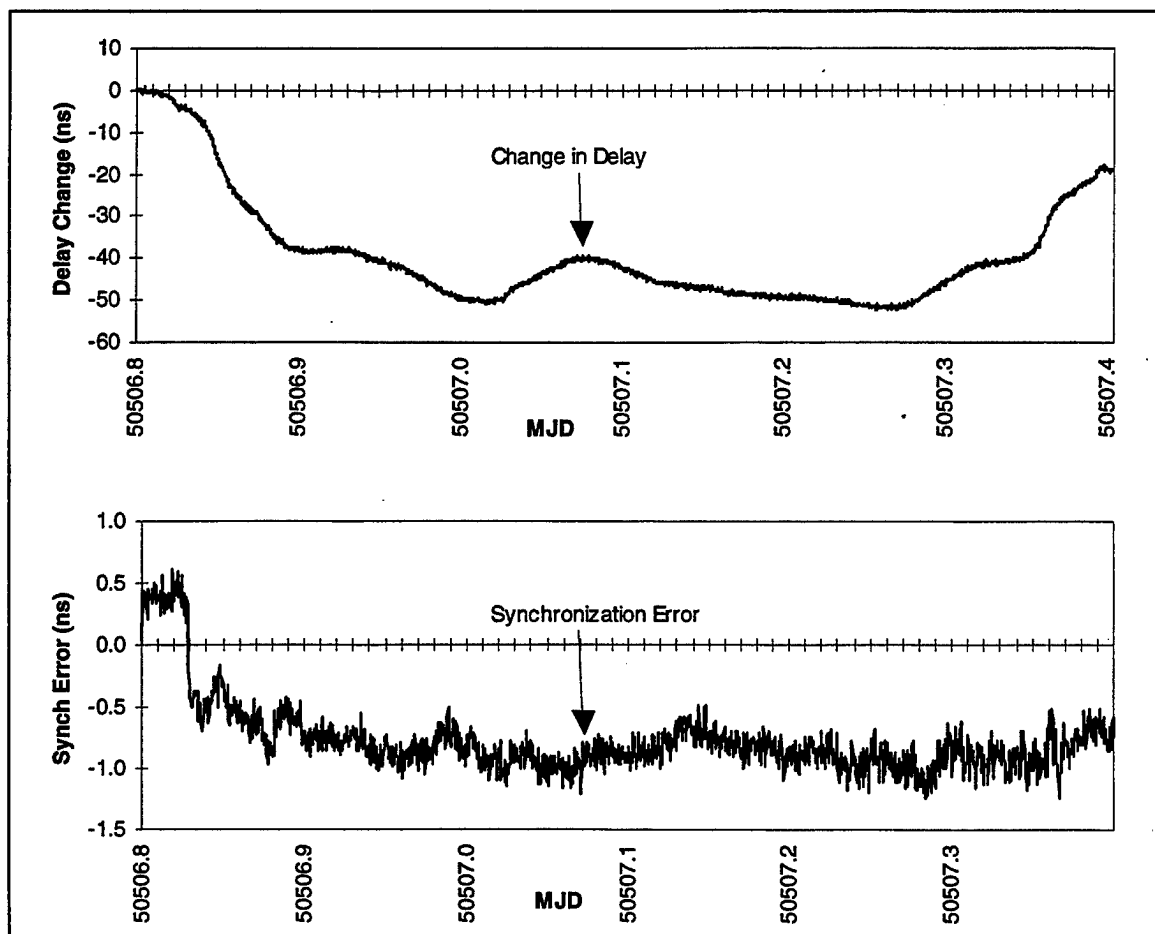


Figure 8: System Performance vs. Delay Change (102 km AON link)

Questions and Answers

MASAMI KIHARA (NTT): I would like to ask about fiber dispersion. You tested a long distance, and you used a very crossed wave length. It is okay. But if you wanted to expand the system to a long way, I think that you have to think about fiber dispersion. What do you think about that?

SAM STEIN (TIMING SOLUTIONS): You are right. For instance, fiber dispersion would probably be the limiting factor for use in an undersea cable. We looked at that a little bit because the optical terminals on the WDM system, the AON, are tunable. So we were able to actually offset the frequencies while the system was running and study the dispersion.

DAVE HOWE (NIST): Sam, it looks like there is a scaling between the round-trip delay and the noise that you encounter with two-way. Can you predict what levels of noise you might see if the round-trip delays are extended beyond 50 nanoseconds in their variations and what situations that might occur?

SAM STEIN: I guess I do not understand why you think there is a scaling.

DAVE HOWE: It just appeared from your plots, but maybe you have not experienced that generally.

SAM STEIN: Normally, for instance, in manufacturing, we evaluate these systems with 20 feet of fiber; we ship them to a customer where they are typically installed with one or two kilometers of fiber; and here we show data with 100 kilometers of fiber. I would say there is not a noticeable difference in performance in the three cases.

PTTI '97

ATTENDEES' LIST

Charles Abell
NASA
906 Old Barn Road
Orlando, FL 32825
Tel: 407-867-4457
Fax: 407-867-7133

Tim R. Armstrong
Industrial Research LTD
PO Box 31-310
Lower Hutt
NEW ZEALAND
Tel: 64 4 5690000
Fax: 64 4 5690194
t.armstrong@irl.cri.nz

Franklin Ascarrunz
Spectra Dynamics, Inc
440 Wellington Avenue
Lafayette, CO 80026
Tel: 303-604-6088
Fax: 303-604-6088

Floyd Ashbaugh
Efratom Time & Frequency Products
3 Parker
Irvine, CA 92618
Tel: 714-598-7758
Fax: 714-598-7676
fashbaugh@efratom.com

Glenn J. Atkinson
AlliedSignal Technical Services
4060 E. Bijou St.
Colorado Springs, CO 80909
Tel: 719-637-6182
Fax: 719-380-7144
glenn.atkinson@alliedsignal.com

Heinz Badura
Datum, Inc.
3 Parker
Irvine, CA 92618
Tel: 714-498-7660
Fax: 714-598-7650

Rich Bailey
Datum, Inc.
Bancomm-Timing Division
6781 Via Del Oro
San Jose, CA 95119
Tel: 408-578-4161
Fax: 408-574-4950
bt-sales@datum.com

Francoise S. Baumont
Observatoire de la Cote D'Azur
OCA/CERGA
Av. N. Copernic
06130 Grasse
FRANCE
Tel: 33 49 340 5338
Fax: 33 49 340 5333
baumont@obs-azur.fr

Ronald Beard
U.S. Naval Research Lab
4555 Overlook Avenue
Washington, DC 20375
Tel: 202-404-7054
Fax: 202-767-2845
beard@juno.nrl.navy.mil

Don J. Berg
AlliedSignal Technical Services
4060 E. Bijou St.
Colorado Springs, CO 80909
Tel: 719-637-6182
Fax: 719-380-7144

Laurent-Guy Bernier
Observatoire Cantonal de Neuchatel
Rue de l'Observatoire 58
Neuchatel CH-2000
SWITZERLAND
Tel: 41 32 8896870
Fax: 41 32 8896281
Laurent-Guy.Bernier@on.unine.ch

Jacques Beser
3S Navigation
4 Executive Circle, #200
Irvine, CA 92614
Tel: 714-862-5900
Fax: 714-862-5908
nav3s@aol.com

Olivier Bignon
2 rue Robert Keuer
Pont Sainte Faie France
FRANCE
Tel: 33-325-764500
Fax: 33-325-803-457
non615.173@compuserve.com

James Bleich
NELO Det PS
476 W Street
Bremerton, WA 98314
Tel: 360-476-4052

Reeves E. Bower
2 SOPS/USAF
300 O'Malley Avenue
Suite 41
Falcon AFB, CO 80912
Tel: 719-567-6377
Fax: 719-567-6307
bowerre@fafb.af.mil

Lee A. Breakiron
U.S. Naval Observatory
3450 Massachusetts Avenue, NW
Washington, DC 20392-5420
Tel: 202-762-1092
Fax: 202-762-1511
lab@tycho.usno.navy.mil

Gabriel Briceno
Efratom Time and Frequency Products
3 Parker
Irvine, CA 92618
Tel: 598-7675
Fax: 714-598-7676
gbriceno@efratom.com

Wayne Bui
Efratom Time and Frequency Products
3 Parker
Irvine, CA 92618
Tel: 714-598-7764
Fax: 714-598-7676
wbui@efratom.com

James Buisson
Antoine Enterprises, Inc
6220 Julian Lane
Mineral, VA 23117
Tel: 202-404-7062
Fax: 202-767-2845
buisson@juno.nrl.navy.mil

Eric A. Burt
U.S. Naval Observatory
3450 Massachusetts Avenue, NW
Washington, DC 20392-5420
Tel: 202-762-0308
Fax: 202-762-1511
burt@atom.usno.navy.mil

Edgar W. Butterline
Telecom Solutions
1461 Carlisle Road
North Brunswick, NJ 08902
Tel: 732-246-7891
Fax: 732-246-7277
butterline1@attmail.com

Otokar Buzek
Institute of Radioengineering and
Electronics-Prague
Czech Academy of Sciences
Chaberska 57
182-51 Praha
CZECH REPUBLIC
Tel: 420 2 6880144
Fax: 420 2 6880222
buzek@ure.cas.cz

Malcolm D. Calhoun
Jet Propulsion Laboratory
4800 Oak Grove Drive
MS 298
Pasadena, CA 91109
Tel: 818-354-9763
Fax: 818-393-6773
Malcolm.d.Calhoun@jpl.nasa.gov

Hank W. Cannella
AT&T Corp.
1316 Camelot Drive
Easton, PA 18045-2134
Tel: 610-559-9344
Fax: 610-559-7328
hcannella@att.com

Rick A. Cannon
ITT/FSC
1415 N. Bradley Road
Santa Maria, CA 93454

Peter E. Cash
Frequency and Time Systems, Inc.
34 Tozer Road
Beverly, MA 01915
Tel: 978-927-8220
Fax: 978-927-4099

William F. Cashin
Efratom Time & Frequency Products
3 Parker
Irvine, CA 92618
Tel: 714-598-7600
wcashin@efratom.com

Thomas P. Celano
Timing Solutions Corporation
5335 Sterling Drive
Boulder, CO 80301
Tel: 303-939-8481
Fax: 303-443-5152
celano@iname.com

Harold Chadsey
U.S. Naval Observatory
3450 Massachusetts Avenue, NW
Washington, DC 20392-5420
Tel: 202-762-1450
Fax: 202-762-1511
hc@planck.usno.navy.mil

Ling C. Chan
GPS World Magazine
859 Willamette Street
Eugene, OR 97401
Tel: 541-343-1200
Fax: 541-344-3514
editmail-gps@gpsworld.com

Yat C. Chan
The Aerospace Corp.
El Segundo Blvd.
El Segundo, CA
Tel: 310-336-4535
yat.c.chan@aero.org

Lee Chenoweth
Odetics Telecom
1585 S. Manchester Avenue
Anaheim, CA 92802
Tel: 714-780-7632
Fax: 714-780-7696
lac3@odetics.com

Hock Ann Chua
Singapore Productivity and Standards
Board
1 Science Park Drive 118221
SINGAPORE
Tel: 65 772 9602
Fax: 65 778 3798
sisirmisc@po.pacific.net.sg

Michael Cimafronte
System Technology Associates, Inc.
1631 South Murray Blvd.
Colorado Springs, CO 80916
Tel: 719-596-8550
Fax: 719-596-4588
mcimafron@stat.com

Franco Cordara
Istituto Elettrotecnico Nazionale
Strada Delle Cacce, 91
Turin 10135
ITALY
Tel: 39 11 3919239
Fax: 39 11 346384
cordara@tf.ien.it

Michael Costa
Lockheed Martin
6030 Boone Drive
Castro Valley, CA 94552
Tel: 408-742-8928
Fax: 408-742-4435

David T. Crater
2 SOPS/USAF
300 O'Malley Avenue
Suite 41
Falcon AFB, CO 80912
Tel: 719-567-2541
Fax: 719-567-6307
craterdt@fafb.af.mil

Jeffrey D. Crum
2 SOPS/USAF
300 O'Malley Avenue
Suite 41
Falcon AFB, CO 80912
Tel: 719-567-6369
Fax: 719-567-6307
crumjd@fafb.af.mil

Leonard S. Cutler
Hewlett-Packard Laboratories
3500 Deer Creek Road
MS 26M-9
Palo Alto, CA 94304
Tel: 650-857-5259
Fax: 650-813-3448
Len_Cutler@hpl.hp.com

Zhongning Dai
Singapore Productivity and Standards
Board
1 Science Park Drive 118221
SINGAPORE
Tel: 65 772 9602
Fax: 65 778 3798
sisirmisc@po.pacific.net.sg

Theodore C. Dass III
ITT ACD
6974 Los Reyes Circle
Colorado Springs, CO 80918-6009
Tel: 719-567-3928
Fax: 719-567-3927
dasstc@afmc.fafb.af.mil

John A. Davis
National Physical Laboratory
Queens Road
Teddington Middlesex TW11 0LW
UNITED KINGDOM
Tel: 44 181 943 7137
Fax: 44 181 943 7138
John.Davis@npl.co.uk

Thomas L. Davis
Raytheon TI Systems
Advanced Weapons Programs
2730 Timberleaf
Carrollton, TX 75006
Tel: 972-575-4958
Fax: 972-575-6809
E-mail: tom-l-davis

Gerrit de Jong
NMI Van Swinden Laboratorium
PO Box 054
Delft 2600 AR
NETHERLANDS
Tel: 31 15 2601623
Fax: 31 15 261 2971
gdejong@nmi.nl

Edoardo Detoma
Allied Signal Technical Services
Corso Montecucco 95
Torino, Italy 10141
ITALY
Tel: 39-11-3854579
dtomae@computer.org

G. John Dick
Jet Propulsion Laboratory
4800 Oak Grove Drive
MS 298-100
Pasadena, CA 91109
Tel: 818-354-6393
Fax: 818-393-6773
John.Dick@jpl.nasa.gov

Rick Dielman
TrueTime, Inc.
2835 Duke Court
Santa Rosa, CA 95407
Tel: 707-528-1230
Fax: 707-527-6648

William A. Diener
Jet Propulsion Laboratory
4800 Oak Grove Drive
MS 298
Pasadena, CA 91109
Tel: 818-354-6770
Fax: 818-393-6773
bdiener@jpl.nasa.gov

Raymond DiEsposti
The Aerospace Corp.
PO Box 92957
Los Angeles, CA 90009
Tel: 310-336-8404
Fax: 310-336-2957, ext. 5076
diesposti@courier3.aero.org

Gary L. Dieter
Boeing
440 Discoverer Avenue
Suite 38
Falcon AFB, CO 80918
Tel: 719-567-3176
Fax: 719-567-2664
dietergl@afamcfa.fb.af.mil

Thomas P. Donaher
Spectracom Corp.
101 Despatch Drive
East Rochester, NY 14445
Tel: 716-381-4827
Fax: 716-381-4998
tdonaher@spectracomcorp.com

Rob Douglas
National Research Council of Canada
Room 1108 Bldg M-36
Ottawa, Canada K1A 0R6
CANADA
Tel: 613-993-5186
Fax: 613-952-1394
rob.douglas@nrc.ca

James V. Duffy
Absolute Time Corp.
800 Charcot Avenue, #110
San Jose, CA 95131
Tel: 408-383-1520
Fax: 408-383-0706

Steve Edwards
Odetics Telecom
1585 S. Manchester Avenue
Anaheim, CA 92802
Tel: 714-780-7640
Fax: 714-780-7696
swe@odetics.com

Willem N. Emmer
Boeing Defense & Space Group
2600 Westminster Blvd.
MS SN-12
Seal Beach, CA 90740-7644
Tel: 562-797-3387
Fax: 562-797-4651
willem.n.emmer@boeing.com

Thomas English
Efratom Time & Frequency Products
3 Parker
Irvine, CA 92618
Tel: 714-598-7600
tenglish@efratom.com

Sheila Faulkner
MEETINGS CONSULTANT
3159 Patrick Henry Drive
Falls Church, VA 22044
Tel: 703-532-6411
Fax: 703-532-6338
bopenyan@aol.com

Peter Fisk
CSIRO Australia
PO Box 218
Lindfield NSW 2070
AUSTRALIA
peterf@tip.csiro.au

Dick Flamm
United Space Alliance
USK 350
Kennedy Space Center 32899
Tel: 407-867-3145

Walt Fowler
Starlink Incorporated
6400 Hwy. 290 East
Suite 202
Austin, TX 78723
Tel: 512-454-5511
Fax: 512-454-5570

Gerald L. Freed
ITT Aerospace/Comm
100 Kingsland Road
Clifton, NJ 07014-1993
Tel: 973-284-2104
Fax: 973-284-3394
gfreed@acd.nj.itt.com

Hugo Fruehauf
Odetics Telecom
1585 S. Manchester Avenue
Anaheim, CA 92802
Tel: 714-780-7960
Fax: 714-780-7696
hxf@odetics.com

Robert Frueholz
The Aerospace Corp.
P.O. Box 92957
Los Angeles, CA 90009
Tel: 310-336-6801
Fax: 310-336-6801

Ed Fudurich
Efratom Time & Frequency Products
3 Parker
Irvine, CA 92618
Tel: 714-598-7801
Fax: 714-598-7676
efdurich@efratom.com

Jean C. Gaignebet
OCA/CERGA
Av. N. Copernic
06130 Grasse
FRANCE
Tel: 33 49 340 5338
Fax: 33 49 340 5333
gaignebet@obs-azur.fr

R. Michael Garvey
Frequency and Time Systems, Inc.
34 Tozer Road
Beverly, MA 01915
Tel: 978-927-8220
Fax: 978-927-4099

Dick Gast
TRAK Systems
4726 Eisenhower Blvd.
Tampa, FL 33129
Tel: 813-884-1411
Fax: 813-884-0981
dgast@trak.com

Gary Geil
Geil Marketing
27134 Paseo Espada
Ste. B223
San Juan Capistrano, CA 92675
Tel: 714-489-7644
Fax: 714-489-7646

Al Gifford
U.S. Naval Observatory
1101 Maryland Avenue, NW
Washington, DC 20002
Tel: 703-808-2606
algifford@aol.com

William Gilbert
US Army White Sands Missile Range
Stews Neo-Dt-0 Bldg 1530
White Sands, NM 88002
Tel: 505-768-3396
Fax: 505-768-0237
gilbertw@wsmr.army.mil

Charles A. Greenhall
Jet Propulsion Laboratory
4800 Oak Grove Drive
MS 298-100
Pasadena, CA 91109
Tel: 818-393-6944
Fax: 818-393-6773
cgreen@pop.jpl.nasa.gov

Allen Gross
WR Inc.
7104 West 4th St.
Pueblo, CO 81003
Tel: 719-595-9880
Fax: 719-595-9890

Jeff Grous
Spectrum Geophysical Instruments
18271 W. McDermott #F
Irvine, CA 92614
Tel: 714-544-3000
Fax: 714-544-8307
joesmie@pacbell.net

Bernard Guinot
Observatoire de Paris
2 rue de sourins
F 77590 Chartrettes
FRANCE
Tel: 331-6066-3693
bguinot@compuserve.com

Joerg Hahn
DLR Oberpfaffenhofen
PO Box 1116
Wessling D-82230
GERMANY
Tel: 49 8153 282335
Fax: 49 8153 281135
joerg.hahn@dlr.de

Thomas Heaton
California Institute of Technology
Mail Code 104-44
Pasadena, CA 91125
Tel: 426-568-4232
Fax: 426-568-2719
heaton@bombay.gps.caltech.edu

Helmut Hellwig
SAF/AQR
1919 South Eads Street
Suite 100
Arlington, VA 22202-3053
Tel: 703-602-9301
Fax: 703-602-4845
hellwig@af.pentagon.mil

Fred Hesse
Efratom Time and Frequency Products
3 Parker
Irvine, CA 92618
Tel: 714-598-7676
Fax: 714-598-7676
fhesse@efratom.com

Peter Hetzel
PTB
Bundesallee 100
Braunschweig 38116
GERMANY
Tel: 49 53 1 5924330
Fax: 49 53 1 5924479
time@ptb.de

David L. Hirsch
Starlink Incorporated
6400 Hwy. 290 East
Suite 202
Austin, TX 78723
Tel: 512-454-5511
Fax: 512-454-5570

Dieter Hoechtl
Technical University of Vienna
Treitlstrasse 1
A-1040 Vienna
AUSTRIA
Tel: 43 1 58801 8189
Fax: 43 1 586 3260
hoechtl@auto.tuwien.ac.at

Douglas W. Hogarth
20241 194th Place, NE
Woodinville, WA 98072-8889
Tel: 425-788-1507
DougHo@niceties.com

Dave Howe
NIST
325 Broadway
Boulder, CO 80303
Tel: 303-497-3277
dhowe@nist.gov

Steven T. Hutsell
U.S. Naval Observatory
400 O'Malley Avenue, Ste 44
Falcon AFB, CO 80912-4044
Tel: 719-567-6740
Fax: 719-567-6763
hutsellst@fafb.af.mil

Jeffrey Ingold
Allied Signal Technical Services
1 Bendix Road
Columbia, MD
Tel: 410-964-7188
Fax: 410-964-7187

Marilyn Ison
NYMA
2435 Vela Way Suite 1613
Los Angeles CA 90245
Tel: 310-363-2284
isonms@gpst.laafb.af.mil

Nicolette M. Jardine
U.S. Naval Observatory
Washington, DC 20392-5420
Tel: 202-762-1414

Kenneth J. Johnston
U.S. Naval Observatory
3450 Massachusetts Avenue, NW
Washington, DC 20392-5420
Tel: 202-762-1513
Fax: 202-762-1461
kjj@astro.usno.navy.mil

Sarunas K. Karuza
The Aerospace Corp.
2350 E. El Segundo Blvd.
El Segundo, CA 90245-4691
Tel: 310-336-6837
Fax: 310-336-6225

Shalom Kattan
Guide Technology
1630 Zanker Road
San Jose, CA 95112
Tel: 408-453-8511
Fax: 408-453-8515
shalom@guidetech.com

Scott A. Kier
TRAK Systems
4726 Eisenhower Blvd.
Tampa, FL 33634
Tel: 813-884-1411
Fax: 813-884-0981
skier@trak.com

Masami Kihara
NTT Optical Network Systems
Laboratories
1-1 Hikari-no-oka
Yokosuka Kanagawa 239
JAPAN
Tel: 81-468-59-3164
Fax: 81-468-55-1282
kihara@exa.onlab.ntt.co.jp

Gerald Kim
TRW Inc.
One Space Park Drive
S/B383
Redondo Beach, CA 90278
Tel: 310-812-2274

Sonia Kim
3S Navigation
4 Executive Circle, #200
Irvine, CA 92614
Tel: 714-862-5900
Fax: 714-862-5908
nav3s@aol.com

Albert Kirk
Jet Propulsion Laboratory
4800 Oak Grove Drive
MS 298-100
Pasadena, CA 91109
Tel: 818-354-3038
Fax: 818-393-6773
Albert.Kirk@jpl.nasa.gov

William Klepczynski
Innovative Solutions International
1608 Spring Hill Road, Suite 200
Vienna, VA 22182
Tel: 202-651-7670
Fax: 202-651-7699
wklepczy@aol.com

Paul A. Koppang
Datum, Inc.
1711 Holt Road
Tuscaloosa, AL 35404
Tel: 205-553-0038
Fax: 205-553-2768
pak@wwisp.com

Guenter Kramer
PTB
PO Box 3145
Braunschweig D-38023
GERMANY
Tel: 49 53 15924340
Fax: 49 53 5924423
guenter.framer@ptb.de

Greg Kret
TrueTime, Inc.
2835 Duke Court
Santa Rosa, CA 95407
Tel: 707-528-1230
Fax: 707-527-6648

Paul F. Kuhnle
Jet Propulsion Laboratory
4800 Oak Grove Drive
MS 298-100
Pasadena, CA 91109
Tel: 818-354-2715
Fax: 818-393-6773
Paul.F.Kuhnle@jpl.nasa.gov

Hans J. Kunze
Allen Osborne Associates
756 Lakefield Road
West Lake Village, CA 91361
Tel: 805-495-8420
Fax: 805-373-6067

E. F. Charles LaBerge
AlliedSignal
1300 E. Joppa Road
Baltimore, MD 21204
Tel: 410-583-4292
Fax: 410-583-4332
efclaberge@aol.com

Francois Lahaye
Natural Resources Canada
615 Booth Street
Ottawa Ontario K1A 0E9
CANADA
Tel: 613-995-4488
Fax: 613-995-3215
lahaye@geod.emr.ca

Marie Largay
Naval Research Laboratory
4555 Overlook Avenue, SW
Washington, DC 20375-5320
Tel: 202-767-9133
Fax: 202-767-2845
largay@juno.nrl.navy.mil

Dennis G. Larsen
U.S. Naval Observatory
3450 Massachusetts Avenue, NW
Washington, DC 20392-5420
Tel: 202-762-1538
Fax: 202-762-1461
dgl@spica.usno.navy.mil

Kristine Larson
University of Colorado at Boulder
Campus Box 440
Boulder, CO 80309-0440
Tel: 303-492-5141
Kristine@spot.colorado.edu

Ming Lee
Lockheed Martin
1111 Beltevia Rd.
Santa Maria, CA 93455
Tel: 805-348-2107
Fax: 805-348-2047
minglee@lmco.com

Albert Leong
The Aerospace Corp.
2350 E. El Segundo Blvd.
El Segundo, CA 90245-4691
Tel: 310-336-6444
Fax: 310-336-6225

Judah Levine
NIST
Time & Frequency Division
MS 847
325 Broadway
Boulder, CO 80303
Tel: 303-497-3903
Fax: 303-497-6461
jlevine@boulder.nist.gov

Wlodzimierz Lewandowski
BIPM
Pavillon de Breteuil
92312 Sevres Cedex
FRANCE
Tel: 33 1 45 077063
Fax: 33 1 45 077059
wlewandowski@bipm.fr

Funming Li
Efratom Time & Frequency Products
3 Parker
Irvine, CA 92618
Tel: 714-598-7678
Fax: 714-598-7676
fli@efratom.com

Chuck Little
Hewlett-Packard Co.
5301 Stevens Creek Blvd.
Santa Clara, CA 95052
Tel: 408-553-2506
Fax: 408-553-2058
Chuck_Little@hp.com

Patrick Logan
EG&G Special Projects
821 Grier Drive
Las Vegas, NV 89108
Tel: 702-361-1660

Douglas Lowrie
EG&G
35 Congress Street
Salem MA 01970
Tel: 508-745-3200
Fax: 508-741-4923

John McK. Luck
AUSLIG
Orroal Geodetic Observatory
Scrivener Building
Dunlop Court
2616 BRUCE A.C.T.
AUSTRALIA
Tel: 61 2 6201-4349
Fax: 61 2 6201-4221
johnluck@auslig.gov.au

Landa Luong
Hewlett Packard
5301 Stevens Creek
Santa Clara, CA 95052
Tel: 408-553-2911
Fax: 408-553-6891
landa@sc.hp.com

Phu V. Mai
U.S. Naval Observatory
3450 Massachusetts Avenue, NW
Washington, DC 20392-5420
Tel: 202-762-1593
Fax: 202-762-1511
phu@mycroft.usno.navy.mil

Leo A. Mallette
Hughes Space & Communications
2309 S. Santa Anita Avenue
Arcadia, CA 91006
Tel: 310-364-9243
Fax: 310-364-9048
lmallette@ccgate.hac.com

Demetrios N. Matsakis
U.S. Naval Observatory
3450 Massachusetts Avenue, NW
Washington, DC 20392-5420
Tel: 202-762-1587
Fax: 202-762-1511
dnm@orion.usno.navy.mil

Dennis D. McCarthy
U.S. Naval Observatory
3450 Massachusetts Avenue, NW
Washington, DC 20392-5420
Tel: 202-762-1837
Fax: 202-762-1511
dmc@maia.usno.navy.mil

Gary McIntire
6714 Doane Ave
Springfield, VA 22152
Tel: 703-321-0008
Fax: 703-321-7521
GBMcintire@aol.com

Angela D. McKinley
U.S. Naval Observatory
3450 Massachusetts Avenue, NW
Washington, DC 20392-5420
Tel: 202-762-1457
Fax: 202-762-1511
amd@tycho.usno.navy.mil

Jack McNabb
Trak Systems
4726 Eisenhower Blvd.
Tampa FL 33634
Tel: 813-884-1411
Fax: 813-884-0981
jsmcnabb@juno.com

Debbie Melnick
Meetings Verbatim
PO Box 941221
Atlanta, GA 31141
Tel: 770-414-5677

Amy Michel
University of Colorado
440 Wellington Avenue
Lafayette, CO 80026
Tel: 303-665-1582

Steven R. Mihelic
Arbiter Systems, Inc.
PO Box 2279
Paso Robles, CA 93447
Tel: 805-237-3831
Fax: 805-238-5717
arbiter@arbiter.com

David L. Mills
University of Delaware
Electrical Engineering Department
Newark, DE 19716
Tel: 302-831-8247
Fax: 302-831-4316
mills@udel.edu

Mihran Miranian
U.S. Naval Observatory
3450 Massachusetts Avenue, NW
Washington, DC 20392-5420
Tel: 202-762-1452
Fax: 202-762-1511
mm@aitken.usno.navy.mil

Donald H. Mitchell
TrueTime, Inc.
2835 Duke Court
Santa Rosa, CA 95407
Tel: 707-528-1230, ext. 118
Fax: 707-527-6648
dmitchell@truetime.com

H. Shawn Mobbs
2 SOPS/USAF
300 O'Malley Avenue
Suite 41
Falcon AFB, CO 80912
Tel: 719-567-2529
Fax: 719-567-6307
mobbs@fafb.af.mil

Philip J. Moore
University of Bath
Dept. of Electronic & Electrical
Engineering
Bath BA2 7AY
UNITED KINGDOM
Tel: 44 1225 826109
Fax: 44 1225 826305
p.j.moore@bath.ac.uk

David Munton
Applied Research Laboratory
10000 Burnet Road
Austin, TX 78713
Tel: 512-835-3831
Fax: 512-835-3259
dmunton@arlut.utexas.edu

Leonardo Mureddu
Stazione Astronomica
Str. 54 Loc. Poggio dei Pini
09012 Capoterra (CA)
ITALY
Tel: 39 70 725246
Fax: 39 70 725425
mureddu@ca.astro.it

Steven L. Myers
Arbiter Systems, Inc.
PO Box 2279
Paso Robles, CA 93447
Tel: 805-237-3831
Fax: 805-238-5717
arbiter@arbiter.com

Jerzy Nawrocki
Astrogeodynamical Observatory
Space Research Center Borowiec
62-035 Kornik near Poznan
POLAND
Tel: 48 61 8170187
Fax: 48 61 8170219
nawrocki@cbk.poznan.pl

Lisa M. Nelson
NIST
325 S. Broadway
Mailstop 847.4
Boulder, CO 80303-3328
Tel: 303-497-3378
Fax: 303-497-3228
lnelson@boulder.nist.gov

Robert Nelson
Sat Engr Res Corp.
7701 Woodmont Avenue #208
Bethesda, MD 20814
Tel: 301-657-9641
Fax: 301-657-9642
RobtNelson@aol.com

Karen F. O'Donoghue
Naval Surface Warfare Center
Code B35
17320 Dahlgren Road
Dahlgren, VA 22448
Tel: 540-653-1567
Fax: 540-653-8673
kodonog@nswc.navy.mil

Steve O'Neal
TRW Inc.
RS/2120
One Space Park
Redondo Beach, CA 90278
Tel: 310-814-3831

Orville J. Oaks
Naval Research Laboratory
4555 Overlook Avenue, SW
Washington, DC 20375-5320
Tel: 202-767-9133
Fax: 202-767-2845
oaks@juno.nrl.navy.mil

Bing Ong
Efratom Time & Frequency Products
3 Parker
Irvine, CA 92618
Tel: 714-598-7600
bong@efratom.com

Skip Osborne
Allen Osborne Associates
756 Lakefield Drive Bldg J
Westlake Village, CA 91361
Tel: 805-495-8420
Fax: 805-373-6667

Terry N. Osterdock
Absolute Time Corp.
800 Charcot Avenue, #110
San Jose, CA 95131
Tel: 408-383-1520
Fax: 408-383-0706
terry@absolutetime.com

Juan Palacio
Real Observatorio de la Armada
Seccion de Hora
Cecilio Pujazon S/N
San Fernando 11.110 Cadiz
SPAIN
Tel: 34 56 599 286
Fax: 34 56 599 366
jpalacio@roa.es

Paul Paquet
Royal Observatory of Belgium
Av. Circulaire 3
1180 Brussel
BELGIUM
Tel: 32 2 3730211
Fax: 32 2 3749822
paquet@oma.be

Nimisha D. Parikh
Odetics Telecom
1585 S. Manchester Avenue
Anaheim, CA 92802
Tel: 714-780-7684
Fax: 714-780-7696
ndp@odetics.com

Thomas Parker
NIST
325 Broadway
Boulder, CO 80303
Tel: 303-497-7881
Fax: 303-497-6461
tparker@bldrdoc.gov

Peter Paulovich
SPAWARSSYSCEN Charleston
Bldg. 165, Code 625PP
PO Box 1376
Norfolk, VA 23501-1376
Tel: 757-396-0287
Fax: 757-396-0518
paulovip@spawar.navy.mil

Alexander Pawlitzki
TimeTech GmbH
Nobelstr. 15
70569 Stuttgart
GERMANY
Tel: 49 711 67 8080
Fax: 49 711 67 80899

Gerard Petit
BIPM
Pavillon de Breteuil
92312 Sevres Cedex
FRANCE
Tel: 33 14 5077067
Fax: 33 14 5077059
gpetit@bipm.fr

Long Pham
Efratom Time and Frequency
3 Parker
Irvine, CA 92618
Tel: 714-598-7756
Fax: 714-598-7676
lpham@efratom.com

Daniel R. Pinda
Raytheon TI Systems
Advanced Programs
6600 Chase Oaks Blvd.
MS 8490
Plano, TX 75023
Tel: 972-575-0425
Fax: 972-575-6809
pinda@ti.com

Edward D. Powers
U.S. Naval Observatory
3450 Massachusetts Avenue, NW
Washington, DC 20392-5420
Tel: 202-762-1451
Fax: 202-762-1511
powers@drake.usno.navy.mil

Bruce Procter
US Army Yuma Proving Ground
4024 13th Place
Yuma, AZ 85364
Tel: 520-328-6381
Fax: 520-328-6388
bprocter@yuma-umn1.army.mil

David Rea
Spectrum Geophysical Instruments
18271 W. McDermott Suite F
Irvine, CA 92614
Tel: 714-544-3000
Fax: 714-544-8307
drea@spintime.com

Wilson G. Reid
SFA
6346 Lakewood Drive
Falls Church, VA 22041
Tel: 202-404-4015
Fax: 202-767-2845
reid@juno.nrl.navy.mil

Karl R. Reuning
Datum/FTS
34 Tozer Road
Beverly, MA 01915-5510
Tel: 978-927-8220
Fax: 978-927-4097
marketing@datum.com

William Riley
EG&G Inc.
35 Congress Street
Salem, MA 01970
Tel: 978-745-3200
Fax: 978-741-4923
wjr@egginc

Dave Robinson
Datum, Inc.
Bancomm-Timing Division
6781 Via Del Oro
San Jose, CA 95119
Tel: 408-578-4161
Fax: 408-574-4950
bt-sales@datum.com

Pascal Rochat
Tenelec Neuchatel
Mail 59
2000 Neuchatel Switzerland
SWITZERLAND
tekelec@vtx.ch

Steve Saks
The Aerospace Corp.
PO Box 92957
Los Angeles, CA 90009
Tel: 310-336-1883
Fax: 310-336-5076
saks@courier3.aero.org

Ken Sandfeld
Odetics Telecom
1585 S. Manchester Avenue
Anaheim, CA 92802
Tel: 714-780-7684
Fax: 714-780-7696
kps@odetics.com

Wolfgang Schafer
TimeTech GmbH
Nobelstr. 15
70569 Stuttgart
GERMANY
Tel: 49 711 67 8080
Fax: 49 711 67 80899

Richard E. Schmidt
U.S. Naval Observatory
3450 Massachusetts Avenue, NW
Washington, DC 20392-5420
Tel: 202-762-1578
Fax: 202-762-1511
res@tuttle.usno.navy.mil

Bill Schuh
ITT/FSC
PO Box 5728
MS 5250
Vandenberg AFB, CA 93437
Tel: 805-734-8232, ext. 6-3166

Ron Sigura
Guide Technology
1630 Zanker Road
San Jose, CA 95112
Tel: 408-453-8511
Fax: 408-453-8515
ron@guidetech.com

Gary Smith
Brandywine
3191-C Airport Loop Drive
Costa Mesa, CA 92626
Tel: 714-755-1050
Fax: 714-755-0713
brandywine@compuserve.com

Armin Soering
Deutsche Telekom AG
Zentrale, TN 236-5
Am Kavalleriesand 3 64295 Darmstadt
GERMANY
Tel: 49 6151 83-4549
Fax: 49 6151 83-3834
soering@usa.net

Samuel R. Stein
Timing Solutions Corporation
5335 Sterling Drive
Boulder, CO 80301
Tel: 303-939-8481
Fax: 303-443-5152
srstein@ibm.net

Michael J. Stone
Computer Sciences Raytheon
KSC Timing
Box 4127
Patrick AFB, FL 32925-0127
Tel: 407-861-1237
Fax: 407-861-1238
michael-stone@pafb.af.mil

Richard L. Sydnor
Jet Propulsion Laboratory
4800 Oak Grove Drive
MS 298-100
Pasadena, CA 91109
Tel: 818-354-0965
Fax: 818-393-6773
sydnor@horology.jpl.nasa.gov

Philip E. Talley
SFA/NRL
Space Technology
1022 Eagle Crest
Macon, GA 31211
Tel: 912-745-3415
petalley@mylink.net

Claudine Thomas
BIPM
Pavillon de Breteuil
92312 Sevres Cedex
FRANCE
Tel: 33 1 45 077073
Fax: 33 1 45 077059
cthomas@bipm.fr

Massimo Tinto
Jet Propulsion Laboratory
4800 Oak Grove
MS 161-260
Pasadena, CA 91109
Tel: 818-354-0798
Fax: 818-393-4643

Mike Tope
TrueTime, Inc.
2835 Duke Court
Santa Rosa, CA 95407
Tel: 707-528-1230
Fax: 707-527-6648

Minh Q. Tran
U.S. Naval Observatory
3450 Massachusetts Avenue, NW
Washington, DC 20392-5420
Tel: 202-762-0913
Fax: 202-762-1511
mtran@tsee11.usno.navy.mil

Marnius J. Van Melle
Boeing
5505 Flintridge Drive
Colorado Springs, CO 80918
Tel: 719-567-2705
Fax: 719-567-2664
vanmellemj@afamcfa.fb.af.mil

Francine M. Vannicola
U.S. Naval Observatory
3450 Massachusetts Avenue, NW
Washington, DC 20392-5420
Tel: 202-762-1455
Fax: 202-762-1511
fmv@cassini.usno.navy.mil

François Vernotte
Observatoire de Besançon
41 bis avenue de l'Observatoire
BP 1615
BESANCON 25410
FRANCE
Tel: 33-3-81-66-69-22
Fax: 33-3-81-66-69-44
francois@obs-besancon.fr

Frank J. Voit
The Aerospace Corp.
2350 E. El Segundo Blvd.
El Segundo, CA 90245-4691
Tel: 310-336-6764
Fax: 310-336-6225
voit@courier8.aero.org

Steven Waite
WR Inc
710 A West 4th Street
Pueblo, CO 81003
Tel: 719-595-9880
Fax: 719-595-9890
gpsman@fleetpc.com

Dennis Wakakuwa
EG&G Special Projects
821 Griek Drive
Las Vegas, NV 89101
Tel: 702-361-1660

Warren Walls
Femtosecond Systems
690 Arbutus Street
Golden, CO 80401
Tel: 303-462-0799
Fax: 303-462-6766
femtosecond@compuserve.com

Buell Walter
The Aerospace Corporation
P.O. Box 92957, MS M2-253
Los Angeles CA 90009-2957
Tel: 310-336-6942
Fax: 310-336-6801
walter.f.buell

Clark Wardrip
726 Foxenwood Drive
Santa Maria, CA 93455
Tel: 805-937-6448
Fax: 805-937-9601
skyclark@aol.com

Eric T. Watts
Boeing Defense & Space Group
2600 Westminster Blvd., MS SN-12
Seal Beach, CA 90740-7644
Tel: 562-797-3627
Fax: 562-797-4651
eric.t.watts@boeing.com

Robert Weaver
University of Southern California
MC 2565 / EEB516
Los Angeles, CA 90089-2565
Tel: 213-740-4686
Fax: 213-740-8729
rweaver@scf.usc.edu

Werner Weidemann
Datum Inc.
3 Parker
Irvine, CA 92618

Marc A. Weiss
NIST
325 S. Broadway
Mailstop 847
Boulder, CO 80303-3328
Tel: 303-497-3261
Fax: 303-497-6461
mweiss@boulder.nist.gov

Paul J. Wheeler
U.S. Naval Observatory
3450 Massachusetts Avenue, NW
Washington, DC 20392-5420
Tel: 202-762-1581
Fax: 202-762-1511
paul@tsee2.usno.navy.mil

Joseph D. White
Naval Research Laboratory
4555 Overlook Avenue, SW
Washington, DC 20375-5320
Tel: 202-767-5111
Fax: 202-767-2845
white@juno.nrl.navy.mil

Gernot M. R. Winkler
8517 Brickyard Road
Potomac, MD 20854
gmrwin@worldnet.att.net

William Wooden
NIMA
4600 Sangamore Rd. D-33
Bethesda, MD 20816
Tel: 301-227-3492
Fax: 301-227-4735
woodenb@nima.mil

Gary Wright
EG&G Special Projects
821 Grier Drive
Las Vegas, NV 89114
Tel: 702-369-3000

Andy C. Wu
The Aerospace Corp.
4452 Canoga Dr.
Woodland Hills, CA 91364
Tel: 310-336-0437
Fax: 310-336-5076
wu@courier3.aero.org